

4/26/96

SANDIA REPORT

SAND93-1000 • UC-721

Unlimited Release

Printed March 1996

RECEIVED

MAY 15 1996

OSTI

Data Report on the Waste Isolation Pilot Plant Small-Scale Seal Performance Test, Series F Grouting Experiment

E. H. Ahrens, T. F. Dale

Prepared by
Sandia National Laboratories
Albuquerque, New Mexico 87185 and Livermore, California 94550
for the United States Department of Energy
under Contract DE-AC04-94AL85000

Approved for public release; distribution is unlimited.



SF2900Q(8-81)

MASTER

DISTRIBUTION OF THIS DOCUMENT IS UNLIMITED

Die

Issued by Sandia National Laboratories, operated for the United States Department of Energy by Sandia Corporation.

NOTICE: This report was prepared as an account of work sponsored by an agency of the United States Government. Neither the United States Government nor any agency thereof, nor any of their employees, nor any of their contractors, subcontractors, or their employees, makes any warranty, express or implied, or assumes any legal liability or responsibility for the accuracy, completeness, or usefulness of any information, apparatus, product, or process disclosed, or represents that its use would not infringe privately owned rights. Reference herein to any specific commercial product, process, or service by trade name, trademark, manufacturer, or otherwise, does not necessarily constitute or imply its endorsement, recommendation, or favoring by the United States Government, any agency thereof or any of their contractors or subcontractors. The views and opinions expressed herein do not necessarily state or reflect those of the United States Government, any agency thereof or any of their contractors.

Printed in the United States of America. This report has been reproduced directly from the best available copy.

Available to DOE and DOE contractors from
Office of Scientific and Technical Information
PO Box 62
Oak Ridge, TN 37831

Prices available from (615) 576-8401, FTS 626-8401

Available to the public from
National Technical Information Service
US Department of Commerce
5285 Port Royal Rd
Springfield, VA 22161

NTIS price codes
Printed copy: A15
Microfiche copy: A01

SAND93-1000
Unlimited Release
Printed March 1996

Distribution
Category UC-721

Data Report on the Waste Isolation Pilot Plant Small-Scale Seal Performance Test, Series F Grouting Experiment

E. H. Ahrens
Nuclear Waste Technology Repository Isolation Systems
Sandia National Laboratories
Albuquerque, NM 87185

T. F. Dale
R. S. Van Pelt
INTERA, Inc.
Austin, TX 78731

ABSTRACT

The Small-Scale Seal Performance Test, Series F (SSSPT-F) was designed to evaluate sealing materials at the Waste Isolation Pilot Plant (WIPP). SSSPT-F demonstrated: (1) the ability to practically and consistently produce ultrafine cementitious grout at the grouting site; (2) successful, consistent, and efficient injection and permeation of the grout into fractured rock at the repository horizon; (3) the ability of the grout to penetrate and seal microfractures; (4) procedures and equipment used to inject the grout. Additionally, techniques to assess the effectiveness of the grout in reducing the gas transmissivity of the fractured rock were evaluated. These included gas-flow/tracer testing, post-grout coring, pre- and post-grout downhole televiewer logging, slab displacement measurements, and increased loading on jacks during grout injection. Pre- and post-grout diamond drill core was obtained for use in ongoing evaluations of grouting effectiveness, degradation, and compatibility. Diamond drill equipment invented for this test successfully prevented drill cuttings from plugging fractures in grout injection holes.

ACKNOWLEDGMENTS

The authors wish to express appreciation for the enthusiastic support received from the following people:

- Denny Just, Arno Szegvari, Margaret Yang, and Rick Wolcke of Union Process, Inc., Akron, OH, for their aid during laboratory evaluation and pilot testing of the Szegvari Attritor.
- Maria Onofrei and Barry Shenton of Whiteshell Laboratories, Pinawa, Manitoba, for their aid in the successful development, optimization, and testing of the ultrafine cementitious grout.
- Harvey Ogden and Lee Jensen of Sandia National Laboratories (SNL) for their invaluable aid in properly configuring the data acquisition system.
- Ray Finley and Tim George of SNL for their help in site and equipment selection.
- Westinghouse personnel at the WIPP, especially the Experimental Operations employees whose suggestions and hard work expedited the experiment.
- Bill Horvath, Angus Robb, and Wesley DeYonge of RE/SPEC, Inc. for their valuable aid in properly instrumenting the test.
- Scott Evans of Christensen Diamond Products for his help with fabrication of the reverse-circulation diamond drill equipment.
- Cliff Howard of RE/SPEC, Inc. for his dedication to the task of Cognizant Engineer, including preparation of the numerous documents and forms required.
- Joe Tillerson, Frank Hansen, and Rudolph Matalucci of SNL for their helpful draft review comments.

CONTENTS

1.0	INTRODUCTION.....	1
1.1	Background.....	1
1.2	WIPP Sealing Strategy.....	5
1.3	Test Objectives.....	6
1.4	Test Description.....	6
2.0	PRE-GROUT ACTIVITIES.....	11
2.1	Selection of Test Location.....	11
2.2	Concrete Slab and Floor Jacks.....	12
2.3	Drilling.....	14
2.4	Borehole Array.....	16
2.5	On-Slab Permeability Tests.....	21
3.0	GROUTING	23
3.1	Sequence of Work.....	25
3.2	Grouting Summary.....	30
3.2.1	Particle Size Determination and Rheology.....	30
3.2.2	Grout Characterization.....	31
4.0	FORMATION CHARACTERIZATION TESTS.....	39
4.1	Gas-Injection Tests.....	39
4.2	Constant-Pressure Gas-Injection Permeability Tests.....	40
4.2.1	Testing Procedure.....	40
4.2.2	Test-Zone Pressure Responses to Injection.....	41
4.3	Tracer-Gas-Injection Testing.....	46
4.3.1	Tracer-Gas-Injection Procedure.....	46
4.3.2	Tracer-Gas-Recovery Data.....	47
4.4	Interpretation Methodology.....	48
4.4.1	Well-Test Simulation Model.....	48
4.4.2	Gas-Permeability Testing Analysis Procedures.....	48
4.4.3	Individual Test Interpretations.....	50
4.4.4	Sensitivity Analyses.....	52
5.0	SUMMARY AND CONCLUSIONS.....	59
5.1	Results.....	59
5.2	Conclusions and Recommendations.....	67
5.2.1	Conclusions.....	67
5.2.2	Suggestions for Future Work.....	67
6.0	REFERENCES.....	69

CONTENTS (Continued)

APPENDIX A:	Grout Development.....	A-1
APPENDIX B:	Floor Restraint System Development.....	B-1
APPENDIX C:	Diamond Drilling Equipment.....	C-1
APPENDIX D:	Gas-Flow/Tracer-Gas Test Equipment.....	D-1
APPENDIX E:	Grouting Equipment.....	E-1
APPENDIX F:	Extensometer Data.....	F-1
APPENDIX G:	Grout Injection Data.....	G-1
APPENDIX H:	Grout Distribution Data.....	H-1
APPENDIX I:	Gas-Flow/Tracer-Gas Test Results.....	I-1
APPENDIX J:	GTFM Flow Model.....	J-1

Photographs

2-1	Reverse-circulation diamond drill.....	17
5-1	Electron microphotograph showing grout "pinch out" at ± 10 microns...	61
5-2	Electron microphotograph showing grout passing through a 7.9-micron constriction.....	61
5-3	Electron microphotograph showing a grout-filled fracture 6 microns wide.....	62
5-4	Electron microphotograph showing a grout-filled fracture 3 microns wide.....	62

Tables

2-1	Hole Coordinate and Drilling Summary.....	18
3-1	Batching and Injection Times for all Grouted Holes.....	23
3-2	Grout Hole Volumes.....	28
3-3	Rheology Data at Lowest Measured Shear Rate (24 1/s).....	32
3-4	Grout Characterization.....	38

Figures

1-1	The WIPP facility (with location of Room L3).....	2
1-2	Disturbed rock zone adjacent to WIPP underground excavations.....	4
1-3	Local stratigraphy around Room L3.....	7
1-4	Plan and elevation views of Room L3, showing slab location.....	9
1-5	Three-dimensional representation of the slab, test holes, DRZ, and stratigraphy below Room L3.....	10
2-1	Typical floor jack arrangement at a grout hole.....	13
2-2	Diagram of reverse circulation drilling system.....	15
2-3	Location of holes drilled for SSSPT-F.....	20
3-1	Attritor tank principle.....	24
3-2	Grout pulverization and injection system.....	26
4-1	Tracer gas injection and sampling equipment.....	42
4-2	Gas-permeability testing results for borehole L3X10 during the third round of testing on April 10, 1993.....	44
4-3	Gas-permeability testing results for borehole L3215 during the first round of testing on January 20, 1993.....	44
4-4	Gas-permeability testing results for borehole L3202 during the second round of testing on March 3, 1993.....	45
4-5	Gas-permeability testing results for borehole L3212 during the third round of testing on April 6, 1993.....	45
4-6	Permeability sensitivity analysis for gas-permeability testing of borehole L3X10 on April 10, 1993.....	54
4-7	Permeability sensitivity analysis for gas-permeability testing of borehole L3215 on January 20, 1993.....	54
4-8	Permeability sensitivity analysis for gas-permeability testing of borehole L3202 on March 3, 1993.....	55
4-9	Permeability sensitivity analysis for gas-permeability testing of borehole L3212 on April 6, 1993.....	55
4-10	Test-zone volume sensitivity analysis for gas-permeability testing of borehole L3X10 on April 10, 1993.....	57
4-11	Test-zone volume sensitivity analysis for gas-permeability testing of borehole L3215 on January 20, 1993.....	57
4-12	Test-zone volume sensitivity analysis for gas-permeability testing of borehole L3202 on March 3, 1993.....	58
4-13	Test-zone volume sensitivity analysis for gas-permeability testing of borehole L3212 on April 6, 1993.....	58
5-1	Qualitative spectral peaks produced by energy dispersive x-ray, verifying that material in fracture is grout.....	63
5-2	Log permeability contours derived from pre-grout (January 1993) gas-flow tests.....	65
5-3	Log permeability contours derived from post-primary grout (March 1993) gas-flow tests.....	65
5-4	Log permeability contours derived from post-secondary grout (April 1993) gas-flow tests.....	66
5-5	Order-of-magnitude change in permeability achieved by grouting.....	66

This page intentionally left blank.

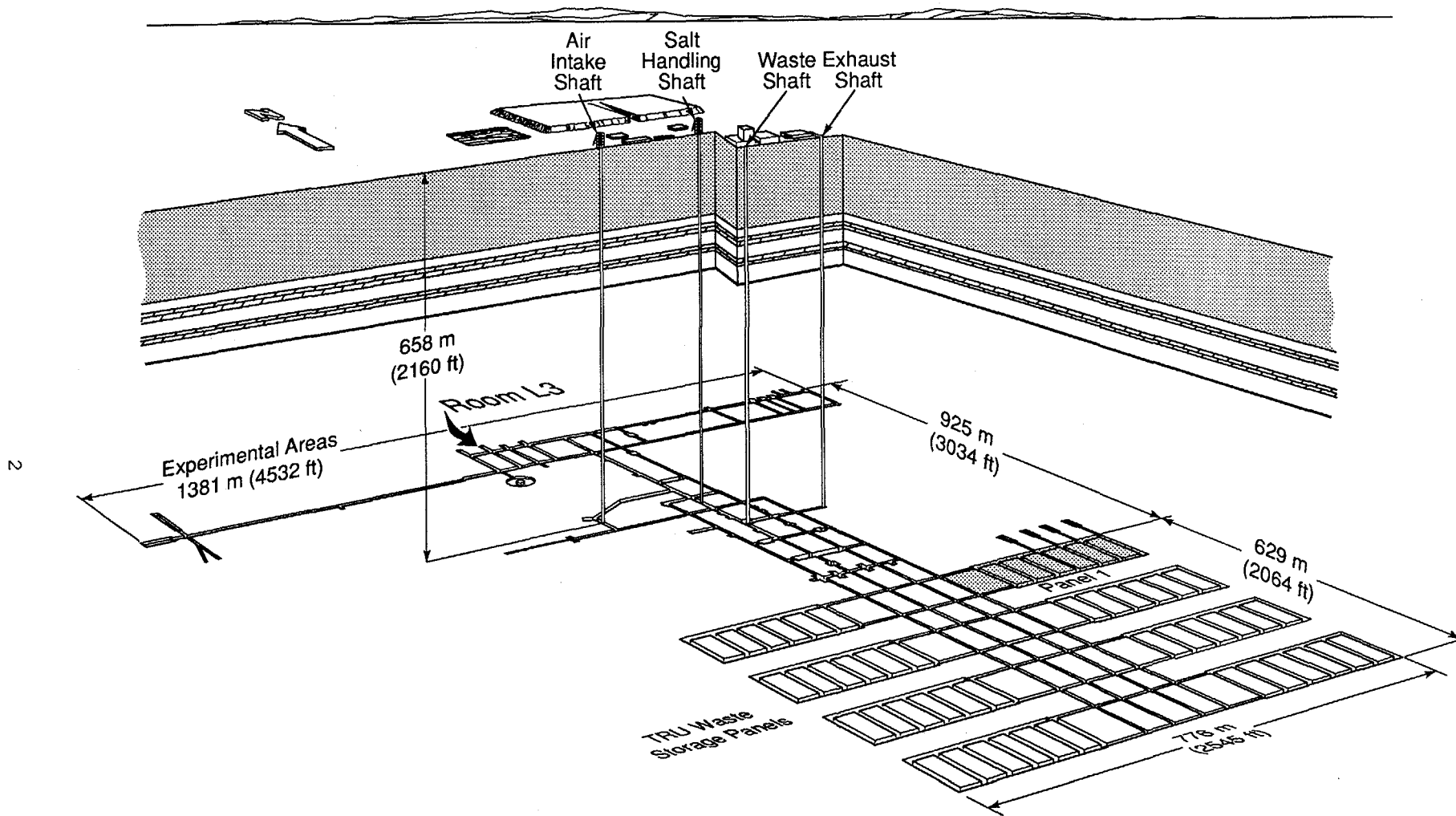
1.0 INTRODUCTION

This report presents data from tests conducted at the Waste Isolation Pilot Plant (WIPP) in southeastern New Mexico. The WIPP is a US Department of Energy (DOE) research and development facility designed to examine methods for safe long-term storage of transuranic (TRU) radioactive wastes generated by US defense programs.

The underground part of the WIPP development is divided into two sections: the north experimental area and the south operational area (Figure 1-1). The test described in this data report is the Small-Scale Seal Performance Test, Series F (SSSPT-F), which was conducted in test Room L3 in the experimental area. The SSSPTs are a set of in situ experiments designed to evaluate the performance of various candidate sealing materials. Results from these tests will be assessed using structural and flow data generated under expected repository conditions. SSSPT-F was designed to demonstrate equipment and techniques for producing, injecting, and evaluating ultrafine cementitious grout. The information presented in this data report is intended to support the development of the Alcove Gas Barrier System (AGBS), the design of upcoming large-scale seal tests, and ongoing laboratory evaluations of grouting efficacy. This data report contains a comprehensive description of the SSSPT-F experiment, including site preparation operations, grouting activities, and formation characterization tests. More specific details about the individual components of the experiment are described in the appendices. Appendix A explains the process used to develop the grout for SSSPT-F. Appendices B, C, D, and E describe the equipment developed for and used in the experiment. Appendices F and G contain plots representing the significant data collected during the experiment. Appendix H describes the post-experiment methods used to determine the scope of grout permeation. Appendix I describes the gas-flow and tracer-gas tests that were used to characterize formation permeability; it also contains memoranda that pertain to these tests. Appendix J contains a description of the flow model used to interpret the permeability tests.

1.1 Background

The WIPP disposal horizon is located approximately 658 m below ground surface in the Salado Formation. The Salado is a 600-m-thick sequence of bedded evaporites (sedimentary salts) that were deposited during the Permian period over 225 million years ago. One advantage of salt as a host for radioactive waste isolation is its ability to deform by creep and ultimately enclose the waste. Creep closure of all excavated WIPP openings begins



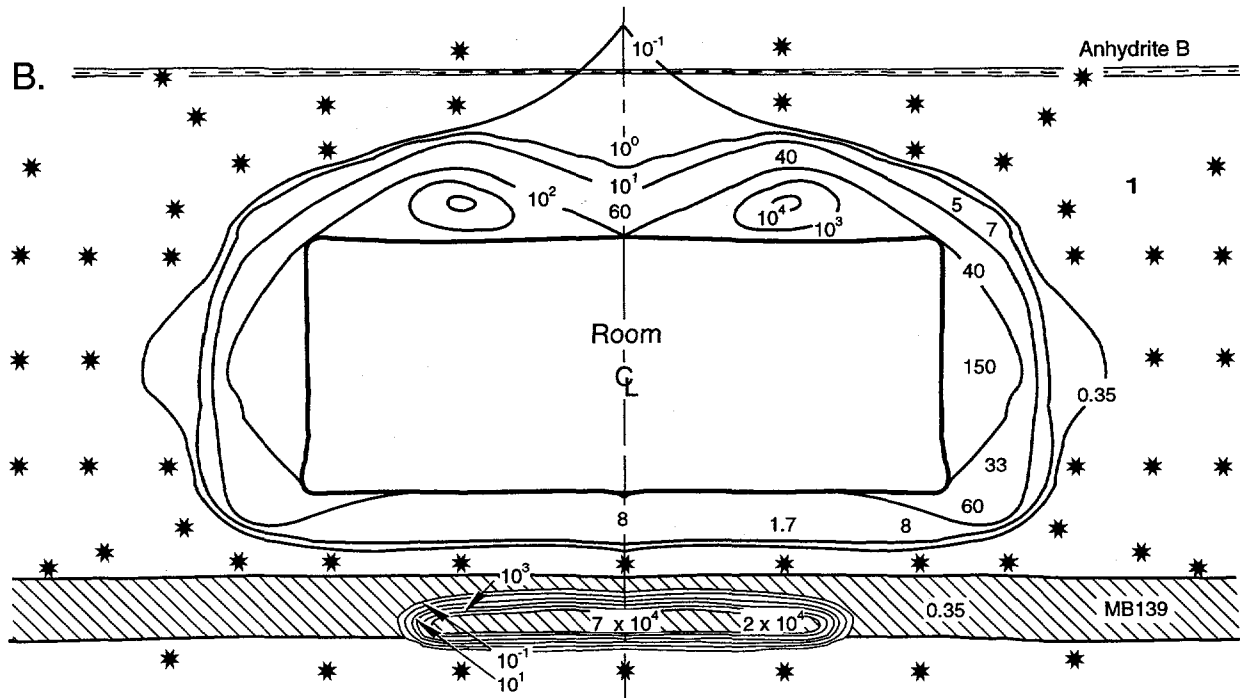
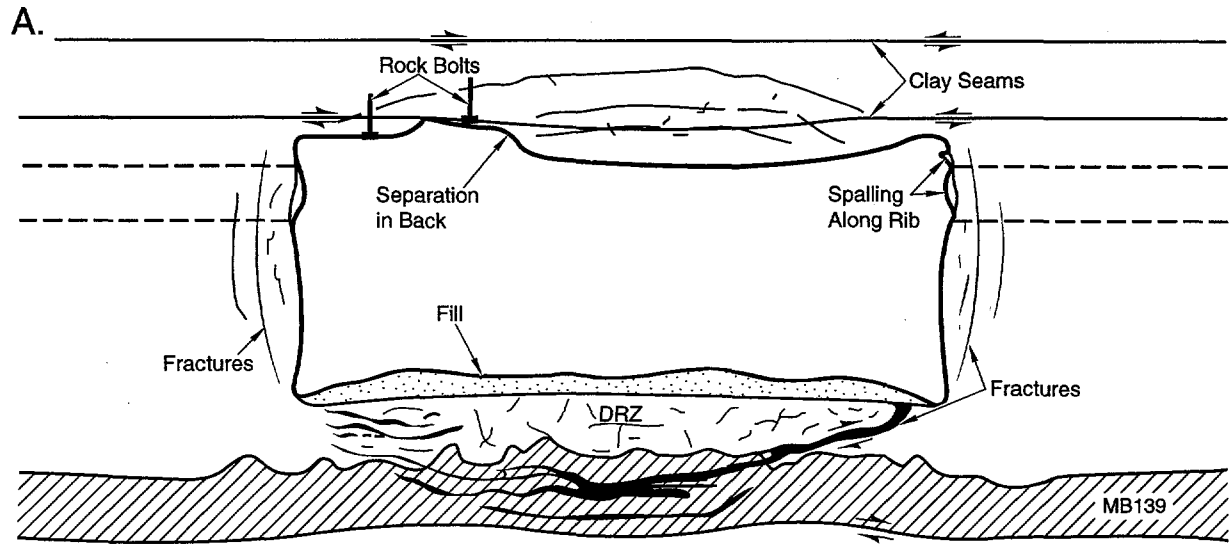
TRI-6346-59-25

Figure 1-1. The WIPP facility (with location of Room L3).

immediately after excavation, with early time closure rates on the order of several cm per year (Munson et al., 1989). Given sufficient time, fracturing from excavation-related stress redistribution creates a near-field zone of mechanically altered rock within the first few meters of the excavations.

Within the disturbed rock zone (DRZ), fractures can increase the permeability of the rock by a few orders of magnitude (Borns and Stormont, 1988). Although the DRZ in halite will eventually heal by creep closure, the local stratigraphy at the repository horizon contains several, almost horizontal layers of anhydrite, polyhalite, and halite, as well as thin clay seams. Of particular note are (1) Marker Bed 139 (MB139), the heterogeneous interbed approximately 2 m below the floor of the repository horizon, and (2) the intervening halite, which commonly exhibits fracturing (Stormont et al., 1987). MB139 is nominally a multilithologic unit consisting of laterally discontinuous lenses of halite, polyhalite, anhydrite, minor gypsum, and thin clay seams. This interbed is approximately 1 m thick and is parallel to the repository floor at depths varying between 2 and 3 m.

Stress redistribution around all excavations induces movement that results in dilation, primarily along depositional interfaces and/or existing flat-lying fractures in relatively hard and brittle units like MB139, as represented in Figure 1-2. Current evidence suggests that continued closure of WIPP excavations over time may result in separations or fractures along the marker-bed/salt interface or within the marker bed (Stormont, 1990). DRZ development has been observed around all excavations, but is more extensive around the wider (>7 m) underground openings within 5 years after excavation (Borns and Stormont, 1988). Additionally, fractures have been observed in interbed layers surrounding the WIPP facility horizon (principally MB139). Bechtel National, Inc. investigated the presence of fractures above and below repository horizon excavations (US DOE, 1986) and found horizontal fractures and separations ranging from microfractures of less than 100 microns to fractures as large as 1 cm in both MB139 and the intervening halite below all test rooms. Similar fracturing was observed in diamond drill core obtained at the test site. Dilation and separations occur in MB139 when it deforms upward into the excavations. Fractures in the DRZ provide potential gas pathways for gas flow from waste emplacement areas and for brine flow to or from these areas (Deal et al., 1987). Grouting may be necessary to control increased permeability resulting from creation of strain-induced fractures in the DRZ around WIPP seals. To demonstrate the ability to control gas and fluid movement within the DRZ, the SSSPT-F experiment included tracer-gas testing, using gas of known density and viscosity, to provide data for determining estimated permeability. For evaluation of grouting effectiveness, tracer-gas testing was conducted before and after grout injection. The pre- and post-grouting permeability measurements were compared to demonstrate the effectiveness of grout injection for sealing the strain-induced fracture permeability within the DRZ.



* = Reading below Resolution of Equipment (less than 0.1 SCCM) Units are in Standard cm^3/min (SCCM)

TRI-6330-82-7

Figure 1-2. Disturbed rock zone adjacent to WIPP underground excavations. (A) fracture patterns; (B) contours of gas-flow rate for gas injected at less than 1 MPa (adapted from Borns and Stormont, 1988).

It should be noted that the pressures used in the gas-testing equipment are too low to displace brine. The fractures near the eastern rib of Room L3 are known to locally contain brine. The SSSPT-F formation characterization tests evaluated the permeability of that portion of the fractured assemblage that did not contain brine and thus included potential pathways for gas movement. Although grout injection pressures during secondary grouting were high enough to displace some brine, the gas-flow test equipment cannot detect whether a fracture is filled with grout or with brine.

1.2 WIPP Sealing Strategy

The WIPP sealing program has developed a sealing strategy to limit the release of radionuclides and other hazardous waste species from the WIPP horizon and to limit the flow of groundwater into the repository horizon and shafts. The WIPP reference sealing strategy is described in Nowak et al. (1990). The sealing system is divided into three subsystems.

The drift/panel sealing subsystem will be located in the drift and panel entryways and in the surrounding host rock salt at the waste disposal horizon. This subsystem is designed to control waste release over the short term (i.e., to meet regulatory requirements during the operational period and until long-term shaft seals are emplaced and effective). The reference seal components for the drift and panel sealing subsystem may include crushed salt members and concrete, with grout in the surrounding DRZ (Van Sambeek et al., 1993).

The lower shaft sealing subsystem will be situated in the lower portion of the shafts and surrounding host rock salt within the Salado Formation. This subsystem provides long-term seals to meet regulatory requirements for 10,000 years. The long-term reference seal component is compacted crushed salt that will be further consolidated by creep closure of the shaft. Sealing the DRZ with this subsystem will involve host rock salt healing (by creep) and may include grouting at major interbeds.

The upper shaft sealing subsystem will be located in the upper portion of the shafts and surrounding host rock within the Rustler Formation and at the top of the Salado Formation. This subsystem is designed to control the downflow of brine from the water-bearing zones of the Rustler over the short term (i.e., while the long-term component, crushed salt, reconsolidates in the lower shaft). The reference short-term components for the upper shaft subsystem consist of precompact bentonite clay with concrete constraining structures and grout in the surrounding DRZ.

Grout-based sealing of the DRZ is currently perceived as essential in all three subsystems, making SSSPT-F a fundamental component of the WIPP Seal System Development Program.

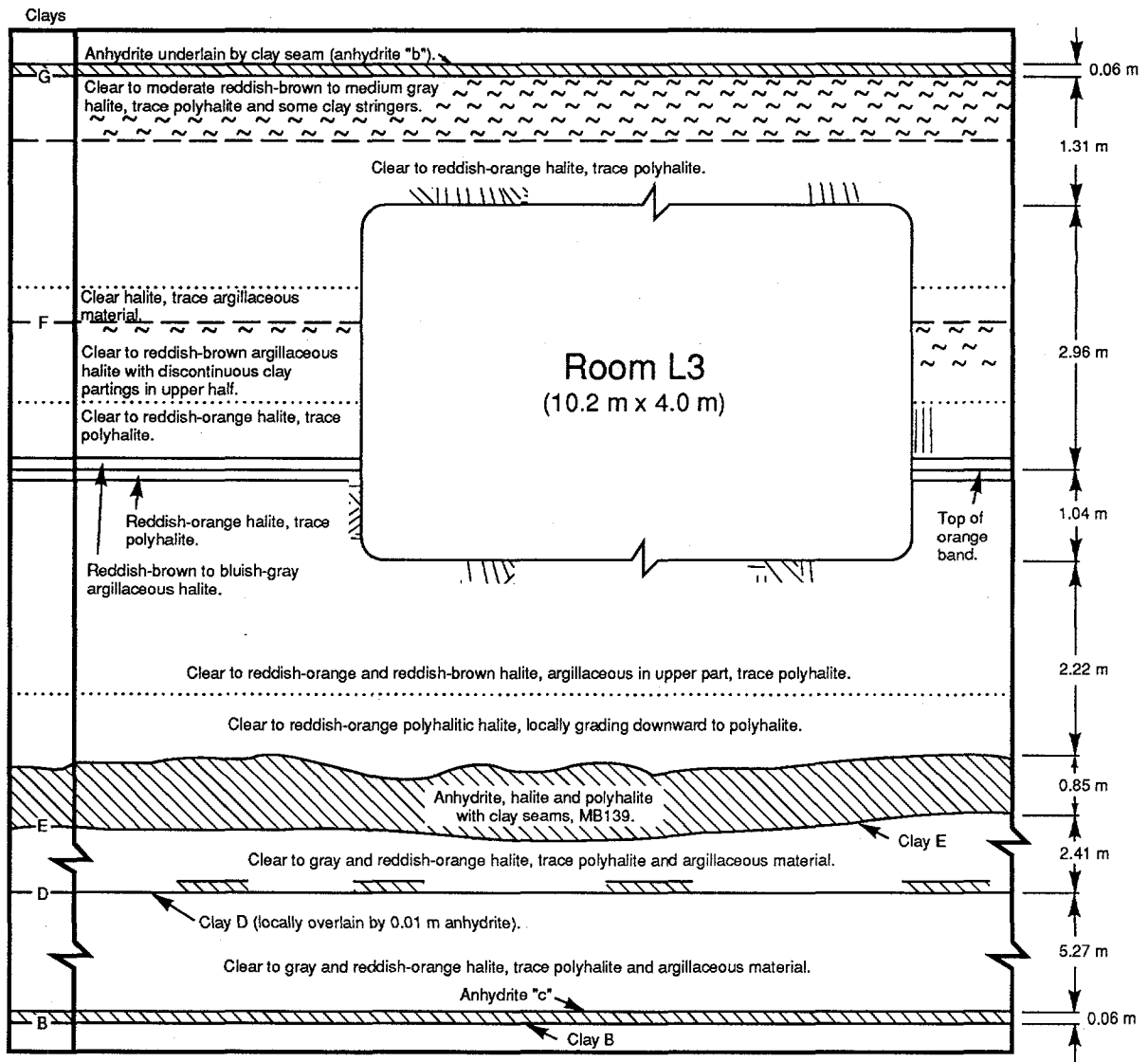
1.3 Test Objectives

The four primary objectives of SSSPT-F are (1) to demonstrate the ability to produce ultrafine, cementitious grout in the WIPP underground in a practical and consistent manner; (2) to demonstrate the ability to inject this grout into fractured rock at the WIPP repository horizon consistently and efficiently; (3) to gather data on the ability of the grout to penetrate and seal macro- and microfractures (aperture \leq 100 microns); (4) to evaluate procedures and equipment for injecting grout into fractured WIPP rock.

Additionally, SSSPT-F has two supporting objectives: (1) evaluation of techniques to assess the effectiveness of ultrafine grout in reducing the gas transmissivity of fractured WIPP rock; the techniques include gas-flow/tracer testing, pre- and post-grout coring, geologic and downhole televiewer logging, slab displacement measurements, and jack loading measurements during grout injection; (2) recovery of pre- and post-grout, diamond-drill core for use in ongoing laboratory evaluations of grouting effectiveness, degradation, and compatibility.

1.4 Test Description

SSSPT-F was conducted in test Room L3 in the experimental area of the WIPP underground. The room position relative to the local stratigraphy is shown in Figure 1-3. Room L3 was chosen as the experimental site because the time since excavation (>5 years) and the room width (10 m) suggested that the DRZ in the salt and anhydrite around Room L3 would be substantial. This DRZ development suggests that high gas-flow rates could be expected in MBL39 beneath the room centerline. To assess the location, a general gas-flow characterization study was conducted between May and July of 1992. Results indicated that a location between 23 and 31 m into the room should be used for the experiment because it exhibited a large range of gas permeabilities. Results of an electrical geophysical survey, conducted simultaneously by the Colorado School of Mines, closely matched gas-flow data near the gas-flow characterization holes. The Test Plan (Ahrens, 1992b) called for the emplacement of a concrete slab on the floor of Room L3 at the experiment site. The slab was to serve as a staging area for the experiment. Prior to slab installation, 18 coreholes were drilled into the formation at points surrounding the proposed location. These holes were used for gas-flow and tracer-gas tests; they furnished data on the variability and interconnectivity of fractures in the formation under Room L3. The



TRI-6334-257-10

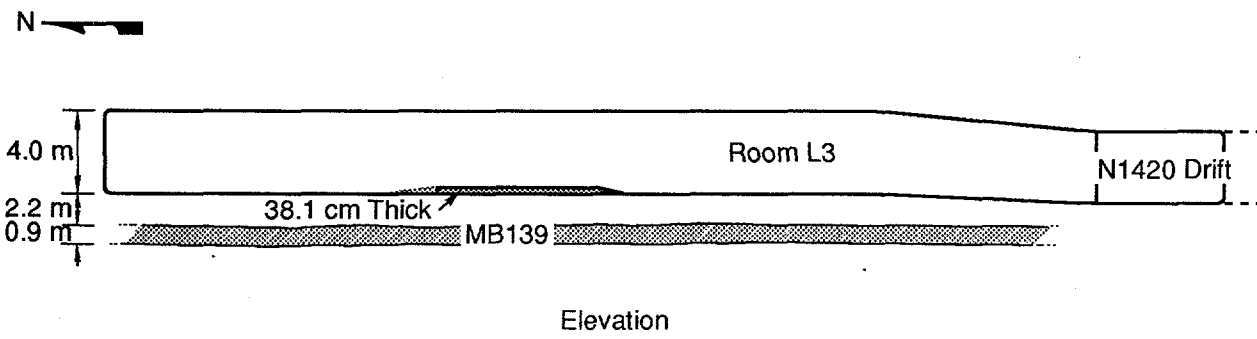
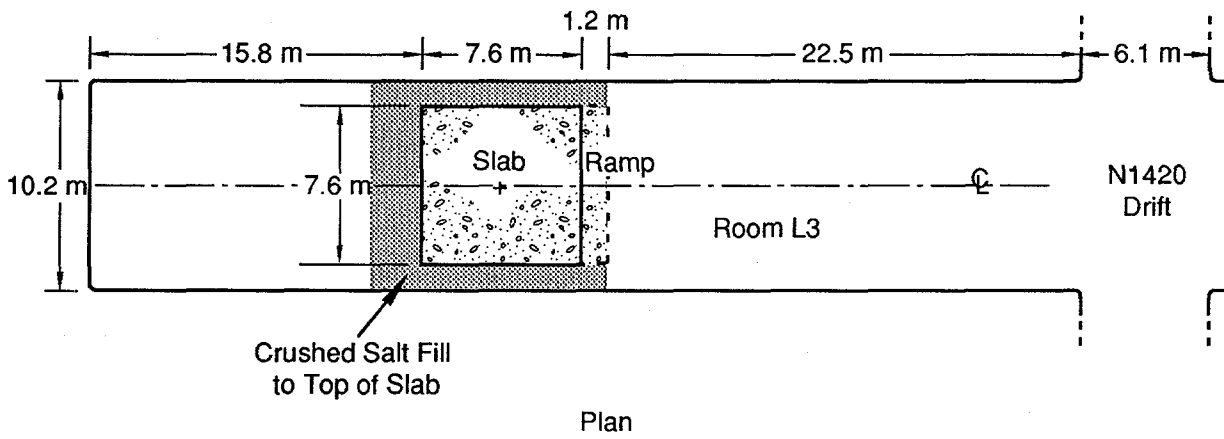
Figure 1-3. Local stratigraphy around Room L3.

electrical geophysical survey was extended across the proposed slab location, where resistivity measurements indicated suitable gas transmissivity for the grouting experiment. Figure 1-4 shows plan and elevation views of Room L3 with the final location chosen for the slab.

After baseline tests were completed, the slab was emplaced, providing a smooth staging area for grouting and later gas-flow testing. The slab was not designed as a structure to be pushed against, i.e., it was known that the slab would provide little resistance to uplift from grout injection (except in the immediate vicinity of the injection). The grouting experiment was not an attempt to define how well the rock could be grouted, because injection pressures were deliberately limited.

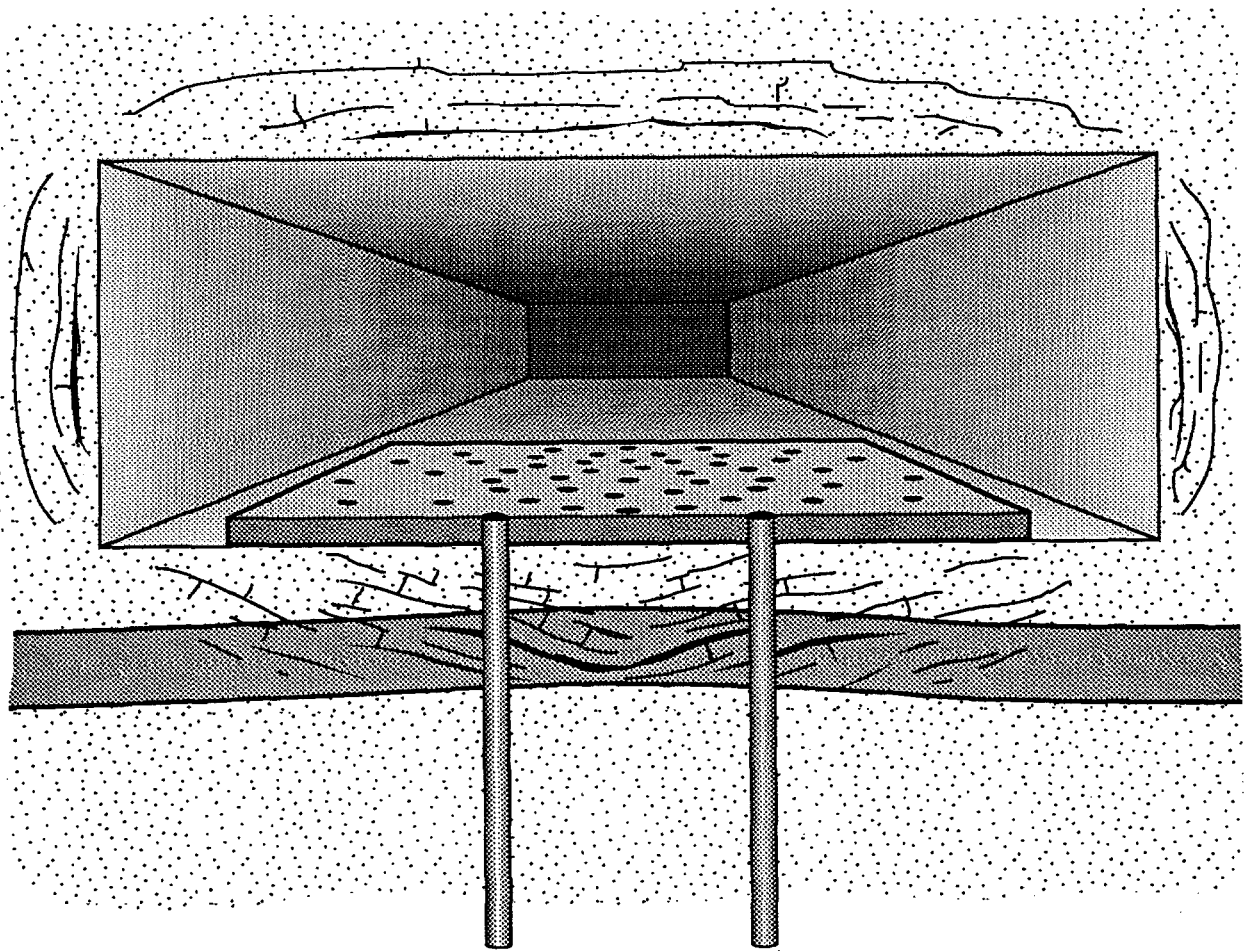
After slab emplacement, a central gas-injection hole and 16 receiver holes were drilled through the concrete and into the formation below Room L3 so that additional baseline gas-flow and tracer tests could be conducted. A three-dimensional representation of this stage of the experiment, showing the slab, test holes, and stratigraphy below Room L3, is given in Figure 1-5.

Grouting activities began with the drilling and grouting of eight primary and eight secondary grout holes. A different color of grout was injected into each hole to aid in determining grout permeation, which was accomplished with post-grout core examinations. After completion of grouting activities, 24 post-grout coreholes were drilled. The cores were examined for evidence of grout, and the holes were tested for gas transmissivity.



TRI-6346-156-1

Figure 1-4. Plan and elevation views of Room L3, showing slab location.



TRI-6121-204-0

Figure 1-5. Three-dimensional representation of the slab, test holes, DRZ, and stratigraphy below Room L3.

2.0 PRE-GROUT ACTIVITIES

2.1 Selection of Test Location

Room L3 was excavated in late March 1989. The room was mined in such a way that the floor inclined up from the adjoining access drift, the N1420 drift. The incline allowed for an additional 1-m thick layer of halite over MB139 compared to that found in the drift. The dimensions of Room L3 as mined were approximately 4 m high by 10 m wide by 45 m long. Room L3 was chosen for the grouting experiment because the size of the room and the time since excavation were expected to facilitate the amount of DRZ development needed for successful grout-injection experimentation.

The N1420 drift was excavated in early 1984. The original location chosen for the grouting test was very near the intersection of the drift and Room L3. However, preliminary gas-flow tests showed that the formation under the floor at this location had very low gas permeabilities. This finding was contradictory to the general observation of higher gas permeabilities near the intersections of perpendicular excavations. To find an ideal location for the test, other locations in Room L3 were subsequently gas-flow tested. Based on the results of these tests, the location for slab placement was chosen between 23 and 31 m into the room, as shown in Figure 1-4. The site selection decision is explained in a memorandum attached to Appendix I.

Before the slab was emplaced, gas-flow testing was conducted near but exterior to the proposed slab location to obtain baseline gas-transmissivity data. Pre-slab testing showed estimated permeabilities from 2.3×10^{-15} to 2.8×10^{-13} m². Twelve 15.2-cm-diameter vertical boreholes, 3.6 m deep, were drilled, 6 north and 6 south of the slab location. After drilling, these holes were examined for fractures with the downhole video camera. Then a series of short-duration order-of-magnitude gas-flow tests was conducted using the four-packer test tool in the downhole configuration (two end packers inflated and gas injected from the end port). The downhole configuration tested the gas transmissivity of the fractured rock by utilizing a gas-pressurized test interval between the bottom of the hole and the lower packer, 1.3 m below the drift floor. At a constant pressure, the gas flow rate into the test interval is a function of the gas transmissivity of the rock into which the borehole is drilled.

Initial test-zone target pressures of 0.14 MPa were used. Generally, in halite near the drift ribs or in the far field, gas transmissivity is sufficiently small for accurate pressure-decay estimates using one isolated test interval. However, when the maximum gas-flow rate from the four-packer test tool could not pressurize the test region because of excessive formation gas transmissivity, borehole areas had to be isolated to locate the

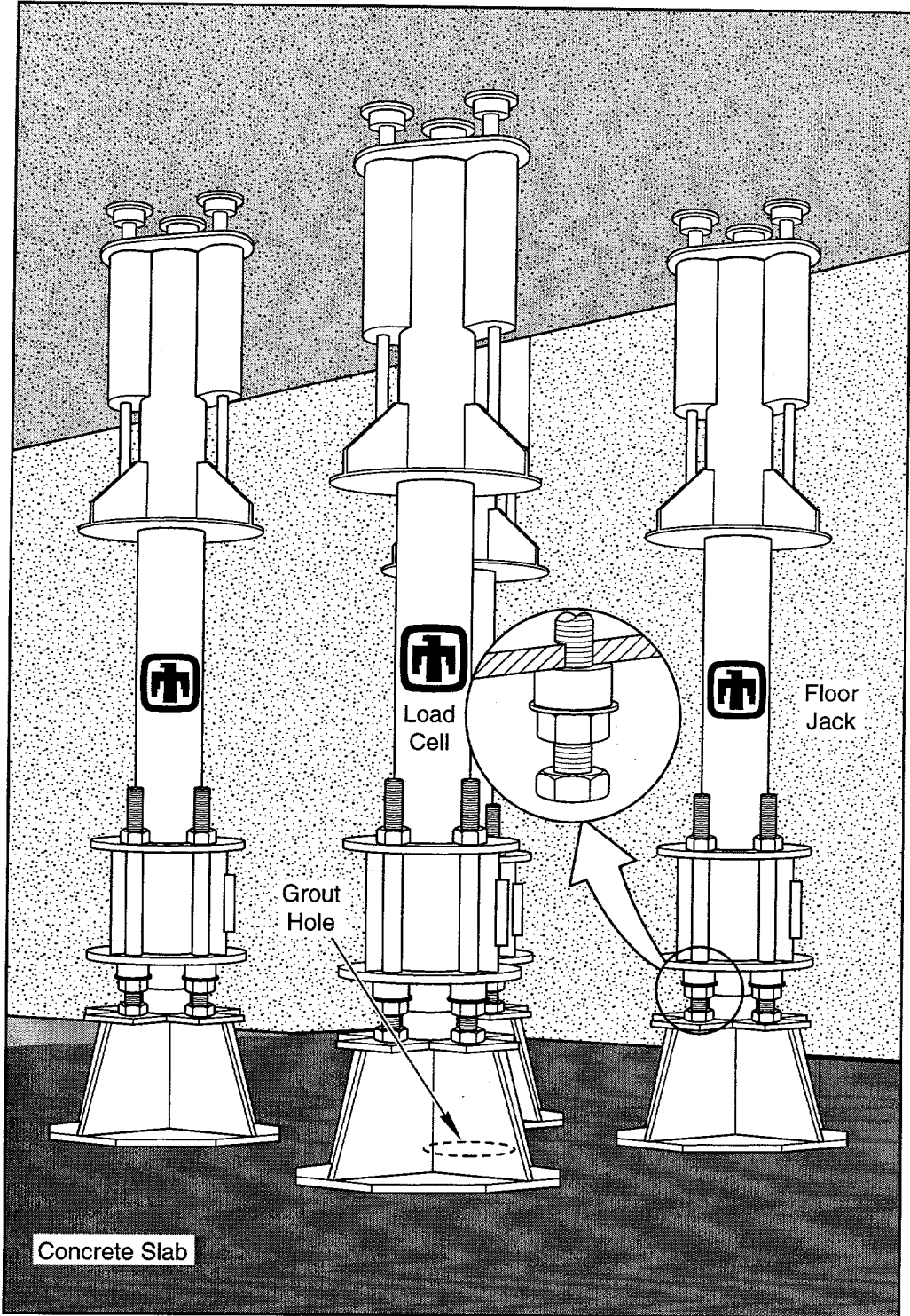
excessively permeable region. Four boreholes were subjected to complete isolated interval testing as part of the baseline study. These four were chosen to represent the range of DRZ development based on core and downhole video observations.

A second series of baseline tests was conducted after slab emplacement. These tests are described in Section 2.4. Specific details of the baseline gas-flow tests in the near- and on-slab boreholes can be found in Appendix I. The holes were retested subsequent to grout injection. Comparisons of the results are given in Appendix I.

2.2 Concrete Slab and Floor Jacks

The central component of the SSSPT-F system (to allow moderate pressurized grout injection) was the concrete slab, which was emplaced on the leveled floor of Room L3. Grout injection pressures planned for this demonstration were capable of hydrodilation and hydrofracturing of the unconstrained floor. In addition, the demonstration was designed to simulate injection of grout around a rigid inclusion. Thus, to stabilize the floor and to provide a reasonably rigid source of backpressure, a heavily reinforced concrete slab stabilized with portable floor-to-ceiling jacks was used. The design provided for a monolithic slab that would transfer upward forces of grout injection through the jacks and into the ceiling of Room L3. The slab was heavily reinforced and designed not to crack. The composition of the concrete was supplied by the Principal Investigator (PI). Plans for the slab were submitted to Constructors, Inc. of Carlsbad, NM, who then supplied, mixed, and emplaced the concrete, aided by Westinghouse Mining Operations. Cyclone mesh safety net was installed on the sides of the room with rock bolts, and the slab was poured in September 1992. The completed slab measured 7.6 x 7.6 m, with a depth of 0.38 m. Extensometers were installed from the slab corners down to stable anchor points 4.5 and 16 m below the floor level. A concrete ramp was poured on the south side of the slab to provide easy access for machinery and materials. A detailed description of the slab construction process is presented in Appendix B. Compressive strength of the concrete was determined prior to grouting. The slab resisted injection pressures as high as 8.2 MPa and remained crack-free throughout the experiment.

Four hydraulically actuated floor jacks were designed and built for this test. The jacks and their arrangement around a grout hole are depicted in Figure 2-1. Design drawings for the jacks were supplied to Hall Machinery in Carlsbad, NM. After approval of shop drawings by the PI, Hall built the jacks and delivered them to the WIPP. Each jack weighs approximately 14 kN and can withstand a load of 3,736 kN. Prior to each grouting event, the



TRI-6121-200-0

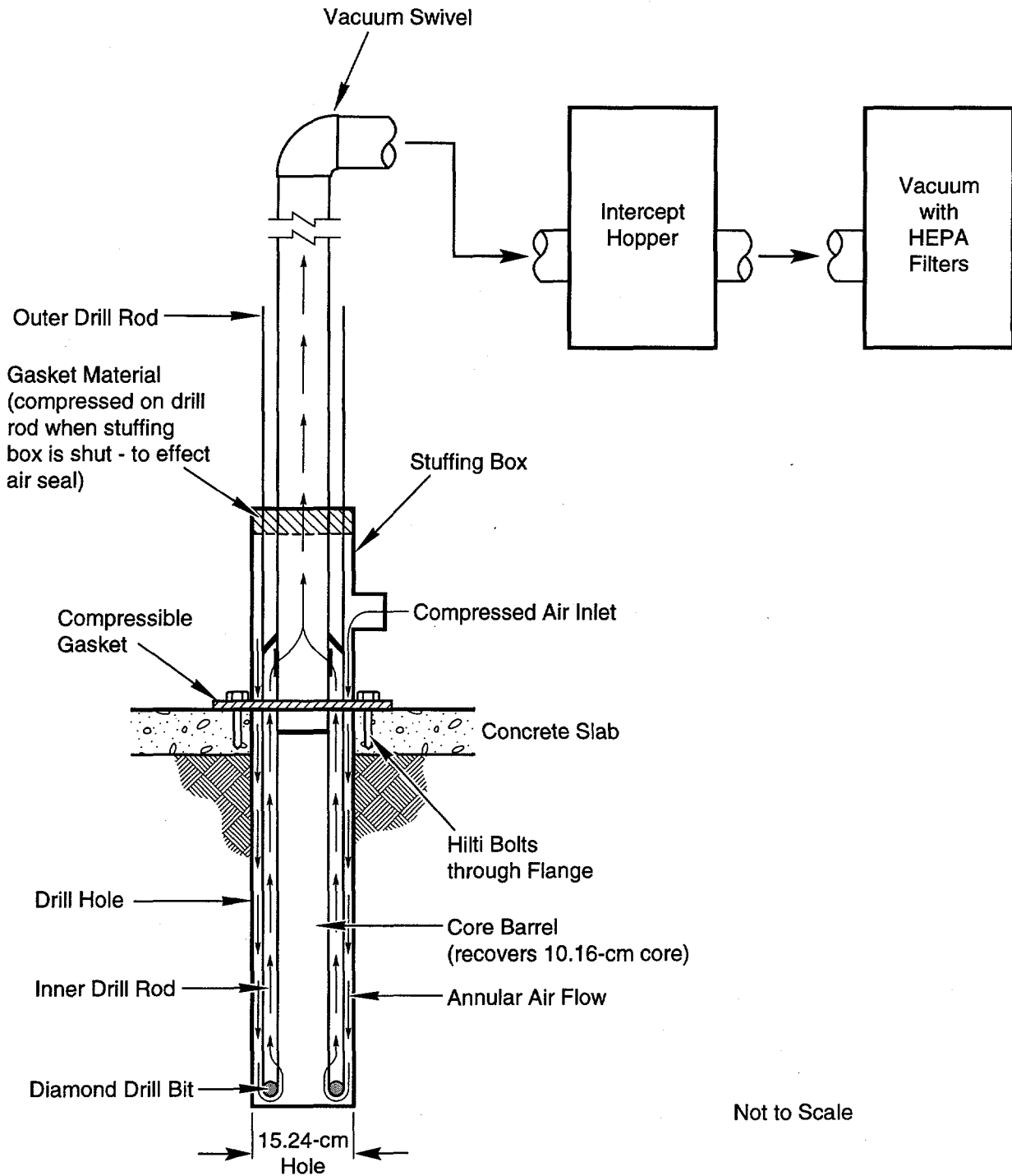
Figure 2-1. Typical floor jack arrangement at a grout hole.

jacks were positioned around the grout injection hole and set at approximately 44.6 kN to remove any mechanical play. The jacks were braced against the ceiling of the room to restrict (but not totally eliminate) upward hydraulic displacement caused by the subjacent injection of pressurized grout. Upward movement of the slab (away from the jacks) was monitored by rod extensometers positioned at each corner of the slab. Jacks were always positioned by the Experimental Operations drilling crew and then checked for safety by the grouting crew. No unsafe setups occurred. Again, maximum grouting efficiency was not possible because the slab/jack system limits the grout pressure that can be used.

2.3 Drilling

The SSSPT-F experiment made use of diamond drilling equipment specifically invented for this test. This equipment allowed operators to recover core while drilling a "clean" hole (i.e. one in which the microfractures remain unplugged by drill cuttings). Clean holes were necessary because one objective of SSSPT-F was to determine the effectiveness of grout for sealing microfractures.

Diamond drill cuttings are very fine-grained. Standard drilling systems use a configuration that blows compressed air down a single hollow drill rod and outward across the diamond bit, cooling the bit (to prevent fusing the salt, which then adheres to the bit and reduces drilling efficiency) but then driving the cuttings up the annular space between the drill rod and the hole wall, where they can plug fractures and block the entrance of grout. Cuttings that do not lodge in fractures are forcibly ejected from the hole collar and dispersed into the drilling area, creating a very dusty work environment. Drillers must wear protective masks, and salt dust is detrimental to electronic equipment. To overcome these drawbacks, special drilling equipment was developed for SSSPT-F. The equipment incorporates a reverse-circulation air-flow system (shown schematically in Figure 2-2) that leaves fractures open in the hole wall. During drilling, compressed air is passed down the annulus between the outer rod and the drillhole wall and then swept inward across the drill bit, carrying the cuttings between the inner and outer drill rods for approximately 1.2 m (the length of the core barrel). The cuttings are then deflected into the center rod and carried to the swivel above the drill where a hose connects the drill to a powerful vacuum. The vacuum promotes movement of the cuttings from the swivel to an intercept hopper where the coarser particles are retained; the finer particles then pass through multiple high-efficiency particulate air (HEPA) filters. The discharge is relatively clean air, which benefits both the workers and the sensitive electronic equipment used in the experiment.



Not to Scale

TRI-6121-201-0

Figure 2-2. Diagram of reverse circulation drilling system.

The drilling equipment design and fabrication process is described in Appendix C. The drilling system was built by Christensen Diamond Products of Salt Lake City, UT. Because of the innovative nature of the drilling equipment, a patent application was filed by SNL. The custom equipment drilled a 15.24-cm-diameter hole and recovered a 10.16-cm-diameter core. Drilling efficiency was high: holes could be drilled through 0.38 m of concrete and 3.28 m of rock in one hour. The drilling rig is shown in Photo 2-1 (behind the drill in the photo is one of the hydraulic floor jacks). This equipment was used to drill all the on-slab holes except the four extensometer holes. A drilling summary with all hole coordinates is presented in Table 2-1.

Table 2-1 was created from actual survey results. Underground surveys at the WIPP utilize a rectangular coordinate system established by WIPP engineers, as described in Gonzales (1989). In this system, coordinates are based on a marker located at the corner common to sections 20, 21, 28, and 29 in Township 22S, Range 31E. WIPP engineers modified the state-plane coordinates of this marker by subtracting 13,530 m from the east coordinate and 14,945 m from the north coordinate. The resulting coordinate numbers have fewer digits and are therefore easier to use. They are also more appropriate to the scale of the WIPP underground. Table 2-1 was developed from survey results reported in U.S. units of feet and inches. For this report, the units were converted to metric units for consistency.

2.4 Borehole Array

Following emplacement of the concrete slab, the drilling equipment was used to core a central gas-injection hole and 16 receiver holes. The locations of all the holes drilled for SSSPT-F are shown in Figure 2-3. On-slab boreholes were placed radially around a central gas-injection hole. The radially placed holes allowed for an equal distance between the gas-injection hole (L3001) and the 16 gas-receiver holes (L3202-L3217) so that differences noted in tracer gas breakthrough curves would represent the differences in the magnitude and nature of the permeable pathways.

The grout injection holes (L3418 - L3425 and L3526 - L3533) were placed radially between the central injection hole and the circle of receiver holes. It was expected that this geometry would result in a continuous grout curtain sealing the central injection hole and isolating it from the ring of receiver holes.

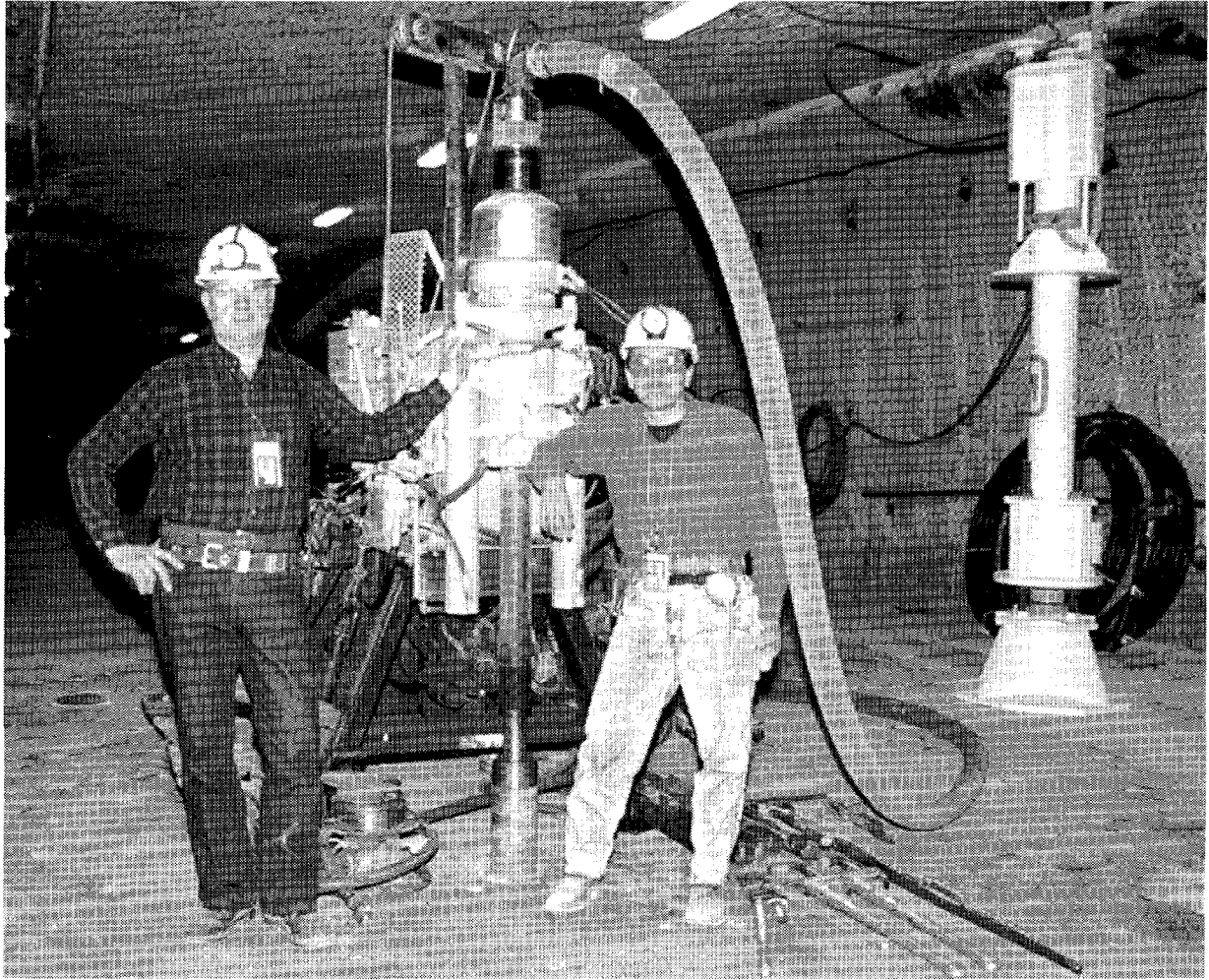


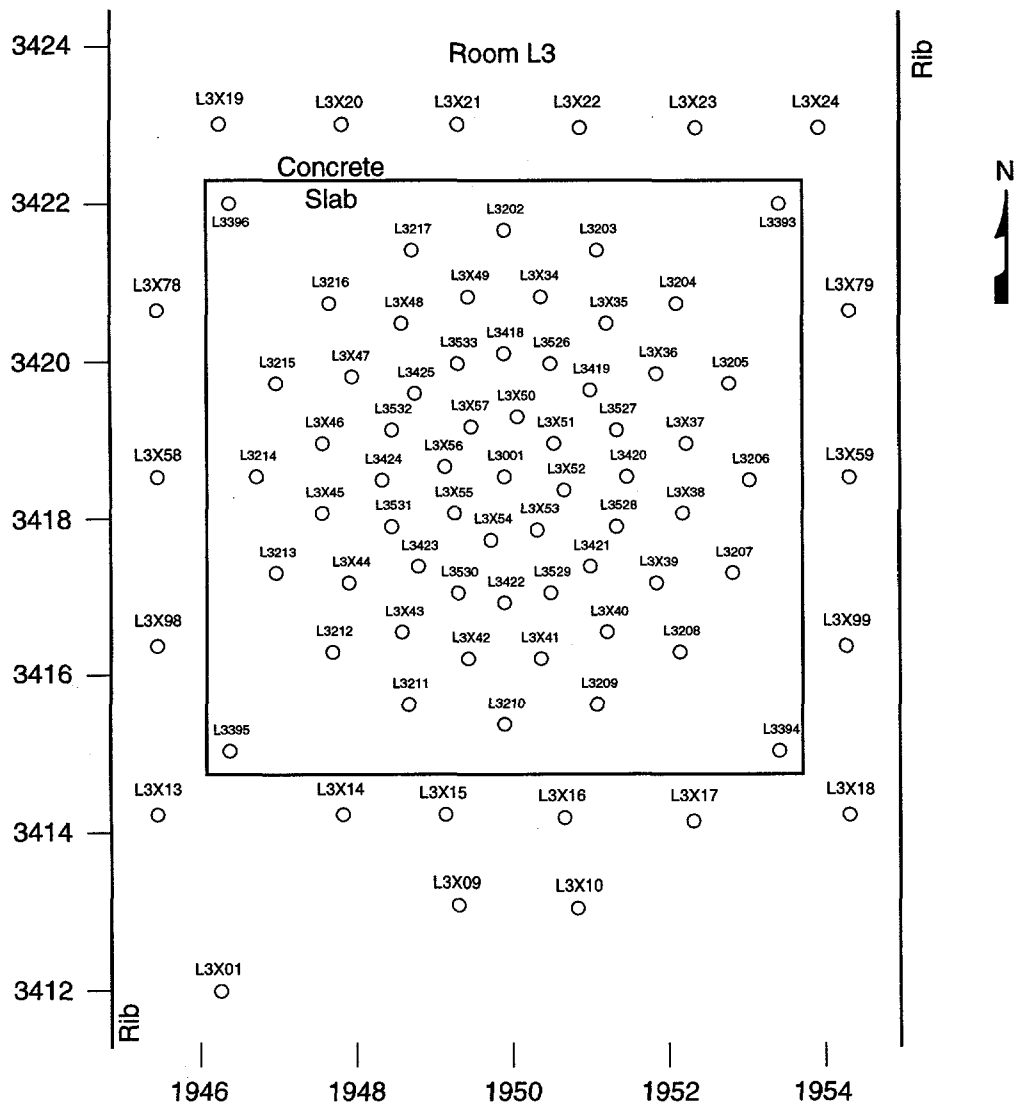
Photo 2-1. Reverse-circulation diamond drill.

Table 2-1. Hole Coordinate and Drilling Summary

Hole	Collar East (m)	Bottom East (m)	Collar North (m)	Bottom North (m)	Collar Elevation (m)	Bottom Elevation (m)	Length (m)	Diam. (cm)	Purpose	Drill Completion Date
L3001	1949.90	1949.90	3418.47	3418.47	396.22	392.56	3.66	15.24	Tracer Injection	10/31/92
L3202	1949.90	1949.90	3421.61	3421.61	396.22	392.56	3.66	15.24	Sniffer	12/4/92
L3203	1951.11	1951.11	3421.37	3421.37	396.22	392.57	3.66	15.24	Sniffer	12/7/92
L3204	1952.13	1952.13	3420.69	3420.69	396.22	392.51	3.71	15.24	Sniffer	12/7/92
L3205	1952.80	1952.80	3419.68	3419.68	396.22	392.54	3.68	15.24	Sniffer	12/7/92
L3206	1953.05	1953.05	3418.46	3418.46	396.22	392.59	3.63	15.24	Sniffer	12/8/92
L3207	1952.82	1952.82	3417.25	3417.25	396.22	392.51	3.71	15.24	Sniffer	12/9/92
L3208	1952.14	1952.14	3416.24	3416.24	396.21	392.51	3.71	15.24	Sniffer	12/9/92
L3209	1951.11	1951.11	3415.56	3415.56	396.22	392.63	3.58	15.24	Sniffer	12/10/92
L3210	1949.89	1949.89	3415.31	3415.31	396.21	392.4	3.81	15.24	Sniffer	11/19/92
L3211	1948.70	1948.70	3415.56	3415.56	396.22	392.43	3.78	15.24	Sniffer	10/20/92
L3212	1947.70	1947.70	3416.24	3416.24	396.22	392.44	3.78	15.24	Sniffer	11/23/92
L3213	1946.99	1946.99	3417.26	3417.26	396.22	392.54	3.68	15.24	Sniffer	11/23/92
L3214	1946.75	1946.75	3418.48	3418.48	396.22	3982.51	3.71	15.24	Sniffer	11/25/92
L3215	1947.00	1947.00	3419.67	3419.67	396.21	392.51	3.71	15.24	Sniffer	12/2/92
L3216	1947.66	1947.66	3420.68	3420.68	396.22	392.53	3.69	15.24	Sniffer	10/15/92
L3217	1948.70	1948.70	3421.38	3421.38	396.22	392.51	3.71	15.24	Sniffer	12/3/92
L3393	1953.42	1953.42	3421.98	3421.98	396.21	380.85	15.36	7.62	Extensometer	10/12/92
L3394	1953.41	1953.41	3414.97	3414.97	396.22	380.82	15.39	7.62	Extensometer	10/8/92
L3395	1946.39	1946.39	3414.99	3414.99	396.21	380.87	15.34	7.62	Extensometer	10/15/92
L3396	1946.40	1946.40	3421.97	3421.97	396.21	380.95	15.26	7.62	Extensometer	10/13/92
L3418	1949.91	1949.91	3420.04	3420.04	396.22	392.36	3.86	15.24	Grout Hole	3/22/93
L3419	1951.01	1951.01	3419.58	3419.58	396.23	392.44	3.79	15.24	Grout Hole	3/15/93
L3420	1951.48	1951.48	3418.47	3418.47	396.22	392.46	3.76	15.24	Grout Hole	3/17/93
L3421	1951.01	1951.01	3417.35	3417.35	396.22	392.43	3.78	15.24	Grout Hole	3/19/93
L3422	1949.90	1949.90	3416.89	3416.89	396.22	392.50	3.72	15.24	Grout Hole	3/23/93
L3423	1948.78	1948.78	3417.35	3417.35	396.22	392.49	3.73	15.24	Grout Hole	3/12/93
L3424	1948.33	1948.33	3418.46	3418.46	396.22	392.49	3.73	15.24	Grout Hole	3/16/93
L3425	1948.78	1948.78	3419.56	3419.56	396.22	392.54	3.67	15.24	Grout Hole	3/18/93
L3526	1940.51	1940.51	3419.92	3419.92	396.22	392.44	3.79	15.24	Grout Hole	2/2/93
L3527	1951.36	1951.36	3419.07	3419.07	396.22	392.46	3.76	15.24	Grout Hole	2/22/93
L3528	1951.37	1951.37	3417.85	3417.85	396.22	392.43	3.78	15.24	Grout Hole	2/10/93
L3529	1950.51	1950.51	3417.02	3417.02	396.22	392.49	3.76	15.24	Grout Hole	2/18/93
L3530	1949.31	1949.31	3417.01	3417.01	396.22	392.41	3.81	15.24	Grout Hole	2/1/93
L3531	1948.45	1948.45	3417.86	3417.86	396.22	392.46	3.76	15.24	Grout Hole	2/19/93
L3532	1948.45	1948.45	3419.07	3419.07	396.22	392.48	3.76	15.24	Grout Hole	2/9/93
L3533	1949.30	1949.30	3419.92	3419.92	396.22	392.44	3.78	15.24	Grout Hole	2/24/93
L3X01	1946.14	1946.14	3411.91	3411.91	395.96	392.43	3.53	15.24	Gas Test Hole	7/2/92
L3X06	1953.88	1953.88	3411.82	3411.82	395.97	392.52	3.45	15.24	Gas Test Hole	7/16/92
L3X09	1949.31	1949.31	3413.01	3413.01	396.07	392.59	3.48	15.24	Gas Test Hole	7/9/92
L3X10	1950.86	1950.86	3412.97	3412.97	396.06	392.58	3.48	15.24	Gas Test Hole	7/10/92

Table 2-1. Hole Coordinate and Drilling Summary (continued)

Hole	Collar East (m)	Bottom East (m)	Collar North (m)	Bottom North (m)	Collar Elevation (m)	Bottom Elevation (m)	Length (m)	Diam. (cm)	Purpose	Drill Completion Date
L3X13	1945.47	1945.47	3414.17	3414.17	395.83	392.35	3.48	15.24	Gas Test Hole	11/10/92
L3X14	1947.83	1947.83	3414.17	3414.17	396.18	392.70	3.48	15.24	Gas Test Hole	7/6/92
L3X15	1949.14	1949.14	3414.14	3414.14	396.17	392.69	3.48	15.24	Gas Test Hole	11/13/92
L3X16	1950.67	1950.67	3414.11	3414.11	396.16	392.61	3.56	15.24	Gas Test Hole	11/16/92
L3X17	1952.34	1952.34	3414.10	3414.10	396.18	392.72	3.45	15.24	Gas Test Hole	7/15/92
L3X18	1954.33	1954.33	3414.16	3414.16	395.83	392.29	3.53	15.24	Gas Test Hole	11/9/92
L3X19	1946.29	1946.29	3422.98	3422.98	395.84	392.41	3.43	15.24	Gas Test Hole	7/30/92
L3X20	1947.83	1947.83	3422.96	3422.96	395.84	392.25	3.58	15.24	Gas Test Hole	7/30/92
L3X21	1949.33	1949.33	3422.96	3422.96	395.84	392.46	3.38	15.24	Gas Test Hole	7/29/92
L3X22	1950.88	1950.88	3422.94	3422.94	395.83	392.38	3.45	15.24	Gas Test Hole	7.28/92
L3X23	1952.37	1952.37	3422.93	3422.93	395.83	392.25	3.58	15.24	Gas Test Hole	7/24/92
L3X24	1953.93	1953.93	3422.94	3422.94	395.83	392.46	3.38	15.24	Gas Test Hole	7/27/92
L3X34	1950.36	1950.36	3420.78	3420.78	396.22	392.52	3.71	15.24	Core Hole	4/29/93
L3X35	1951.22	1951.22	3420.43	3420.43	396.22	392.57	3.66	15.24	Core Hole	9/15/93
L3X36	1951.87	1951.87	3419.79	3419.79	396.23	392.57	3.66	15.24	Core Hole	9/15/93
L3X37	1952.22	1952.22	3418.92	3418.92	396.22	392.56	3.66	15.24	Core Hole	9/14/93
L3X38	1952.21	1952.21	3418.01	3418.01	396.22	392.56	3.66	15.24	Core Hole	9/13/93
L3X39	1951.86	1951.86	3417.15	3417.15	396.22	392.53	3.68	15.24	Core Hole	4/13/93
L3X40	1951.21	1951.21	3416.50	3416.50	396.22	392.33	3.89	15.24	Core Hole	4/15/93
L3X41	1950.36	1950.36	3416.16	3416.16	396.22	392.48	3.73	15.24	Core Hole	4/16/93
L3X42	1949.44	1949.44	3416.15	3416.15	396.22	392.46	3.76	15.24	Core Hole	4/16/93
L3X43	1948.59	1948.59	3416.51	3416.51	396.22	392.46	3.76	15.24	Core Hole	4/20/93
L3X44	1947.93	1947.93	3417.16	3417.16	396.22	392.46	3.76	15.24	Core Hole	4/22/93
L3X45	1947.59	1947.59	3418.01	3418.01	396.22	392.54	3.68	15.24	Core Hole	4/23/93
L3X46	1947.58	1947.58	3418.93	3418.93	396.22	392.51	3.71	15.24	Core Hole	4/23/93
L3X47	1947.94	1947.94	3419.77	3419.77	396.22	392.50	3.72	15.24	Core Hole	4/26/93
L3X48	1948.58	1948.58	3420.42	3420.42	396.22	392.46	3.76	15.24	Core Hole	4/27/93
L3X49	1949.45	1949.45	3420.78	3420.78	396.22	392.52	3.71	15.24	Core Hole	4/28/93
L3X50	1950.06	1950.06	3419.24	3419.24	396.22	392.56	3.66	15.24	Core Hole	9/1/93
L3X51	1950.56	1950.56	3418.91	3418.91	396.23	392.57	3.66	15.24	Core Hole	8/30/93
L3X52	1950.68	1950.68	3418.31	3418.31	396.22	392.56	3.66	15.24	Core Hole	8/30/93
L3X53	1950.34	1950.34	3417.80	3417.80	396.22	392.56	3.66	15.24	Core Hole	8/24/93
L3X54	1949.75	1949.75	3417.69	3417.69	396.22	392.56	3.66	15.24	Core Hole	8/20/93
L3X55	1949.25	1949.25	3418.02	3418.02	396.22	392.56	3.66	15.24	Core Hole	8/19/93
L3X56	1949.13	1949.13	3418.61	3418.61	396.22	392.56	3.66	15.24	Core Hole	8/8/93
L3X57	1949.47	1949.47	3419.12	3419.12	396.22	392.57	3.66	15.24	Core Hole	8/11/93
L3X58	1945.49	1945.49	3418.46	3418.46	395.83	392.30	3.53	15.24	Gas Test Hole	11/11/92
L3X59	1954.33	1954.33	3418.47	3418.47	395.83	392.37	3.45	15.24	Gas Test Hole	10/30/92
L3X78	1945.49	1945.49	3420.60	3420.60	395.83	392.30	3.53	15.24	Gas Test Hole	11/12/92
L3X79	1954.32	1954.32	3420.61	3420.61	395.83	392.33	3.51	15.24	Gas Test Hole	11/2/92
L3X98	1945.48	1945.48	3416.34	3416.34	395.83	392.32	3.51	15.24	Gas Test Hole	11/2/92
L3X99	1954.28	1954.28	3416.33	3416.33	395.83	392.25	3.58	15.24	Gas Tes Hole	10/27/92



Key:

Room Designation
 Hole Number

L3X10

Hole Type

X = Post-grout core or off-slab gas-test
 0 = Central gas injection
 2 = Sniffer
 3 = Extensometer
 4 = Primary grout
 5 = Secondary grout

Note: All coordinates are given in meters.

TRI-6121-154-1

Figure 2-3. Location of holes drilled for SSSPT-F.

Boreholes adjacent to the slab along the east and west ribs of Room L3 (L3X13, L3X59, L3X99, and L3X18, L3X58, L3X78, L3X98 respectively), as well as two additional boreholes to the south of the slab (L3X15 and L3X16) were drilled in early October 1992 and were later collared or included in the ramp structure.

The locations of the remaining boreholes (all of which were on the slab) including the central-gas injection hole, tracer-gas receiver holes, and grout-injection holes, were surveyed and marked in early October 1992. The concrete cores from the slab were drilled for the central gas-injection hole (L3001) and tracer-gas-receiver holes (L3202 - L3217) on October 12, 1992. Drilling of the underlying formation for these 17 boreholes was performed during late November and early December 1992.

2.5 On-Slab Permeability Tests

After drilling the borehole array, gas-flow and tracer-gas tests were conducted to obtain permeability data on the formation beneath the slab. Gas-flow testing was conducted as described in Section 2.1. Tracer gas testing was performed by injecting nitrogen spiked with isobutene at 0.14 MPa into the central gas injection hole (L3001) and sampling at the receiver holes. The tracer-gas testing is described in greater detail in Section 4.1.1. Both types of tests were used to determine pre-grout formation gas-transmissivity and gas-flow characteristics.

Four tests were performed: high- and low-pressure formation characterization, and high- and low-pressure tracer gas testing. Gas-flow testing was conducted in all boreholes on the slab prior to grout injection. Tracer-gas testing was conducted prior to the first grout injection, after each of the first four primary grout injections, after completion of the eight primary grout injections, and again after completion of the eight secondary grout injections. Tests conducted during and after grouting are discussed in Section 4. Results of all gas-flow and tracer-gas tests are presented in Appendix I.

This page intentionally left blank.

3.0 GROUTING

The SSSPT-F grouting activity began February 3, 1993 and was completed March 24, 1993. Table 3-1 shows the grouting date, time, and injection data for all holes, as taken from the drilling contractor records, which are filed at the Nuclear Waste Management Information Center. The objectives of SSSPT-F (as noted in Section 1.3) required the development of an ultrafine cement-based grout and innovative grout pulverization and injection equipment. The grout research and development process is described in Appendix A. The grouting equipment is described in Appendix E.

Table 3-1. Batching and Injection Times for all Grouted Holes

Hole No.	Date	Batch Start Time	Batch Stop Time	Elapsed Time (minutes)	Finish	Elapsed Time (minutes)	Injection Start Time	Elapsed Time (minutes)	Injection Stop Time	Elapsed Time (minutes)
					Transfer to Agitation Tank					
L3418	8-Feb	9:28	10:53	85	11:03	95	11:14	106	14:00	272
L3419	24-Feb	8:22	9:46	84	9:56	94	10:08	106	12:30	248
L3420	16-Feb	10:22	12:00	98	12:06	104	12:15	113	14:26	244
L3421	19-Feb	8:33	10:04	91	10:10	97	10:28	115	11:26	173
L3422A	3-Feb	9:42	10:53	71	11:03	81	11:17	95	11:20	98
L3422B	4-Feb	9:24	10:44	80	10:54	90	11:04	100	13:03	219
L3423	23-Feb	8:36	10:00	84	10:07	91	10:17	101	11:05	149
L3424A	11-Feb	9:05	10:28	83	10:35	90	10:44	99	10:59	114
L3424B	12-Feb	9:54	11:22	88	11:32	98	11:50	116	13:10	196
L3425	25-Feb	8:33	10:01	88	10:09	96	10:27	114	11:21	168
L3526	16-Mar	9:49	11:13	84	11:24	95	11:35	106	12:45	176
L3527	18-Mar	9:47	11:13	86	11:20	93	11:30	103	13:40	233
L3528	22-Mar	9:04	10:27	83	10:35	91	10:46	102	12:10	186
L3529	24-Mar	8:34	9:55	81	10:04	90	10:19	105	10:53	139
L3530	15-Mar	9:45	11:13	88	11:22	97	11:39	114	13:05	200
L3531	17-Mar	8:45	10:13	88	10:21	96	10:32	107	12:42	237
L3532	19-Mar	8:39	10:03	84	10:10	91	10:28	109	11:57	198
L3533	23-Mar	8:33	9:57	84	10:07	94	10:15	102	11:16	163

The grouting equipment was selected and developed specifically for SSSPT-F. Grout was pulverized on site and then pumped into the formation below Room L3 through the grout boreholes. A Szegvari 50S Attritor was set up in Room L3 and used to simultaneously pulverize and mix the grout. The attritor was purchased after laboratory work and pilot tests showed that it would efficiently accomplish the required particle size reduction. The 50S pulverized and mixed grout wet by grinding the grout components in a stationary tank together with 681 kg of grinding media (3-mm-diameter, #316 stainless-steel spheres). Six tungsten carbide cross-arms attached to a vertical shaft stirred the contents, imparting random motion to the grinding media. Pulverization resulted from impact and shear between the spheres, and size reduction was accomplished in about 85 minutes. The attritor pulverization principle is shown in Figure 3-1. During mixing, the tank is cooled by chilled water to prevent premature setting of the grout.

Constant agitation of the mix was required because the thixotropic grout must be kept in motion to remain fluid. After pulverization, the grout was transferred from the attritor to a water-cooled agitation tank where it was stirred constantly until injection.

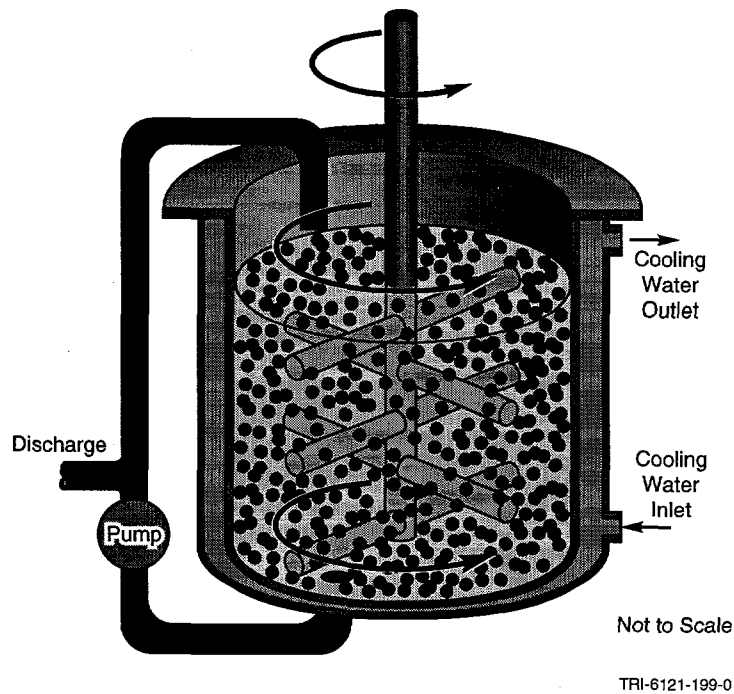


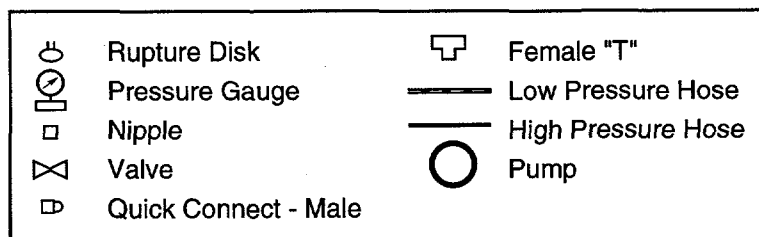
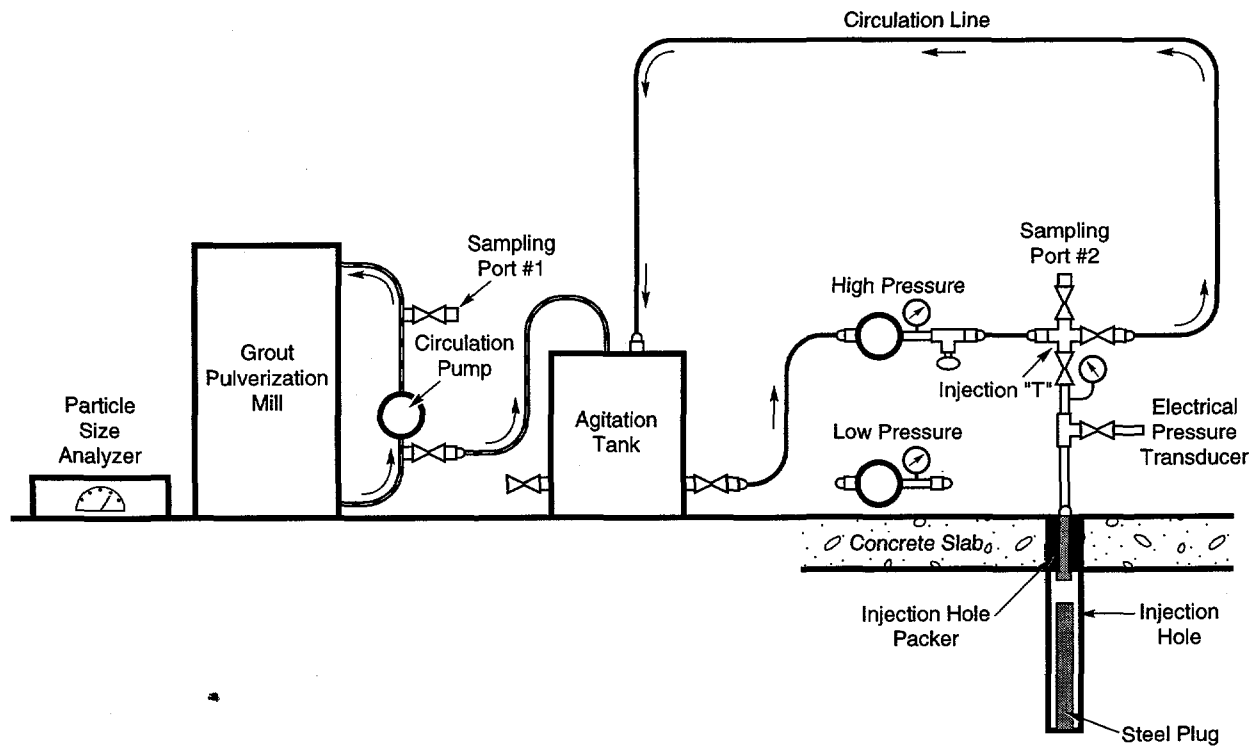
Figure 3-1. Attritor tank principle.

Grout injection was accomplished by sealing the designated injection hole with a packer and pumping the grout through the packer into the hole, where it then dispersed through fractures. The grout pulverization and injection system is shown schematically in Figure 3-2. The grout injection process was repeated 18 times (see Table 3-1). The typical sequence of events is described in section 3.1.

3.1 Sequence of Work

Grouting occurred during the day shift. Drilling of the next injection hole and repositioning of the floor jacks took place on the following shift. Prior to any other activity on the day shift, the ceiling of Room L3 was sounded with a scaling bar to check its integrity, and barriers and warning signs were checked to be sure they were properly placed. The following activities then occurred concurrently:

- Floor jack set-ups were checked for safety.
- Pre-weighed grout components were check-weighed on a calibrated electronic scale prior to loading into the attritor.
- The attritor, laser particle size analyzer, and data acquisition system (DAS) were activated and their operations checked.
- The rotary viscometer was started and (if necessary) calibrated for residual torque and temperature.
- The laser particle size analyzer was checked and cleaned if dirty.
- All instrumentation was checked via the DAS.
- The water chiller was started and its outlet temperature checked; circulation of water through the attritor cooling jacket was initiated at 20 gpm.
- Inflation pressure in the central injection hole guard packer was checked and adjusted if necessary.
- A hermetically sealed steel plug (shown in Figure 3-2 and described below) was placed in the hole to be grouted. The sliding-end injection packer was positioned above the plug and inflated, and a mechanical restraint was attached to anchor the packer to the slab.
- The injection "T" was inserted into the top of the packer and all grout hoses were connected via quick-connect fittings.
- Five gallons of water containing superplasticizer were placed in the agitation tank, pumped through the grout hoses, and then drained. This flush "lubricated" the system and aided grout flow. Note: Water was used throughout the experiment rather than brine (as stated in the SOP) because laboratory tests prior to the field experiment indicated that brine was unacceptable. Additionally, the Moyno pump was found to generate heat during grouting of the first hole. Use of the Moyno was immediately discontinued because heat greatly reduces the period during which the grout remains injectable.



TRI-6346-158-1

Figure 3-2. Grout pulverization and injection system.

- Grout components were added to the attritor as soon as possible after it attained operating speed. Optimum time to achieve a grout mix with 90% of the particles smaller than 8.5 microns was approximately 85 minutes, and timing of the mixing process began with the addition of the last component. Stop watches for the PI and the DAS, viscometer, and laser operators were synchronized by the attritor operator.
- For the initial 60 minutes of pulverization, samples were drawn from the recirculation loop on the attritor (sample port #1) every 15 minutes and analyzed for particle size and rheology.
- The sampling interval was then reduced to 10 minutes until the completion of pulverization. Every sample was weighed and all grout was taken into account.
- When the particle size was 90% smaller than 8.5 microns, the grout was transferred to the agitation tank. Prior to transfer, chilled water was circulated through the tank cooling jacket. During transfer, attritor speed was reduced to minimize frictional heat and the agitation tank paddle rotation speed was maintained at approximately 60 rpm.
- Grout was then pumped from the agitation tank through the grout hoses and fittings, across the top of the injection "T" and back into the agitation tank in a closed recirculation loop as shown in Figure 3-2. The valve into the grout hole remained closed during this procedure. Cleaning of the attritor began immediately following grout transfer.

Note: The "gas Lugeon" test described in the SOP (Ahrens, 1992a) proved impractical and was not conducted during the grouting.

The 50S attritor can pulverize and mix 129 to 140 liters of grout per batch, but the time required increases with the volume. Because volume requirements were believed to be small, the lowest batch size was selected for this experiment. After pulverization and transfer to the agitation tank, approximately 25 liters were retained on the surface area of the grinding media in the attritor tank, leaving about 104 liters for injection. The average volume of the injection holes (3.6-m deep and 15.2-cm in diameter) was approximately 66.8 liters. To decrease the volume of grout required to fill the hole, sealed steel plugs were fabricated and placed in all injection holes except the first two (L3418 and L3422). The plugs were made from 14.1-cm outside diameter, schedule 80 carbon steel pipe, 2.5 m in length. After the plugs and packer were in place, approximately 17 liters of grout filled the hole, leaving 87 liters for injection into the formation. The plugs were left in the hole after grouting. The packer was removed and the hole was filled with grout to the top of the concrete slab. Plug volumes, together with data on hole volume, are shown in Table 3-2.

After steady-state flow was achieved in the recirculation loop, the valve to the injection packer was opened and the hole filled by gravity flow (the return valve to the agitation tank remained open during this operation). The hole was considered full when grout extruded from the 6.3-mm stainless steel tube/valve assembly that passed through the packer and out its top.

Table 3-2. Grout Hole Volumes

Hole Number	Diameter (cm)	Length (m)	Volume of Empty Hole (L)	Volume of Packer in Hole (L)	Core Stub Volume (L)	Plug Volume (L)	Volume of Grout in Hole (L)	Test Date
L3422A	15.24	3.72	67.89	7.41	no info	0.00	60.47	2/3/93
L3422B	15.24	3.72	67.89	7.41	no info	0.00	60.47	2/4/93
L3418	15.24	3.86	70.43	7.41	no info	0.00	63.02	2/8/93
L3424A	15.24	3.73	68.12	7.41	no info	39.44	21.27	2/11/93
L3424B	15.24	3.73	68.12	7.41	no info	39.44	21.27	2/12/93
L3420	15.24	3.76	68.58	7.41	no info	39.44	21.73	2/16/93
L3421	15.24	3.78	69.04	7.41	no info	39.44	22.19	2/19/93
L3423	15.24	3.81	69.51	7.41	0.62	39.44	22.04	2/23/93
L3419	15.24	3.81	69.51	7.41	0.41	39.44	22.25	2/24/93
L3425	15.24	3.76	68.58	7.41	0.82	39.44	20.91	2/25/93
L3530	15.24	3.86	70.43	7.41	0.00	29.36	33.66	3/15/93
L3526	15.24	3.81	69.51	7.41	0.41	29.36	32.32	3/16/94
L3531	15.24	3.76	68.58	7.41	0.41	39.44	21.32	3/17/93
L3527	15.24	3.76	68.58	7.41	0.82	39.44	20.91	3/18/93
L3532	15.24	3.78	69.04	7.41	0.41	39.44	21.78	3/19/93
L3528	15.24	3.78	69.04	7.41	0.00	39.44	22.19	3/22/93
L3533	15.24	3.78	69.04	7.41	0.21	39.44	21.99	3/23/93
L3529	15.24	3.73	68.12	7.41	0.41	39.44	20.86	3/24/93

When extrusion occurred, the injection valve was closed and the DAS operator instructed the system to begin weighing the agitation tank (which was suspended from a sensitive load cell) every five seconds for three minutes. Average weight was determined, and the DAS then reduced the jack and agitation tank load cell readings to numbers approaching zero. When the DAS operator was satisfied that all systems were operating properly, he signaled the grouting supervisor to initiate grout injection. This was accomplished by pumping at a pressure higher than needed and controlling injection pressure by simultaneously manipulating the injection and recirculation valves on the injection "T."

The grouting supervisor monitored procedures on a color monitor while operating the injection valves. Extensometer readings, grout injection rate and pressure, floor jack loadings, total weight of injected grout, and water chiller outlet temperature were displayed graphically and/or numerically on one of two monitor screens positioned close to the injection "T." Screens were changed by the DAS operator as requested by the grouting supervisor. All instrumentation data from this procedure are presented in Appendix E.

Injection pressure, initiated at approximately 0.03 MPa, was slowly increased as required to maintain relatively steady injection rates. During grouting of the first eight grout holes (termed "primary" grout holes), pressure was limited to 3.4 MPa by a rupture disk. Equipment changes allowed pressure to be increased to 8.2 MPa during grouting of the second eight holes (termed "secondary" grout holes). Jack load increases enabled operators to deduce that a volume of high-pressure grout was usually created near the injection hole, and the variation in jack load increase frequently suggested the direction of grout movement away from the hole. When injection ended, most of this pressure dissipated in about 30 minutes, indicating that the grout was slowly moving out through the fractured rock. After pressure dissipation, the injection packer was removed and cleaned.

Fixed-end, 3.6-m-long guard packers were used to seal the central gas injection hole and any non-injection holes that showed grout communication during injection. These packers were inflated with pressurized nitrogen to approximately 4.1 MPa during primary-hole grouting and approximately 6.9 MPa during grouting of the secondary injection holes. When any open hole showed grout communication, injection was temporarily stopped while workers noted the depth, quadrant, and approximate flow rate and then set a guard packer to block the flow. The procedure required about 5 minutes, after which injection was resumed. Grout communication information is presented in Appendix D.

The open-hole guard packer procedure was not used for the first and third primary grout holes (L3422 and L3424). When grout communication was observed in these early holes, injection was terminated and the grout was vacuumed from the hole. The grout was allowed to harden overnight and a second injection was attempted the next day. As shown in Table 3-1, L3422A and L3424A refer to the initial grouting and L3422B and L3424B refer to the second grouting effort. This procedure proved unsatisfactory, probably because the initial grout injection had sealed most of the fracturing near the injection hole, inhibiting grout injection during the second attempt. Therefore, this procedure was revised to allow the use of the guard packers, which sealed the hole from the bottom to approximately 0.15 m below the top of the concrete slab. Early in the experiment, efficient grouting was hindered by an insufficient number of guard packers. Additional guard packers were obtained as quickly as possible.

To aid post-test determinations of grout permeation, grout in each of the sixteen injection holes was dyed a different color. The dyes and their characteristics are described in Appendix A. Post-experiment analyses of grout diffusion patterns (based on dyes) are explained in Appendix H.

The grouting sequence was such that the hole being grouted was located the maximum distance from the previously grouted hole. After the grouting of

hole L3422, for example, L3418 (the diametrically opposed hole) was grouted. This procedure was used throughout the grouting experiment. As shown in Table 3-1, injection times ranged from 93 to 115 minutes. Injection was terminated when:

- the injection rate became too low,
- grout communication with an open hole could not be countered by the insertion of a guard packer,
- rod extensometer readings reached 12.5 mm (one occurrence), or
- grout supply was spent (one occurrence).

Flash set never occurred, so injection was never terminated because of setting of the grout. All grouting equipment was disassembled and cleaned thoroughly immediately after its use. Cleaning procedures are described in Appendix E.

3.2 Grouting Summary

All critical data collected during grouting are presented graphically in Appendix G. The plots present information on grout particle size and rheology, grout volume and pressure, jack loading and temperature, and attritor torque and temperature. Data from the rod extensometers are presented in Appendix F. Grout distribution patterns are discussed in Appendix H.

3.2.1 Particle Size Determination and Rheology

An important component of quality control during grouting was the determination of grout rheological properties and grout particle size (and the percent distribution of sizes). Rheological characteristics were assessed with a Bohlin Visco 88 rotary viscometer in conjunction with its dedicated computer, printer, and Bohlin VISCOSOFT proprietary software. VISCOSOFT is commercially available, off-the-shelf software that meets the requirements of QAPD Section 19 and QAP 19-1. The viscometer was calibrated for temperature and residual torque immediately prior to each grouting event as directed by the manufacturer. Additionally, instrument performance and accuracy were verified by determining the viscosity of three Brookfield oils whose viscosity is traceable to the National Institute of Standards and Testing (NIST). The viscosities of these standards covered the entire range encountered during the experiment. Calibration documentation is filed with WIPP Quality Assurance. The Visco 88 employed a precise and fixed concentric geometry with a rotating inner "bob" in a stationary outer cylinder. Torque, developed on the cylinder by the grout as the bob revolves, is directly related to the sample's plastic viscosity and shear stress through a measuring system geometric constant.

Rheology of the thixotropic grout was determined at eight different shear rates, and plastic viscosity and shear stress were plotted as a function of time for each sample. The data, which were displayed on the computer monitor and printed as hard copy, are presented numerically in Table 3-3 and graphically in Appendix G. Table 3-3 shows rheology at the lowest shear rate (24 1/s).

Particle size analyses were conducted on a Malvern 3200E Mastersizer laser particle size analyzer, which operated with a dedicated computer and printer using commercially available off-the-shelf Malvern software that meets the requirements of Quality Assurance Program Description Section 19 and Quality Assurance Procedure 19-1. If the laser/software combination determines the size correctly anywhere within the instrument's range, (1 to 600 microns), the readings are correct for any other size. Mono-modular (all particles the same size) standards traceable to NIST were obtained in 2, 4, and 10 micron sizes. These were run five times during the experiment and the laser analyzer was always correct. Calibration documentation is filed with WIPP Quality Assurance. The Malvern displayed the analyses graphically and numerically on a monitor screen and printed them in hard copy as well. Analyses were completed in approximately 5 minutes, yielding "real time" data.

Particle size averaged 90% smaller than 8 microns, with the average particle size approximately 4 microns. Plastic viscosity and shear strength were suitable for two hours of injection.

3.2.2 Grout Characterization

Information about grout color, particle size, and injected volume are presented in Table 3-4. Less than one micron variation in particle size among the 18 grout batches illustrates excellent quality control of the simultaneous pulverization and mixing processes.

Table 3-3. Rheology Data at Lowest Measured Shear Rate (24 1/s)

Hole Number	Batch Start & Sampling Times	Analysis Duration (sec)	Time from Batch Start (min)	Grout Temp. (°C)	Shear Stress (Pa)	Viscosity (Pa*s)
L3418	9:28 AM		0.00			
	9:46 AM	20.4	18.35	27.4	0.588	0.025
	9:59 AM	20.3	31.73	26.3	0.649	0.027
	10:14 AM	20.4	46.72	26.4	1.150	0.048
	10:29 AM	20.4	61.73	26.5	1.850	0.077
	10:40 AM	20.3	72.20	25.7	2.760	0.115
	10:50 AM	20.3	82.30	25.5	5.310	0.221
	11:01 AM	20.3	93.43	25.3	4.800	0.200
	11:10 AM	20.3	102.95	24.9	4.750	0.198
	11:21 AM	20.4	113.05	25.2	4.730	0.197
	11:38 AM	20.3	130.27	26.5	5.430	0.226
	11:52 AM	20.4	144.22	26.8	5.030	0.210
	12:07 PM	20.4	159.43	27.6	5.280	0.220
	12:21 PM	20.3	173.62	28.3	5.610	0.233
	12:38 PM	20.4	190.82	28.9	5.950	0.248
	12:54 PM	20.3	206.55	29.0	5.970	0.248
	1:09 PM	20.3	221.57	29.0	5.980	0.249
1:24 PM	20.3	236.82	29.5	6.420	0.267	
1:40 PM	20.4	252.73	29.2	6.630	0.276	
1:56 PM	20.3	268.62	29.5	6.750	0.281	
L3419	8:22 AM		0.00			
	8:40 AM	20.4	18.00	26.7	0.733	0.031
	8:53 AM	20.4	31.80	25.4	0.737	0.031
	9:09 AM	20.3	47.32	25.4	1.150	0.048
	9:25 AM	20.3	63.23	25.1	2.200	0.092
	9:35 AM	20.3	73.00	24.4	3.300	0.137
	9:44 AM	20.3	82.20	24.6	5.380	0.224
	10:01 AM	20.3	99.95	24.2	6.560	0.273
	10:16 AM	20.2	114.83	24.7	7.510	0.312
	10:32 AM	20.4	130.07	25.3	8.390	0.349
	10:45 AM	20.3	143.67	24.8	8.720	0.363
	11:02 AM	20.3	160.63	24.0	9.030	0.376
	11:16 AM	20.3	174.68	25.5	9.640	0.401
	11:34 AM	20.3	192.00	25.5	10.200	0.423
	11:50 AM	20.3	208.80	26.9	10.900	0.453
12:06 PM	20.3	224.13	27.5	11.600	0.484	
12:21 PM	20.2	239.25	28.2	12.100	0.503	

Table 3-3. Rheology Data at Lowest Measured Shear Rate (24 1/s) (continued)

Hole Number	Batch Start & Sampling Times	Analysis Duration (sec)	Time from Batch Start (min)	Grout Temp. (°C)	Shear Stress (Pa)	Viscosity (Pa*s)
L3421	8:33 AM		0.00			
	9:09 AM	20.3	36.32	25.0	0.781	0.033
	9:24 AM	20.3	51.45	24.5	1.350	0.056
	9:39 AM	20.4	66.88	23.6	2.170	0.091
	9:50 AM	20.3	77.15	23.7	2.320	0.097
	9:59 AM	20.3	86.13	23.7	7.450	0.311
	10:09 AM	20.3	96.93	24.0	17.200	0.718
	10:21 AM	20.2	108.75	22.5	15.600	0.651
	10:36 AM	20.4	123.65	22.4	18.700	0.781
	10:52 AM	20.3	139.77	22.8	25.800	1.070
	11:08 AM	20.3	155.70	24.5	40.200	1.680
11:23 AM	20.3	170.25	24.9	36.500	1.520	
L3422A	9:42 AM		0.00			
	9:53 AM	20.3	11.73	27.7	0.484	0.020
	10:08 AM	21.6	26.50	26.9	0.498	0.021
	10:24 AM	20.3	42.18	26.7	0.811	0.034
	10:38 AM	20.3	56.73	26.5	1.220	0.051
	10:49 AM	20.3	67.62	26.2	1.930	0.080
	11:03 AM	21.6	81.33	26.0	2.150	0.090
	11:17 AM	20.3	95.32	26.0	2.160	0.090
	11:25 AM	20.4	103.68	26.2	2.300	0.096
	11:39 AM	20.3	117.23	26.9	2.230	0.093
	11:49 AM	20.3	127.58	27.0	2.190	0.091
	12:02 PM	20.3	140.97	26.9	1.800	0.075
	12:12 PM	20.4	150.23	27.5	2.380	0.099
L3422B	9:24 AM		0.00			
	9:37 AM	20.3	13.23	28.0	0.617	0.026
	9:51 AM	20.3	27.30	27.3	0.598	0.025
	10:06 AM	20.3	42.02	27.5	0.909	0.038
	10:20 AM	20.3	56.85	26.6	1.550	0.065
	10:31 AM	20.3	67.07	26.5	2.450	0.102
	10:41 AM	20.3	77.55	26.5	4.490	0.187
	10:50 AM	20.4	86.97	26.1	5.520	0.230
	11:08 AM	20.3	104.75	26.4	6.280	0.262
	11:09 AM	20.3	105.43	26.4	6.280	0.262
	11:20 AM	20.3	116.92	26.3	7.130	0.297
	11:33 AM	20.3	129.23	27.2	6.850	0.285
	11:48 AM	20.3	144.90	27.0	7.490	0.312
	12:04 PM	20.4	160.37	27.4	9.470	0.394
	12:22 PM	20.3	178.17	26.9	9.930	0.413
	12:41 PM	20.4	197.50	27.7	10.800	0.450
	12:55 PM	20.3	211.02	28.6	12.900	0.536
1:06 PM	20.4	222.18	28.7	12.700	0.528	

Table 3-3. Rheology Data at Lowest Measured Shear Rate (24 1/s) (continued)

Hole Number	Batch Start & Sampling Times	Analysis Duration (sec)	Time from Batch Start (min)	Grout Temp. (°C)	Shear Stress (Pa)	Viscosity (Pa*s)
L3423	8:36 AM		0.00			
	8:53 AM	20.3	17.30	26.4	0.864	0.036
	9:07 AM	20.4	31.80	25.7	0.867	0.036
	9:22 AM	20.3	46.57	24.7	1.190	0.050
	9:37 AM	20.4	61.48	24.6	1.820	0.076
	9:47 AM	20.3	71.75	24.5	3.230	0.135
	9:57 AM	20.3	81.87	23.3	5.580	0.232
	10:14 AM	20.3	98.90	24.2	9.720	0.405
	10:28 AM	20.3	112.15	23.5	10.200	0.423
	10:44 AM	20.3	128.82	23.0	9.920	0.413
	11:01 AM	20.3	145.15	22.8	10.500	0.439
L3424A	9:05 AM		0.00			
	9:23 AM	20.3	18.93	27.0	0.760	0.032
	9:36 AM	20.3	31.97	26.5	0.610	0.025
	9:51 AM	20.3	46.82	26.7	0.990	0.041
	10:06 AM	20.3	61.55	26.1	1.810	0.075
	10:16 AM	20.4	71.68	25.7	3.100	0.129
	10:27 AM	20.3	82.03	25.8	5.540	0.231
	10:27 AM	20.4	82.97	26.9	0.600	0.025
	10:36 AM	20.2	91.90	25.4	5.810	0.242
	10:51 AM	20.3	106.72	25.6	6.610	0.275
	11:02 AM	20.2	117.73	24.5	6.350	0.264
L3424B	9:54 AM		0.00			
	10:13 AM	20.4	19.50	27.1	0.562	0.023
	10:43 AM	20.3	49.20	26.5	0.861	0.036
	10:58 AM	20.3	64.68	26.5	1.600	0.067
	11:10 AM	20.3	76.38	26.5	2.500	0.104
	11:18 AM	20.3	84.18	25.6	3.800	0.158
	11:33 AM	20.3	99.92	25.3	5.520	0.230
	11:44 AM	20.4	110.75	24.7	6.070	0.253
	12:01 PM	20.3	127.10	26.0	8.750	0.365
	12:17 PM	20.3	143.32	27.2	10.200	0.426
	12:34 PM	20.4	160.67	28.0	12.700	0.528
	12:51 PM	20.4	177.77	28.0	12.600	0.523

Table 3-3. Rheology Data at Lowest Measured Shear Rate (24 1/s) (continued)

Hole Number	Batch Start & Sampling Times	Analysis Duration (sec)	Time from Batch Start (min)	Grout Temp. (°C)	Shear Stress (Pa)	Viscosity (Pa*s)
L3425	8:33 AM		0.00			
	8:51 AM	20.3	18.65	24.5	1.460	0.061
	9:23 AM	20.3	50.88	23.8	2.040	0.085
	9:35 AM	20.3	62.58	23.3	2.380	0.099
	9:45 AM	20.4	72.90	23.1	3.350	0.139
	9:55 AM	20.3	82.87	22.7	5.000	0.208
	10:15 AM	20.4	102.05	23.3	3.660	0.152
	10:32 AM	20.4	119.20	23.3	3.850	0.160
	10:51 AM	20.3	138.23	22.8	4.170	0.173
11:08 AM	20.3	155.10	23.2	3.760	0.156	
L3526	9:49 AM		0.00			
	10:05 AM	20.4	16.65	26.7	0.952	0.040
	10:20 AM	20.2	31.48	25.6	0.841	0.035
	10:35 AM	20.3	46.52	25.8	1.590	0.066
	10:50 AM	20.3	61.13	25.1	2.350	0.098
	11:05 AM	20.3	76.13	25.1	5.210	0.217
	11:12 AM	20.3	83.23	24.9	6.230	0.259
	11:28 AM	20.3	99.48	25.1	3.040	0.126
	11:44 AM	20.3	115.80	25.0	5.870	0.244
	12:00 PM	20.4	131.43	26.8	7.070	0.294
	12:17 PM	20.4	148.23	27.4	7.260	0.302
	12:33 PM	20.3	164.22	28.0	7.610	0.316
L3527	9:47 AM		0.00			
	10:04 AM	20.4	17.00	26.4	0.687	0.029
	10:18 AM	20.3	31.95	25.9	0.856	0.036
	10:33 AM	20.3	46.43	25.5	1.300	0.054
	10:48 AM	20.4	61.57	25.3	2.100	0.087
	10:58 AM	20.2	71.82	25.0	3.670	0.153
	11:08 AM	20.4	81.72	24.5	5.730	0.238
	11:27 AM	24.5	100.92	24.5	6.740	0.280
	11:44 AM	20.4	117.65	24.3	6.460	0.269
	12:01 PM	20.2	134.98	24.4	6.750	0.281
	12:18 PM	20.3	151.62	27.3	8.150	0.339
	12:37 PM	20.3	170.83	23.5	7.400	0.308
	12:55 PM	20.3	188.07	26.5	9.400	0.391
	1:10 PM	20.3	203.02	26.3	9.510	0.396
1:27 PM	20.3	220.38	26.4	9.780	0.407	

Table 3-3. Rheology Data at Lowest Measured Shear Rate (24 1/s) (continued)

Hole Number	Batch Start & Sampling Times	Analysis Duration (sec)	Time from Batch Start (min)	Grout Temp. (°C)	Shear Stress (Pa)	Viscosity (Pa*s)
L3528	9:04 AM		0.00			
	9:19 AM	20.3	15.67	25.2	0.632	0.026
	9:36 AM	20.4	32.37	24.7	0.774	0.032
	9:48 AM	20.4	44.92	24.5	0.955	0.040
	10:03 AM	20.3	59.98	24.2	1.550	0.064
	10:14 AM	20.3	70.62	23.9	2.650	0.110
	10:23 AM	20.4	79.97	23.3	4.510	0.188
	10:41 AM	20.4	97.65	23.6	5.400	0.225
	10:57 AM	20.4	113.70	23.3	5.470	0.228
	11:14 AM	20.2	130.17	22.7	5.270	0.219
	11:29 AM	20.3	145.82	24.8	6.850	0.285
	11:45 AM	20.4	161.03	25.2	8.490	0.353
	12:11 PM	20.3	187.65	24.3	6.950	0.289
L3529	8:34 AM		0.00			
	8:51 AM	20.3	17.02	25.7	0.729	0.030
	9:04 AM	20.3	30.08	24.8	0.739	0.031
	9:18 AM	20.4	44.87	24.0	0.991	0.041
	9:35 AM	20.3	61.15	24.2	1.590	0.066
	9:43 AM	20.4	69.68	23.6	2.190	0.091
	9:53 AM	20.3	79.70	23.5	3.650	0.152
	10:11 AM	20.3	97.70	23.9	4.560	0.190
	10:29 AM	20.3	115.08	24.8	5.190	0.216
	10:45 AM	20.3	131.32	24.4	5.840	0.243
	11:03 AM	20.3	149.10	23.8	5.210	0.217
	11:19 AM	20.3	165.70	23.9	5.120	0.213
	L3530	9:45 AM		0.00		
10:02 AM		20.4	17.10	26.2	1.200	0.050
10:15 AM		20.3	30.47	25.0	1.300	0.054
10:30 AM		20.4	45.47	24.1	1.350	0.056
10:48 AM		25.4	63.87	24.5	2.110	0.088
10:56 AM		20.4	71.23	24.3	2.500	0.104
11:05 AM		20.4	80.53	24.3	3.740	0.156
11:13 AM		20.3	88.38	24.1	4.940	0.206
11:29 AM		20.3	104.18	23.3	3.840	0.160
11:45 AM		20.3	120.45	23.5	4.210	0.175
12:00 PM		20.4	135.50	21.7	3.860	0.161
12:17 PM		20.3	152.32	23.9	4.380	0.182
12:34 PM		20.3	169.35	24.0	4.620	0.192
12:50 PM	20.3	185.08	24.8	5.060	0.211	
1:09 PM	20.3	204.13	21.9	4.400	0.183	

Table 3-3. Rheology Data at Lowest Measured Shear Rate (24 1/s) (continued)

Hole Number	Batch Start & Sampling Times	Analysis Duration (sec)	Time from Batch Start (min)	Grout Temp. (°C)	Shear Stress (Pa)	Viscosity (Pa*s)
L3531	8:45 AM		0.00			
	9:01 AM	20.3	16.28	27.2	0.608	0.025
	9:16 AM	20.3	31.62	26.1	0.686	0.029
	9:32 AM	20.2	47.43	25.9	0.980	0.041
	9:46 AM	20.3	61.35	25.7	1.820	0.076
	9:56 AM	20.4	71.65	24.9	2.930	0.122
	10:06 AM	20.3	81.38	24.6	4.890	0.203
	10:28 AM	20.2	103.08	25.9	7.070	0.294
	10:42 AM	20.2	117.83	25.1	7.280	0.303
	11:00 AM	20.4	135.47	26.8	8.950	0.372
	11:01 AM	20.4	136.13	26.8	8.950	0.372
	11:17 AM	20.3	152.98	28.0	9.500	0.395
	11:32 AM	20.3	167.58	28.1	10.000	0.417
	11:48 AM	20.3	183.27	28.3	10.000	0.417
	12:02 PM	20.3	197.93	27.9	9.780	0.407
12:18 PM	20.4	213.38	27.4	9.740	0.405	
L3532	8:39 AM		0.00			
	8:57 AM	20.3	18.88	24.4	0.684	0.029
	9:10 AM	20.3	31.23	23.8	0.729	0.030
	9:25 AM	20.4	46.50	23.7	1.010	0.042
	9:41 AM	20.4	62.12	24.0	2.570	0.107
	9:51 AM	20.3	72.13	23.7	3.480	0.145
	10:00 AM	20.3	81.10	23.6	5.630	0.234
	10:22 AM	20.3	103.40	23.2	6.440	0.268
	10:39 AM	20.4	120.12	22.4	5.610	0.233
	10:54 AM	20.4	135.73	22.4	5.950	0.248
	11:09 AM	20.3	150.98	22.5	6.260	0.261
	11:28 AM	20.3	169.48	23.0	5.820	0.242
L3533	8:33 AM		0.00			
	8:50 AM	20.2	17.02	25.3	0.766	0.033
	9:04 AM	20.4	31.35	24.9	0.806	0.034
	9:18 AM	21.6	45.95	24.1	0.983	0.041
	9:33 AM	20.3	60.67	23.9	3.330	0.138
	9:44 AM	20.4	71.00	24.1	2.700	0.112
	9:54 AM	20.3	81.37	23.6	4.790	0.199
	10:17 AM	20.3	104.73	23.1	6.300	0.262
	10:41 AM	20.2	128.30	23.9	6.440	0.268
	10:59 AM	20.3	146.70	24.8	10.000	0.416
11:16 AM	20.4	163.62	23.3	8.760	0.365	

Table 3-4. Grout Characterization

	Hole Number	Injection Date	Grout Colorization		Injected Grout Particle Size (μm)		Volume Injected (L)	
			Percent Dye by Weight	Dye Color(s)	Resulting Grouting Color	90% Smaller Than		Average
Primary Grout Holes	L3418	2/8/93	5.0	Blue - 5556	Steel Blue	7.9	4.2	16
	L3419	2/24/93	5.0	Orange - 110	Dark Orange	7.8	4.1	13
	L3420	2/16/93	5.0	Black - 490	Black	8.3	4.8	23
	L3421	2/19/93	5.0	Green - 329	Green	7.6	4.5	13
	L3422A	2/3/93	N/A	None	Light Gray	8.6	4.2	10
	L3422B	2/4/93	N/A	None	Light Gray	7.9	4.1	10
	L3423	2/23/93	5.0	Yellow - 420	Dark Yellow	8.2	4.5	87
	L3424A	2/11/93	2.5	Blue - 5556	Light Blue	7.9	4.1	17
	L3424B	2/12/93	5.0	Dark Red - 180	Dark Red	7.7	4.2	8
	L3425	2/25/93	5.0	Dark Brown - 686	Dark Brown	8.3	4.2	51**
Primary Average					8.1*	4.4*		
Secondary Grout Holes	L3526	3/16/93	5.0	Light Brown - 610	Light Brown	8.1	4.1	8
	L3527	3/18/93	5.0	Orange-Red - 130	Orange-Red	7.9	4.1	26
	L3528	3/22/93	5.0	Purple (Blue - 5556 + Dark Red - 180)	Dark Lavender	8.0	4.6	29
	L3529	3/24/93	2.5	Dark Red - 180	Brown	8.1	4.4	5
	L3530	3/15/93	5.0	Brown - 663/4	Brown	8.1	4.4	22
	L3531	3/17/93	2.5	Green - 329	Light Green	7.6	4.1	10
	L3532	3/19/93	5.0	Gold - 960/4	Golden Brown	8.0	4.2	73
	L3533	3/23/93	2.5	Aqua (Blue - 5556 + Green - 329)	Olive Green	7.9	4.1	10**
Secondary Average					8.0*	4.3*		

4.0 FORMATION CHARACTERIZATION TESTS

Gas-flow and tracer-gas tests were conducted during and after grouting activities to determine the effectiveness of the techniques and the test equipment. Data from these tests were compared to the pre-grout baseline data collected before and immediately after slab emplacement, as described in Section 2. Gas-flow testing was performed in all boreholes on the slab prior to the first grout injections.

Cross-hole tracer-gas testing was conducted immediately before grouting activity to provide information about the nature of the gas-permeability and pre-grout flow pathways. Tracer-gas testing was repeated five times during grouting: after the first four primary grout-injection holes (L3422, L3418, L3424, L3420) had been drilled and grouted individually, and after the remaining four primary holes (L3419, L3421, L3423, L3425) had been drilled and grouted as a group. About three weeks later, after the eight secondary holes (L3526 through L3533) were drilled and grouted, a final series of cross-hole tracer-gas tests was conducted.

Gas-flow/tracer tests were conducted throughout the experiment, and additional testing continued after all grouting activities were completed. Gas-flow tests were conducted prior to, during, and after grouting. After completion of all grouting activities, 24 post-grout boreholes (15-cm-diameter) were drilled and a series of gas-flow tests were conducted. A delay of approximately 6 months occurred during this work because of the priority of other SNL testing. Rod extensometer readings during this period were recorded, and they indicated continuing deformation of the volume grouted, as a result of ongoing DRZ formation. This deformation may produce additional strain-induced permeability, thus affecting the later gas-flow readings. At this time, these gas-flow tests have not been analyzed.

4.1 Gas-Injection Tests

Two types of gas-injection tests were conducted for SSSPT-F. The first was gas-permeability testing in which gas was injected into a sealed borehole interval while the borehole pressures and the flow-rate response were monitored. The second was a tracer-gas test, which was conducted by injecting a detectable tracer gas into a central borehole and monitoring the gas breakthrough at numerous boreholes surrounding the injection borehole. The gas-permeability tests were used to demonstrate the quantitative effects of the grouting experiments on formation gas permeability. The tracer-gas tests results were used to qualitatively describe the effect of the grouting experiments on the gas-travel paths. Both provided a means to describe the efficiency of grout injection for restricting the movement of gas through the DRZ under Room L3.

Initial gas-permeability testing (of the boreholes drilled from October through December 1992) was performed from January 20 to 28, 1993. The first tracer-gas testing was performed on January 29. This first round of testing provided information about the nature of the gas permeability and flow pathways existing prior to any grouting activities.

The first grout-injection sequence consisted of drilling and grouting four boreholes located at 90° to each other as measured from the central injection borehole. Borehole L3422 was drilled February 1, 1993 and was grouted in two separate events on February 3 and 4. The first post-grout tracer-gas test was performed on February 5. Borehole L3418 was drilled and sealed with a guard packer on February 2. Grout was injected into this borehole on February 8, and the second post-grout tracer-gas test was performed on February 9. Borehole L3424 was drilled on February 10, grouted in two separate events on February 11 and 12, and the post-grout tracer-gas test was performed on February 15. The fourth grouted borehole, L3420, was drilled on February 15 and grouted on February 16.

Boreholes L3421, L3423, L3419, and L3425 were drilled on February 18, 19, 23, and 25 and were grouted on February 19, 23, 24, and 25 respectively. Gas-permeability tests were performed from March 3 through 8. A tracer-gas test performed on March 10 showed that sufficient formation blockage had been produced by the grouting events to necessitate an increase of tracer gas injection pressure from 0.23 MPa to 0.43 MPa. An additional tracer-gas test was performed at the higher pressure on March 11 to allow a benchmark comparison of tests performed at the two pressures.

Secondary grout-injection boreholes L3526 through L3533 were drilled and grouted between March 12 and 24. Final gas-permeability testing of all boreholes drilled before January 1993 was conducted between March 26 and April 22. The final tracer-gas test was performed on April 5.

4.2 Constant-Pressure Gas-Injection Permeability Tests

4.2.1 Testing Procedure

To estimate the formation permeability to gas, constant-pressure gas-injection permeability tests were performed in boreholes located on and adjacent to the SSSPT-F slab. These tests were conducted prior to grout injection, after the first eight grout-injection boreholes had been grouted, and again after all sixteen grout-injection boreholes had been grouted.

Differences noted between the series of tests were expected to quantify the effectiveness of the progressive grout curtain for reducing gas permeability in the DRZ under the slab.

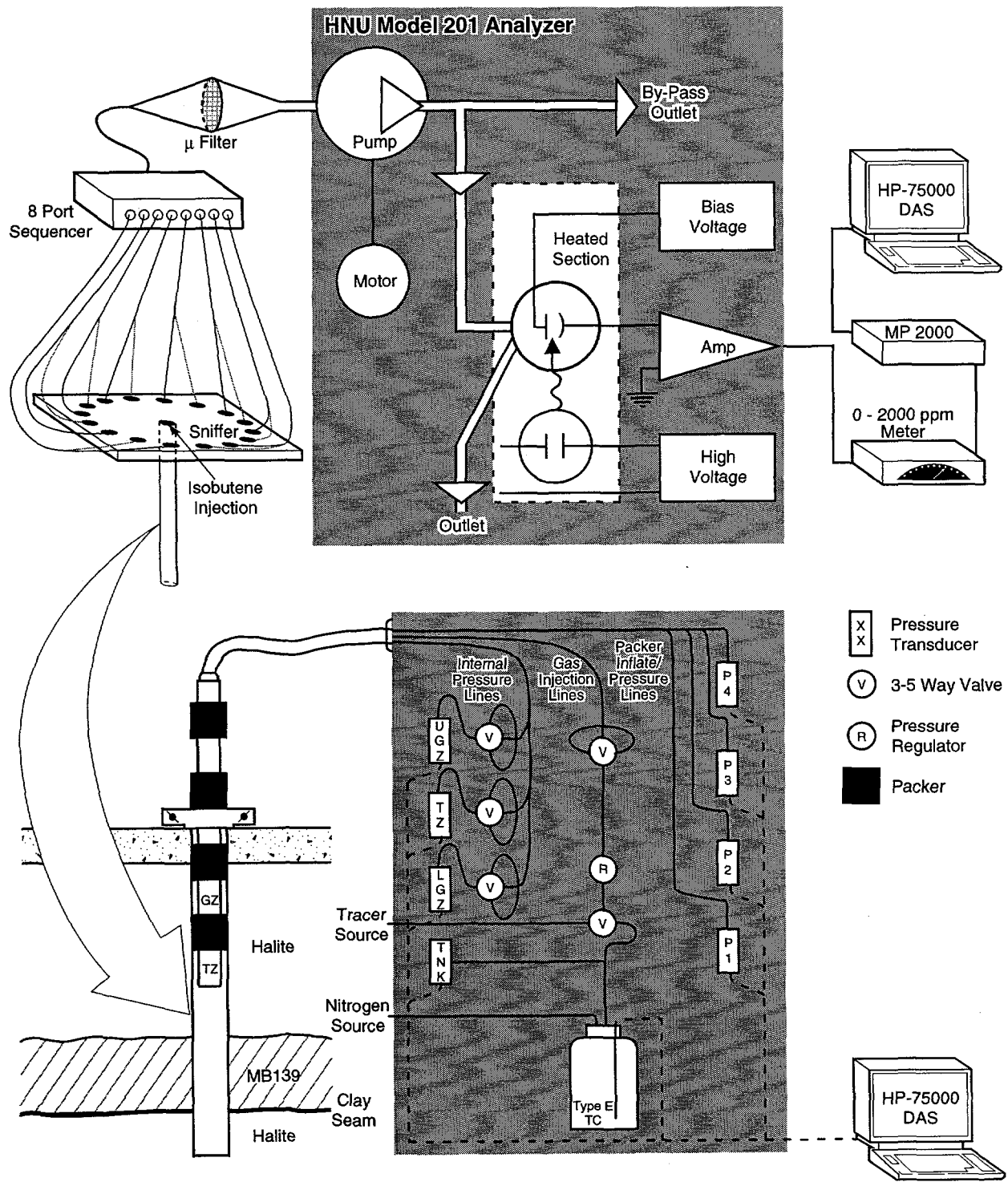
The gas-injection and sampling equipment configuration is shown in Figure 4-1. This equipment is described in Appendix D. The straddle-packer assembly (also described in Appendix D) was set so that the top of the test zone was approximately 1.37 m below the borehole collar, and a split clamp was placed on the packer tool to maintain that depth throughout the test sequence. Packers P1 and P2 were inflated to 0.69 to 0.86 MPa and allowed to set for a period of 15 to 30 minutes, the noted time of packer compliance for this tool. The digital gas-flow tool (DGFT) was configured to deliver gas from the internal reservoir to the test zone. Prior to testing, the internal reservoir was filled to $7.0 \text{ MPa} \pm 0.07 \text{ MPa}$ and the heat of compression was allowed to dissipate from the reservoir. The panel regulator was set to $0.23 \text{ MPa} \pm 6895 \text{ Pa}$.

When the heat of compression had dissipated from the reservoir, the panel valve controlling flow to the test zone was activated and the time of test initiation was noted on the test quality assurance (QA) form for future reference. After 90 minutes of constant-pressure gas injection into the test zone or after the reservoir bottle had depressurized to 1.7 MPa, whichever came first, the flow of gas into the test zone was stopped. The pressure in the test zone was then allowed to decay and the rate of test-zone pressure decay was monitored for a period of one hour or until the test zone returned to ambient atmospheric pressure. After this pressure decay portion of the test, the DAS was turned off, the test and guard zones were vented, the packers were deflated, and preparations were made for the next test.

4.2.2 Test-Zone Gas-Pressure Responses to Injection

The buildup of gas pressure in the test zone during a constant-pressure gas-injection test is a function of the flow rate into the test zone and the characteristics of the formation tested. The ability of the formation to dissipate the gas is a function of several items including the formation gas permeability. If the flow rate is greater than the ability of the formation to dissipate the gas, gas pressure in the test zone will rise, creating a gradient to induce flow through the pathways in the formation.

The DGFT and packer tool combination used for this series of gas-flow tests had a maximum flow rate of approximately 36 L/min of nitrogen gas at standard pressure and temperature when the panel regulator was set to 0.23 MPa. The test-zone lengths for this series of tests were approximately



TRI-6121-99-0

Figure 4-1. Tracer gas injection and sampling equipment.

2.5 m. Appendix I presents the tabulated and charted results of the gas-permeability testing.

The observed borehole pressure responses to the gas-injection tests can be grouped into four basic categories. These categories are differentiated by the rate of pressure buildup, behavior of pressure response after initial buildup, and magnitude of pressure buildup. The four different pressure response curves are a function of the gas permeability within the formation surrounding the individual boreholes.

Figures 4-2 through 4-5 present an example of four test response categories. Figure 4-2 presents the first typical response as seen in borehole L3X10 during the third round of gas-permeability testing. This borehole pressure response is termed the no-rise response. The borehole pressure response in L3X10 does not build up above 5000 Pa even though the gas-injection flow rate into the borehole stays close to the maximum of the gas delivery system for the entire test. This response is typical for a borehole located in a region of high permeability. The permeability is sufficiently large enough that only a small pressure gradient is needed to drive the gas into the formation.

Figure 4-3 presents the second response behavior as seen in the gas-permeability testing of borehole L3215 during the first round of testing. This borehole pressure response is termed the slow-rise response. This response is typical for a borehole that is within a region of slightly lower permeability than those regions demonstrating the no-rise response. The gas-permeability is still sufficient to allow gas flow into the formation, as shown by the high gas-injection flow rates over the entire test. However, the permeability is low enough to result in a buildup in the borehole pressure. The maximum pressure buildup in a slow-rise-response borehole is typically less than 40,000 to 50,000 Pa.

Figure 4-4 presents an example of the third response behavior, termed the continual-rise response. The gas-permeability test presented in Figure 4-4 is for the second round of testing in borehole L3202. In the continual-rise response, the formation surrounding the borehole has a permeability low enough that the wellbore must be partially pressurized before gas will start flowing into the formation. The gas-injection rate behavior includes a high gas-injection rate at early time. This injection rate then decreases to a low flow rate after the wellbore storage effects are overcome enough by the gas-pressure buildup in the borehole so that flow into the formation can occur. The maximum buildup pressure observed for the continual-rise response is typically around 150,000 Pa.

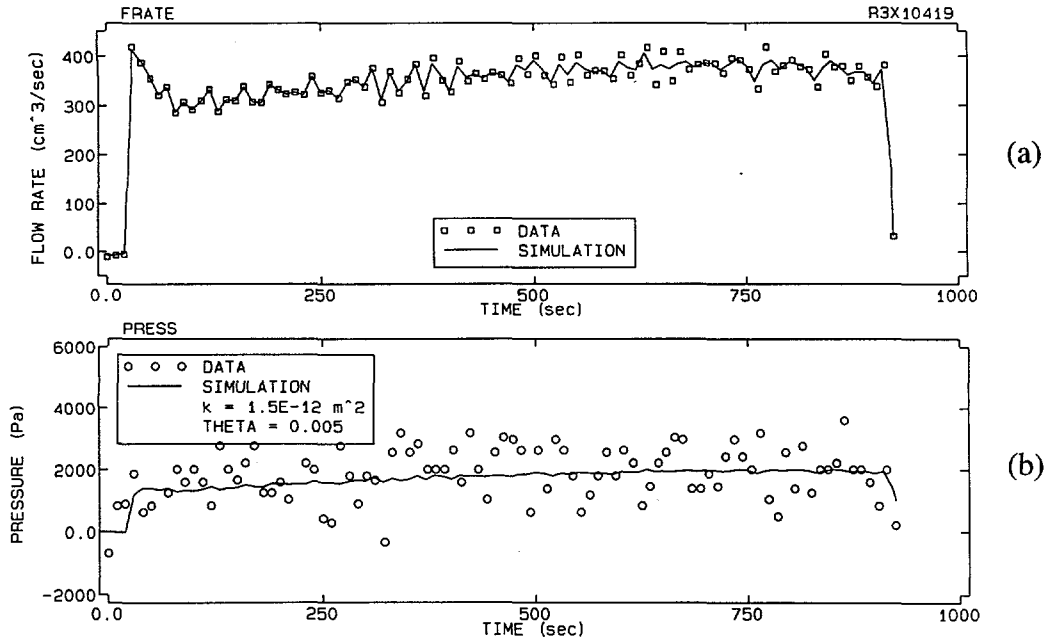


Figure 4-2. Gas-permeability testing (a) gas-injection flow rate and (b) test-zone pressure results for borehole L3X10 during the third round of testing on April 10, 1993.

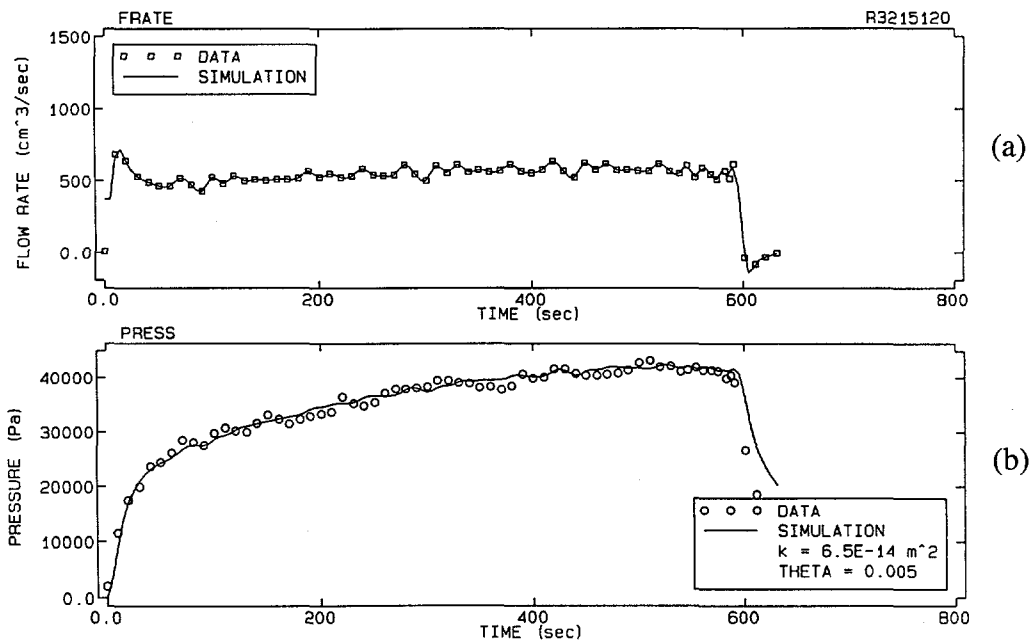


Figure 4-3. Gas-permeability testing (a) gas-injection flow rate and (b) test-zone pressure results for borehole L3215 during the first round of testing on January 20, 1993.

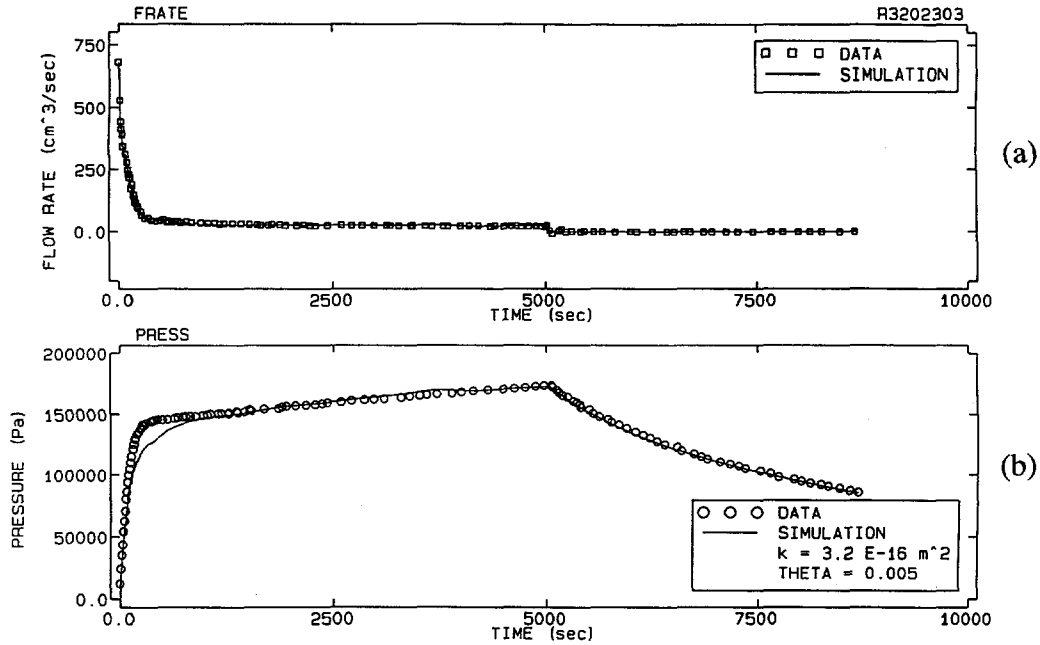


Figure 4-4. Gas-permeability testing (a) gas-injection flow rate and (b) test-zone pressure results for borehole L3202 during the second round of testing on March 3, 1993.

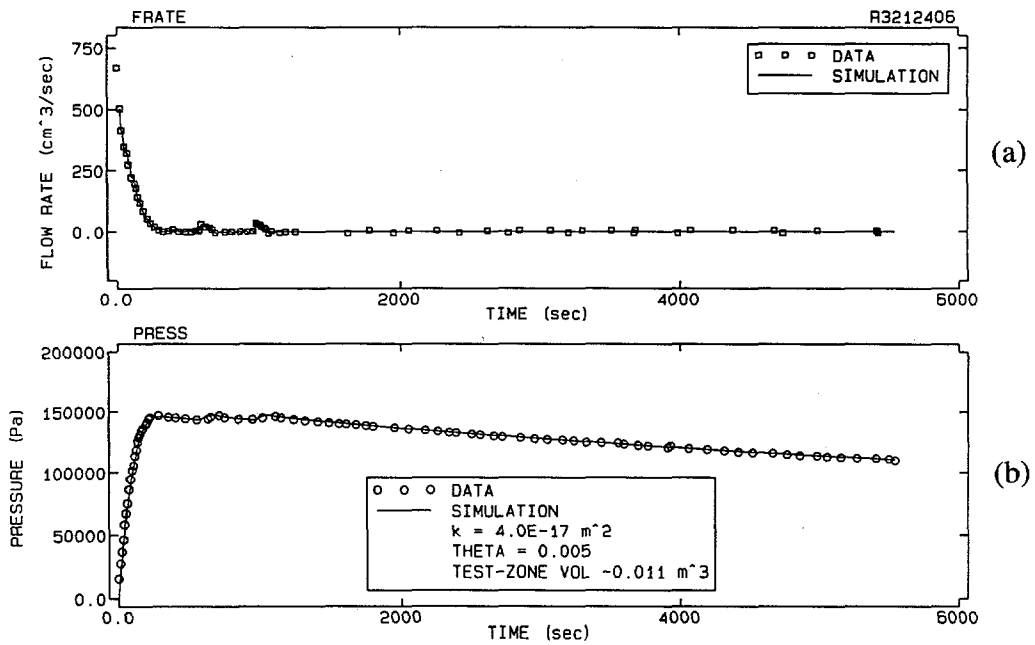


Figure 4-5. Gas-permeability testing (a) gas-injection flow rate and (b) test-zone pressure results for borehole L3212 during the third round of testing on April 6, 1993.

Figure 4-5 presents the last response behavior, termed the rise-and-fall response. The gas-permeability test results presented are for the third and final round of testing in borehole L3212. The rise-and-fall response is typical for the injection tests conducted in a region with very low formation gas permeability. The pressure-buildup curve is similar to the continual-rise response, but the rate of pressure buildup in the borehole is faster for the rise-and-fall response with the same maximum borehole pressure achieved. In the rise-and-fall response, when the borehole had been pressurized to approximately the maximum achievable gas-injection pressure, the gas-injection test was terminated. Once the test was terminated, the pressure in the borehole began to dissipate at a very slow rate compared to the previously described responses.

The four gas-permeability tests presented above will be used to demonstrate the test interpretation procedures followed and the typical interpretation results. A more detailed description of the gas-permeability test interpretations is presented in Section 4.4.

4.3 Tracer-Gas-Injection Testing

4.3.1 Tracer-Gas-Injection Procedure

Tracer-gas-injection testing was performed using the straddle-packer assembly set in borehole L3001 and the DGFT configured as described in Appendix D. Gas-injection pressures were 0.23 MPa for the first 6 tracer-gas tests and were 0.43 MPa for the last two tests.

Tracer-gas tests were performed by injecting instrument grade air at constant flow/pressure for a period of 1.5 hours into the central gas-injection hole to achieve a quasi-steady-state pressure gradient in the formation. This initial flow period was followed by a 0.5-hour constant flow/pressure pulse of instrument grade air with a 200 mg/Kg spike of isobutene that was followed with a 2-hour constant flow/pressure injection of the instrument grade air. The final 2-hour pulse of air was intended to chase the majority of the tracer gas beyond the location of the receiver boreholes.

Gas was withdrawn from the 16 tracer-gas receiver holes arranged radially around the central gas-injection hole at a rate of 0.075 L/min per hole to a sequencing manifold that serviced a photo ionization detector (PID). A total of eight holes could be sampled per test, with the remaining eight holes ventilated at atmospheric pressure through a manifold system that prevented cross-flow between the holes. After the test, the tracer-gas detecting equipment was removed and placed in the remaining eight receiver

holes and the test was repeated. Breakthrough concentration data collection started at the initiation of tracer-gas injection and continued for a period of 2 hours following the end of the injection. After the 2-hour final air injection period or when sampled concentrations dropped to initial levels, air flow was stopped and the test was terminated.

4.3.2 Tracer-Gas-Recovery Data

The tracer-gas breakthrough concentrations measured in the receiver boreholes over the duration of the test led to a tracer-gas breakthrough curve for each borehole. The breakthrough concentrations were normalized to the concentration of the injected tracer gas. The maximum relative concentration noted in the course of testing was 0.3. The observed data from each of the receiver holes are plotted in Appendix I.

The progressive grouting of the formation below the slab was expected to limit the larger pathways of gas transport first and, as the larger fractures had been filled and injection pressures were increased, then to limit the smaller pathways for gas transport. This limitation of pathways should manifest itself in the progressive lessening of the peak concentrations observed in the receiver holes, a lengthening of the time to peak concentration, and a lengthening of the period required to flush the tracer pulse from the formation. In general, this trend was observed during the implementation of SSSPT-F.

The tracer-gas breakthrough history of receiver hole L3209 is ideally behaved. The first grouting event conducted (borehole L3422) lengthened the time to peak concentration and the time required to flush the tracer-gas pulse from the formation during the February 5 test. The second grouting event (borehole L3418) lessened the peak concentration observed in the receiver hole during the February 9 test. The third grouting event (borehole L3424) had little or no apparent effect on the flow properties, as indicated by the breakthrough curve of the February 15 test and its similarity to the February 9 curve. The fourth grouting event (borehole L3420) was more effective at limiting the flow pathways between the injection borehole and this receiver hole than any previous events, as indicated by the lower peak concentration and longer time to flush the tracer pulse from the formation between these two boreholes. Similarly, the grouting of the next four grout-injection holes (L3421, L3423, L3419, and L3425) further limited the pathways, as did the final grout-injection sequence in the last eight of the sixteen grout-injection boreholes (L3530, L3526, L3431, L3527, L3532, L3528, L3533, and L3529).

The tracer-gas breakthrough history of receiver hole L3210 exhibits behavior similar to L3209 with two major differences. The primary difference is that the first grouting event was, by far, the most effective at limiting the flow pathways between the injection borehole and L3210. Successive grouting events, while producing some further effects, did not create as drastic a change in the nature of the curve. The second difference was an indication that the grouting of the last eight of the sixteen grout injection boreholes may have actually increased the pathways available for gas transport between the tracer-gas-injection borehole and L3210. This observed increase in the breakthrough of tracer gas, relative to the prior test, is present in the breakthrough histories of other receiver holes as well. This increase could result from the overall decrease in flow volume in the formation available in the system because of grouting, which resulted in a higher concentration and more rapid transport in the pathways left open to flow.

4.4 Interpretation Methodology

4.4.1 Well-Test Simulation Model

The gas-permeability test data were interpreted using the Graph Theoretic Field model (GTFM) of Pickens et al. (1987). GTFM allows complex pre-test borehole pressure history and boundary conditions to be incorporated into the solution. Details on GTFM assumptions and properties used in the analysis of gas-flow data are found in Appendix J.

4.4.2 Gas-Permeability Testing Analysis Procedures

A consistent set of analysis procedures was followed for each of the gas-permeability tests performed for the Room L3 boreholes. The calculated gas-injection flow rate and the observed test-zone pressure values for each time step were input into GTFM as data against which to check the simulation. The time when the interpretation simulation started usually coincided with the start of data collection. However, in a few cases the start of data collection did not coincide with the start of the test; thus the tests were all scaled in time so that a time of zero seconds corresponded with the actual start of the gas-permeability test.

An option within GTFM allows for the generation of history curves that represent curve fits through a set of data points (e.g., pressure or flow rate) that vary in time. In each simulation, a history curve of the gas-injection flow rate into the borehole was generated. The use of this history

curve in the GTFM simulation forces a transient gas-injection flow rate boundary condition within the wellbore. The history curve was specified only during the gas-injection portion of the test.

The specification of consecutive test sequences within GTFM consisted of a flow period followed by a pulse period. The flow period was specified during the gas-injection portion of the test. The pulse period was specified during the pressure-recovery portion. During the flow period, the gas-injection-flow rate was specified within the wellbore, and the resulting pressure distributions generated within the wellbore and formation were calculated. When the gas-injection portion of the test was terminated, the specified boundary condition within the wellbore was removed and the pressure recovery within the wellbore and the formation was calculated.

After the check data were entered and the history-curve files were generated, the borehole configuration parameters, formation hydraulic parameters, injection-gas parameters, and model-grid parameters were input to the model. The borehole configuration parameters consisted of the borehole radius and the length of the testing interval. A borehole radius of 7.62 cm was specified for each test analysis. The test-zone length was borehole-specific, with the range of lengths varying from 229 to 267 cm. The formation hydraulic parameters used as input were the formation permeability to gas, formation porosity, and formation-gas pressure. The formation-gas pressure was specified at 0.0 MPa for each test analysis. The formation gas-permeability and porosity were the two principal fitting parameters used in the analyses. The values for formation gas-permeability and porosity ranged over several orders of magnitude and were dependent on the sequencing and proximity of the individual boreholes to the grout-injection experiments and the location of the borehole within the room. The gas viscosity and reference temperature and pressure for the injected gas were maintained consistent and constant for each test analysis at 1.8×10^{-5} Pa·s, 27°C, and 0.09 MPa, respectively. The model grid parameters consisted of the location of the outer radial constant-pressure boundary and the number of radial grid blocks in the system. These parameters were held constant for each test analysis at 1000 m and 100, respectively.

The use of GTFM in the testing analysis provided for a flexible tool to capture occurrences within the entire testing system. The majority of the simulation results consisted of linear-linear plots of gas-injection, flow-rate, and wellbore-pressure within the borehole versus time. These curves showed the comparison of the observed data and the GTFM simulation results. Another generated result was pressure-profile curves. These curves showed the pressure distribution generated within the formation during the simulation. Curves of pressure versus radial distance from the wellbore at

various times during the simulation provided the distance to the radius of influence and thus aided in determining the location of the outer radial constant-pressure boundary.

4.4.3 Individual Test Interpretations

Appendix I describes the sequence of gas-permeability testing that occurred in each of the boreholes in Room L3. Each of these tests was interpreted using GTFM and the interpretation procedures described in Appendix J. The significant interpretation parameters for each gas-permeability test are formation gas-permeability, formation porosity, and test-zone volume modification. In some cases, the test-zone volume modification parameter was necessary to add or subtract volume from the test zone in order to better characterize the borehole storage effects and initial borehole pressure buildup. This modification was almost always limited to the tests conducted in a region at the lower end of the gas-permeability range. Each gas-permeability test interpretation versus the observed data is plotted in Appendix I.

Section 4.3.2 described the borehole pressure response for four of the gas-permeability tests conducted in Room L3. Only these four interpretations will be discussed in detail. The remaining test interpretations can be categorized into one of these four response groups.

The gas-permeability test conducted in borehole L3X10 during the third round of testing is the example interpretation for the no-rise pressure response category. The interpretations for the no-rise response group were the most difficult to use for obtaining an estimate of the significant parameters. The permeability estimates for these tests could have an uncertainty range over several orders of magnitude because of the unstable pressure conditions within the wellbore during testing. These unstable conditions result from the ability of the formation to rapidly move the gas away from the borehole, which stresses the upper limits of the gas delivery system. The system could not deliver the injectate gas at an adequate rate to pressurize the borehole. The gas-permeability estimates for the no-rise response group were usually set at $1 \times 10^{-12} \text{ m}^2$.

Results of the gas-permeability test conducted in borehole L3215 during the first round of testing are consistent with the gas-permeability tests conducted in the slow-rise response group. The estimate of the gas permeability for borehole L3215 was $6 \times 10^{-14} \text{ m}^2$. This value falls within the range of gas permeabilities estimated for this group, which range from 1×10^{-13} to $1 \times 10^{-15} \text{ m}^2$. A formation porosity of 0.005 was estimated. This very low porosity value is assumed to be the fracture porosity within

the region surrounding the borehole, with most of the gas flow occurring within the local fractures. The formation porosity estimated for all gas-permeability tests ranged from 0.015 to 0.001 with a value of 0.005 being the most common fitted value.

The interpretation of the gas-permeability test conducted in borehole L3202 during the second round of testing is typical of the continuous-rise response group. The range of gas permeabilities estimated for this group varies from 1×10^{-14} to $1 \times 10^{-17} \text{ m}^2$ with an estimate of $3 \times 10^{-16} \text{ m}^2$ for the test conducted in borehole L3202. This range of gas permeabilities was sufficiently low to allow for significant pressure buildup within the borehole and sufficiently high to allow for significant borehole pressure falloff to occur within the testing period.

The interpretation of the gas-permeability test conducted in borehole L3212 during the third round of testing is consistent with those of the rise-and-fall group. The rise-and-fall response is characterized by a very fast pressurization of the borehole and a very slow dissipation rate of the borehole pressure. The gas permeability estimate for the simulation of L3212 was $4 \times 10^{-17} \text{ m}^2$, which is within the 1×10^{-17} to $1 \times 10^{-18} \text{ m}^2$ range estimated for the rise-and-fall response group. This range of gas permeabilities is the lowest estimated for all the tests conducted in Room L3. As the gas permeability in the formation is lowered, the rate of pressure buildup in the borehole increases, but the rate of pressure dissipation out of the borehole into the formation decreases significantly. The volume of the test zone was decreased by 0.011 m^3 to obtain a better match to the initial pressurization of the borehole. This volume reduction is approximately 24% of the actual test-zone volume and was necessary on several of the tests conducted in the very low permeability range.

The four interpretations of the gas-permeability tests demonstrate the basic behavior of the suite of gas-permeability tests conducted in Room L3. The gas-permeability estimates ranged from 1×10^{-12} to $1 \times 10^{-18} \text{ m}^2$, spanning six orders of magnitude. As the estimate of the gas permeability increased, the borehole pressure response changed from that of a quickly pressurized borehole with low flow into the formation into that of a borehole that could not hold pressure because of high flow into the formation.

4.4.4 Sensitivity Analyses

4.4.4.1 BOUNDARY EFFECTS

The proximity of a borehole to the ribs and centerline of Room L3 has a distinct controlling factor on the estimated gas permeability in the vicinity of the borehole. The relationship is shown in contour maps of the gas permeability distribution in Room L3 before and after grouting, which are presented in Section 5.1. The gas permeability distribution is such that higher permeabilities exist along the centerline of the room and decrease by up to six orders of magnitude towards the ribs. This distribution results from the stress loading of the floor, which causes the floor to rise in elevation in an attempt to seal the open excavation. This process of sealing has led to high permeabilities in the center of the room. As the floor rises, fractures and layer separation are generated within the formation and along the formation bedding planes. This behavior is similar to behavior exhibited in the back of other WIPP excavations. Stensrud et al. (1992) present results from brine-permeability testing (sequence S1P73-A) performed in the back, close to the centerline of Waste Panel 1, Room 7. Brine was injected into a packer-sealed borehole that intersected anhydrites "b" and "c." The pressure within the borehole did not build, and brine was observed flowing from roof-bolt holes approximately 1 m away. Stensrud et al. concluded that separation between the anhydrite layers and the halite was allowing a free-flow path for the brine to travel through the formation and down the roof-bolt drill holes. The contour maps in Section 5.1 show that the gas-permeability in Room L3 decreases from the center of the room towards the side ribs and back rib. Under the ribs the formation is closer to in-situ conditions; therefore little separation from stress redistribution is occurring. For the boreholes close to the rib, the gas injected during the gas-permeability testing most likely traveled into and parallel to the center of the room and towards the N1420 drift. These travel paths would be the paths of least resistance, away from the ribs.

The two grouting events in Room L3 had an effect on the gas-permeability values estimated for the region surrounding most of the boreholes. As the grouting experiments progressed, a grout curtain was developed around the central gas-injection borehole. The contour plots in Appendix I show that the estimated gas permeability in the region surrounding the central gas-injection borehole dropped by three orders of magnitude. This decrease is caused by the grout effectively sealing the formation surrounding the grouting boreholes and essentially creating a no-flow boundary between the grouting boreholes and the central gas-injection borehole. This is also evidenced by the decrease in the gas-permeability estimates for the boreholes between the ribs and the central gas-injection borehole. As the grout curtain developed, the pathways of least resistance to flow within the room

(towards the center of the room) were sealed by the grouting experiment, resulting in a lower estimate of gas permeability in those regions. The area along the centerline of the room and closest to the N1420 drift was least affected by the grouting curtain because the grout curtain was closer to the back rib than the boreholes; sufficient permeability existed between the boreholes and the drift to allow for the high flow rates (and thus high gas permeabilities) observed. These boreholes exhibited the characteristics of the no-rise response during all three gas-permeability testing sequences.

4.4.4.2 PERMEABILITY

The estimates for gas-permeability in the northern end of Room L3 ranged over six orders of magnitude. Four characteristic wellbore pressure responses to the gas-permeability testing were observed. These responses were discussed in Section 4.3.2. Each gas-permeability interpretation was performed and a single value was estimated for the gas permeability in the region surrounding the borehole.

Plots of the four example responses, where the estimated gas-permeability has been increased and decreased by one order of magnitude about the best-fit permeability value, are presented in Figures 4-6 through 4-9. The additional GTFM simulations show that a significant change in the borehole pressure response is generated by changing the estimate of the gas permeability by one order of magnitude. These plots show that the results from the gas-permeability tests provided good order-of-magnitude estimates of the gas permeability and the changes in gas permeability with time.

4.4.4.3 TEST-ZONE VOLUME

The borehole volume of the isolated test zone was calculated based on the placement of the packer that isolated the test interval with respect to the bottom of the borehole. The volume of the test tool below that packer assembly was assumed to be insignificant to the testing interpretations. The test-zone volume varied slightly between each test because of variations in the total depth of the borehole and the location of the anhydrite unit. Assuming average parameters of a 7.62-cm borehole radius and a 2.48-m test-zone length, a typical test-zone volume of 0.045 m³ is obtained. In some of the gas-permeability testing analyses, the volume of the test zone was modified to obtain a better fit to the early-time borehole pressure response. This modification decreased the test-zone volume used in the pressure response simulation. By decreasing the test-zone volume, the rate of pressure increase within the borehole is increased because of the smaller

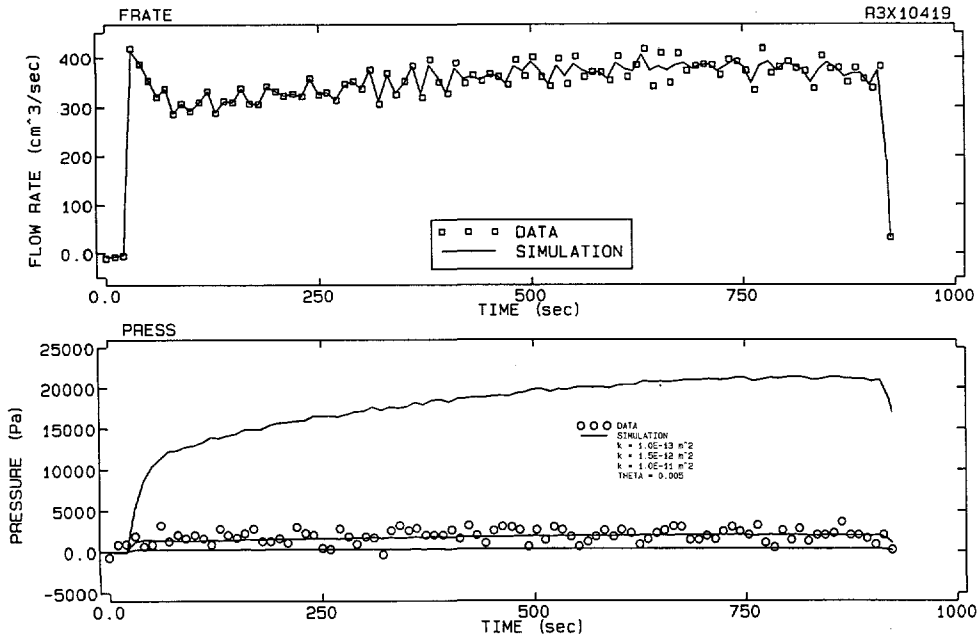


Figure 4-6. Permeability sensitivity analysis for gas-permeability testing of borehole L3X10 on April 10, 1993.

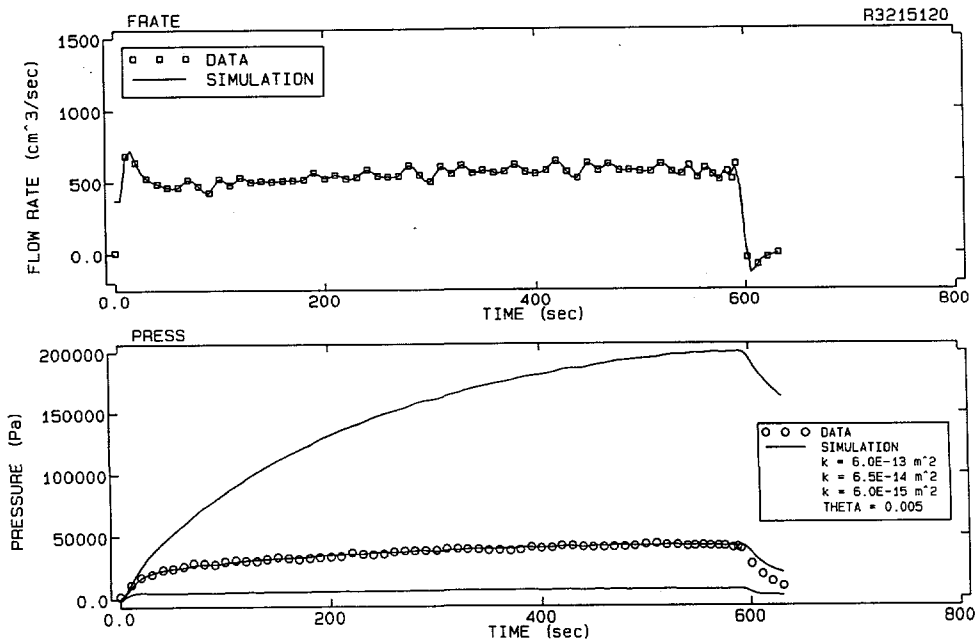


Figure 4-7. Permeability sensitivity analysis for gas-permeability testing of borehole L3215 on January 20, 1993.

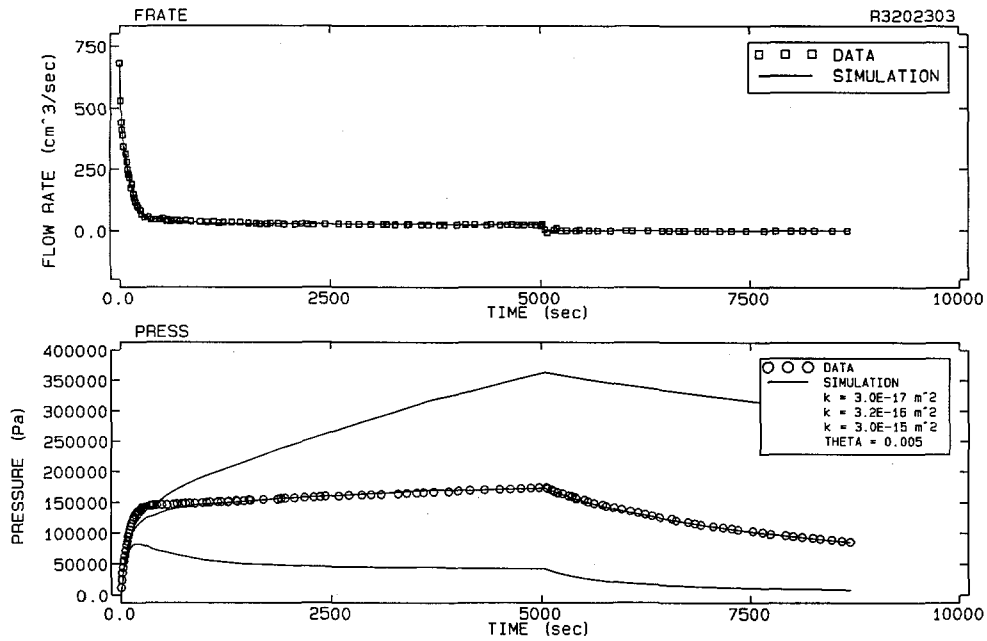


Figure 4-8. Permeability sensitivity analysis for gas-permeability testing of borehole L3202 on March 3, 1993.

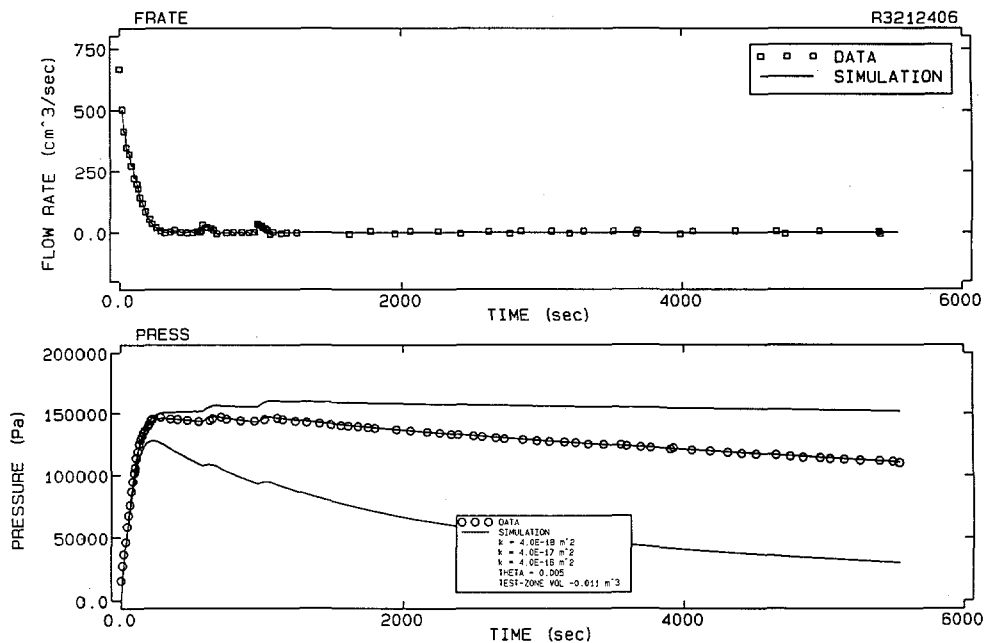


Figure 4-9. Permeability sensitivity analysis for gas-permeability testing of borehole L3212 on April 6, 1993.

storage effects. As the test-zone volume decreases, the necessary amount of gas injected into the test zone to overcome the storage effects decreases, resulting in an increased rate of pressurization.

Of the four example test responses discussed, only one had a modified test-zone volume in the best-fit simulation (L3212). The test-zone volume of the other three simulations were not modified. As the estimated gas permeability decreases, the impact of modifying the test-zone volume increases. Figures 4-10 through 4-13 present plots demonstrating the effect of modifying the test-zone volume on the pressure response. For the no-rise response, there is no sensitivity of the simulation results to the change in test-zone volume. However, the rise-and-fall response shows the most sensitivity to a change in test-zone volume. For the low permeability case, the rate of pressure dissipation into the formation decreases, thereby increasing the wellbore storage effects on the test interpretation. In order to accurately incorporate the effects of wellbore storage, the test-zone volume was modified to match the observed pressure buildup. In the gas-permeability test interpretations in which the test-zone volume was modified, the test-zone volume was decreased and the majority of the estimated gas-permeability values ranged between 1×10^{-16} and 1×10^{-17} m².

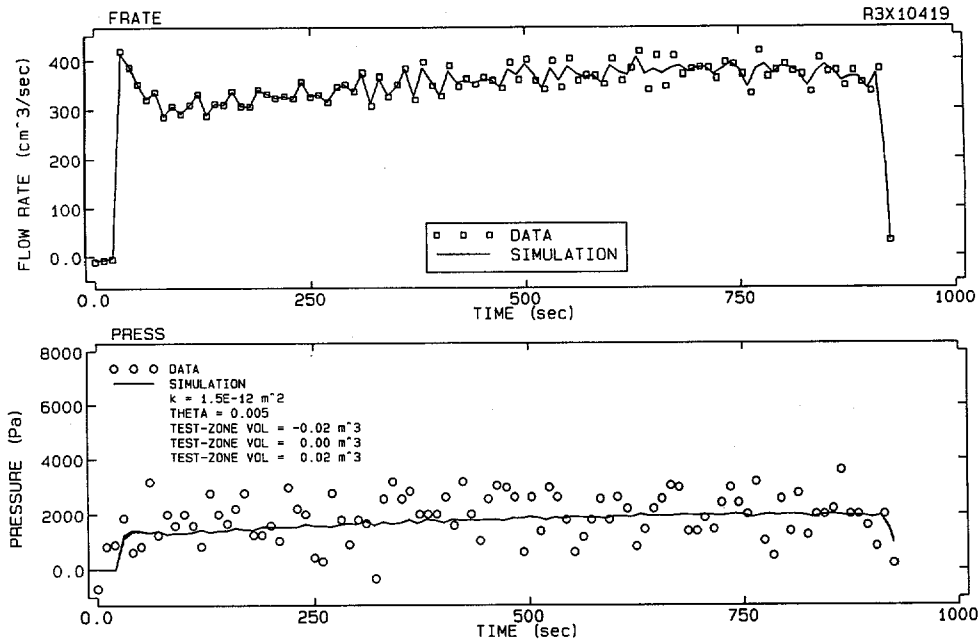


Figure 4-10. Test-zone volume sensitivity analysis for gas-permeability testing of borehole L3X10 on April 10, 1993.

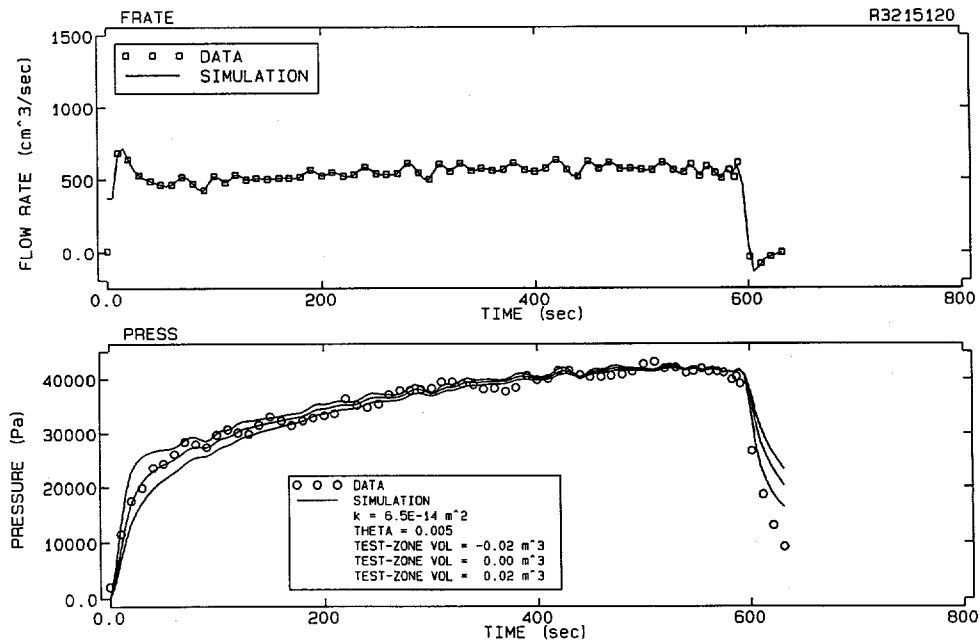


Figure 4-11. Test-zone volume sensitivity analysis for gas-permeability testing of borehole L3215 on January 20, 1993.

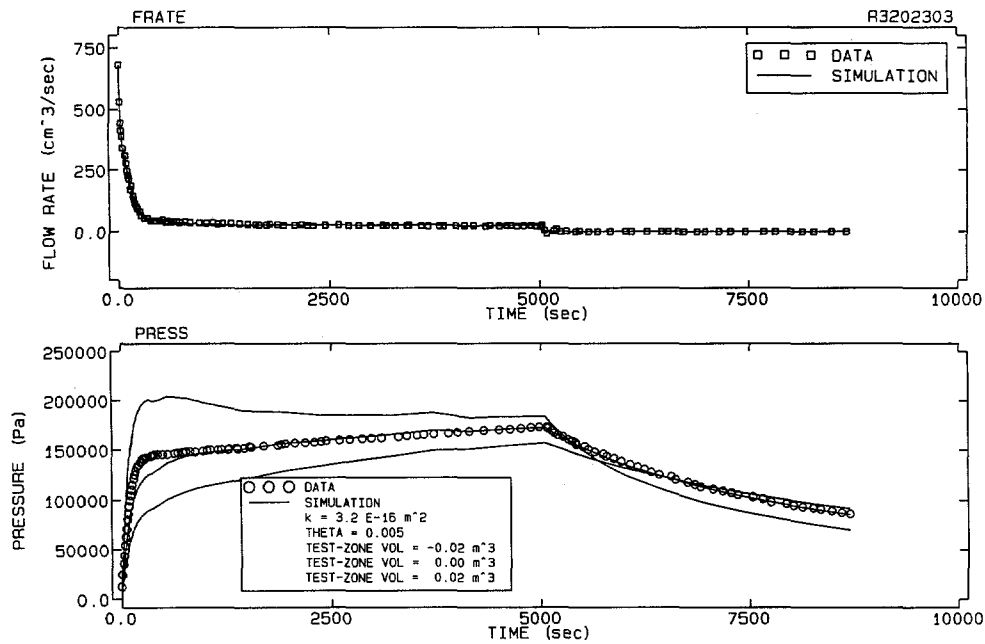


Figure 4-12. Test-zone volume sensitivity analysis for gas-permeability testing of borehole L3202 on March 3, 1993.

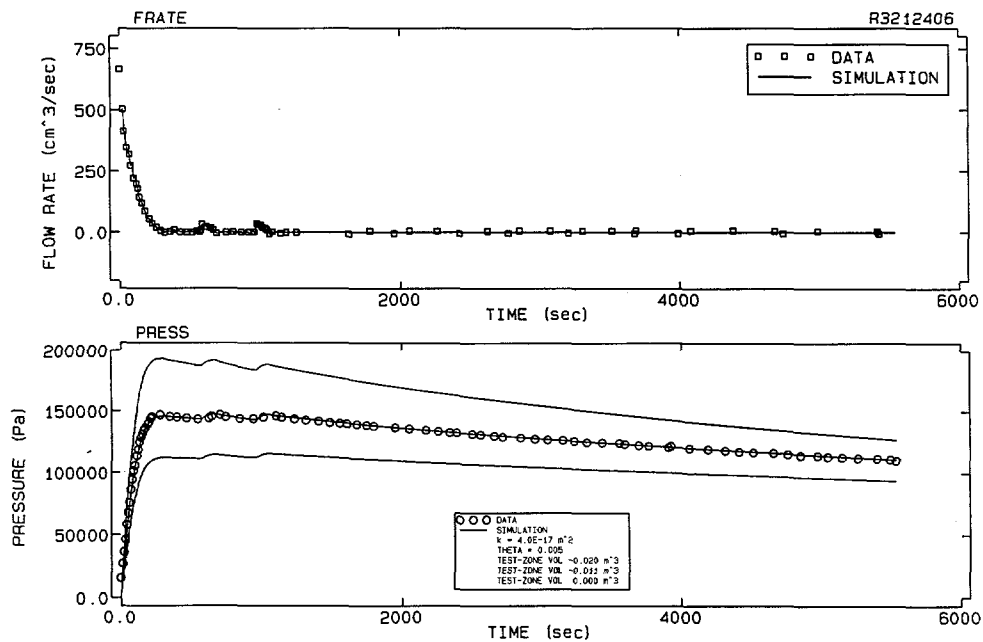


Figure 4-13. Test-zone volume sensitivity analysis for gas-permeability testing of borehole L3212 on April 6, 1993.

5.0 SUMMARY AND CONCLUSIONS

5.1 Results

The ability to practically and consistently produce ultrafine cementitious grout at the grouting site was demonstrated in SSSPT by the success of 18 separate grouting events. Consistency is evidenced by the less than one micron variation in particle size throughout, as shown in Table 3-3.

Consistent and efficient permeation of ultrafine cementitious grout into fractured rock at the WIPP repository horizon was indicated by observations of the grout in post-grout diamond drill cores. Each grout injection hole utilized a different color of grout, which enabled an approximation of permeation distance achieved. Additionally, each post-grout hole was scanned with the down-the-hole televiewer. This system, which utilizes a high-resolution camera and monitor, clearly shows the various colors of grout in the holes.

Effective permeation and sealing of microfractures was verified by the following observation methods:

- down-the-hole televiewer,
- megascopic (hand lens) observation,
- optical microscopy,
- scanning electron microscopy (SEM) in conjunction with energy dispersive x-ray (EDX). EDX was used to verify that the material sealing the fracture was grout. The EDX technique produces a qualitative spectral graph in which a high peak for silica and calcium verifies that the examined material is grout.

To perform the SEM/EDX procedure, the eight samples that appeared to have the smallest grouted fractures were selected by a combination of megascopic and optical examinations. These samples were then examined under the SEM with the assistance of EDX. The examination revealed that fractures with an aperture of 10 or more microns were routinely penetrated and sealed by grout. In one rare instance, a fracture 3 microns in width was completely filled by the smaller particles in the grout (3 microns equal approximately 1/1000th of 1/8 inch).

Procedures and equipment used to inject ultrafine cementitious grout were thoroughly evaluated by use. Very little modification of equipment and procedures was required. Minor departures from the Standard Operating Procedure (Ahrens, 1992a) are described in Section 3.0.

Gas-flow/tracer equipment, specially designed and constructed for this test, permitted near "real time" determination of gas transmissivity and the

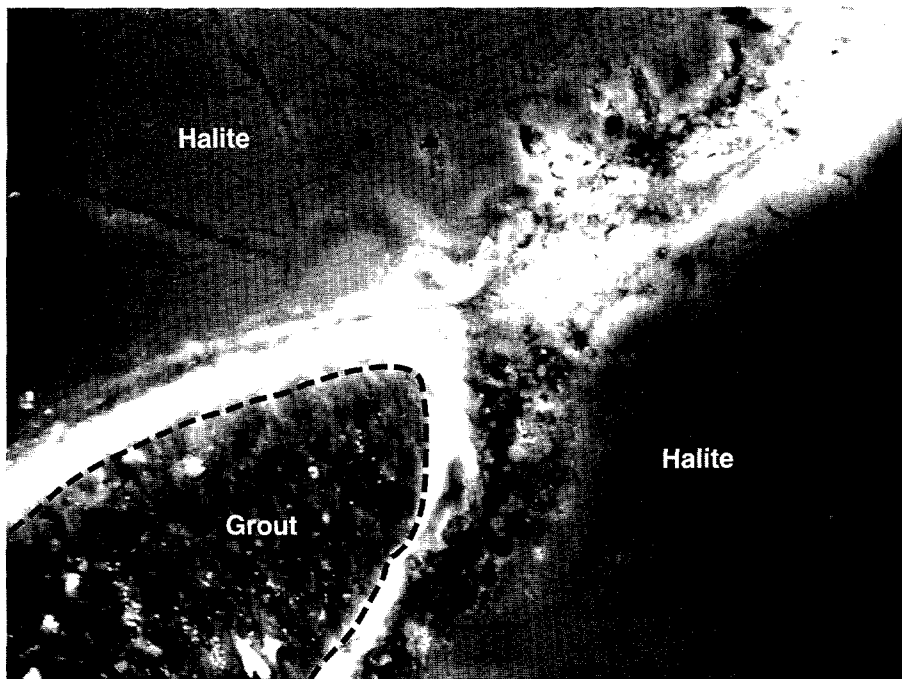
changes therein caused by grouting. This system shows promise as a technique for discerning preferential flow paths in the DRZ around seals and for determining the reduction of gas transmissivity achieved by the injection of ultrafine grout. Pre- and post-grout diamond drill core was extremely useful: it provided test specimens for optical and SEM/EDX examination as well as ongoing laboratory evaluation of grouting and sealing effectiveness and grout degradation and compatibility. An excellent visual verification of grouting permeation was provided by pre- and post-grout downhole inspection utilizing a high-resolution televiewer in conjunction with a recorded voice commentary. Proper viewing of the tapes requires the use of a high-resolution color video monitor.

Slab displacement measurements, provided by the eight rod extensometers, were useful in affording some control over the injection pressures used. Additionally, they indicated that deformation in response to stress redistribution continued unabated throughout the experiment. Two disadvantages of the test were:

- The slab/floor jack combination did not allow the use of higher injection pressures, which would have resulted in greater grouting effectiveness. This factor was recognized prior to the test; however, because it was thought the test objectives could be met with this system, the additional costs were not thought warranted.
- The wet pulverization/mixing procedure that was used limits the volume of grout available for injection. Although volume was not a problem with this experiment, the mill cost and limited volume would severely limit commercial use. Efforts to achieve cost-effective dry pulverization will be continued. Success could result in a process that would enable the production of bagged grout, which could impact the market.

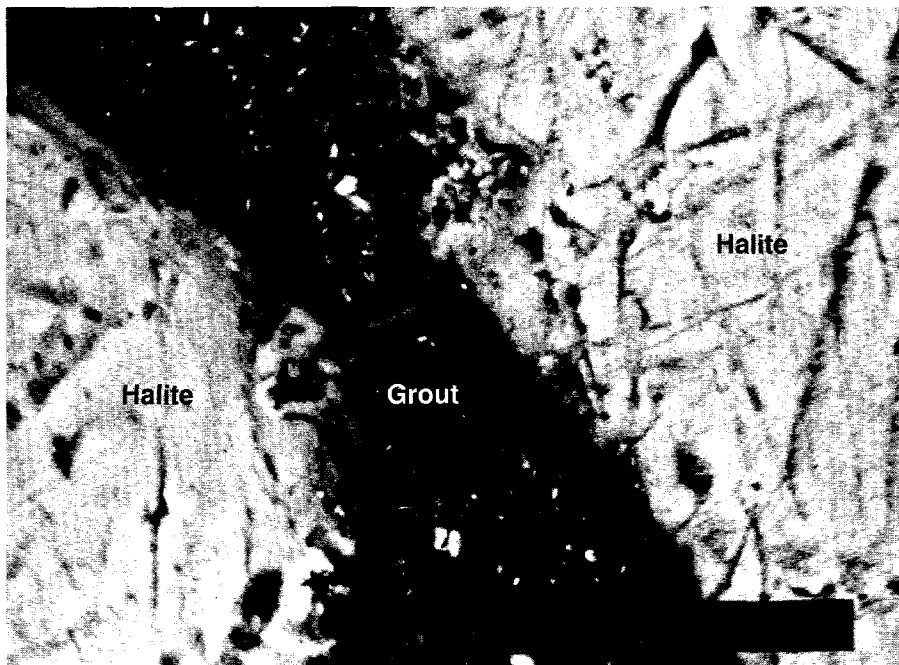
The grouting results can be seen in Photos 5-1 through 5-4, which are scanning electron microphotographs showing fracture widths from 3 to 10 microns completely filled with grout. The graphical scale bar on each photo varies in length with the magnification. Bar length in microns is denoted by the number at the lower left of the scale.

Photo 5-4 shows a 3-micron microfracture in hole L3X43, at a depth of 3.61 m, filled with grout injected through hole L3421. The accompanying spectral analysis graph (Figure 5-1, following page), made with the EDX, confirms that the material filling the fracture is grout. Similar graphs were obtained for all SEM specimens shown. Additional information on grout distribution is presented in Appendix H.



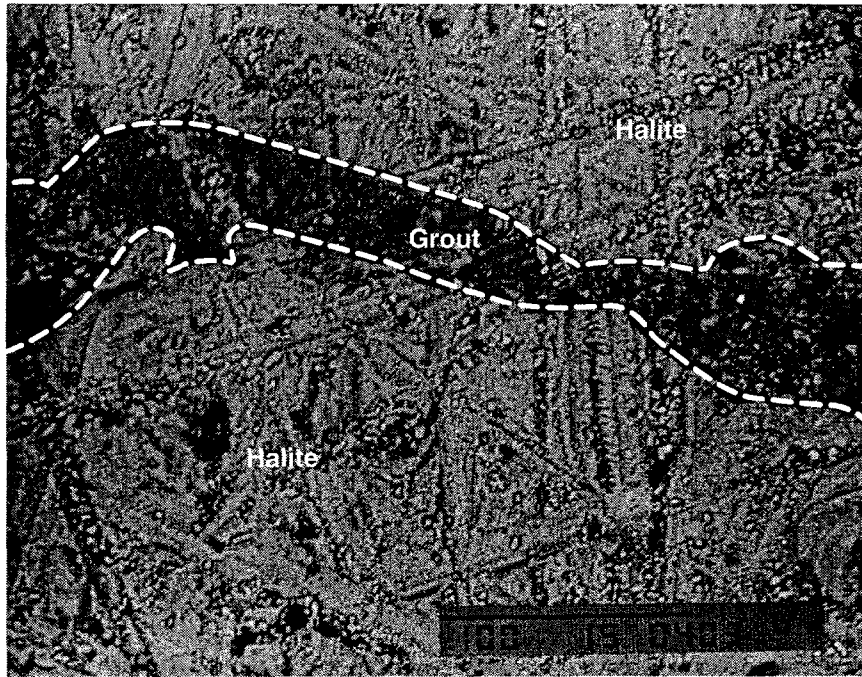
1890-2

Photo 5-1. Electron microphotograph showing grout "pinch out" at ± 10 microns.



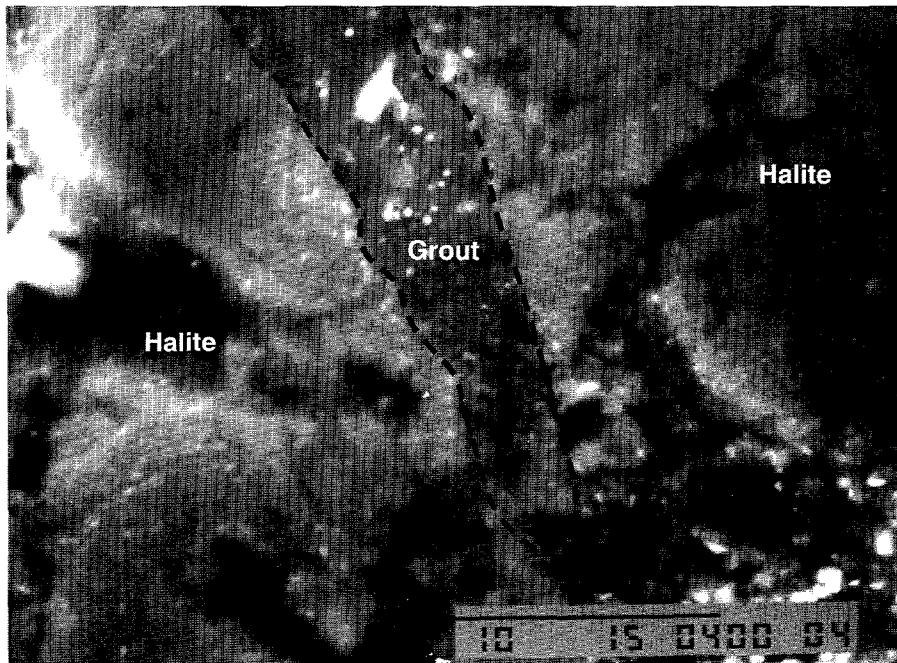
1889-2

Photo 5-2. Electron microphotograph showing grout passing through a 7.9 micron constriction.



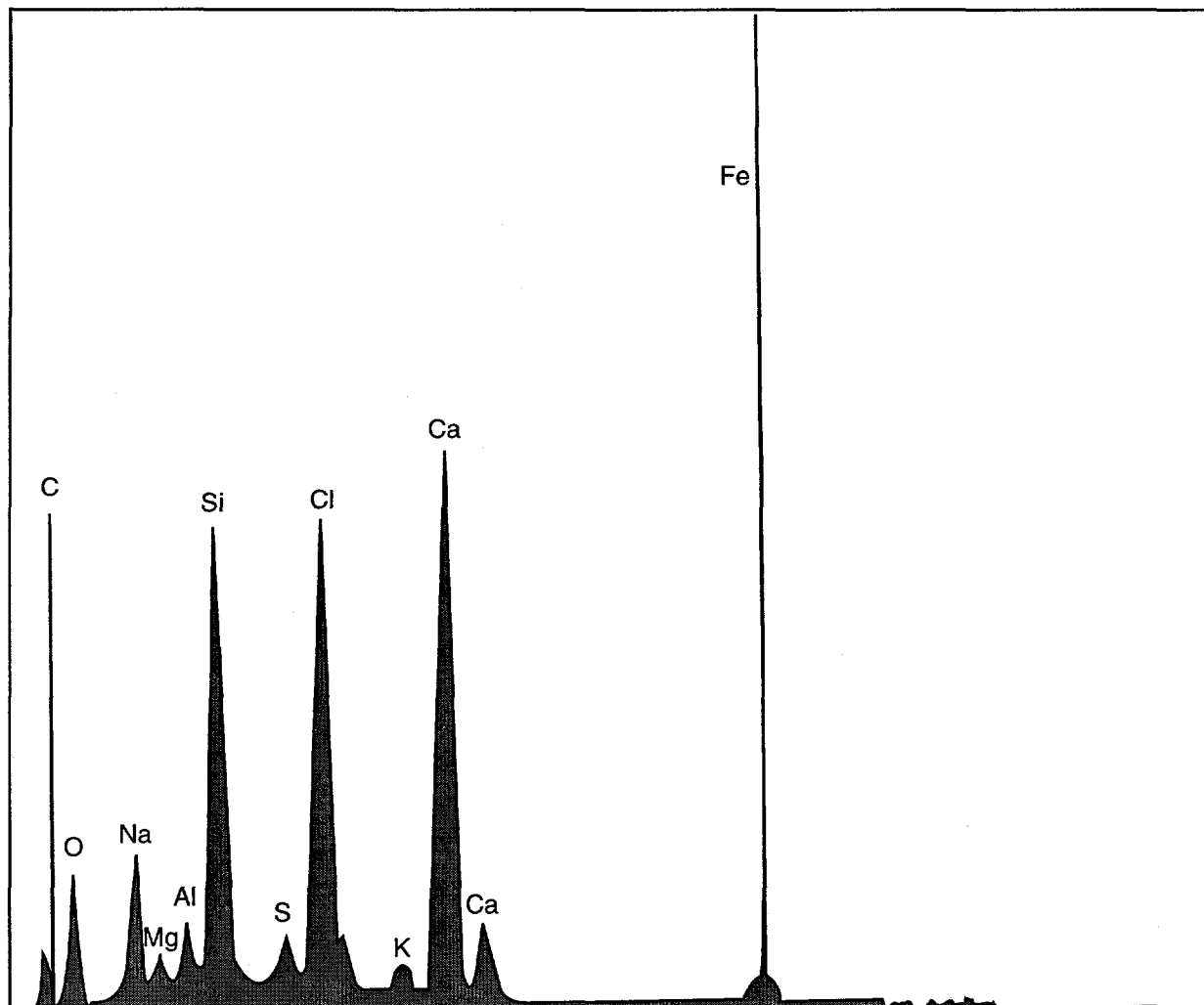
TRI-6121-310-0

Photo 5-3. Electron microphotograph showing a grout-filled fracture 6 microns wide.



1891-2

Photo 5-4. Electron microphotograph showing a grout-filled fracture 3 microns wide.



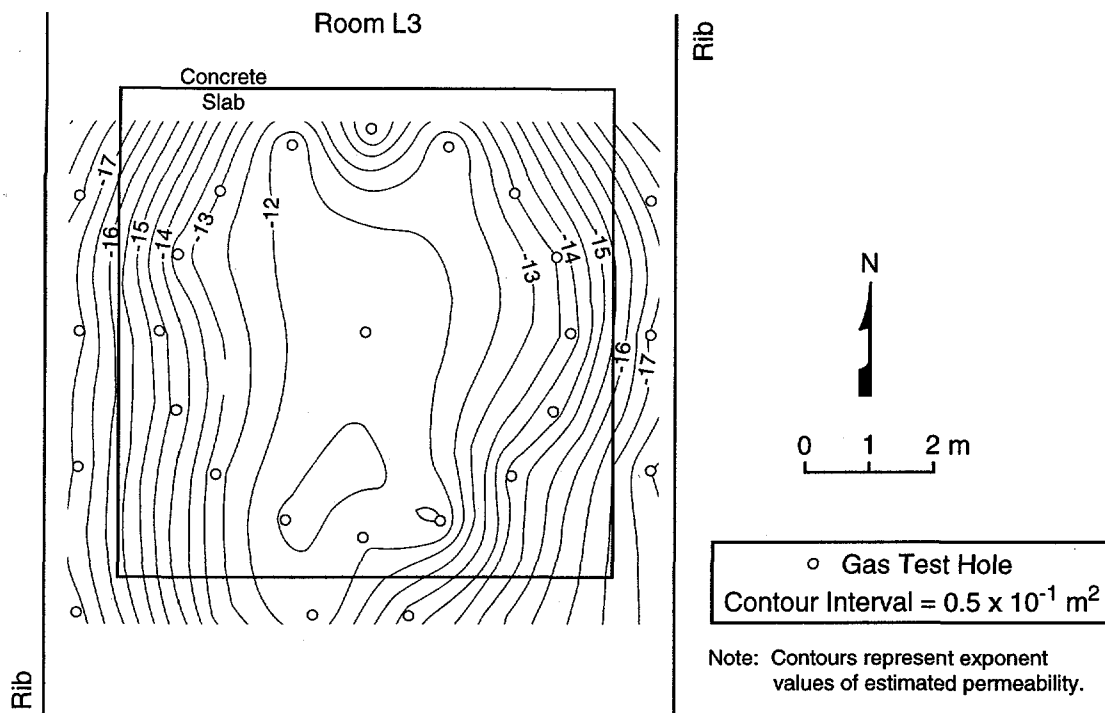
TRI-6121-205-0

Figure 5-1. Qualitative spectral peaks produced by energy dispersive x-ray, verifying that material in fracture is grout.

Results from formation permeability tests are represented in Figures 5-2 through 5-5, which are plan views of Room L3 with permeability contours superimposed on the slab region. Data used to generate these figures are from the derived permeability tables (m^2) in Appendix I. The contours in Figure 5-2 represent pre-grout permeability. Only the holes used for data collection are indicated in the figure. The contours reveal that, before grouting, a north-south-trending zone of higher permeability existed in MB139 along the room centerline, with permeability decreasing towards the sides of the room. The north-south-trending zone exhibited a permeability of $1 \times 10^{-13} m^2$, whereas the permeability of the formation near the sides of the room measured $1 \times 10^{-16} m^2$.

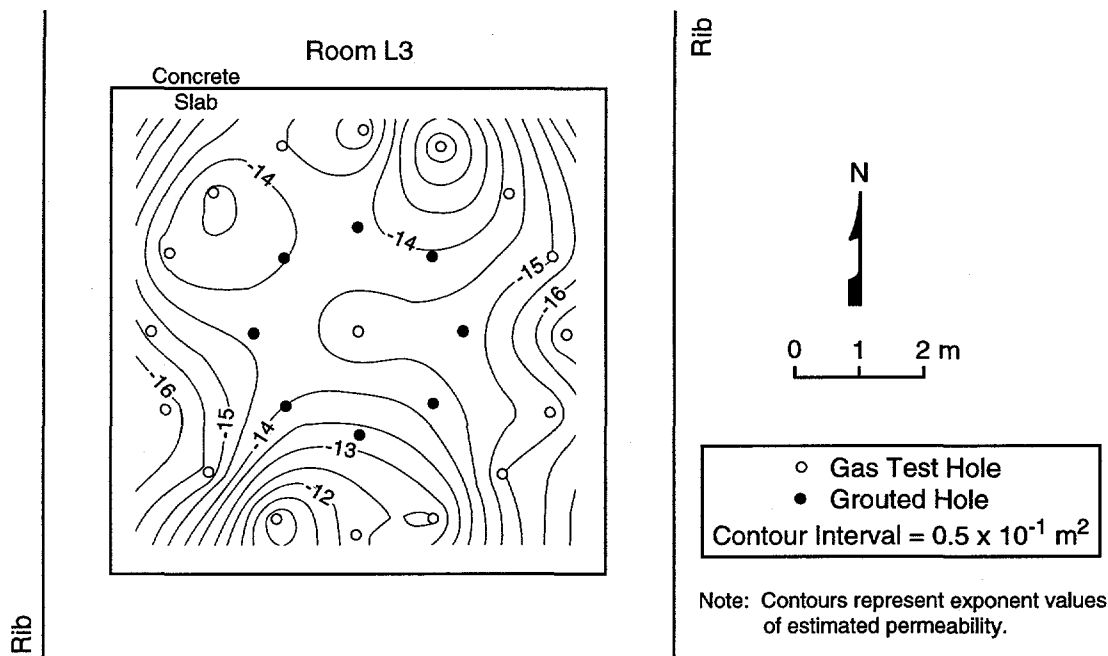
Figure 5-3 shows log permeability contours derived from March 1993 test data, after grouting of the primary holes. Only the on-slab holes were tested in March. Figure 5-4 shows both off-slab and on-slab gas-flow test data from April 1993. Note that the locations of the grout holes are also shown on these figures. When Figure 5-2 is compared to Figures 5-3 and 5-4, it is evident that the area delineated by the 10^{-13} contour is significantly reduced and that the exponent values listed as contours are becoming more negative, indicating a reduction in permeability. Figure 5-3 shows that most of this reduction was achieved by the primary grouting. Figure 5-4 shows that after the secondary grouting only a small area of the slab along the southern edge showed permeability greater than 10^{-13} .

Figure 5-5 shows the order-of-magnitude decrease in permeability between the pre-grout and post-secondary-grout gas-flow tests. Only the holes tested in both investigations are compared. Figure 5-5 shows that most of MB139 under the slab experienced a permeability reduction at least 2 orders of magnitude and that about one-quarter of the tested zone experienced a 3 order-of-magnitude decrease in permeability after grouting.



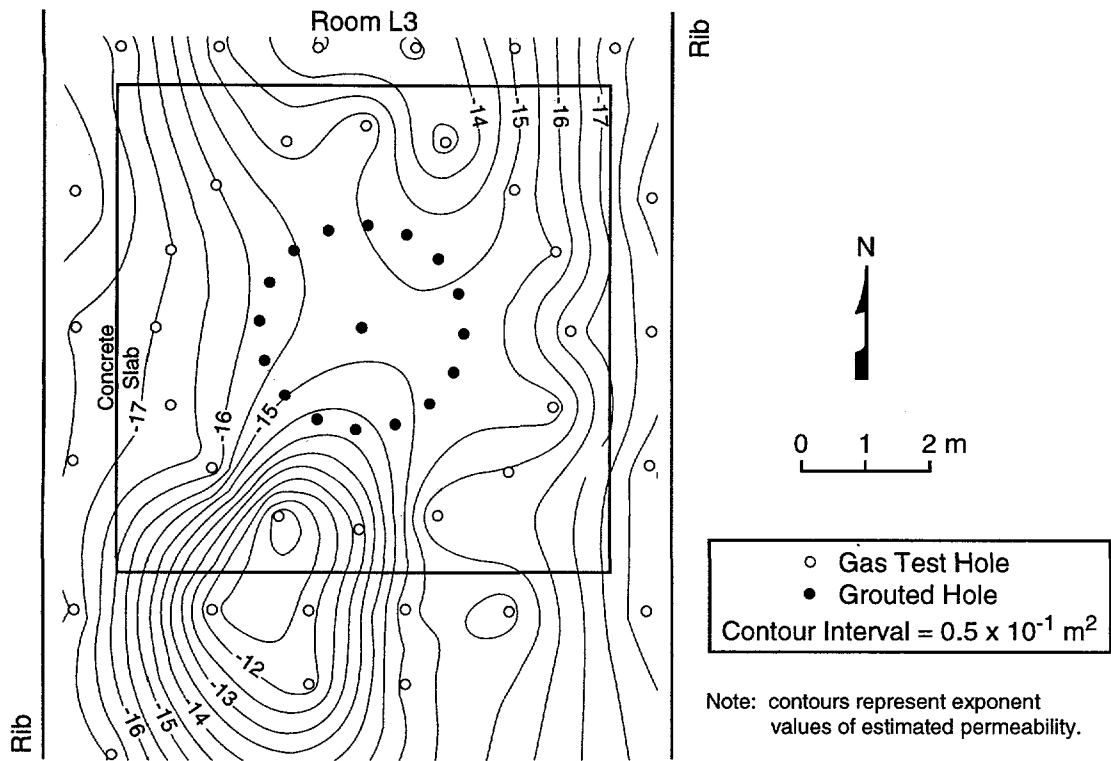
TRI-6121-317-0

Figure 5-2. Log permeability contours derived from pre-grout (January 1993) gas-flow tests.



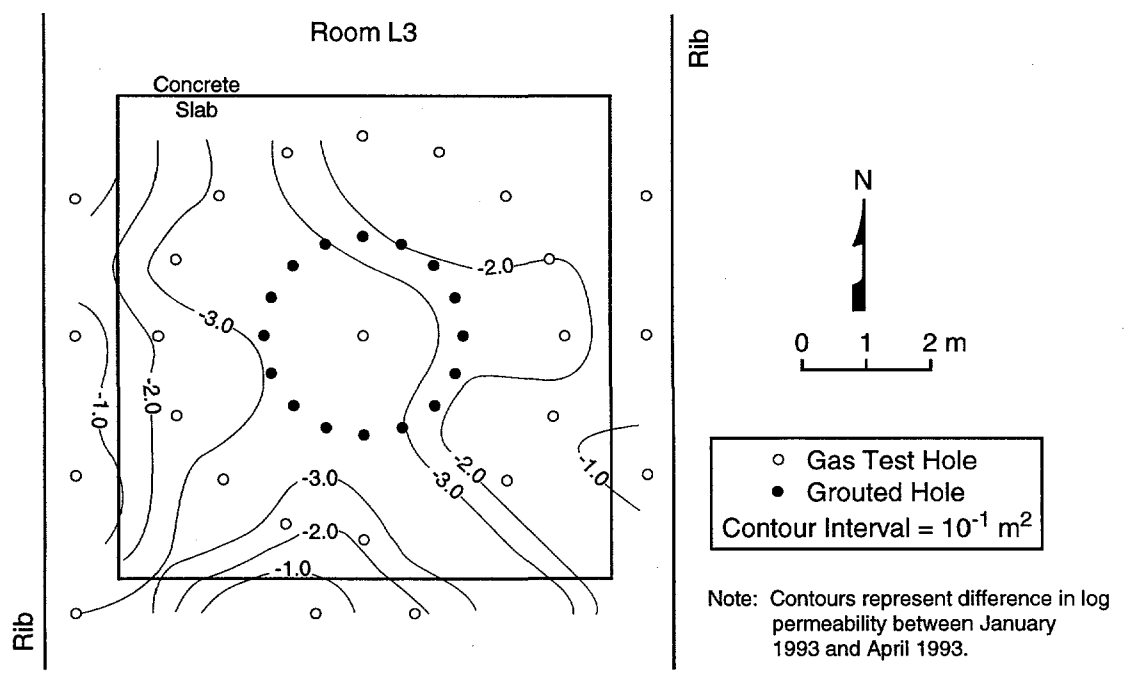
TRI-6121-318-0

Figure 5-3. Log permeability contours derived from post-primary grout (March 1993) gas-flow tests.



TRI-6121-319-0

Figure 5-4. Log permeability contours derived from post-secondary grout (April 1993) gas-flow tests.



TRI-6121-209-0

Figure 5-5. Order-of-magnitude change in permeability achieved by grouting.

5.2 Conclusions and Recommendations

5.2.1 Conclusions

- The ability to practically and consistently produce ultrafine cementitious grout at the grouting site was demonstrated.
- Injection and permeation of ultrafine cementitious grout into fractured rock at the WIPP repository horizon was accomplished consistently and efficiently.
- Data were obtained on the ability of ultrafine cementitious grout to penetrate and seal microfractures. Ten-micron fractures were routinely sealed and, in one instance, a 3-micron fracture was successfully grouted.
- Procedures and equipment used to inject ultrafine cementitious grout into fractured WIPP rock were evaluated and found acceptable.
- Techniques to assess the effectiveness of ultrafine cementitious grout in reducing the permeability of fractured WIPP rock were evaluated. These include gas-flow/tracer testing, post-grout coring, pre- and post-grout downhole televiwer logging, slab displacement measurements, and increased loading on jacks during injection.
- Pre- and post-grout diamond drill core was obtained for use in ongoing laboratory evaluations of grouting effectiveness, degradation, and compatibility.

5.2.2 Suggestions for Future Work

Simultaneously pulverizing and mixing the grout wet at the grouting site as needed is possible, but it has the following limitations:

1. Volume is limited to approximately 102 liters every three hours.
2. An expensive pulverization mill (Szegvari or acceptable alternate) must be used.

Dry pulverization, resulting in a bagged product ready to mix, is required by the grouting industry. Problems that SNL encountered in dry pulverization were solved subsequent to the SSSPT-F experiment. Dry pulverization in conjunction with air classification can produce a bagged ultrafine cementitious grout with 90% of the particles smaller than 5 microns. Theoretically, this grout will penetrate smaller openings than the grout used in SSSPT-F.

Because the surface area of cement is much greater at the 5 micron size, the water/cement ratio and the weight percent of superplasticizer used in the Type K grout (used in SSSPT-F) must be adjusted slightly. This will

necessitate additional laboratory work. Additionally, the physical parameters must be redetermined.

If additional field testing is to be done, SNL should purchase a 0.12 m³ Colcrete "colloidal" grout mixer (or acceptable alternative). This, in conjunction with dry pulverization and bagging, will facilitate the use of ultrafine grout and simultaneously permit large-volume grouting using standard, less costly grout, which is suitable for sealing large voids. Because tests to date indicate that the dry pulverized grout can be produced at a competitive price, it will have an impact on the market. SNL should attempt to transfer this technology to private industry.

A non-coring version of the reverse-circulation diamond drill equipment has been invented (SNL is seeking a patent) but not constructed. This equipment will be used in the production drilling of grout injection holes that may be required around WIPP seals. Construction and evaluation of this equipment is recommended.

6.0 REFERENCES

- Ahrens, E.H. 1992a. "Activity Specific ES&H Standard Operating Procedure for Test Plan 'Sealing of the Disturbed Rock Zone (DRZ), Including Marker Bed 139 (MB139) and the Overlying Halite, Below the Repository Horizon, at the WIPP'." WP472218. Albuquerque, NM: Sandia National Laboratories. (Copy on file at the Sandia WIPP Central Files, Sandia National Laboratories, Albuquerque, NM.)
- Ahrens, E.H. 1992b. "Test Plan: Sealing of the Disturbed Rock Zone (DRZ), Including Marker Bed 139 (MB139) and the Overlying Halite, Below the Repository Horizon, at the Waste Isolation Pilot Plant: Small-Scale Seal Performance Test-Series F." WP07843. Albuquerque, NM: Sandia National Laboratories. (Copy on file at the Sandia WIPP Central Files, Sandia National Laboratories, Albuquerque, NM.)
- Baker, W.H., ed. 1982. *Grouting in Geotechnical Engineering*. New York, NY: American Society of Civil Engineers.
- Borns, D.J. 1985. *Marker Bed 139: A Study of Drillcore From a Systematic Array*. SAND85-0023. Albuquerque, NM: Sandia National Laboratories.
- Borns, D.J., and J.C. Stormont. 1988. *An Interim Report on Excavation Effect Studies at the Waste Isolation Pilot Plant: The Delineation of the Disturbed Rock Zone*. SAND87-1375. Albuquerque, NM: Sandia National Laboratories.
- Davies, P.B. 1991. *Evaluation of the Role of Threshold Pressure in Controlling Flow of Waste-Generated Gas into Bedded Salt at the Waste Isolation Pilot Plant*. SAND90-3246. Albuquerque, NM: Sandia National Laboratories.
- Deal, D.E., J.B. Case, R.M. Deshler, P.E. Drez, J. Meyers, and J.R. Tybursky. 1987. *Brine Sampline and Evaluation Program Phase II Report*. DOE-WIPP-87-010. Carlsbad, NM: Westinghouse Electric Corporation.
- Deal, D.E., R.J. Abitz, D.S. Belski, J.B. Case, M.E. Crawley, R.M. Deshler, P.E. Drez, C.A. Givens, R.B. King, B.A. Lauctes, J. Myers, S. Niou, J.M. Pietz, W.M. Roggenthen, J.R. Tyburski, and M.G. Wallace. 1989. *Brine Sampling and Evaluation Program 1988 Report*. DOE/WIPP 89-015. Carlsbad, NM: Westinghouse Electric Corporation.
- Gonzales, M.M. 1989. *Compilation and Comparison of Test-Hole Location Surveys in the Vicinity of the Waste Isolation Pilot Plant Site*. SAND88-1065. Albuquerque, NM: Sandia National Laboratories.
- Lappin, A.R., R.L. Hunter, D.P. Garber, and P.B. Davies, eds. 1989. *Systems Analysis, Long-Term Radionuclide Transport, and Dose Assessments, Waste Isolation Pilot Plant (WIPP), Southeastern New Mexico; March 1989*. SAND89-0462. Albuquerque, NM: Sandia National Laboratories.

- Munson, D.E., A.F. Fossum, and P.E. Senseny. 1989. "Approach to First Principles Model Prediction of Measured WIPP In Situ Room Closure in Salt," *Rock Mechanics as a Guide for Efficient Utilization of Natural Resources: Proceedings of the 30th U.S. Symposium, West Virginia University, Morgantown, WV, June 19-22, 1989*. Ed. A.W. Khair. SAND88-2535C. Brookfield, VT: A.A. Balkema. 673-680.
- Nowak, E.J., J.R. Tillerson, and T.M. Torres. 1990. *Initial Reference Seal System Design: Waste Isolation Pilot Plant*. SAND90-0355. Albuquerque, NM: Sandia National Laboratories.
- Onofrei, M., B. Shenton, B. Walker, and L. Roe. 1993. "Final Report on the Development of Cement-Based Microfine Grout for the Sandia National Laboratories." Pinawa, Manitoba: Whiteshell Laboratories. (Copy on file at the Sandia WIPP Central Files, Sandia National Laboratories, Albuquerque, NM.)
- Peterson, E.[W.], P.[L.] Lagus, J. Brown, and K. Lie. 1985. *WIPP Horizon In Situ Permeability Measurements Final Report*. SAND85-7166. Albuquerque, NM: Sandia National Laboratories.
- Pickens, J.F., G.E. Grisak, J.D. Avis, D.W. Belanger, and M. Thury. 1987. "Analysis and Interpretation of Borehole Hydraulic Tests in Deep Boreholes: Principles, Model Development, and Applications," *Water Resources Research*. Vol. 23, no. 7, 1341-1375.
- Sepulveda-Jiminez, J.L. 1981. "A Detailed Study on Stirred Ball Mill Grinding." PhD dissertation. Salt Lake City, UT: University of Utah.
- Stensrud, W.A., T.F. Dale, P.S. Domski, J.B. Palmer, R.M. Roberts, M.D. Fort, G.J. Saulnier, Jr., and A.L. Jensen. 1992. *Waste Isolation Pilot Plant Salado Hydrology Program Data Report #2*. SAND92-7072. Albuquerque, NM: Sandia National Laboratories.
- Stormont, J.C. 1990. *Summary of 1988 WIPP Facility Horizon Gas Flow Measurements*. SAND89-2497. Albuquerque, NM: Sandia National Laboratories.
- Stormont, J.C., E.W. Peterson, and P.L. Lagus. 1987. *Summary of and Observations About WIPP Facility Horizon Flow Measurements Through 1986*. SAND87-0176. Albuquerque, NM: Sandia National Laboratories.
- U.S. Department of Energy. 1986. *Design Validation Final Report*. DOE-WIPP-86-010. San Francisco, CA: Bechtel National, Inc.
- U.S. Department of Energy. 1988. *Geotechnical Field Data and Analysis Report, July 1986-June 1987*. DOE/WIPP 87-017. Carlsbad, NM: Westinghouse Electric Corporation. Vols. 1-2.
- U.S. Department of Energy. 1989. *Geotechnical Field Data and Analysis Report, July 1987-June 1988*. DOE/WIPP 89-009. Carlsbad, NM: Westinghouse Electric Corporation. Vols. 1-2.

Van Sambeek, L.L., D.D. Luo, M.S. Lin, W. Ostrowski, and D. Oyenuga. 1993.
Seal Design Alternatives Study. SAND92-7340. Albuquerque, NM: Sandia
National Laboratories.

This page intentionally left blank.

APPENDIX A: GROUT DEVELOPMENT

This page intentionally left blank.

APPENDIX A: GROUT DEVELOPMENT

Cementitious grout is being investigated as a plugging and sealing material for the WIPP because of its low permeability and its compatibility with the underground environment. In a general sense, the performance objectives for ultrafine grout include its:

- ability to reduce the gas transmissivity (and ultimately the radionuclide transport properties) of the host rock altered by excavation,
- acceptably low hydraulic conductivity,
- ability to penetrate very fine fractures within the host rock,
- physical and chemical compatibility with the host environment,
- long-term physical stability.

The grout used in SSSPT-F was developed, optimized, and tested over a seven-month period at Whiteshell Laboratories in Manitoba, Canada. The final laboratory results were verified at Union Process, Inc. in Akron, OH, where pilot tests were conducted in a larger grout mill. Verification was necessary because the large mill ultimately used for SSSPT-F could not be properly designed from the data generated by the small mill used in the laboratory work. The SSSPT-F objectives required development of a highly specialized, ultrafine cementitious grout that could effectively permeate and seal both macro- and microfractures in MB139 and the surrounding rock beneath WIPP test Room L3. Cementitious grout was chosen for this task because of its proven utility and resistance to degradation.

The normal degradation mode for hardened grout is as follows:

- Because of its permeability, water (or brine) enters the hardened grout and dissolves the most soluble constituent, calcium hydroxide.
- By mass transfer, the calcium and hydroxyl ions migrate to a region of lower concentration (in this case, from within the hardened grout to the fluid outside).
- The ions leave the grout, and the outer portion of the grout degrades.
- Secondary minerals simultaneously deposit on the exterior of the grout, possibly impeding the ion migration.
- The pozzolan (amorphous silica) reacts with calcium hydroxide, converting it to a low-solubility calcium tri-silicate. Physically, addition of the pozzolan results in smaller and more disconnected pores, further reducing the permeability of the grout.

Degradation tests of the grout developed for SSSPT-F are currently being conducted.

For effective grouting, the largest grout particle should be no larger than one-third the aperture of the smallest fractures to be sealed (Baker, 1982). To seal microfractures, an ultrafine grout with a composition of 90% less than 8 microns was developed. (Actual particle size distribution data are presented in Appendix G.) The grout developed and used for SSSPT-F met the following criteria:

- 90% of particles smaller than 8 microns;
- "stable" grout (i.e., no water separates when grout hardens);
- no measurable dissolution of halite by fluid grout;
- no measurable agglomeration for three hours after pulverization;
- permeability of 10^{-9} darcy or less;
- injectable for a minimum of three hours after pulverization;
- initial Vicat needle set in approximately 14 hours and final Vicat needle set in approximately 15 hours;
- unconfined uniaxial compressive strength greater than 40 MPa;
- less than 1% linear shrinkage (in a totally desiccating environment);
- chemical compatibility with halite, polyhalite, clay, dolomite, and anhydrite;
- grout comprised of common, inexpensive, easily obtained components;
- compatible with chemically inert dyes.

Two ultrafine grout production methods exist: dry and wet. The dry grout pulverization process was examined first but rejected because of (1) high equipment costs, (2) the highly hygroscopic nature of the dry grout (which would necessitate hermetic packaging), (3) material compaction problems, and (4) the inability to identify a dry grinding aid (to keep fines from agglomerating and sticking to the pulverization media and the mill). Several wet pulverization mills were subsequently investigated to locate a process for economically producing ultrafine grout. Such a process would incorporate simultaneous mixing and pulverization while using simple, dependable equipment that is easy to clean. Based on these criteria, the attritor was selected for laboratory grout development and optimization.

Laboratory Development and Optimization

Attritors function by agitating pulverization media together with the materials to be pulverized in a stationary vertical tank. Attritors are widely used in the food, paint, rubber, pharmaceutical, and ceramic industries. A Union Process Model 1S Batch Attritor was acquired for the SSSPT-F laboratory development work. The 1S holds a vertical, 316 stainless steel tank that is open on the top. Extending downward into the tank is a vertical shaft equipped with six tungsten carbide cross-arms. Pulverization media (spheres) are placed in the tank until they just cover the upper arms

when the machine is at rest. An electric motor turns the shaft, and the cross-arms move through the media, imparting random motion to the spheres. (The 1S tank configuration is shown in Section 3 of this report.) Pulverization results from impact and shear between the balls. The attritor process reduces particle size approximately five times as fast as an ordinary ball mill and is more energy-efficient. A detailed study of stirred ball mill grinding can be found in Sepulveda-Jimenez (1981).

To develop and optimize an ultrafine cementitious grout using the attritor, the laboratory was asked to optimize the following variables:

1. composition and diameter of the grinding media;
2. type and wt% of:
 - portland cement
 - superplasticizer
 - pozzolanic material
 - water;
3. rotational speed and duration of pulverization;
4. amount of mechanical and hydrational heat that must be removed from the grout during pulverization and subsequent agitation (heat initiates hardening of the grout).

Because of the many variables, the solution was labor-intensive, requiring many mixes. Optimal grout components were Canadian (LeFarge) Type 50 sulfate-resistant portland cement, Dowell-Schulumberger D-65 (sulfonated naphthalene formaldehyde) superplasticizer, and -325 mesh pumice. The grout optimization process is described in Onofrei et al. (1993).

Pulverization media were suggested by Union Process, Inc. during initial grout pulverization experiments in their laboratory. Their suggestions were based on extensive experience and essentially followed their publication "How to Select Your Grinding Media." The following media were evaluated:

- 3-mm-diameter zirconium oxide, stabilized with rare earths;
- 6-mm-diameter zirconium oxide, stabilized with rare earths;
- 3-mm-diameter carbon steel;
- 3-mm-diameter, 440C, 316 stainless steel.

The 3-mm-diameter stainless steel spheres were chosen on the basis of performance, specific gravity, cost, and longevity. This type of media pulverized approximately 3 L of grout to 90% smaller than 8 microns in 15 minutes in the laboratory 1S batch attritor. Records of these tests are filed with WIPP Quality Assurance.

Particle size analysis was essential to optimization. After evaluating several methods of particle size analysis and field testing four Laser Particle Size Analyzers and one Coulter unit, a Malvern 3200E Mastersizer was selected and purchased. Following evaluation at Whiteshell, a Bohlin Visco

88 Rotary Viscometer was purchased for rheological determinations. Both these instruments are described in Appendix E.

The first step in assessing the applicability of the Szegvari Attritor to grout pulverization was to evaluate the process in a laboratory-sized 1S Attritor, which is a small (3-L tank) mill. It is not possible to extrapolate data from this test to allow the selection of a production-sized mill. For that reason, it was necessary to conduct a pilot test in a much larger 30S Attritor. Union Process, Inc. maintains a laboratory section, a pilot mill test section, and manufacturing facilities. Pilot tests were conducted there with a 30S batch attritor (94.6-L tank). These tests supplied the operating data required for proper design of the larger 50S Attritor that was used for the SSSPT-F grouting experiment at the WIPP.

The grout used for the experiment is thixotropic (i.e., not like water, which is a Newtonian fluid). Thixotropic fluids are termed Binghamian, and thicken when at rest. Re-liquefaction is then achieved by applying sufficient force (pressure) to slightly exceed the shear stress. Therefore, during the field experiment, the grout was always kept in motion to avoid thickening. An agitation tank was employed in conjunction with a recirculation system. No agitation tank was available at Whiteshell Laboratories for the development and optimization of the grout, which preceded the field experiment. An electric ice cream maker was supplied by SNL as a temporary solution to this problem. Although its planned use was provisional, this low cost unit performed reliably and satisfactorily throughout the laboratory work.

Grout Evaluation

The grout development process was complex, requiring a large number of pulverizations and many physical tests of the grout produced. This work, accomplished at Whiteshell Laboratories under SNL direction, included the following specific SNL guidance:

- Use of the Szegvari: a laboratory-sized 1S attritor was suggested and supplied by SNL (this equipment had never been used for this purpose before).
- Optimum pulverization media: selected and supplied by SNL.
- Water-cooled agitation tank and laser particle size analyzer: selected and supplied by SNL.
- Appropriate rotational speed for the Szegvari attritor.
- SNL identified and supplied the material (pumice) that proved to be the most effective pozzolan and a dry-grinding aid. Success was achieved in dry pulverization subsequent to the field experiment described in this report.

- SNL identified and supplied the sodium condensate (salt) of sulphonated naphthalene formaldehyde, which served as (1) a retarder, (2) a water-reducing agent, and (3) a dry grinding aid.
- SNL supplied the basic Statement of Work (SOW) that guided the laboratory effort.

The simultaneous wet pulverization and mixing procedure was not obvious, as demonstrated by the fact that approximately 7 months of laboratory effort were required to optimize it. Therefore, a technology advance disclosure describing the method was submitted to the SNL patent department, and a patent application is being filed.

Work at Whiteshell produced the grout used in the field experiment described in this report. This grout met or exceeded all criteria as stated in the SOW. The optimized grout components are easily obtained, inexpensive materials that can be simultaneously mixed and pulverized at the grouting site as required. Particles in the fluid grout are 90% smaller than 8 microns and the average particle size is approximately 4 microns. Additionally, the grout exhibits no measurable agglomeration (particles clumping together) for at least three hours subsequent to mixing. The unconfined, uniaxial compressive strength (at 28 days) exceeds 40 MPa; maximum linear shrinkage (at 50% relative humidity) is 1%; and permeability is very low (10^{-9} darcy, approximately 10^{-16} m/s) and decreases with time, probably because of continuing hydration resulting in less pore volume. The grout also remains injectable for 3 to 4 hours after pulverization/mixing.

Chemically Inert Dyes

A distinct grout color was desired for each of the 16 grout injection holes. If a visually discernible color could be assigned to each hole, permeation studies would be enhanced. Several supposedly chemically inert dyes were obtained and used to achieve 16 different grout colors. The grout colors, dye percentages, and resulting colors for the eight primary and eight secondary holes are described in Section 3.2.2.

Because fluorescein ($C_{20}H_{12}O_5$) initiated flocculation and precipitation, it was not used. The black dye evolved an organic gas (type unknown) until the grout was set. This gas rendered operation of the gas-flow/tracer photo ion detector (PID) impossible. A "flush" of nitrogen, maintained overnight in the central gas-injection hole to remove this gas, permitted operation of the PID the following morning. Green dye was used in one batch that exhibited a three-fold increase in shear stress and plastic viscosity. The simultaneous wet pulverization/mixing process is sensitive to pulverization time, which in this case was 6 minutes longer than the optimum 85 minutes. However, the increase in viscosity and shear stress were too excessive to

have resulted from this relatively small increase in pulverization time. The increases may have been caused by the supposedly chemically inert green dye. In spite of the increased viscosity and shear stress, the grout successfully permeated and sealed microfractures smaller than 10 microns in halite, and in one rare instance it completely sealed the 3-micron fracture shown in Photo 5-3.

Dyes were incorporated into the grout by weighing 2.5 to 5.0 wt% on an electronic balance calibrated with weights traceable to the National Institute for Standards and Testing (NIST). The dry, powdered dye was added to the attritor as the final grout component. The attritor and ancillary grouting equipment are described in Appendix E of this report.

APPENDIX B: FLOOR RESTRAINT SYSTEM DEVELOPMENT

This page intentionally left blank.

APPENDIX B: FLOOR RESTRAINT SYSTEM DEVELOPMENT

The SSSPT-F floor-slab/floor-jack system was devised to restrict the formation and improve control over the grout during the injection of pressurized grout. The system consisted of four hydraulically actuated (and then mechanically locked) floor jacks and a reinforced concrete slab. The slab, emplaced on the leveled floor of Room L3, was heavily reinforced and designed not to crack. Prior to grouting, the jacks were positioned around the injection hole and braced against the ceiling of the room. These jacks were used to resist upward displacement of the slab that resulted from the subjacent injection of pressurized grout; they were not intended to push the slab down. Vertical movement of the slab was measured by rod extensometers placed near each of the four corners of the slab. Two extensometers were situated in a vertical hole approximately 15.4 m deep in each corner. One extensometer was anchored at a depth of 15.2 m and the second was anchored at 4.3 m. These could detect vertical movement as small as 0.025 mm. Extensometers were constantly monitored via the video monitor at the injection "T" and the data were simultaneously recorded by the DAS. The extensometers provided useful information permitting improved control of injection pressures.

Design Development and Analysis

The floor restraint system was designed and structurally analyzed by Parsons Brinckerhoff Quade & Douglas, Inc. (PB) of San Francisco, CA. The PB engineer supplied drawings of the jacks. Hall Machinery of Carlsbad, NM prepared shop drawings, which were checked and approved by the Principal Investigator. Hall then built the jacks and delivered them to the WIPP. PB supplied plans for the slab. Constructors, Inc. of Carlsbad supplied, mixed, and emplaced the concrete, aided by Westinghouse Mining Operations.

The location of the slab within Room L3 was determined following the results of preliminary gas-flow and electrical geophysical surveys. The slab was placed above the most permeable zone in the room. The concrete was analyzed for unconfined uniaxial compressive strength by Pettigrew and Associates of Hobbs, NM (analyses were filed in the WIPP Quality Assurance SSSPT-F file).

Slab Construction and Emplacement

A plan view of the slab showing the location of all coreholes is presented in Section 2. After the slab location was finalized, the area was

marked by the WIPP engineering department, and the floor of the room was leveled by Westinghouse Mining Operations. Cyclone mesh, extending 7.62 m horizontally from the slab, was installed on the sides of the room with rock bolts before slab emplacement. The concrete composition, determined by SNL, is shown in Table B-1.

Table B-1. Composition of Concrete Slab

Materials	1 yd ³ wt. (lb)	1 yd ³ vol. (ft ³)
Cement, Type I-II/V	564.	2.87
Silica Fume	62.5	0.44
Water	350.	5.61
Coarse aggregate	1520.	8.86
Fine aggregate	1490.	9.23
Reobuild 1000	138.	0.00
Fibermesh	3.	0.00
TOTALS	3990	27

Water (+ Rheobuild 1000) to Cement Ratio (wt): 0.62/1
 Unit weight: 147.65 lbs/ft²

Materials and sources:

1. Ideal Portland Cement, Type V. Holnam, Inc., Tijeras, NM.
2. Silica Fume, Holnam, Inc., Tijeras, NM.
3. Special Coarse Aggregate, Constructors, Inc., Carlsbad, NM.
4. Special Fine Aggregate, Constructors, Inc., Orla, TX.
5. Rheobuild 1000 (High Range Water Reducer), Master Builders, Inc.

The sequence of events for slab construction was as follows:

- Wooden forms, wire, a concrete conveyor, and 144 pieces of 2.54-cm reinforcement steel (7.62-m long) were delivered to the WIPP and moved to Room L3.
- Forms were erected and rebar installed as shown in the architectural and engineering drawings (below, in this appendix). Rebar was removed from areas where holes would be drilled through the slab.
- Two concrete buckets were modified by welding an extension to their tops, increasing their capacity to about 1.14 m³.
- Two front-end loaders were modified to discharge concrete onto a 61-cm-wide conveyor belt.
- Concrete was dry-batched at Southeast Redi-Mix in Carlsbad, transported to the WIPP in mixer trucks, and mixed in the trucks as needed.

- Slump was measured and compression samples were poured; then the concrete was transferred to the concrete bucket in the Salt Handling shaft.
- The filled bucket was lowered to the repository level, where the concrete was transferred to the modified scoops of the front-end loaders. Using two front-end loaders to transport concrete to Room L3, workers averaged about one bucket every 20 minutes.
- The front-end loaders poured the concrete onto the conveyer, and the conveyer was maneuvered to distribute the concrete where needed.
- The concrete was properly vibrated and trowelled.

Concrete transfer was accomplished during a 12-hour period by Westinghouse Mining Operations, aided by Experimental Operations and Constructors personnel. The completed slab measured 7.62 x 7.62 m and had a depth of .38 m.

Hydraulic Floor Jacks and Load Cells

A schematic diagram and a photo of the floor jacks are presented in Section 2. The jacks were positioned around each grout injection hole prior to grouting. Braced between the concrete slab and the ceiling of the room, they held the slab in place during grouting, thus retarding hydraulic displacement of the formation by counteracting upward thrust caused by the injection of pressurized grout.

Each jack weighs approximately 14 kN and can withstand a load of 3,736 kN, exceeding all established SNL pressure safety requirements. The greatest load recorded on a single jack was approximately 155 kN (see data for holes L3420, L3425, L3527, L3528, L3530 in Appendix G.) To ensure safety, standard Westinghouse Waste Isolation Division Rigging Procedures were used to move and position the jacks.

The floor jacks were actuated by an 890 kN hydraulic cylinder and locked in place with the four lower capstan bolts. The hydraulics were then relieved (preventing possible hydraulic leakage). Each jack was equipped with four load cells (one on each of the four lower capstan bolts), each cell sensitive to a load change of 2 kg. During grouting, these cells indicated that a volume of high-pressure grout formed near the hole. When injection stopped, this pressure decreased significantly during the first 30 minutes, suggesting that the grout was slowly moving away from the hole through microfractured rock. Load cell data showing the pressure rise and dissipation are presented in Appendix G.

Prior to grouting, the jacks were positioned around the injection hole and ordered set at approximately 44 kN to remove any mechanical play. The jacks were anchored by placing about 5 cm of thick, wet Hydrastone Super X on top of the three 25.4-cm-diameter discs located on the three upper capstan bolts, then adjusting the jack until the Hydrastone made complete contact with the ceiling of the room. In about 30 minutes, the unconfined uniaxial compressive strength of the Hydrastone was approximately 41 MPa, and jack set was completed as described above. Jacks were always positioned and set during the afternoon shift by Westinghouse Experimental Operations and checked the following morning for proper setup and safety by the grouting crew. No improper or unsafe setups were encountered.

Rod Extensometers

Four vertical, 15.4-m-deep, 7.6-cm-diameter holes were drilled through the slab near the corners. (Hole locations are shown in Figure 2-1.) Each hole held two rod extensometers to measure vertical displacement of the slab. The extensometer transducers, mounted inside the slab and connected by rods to the two anchors, were capable of detecting vertical movements as small as 0.025 mm. Extensometer data are presented in Appendix F.

The drillholes housing the extensometers were cased with grouted polyvinyl chloride (PVC) pipe to a point 3.66 m below the slab. The top of the transducer housing was set flush with the slab surface. The extensometer system was comprised of downhole hardware and the transducer assembly. Hardware included modified rod extensometer components, borehole anchors, rod set stabilizers, stainless steel rod sets, and protective tubing (which housed the rods inside the grouted casing). Transducer assemblies included two transducers and a mounting fixture. The transducers were linear variable differential transformers (LVDTs) with a DC output. The mounting fixture attached the LVDTs to the borehole collar and provided the necessary adjustments for aligning the units with the rod sets and setting the transducers within their usable range. Each installation contained two LVDTs connected to their anchors via the rods. Three procedures were undertaken to ensure free travel of the rods: (1) The borehole was cased beyond the base of MB139 to protect against grout intrusion. (2) The rods were encased in PVC pipes to total depth, providing complete protection against brine or grout intrusion. (3) The rods were positioned in the center of the hole with rod stabilizers located between the anchors and the transducer housing.

System reliability was expected to be high because all components had been previously used in the WIPP environment. Nonetheless, because the configuration was new, a two-part validation exercise was conducted. The first part involved calibration of the selected LVDT type (to characterize

linearity and repeatability of output) and development of a multiple-point calibration sequence to accommodate the full 2.54-cm range while enhancing resolution in the 0.0 to 13 mm range. The second part of the validation exercise occurred underground with the installation of two prototype gauge systems and connections to a DAS. Two identical gauges were located in adjacent boreholes to provide information on the feasibility of the measurement system. When the gauges demonstrated stable performance, grout was introduced into one of the holes to determine the effect on gauge performance. Installation and operation of these prototypes provided an opportunity to practice the assembly and proper adjustment of the system prior to actual fielding of the experiment. It also assisted procedure development, training, and in situ characterization of the extensometer system.

The floor restraint system functioned perfectly throughout the test period. The slab effectively resisted injection pressures as high as 8.2 MPa and remained crack-free throughout the test.

This page intentionally left blank.

This page intentionally left blank.

APPENDIX C: DIAMOND DRILLING EQUIPMENT

APPENDIX C: DIAMOND DRILLING EQUIPMENT

Portions of the diamond drilling equipment used in SSSPT-F were invented and fabricated to meet specific objectives in this test. The drilling system was designed to allow core recovery while drilling a "clean" hole (i.e., one where fractures in the hole wall are not plugged by drill cuttings).

Concept Development

One objective of SSSPT-F was to determine the efficiency of grout for sealing microfractured rock (aperture equal to or less than 0.1 mm). Diamond drill cuttings are very fine-grained, and the drilling-fluid flow direction of the standard WIPP drilling system allows these cuttings to plug fractures in borehole walls. The standard drilling configuration blows compressed air down a single drill rod and outward across the diamond bit. This flow drives the cuttings up the annular space between the drill rod and the hole wall, where they often plug fractures, potentially blocking the entrance of grout. Cuttings that don't plug fractures are then forcibly ejected from the collar of the hole and dispersed into the drilling area, creating a dusty work environment that is detrimental to both workers and electronic equipment.

To overcome these problems, special drilling equipment was invented for SSSPT-F. The custom equipment incorporates a reverse-circulation air-flow system, which is shown schematically in Section 2. During operation, compressed air is passed down the annulus between the outer rod and the drillhole wall and then sweeps inward across the drill bit, cooling it and carrying cuttings up between the inner and outer drill rods for approximately 1.22 m (to clear the core barrel). The cuttings are then deflected into the center rod and carried up to the swivel (above the drill), where a hose connects the swivel to a powerful vacuum. The vacuum draws the cuttings from the drill rig across an intercept hopper (where the coarser particles are retained) and then pulls the finer particles through multiple HEPA filters. Clean air is discharged, benefitting the workers and sensitive electronic equipment.

Design and Fabrication

The drilling equipment design was based on extensive experience with diamond, down-the-hole hammer, and tri-cone reverse-circulation drills. Development began when SNL created a set of drawings for the proposed system and sent them to Christensen Diamond Products of Salt Lake City, UT, who

fabricated the new equipment. The final product met all design criteria and had the following attributes:

- The system is dual-rod, reverse-circulation, utilizing both compressed air and vacuum-assisted air as the drilling fluid.
- A vacuum is applied at the upper end of the drill rods while compressed air is introduced at the collar of the hole via a "stuffing box"—an air-tight seal between the concrete floor slab and the drill rods.
- The drilling fluid flows down the outer annulus and up through the drill to a vacuum where the cuttings are trapped.
- The equipment drills a 15.24-cm hole and recovers a 10.16-cm core.
- The dual-rod system adds stiffness to the rods, enabling the tool to drill a straighter hole.
- The drilling efficiency is high: holes can be drilled through .38 m of concrete and 3.28 m of rock in one hour (including the time required to position the drill).

Testing and Modification

Minor modifications were indicated during initial evaluation of the new drilling equipment. Cooperation by Christensen Diamond Products was typified by their sending a design engineer to the WIPP site. A meeting was held underground with the drill crew, and suggestions presented were incorporated by the engineer, resulting in equipment that functioned perfectly. The final drill rig design is shown in Section 2, Photo 2-1.

Because of the innovative nature of the drilling equipment developed for SSSPT-F, a technology advance disclosure was filed with the SNL patent department. The SSSPT-F drilling equipment was used to drill a total of 57 on-slab holes. A complete drilling summary showing hole coordinates, lengths, diameters, and drill dates is presented in Section 2.3.

APPENDIX D: GAS-FLOW/TRACER-GAS TEST EQUIPMENT

This page intentionally left blank.

APPENDIX D: GAS-FLOW/TRACER-GAS TEST EQUIPMENT

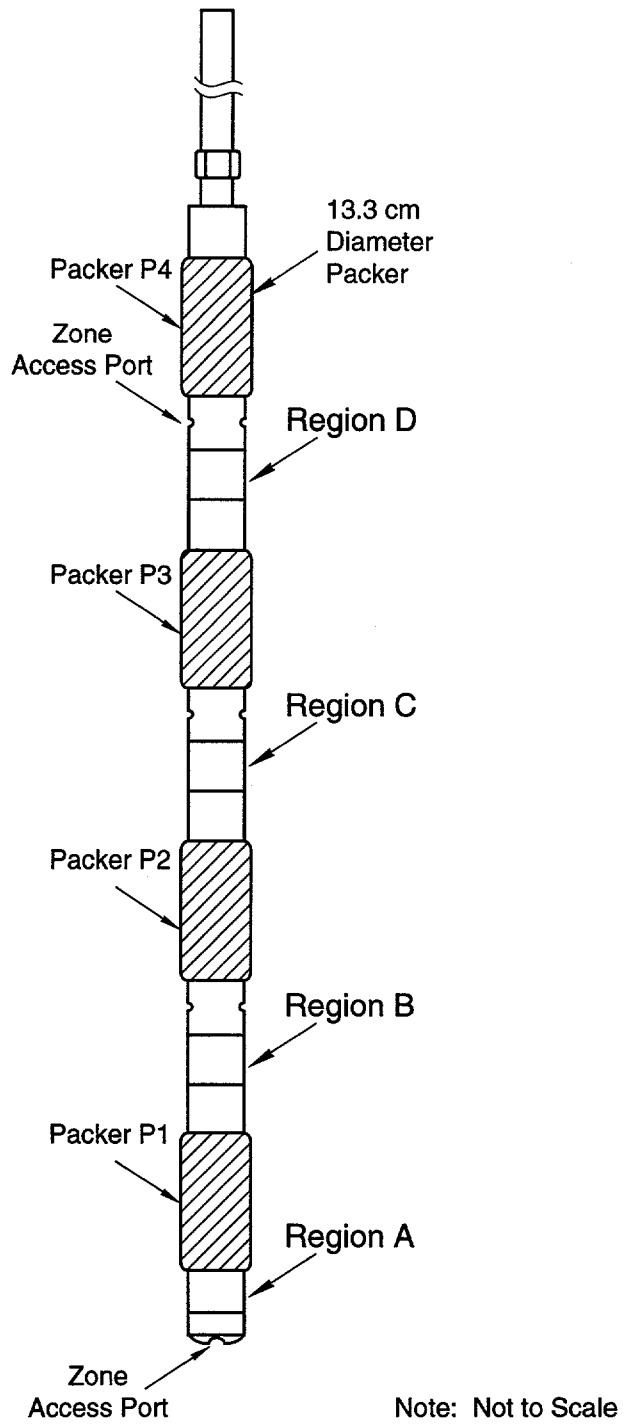
The purpose of gas-flow/tracer testing was primarily to evaluate the testing technique and innovative equipment as a possible method of assessing the effectiveness of ultrafine grout in reducing the gas transmissivity of fractured strata surrounding the WIPP facility. The equipment configurations for the gas-flow and tracer-gas tests are shown in Section 4. The equipment is described in this appendix. Test results are presented in Appendix I.

Packer Assembly

A fixed-end inflatable packer was used during gas-flow and tracer-gas testing to seal the injection hole and permit gas injection. The straddle-packer assembly was used in all gas flow testing conducted in support of SSSPT-F. The packer tool was manufactured by Tam International specifically for gas-flow testing in the WIPP underground. The packer tool features an 8.9-cm mandrel supporting four 13.3-cm-diameter inflatable packer elements. Each element is approximately 35.6 cm in length, is covered with a 70 durometer elastomeric cover, and contains a bladder that has been pressure tested to 2.1 MPa.

The four inflatable packer elements are separated by mandrel sections (intervals) containing plumbing sub-assemblies (subs) and extensions. The subs are fitted with threaded female ports on the inside surface of the tool so that each inter-packer sub can support compression fittings and associated plumbing that facilitate (1) inflation of the attached inflatable element, (2) gas injection into the interval, and (3) a static pressure return/vent line so that interval pressures may be accurately read during testing and vented at the end of individual tests. The end sub, which is approximately 25.5 cm in length and closed at the end, has only two threaded ports because no inflatable element is located beyond it. Inter-packer intervals are approximately 35.6 cm in length.

The use of a multipacker tool allows for testing to be performed in a single zone with the remaining zones used as a check on the quality of the packer seals isolating the testing zone. The packer tool, as configured and used in the SSSPT-F testing, can support three test zones: intervals, A, B, and C (Figure D-1). Use of interval A as the test zone allows for an upper guard zone in interval B. Use of interval B as the test zone allows for an upper guard zone in interval C and a lower guard zone in interval A. Use of interval C as the test zone allows for an upper guard zone in interval D as well as a lower guard zone of equal volume in interval B. Almost all gas



TRI-6121-307-0

Figure D-1. Schematic of SSSPT-F straddle-packer test tool.

permeability testing conducted in support of SSSPT-F utilized interval A as the test zone, a configuration referred to as the down-hole configuration. This configuration allowed assessment of gas permeability of the formation in the effective grout-injection interval that ranged from approximately 137 cm to 366 cm below the top of the concrete slab.

Volumes of the inter-packer internals and the response of these volumes to different pressures were measured in a compliance test chamber. The packers were inflated to 0.34 or 0.69 ± 0.07 MPa. The intervals were filled with fluid through the packer tool plumbing lines, and gas pressures were applied to the top of the columns. Interval pressures were stepped 0.07 MPa to a maximum of 0.34 MPa, and the compliance effects were noted for each pressure step by time. The results of the volume and compliance tests for the packer tool are on file with the SNL/WIPP records department.

The straddle-packer assembly is built on a low pressure fixed-end inflatable element design. Compliance testing revealed several facts about the operation of the packer tool. First, the packer elements are much less compliant with 0.69 MPa inflation pressures than they are with 0.34 MPa inflation pressures. Second, leakage between the inflatable element and the internal surface of the test fixture is negligible unless the interval pressure is greater than about 60 percent of the packer inflation pressure. Finally, the fixed-end design is highly non-compliant. The compliance effects noted were less than 1 percent of interval volume and occurred predominantly in the first fifteen minutes after interval pressures were increased. For these reasons, compliance effects were not expected to cause measurable errors in the gas-flow permeability testing program.

Digital Display Panel

Inflation of the packer elements, control of gas injection into the test zone, and monitoring of pressures in the packers, test zone, and guard zone was accomplished with the Digital Gas Flow Tool (DGFT). The DGFT contains an aluminum pressure cylinder that is filled from an external nitrogen pressure cylinder. When filled to 6.9 MPa, the reservoir holds approximately 0.45 m^3 (416L) of gas at ambient temperature and pressure conditions (20° C and 101300 Pa). This internal reservoir tank is instrumented with pressure and temperature gauges that allow gas-flow rates to be calculated from changes in internal pressure and temperature.

Gas-injection pressure is controlled by a GO-brand zero-leak pressure regulator. The test and guard zones are selected with the multi-way valves on the panel front. Pressures of these zones and the reservoir tank are

displayed on control-panel-mounted digital indicator gauges. Pressures of the inflatable packer elements are shown on analog dial gauges mounted on the right side of the control panel.

Plumbing lines from the straddle-packer assembly are attached to the DGFT by self-sealing quick-disconnect fittings located on the left side panel of the cabinet. A tracer-gas inlet port, also located on the left side panel, is attached to a 3-way valve inside the cabinet that allows the operator to use the DGFT to control tracer-gas injection instead of conducting gas-permeability tests.

Pressure and Temperature Instrumentation

Pressures in the reservoir tank and test and guard zones were monitored with 0.0 to 6.0 MPa-range CEC Model 5500 pressure transducers. The 10-VDC excitation voltage for these transducers was supplied by power supplies internal to their respective digital indicator gauges. These transducers were calibrated with their respective power supplies at the INTERA WIPP-site calibration facility. Calibration records for these transducers are on file with the SNL/WIPP records department.

The packer pressures were monitored with 0.0 to 2000 psig (13.8 MPa) Kulite Model HKM-375 pressure transducers. The 10-VDC excitation voltage for these transducers was supplied by a Hewlett Packard (HP) laboratory power supply. These transducers were calibrated by the SNL Albuquerque calibration facility, and calibration records for these transducers are on file with the SNL/WIPP records department.

The temperature of the gas in the DGFT reservoir tank was monitored with a sealed Type E thermocouple inserted through a sealed port in the tank plumbing head so that the junction was near the center of the tank. This thermocouple was shipped from the manufacturer with a certificate of compliance with stated accuracy standards. A post-test as-found calibration was later performed at the SNL WIPP-site calibration facility. The thermocouple was found to be within stated accuracy limits. The calibration records for this thermocouple are on file with the SNL/WIPP records department.

Data Acquisition System

Signals from all pressure transducers and thermocouples were monitored by an HP 3497a Data Control Unit (DCU) with a 5.5-digit integrating Digital

Volt Meter (DVM) option installed. Signal- and excitation-voltage monitor cables for the pressure transducers were installed on a mux card that connects to the HP 3497a. The thermocouple was installed on a separate mux card that allowed for reference junction compensation of the primary junction voltages.

The HP 3497a DCU was controlled by a personal computer (PC) running an SNL data acquisition code written for permeability testing equipment in use at the WIPP. The data acquisition code initiated HP 3497a scans of the instruments, directed digitized data to storage devices resident in the PC, documented test and instrument information, and provided a real-time display of logged voltages as well as converted engineering units on the PC monitor. Digital displays on the panel front gave indications of real-time pressures of the reservoir tank and test and guard zones as well as the raw voltages being logged.

Tracer-Gas-Injection Testing Equipment

Tracer-gas testing was used to investigate the qualitative aspects of gas-flow pathways in the formation tested during SSSPT-F. The time to maximum relative concentration breakthrough as well as the magnitude of the relative concentration of tracer gas may be interpreted to yield information about the size, directness, and branching of the flow pathways. Successive tracer-gas breakthrough tests were performed prior to, during, and after a set of grout-injection experiments to provide a qualitative indication of the effectiveness of the grout injections for limiting gas flow through the fractured formation.

Tracer Gas

Instrument grade air was prepared with a 200 ppm spike of isobutene. Isobutene was chosen as a tracer because of low toxicity, convenience, low cost, and established detection equipment and procedures that provide for rapid analysis and real-time display of data. Instrument grade air was used as the blank matrix gas injected before and after the tracer-gas pulse.

Tracer-Gas-Injection Configuration

The DGFT was configured to isolate the reservoir tank from the injection system for use as an alternative pressure source. For tracer-gas testing, this configuration was used with a High Purity Switchover Manifold (HPSM)

attached to two pressure cylinders, one containing instrument grade air and the other containing instrument grade air with a 200 ppm spike of isobutene. The reservoir tank and the two cylinders provided the pressure source for gas injection. Pressures in the two cylinders attached to the HPSM were monitored by Kulite Model HKM-375 pressure transducers. Dedicated cables connected these transducers to an HP 75000-based DAS. These transducers were calibrated by the SNL Albuquerque calibration facility. The calibration records are on file with the SNL/WIPP records department office.

The outlet of the HPSM is attached to the tracer-gas inlet port of the DGFT. By selecting the tracer-gas injection option on the pressure source selector valve inside the DGFT cabinet, gas from the inlet port is routed directly to the GO-brand pressure regulator. Other DGFT and packer tool functions were unaffected by the reconfiguration, and all instrumentation, with the exception of reservoir tank pressure and temperature, remained active. Internal connectors allowed the instrument cables to be attached to external cable connectors located on the top of the DGFT cabinet.

Tracer Gas Sampling and Detection System

Tracer-gas receiver boreholes were capped with aluminum plates bored to accept three bulkhead fittings, which allowed controlled gas passage through the plate. The plates were bolted to the slab with foam seals between the borehole collar and the plate. Two 1.3-cm bulkhead connectors provided gas pressure equalization through matched unidirectional check valves connected to individual 4.5-cm intake and exhaust manifolds opened to mine up-ventilation and down-ventilation, respectively, from the test location. This system guaranteed zero pressure in the receiver holes regardless of the flow or aspiration rates and prevented over-the-slab crosstalk between the receiver boreholes.

The above-ground connection of the third bulkhead fitting was attached to one of eight teflon aspiration hoses servicing the Gas Detection Cabinet. These lines were each constantly aspirated at the rate of 0.075 L/min. The below-ground connection of the third bulkhead fitting was connected to a branched manifold built of 6-mm OD teflon tubing. The branches of the manifold were conducted of equal lengths of tubing, but the manifold was constructed so that each of the four branches opened into different depths of the receiver hole. By constructing the manifold this way, the sample aspirated into the above-ground teflon tube was unbiased by location of formation contribution to receiver hole tracer-gas entry.

The tracer-gas detection system consisted of an HNU201 photoionization detector (PID) connected to an MP2000 sequencer/data integrator. The HNU201

utilized a 10.7-electron-volt lamp as the photoionization exciter source. This wavelength lamp is 100% efficient at exciting electrons in isobutene. The HNU201 was zeroed with ambient air and span-calibrated with a sample of the tracer-spiked injection gas. The gain was set to 200 ppm. The HNU201 provided an analog dial gauge indicating the percentage of span and supplied an analog voltage to the MP2000 sequencer/data integrator.

The MP2000 served multiple functions for the tracer-gas detection system. The programmable sequencer opened and closed solenoid valves connected to the eight aspiration lines every 30 seconds so that each of the eight could be sequentially selected for purging and sampling during a four-minute period. The data integrator provided a digital indication of the tracer-gas concentration for the aspiration line being sampled and stored the value until the DAS scanned the memory.

Data Acquisition System and Software

Signals of all DGFT instrumentation, the MP2000/HNU201 tracer-gas detection system, and the gas-cylinder pressure transducers attached to the HPSM were monitored by an HP 75000 DCU with a 6.5-digit DVM option installed. Thus all data sources were integrated with a common time-stamp. Although the HP 75000 is programmable and may be operated in standby mode, a portable PC with an IEEE 488 card installed was used as a terminal interface and data storage driver. Control of data acquisition was provided with the commercial software package Labtech Notebook XE.

The data acquisition software allowed the partitioning of the incoming data stream into two subsets. The first data subset consisted of pressure data from the DGFT and transducers attached to the HPSM. This data stream was stored in a data file written to the fixed disk of the PC and was also converted into engineering units and displayed in real time to the display screen. The second data subset consisted of the tracer-gas concentrations output from the MP2000/HNU201 gas-detection system. This data stream was also stored on the fixed disk of the PC and converted into concentration units of parts per million for real-time display on the screen.

This page intentionally left blank.

APPENDIX E: GROUTING EQUIPMENT

This page intentionally left blank.

APPENDIX E: GROUTING EQUIPMENT

Szegvari 50S Attritor

The Szegvari 50S Attritor (shown in Photo E-1) simultaneously mixed and pulverized cementitious grout at the site as needed. The 50S reduced the grout to 90% smaller than 8.0 microns in one-fifth the time required by a standard ball mill. It was also energy efficient, simple, durable, and easy to clean and maintain. The use of the 50S during the grout development process is described in Appendix A. The field experiment use of the 50S is described in Section 3.

The 50S was selected after seven months of laboratory research and development at Whiteshell Laboratories in Pinawa, Manitoba and pilot tests at Union Process, Inc. in Akron, OH. The 50S is a 1589-kg batch unit with a tank capacity of 284 L and a slurry capacity of 129 to 140 L. The frame is carbon steel, but portions contacting the grout are #316 stainless steel. The 50S pulverizes grout in the wet state by grinding the grout components between moving milling media in its vertical, stationary tank. A diagram of the tank appears in Section 3. The 50S tank contains 681 kg of 3-mm-diameter, 440C, 316 stainless-steel spheres as milling media. Six tungsten carbide cross-arms attached to the vertical internal shaft of the tank stir the spheres, imparting random motion to the media. Pulverization results from impact and shear between the spheres. Because most pulverization occurs from one- to two-thirds of the distance from the central vertical shaft to the tank wall, tank wear is minimal. The durable spheres also experience minimal wear.

A special electric motor with 450% starting torque powers the 50S. This high initial torque is required to start movement of the agitation arms through the heavy steel grinding media. Starting power is 90 HP, which drops to 20 HP when the agitation arms attain operating speed.

Initial Evaluation

Attritor evaluation began at the Union Process, Inc. laboratory. Preliminary tests were performed in a small Szegvari 1S Batch Attritor with a 3.78 L capacity. Grout particle size and distribution were determined with a MicroTrac laser particle size analyzer. After a series of successful tests at Union Process, a Szegvari 1S was purchased by SNL for grout development and optimization studies to be conducted at Whiteshell Laboratories (operated by Atomic Energy of Canada, Ltd.). The grout development process is described in Appendix A.



Photo E-1. Szegvari 50S Attritor.

Whiteshell personnel were requested to produce a zero-bleed grout of the smallest possible particle size to meet the physical criteria listed in Appendix A. Several laser particle size analyzers and one Coulter-principle particle size analyzer were evaluated, leading to the purchase of a Malvern 3200E Mastersizer Laser Particle Size Analyzer. Because Whiteshell Laboratories had successfully used a Bohlin rotary viscometer for rheological analyses for two years with excellent results, one was purchased for the SSSPT-F experiment. The laser analyzer and rotary viscometer were essential quality control instruments.

Attritor Use During Grout Development and Optimization

Seven months of laboratory effort were required to develop an optimum grout. Initial evaluation consisted of a series of trial runs in the Szegvari 1S Attritor. Four different types of grinding media were tested with the 1S:

- 6.34-mm-diameter zirconium oxide stabilized with rare earth,
- 3.17-mm-diameter zirconium oxide stabilized with rare earth,
- 3.17-mm-diameter carbon steel, and
- 3.17-mm-diameter 440C, #316 stainless steel.

The last was selected as optimal for this experiment. Attritor rotation speed was optimized at 400 rpm for the 1S, and the unit succeeded in pulverizing grout to 90% smaller than 8 microns in 15 minutes. Although the correct particle size was achieved in a number of different mixes, physical parameters were not completely satisfied until many batches of varying composition had been processed. After optimization, the decision was made to purchase a customized Szegvari 50S Attritor for the field experiment.

Pilot Tests and Design of 50S Model Used for Field Test

Because it was not possible to design a 50S based on operating data from the small 1S Attritor, pilot tests were conducted in a larger 30S Attritor in the Union Process pilot section (the pilot section had no 50S). Pilot tests were necessary to establish specifications and provide the data required for proper design of the customized 50S.

The 30S Attritor (capacity 94.6 L) was effective in simultaneously pulverizing and mixing the grout components. Data collected during pilot testing (observed and directed by the PI) included power consumption, pulverization time, rotational speed, torque, inlet and outlet temperature of the water used to cool the unit, and particle size analyses. These data were

documented in the Union Process, Inc. test report, which is filed with WIPP Quality Assurance. Results of the pilot tests were utilized to properly modify the 50S Attritor to the customized version ultimately purchased for the in situ experiment.

Agitation Tank and Load Cell

Agitation of the mix was required because the thixotropic grout must be kept in motion to remain fluid. After pulverization, the grout was transferred from the attritor to an agitation tank where it was cooled and constantly stirred at approximately 60 rpm. The custom-built, #316 stainless steel agitation tank used for SSSPT-F was made by the ChemGrout Co.; its custom #316 stainless steel "Temp Plate" cooling jacket was constructed and attached with heat-conducting mastic by the Paul Mueller Co. Grout was transferred from the attritor to the agitation tank, where it was maintained in a fluid state prior to injection into the formation. The tank was capable of variable stirring speeds because it was powered by a top-drive, vane-type air motor acting through a gear reduction box. Tank cooling was accomplished by water chilled to approximately 5°C and circulated through the cooling jacket at a flow rate of 75.6 L/min.

The water chiller used to cool the attritor and the agitation tank was a custom-built Dunham Bush unit rated at 6.8 metric tons (but equipped with the compressor used for a 10-ton unit). It utilized reverse osmosis water as the cooling fluid (deionized water will attack metals). The unit pumped 75.6 L/min of water at 5.1°C, accomplishing a Δt of about 5.5°C. The chilled water circulated through the double-walled custom cooling jacket on the 50S during pulverization and through the cooling jacket on the agitation tank after the grout had been transferred. The chilled water hoses and all cold surfaces on the chiller were insulated to minimize condensation.

Grout Injection Pumps

Two grout injection pumps were used in the SSSPT-F experiment. A constant-pressure, helical screw (Moyno) pump was intended for use at injection pressures below 2 MPa. However, use of the Moyno was discontinued early in the experiment when it generated heat, initiating premature grout set.

A piston-type, positive displacement pump capable of delivering 20.6 MPa pressure was utilized for the remainder of the experiment. Injection pressures during grouting of the primary holes were limited to 3.4 MPa, but

equipment changes prior to the grouting of the secondary holes permitted pressures as high as 8.2 MPa.

Injection Pipes, Valves, and Fittings

The injection equipment setup is shown schematically in Section 3, Figure 3-3. All metal parts contacting the grout were #316 stainless steel. Numerous fittings were necessary to connect the equipment. Components consisted of:

- 1.9-cm ID thermoplastic, nylon 11-lined grout hoses (34 MPa working pressure) equipped with adequate whipchecks (as specified in established SNL pressure safety guidelines);
- "full-flow" Swagelok and other quick-connect fittings;
- Westech in-line, flow-through saddle diaphragms with oil-filled instrument protectors;
- 10.16-cm-diameter Westech pressure gauges;
- 1.9-cm ID schedule 80 pipe and pipe fittings;
- Whitey Series 60 ball valves with "dead space" inserts;
- one way gate valve;
- BS&B Safety Systems rupture disc, complete with rupture disk body;
- concentric reducers;
- low-pressure hose (for transfer of pulverized grout from the 50S to the agitation tank).

The injection system was protected by the rupture disk. During the injection of the primary holes, pressure was limited to 3.4 MPa. This pressure was increased to 6.9 MPa for the grouting of the secondary holes.

Inflatable Packers

Both fixed- and sliding-end inflatable packers were used during grouting. Fixed-end guard packers were used to prevent the flow of grout into the central gas injection hole and any receiver (sniffer) or slab-external holes that showed signs of grout communication. These packers prevented extruding grout from filling nearby open holes instead of permeating adjacent fractured rock. The packers were manufactured by Baski, Inc. of Denver, CO, and were designed to properly seat in the 15.2-cm holes. Metal portions of the Baski packers were #316 stainless steel. The packers were mechanically restrained to prevent vertical movement and were equipped with pressure gauges to monitor element pressures. Guard packers were 3.7 m long with a 3-m inflatable element and were inflated with nitrogen to 4.1 MPa during grouting of the primary holes and to 6.9 MPa during secondary grouting. Two guard packers were on hand at the start of grouting; a third was added during grouting of the primary holes, and two more were obtained prior to grouting the secondary holes.

A lubricated, sliding-end packer was used to seal the injection hole and permit pressurized grout injection. This 14-cm-diameter packer was 1.2 m in total length and had a 45.7-cm-long inflatable element. It was inserted into the hole and inflated prior to grout injection. Inflation pressures ranged from 4.1 to 5.2 MPa for the primary holes, and from 8.9 to 10.3 MPa for the secondary holes. Nitrogen inflated the packer during primary grouting, and water (delivered via an air-powered pressure intensifier pump) was the inflation fluid used during secondary grouting. Construction and pressure testing of all packers were approved by the WIPP SNL Pressure Representative.

Analytical and Data Acquisition/Display Equipment

During grouting activities, all pulverization/mixing, particle size analyses, and rheological analyses were conducted by Westinghouse Experimental Operations personnel as directed by the Principal Investigator. Pumping and injection control were accomplished by Denver Grouting personnel aided by the DAS computer operator, who was either a RE/SPEC, Inc. or Experimental Operations employee.

Data Acquisition System

A state of the art Hewlett Packard 75000 DAS (housed in an air-cooled cabinet) recorded data from the numerous SSSPT-F gauges described below. Test control was accomplished by coordinating manual operation of injection valving with the data obtained from various instruments. Coordination was facilitated by the use of a 17-in. color monitor positioned at the injection "T." The monitor permitted display of (1) injection pressure, (2) injection rate, (3) rod extensometer deflection, (4) jack loading, (5) rate of grout injection, and (6) various system temperatures.

Both the laser particle size analyzer and rotary viscometer were "free standing" (i.e., not connected to the DAS). They were computer operated, utilized commercial software, and had their own printers.

Laser Particle Size Analyzer

An important aspect of quality control during grouting was the constant assessment of grout particle size and the percent distribution thereof, which were determined at least every 15 minutes by the Malvern Laser Particle Size Analyzer. Analyses began after the last grout component was added to the attritor and, once initiated, continued at least once every 15 minutes until grout injection ended. The laser analyzer is shown in Photo E-2. The unit

analyzed particles varying in size from 1.0 to 600 microns and recorded all data, completing the analyses in less than 5 minutes. Data, presented on the monitor, were also printed.

The Malvern Laser Analyzer operates of Fraunhauffer light scattering theory. Light is deflected by particles in the sample, with the degree of deflection determined by the size of the particle. The deflected light then impinges on a series of 65 light detector rings. Particles of cement in the grout are dominantly plate-like, and the effect of spatial orientation on the degree of deflection is obvious. To overcome this, the laser analyzer averages the results of many readings over a 30-second period. If the instrument determines the correct particle size anywhere within its range (1 to 600 microns), analyses are correct for the entire range. Since the range of interest in this experiment was essentially 1 to 10 microns, three monomolecular samples (spheres of the same dimension), traceable to NIST, were obtained and analyzed 5 times. The laser analyzer always yielded the correct size information. Documentation of these determinations is filed with WIPP Quality Assurance. Particle size data are tabulated in Appendix G.

Rotary Viscometer

A Bohlin Visco 88 portable viscometer, shown in Photo E-3, was used to determine the rheological properties of the thixotropic grout. The Viscometer employs a precise and fixed concentric geometry with a rotating inner cylinder and a stationary outer cylinder. The torque developed on the inner cylinder by the grout is directly related to the sample's plastic viscosity and shear stress through a measuring system geometric constant.

Sheer stress analyses of the thixotropic grout were determined at eight shear rates. All samples were analyzed for rheology. Plastic viscosity and shear stress were plotted as a function of time for each sample. Data were graphically displayed on the computer monitor and printed in numerical form.

Injection Monitor

The 17-in. color monitor was placed on a mobile cart and positioned for easy viewing by the grouting supervisor while he operated the injection valves. Data were displayed in color, graphically and numerically, on two screens: the first showed readouts from the four rod extensometers and the grout injection rate and pressure; the second showed increased loading on each of the four floor jacks, volume of grout being injected, and the temperature of the chiller outlet water. Rod extensometer readings were displayed as multi-colored horizontal histograms. The numerical value of the

movement was simultaneously indicated to the right of each histogram. Grouting operations were easily and effectively controlled utilizing information displayed on the monitor.

Audible/Visible Alarm

An audible and visible alarm, mounted on the west wall of Room L3, was activated by either a specified temperature rise in the chiller outlet or the DAS cabinet, or a vertical movement of the slab in excess of 1.3 mm. No temperature-related alarms occurred during testing, and only one alarm resulted from slab lift (during injection of hole L3425), indicating good performance of the floor restraint system.

Instrumentation

Instrumentation data, except those generated by the particle size analyzer and viscometer, were recorded by the free-standing DAS. Several types of measurements were made during the grout injection phase of the experiment: (1) force at the floor jack base; (2) weight of the grout agitation tank; (3) pressure at the grout injection "T"; (4) temperatures of the chiller, room (ambient), mill, injection "T," and agitation tank outflow; (5) mill torque; (6) slab displacement; (7) grout particle size; (8) grout rheological properties.

Rod Extensometers

Two point rod extensometers, housed in each of four, vertical, 15.4-m-deep drill holes situated within and near the corners of the concrete slab, measured vertical displacement. The extensometer rods were anchored 4.3 and 15.2 m below the upper slab surface, and the transducers connected to them were capable of detecting vertical movements as small as 0.025 mm. The system configuration is described in Appendix B. Extensometer data showing the effects of both grouting and creep closure are presented in Appendix F.

Floor Jack Load Cells

Each floor jack was instrumented with four Houston Scientific 3300 load cells, each able to determine a load increase of ± 2 kg. After the jacks were set in preparation for grouting, the load cells were connected to the DAS and their outputs checked and monitored. Jack load data are presented in Appendix G.



Photo E-2. Laser particle size analyzer.



Photo E-3. Rotary viscometer.

Thermocouples

The grouting equipment included thermocouples that measured all temperatures critical to the experiment. Temperatures of the chiller water, grout in the attritor, and ambient air were measured in the fluid itself. These measurements were made with Type E chromel/constantan thermocouples. Temperature of the injection grout stream was monitored with a Watlow Gordon brand pipe-clamp thermocouple positioned on the outside surface of the pipe near the bottom of the injection "T."

Temperature of the grout being pulverized was measured with an RTD brand thermocouple positioned in the recirculation loop. Temperature was displayed on the 50S and simultaneously recorded electronically on the DAS. Attritor temperature data appear in Appendix G.

Agitation Tank Load Cell

Baseline gas-flow test results suggested that low grout injection rates would occur. Because turbine and Doppler-flow meters are inaccurate at low flow, it was decided to suspend the agitation tank from a sensitive load cell and determine injection rate from tank weight decrease. The tank was suspended (over a secondary containment pan) from a tension and compression load cell (model 3100) manufactured by Houston Scientific International, Inc., and weight was added to the base of the tank to increase its inertia. The load cell was calibrated twice during the experiment by filling the tank with grout and weighing specific volumes on a calibrated electronic balance as they were withdrawn.

The load cell is an instrumented cylinder that deforms linearly when stressed. Foil resistor strain gauges are bonded to the active column area of the cylinder core in a Wheatstone bridge configuration. An excitation voltage is applied to the bridge, and the bridge output is monitored. Stress on the gauge cylinder causes deformation that is sensed by the bridge and reflected in the output voltage.

After an injection hole was filled with grout, the DAS recorded the load cell reading every five seconds for three minutes and computed an average tank weight. When injection began, flow rate was determined by the decrease in tank weight. The load cell sensitivity was ± 756 cc, so weight variances as low as 0.2 gpm could be detected. Specific gravity of the grout was determined periodically during grouting operations by weighing a known volume on a calibrated electronic balance.

During the injection of the primary grout holes, load cell data were noisy and questionable. Before grouting the secondary holes, technicians discovered that an electrical ground was acting as an aerial for the electromagnetic field generated by the nearby 460-volt attritor motor (which was operating during cleaning of the unit). The ground was removed, and subsequent weight data were much improved.

Pressure Gauge and Transducer

Two grout injection pressure measurements were made with Ametek oil-filled saddle diaphragms, which transferred fluid pressure in the grout to an instrumented oil reservoir. One reservoir was monitored with a 10-cm dial gauge mounted on the injection "T." The second was electronically monitored with a Kulite MKM-375 miniature pressure transducer. The transducer employed a stainless steel diaphragm instrumented with a Wheatstone bridge strain cell configured as a half-bridge. The pressure gauge served as a check on the electronic pressure transducer located below it. Instrumentation technicians cleaned these units after each grouting event.

Torque Meter

A torque sensor on the 50S attritor allowed torque to be displayed on the attritor and simultaneously relayed to the DAS via cable. The torque sensor is an electronic transducer that produces an electrical signal proportional to the applied torque. The unit consists of a mechanical assembly coupled to the agitator shaft. The torque-sensitive element is a bonded resistance strain gauge: any change in torque produces a corresponding change in the resistance of this gauge. The strain gauge is positioned in the sensor shaft and connected to a Wheatstone bridge circuit, which produces a variable voltage as a linear function of applied torque. In operation, excitation is applied to the bridge and, with no torque exerted, the bridge remains in balance and the output is 0.0. However, when torque is applied, the torsional strain is transmitted to the bonded strain gauges, causing a change in resistance, which unbalances the bridge and produces a voltage. Attritor torque produced a 4 to 20 Ma current proportional to strain on the gauge via a Daytronic Model 3170 strain gauge conditioner with an internal calibration resistor. The cable between the torque sensor and the DAS incorporated a 300 Ohm resistor that converted the signals to voltages suitable for the DAS. Attritor torque data are presented in Appendix G.

Equipment Cleaning

To facilitate the meticulous equipment cleaning required during grouting activities, all grout apparatus could be disconnected in small pieces via quick-connect fittings. Three fiberglass laundry tubs and one commercial parts cleaning setup, supplied with pressurized water by sump pumps, served as cleaning stations. Waste, pumped into 55-gallon steel drums, was removed from the underground by the WID Management and Operating Contractor and delivered on the surface to WID Environmental Safety and Health. Analyzed solid waste is non-hazardous, but the water phase was alkaline and contained trace amounts of metals. It was used to mix concrete for a surface slab.

Secondary containment units (steel pans, adequate to contain spills) were placed under all equipment except hoses and were easily cleaned with water, brushes, and a venturi-type wet/dry vacuum.

APPENDIX F EXTENSOMETER DATA

This page intentionally left blank.

APPENDIX F: EXTENSOMETER DATA

To measure vertical displacement, two point rod extensometers were housed in each of four, -90°, 15.4-m-deep drill holes situated within and near the corners of the concrete slab. The extensometer rods were anchored 4.3 and 15.2 m below the upper slab surface and were connected to transducers capable of detecting vertical movements as small as 0.025 mm.

Data plots in this appendix present rod extensometer data collected during the experiment. The deepest extensometer anchors show about 6% more displacement than the shallow anchors after 30 days. Ignoring the effect of grouting (shown by vertical offset of the extensometer displacement), data are consistent with extensometer measurements acquired in other tests.

During grouting events, usually only one of the four slab corners showed any significant displacement due to injected grout. The most recent grouting event, however, (injection of L3529) affected all four corners (though only the south end of the slab remained permanently displaced). Displacement was a result of injected grout spreading at the slab/salt interface.

During grouting of the primary holes, only the extensometers at the northern corners were affected. Of the 18 grouting events, 7 resulted in measurable slab displacement, with the largest displacement being recorded during injection of L3425, when the northwest slab corner rose over 1.5 mm.

Extensometer displacement attributed to grouting (that is, displacement in excess of what is expected from typical room closures) is given in Table F-1.

Table F-1. Extensometer Displacement Resulting from Grouting

<u>Extensometer No.</u>	<u>Location</u>	<u>Total Displacement</u>
L3393	NE Corner	1.00 mm
L3394	SE Corner	0.72 mm
L3395	SW Corner	0.18 mm
L3396	NW Corner	1.52 mm

Complete extensometer data are presented in Figures F-1 through F-4. The first two plots show the primary grouting data; the next two show data collected during secondary grouting. Icons inserted within each plot depict a plan view of the concrete slab, showing locations of grout and extensometer holes as well as jack locations. In Figure F-1, for example, the box-shaped icon tracks the displacement of the slab's northwest corner. After 22 days of consistent displacement, the influence of hole L3425 grouting is evident. In Figure F-3, the temporary negative displacement seen during grouting of L3529 seems anomalous.

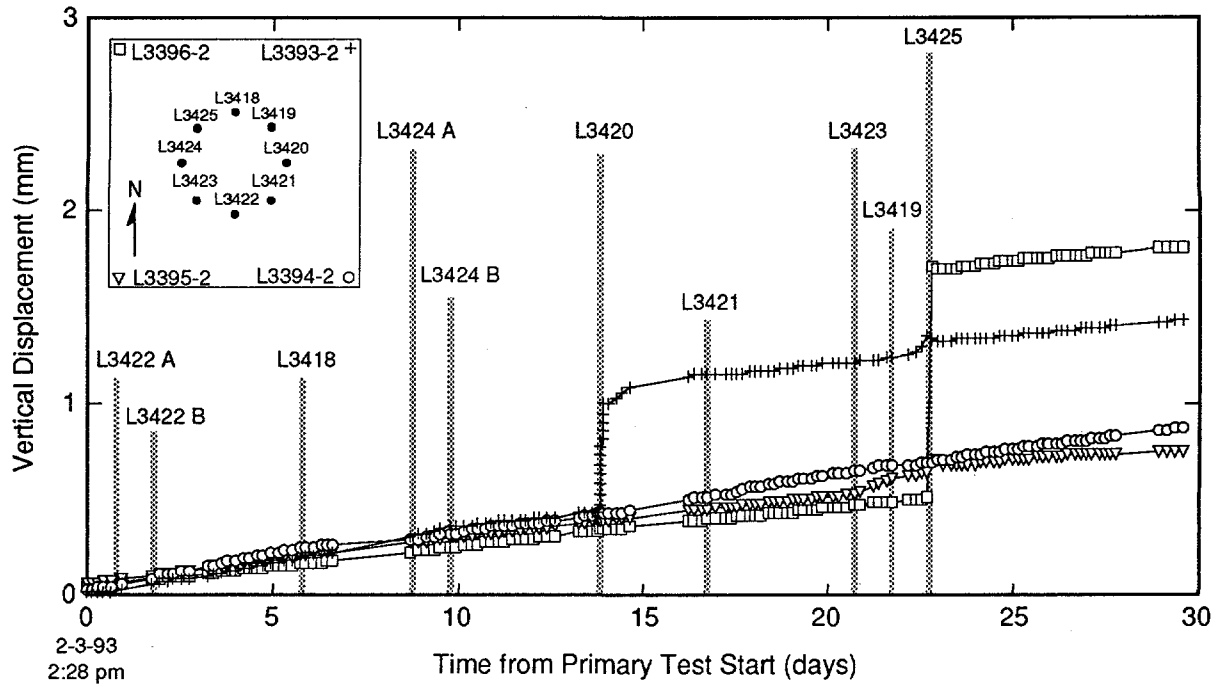


Figure F-1. Displacement of four 4.3 meter long extensometer gauges showing influence from injecting ten primary grout holes.

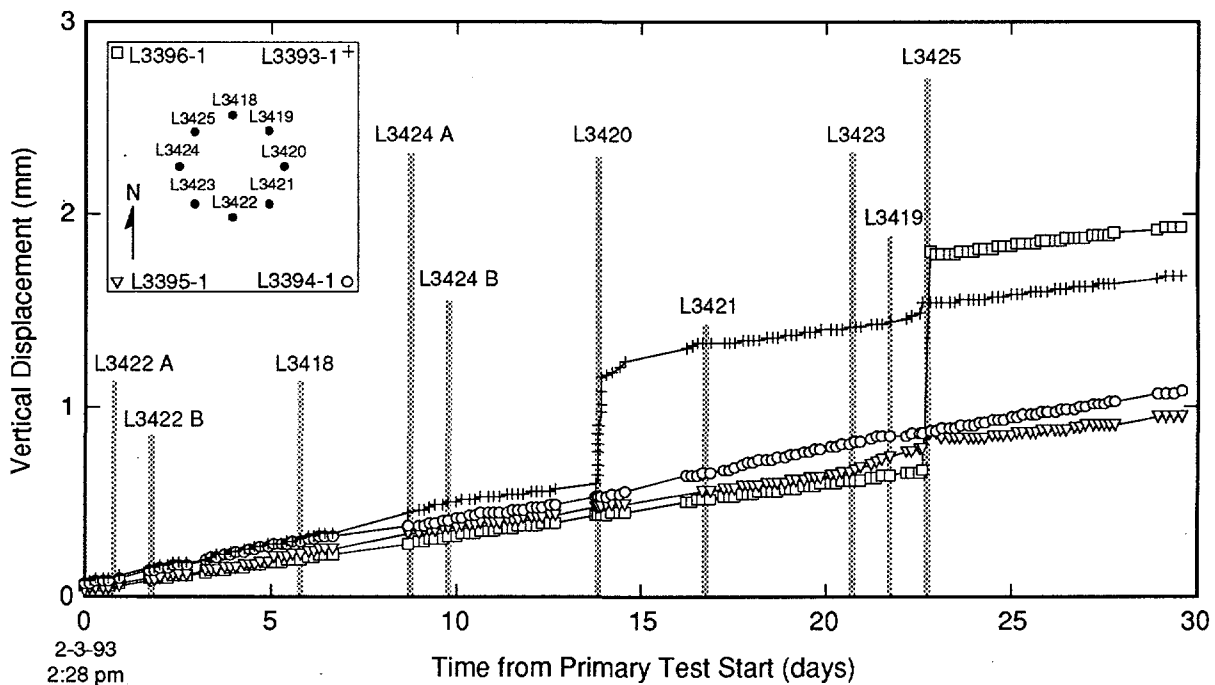


Figure F-2. Displacement of four 15.2 meter long extensometer gauges showing influence from injecting ten primary grout holes.

TRI-6121-162-0

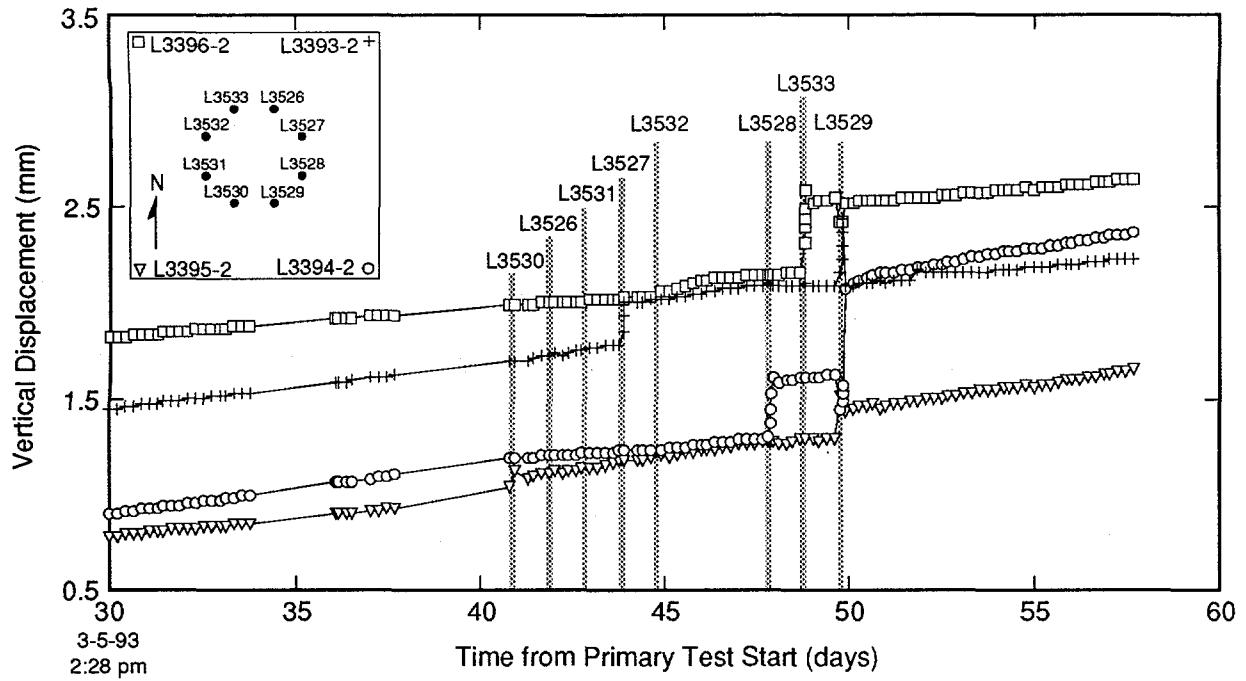


Figure F-3. Displacement of four 4.3 meter long extensometer gauges showing influence from injecting eight secondary grout holes.

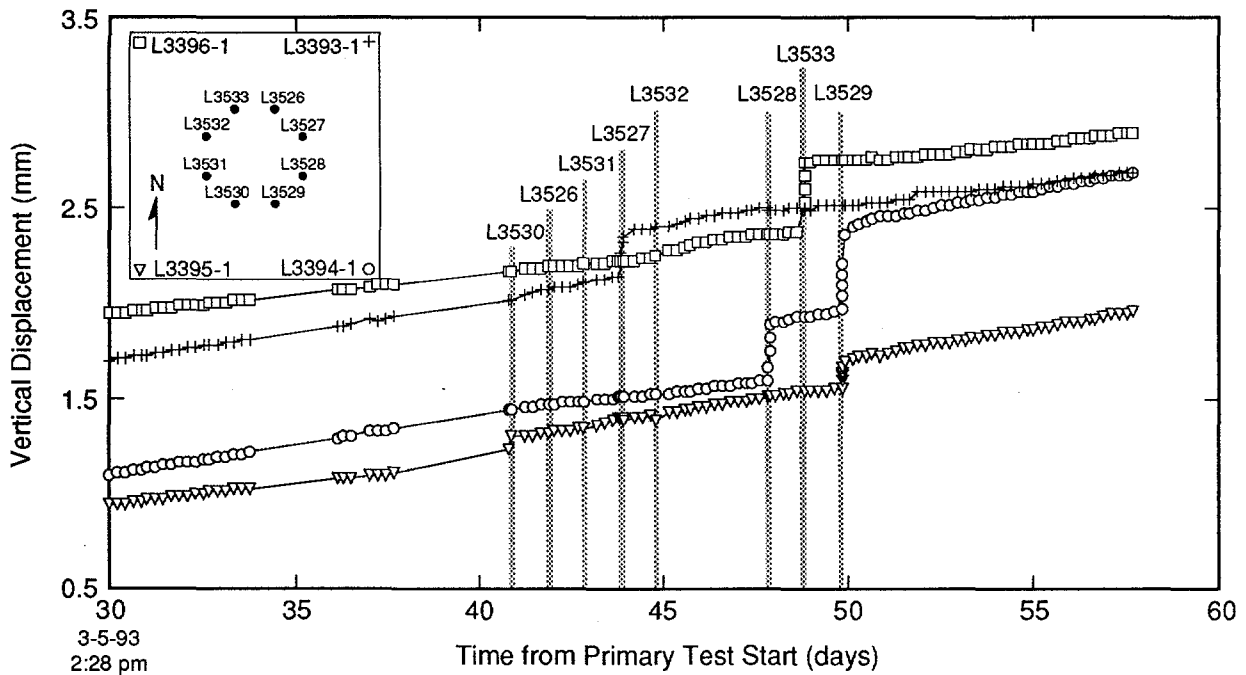


Figure F-4. Displacement of four 15.2 meter long extensometer gauges showing influence from injecting eight secondary grout holes.

TRI-6121-163-0

APPENDIX G: GROUT INJECTION DATA

This page intentionally left blank.

APPENDIX G: GROUT INJECTION DATA

SSSPT-F grouting activity commenced on February 3, 1993 and was concluded March 24, 1993.

Table G-1 presents a summary of the grout injection and extrusion history for all holes. The series of graphs in the following pages, Figures G-1 through G-103, graphically represent the critical data collected during grouting. The graphs are ordered by hole number with six graphs for each hole. Axis scales vary among the plots to show data changes more clearly. The six graphs for each hole are organized as follows:

1. Particle size in microns (μm),
2. Rheology during batching and injection (at slowest recorded shear rate),
3. Measured load increases on the floor jacks (due to the injection of pressurized grout),
4. Temperature of:
 - grout at the agitation tank
 - grout at the base of the injection "T"
 - Room L3 (ambient)
 - cooling water,
5. Grout injection pressure and volume,
6. Torque developed by (and temperature of grout in) the attritor.

Lost and Problematic Data

Attritor torque, jack load cell, grout volume, injection pressure, and grout temperature data were lost for hole L3533. Apparently this loss was the result of a disk failure. Data from the particle size analyzer and the viscometer were not affected because these units recorded data independent from the DAS. Another loss of data occurred while writing disk files for hole L3425. Much of the critical data collected during grout injection was lost. Graphs of data recorded on the DAS lack a critical portion of data from about 20 minutes after the start of injection through the end of grouting. No rheologic data were recorded for hole L3420 because the viscometer was inoperable.

Table G-1. Grout Extrusion in Open Holes

	Injection Hole	Extrusion Hole	Extrusion Depth (m)	Horz. Dist. from Injection to Extrusion (m)	Time from Injection to Extrusion (min)	Volume of Grout Injected (L)	Notes:
Primary Grout Holes	L3418	L3203	2.4	1.80	1	16	
	L3419		not available			13	
	L3420	L3205	1.3	1.79	6	23	During injection of L3420 the slab was lifted ~1 mm.
		L3206	1.3	1.56	6		
		L3204	1.2	2.31	27		
	L3421	none	N/A	N/A	N/A	13	
	L3422A	L3209	2.7	1.80	5	10	
		L3210	2.7	1.59	5		
	L3422B	none	N/A	N/A	N/A	10	
	L3423	L3212	1.2	1.56	8	87	
		L3211	1.8	1.79	20		
		L3X81	1.5	?	20		
		L3X38	0.6	3.48	42		
	L3424A	L3216	3.1	2.31	6	17	
		L3217	3.3	2.94	6		
	L3424B	none	N/A	N/A	N/A	8	
L3425	L3217	2.5	1.82	10	51	During injection of L3425 the slab was lifted ~1.5 mm. An estimated 12L of grout remained under slab.	
	L3X62	2.2	?	22			
	L3215	slab base	1.79	48			
	L3216	slab base	1.58	48			
	L3214	?	2.30	57			
Secondary Grout Holes	L3526	L3202	slab base	1.79	75	8	
	L3527	L3204	2.0	1.79	10	26	During injection of L3527 the slab was lifted ~0.3 mm.
		L3203	2.7	2.31	17		
		L3205	1.9	1.56	53		
	L3528	L3209	2.6	2.31	6	29	During injection of L3528 the slab was lifted ~0.4 mm.
		L3X16	2.6	3.81	21		
		L3207	slab base	1.57	66		
		L3208	slab base	1.79	66		
		L3206	slab base	1.78	81		
	L3529	L3209	slab base	1.58	38	5	During injection of L3529 the slab was lifted ~0.7 mm.
		L3210	slab base	1.82	38		
		L3X16	?	2.91	64		
		L3X15	slab base	3.19	72		
	L3530	L3211	3.3	1.57	17	22	
		L3212	slab base	1.78	82		
		L3213	?	2.33	82		
L3531	none	N/A	N/A	N/A	10		
L3532	L3216	1.8	1.79	8	73		
	L3215	1.7	1.57	20			
	L3X81	2.2	?	29			
	L3213	1.2	2.32	53			
	L3214	0.9	1.80	63			
L3533	L3215	slab base	2.31	15	10	During injection of L3533 the slab was lifted ~0.5 mm.	
	L3216	slab base	1.81	15			
	L3217	slab base	1.58	15			
	L3202	slab base	1.80	61			

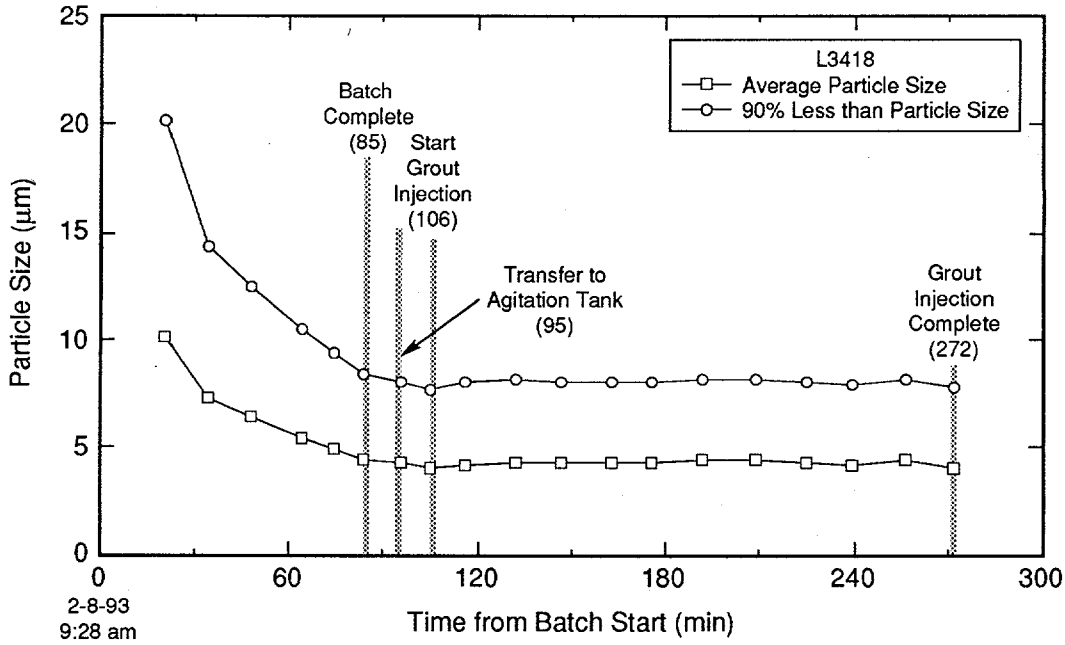


Figure G-1. Grout particle size measured during batching and injection of hole L3418.

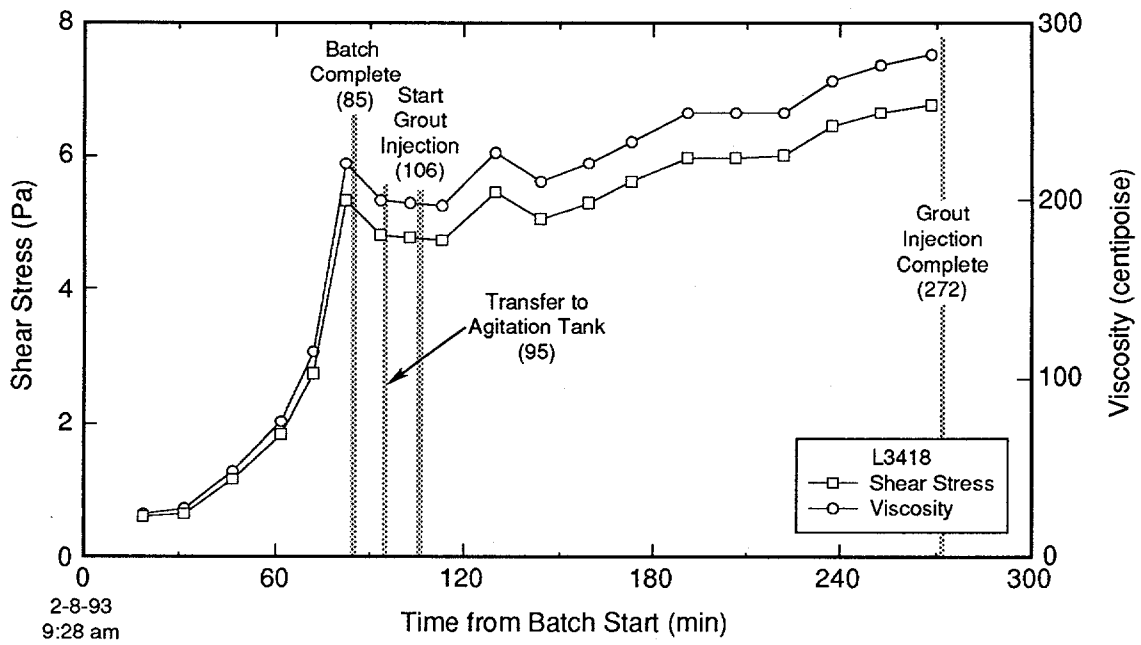


Figure G-2. Grout rheologic properties measured during batching and injection of hole L3418.

TRI-6121-181-0

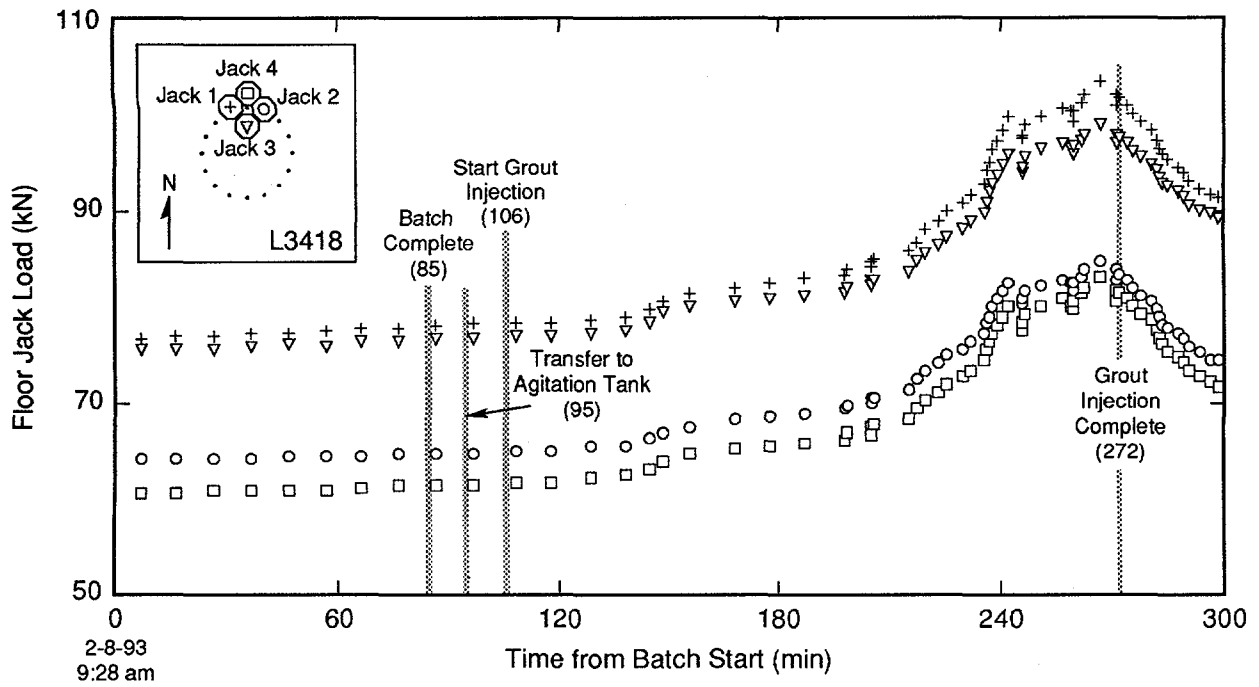


Figure G-3. Load cell measurements acquired during batching and injection of hole L3418.

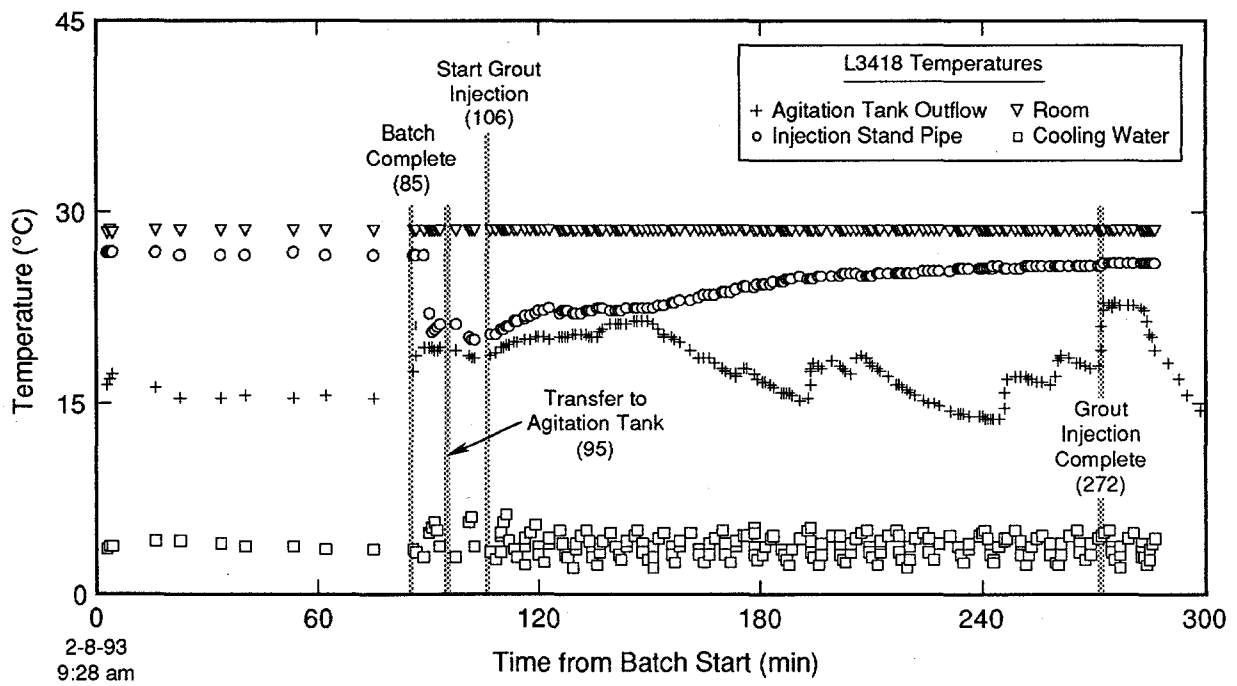


Figure G-4. Temperature measurements acquired during batching and injection of hole L3418.

TRI-6121-144-0

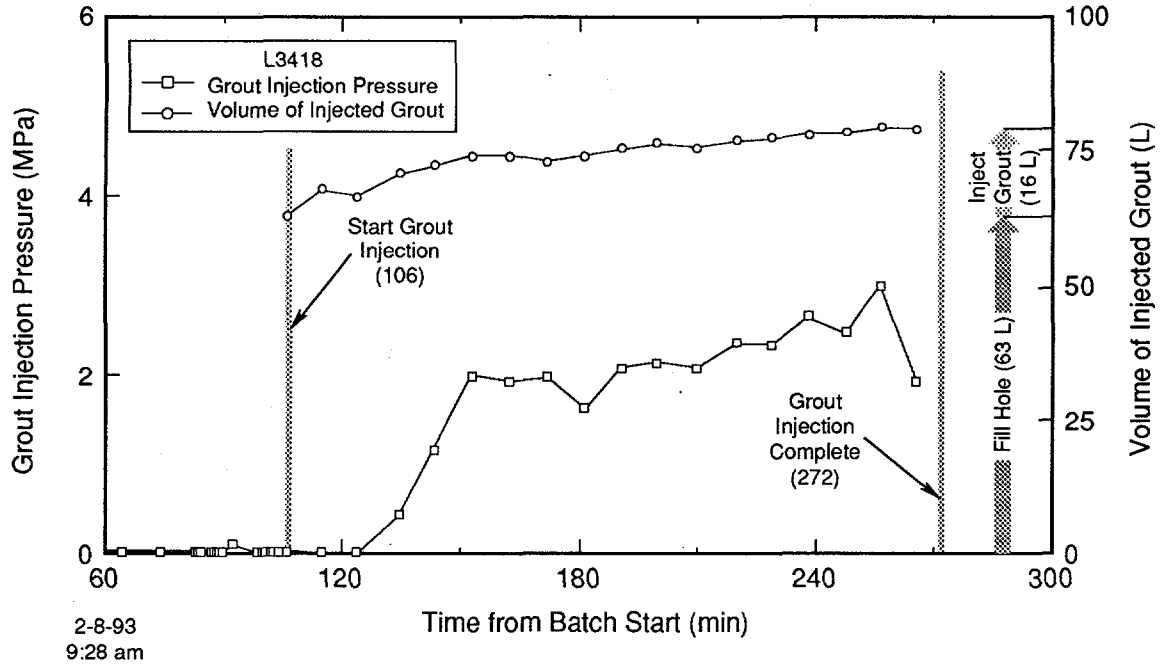
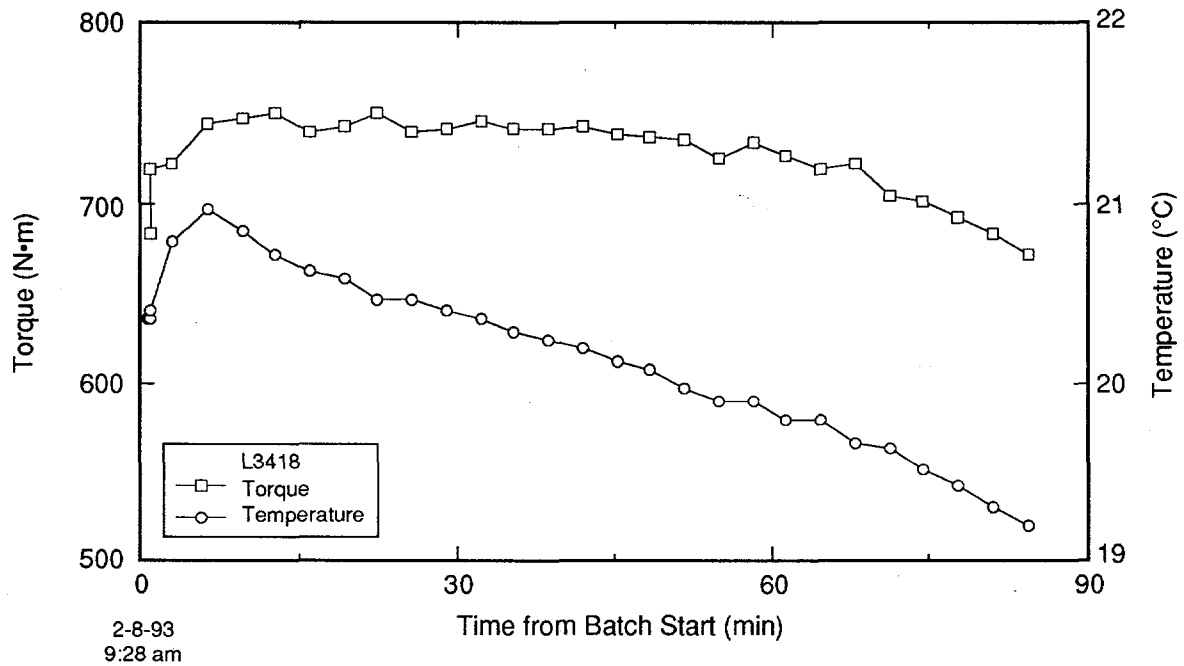


Figure G-5. Grout volume and pressure measured during injection of hole L3418.



TRI-6121-164-0

Figure G-6. Attritor torque and temperature measured during grout batching for hole L3418.

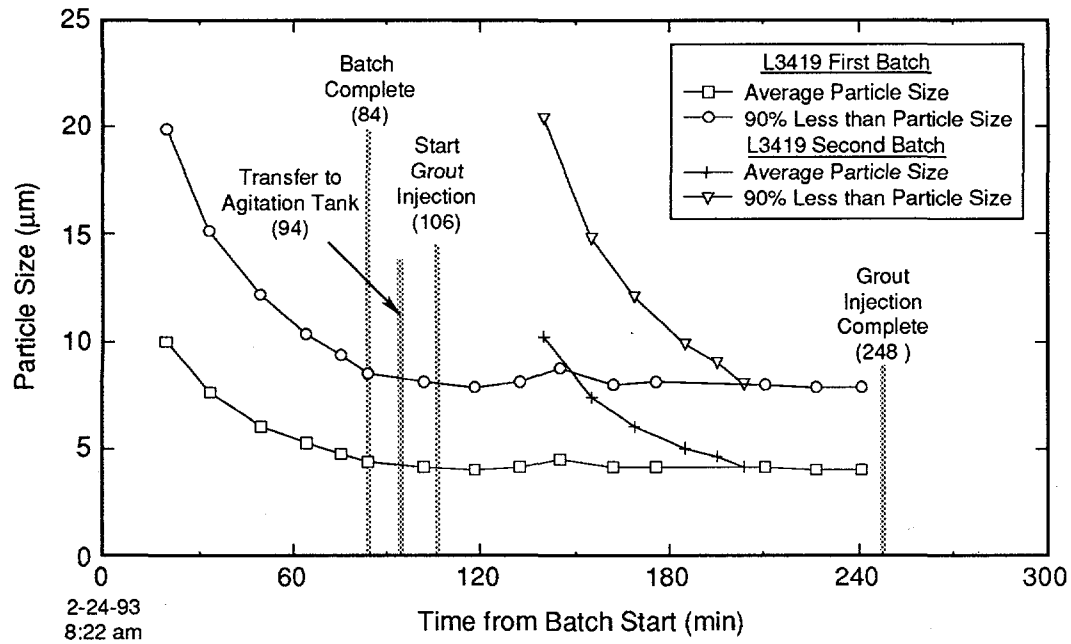
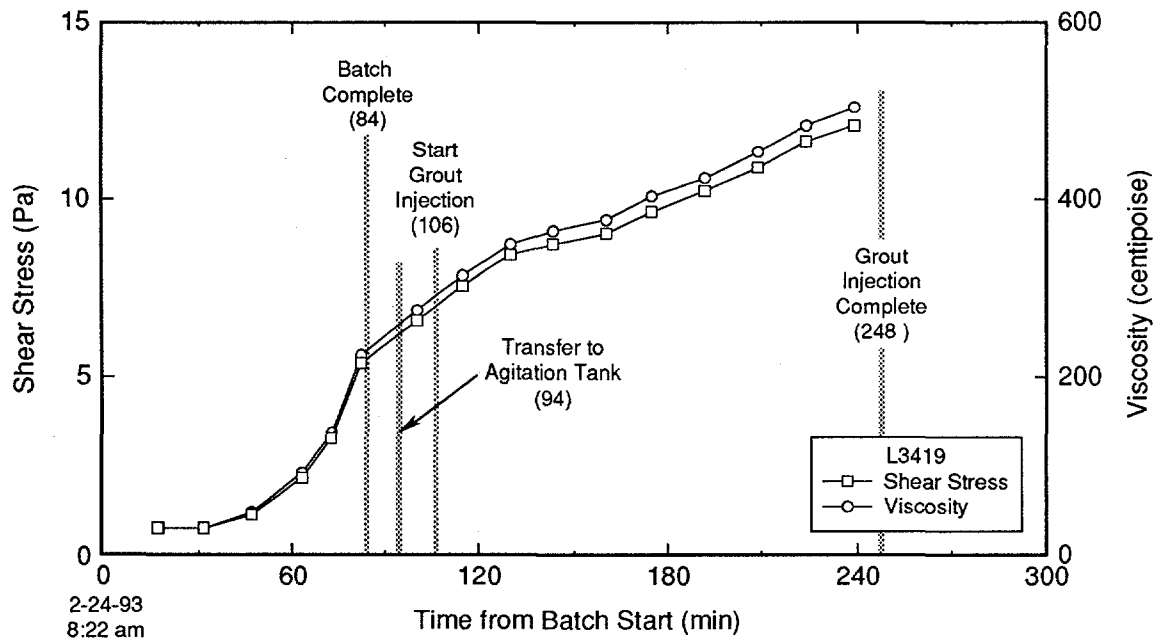


Figure G-7. Grout particle size measured during batching and injection of hole L3419.



TRI-6121-182-0

Figure G-8. Grout rheologic properties measured during batching and injection of hole L3419.

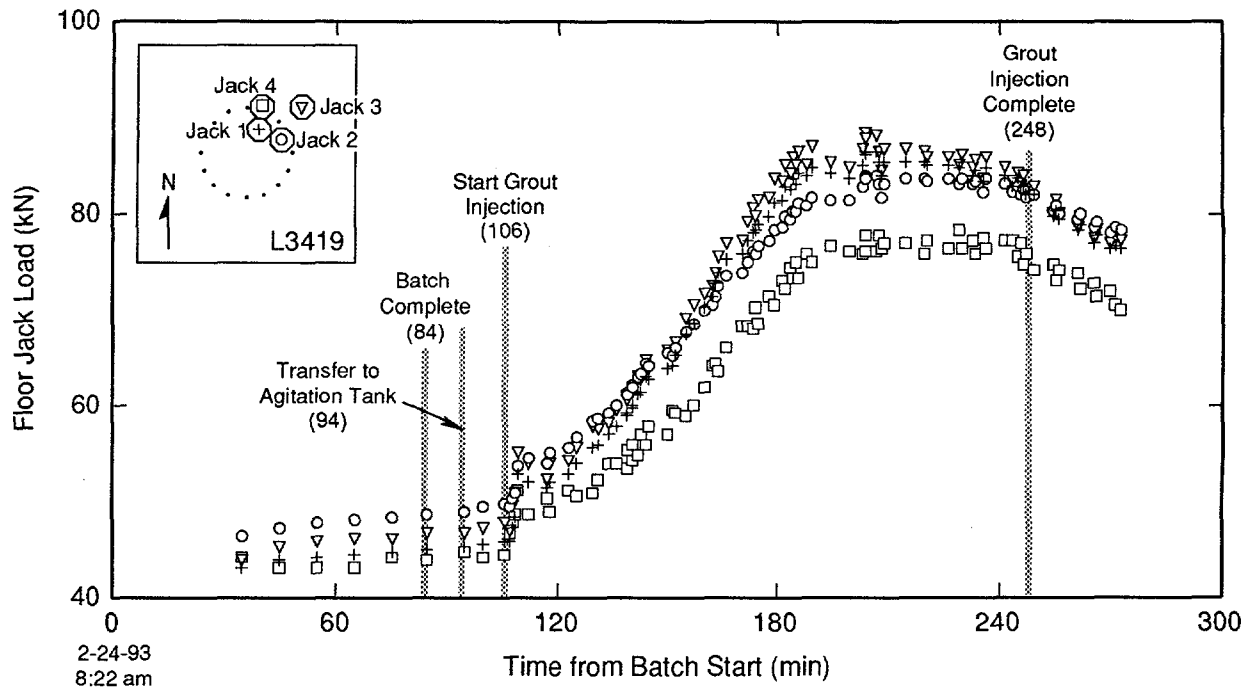


Figure G-9. Load cell measurements acquired during batching and injection of hole L3419.

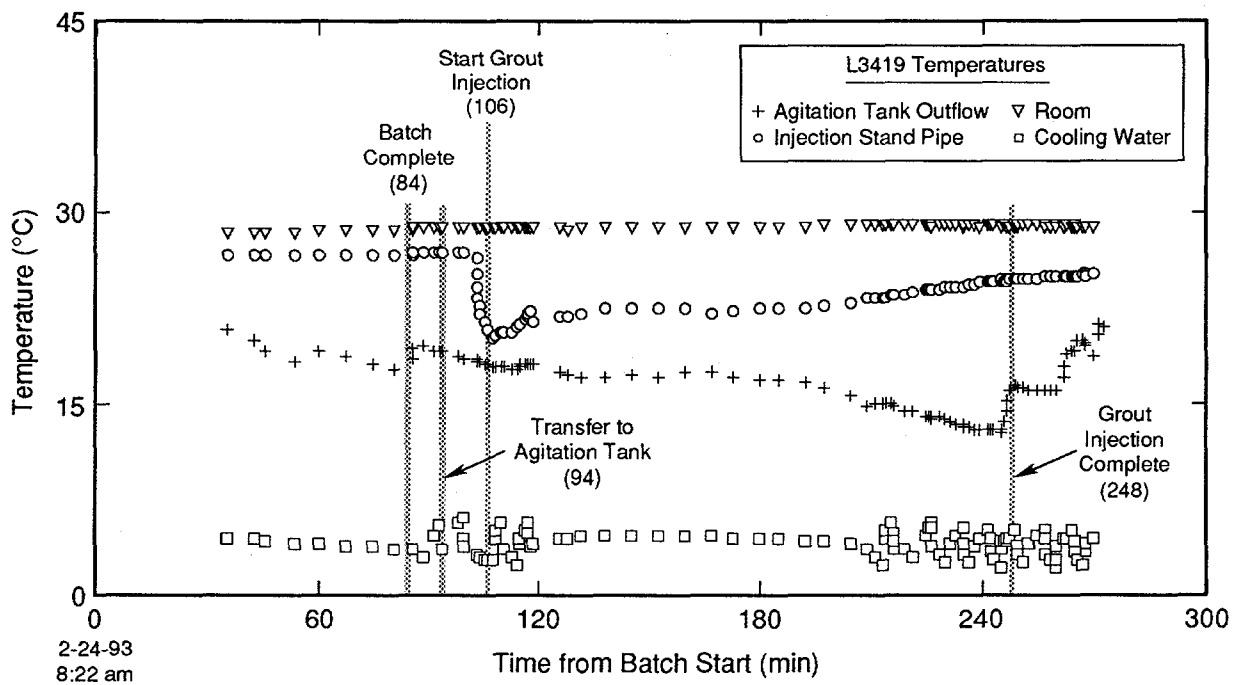


Figure G-10. Temperature measurements acquired during batching and injection of hole L3419.

TRI-6121-145-0

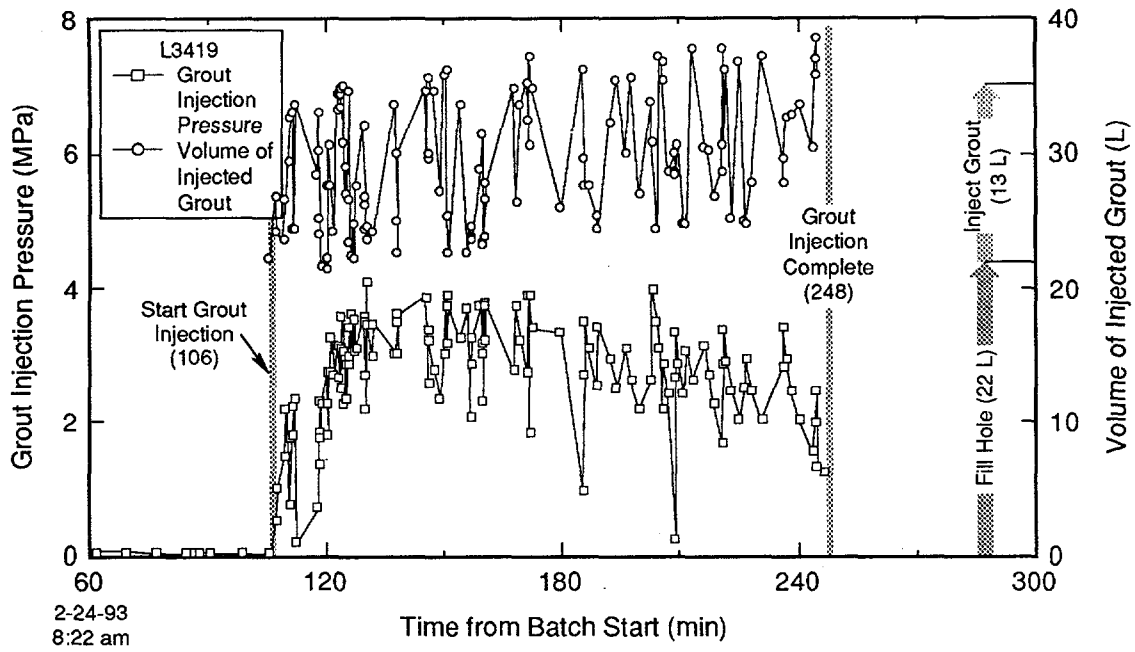
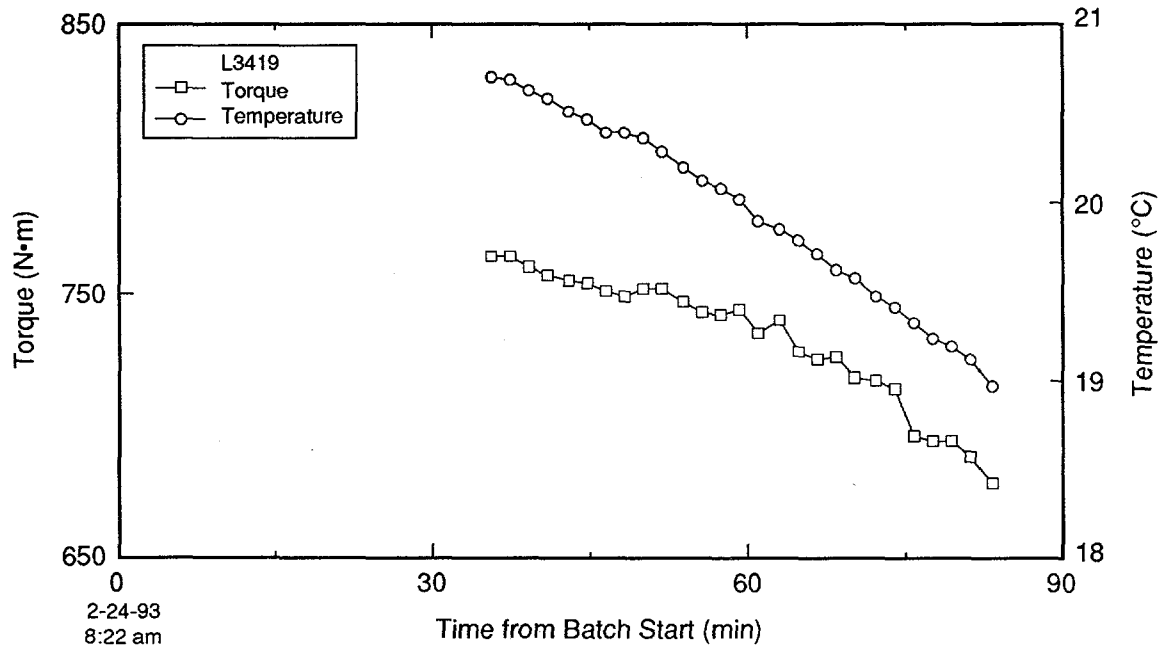


Figure G-11. Grout volume and pressure measured during injection of hole L3419.



TRI-6121-165-0

Figure G-12. Attritor torque and temperature measured during grout batching for hole L3419.

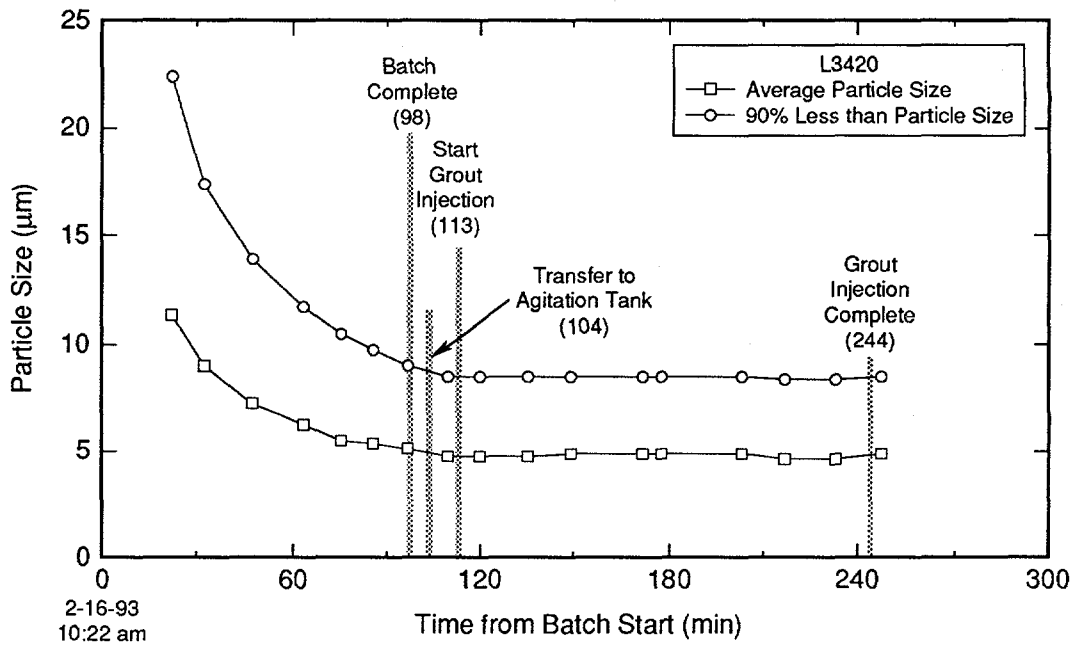


Figure G-13. Grout particle size measured during batching and injection of hole L3420.

No Data Presented for L3420
 Bohlen Viscometer Inoperable

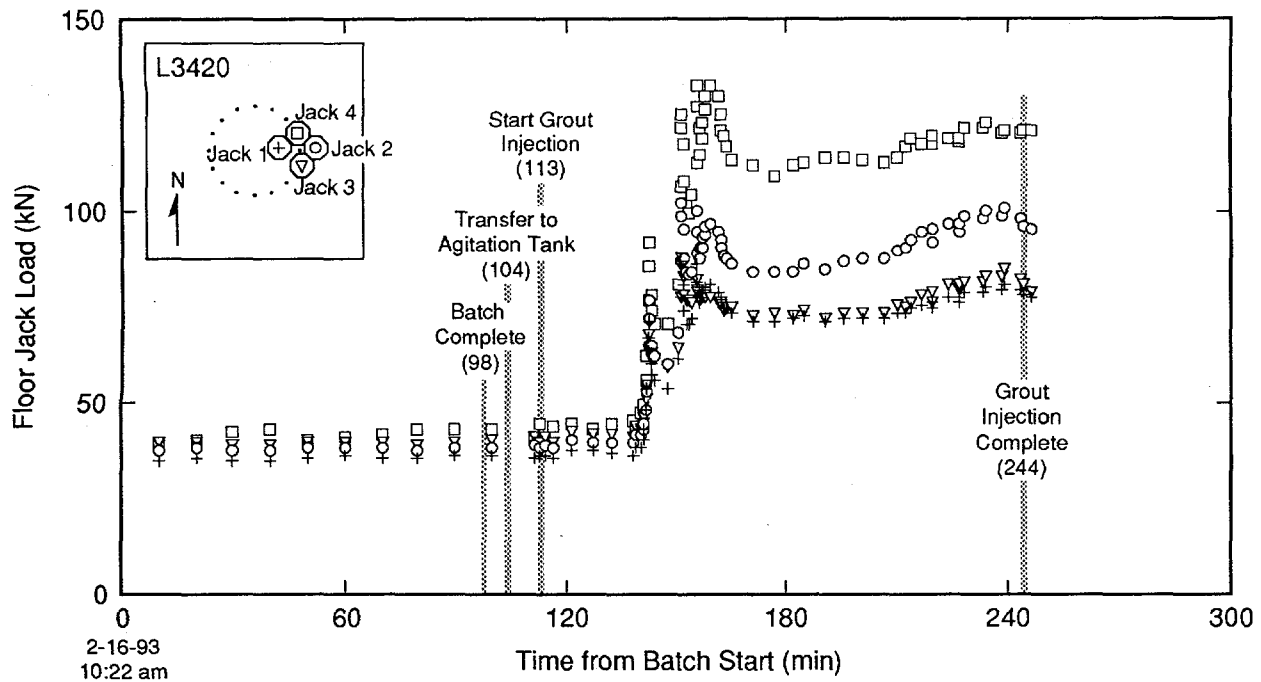


Figure G-14. Load cell measurements acquired during batching and injection of hole L3420.

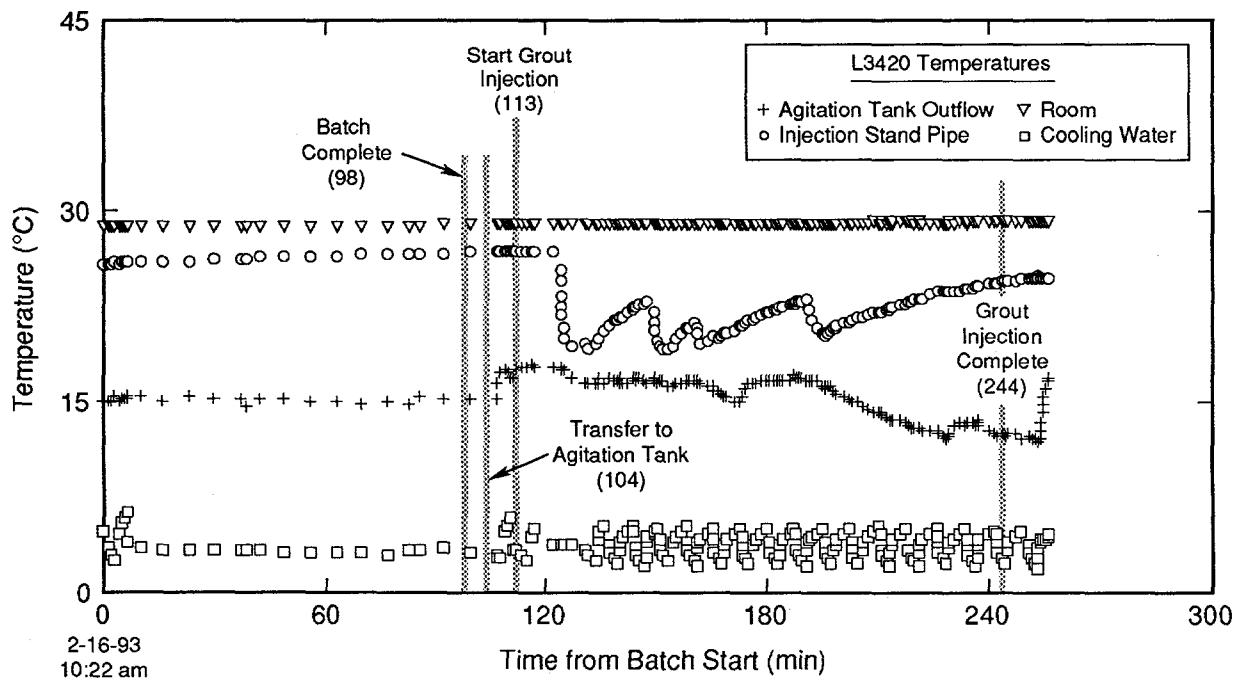


Figure G-15. Temperature measurements acquired during batching and injection of hole L3420.

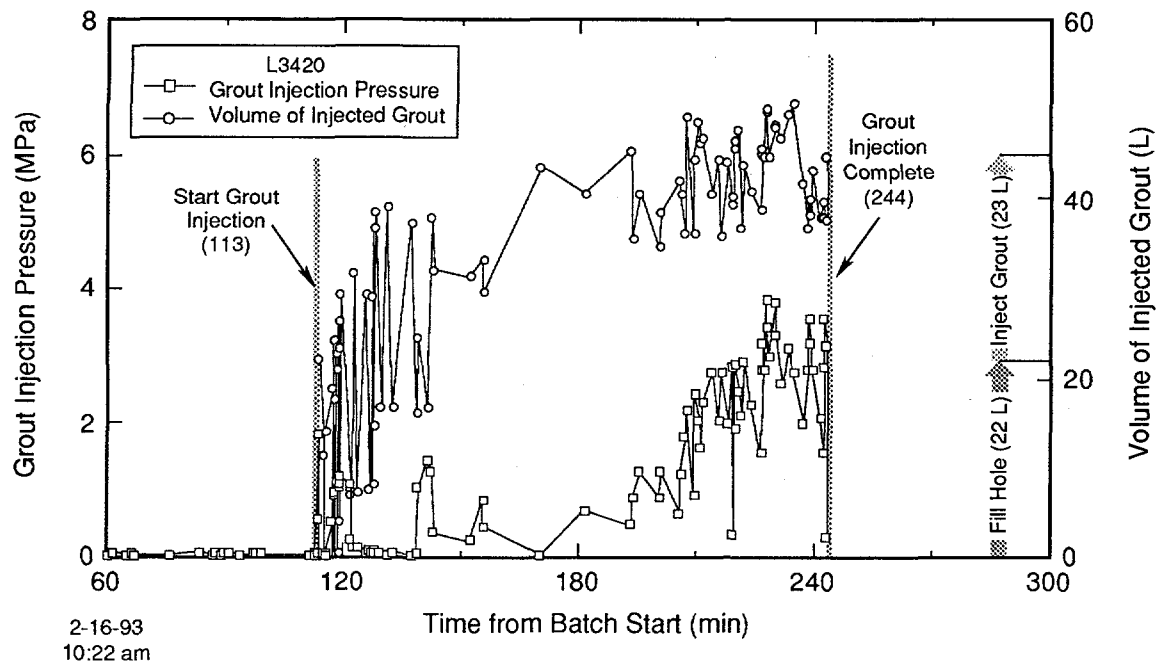
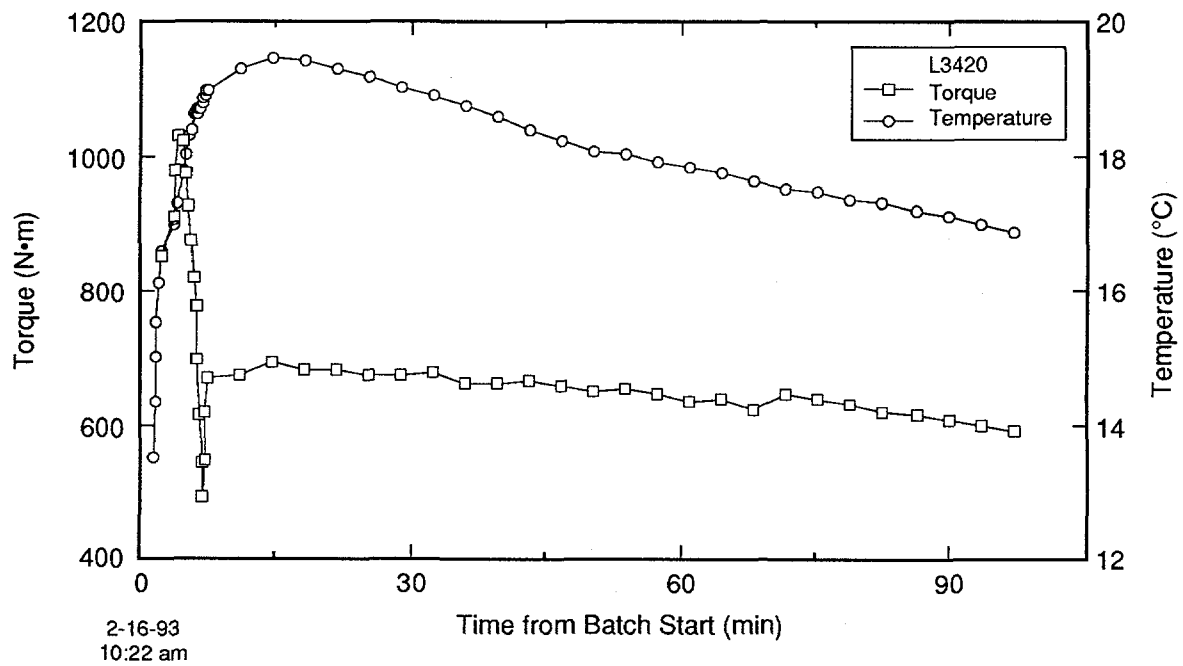


Figure G-16. Grout volume and pressure measured during injection of hole L3420.



TRI-6121-166-0

Figure G-17. Attritor torque and temperature measured during grout batching for hole L3420.

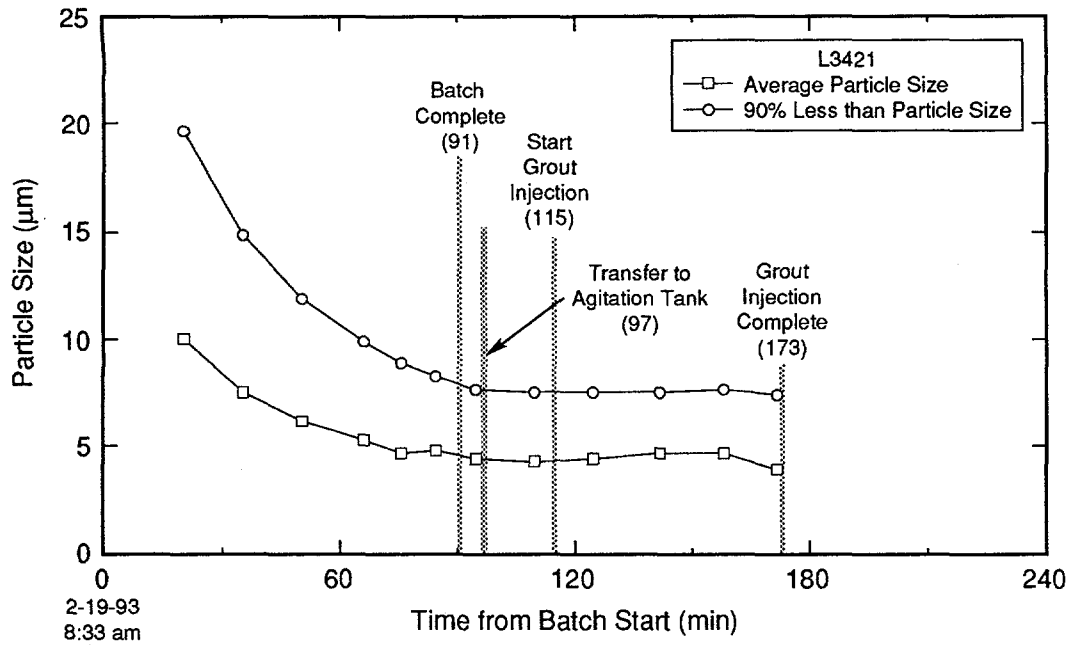


Figure G-18. Grout particle size measured during batching and injection of hole L3421.

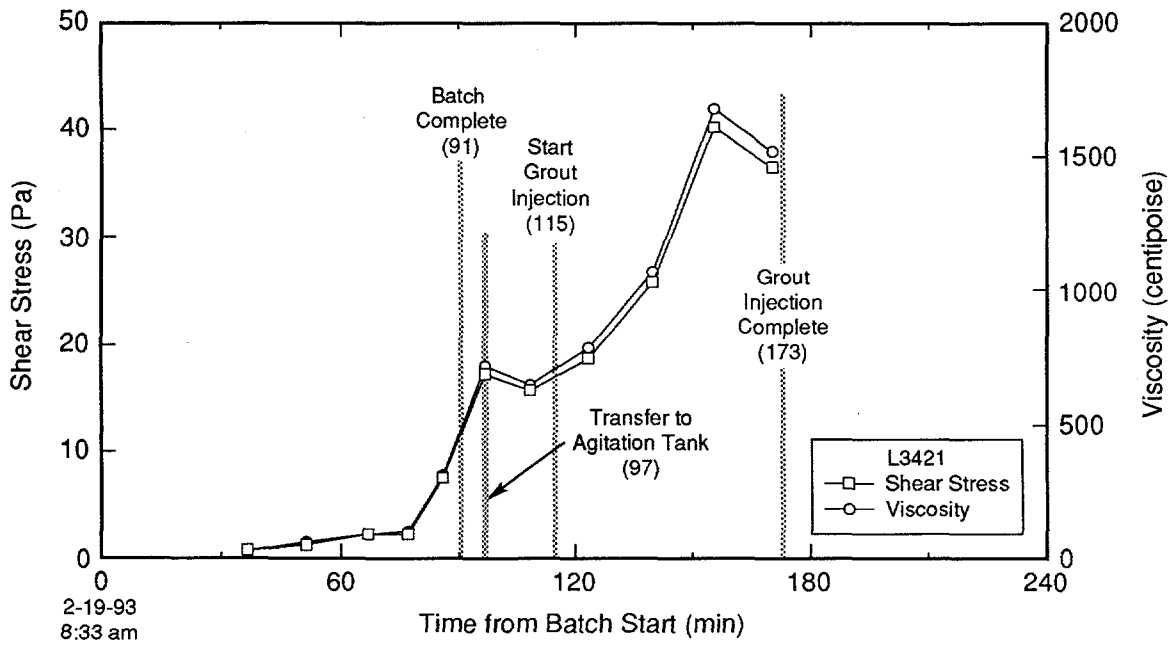


Figure G-19. Grout rheologic properties measured during batching and injection of hole L3421.

TRI-6121-184-0

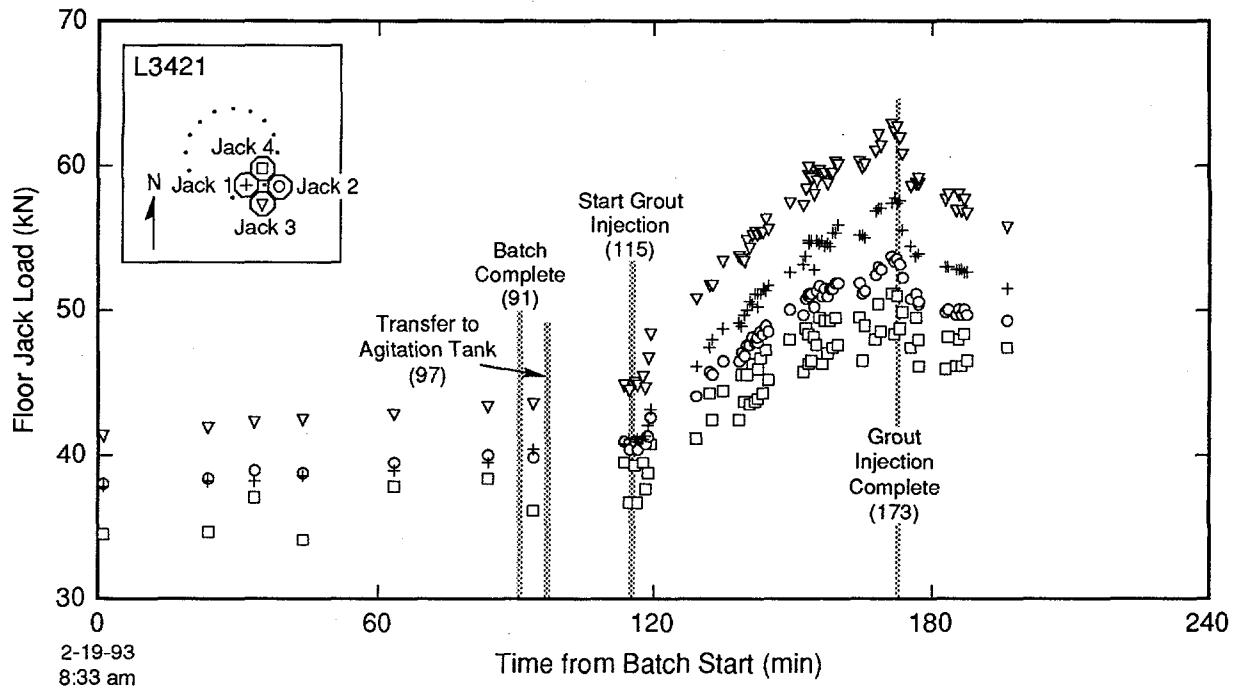


Figure G-20. Load cell measurements acquired during batching and injection of hole L3421.

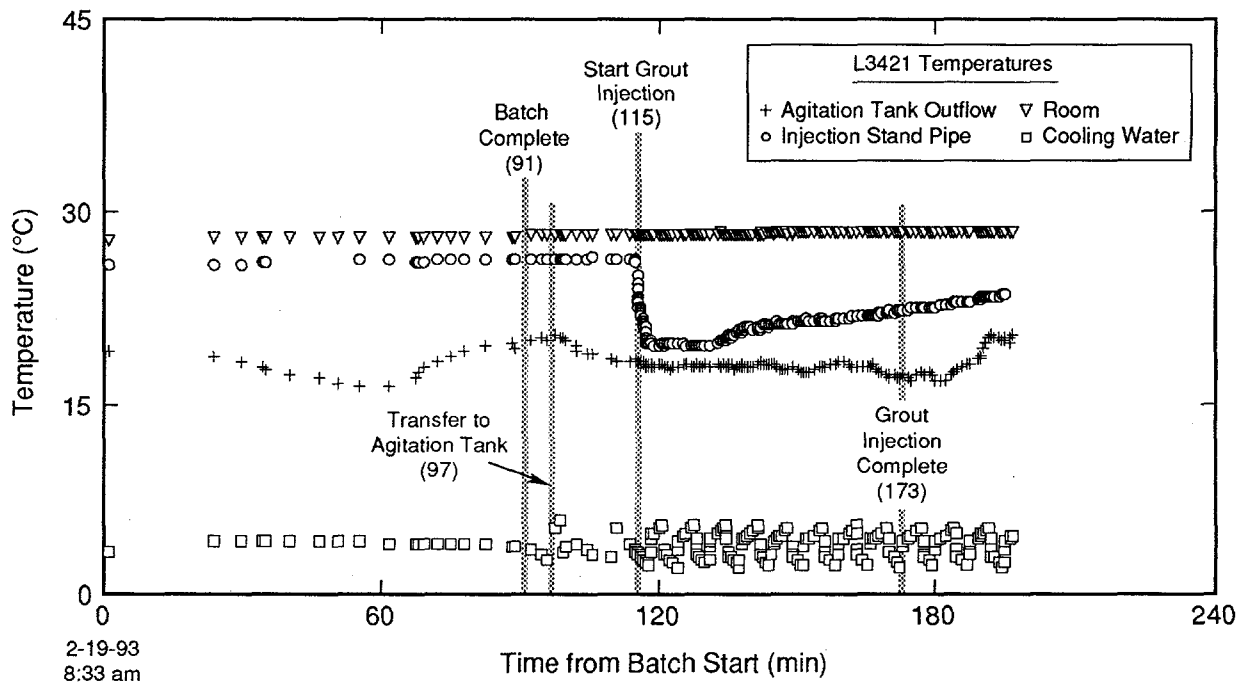


Figure G-21. Temperature measurements acquired during batching and injection of hole L3421.

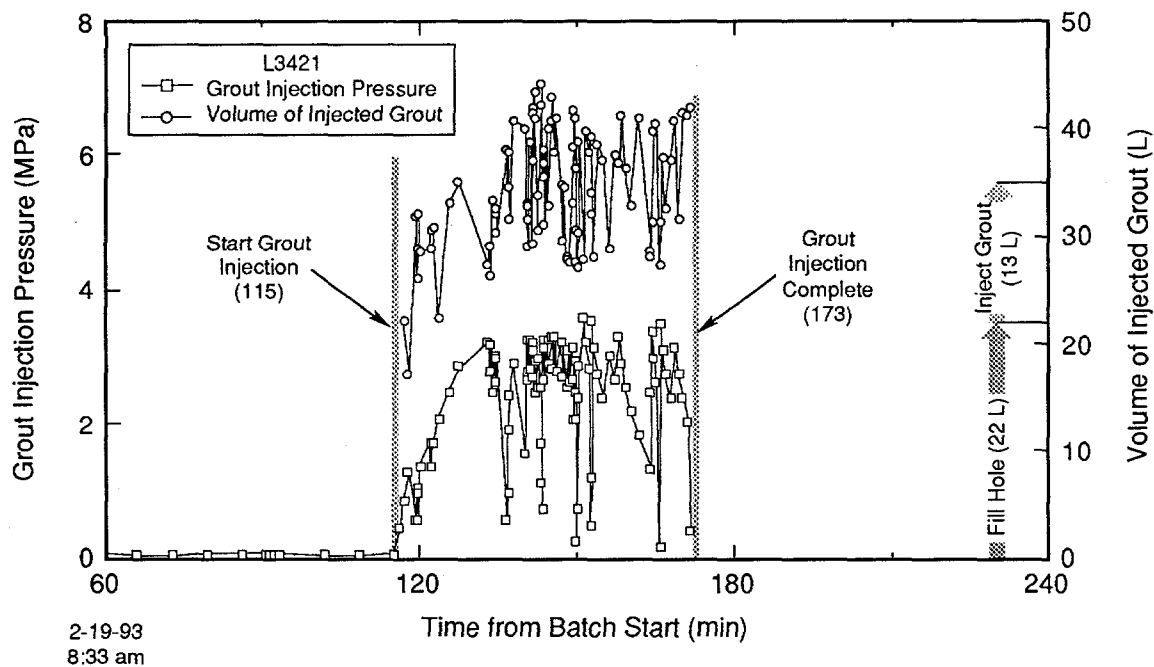


Figure G-22. Grout volume and pressure measured during injection of hole L3421.

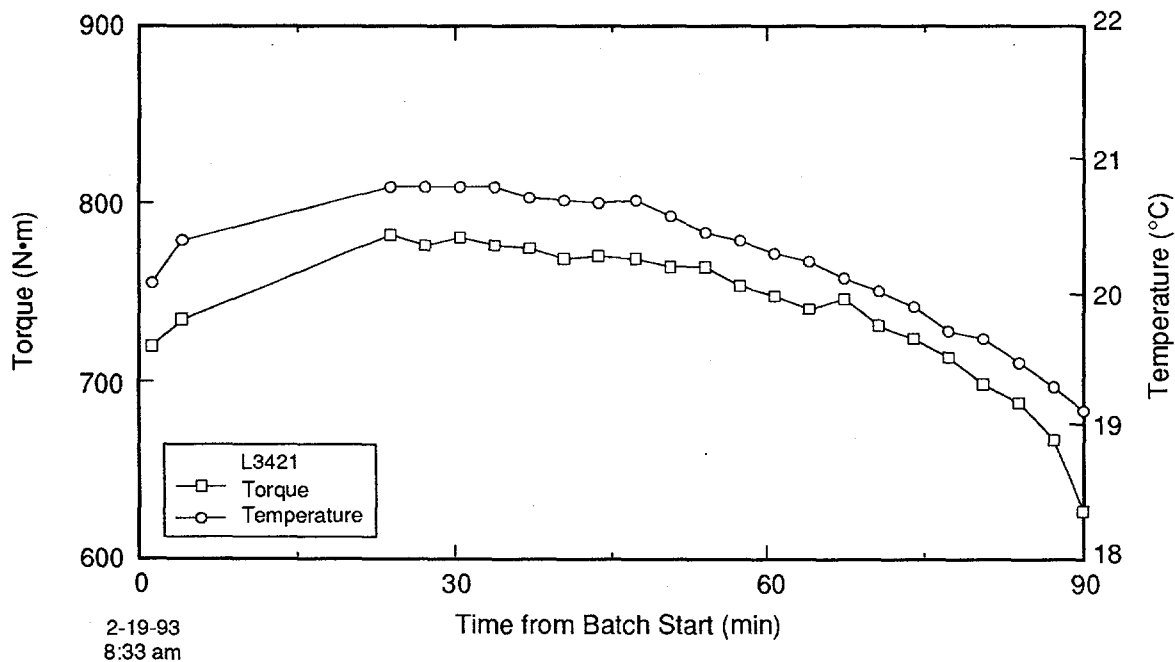


Figure G-23. Attritor torque and temperature measured during grout batching for hole L3421.

TRI-6121-167-0

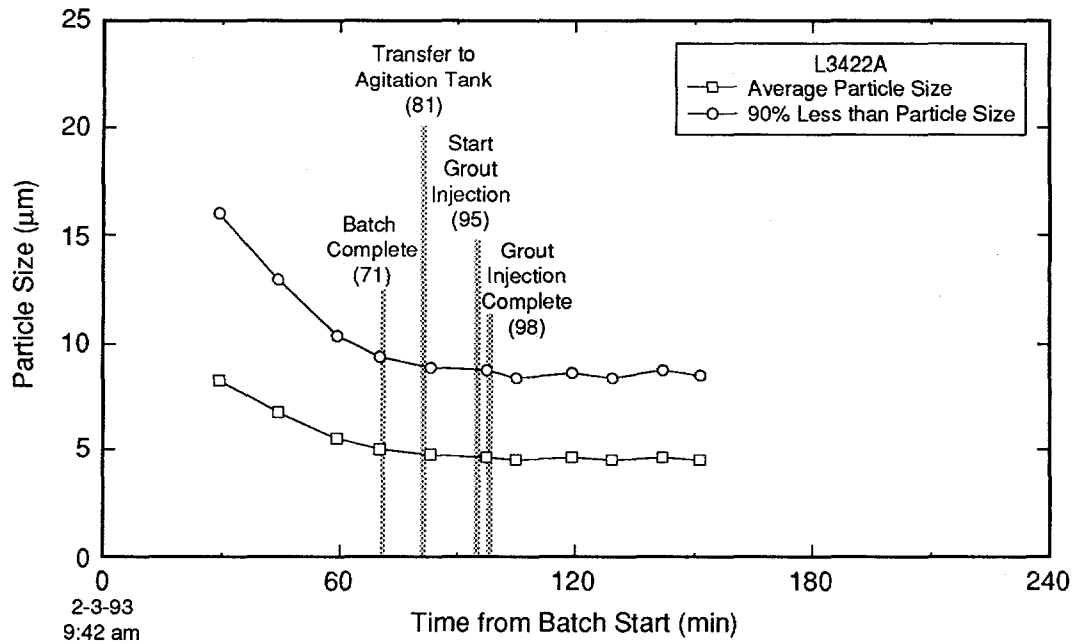
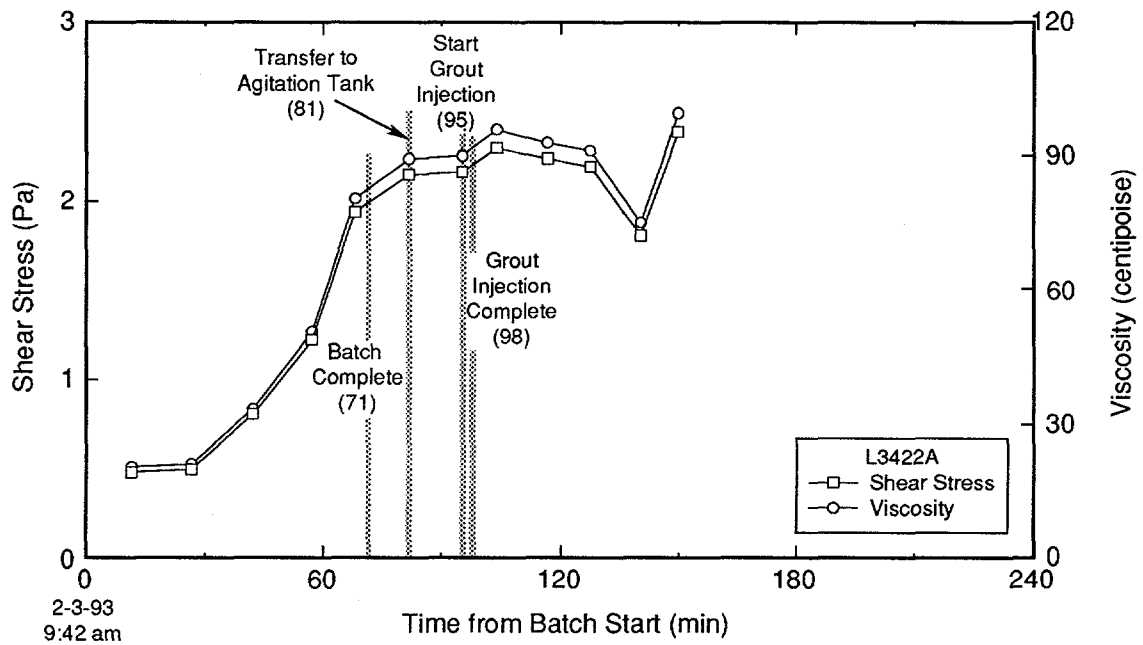


Figure G-24. Grout particle size measured during batching and injection of hole L3422A.



TRI-6121-185-0

Figure G-25. Grout rheologic properties measured during batching and injection of hole L3422A.

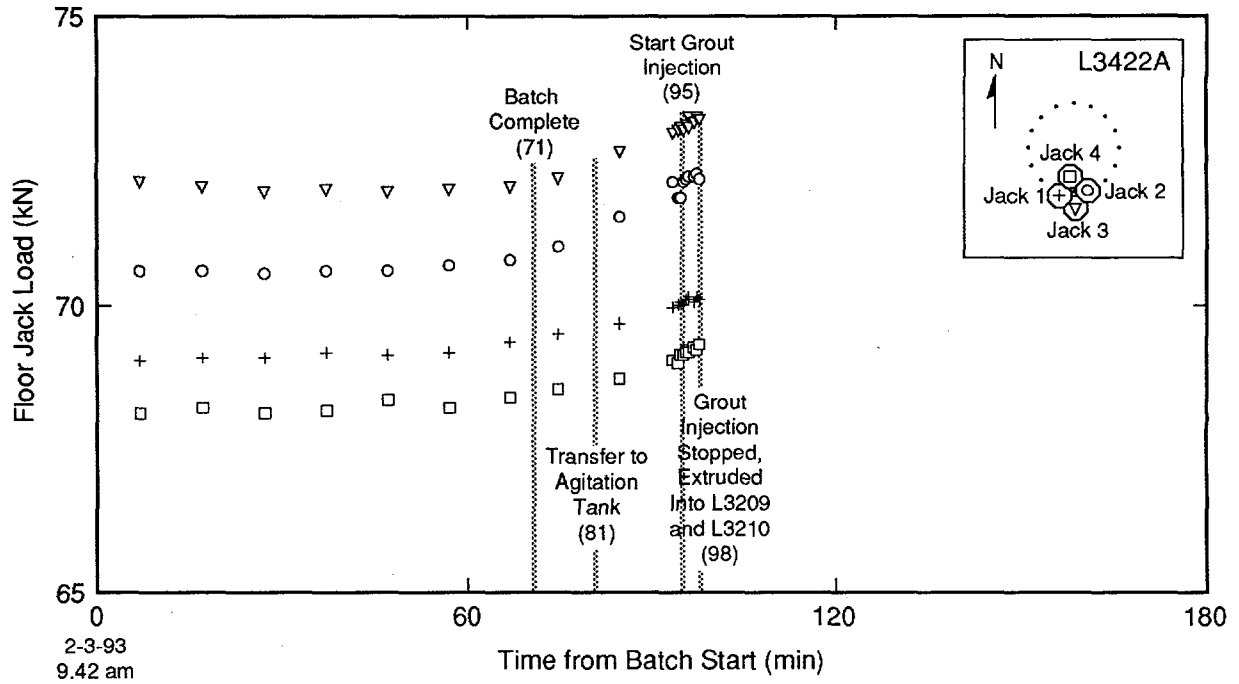


Figure G-26. Load cell measurements acquired during batching and injection of hole L3422A.

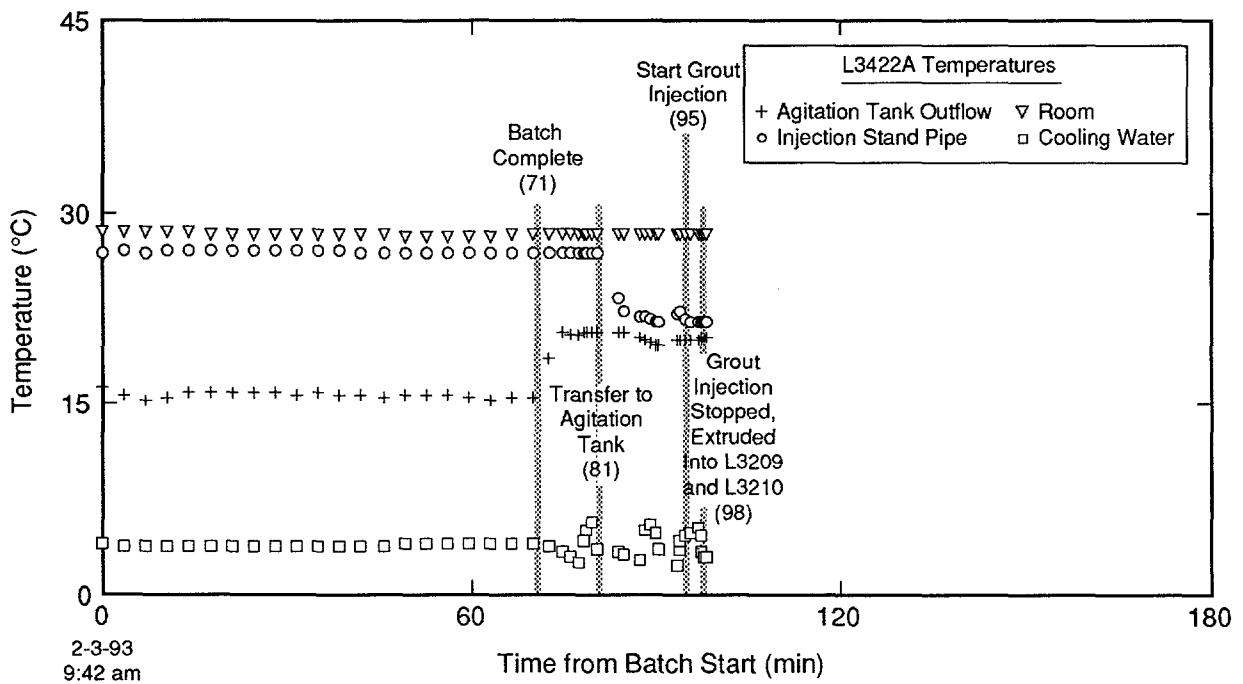


Figure G-27. Temperature measurements acquired during batching and injection of hole L3422A.

TRI-6121-148-0

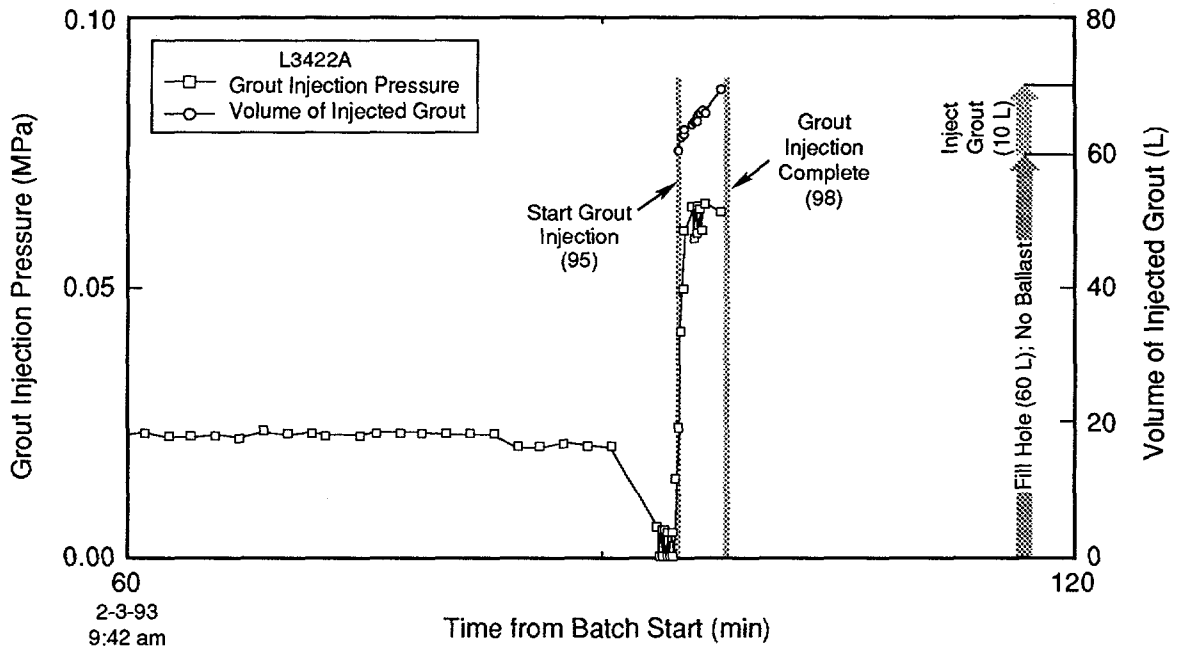


Figure G-28. Grout volume and pressure measured during injection of hole L3422A.

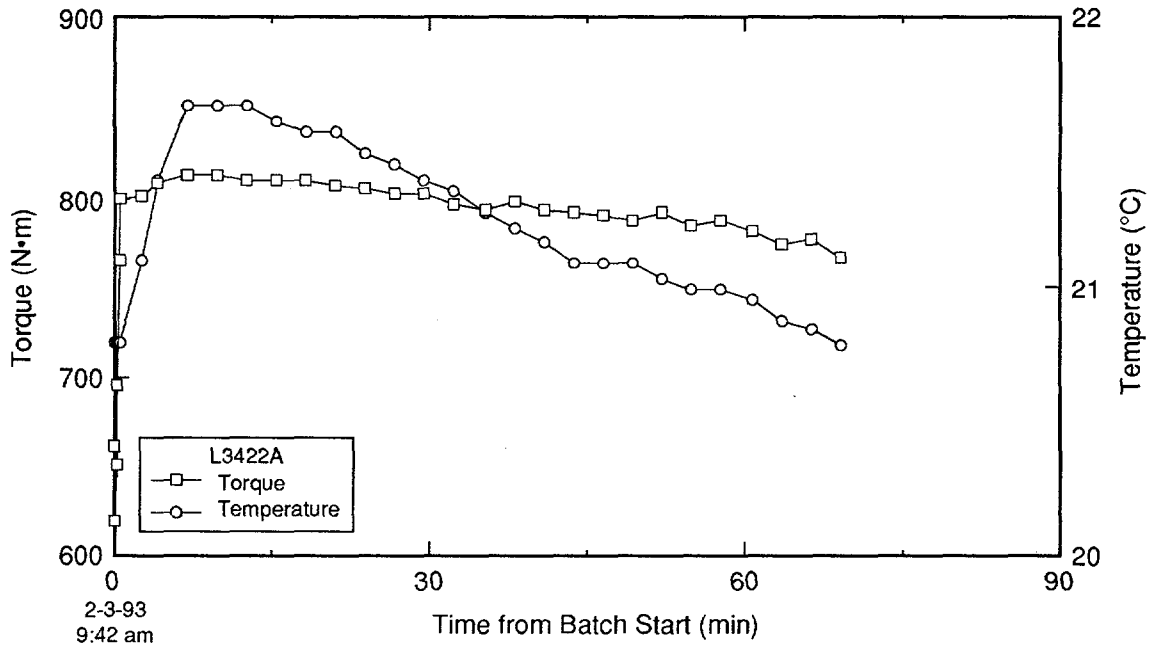


Figure G-29. Attritor torque and temperature measured during grout batching for hole L3422A.

TRI-6121-168-0

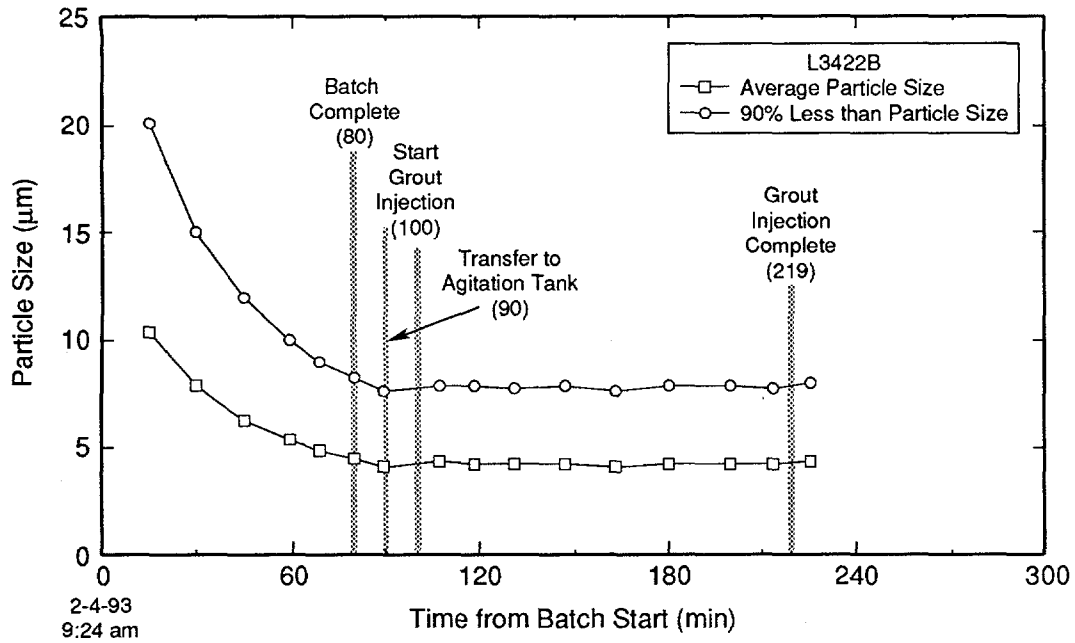


Figure G-30. Grout particle size measured during batching and injection of hole L3422B.

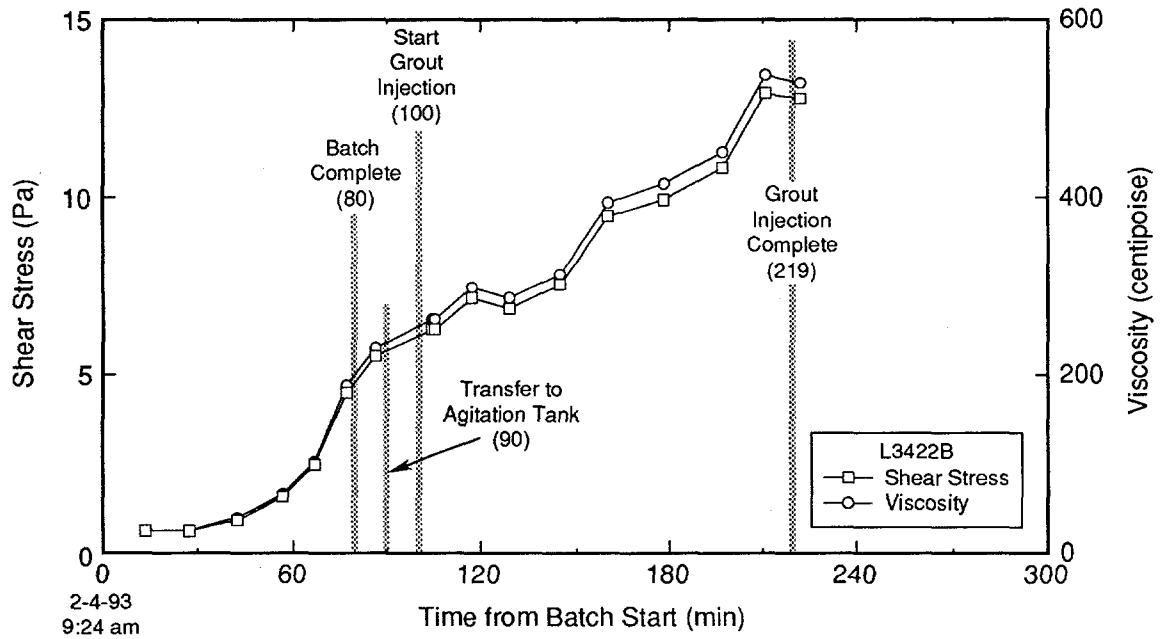


Figure G-31. Grout rheologic properties measured during batching and injection of hole L3422B.

TRI-6121-186-0

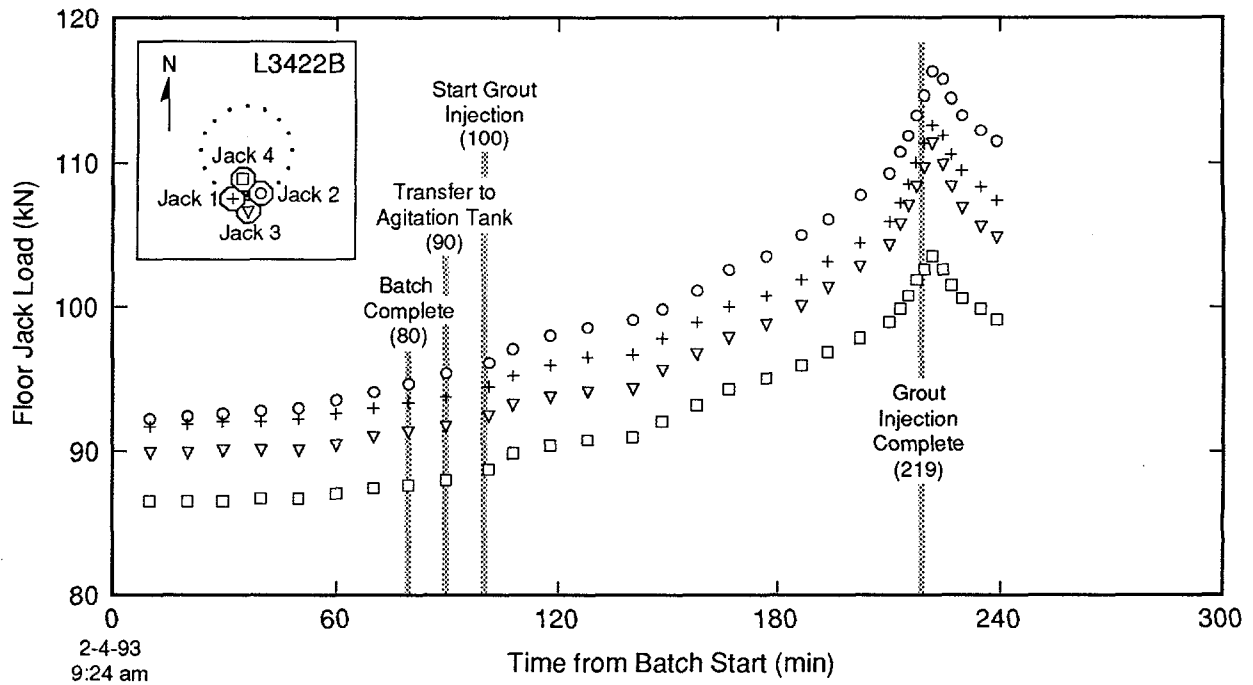


Figure G-32. Load cell measurements acquired during batching and injection of hole L3422B.

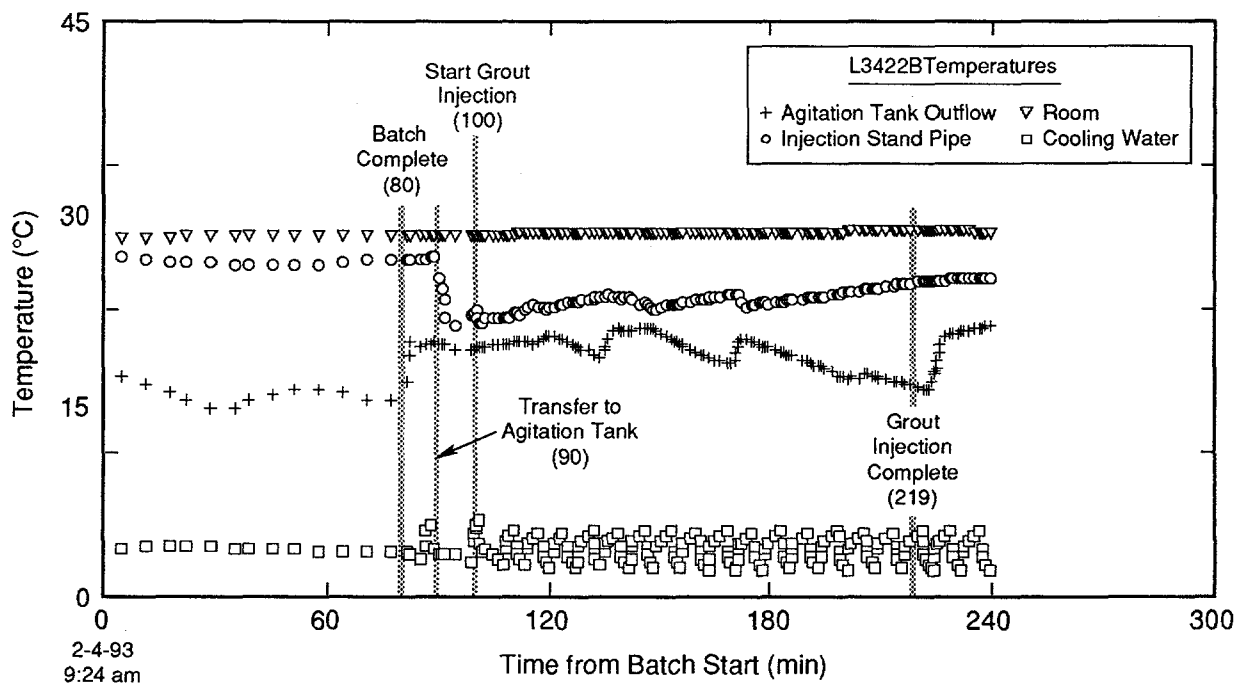


Figure G-33. Temperature measurements acquired during batching and injection of hole L3422B.

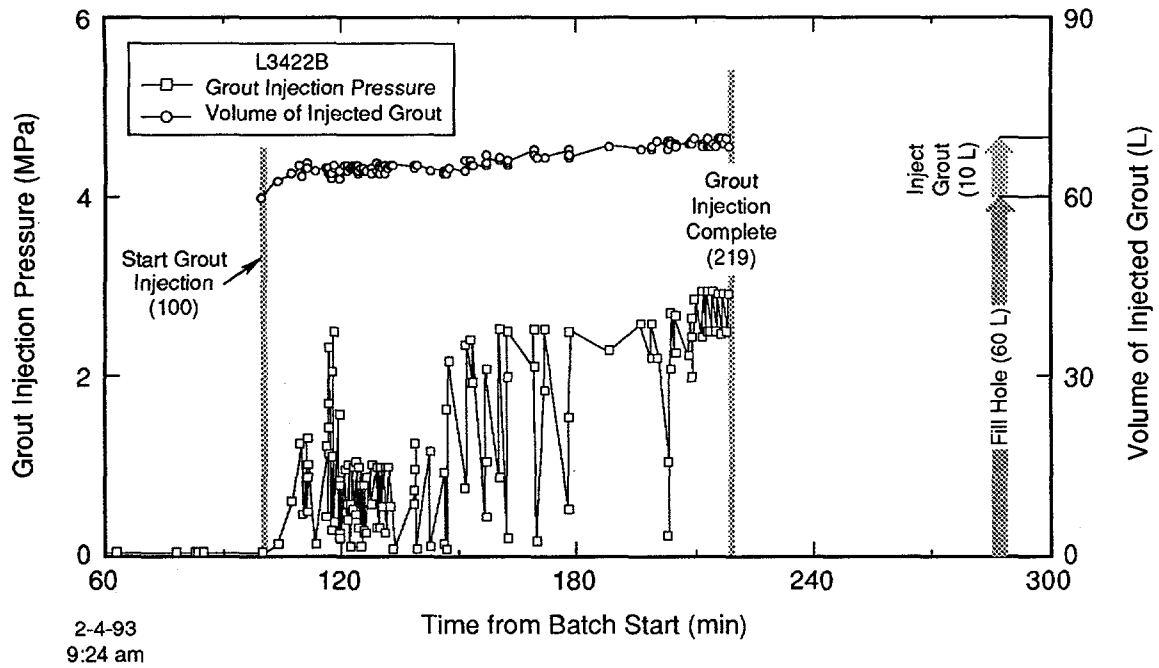
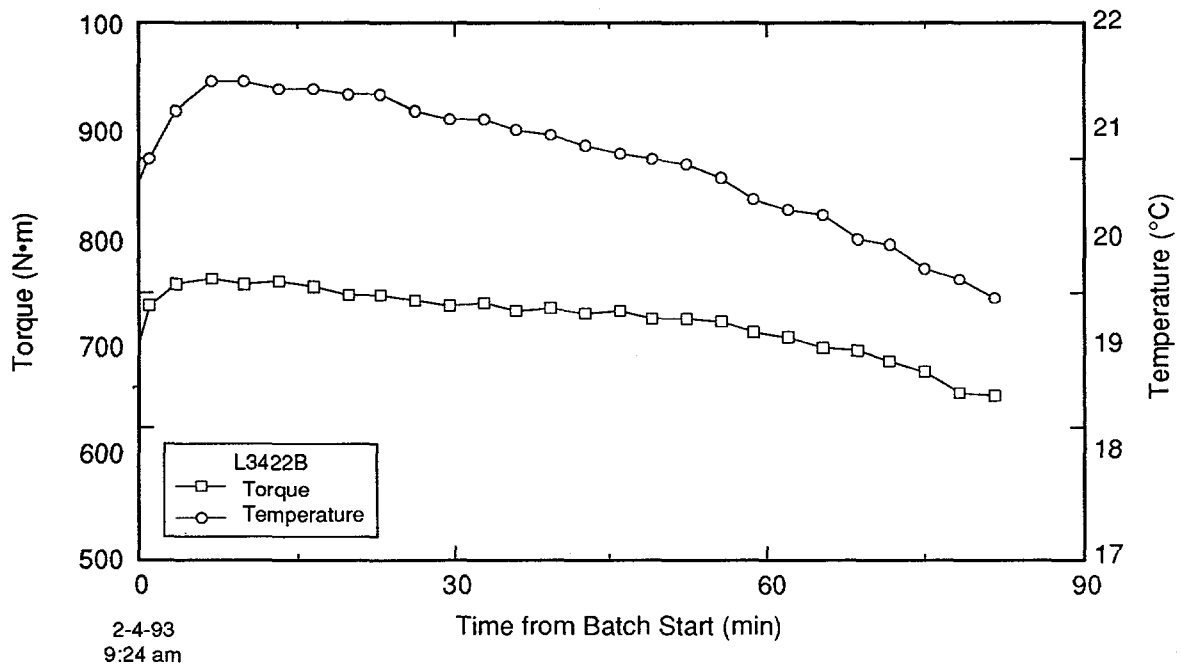


Figure G-34. Grout volume and pressure measured during injection of hole L3422B.



TRI-6121-169-0

Figure G-35. Attritor torque and temperature measured during grout batching for hole L3422B.

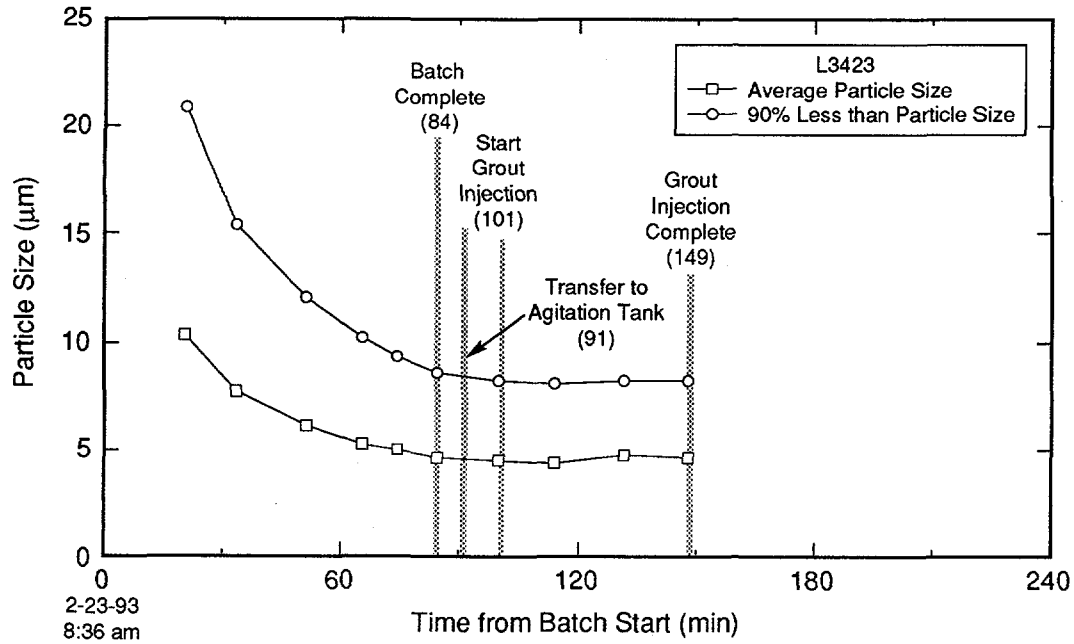


Figure G-36. Grout particle size measured during batching and injection of hole L3423.

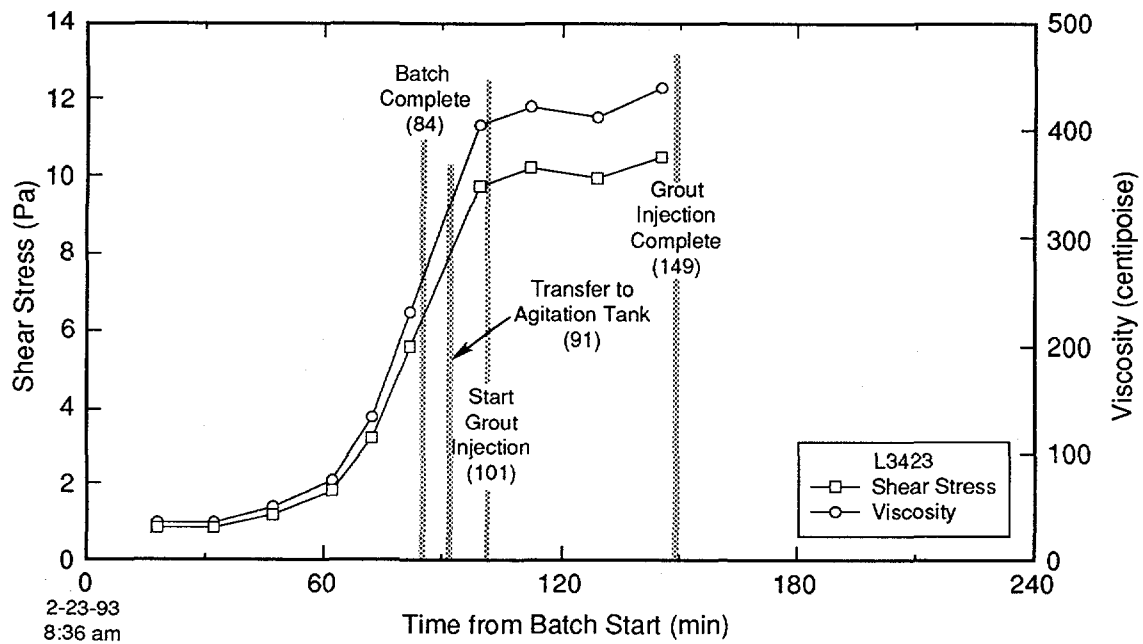


Figure G-37. Grout rheologic properties measured during batching and injection of hole L3423.

TRI-6121-187-0

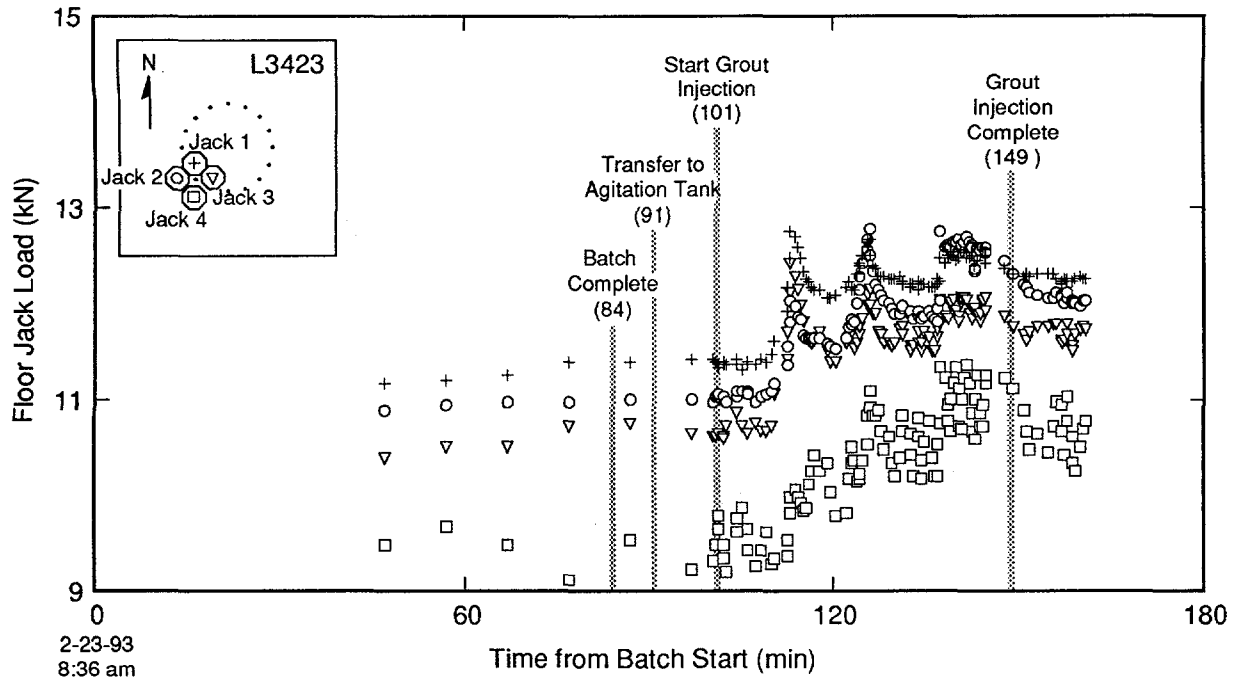


Figure G-38. Load cell measurements acquired during batching and injection of hole L3423.

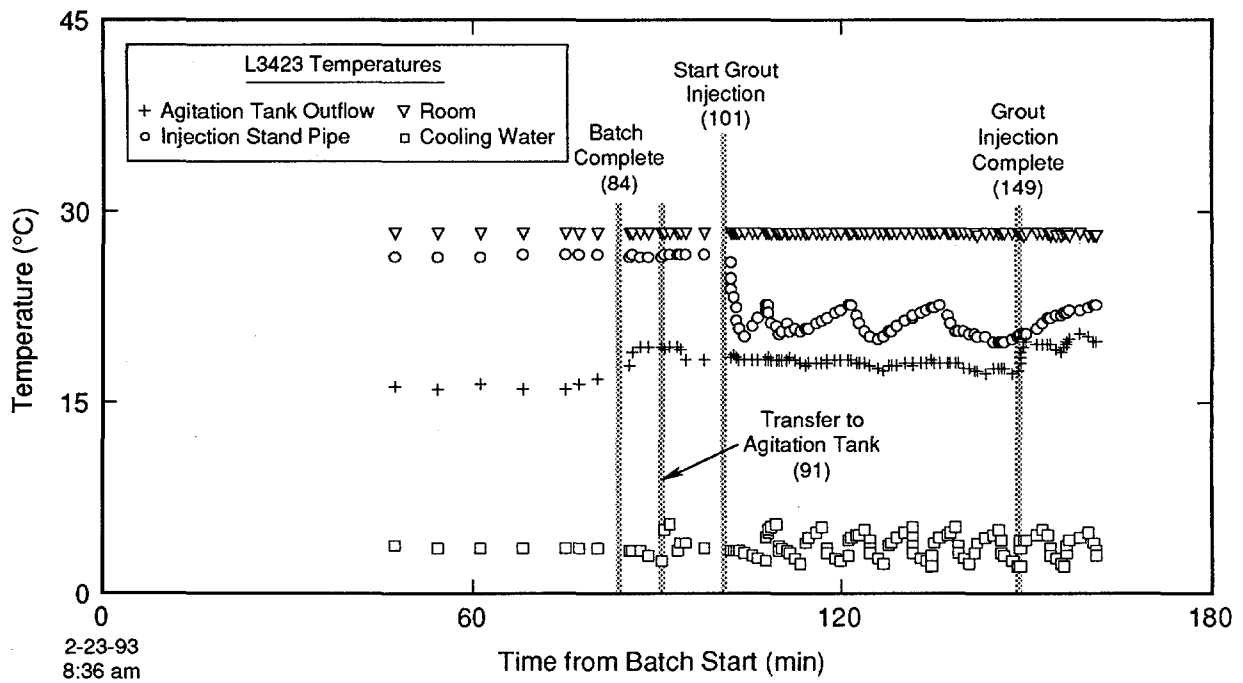


Figure G-39. Temperature measurements acquired during batching and injection of hole L3423.

TRI-6121-150-0

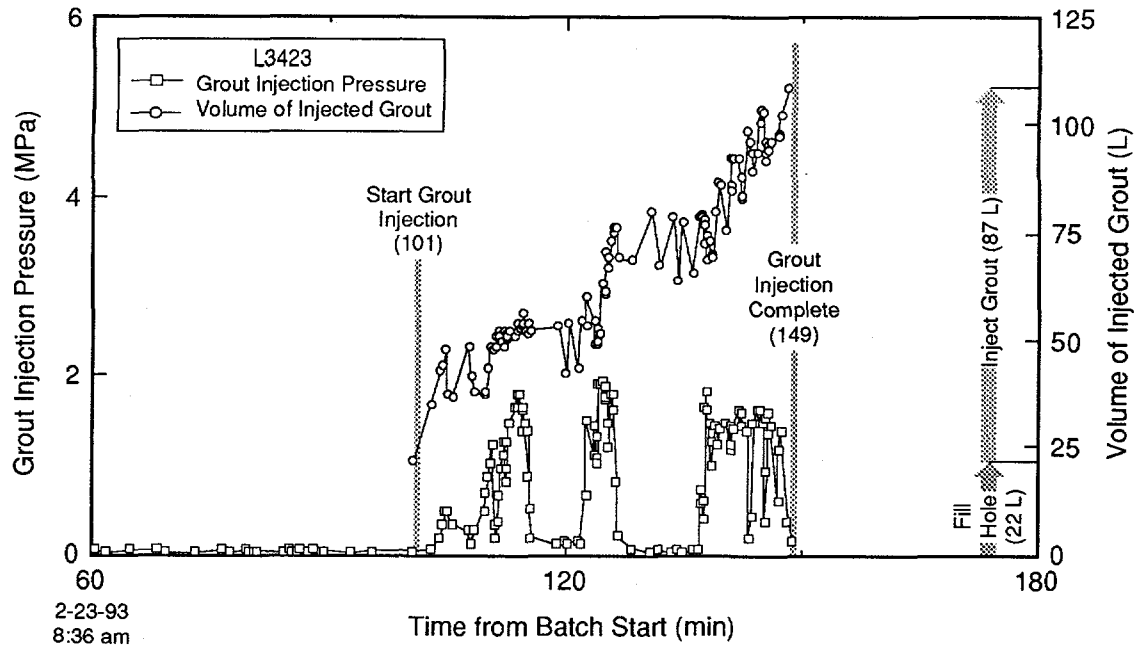


Figure G-40. Grout volume and pressure measured during injection of hole L3423.

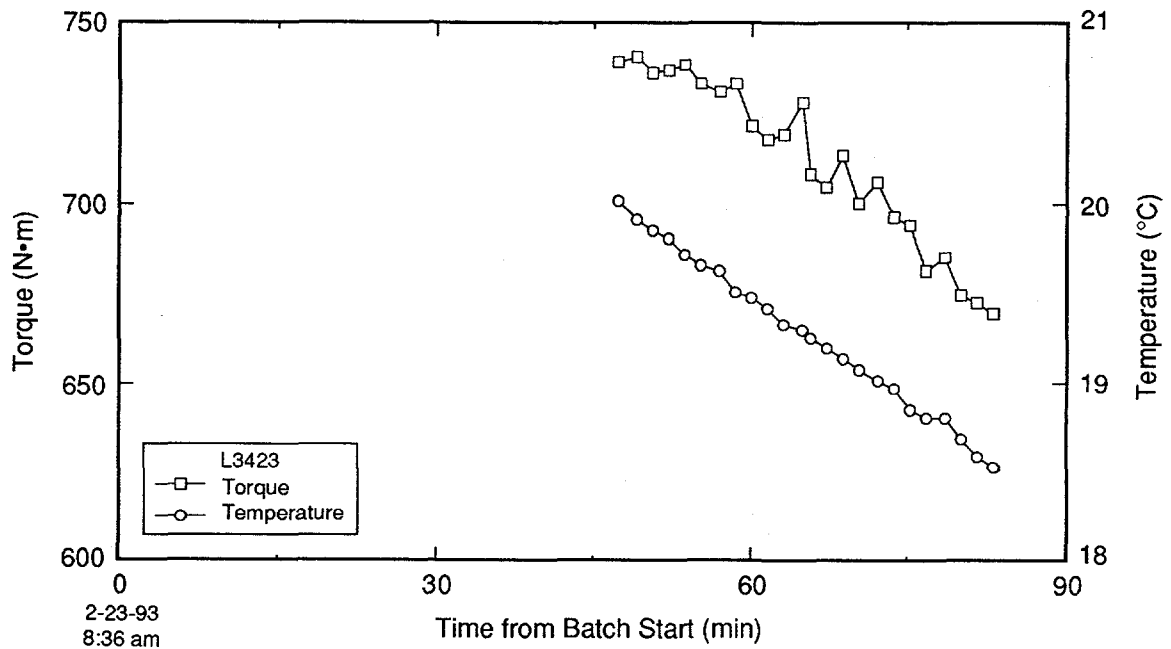


Figure G-41. Attritor torque and temperature measured during grout batching for hole L3423.

TRI-6121-170-0

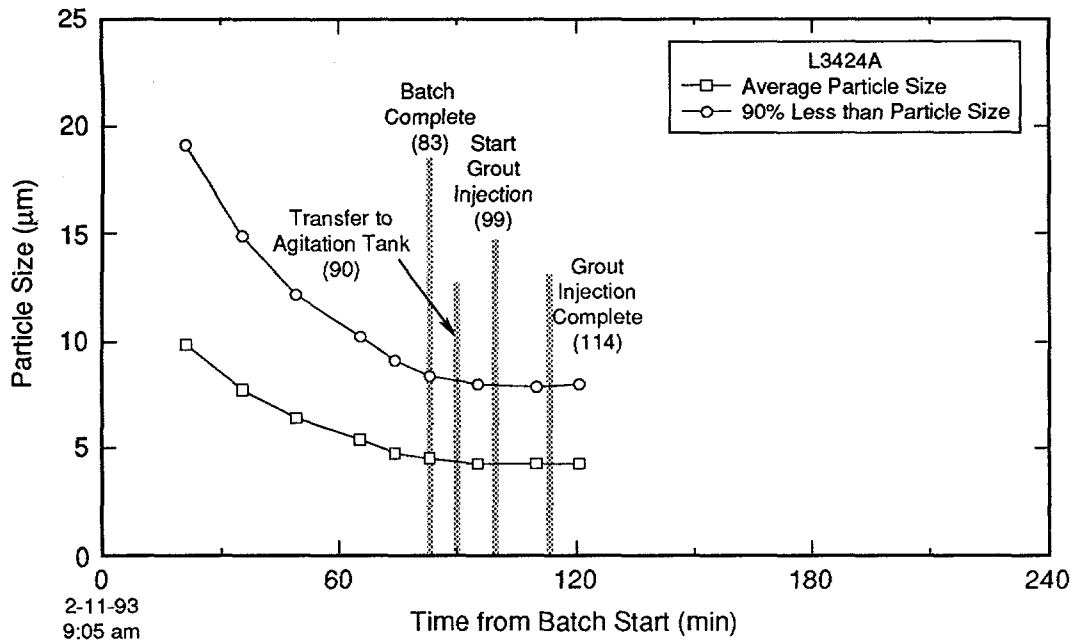


Figure G-42. Grout particle size measured during batching and injection of hole L3424A.

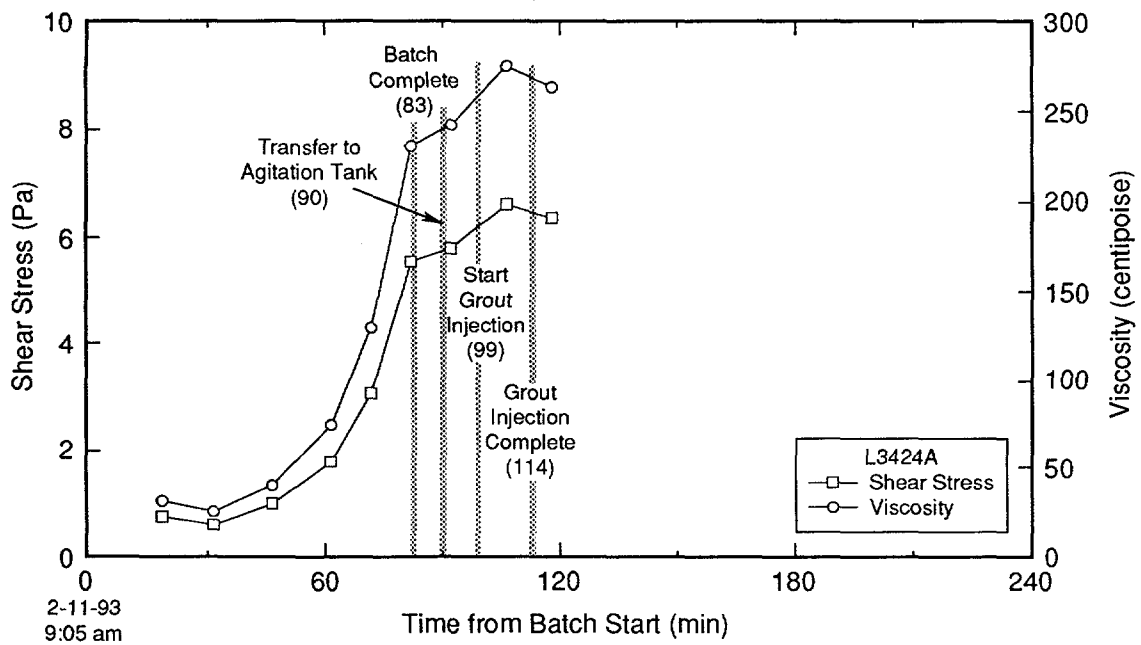


Figure G-43. Grout rheologic properties measured during batching and injection of hole L3424A.

TRI-6121-188-0

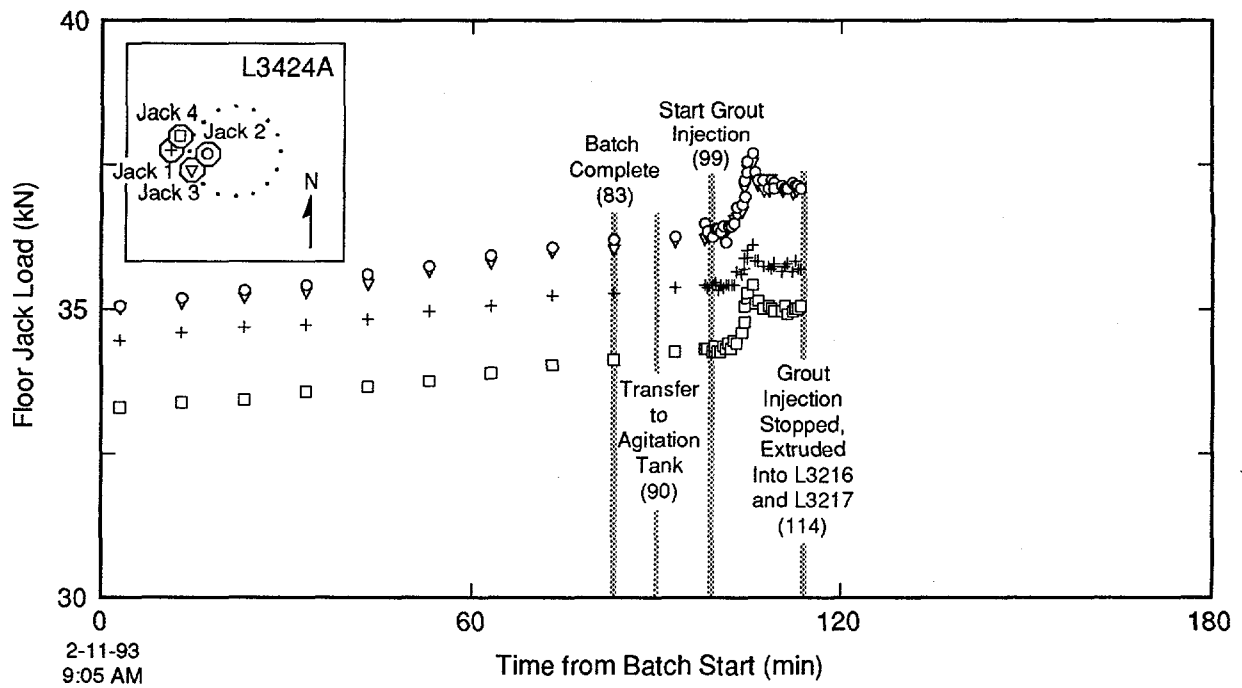


Figure G-44. Load cell measurements acquired during batching and injection of hole L3424A.

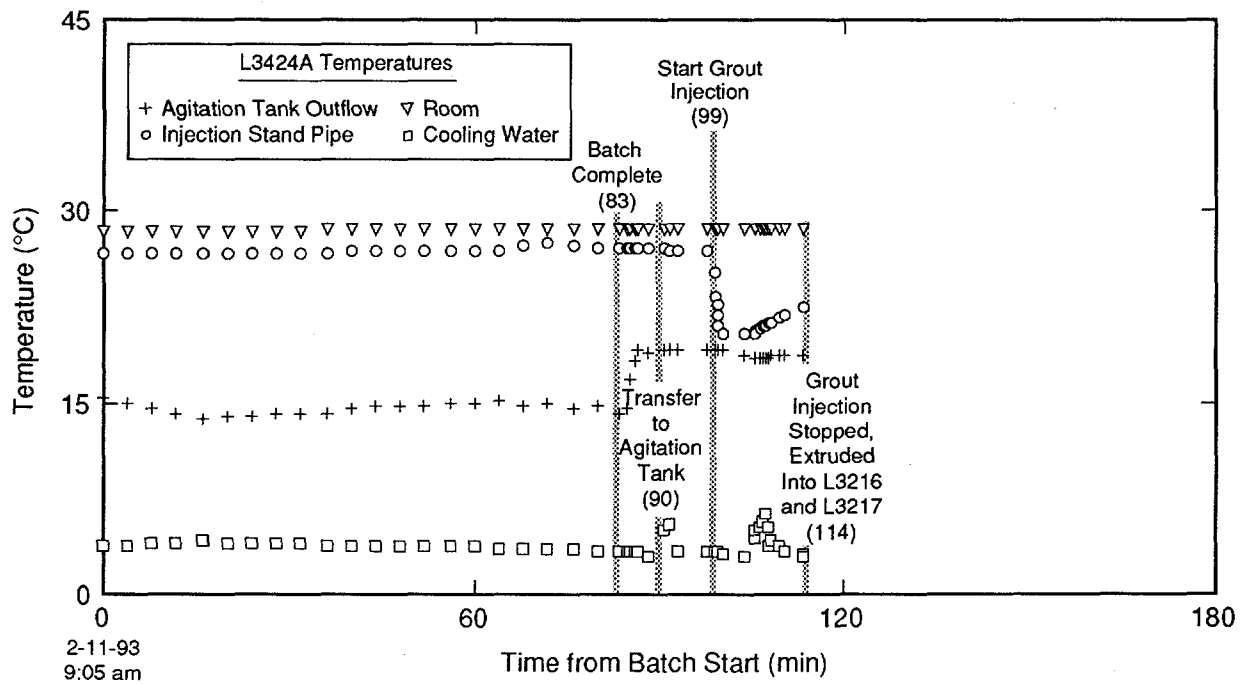


Figure G-45. Temperature measurements acquired during batching and injection of hole L3424A.

TRI-6121-151-0

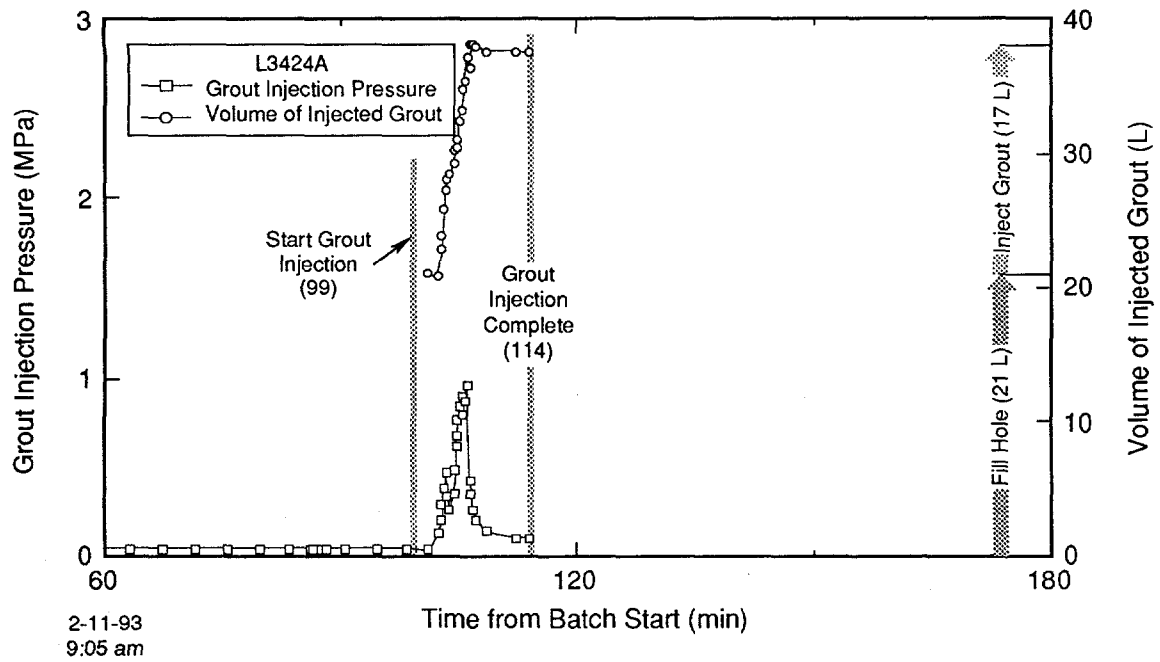


Figure G-46. Grout volume and pressure measured during injection of hole L3424A.

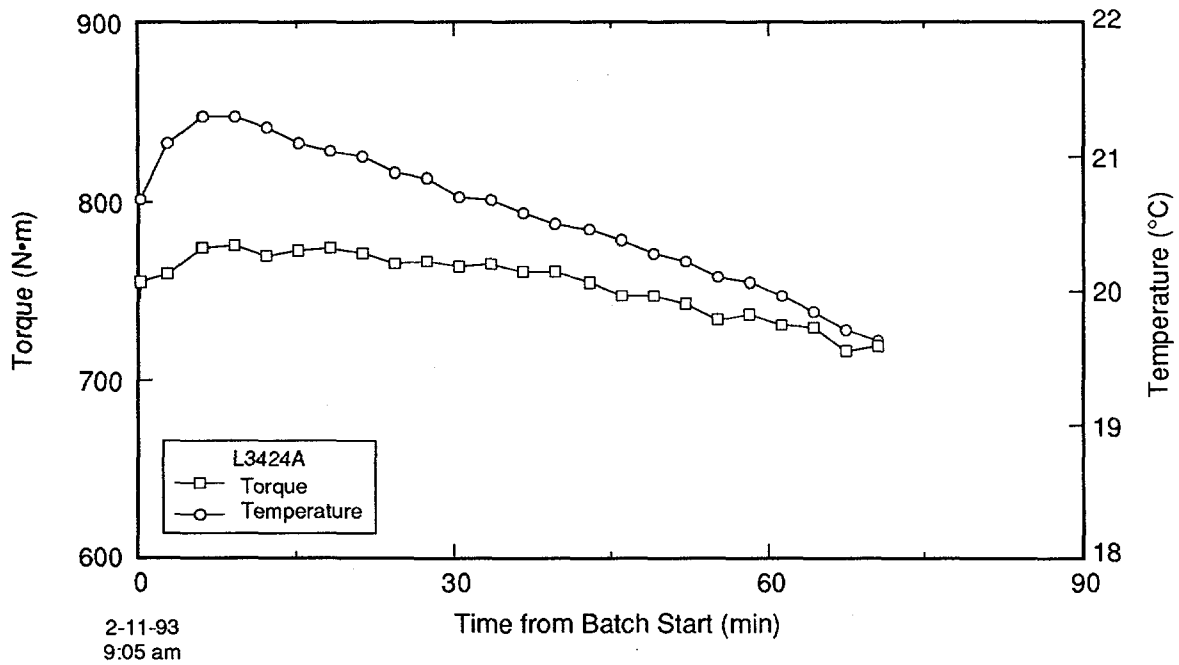


Figure G-47. Attritor torque and temperature measured during grout batching for hole L3424A.

TRI-6121-171-0

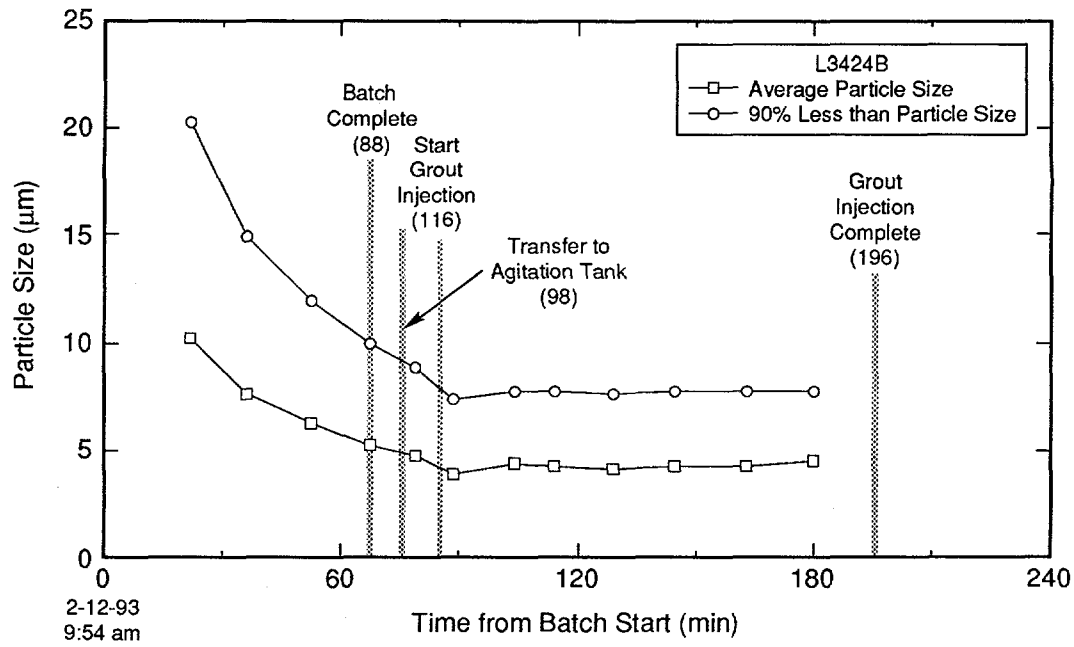


Figure G-48. Grout particle size measured during batching and injection of hole L3424B.

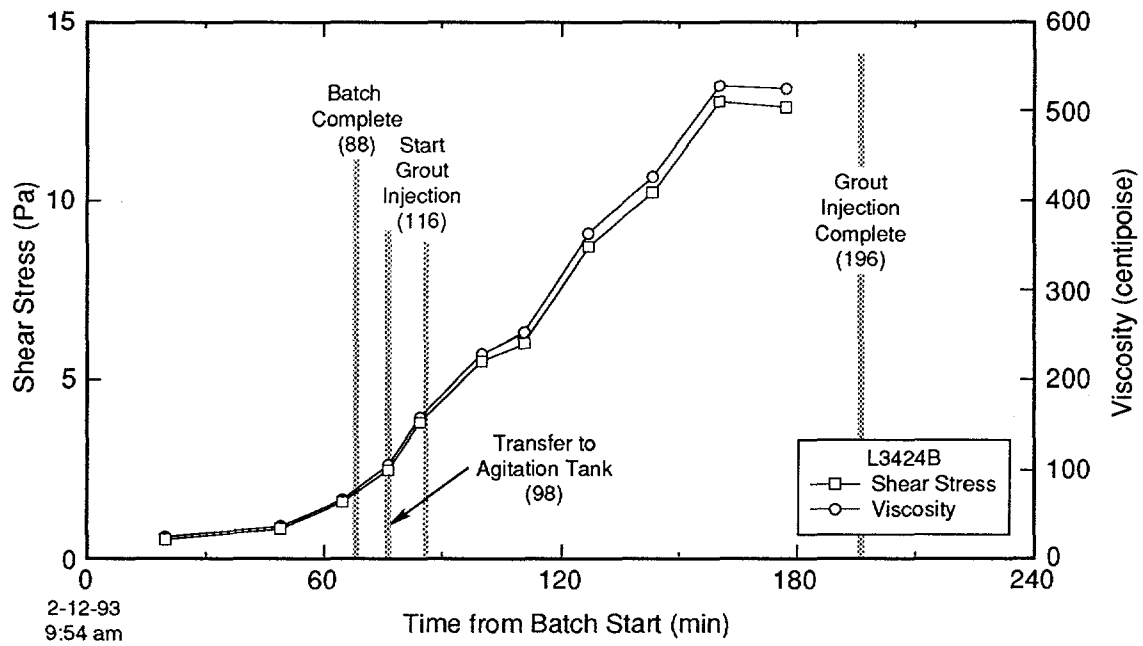


Figure G-49. Grout rheologic properties measured during batching and injection of hole L3424B.

TRI-6121-189-0

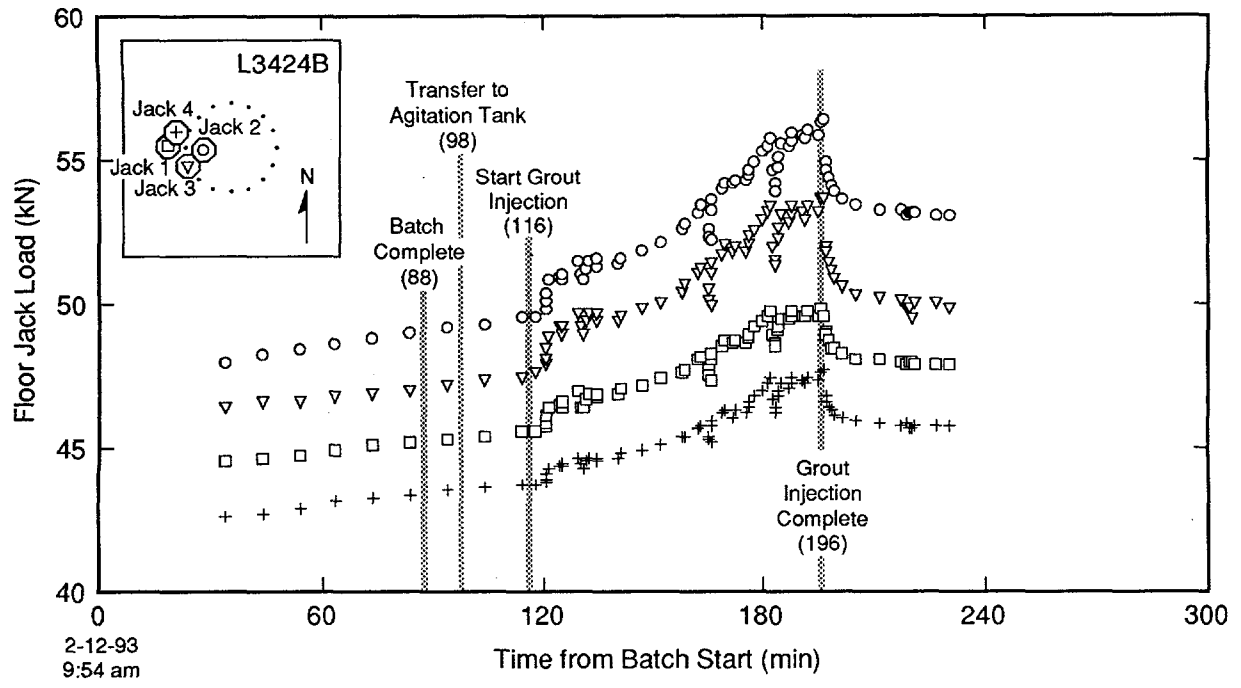


Figure G-50. Load cell measurements acquired during batching and injection of hole L3424B.

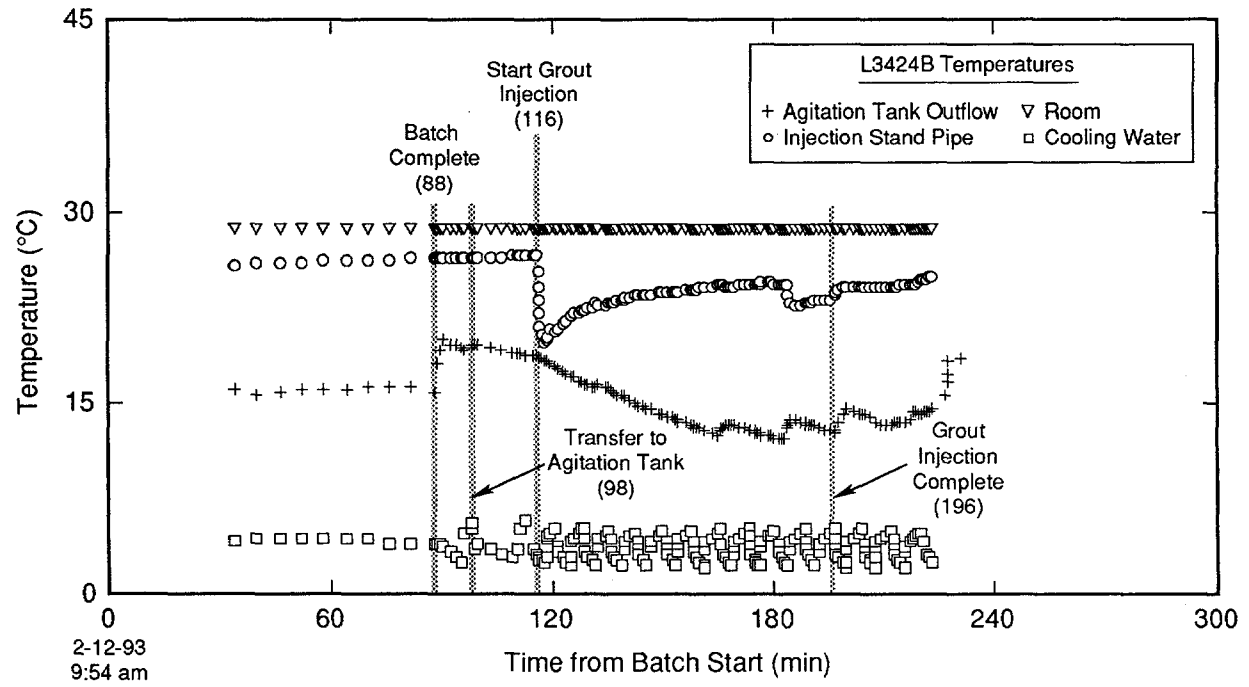


Figure G-51. Temperature measurements acquired during batching and injection of hole L3424B.

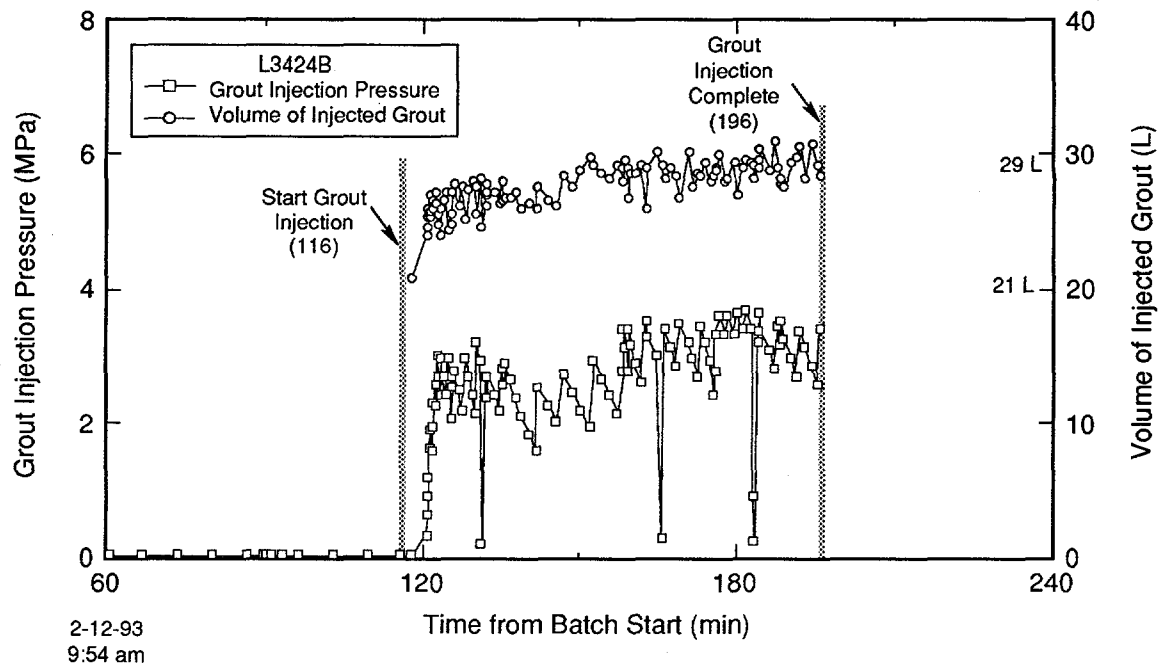


Figure G-52. Grout volume and pressure measured during injection of hole L3424B.

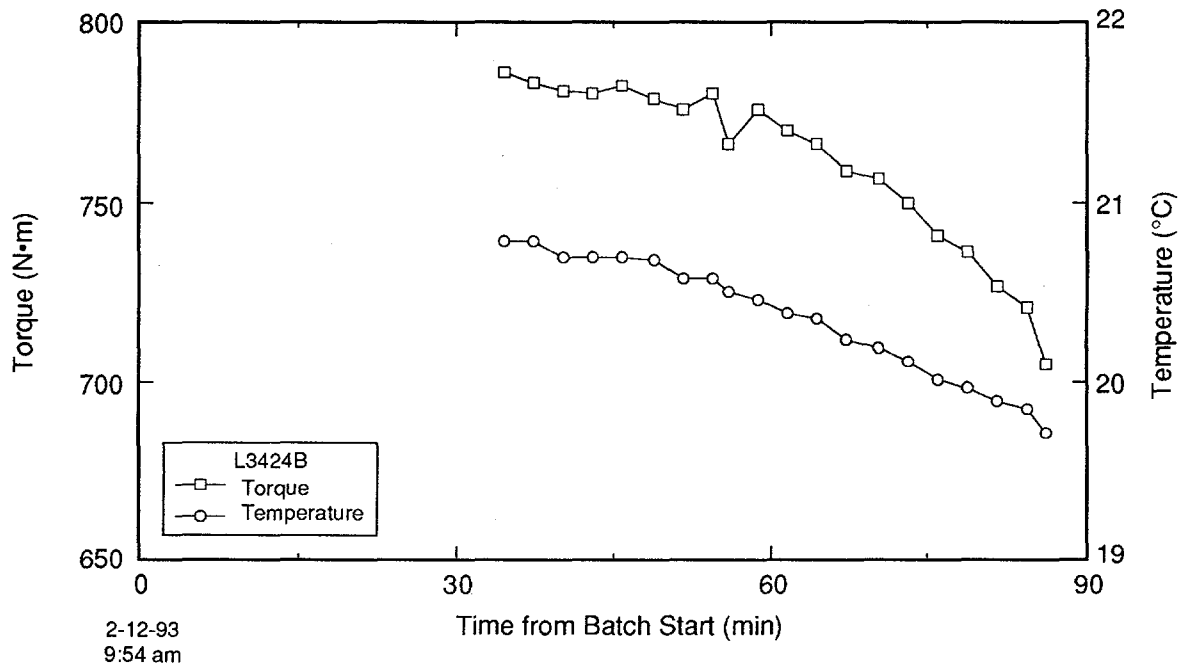


Figure G-53. Attritor torque and temperature measured during grout batching for hole L3424B.

TRI-6121-172-0

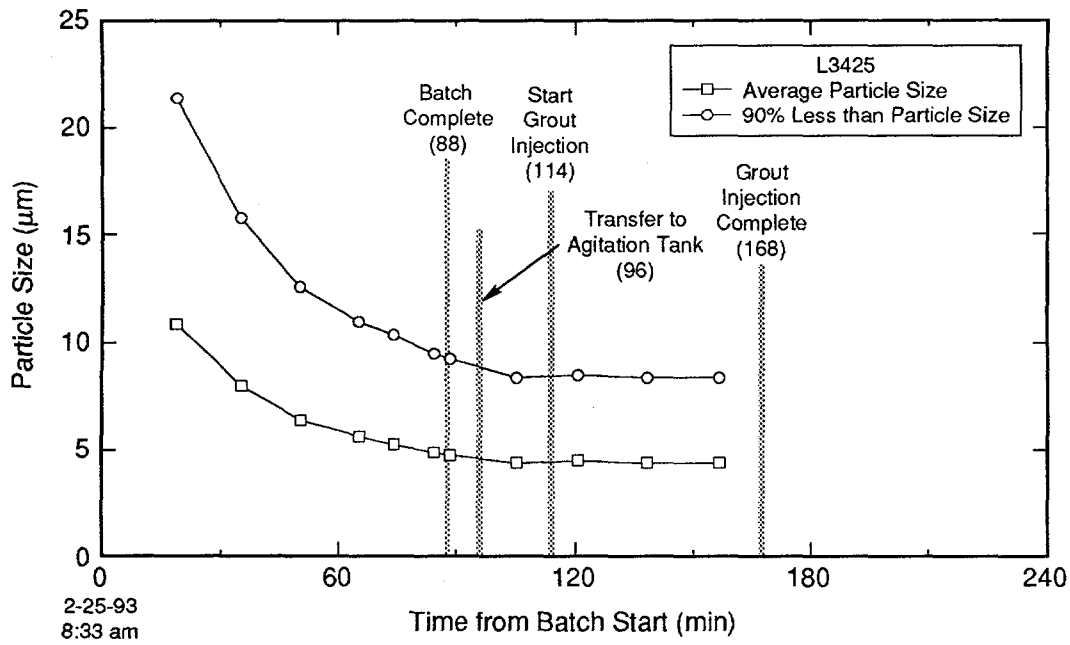


Figure G-54. Grout particle size measured during batching and injection of hole L3425.

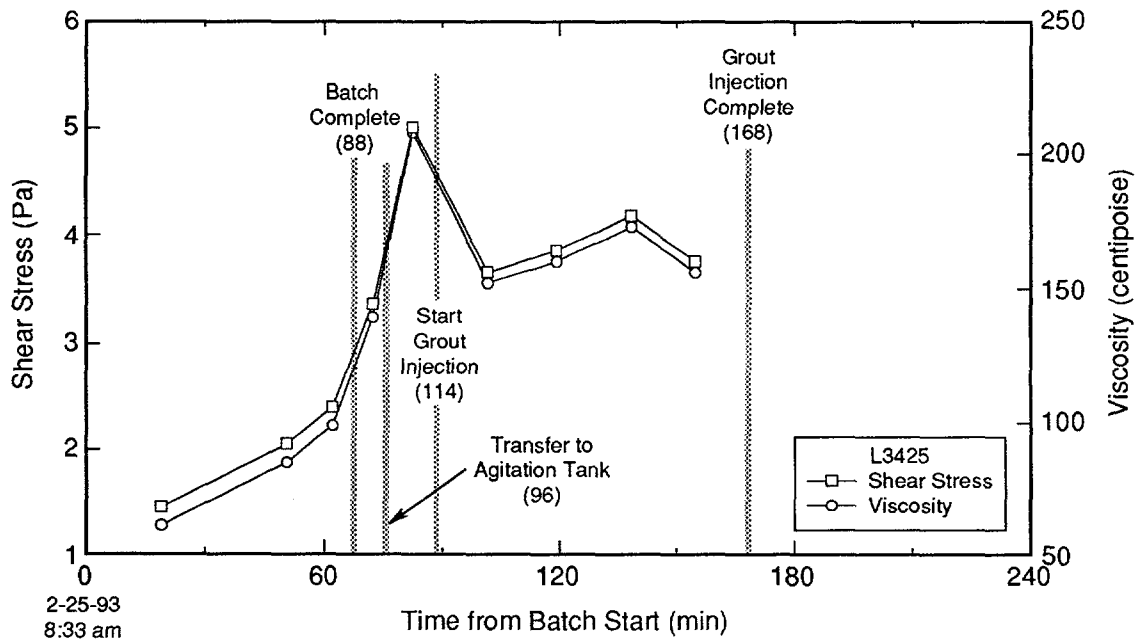


Figure G-55. Grout rheologic properties measured during batching and injection of hole L3425.

TRI-6121-190-0

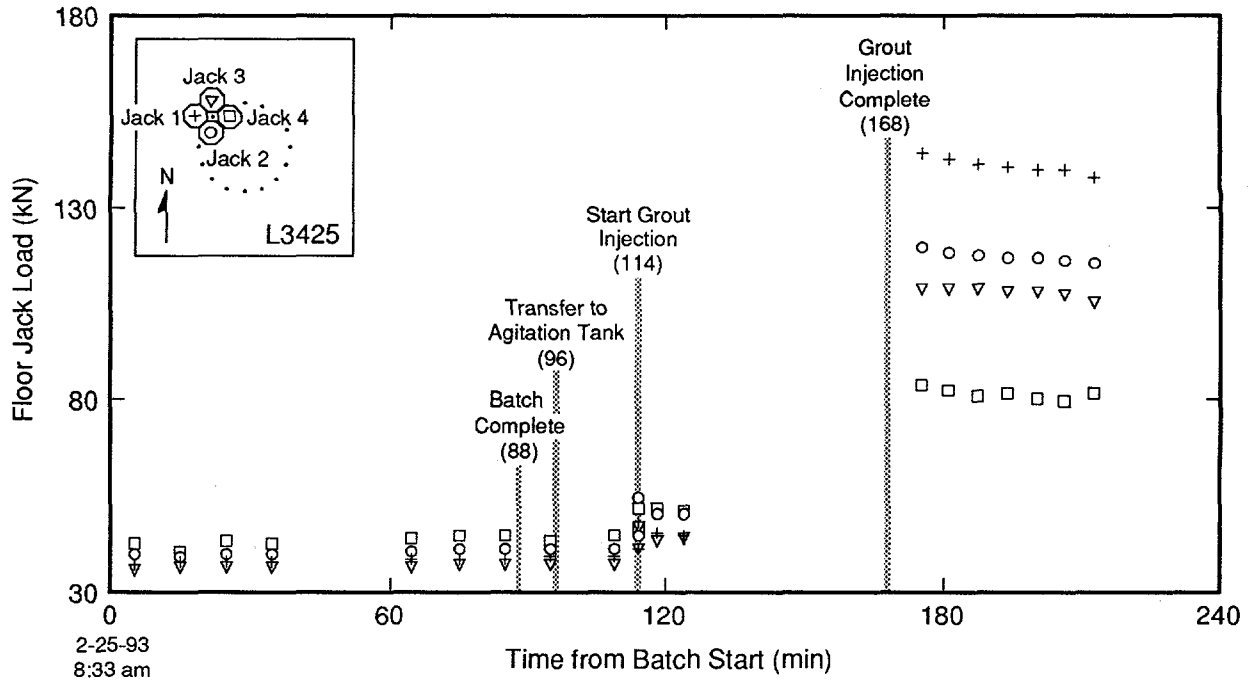


Figure G-56. Load cell measurements acquired during batching and injection of hole L3425.

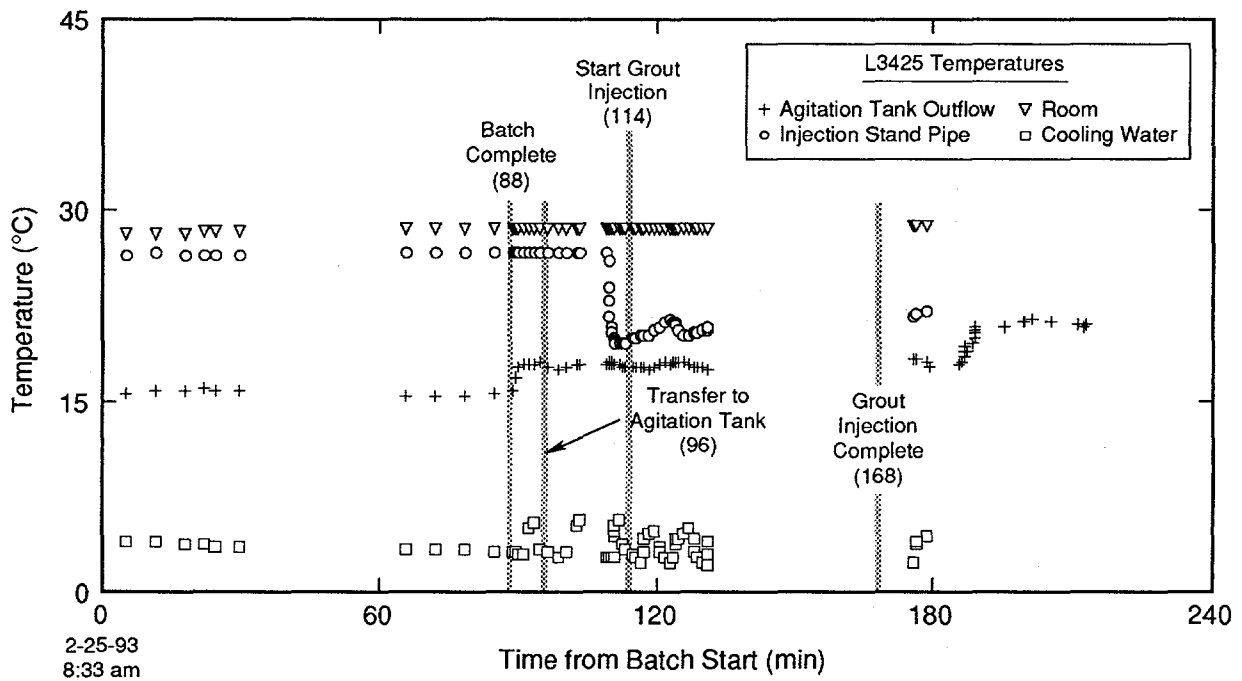


Figure G-57. Temperature measurements acquired during batching and injection of hole L3425.

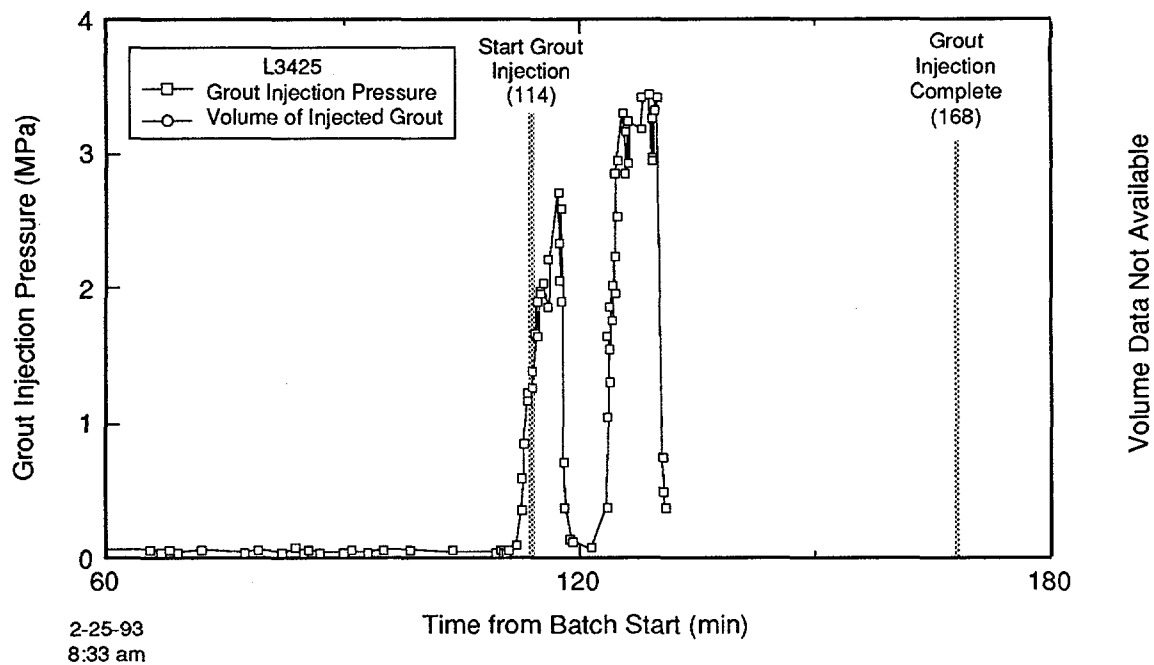
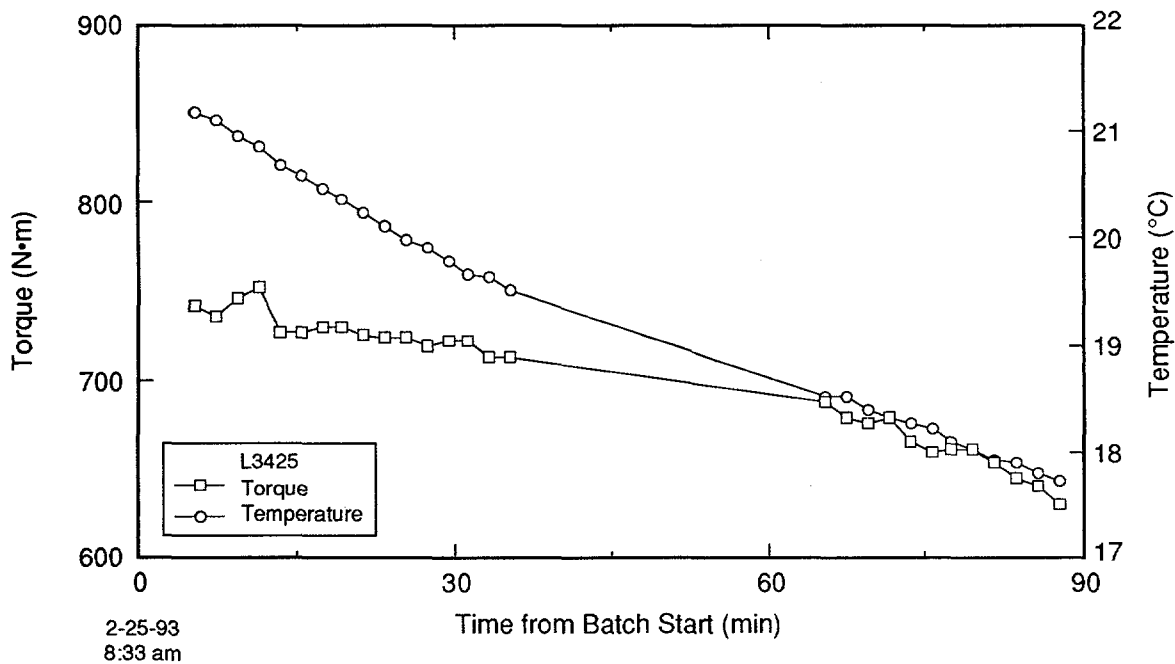


Figure G-58. Grout volume and pressure measured during injection of hole L3425.



TRI-6121-173-0

Figure G-59. Attritor torque and temperature measured during grout batching for hole L3425.

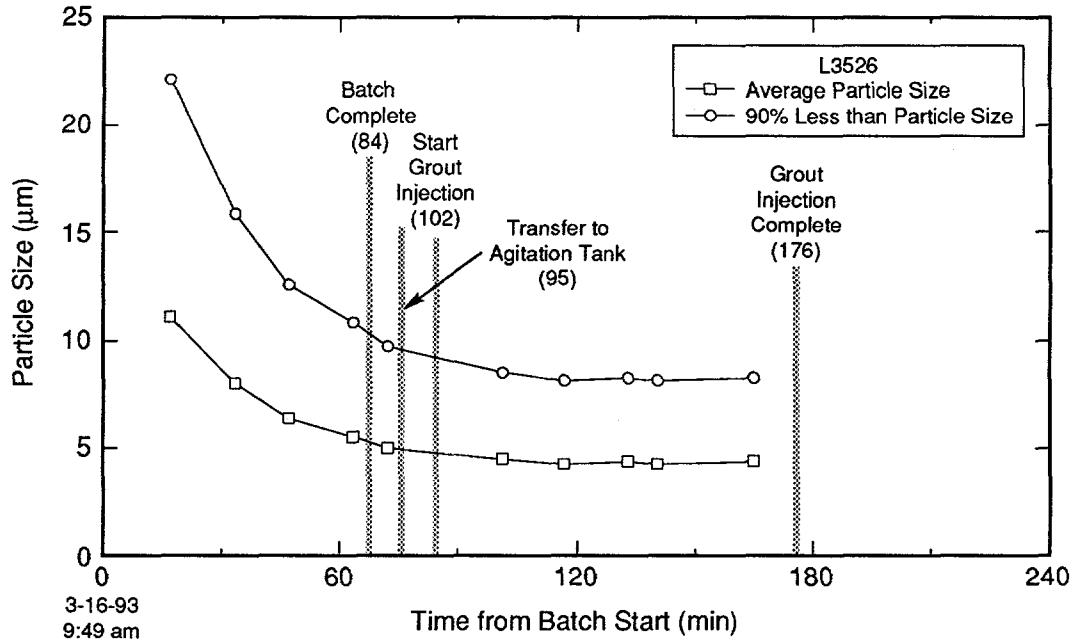


Figure G-60. Grout particle size measured during batching and injection of hole L3526.

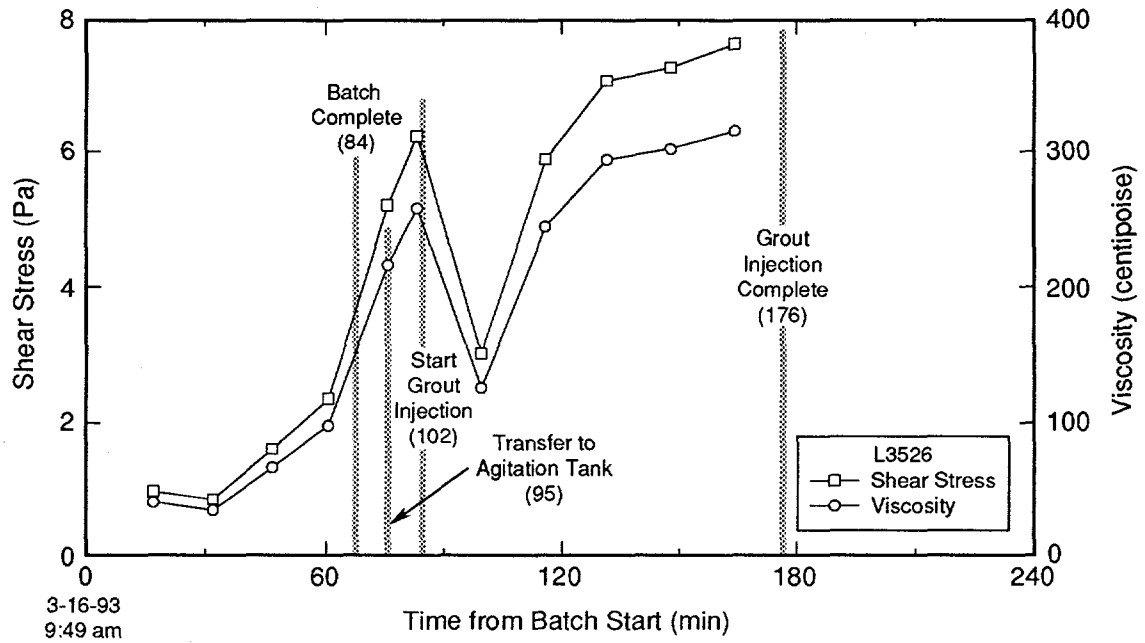


Figure G-61. Grout rheologic properties measured during batching and injection of hole L3526.

TRI-6121-191-0

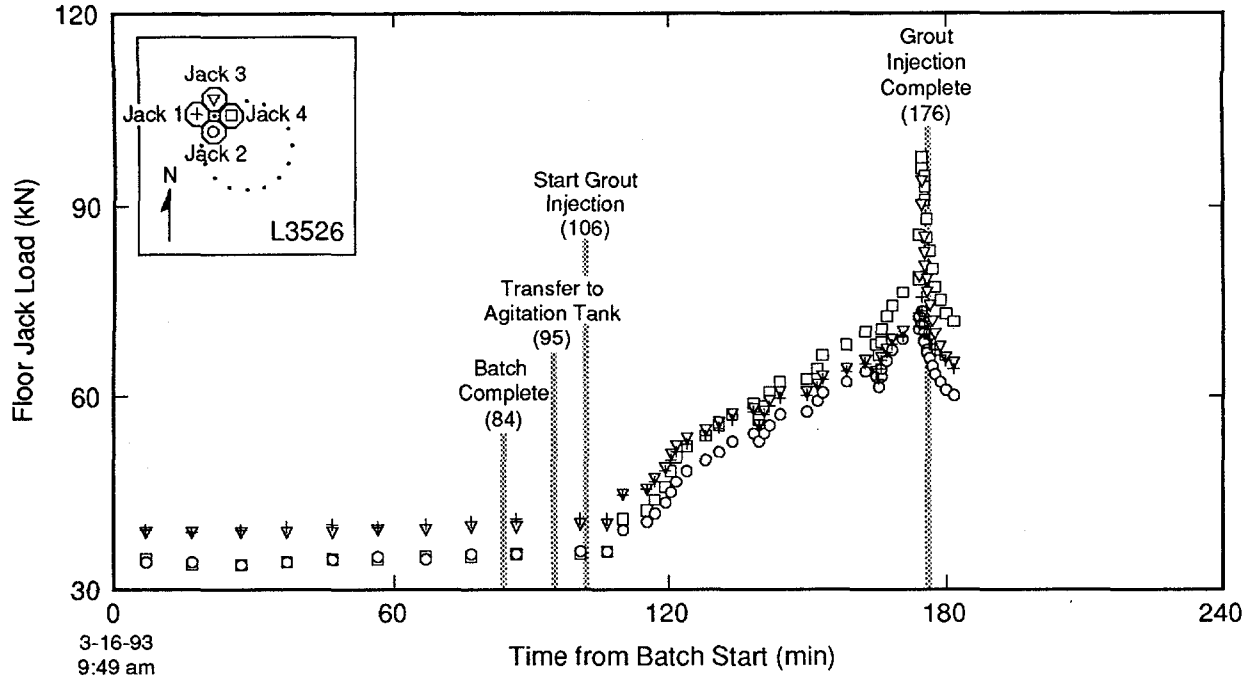


Figure G-62. Load cell measurements acquired during batching and injection of hole L3526.

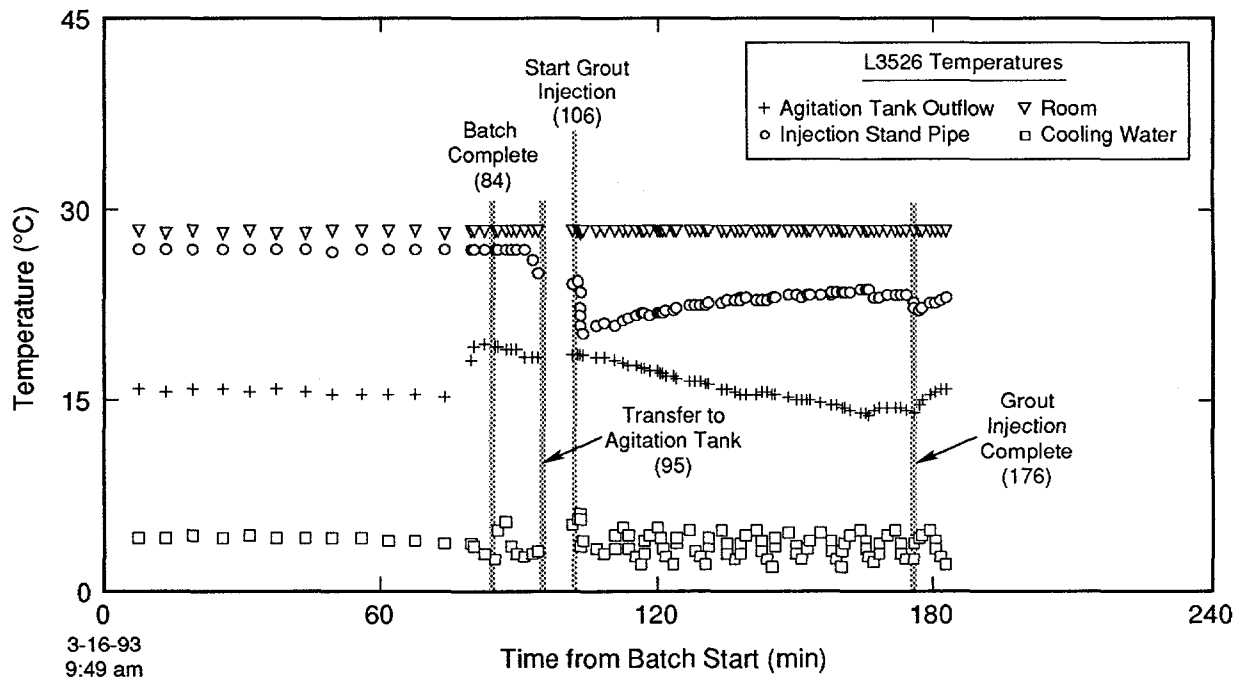


Figure G-63. Temperature measurements acquired during batching and injection of hole L3526.

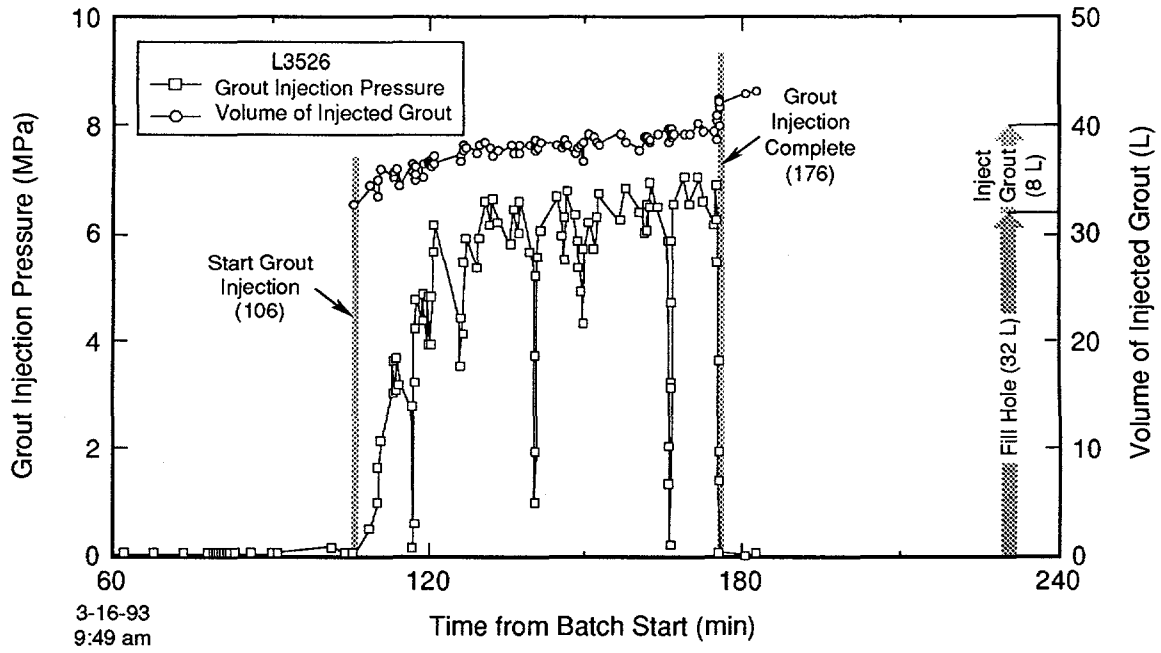


Figure G-64. Grout volume and pressure measured during injection of hole L3526.

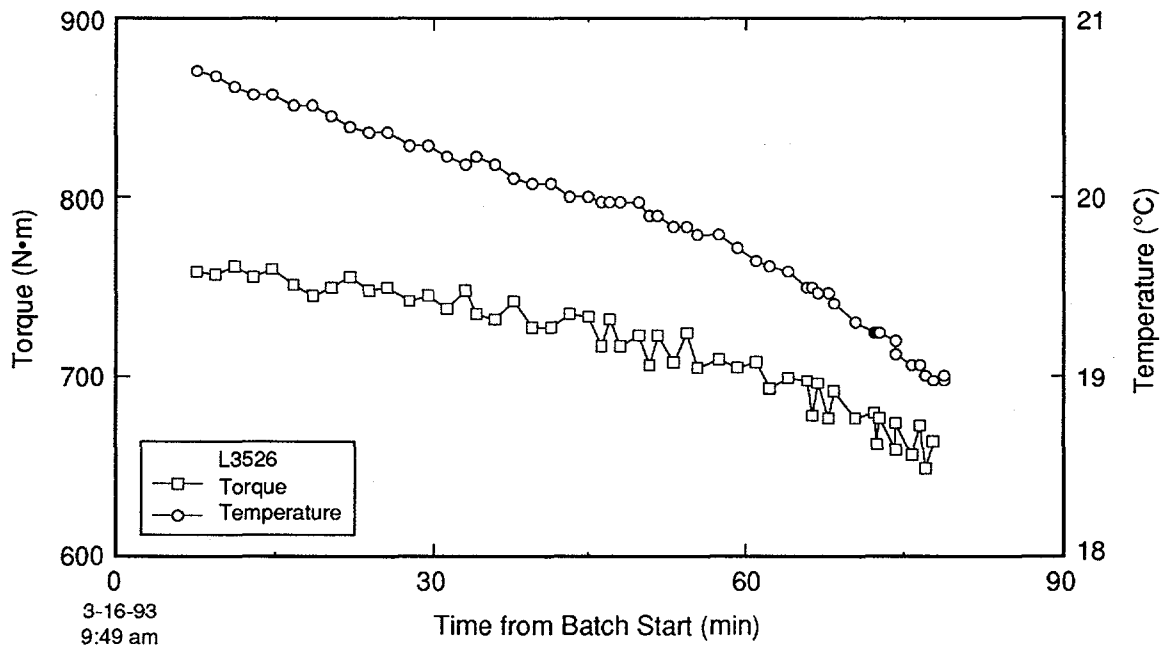


Figure G-65. Attritor torque and temperature measured during grout batching for hole L3526.

TRI-6121-174-0

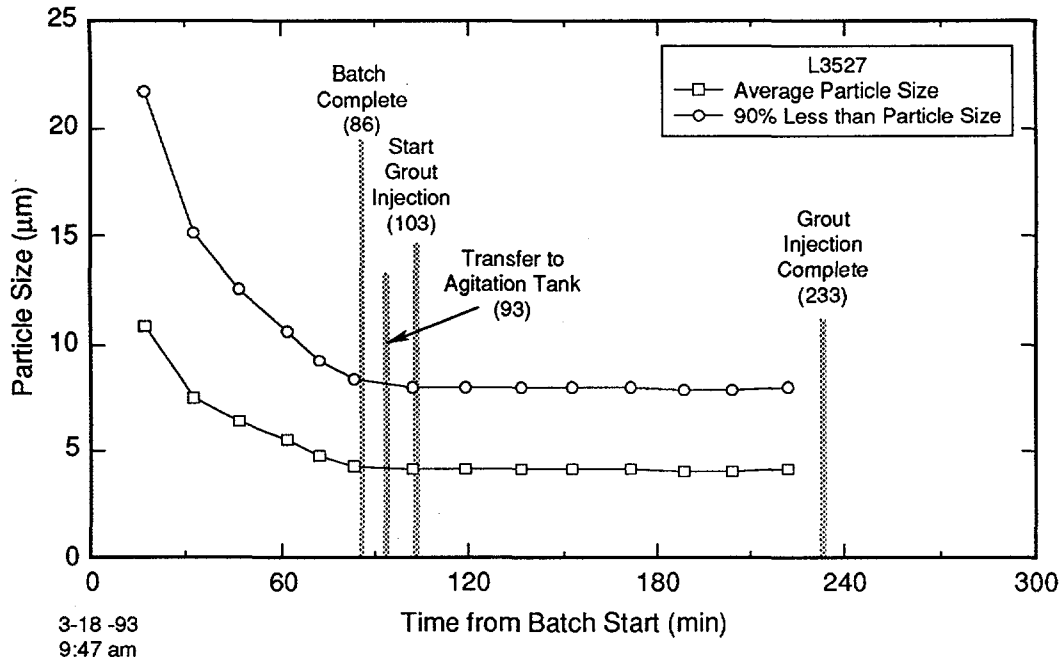
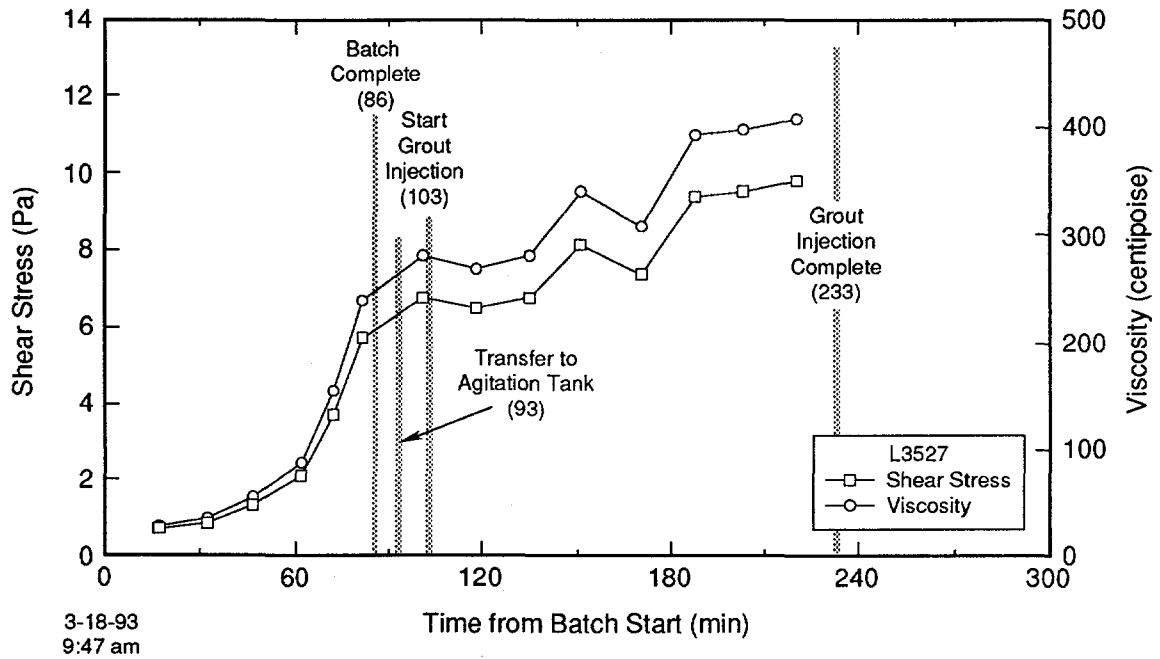


Figure G-66. Grout particle size measured during batching and injection of hole L3527.



TRI-6121-192-0

Figure G-67. Grout rheologic properties measured during batching and injection of hole L3527.

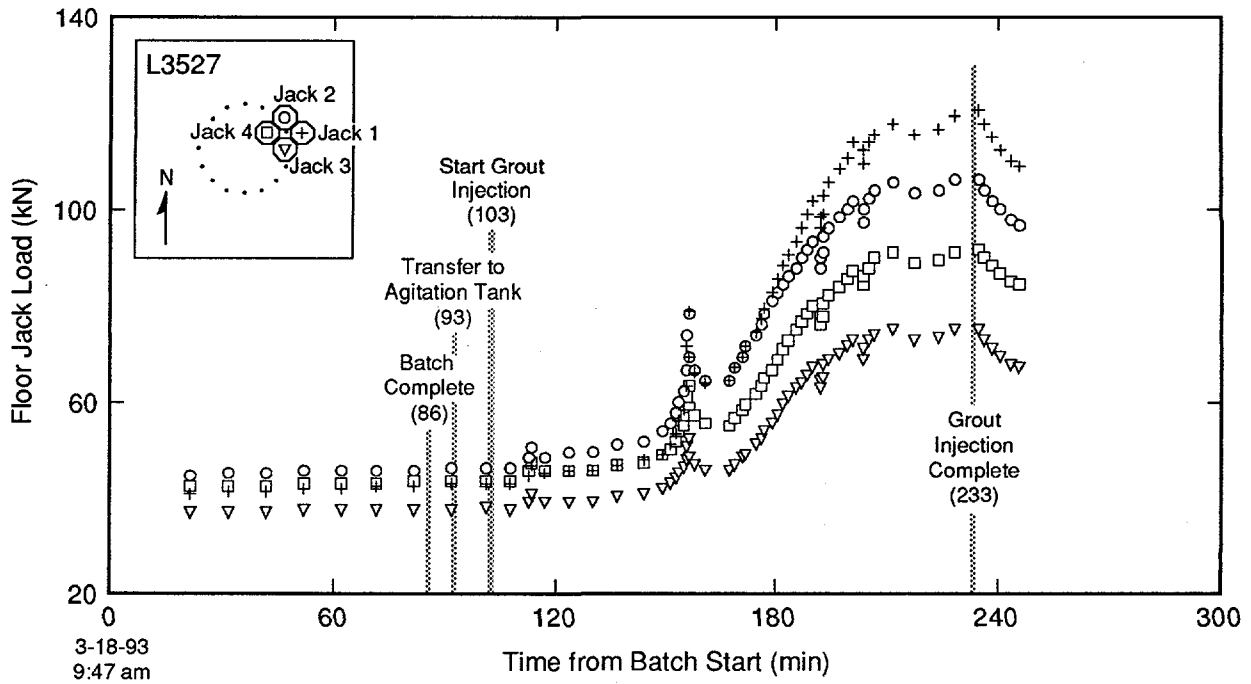


Figure G-68. Load cell measurements acquired during batching and injection of hole L3527.

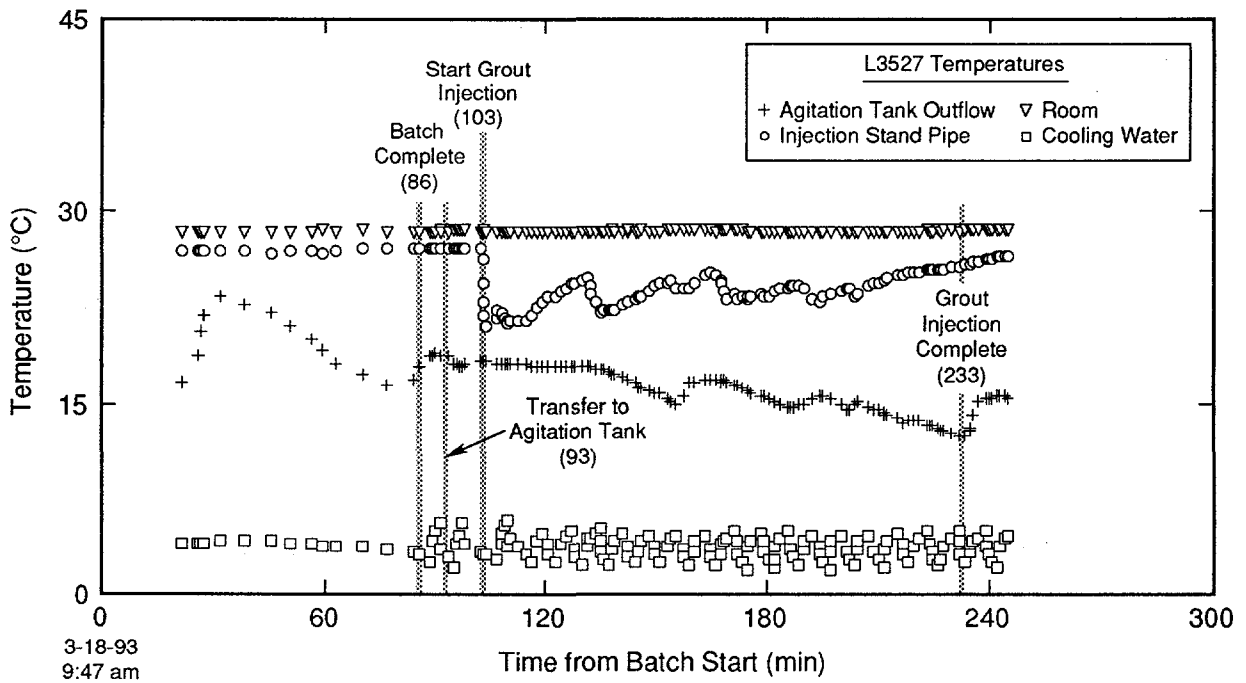


Figure G-69. Temperature measurements acquired during batching and injection of hole L3527.

TRI-6121-155-0

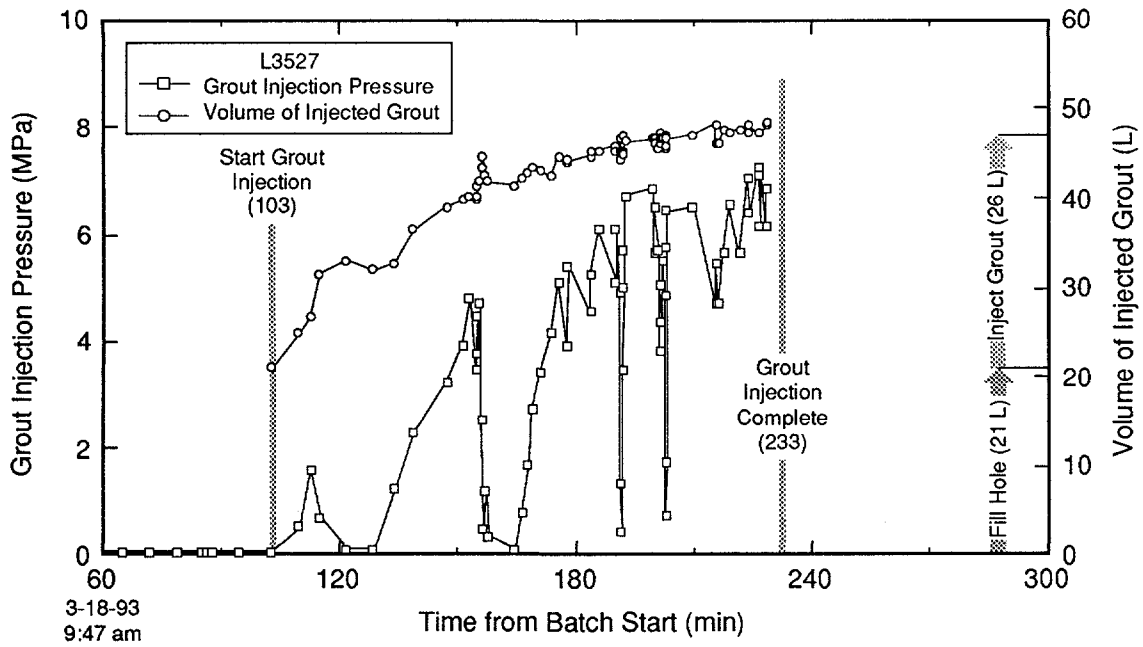
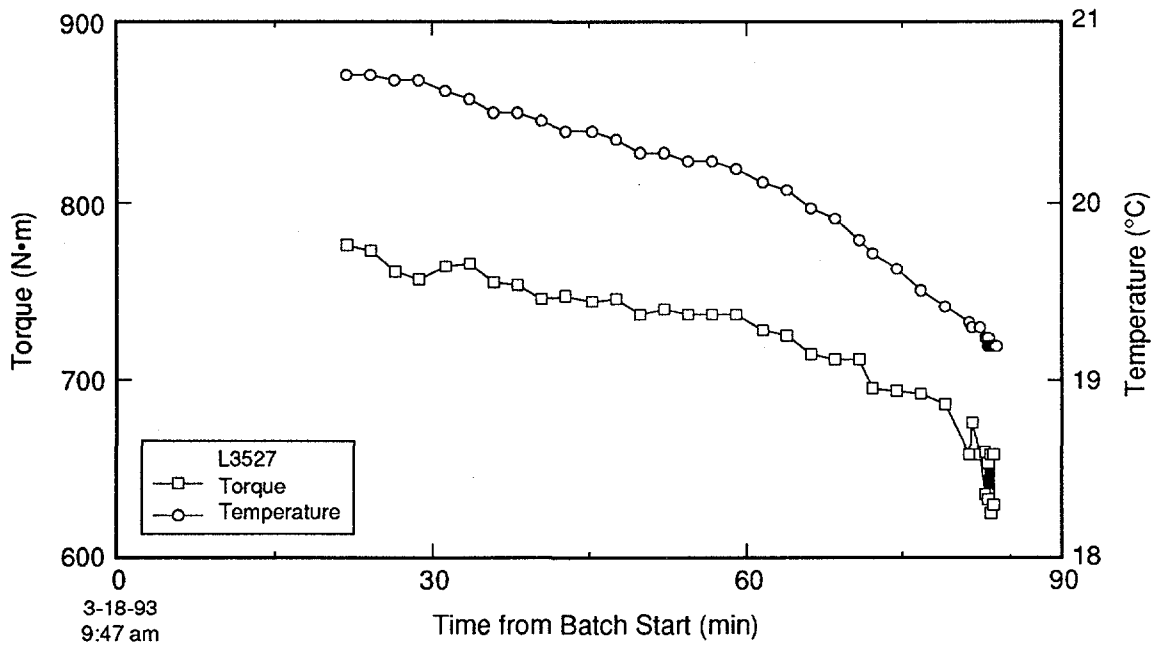


Figure G-70. Grout volume and pressure measured during injection of hole L3527.



TRI-6121-175-0

Figure G-71. Attritor torque and temperature measured during grout batching for hole L3527.

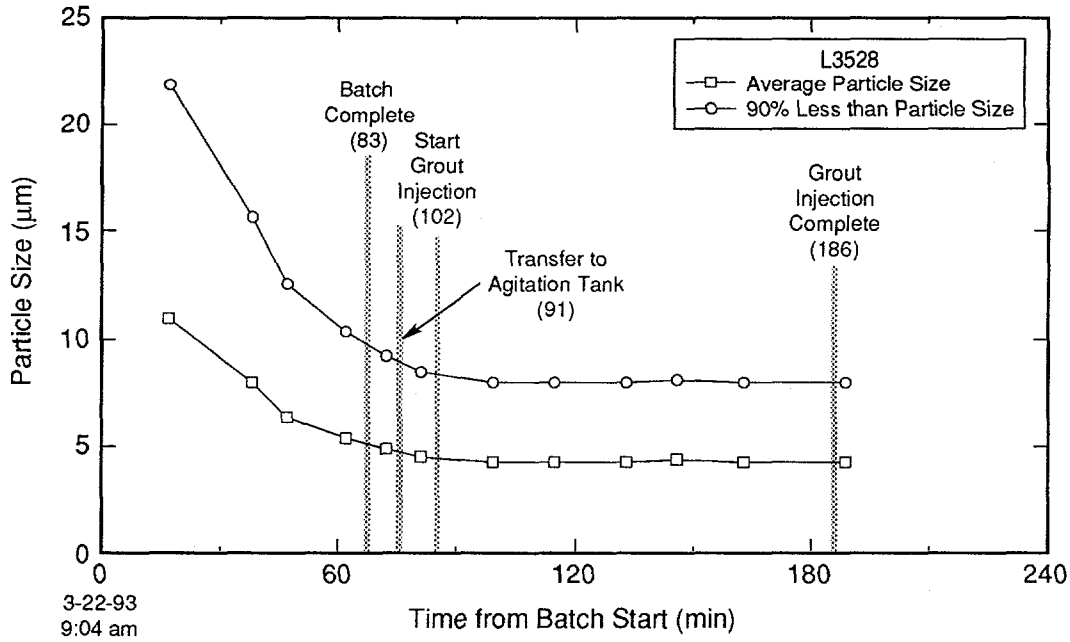


Figure G-72. Grout particle size measured during batching and injection of hole L3528.

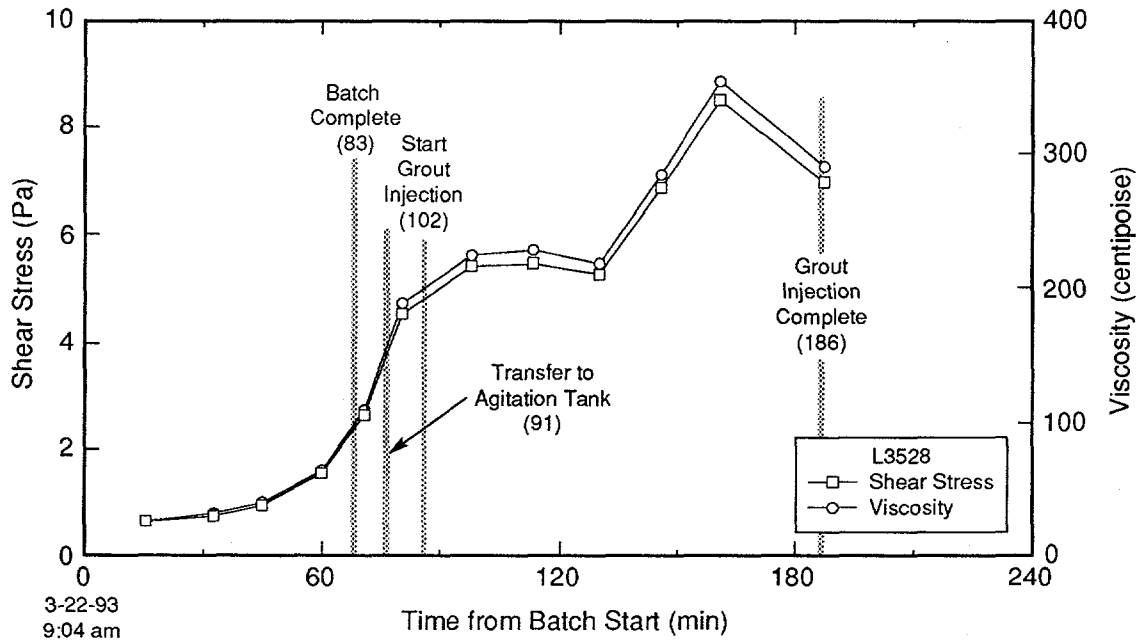


Figure G-73. Grout rheologic properties measured during batching and injection of hole L3528.

TRI-6121-193-0

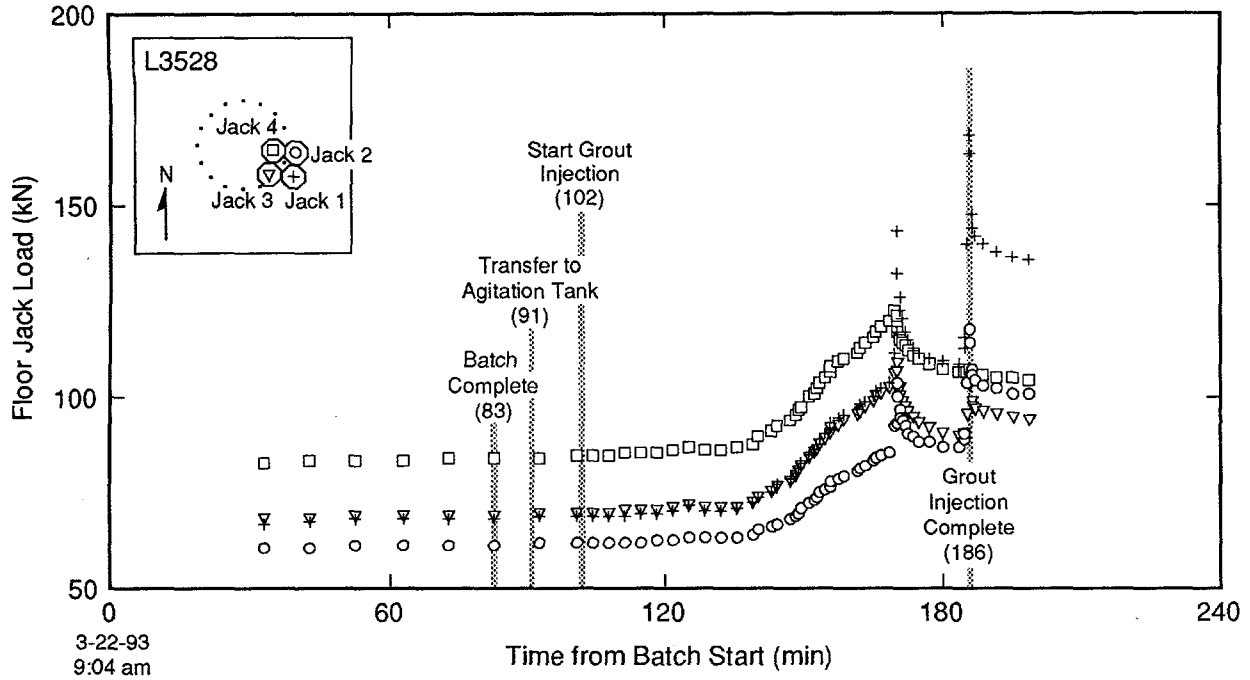


Figure G-74. Load cell measurements acquired during batching and injection of hole L3528.

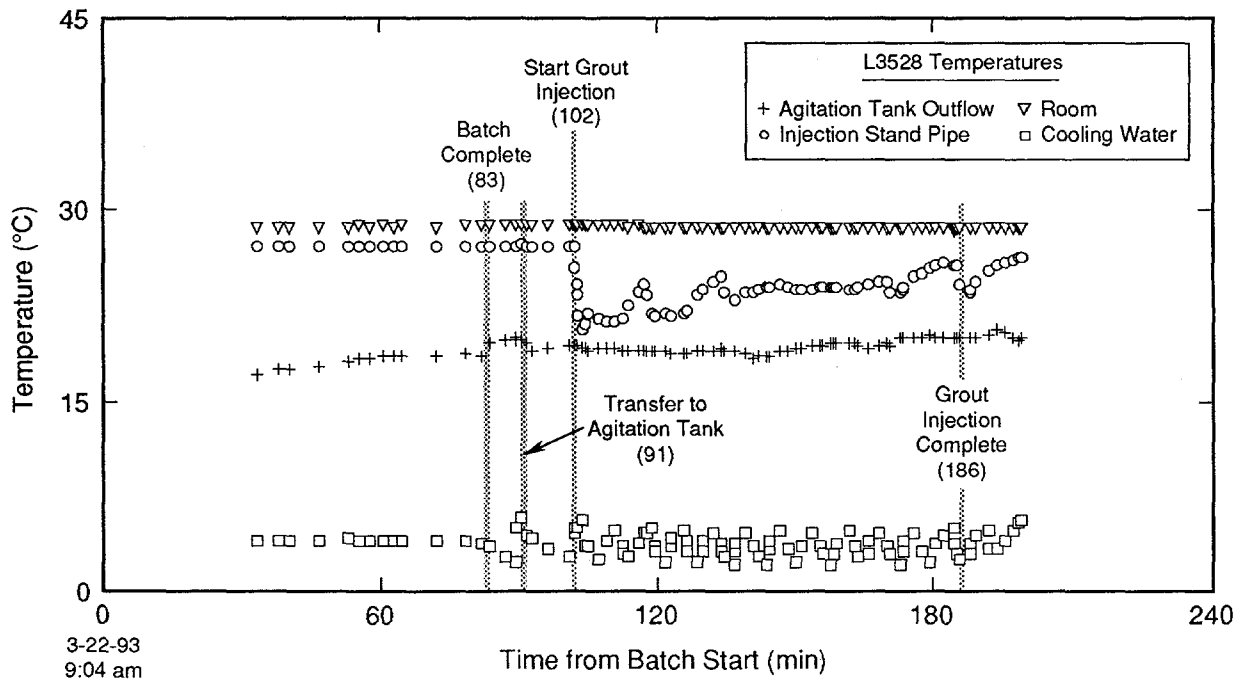


Figure G-75. Temperature measurements acquired during batching and injection of hole L3528.

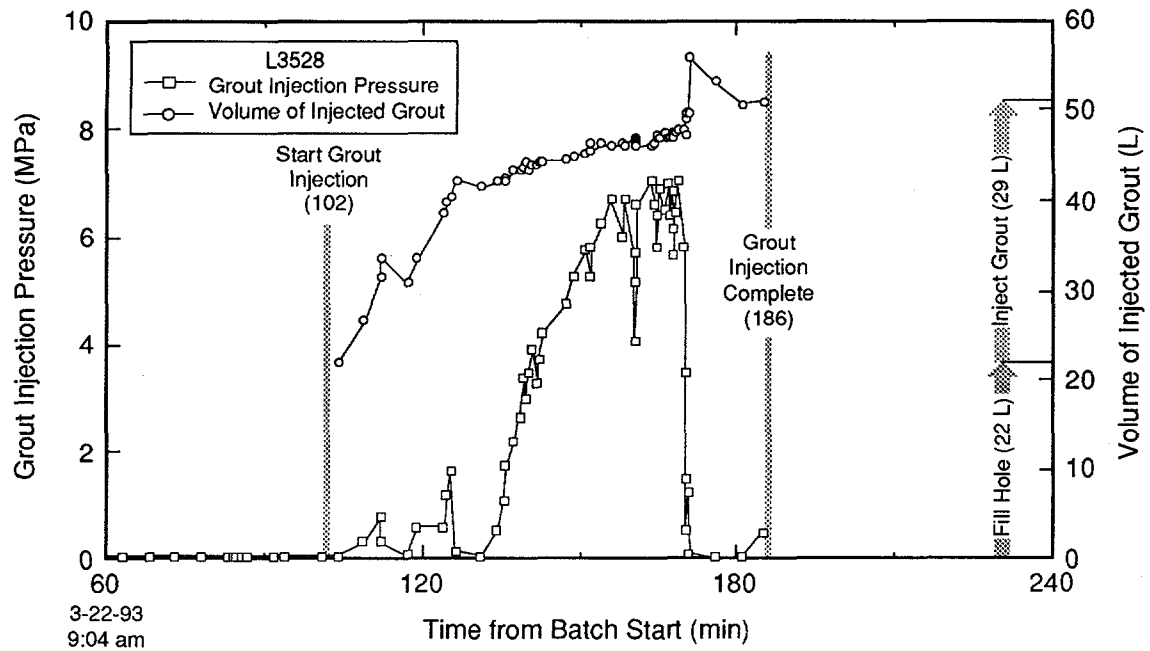


Figure G-76. Grout volume and pressure measured during injection of hole L3528.

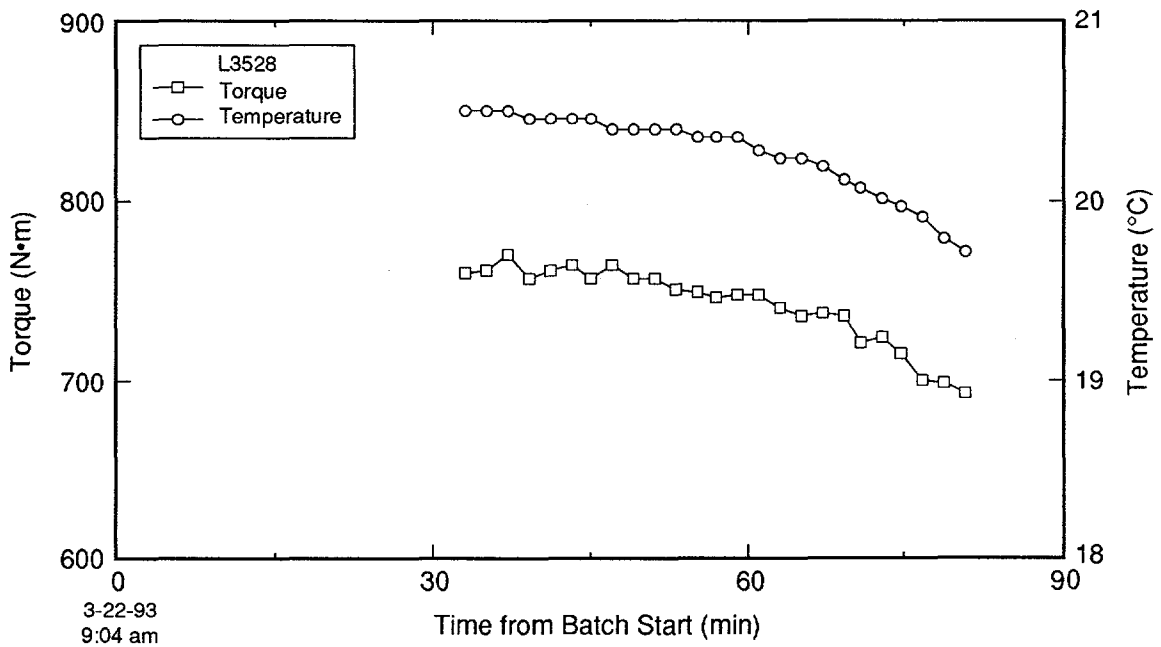


Figure G-77. Attritor torque and temperature measured during grout batching for hole L3528.

TRI-6121-176-0

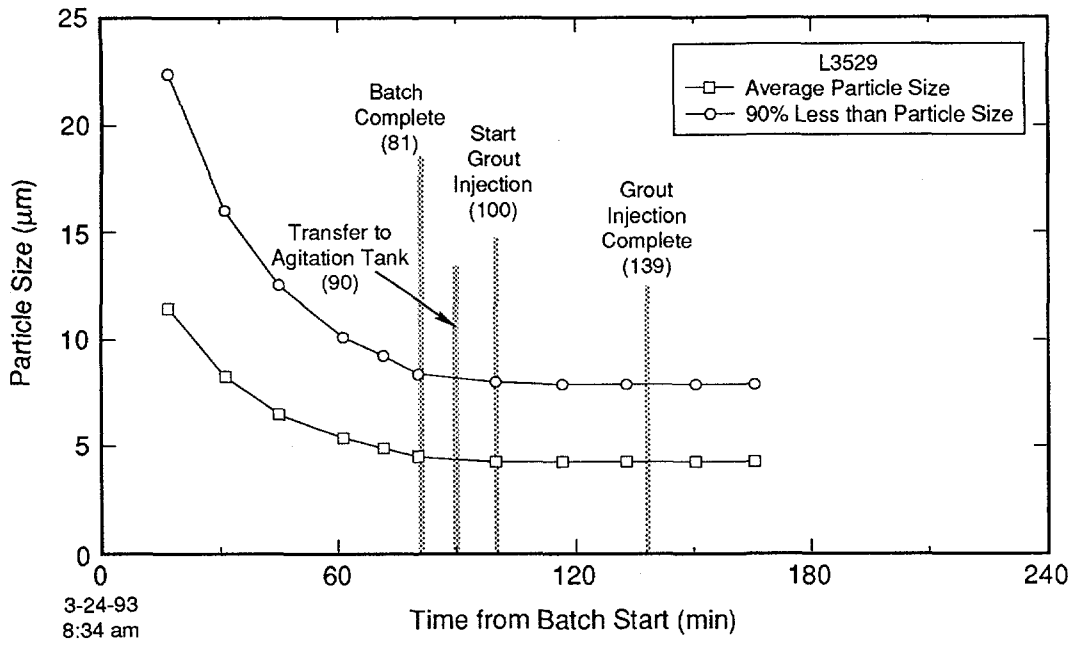


Figure G-78. Grout particle size measured during batching and injection of hole L3529.

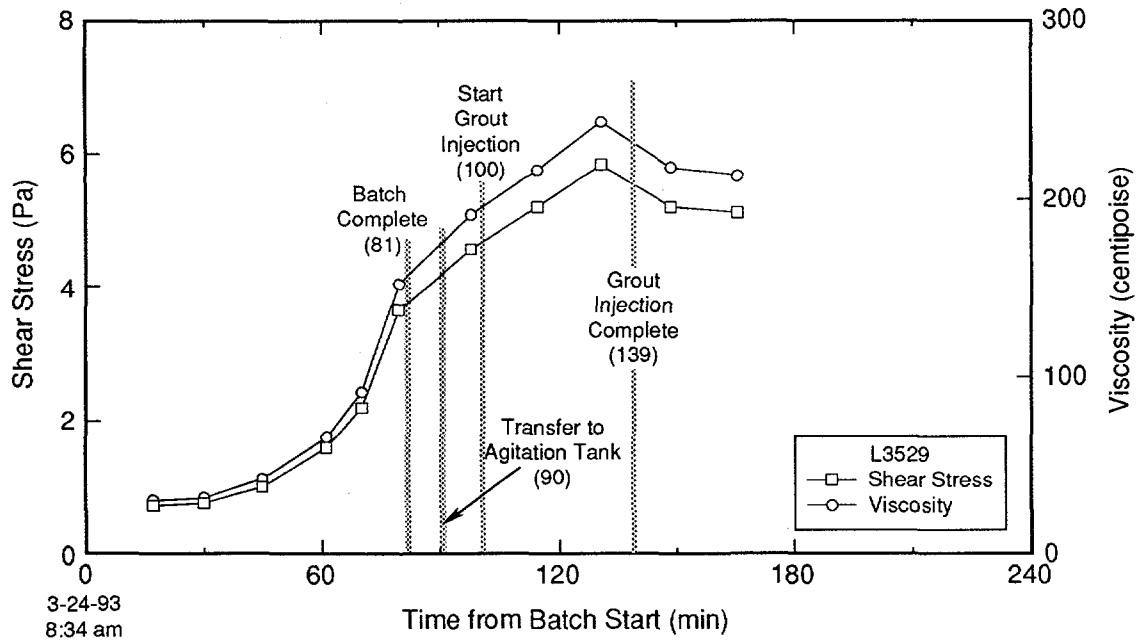


Figure G-79. Grout rheologic properties measured during batching and injection of hole L3529.

TRI-6121-194-0

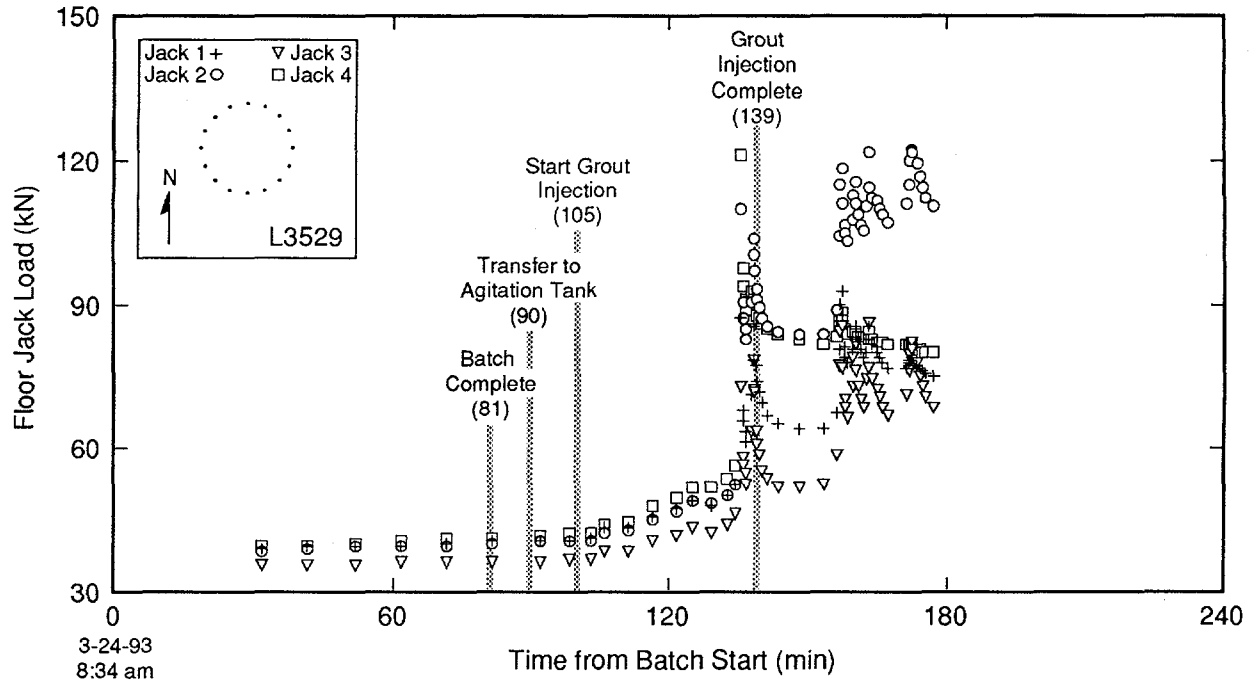


Figure G-80. Load cell measurements acquired during batching and injection of hole L3529.

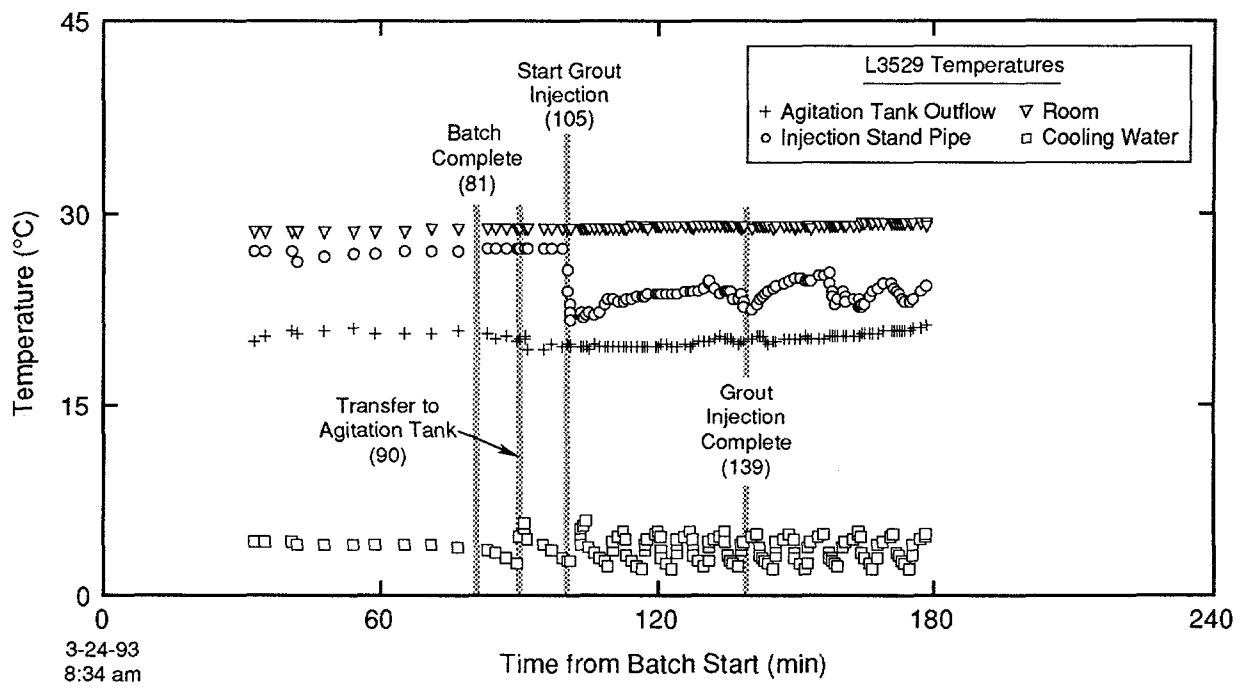


Figure G-81. Temperature measurements acquired during batching and injection of hole L3529.

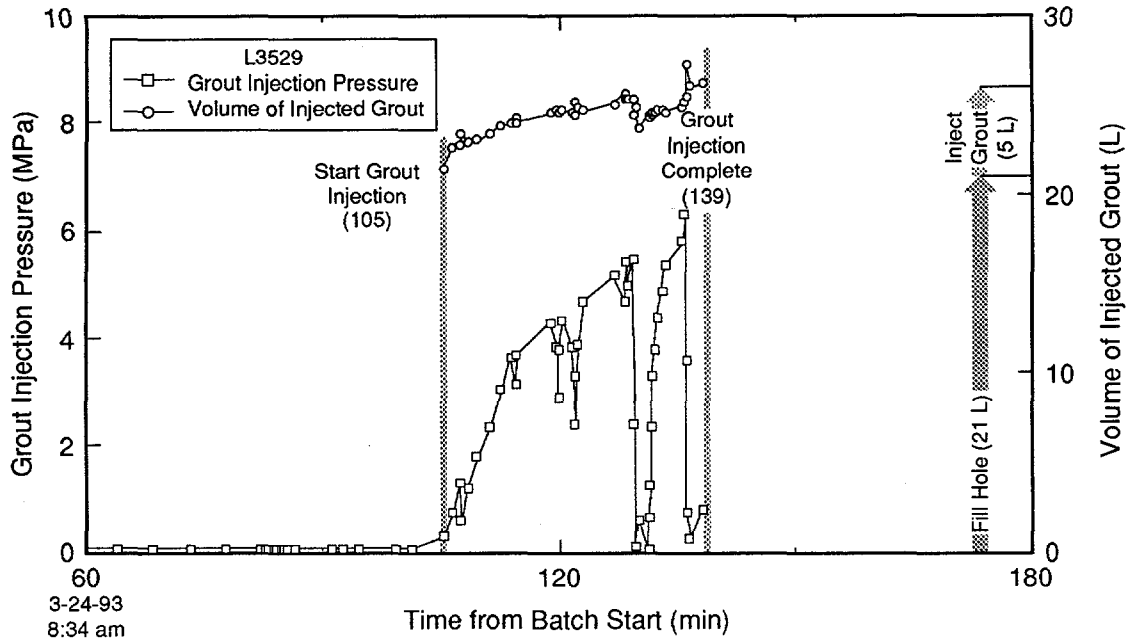


Figure G-82. Grout volume and pressure measured during injection of hole L3529.

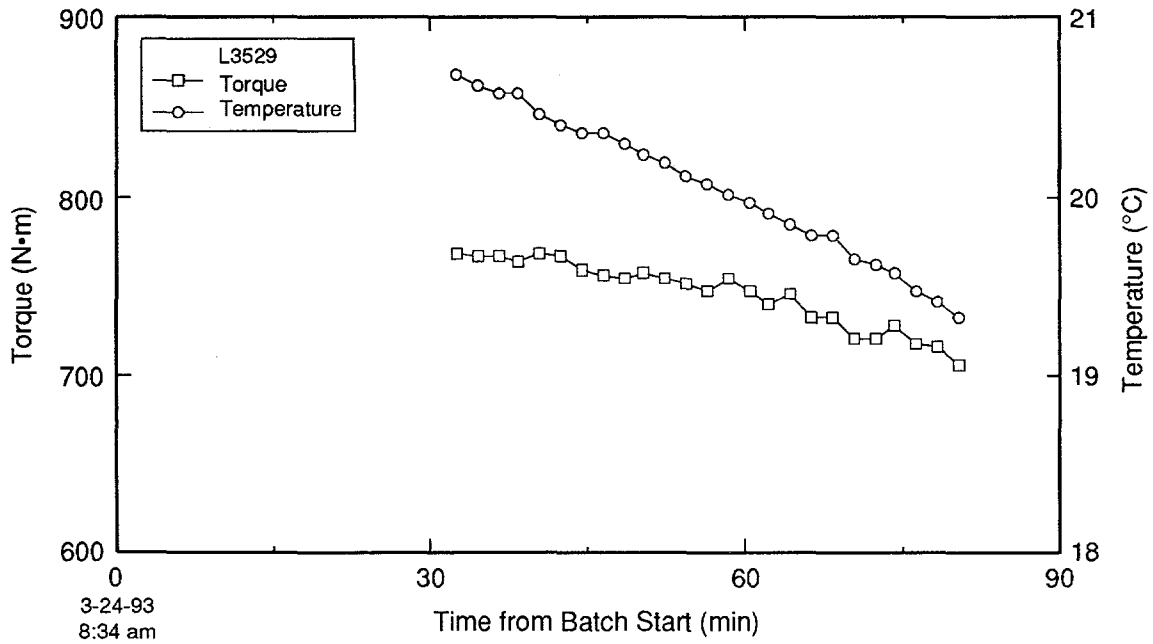


Figure G-83. Attritor torque and temperature measured during grout batching for hole L3529.

TRI-6121-177-0

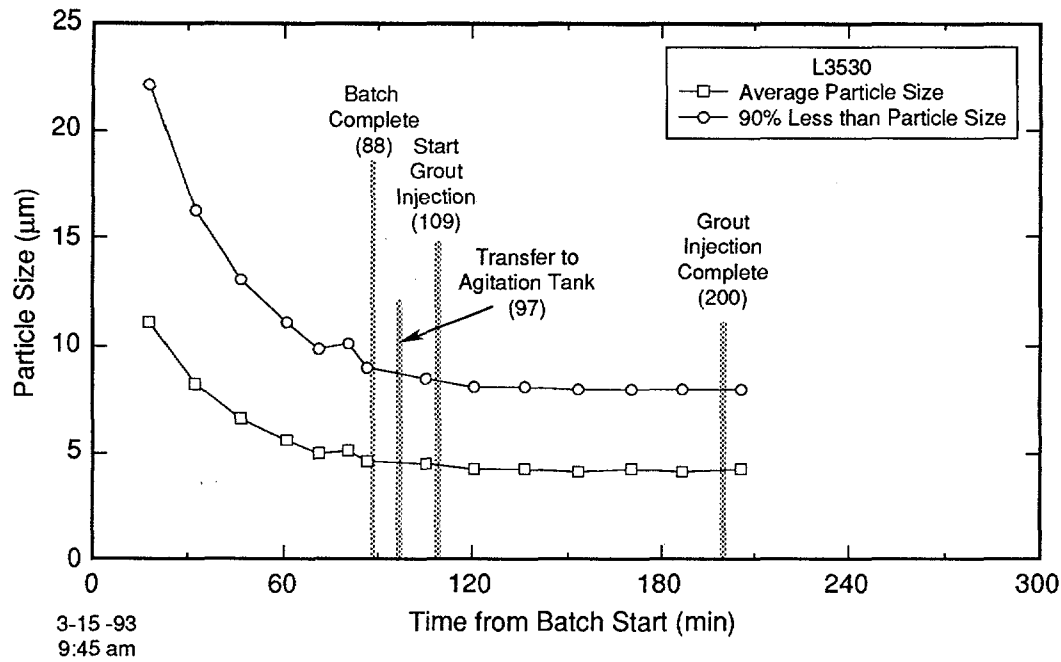


Figure G-84. Grout particle size measured during batching and injection of hole L3530.

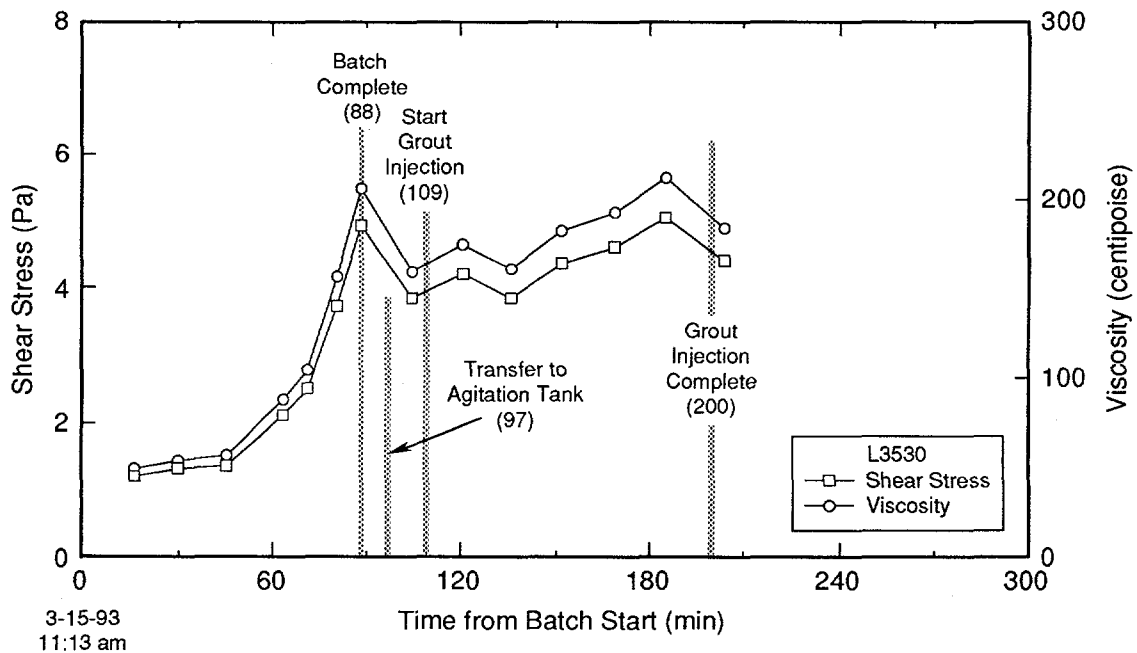


Figure G-85. Grout rheologic properties measured during batching and injection of hole L3530.

TRI-6121-195-0

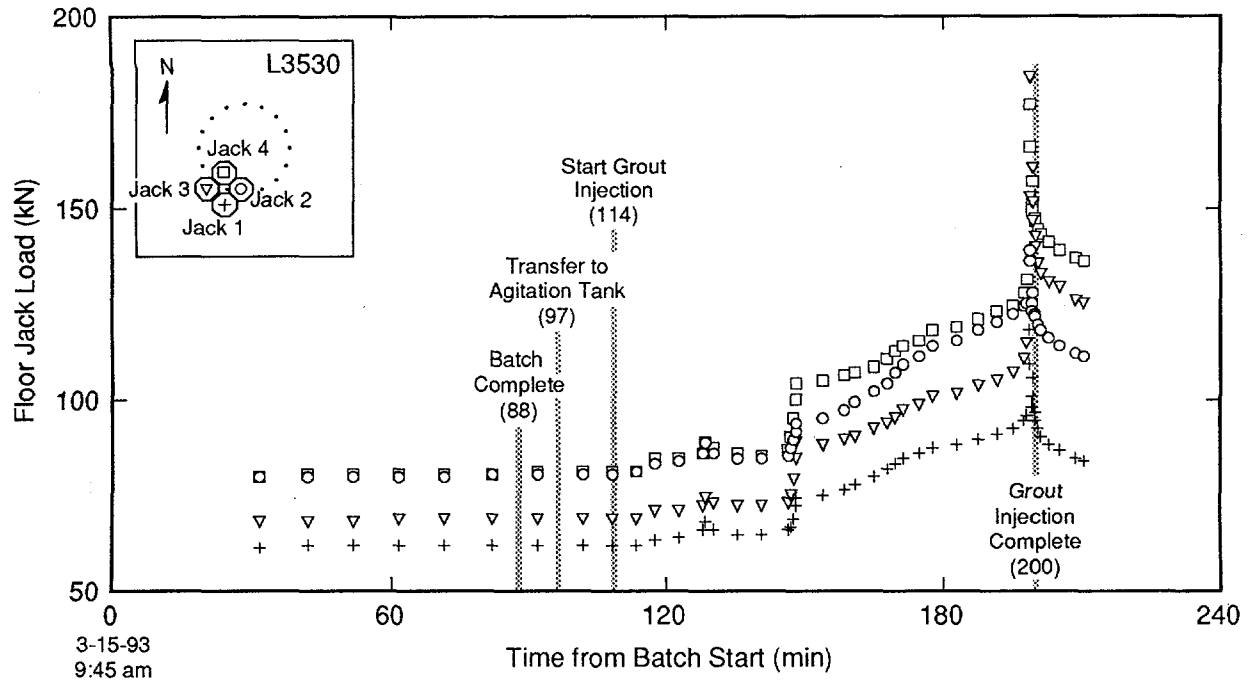


Figure G-86. Load cell measurements acquired during batching and injection of hole L3530.

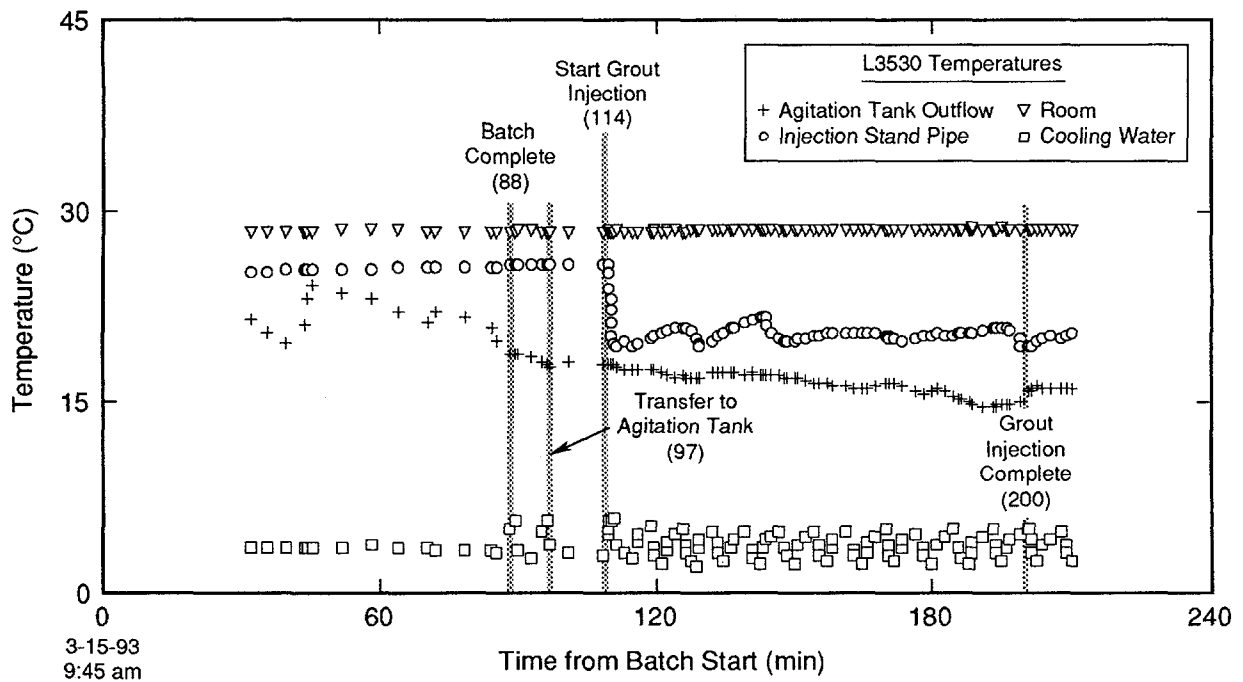


Figure G-87. Temperature measurements acquired during batching and injection of hole L3530.

TRI-6121-158-0

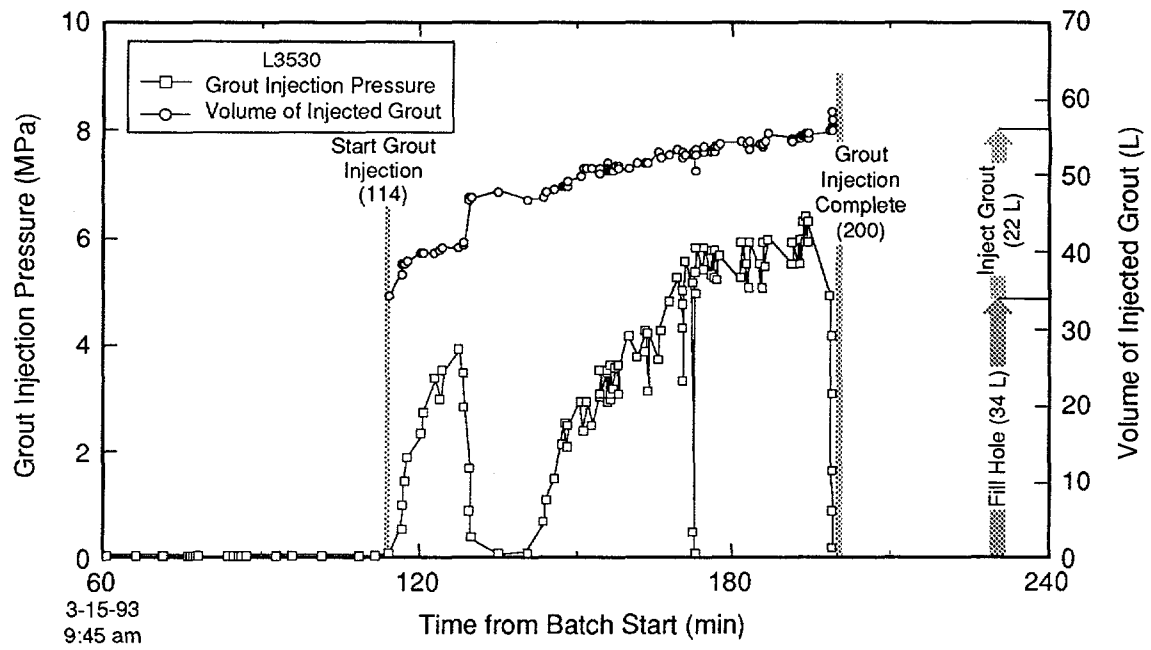


Figure G-88. Grout volume and pressure measured during injection of hole L3530.

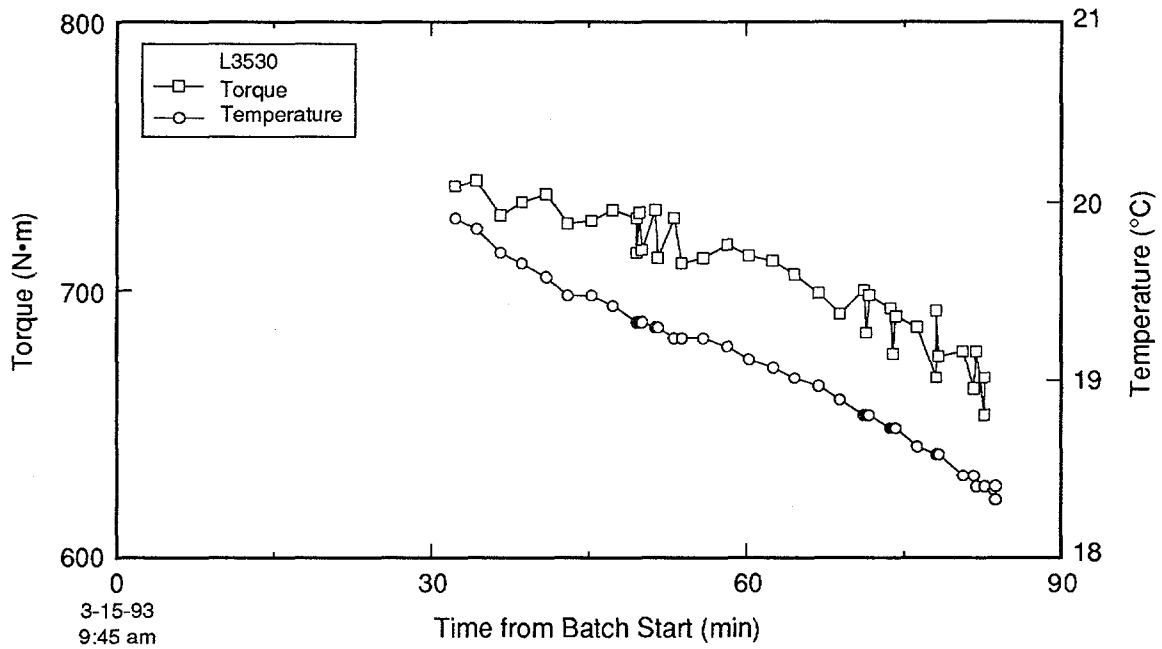


Figure G-89. Attritor torque and temperature measured during grout batching for hole L3530.

TRI-6121-178-0

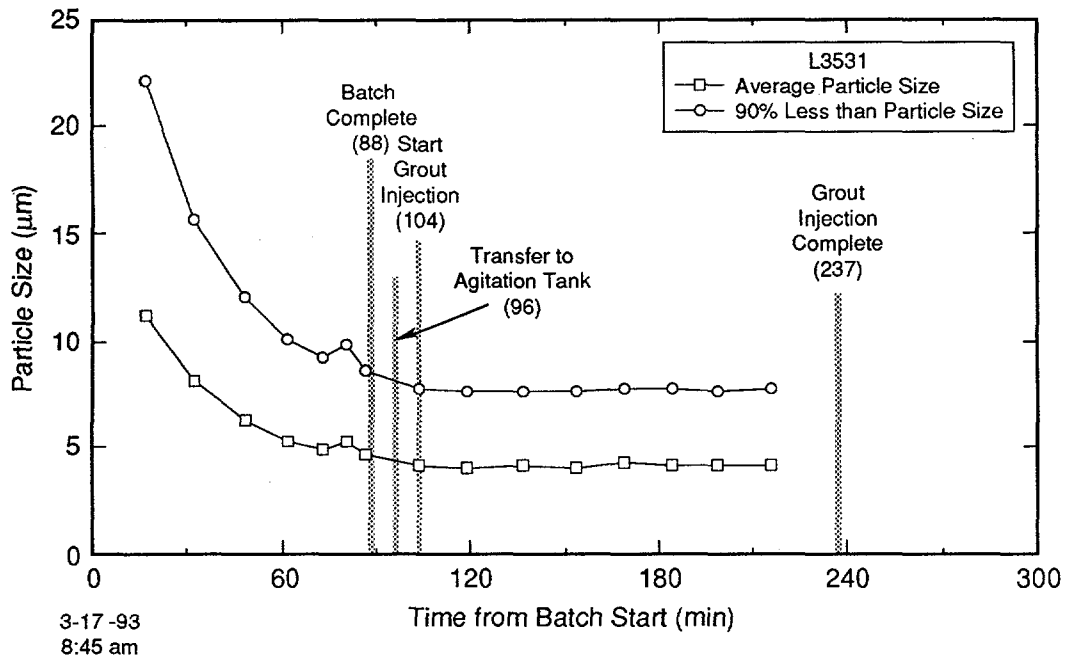
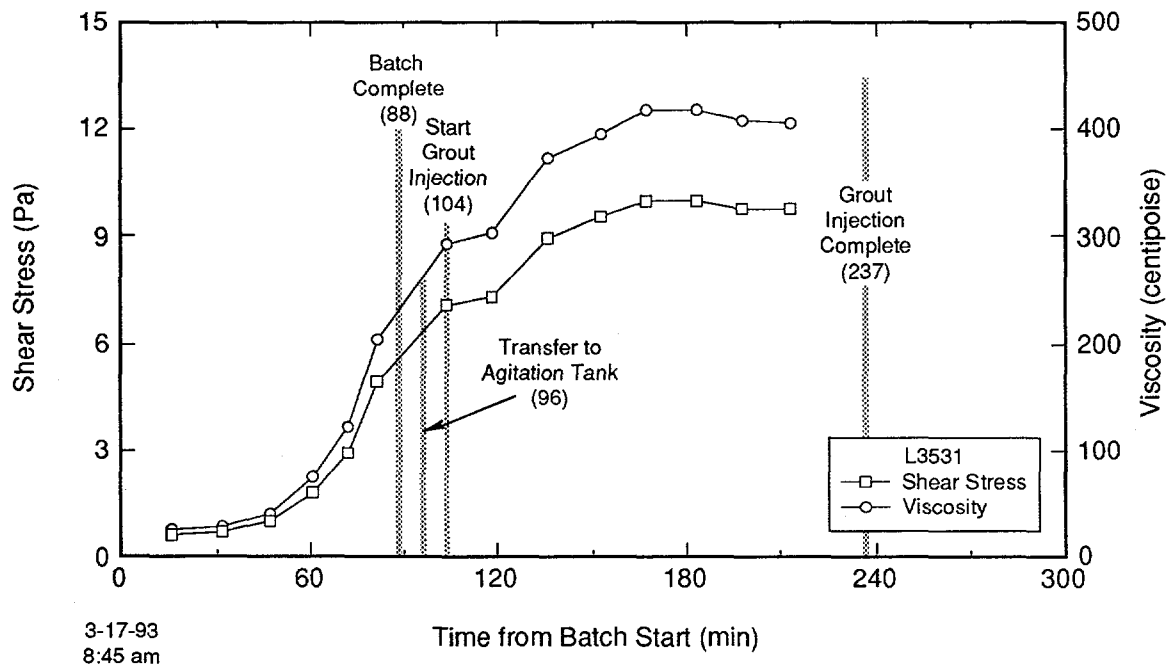


Figure G-90. Grout particle size measured during batching and injection of hole L3531.



TRI-6121-196-0

Figure G-91. Grout rheologic properties measured during batching and injection of hole L3531.

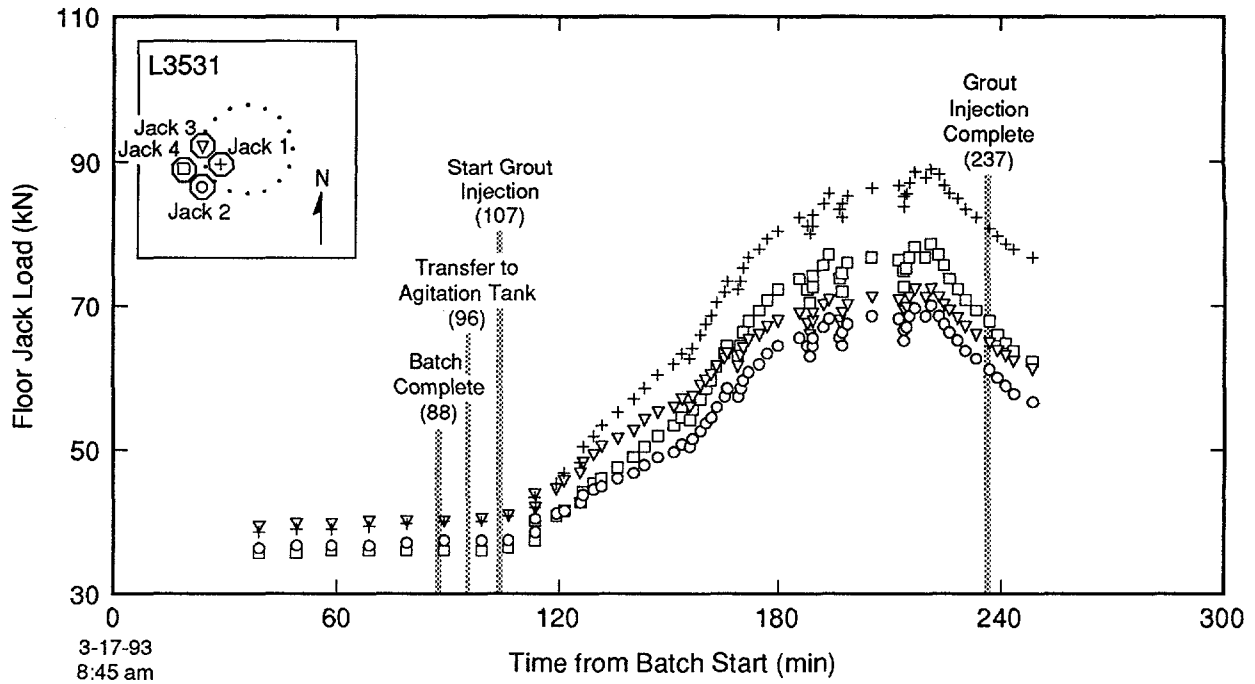


Figure G-92. Load cell measurements acquired during batching and injection of hole L3531.

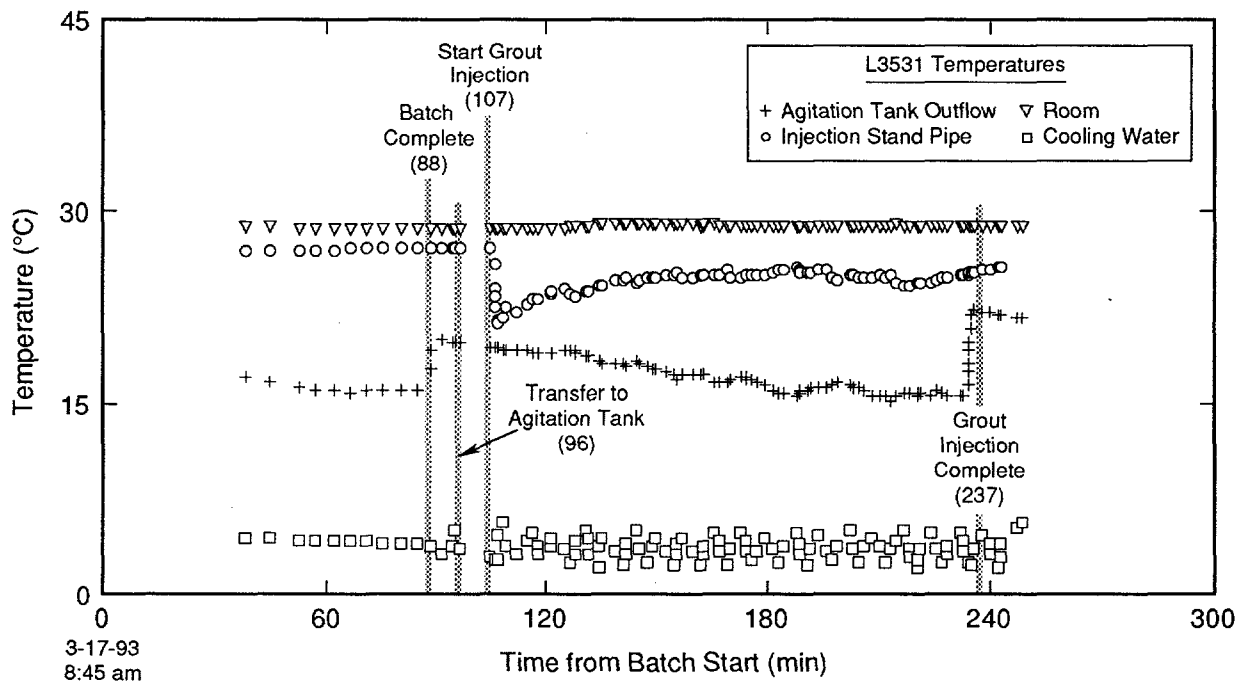


Figure G-93. Temperature measurements acquired during batching and injection of hole L3531.

TRI-6121-159-0

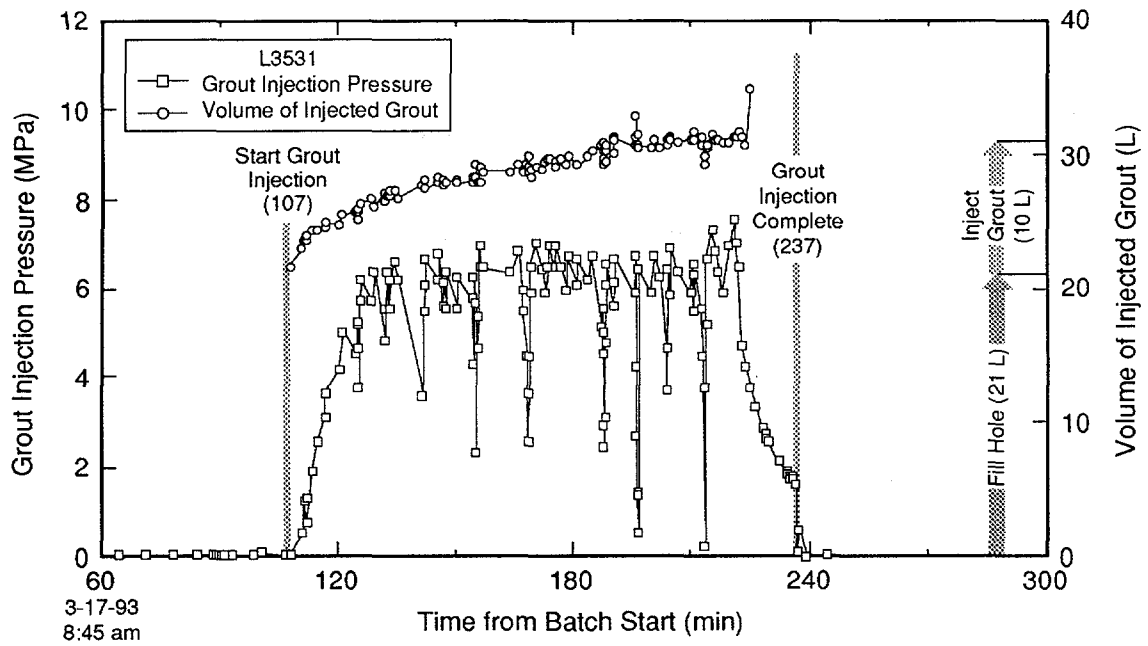
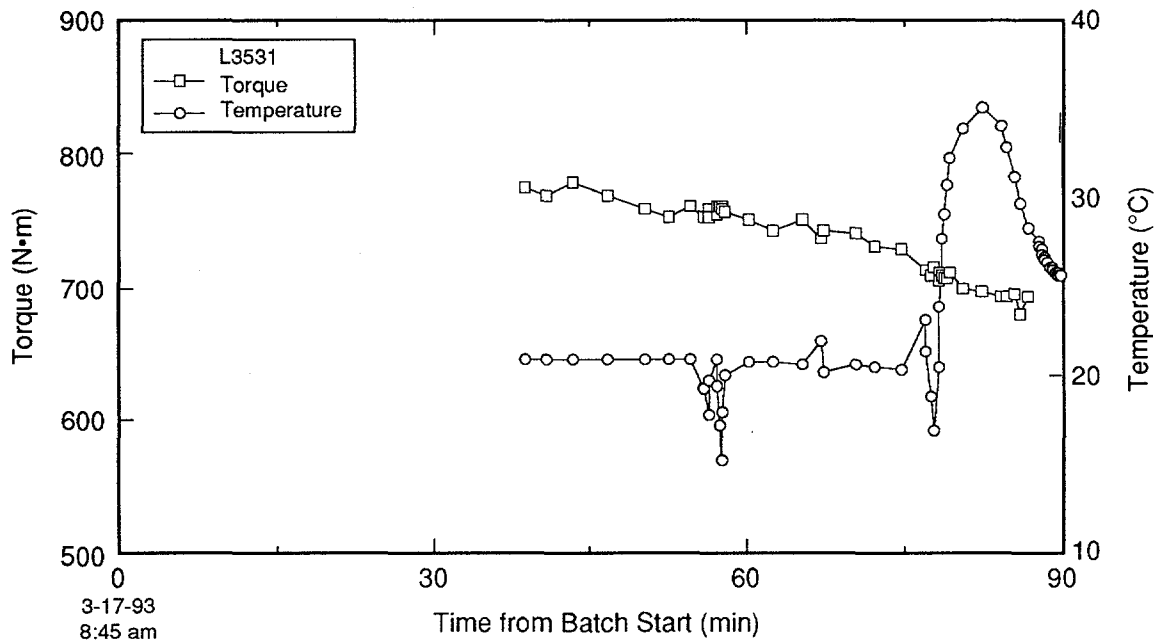


Figure G-94. Grout volume and pressure measured during injection of hole L3531.



TRI-6121-203

Figure G-95. Attritor torque and temperature measured during grout batching for hole L3531.

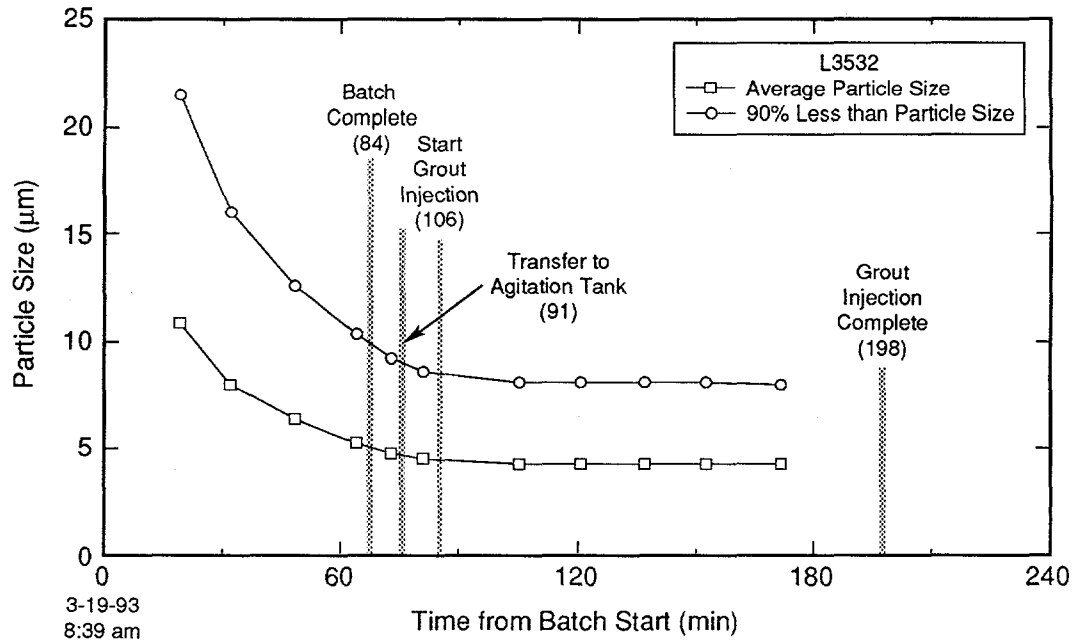


Figure G-96. Grout particle size measured during batching and injection of hole L3532.

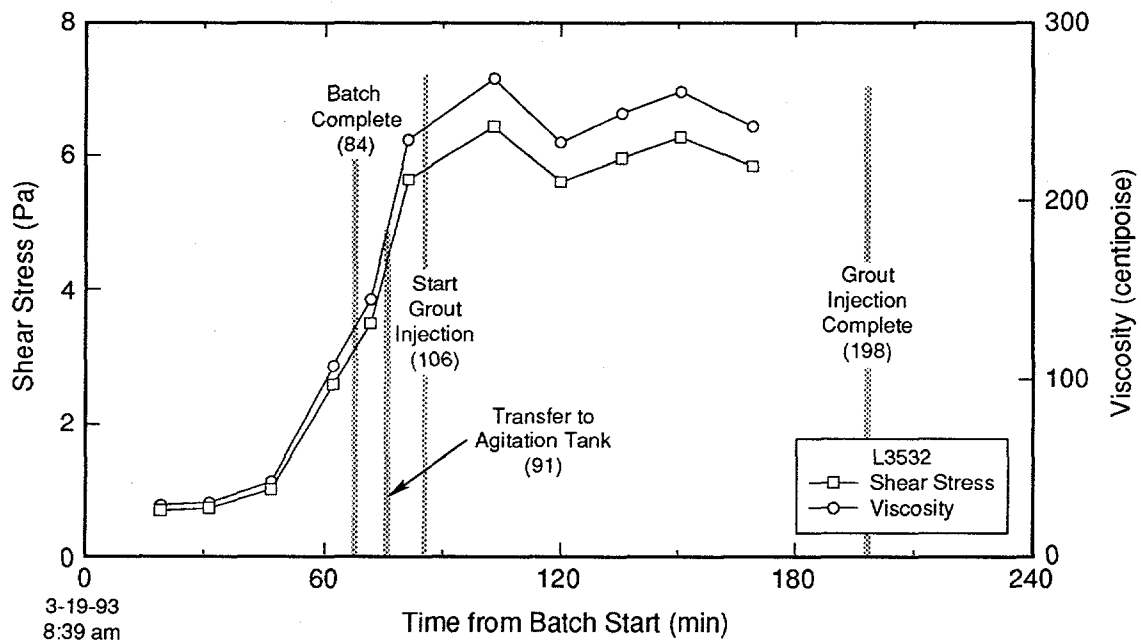


Figure G-97. Grout rheologic properties measured during batching and injection of hole L3532.

TRI-6121-197-0

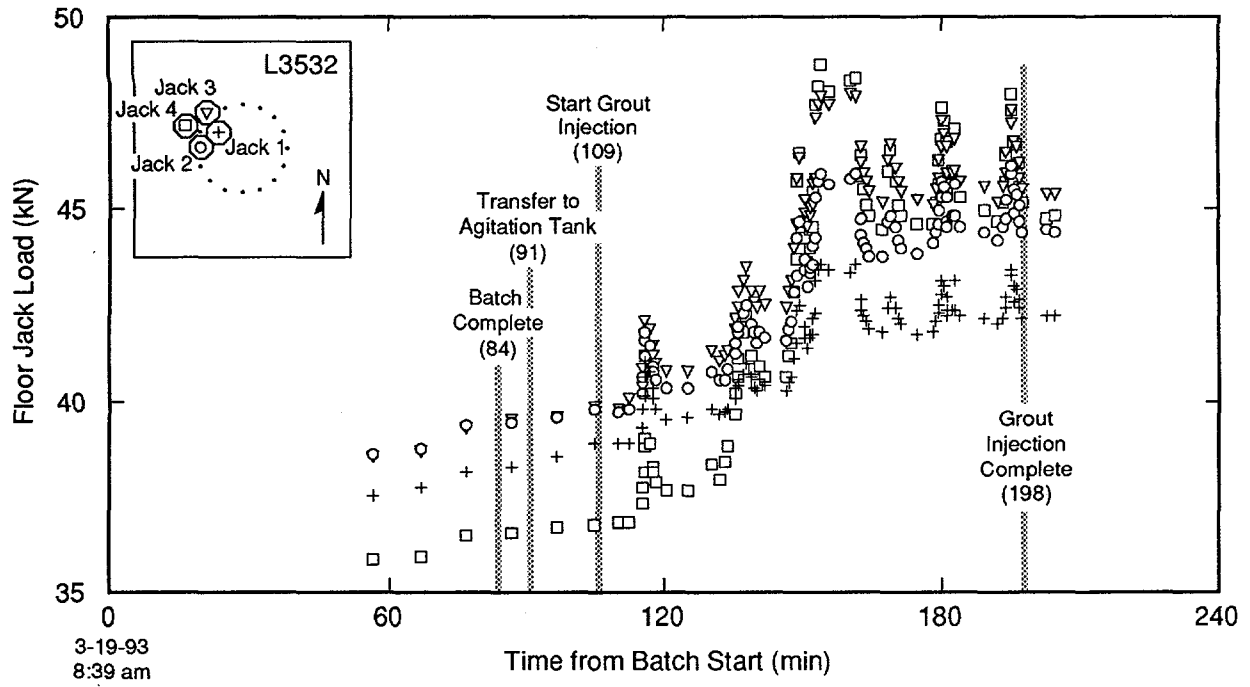


Figure G-98. Load cell measurements acquired during batching and injection of hole L3532.

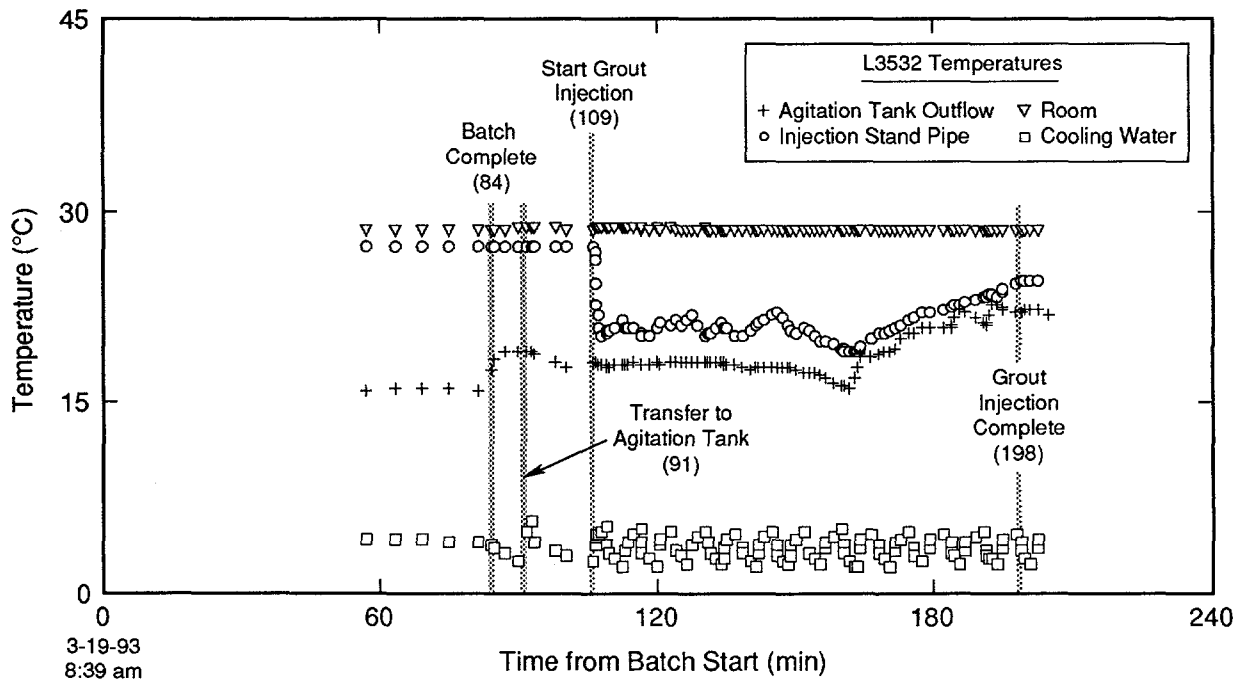


Figure G-99. Temperature measurements acquired during batching and injection of hole L3532.

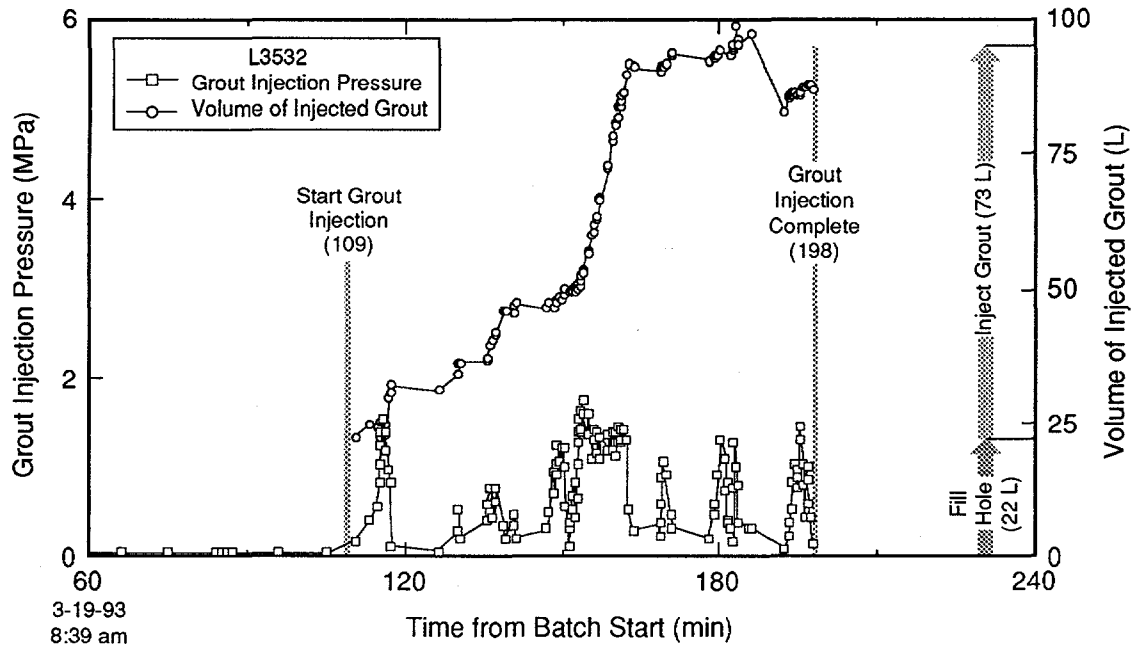


Figure G-100. Grout volume and pressure measured during injection of hole L3532.

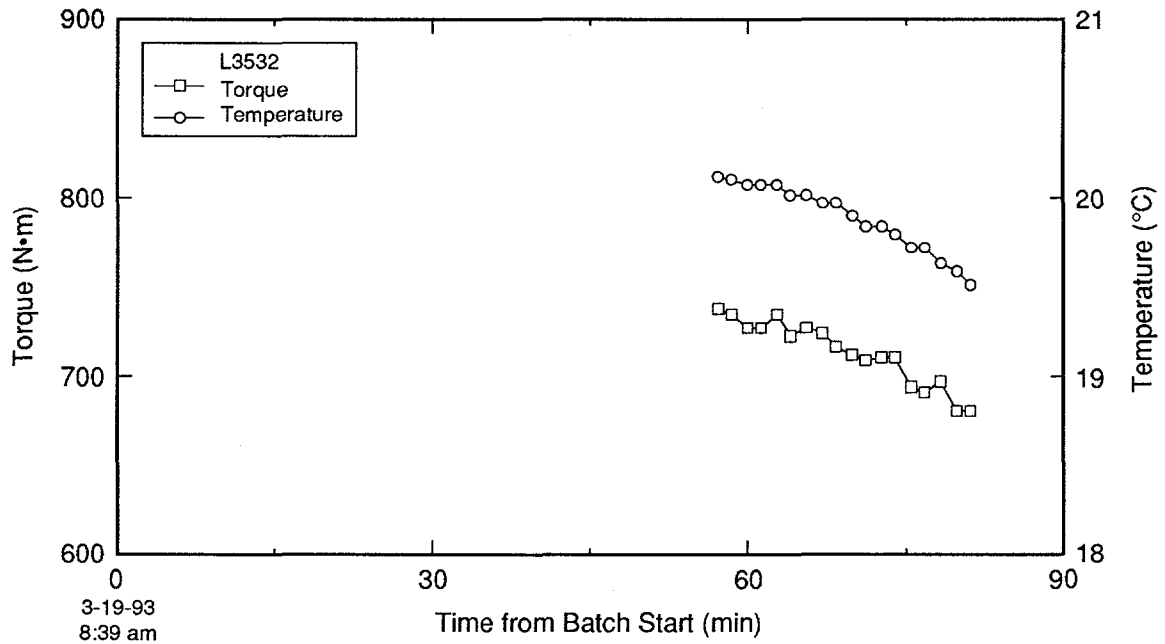


Figure G-101. Attritor torque and temperature measured during grout batching for hole L3532.

TRI-6121-180-0

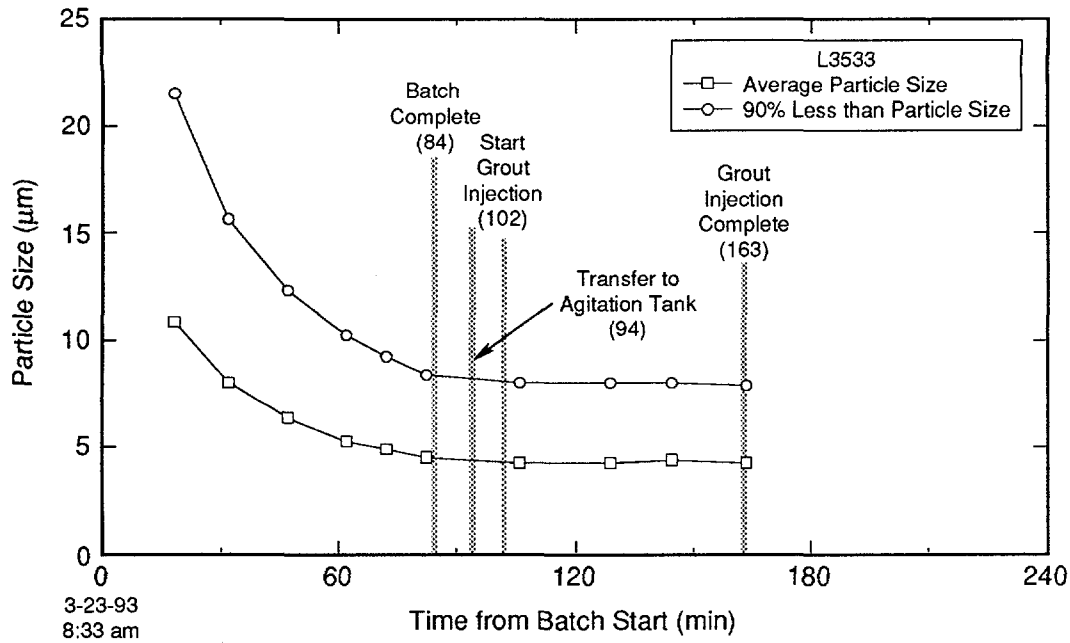


Figure G-102. Grout particle size measured during batching and injection of hole L3533.

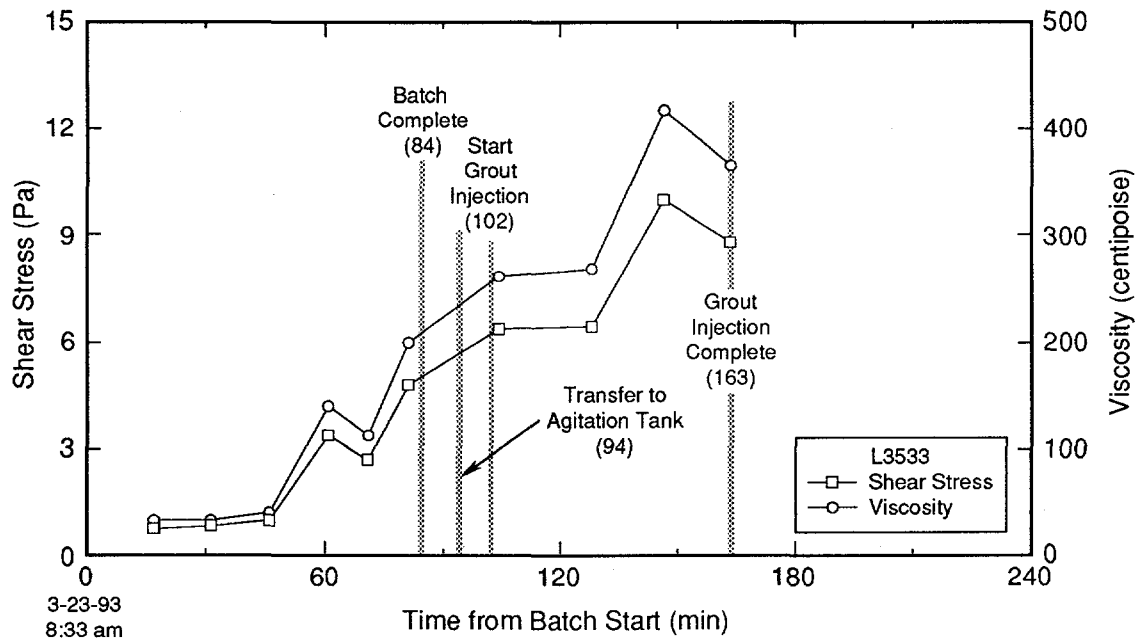


Figure G-103. Grout rheologic properties measured during batching and injection of hole L3533.

TRI-6121-198-0

Particle Size

A review of the graphs verifies that the simultaneous pulverization/mixing procedure resulted in acceptable quality control, as evidenced by the less than 1-micron variation among the 18 batches prepared. The criteria that 90% of the particles be smaller than 8 microns was satisfied. Continued particle size decrease during transfer of the grout to the agitation tank is probably due to additional mill activity (the attritor was operated at slow speed during transfer).

Note: the graph of the L3419 particle size data (Figure G-7) was partly experimental, as it contains information pertaining to the preparation of a second batch of grout. This was done to evaluate the feasibility of rapidly preparing a second batch, in case it proved necessary. (The second batch was simply discarded.)

Rheology

Plastic viscosity and shear stress of the grout were determined at 8 shear rates because both vary with the rate. During grouting, "straight line" (in plan) grout communication distances varied from 1.19 to 4.21 m. For graphic representation, the slowest of the eight shear rates was selected because it was assumed to most closely match the actual rate of grout movement through the formation.

Increased Load on Floor Jacks

Floor jacks were ordered set with an initial load of 44.6 kN. The four load cells on each jack recorded the load (readings from the four were combined to yield the total load). In practice, initial loads varied between 70 and 185 kN. The floor jack graphs show total load on each of the four jacks.

Initial load on each jack is indicated by the values closest to the y-axis. For example, Figure G-4 indicates that jack #4 was set to approximately 60 kN prior to grouting. The highest initial load was set on jacks supporting the grout test in L3422B. These four jacks were balanced at about 90 kN each. The lowest initial load was for jacks supporting grouting of hole L3423, about 10 kN. The maximum increase in jack load due to grouting occurred while injecting L3530. Load values during this event ranged from a low of 70 to a high of 185 kN, a difference of 115 kN. The divergence from the specified 44.6 kN initial load was not noted until after the tests were completed. The variance in initial jack load was 80 kN, and the area of the slab was 58 m², which translates to a variance of 0.00014 kN/cm². This variance is considered too small to affect test results.

Observations of increased jack loading frequently allowed the grouting supervisor to estimate the direction of grout movement.

Agitation Tank Load Cell Data

As noted in Appendix E, during injection of the primary grout holes, load cell data were noisy and questionable. Much of the data recorded on the DAS during this time were affected by a cabling problem discovered later. A "ground loop" acting as an aerial was affected by the electromotive field around the 460-volt attritor motor and apparently caused fluctuations in the electrical signal to the DAS. The problem is most evident in grout volume data (seen as significant fluctuations or instability) in holes L3419, L3420, and L3421. This problem was corrected prior to grouting the secondary grout holes.

Temperature

Temperature data were very consistent throughout the two-month testing period. Room temperatures remained nearly constant at 28.5°C, and cooling water temperatures were generally within a $\pm 2^\circ$ range of 4°C. This variation is believed to be a result of the hysteresis of the thermostat combined with cycling of the compressor. Temperatures measured at the injection "T" typically showed a 7° or 8°C drop (coinciding with initial injection) followed by a slow increase of approximately 2°C over the grout injection period because the near-stationary grout at that point was evolving hydrational heat uncompensated by cooling. Agitation tank outflow temperatures, in contrast, tended to decrease with time because cooling more than counteracted hydrational heat in the moving grout.

Injection Pressure

Marked variations in injection pressure can be seen in the data plots for all holes. The reasons for the variations are listed below:

- The injection operator may stop injection because rod extensometer readings suggest that slab displacement is beginning.
- Injection may be halted because a sudden pressure drop suggests communication with other holes, which may (or may not) be the case.
- A drop in the injection rate occurs; this was usually counteracted by increasing injection pressure.

- Actual grout communication with an open hole (or holes) occurs, requiring cessation of injection while guard packers are set.

Attritor Torque and Temperature

Temperature and torque both decrease with time because, although plastic viscosity and shear stress increase during pulverization and mixing, the torque (force required to rotate the "stirring arms") decreases. This anomalous behavior is currently inexplicable. As the torque decreases, so does the amount of mechanical heat. Since cooling remains constant, the temperature of the grout decreases.

This page intentionally left blank.

APPENDIX H: GROUT DISTRIBUTION DATA

This page intentionally left blank.

Post-grout, Down-the-Hole Televiewer

All post-grout coreholes were examined with a high-resolution down-the-hole televiewer. The resulting videotapes were edited to show only the sections of the hole containing grout. These served as a useful check on the core logs and are filed with WIPP Quality Assurance.

The north, south, east, and west surfaces of the holes were viewed. The number of observed grout occurrences varied, but some surfaces showed as many as 25 occurrences involving 6 different grout colors.

APPENDIX H: GROUT DISTRIBUTION DATA

Post-grout, Diamond Drill Core Logs

After grouting activities were completed, 24 coreholes 15.24-cm in diameter were drilled. The core was logged, with special attention paid to any grout observed. The core was then photographed in color, and the logs and photographs were filed with WIPP Quality Assurance.

Grout occurrences were examined with the petrographic microscope (using reflected light), and with the scanning electron microscope (SEM) and energy-dispersive x-ray (EDX). These examinations helped determine the size of the aperture routinely grouted, as well as indicating the smallest apertures grouted.

Because of the complexity of the macro- and micro-fracture system, flow paths are extremely irregular and impossible to predict. A flow distance of 6 x straight-line was assumed based on previous experience. For this assumed distance, flow rates varied from 0.17 to 3.83 cm/second. The slowest shear rate, 23.7 rpm (equivalent to a flow rate of 3.72 cm/second) was selected for graphical depiction of shear stress and plastic viscosity, as it was assumed to most closely match the actual rate of movement of the grout within the formation.

An EDX analysis used in conjunction with the SEM yields a qualitative analysis of the material in the fracture, verifying that it is grout. Notable examples are presented in Section 5. The SEM and EDX work has revealed these accomplishments:

- Microfractures with apertures ≤ 10 microns were routinely sealed.
- Examination of grouted microfractures by SEM (at Whiteshell Laboratories and SNL) failed to reveal any dissolution of halite due to the injection of grout.
- Although constrictions as small as 7.9 microns were successfully penetrated (Photo 5-1), permeation generally ceased at approximately 10 microns. One highly unusual exception was noted (Photo 5-3) in which the grout completely filled a 3-micron fracture.

APPENDIX I: GAS-FLOW/TRACER-GAS TEST RESULTS

This page intentionally left blank.

APPENDIX I: GAS-FLOW/TRACER-GAS TEST RESULTS

Gas-flow/tracer-gas equipment and test procedures, designed and developed specifically for this experiment, were evaluated to determine the system's ability to quantify the effectiveness of ultrafine cementitious grout in reducing gas transmissivity of fractured WIPP rock.

Preliminary gas-flow testing of Room L3 was conducted to determine the best location for the experiment. A memorandum describing the decision to situate the grout test in the north end of Room L3 is attached to this appendix.

Cross-hole gas-tracer testing was conducted before grouting (on January 29, 1993), six times during grouting, (on February 5, 9, 15, 18 and on March 10 and 11, 1993), and repeated after grouting on April 5, 1993. Gas-flow and cross-hole tracer gas analyses were conducted as detailed in Section 4, and results are summarized in the tables on pages I-30 through I-34.

Most of the reduction in gas transmissivity appears to have been accomplished by grouting the initial four holes (located at 12, 3, 6, and 9 o'clock positions—with 12 o'clock in the north position), which indicates that hole spacing was closer than necessary.

Although secondary grouting (ninth through sixteenth grout holes) was accomplished at higher injection pressure than that used for the eight primary grout holes, much of the later grout simply spread beneath the slab (at the slab/salt interface) and had minimal impact on the gas transmissivity. This is believed to be the result of a decrease in open pathways (fractures) resulting from previous grout injection.

Possible Future Use of Data

Baseline data (core and borehole observations, gas-flow and cross-hole gas tracer test results, analysis of tracer gas movement during and after grout injection, and post-grout core analyses) may provide sufficient information to enable the preliminary development of a qualitative DRZ grout injection and sealing model. Additionally, the study of localized variability in MB139 gas transmissivity (fracture characteristics), coupled with a site-wide study of MB139 variability, could help establish initial estimates of grout hole spacing and formation grouting requirements.

Tracer-Gas Test Results

Tracer-gas test results are presented in terms of the maximum relative received tracer gas concentration (together with the time required to achieve this concentration) in each of the receiver holes. The analyses are presented in a series of "breakthrough" curves in the memorandum of April 29, 1993 included in this appendix. Note that the hole locations shown in Figure 1 of this memorandum are incorrect. The correct locations appear in Section 2, Figure 2-3.

Gas-Flow Analysis

Gas-flow test data were interpreted with the Graph Theoretic Field Model (GTFM) described in Appendix J and fully detailed in Pickens et al. (1987). The GTFM model uses a finite difference technique and assumes a constant formation thickness. A preliminary analysis of the data was conducted in 1993 and then updated in 1994 with a reanalysis of the data using an enhanced version of the test-analysis software. The principal changes in the reanalyses were (1) extension of the model boundaries to beyond the area of influence of the modeled gas injection, (2) simultaneous optimization of porosity and permeability, and (3) inclusion of the effect of wellbore storage on the isolated test intervals. Results of the reanalysis are summarized in the second memorandum attached to this appendix, dated June 16, 1994.

date: April 29, 1993

to: distribution

Ray E. Finley
from: R.E. Finley & J.T. George, 6121
R.S. Van Pelt & G. Saulnier, Intera

subject: Memorandum of Record - Preliminary Results of Gas Flow/Tracer Testing in MB139 and Overlying Halite in Room L3 at the WIPP

1.0 INTRODUCTION

This memorandum describes the equipment, techniques, and preliminary results of gas flow/tracer testing in Marker Bed 139 (MB139) and the overlying halite in Room L3 at the WIPP. This gas flow testing was conducted between May, 1992 and April, 1993 and was performed as an integral part of the grouting demonstration described in Ahrens, 1992. Only the results of gas flow/tracer testing performed through completion of the primary grout injection holes is described in this memorandum. Subsequent gas flow/tracer data will be presented in a later report. The rationale for this test and its relationship to the WIPP sealing program are described in the original test plan and will not be discussed here. The objectives of the grouting demonstration are (from Ahrens, 1992);

- 1) Demonstrate the ability to practically and consistently produce microfine, cementitious grout at the grouting site (Room L3).
- 2) Demonstrate the ability to inject and permeate microfine, cementitious grout into fractured rock at the WIPP repository horizon consistently and efficiently.
- 3) Gain data on the ability of microfine, cementitious grout to penetrate and seal microfractures.
- 4) Evaluate procedures and equipment used to inject microfine, cementitious grout into fractured WIPP rock.
- 5) Evaluate techniques which can assess the effectiveness of microfine grout in reducing the gas permeability of fractured WIPP rock. These include gas flow/tracer testing, post-grout coring, pre- and

post-grout downhole televiewer logging, slab displacement measurements, and increased loading on jacks during grout injection.

- 6) Obtain pre- and post-grout, diamond drill core for use in ongoing laboratory evaluations of grouting effectiveness, degradation, and compatibility.

The information in this memorandum applies directly to objectives 3 and 5 above. Objective 5 is especially important for gas flow/tracer testing because these techniques are being considered for use in evaluating the performance of planned large-scale seal tests at the WIPP. The grouting demonstration provided a unique opportunity to assess SNL's readiness in estimating gas flow potential in the Disturbed Rock Zone on a drift-scale and under changing flow conditions.

2.0 TEST CONFIGURATION

Room L3 was selected as the location for the grouting demonstration based on the results of previous studies that described the nature of the DRZ in MB139 (e.g. Borns, 1985; Borns and Stormont, 1988; Stormont et al, 1987). These studies suggested that high gas flow rates could be expected in MB139 along the drift centerline based on the age (> 5 years) and size (33 ft wide) of Room L3. The exact location for the grouting demonstration was selected based on a general gas-flow characterization program that included holes into MB139 along 5 cross-sections from the Room L3 intersection with N1420 to approximately 100 ft into Room L3. This characterization was completed between May-July 1992 and suggested that a location between 75-100 ft into Room L3 be used for the grouting demonstration because that location exhibited a large range of gas permeabilities.

2.1 TEST GEOMETRY AND GAS FLOW/TRACER EQUIPMENT

Figure 1 shows a plan view of the concrete slab and the location of the boreholes used to conduct gas flow/tracer testing. The figure also shows the locations of the grout injection boreholes. Table 1 provides a description of the function of each borehole along with chronological information on the test.

Figure 2 shows schematically the gas flow and gas tracer equipment used in this test. Figure 2 also shows the approximate geometry of the downhole packer tool relative to MB139, the overlying halite, and the concrete slab. The results presented in this memo are for the downhole configuration shown in figure 2 only. This configuration provided a good overall estimate of the gas flow potential in the entire region under the concrete slab before, during, and after grout injection.

All boreholes drilled in and adjacent to the concrete slab were nominally 6-inches in diameter to a depth of 11.5-12.5 ft. These boreholes were tested with a four-packer assembly with 3.5-inch mandrel and inflatable packers 5.25 inches in diameter. The gas flow/tracer testing described in this memo was performed with only the bottom two packers set in the borehole as shown in figure 2. The effective - pressurized portion (test zone) extended from 51.5 inches below the borehole collar to the bottom of the borehole with a single upper guard zone of 14 inches located between the two inflated packers.

The tracer gas testing was performed by injecting nitrogen spiked with isobutene at 20psi in the central gas injection hole (L3001) and sampling in each of eight alternating tracer receiver holes. The sampling tubes were moved to the other eight tracer receiving boreholes and the tracer test repeated. Thereby, tracer arrival and concentration data were obtained for all sixteen tracer receiver holes prior to the first grout injection, after the first four primary grout injections, and after all eight primary holes were grouted.

The gas flow system is capable of injecting gas flow rates of up to about 30,000 Standard Cubic Centimeters Per Minute (SCCM) for the borehole geometries and injection pressures used in this testing. The tracer detection system is capable of detecting tracer arrivals in concentrations of from 0.1 to 2000 ppm.

2.2 TEST SEQUENCING

The location of the concrete slab for the grouting demonstration was determined from the results of gas flow testing in Room L3 from May through July, 1992. The invert at the slab location was laser levelled in late August 1992 and slab construction begun in September 1992. Concrete for the slab was poured in late September 1992. Table 1 lists the near and on slab boreholes that were used for gas and grout injections and provides information on the chronology of pertinent activities.

Gas flow testing was performed in all boreholes on the slab prior to the first grout injections and following the completion of the primary hole grouting. Gas tracer testing was performed prior to the first primary grout injection, after each of the first four primary grout injections, and after all eight primary grout injections. Results of tests conducted after the secondary grouting are not yet available.

3.0 DATA ANALYSES

3.1 GAS FLOW ANALYSIS

The interpretation of the gas flow data was conducted using the well-test-simulation model GTFM (Graph Theoretic Field Model; Pickens et al, 1987). GTFM has the capability to model single-phase, one-dimensional, radial-flow gas injection from a borehole under specified boundary conditions. The model uses a finite difference technique and assumes a constant formation thickness.

The analyses were performed using two different simulation strategies. Gas flow tests were simulated by specifying the flow rate, as determined from the test data, and simulating the pressure history. The simulated pressure history was then compared with the measured pressure history. Tests were also simulated by specifying the measured pressure data, simulating the flow rate, and comparing the simulated flow rate data with the measured flow rates. For both simulation strategies, permeability and porosity values are varied until the specified simulated output (flow rate or pressure history) best matches the measured data. In general, both methods of gas flow analyses yielded similar permeability estimates.

3.2 TRACER GAS ANALYSIS

Tracer gas injection pulse tests were performed by injecting instrument grade air into the central gas injection hole (L3001) at constant downhole flow/pressure for a period of 1.5 hours to achieve near steady-state conditions. This was then followed by a 30 minute constant flow/pressure pulse of instrument grade air with a "spike" of isobutene followed by a 2 hour pulse of instrument grade air intended to force the isobutene through the formation.

Tracer gas (isobutene) was detected in each of the "sniffer" holes (L3202-L3217) using the sequencing manifold and Photo Ionization Detector (PID) (see figure 2). Output from the tracer gas detection system was described as a time sequence of received tracer gas in each "sniffer" hole expressed as a relative concentration of isobutene. This relative concentration is the sampled concentration divided by the maximum possible concentration.

The tracer gas testing provided results that can be used to qualitatively assess the nature of the flow paths through which the gas travelled. Quantification of the tracer gas results is not possible because of the geometry between the gas injection and "sniffer" holes. This geometry does not allow for a mass balance of injected and received tracer gas.

4.0 RESULTS

Table 2 lists the results of the gas flow characterization conducted in the on-slab boreholes through the completion of the primary grouting. This data is compared with the results of the pre-grouting characterization and the difference in calculated permeabilities is presented. The results show that the permeability in the central gas injection hole was decreased by about three orders of magnitude (from about $1.8E-12 \text{ m}^2$ to about $1.9E-15 \text{ m}^2$) as a result of grout injection in the eight primary grout injection holes. A reduction in permeability was seen in all but one of the "sniffer" holes over the same time period. A very preliminary estimate of the gas flow in the central injection hole was made following completion of the secondary grouting. Measured flowrates suggest little additional reduction in permeability was achieved in the central gas injection hole (L3001) by grouting in the secondary holes.

Table 3 and figures 3 through 18 present data on the tracer gas testing. The results are presented in terms of the maximum relative received tracer gas concentration and the time to achieve this concentration in each of the "sniffer" holes. The results show, in general, that the received concentrations tended to decrease as each grouting episode was completed. The results also show that the flow of gas was redirected to other receiver holes, primarily during the early grouting events. This is seen in increases in arrival concentrations in some holes (e.g. hole L3203). The tracer gas breakthrough curves and data should be used for subjective estimates of the gas flow potential from the central gas injection hole toward each of the "sniffer" holes. Because mass balance of the tracer gas is not possible for this test configuration, exact estimates of flow path geometries are not possible at this time. Figure 19 presents a description of generalized types of breakthrough curves seen during the tracer testing.

Figure 20 presents the tracer gas data in a different format. The peak arrival concentrations are plotted as arrows whose length is proportional to the peak arrival relative concentration for each of the sixteen "sniffer" holes for the pre-grouting and post primary grouting tracer gas tests. The data presented in this form allows a quick evaluation of the changes that occur in flow paths as a function of grout injection. The figure shows clearly that prior to grouting, the predominate flow paths were to the north and south along the drift centerline. Each successive grout injection caused a change in the nature of the gas flow paths. The final gas tracer test showed that the peak arrival concentrations were greatly reduced in all of the "sniffer" holes with minor residual flow paths toward the north and southeast along the drift centerline. In other

words, the tracer gas tests provide some indication as to the relative direction that gas injected into the central gas injection hole permeates.

Results from the gas flow/tracer testing after the grouting of the secondary holes are currently being analyzed. These data will be transmitted as they are available, however preliminary estimates are that the flow rates measured in the central gas injection hole (L3001) are of the same order of magnitude as those measured after the primary grout injections.

5.0 CONCLUSIONS

The conclusions that can be drawn from the gas flow/tracer testing results obtained and analyzed to date are as follows;

- 1) The gas flow characterization equipment, techniques, and procedures used in this testing can be used as an index tool to effectively describe changes in gas permeability as a result of cementitious grouting in the nonsaturated DRZ surrounding WIPP openings.
- 2) The tracer gas testing equipment, techniques, and procedures used in this testing show promise as a tool to describe preferential flow paths in the DRZ around seal components.
- 3) The injection of microfine cementitious grout using the equipment, geometry, and restraint system described in the original test plan (Ahrens, 1992) reduced the gas permeability in the DRZ under Room L3 by about three orders of magnitude over a limited region.

It is known that the concrete slab was uplifted during several of the grouting episodes due to the pressurized injection of the grout. It is not known whether this uplift influenced any of the gas flow/tracer measurements conducted in the on-slab boreholes. This uplift could account for the increase in gas permeability seen in borehole L3211. The gas flow/tracer data will continue to be analyzed in an effort to better understand the results of the grouting demonstration.

6.0 REFERENCES

- Ahrens, E.H., 1992, "Test plan-Sealing of the Disturbed Rock Zone (DRZ), Including Marker Bed 139 (MB139) and the Overlying Halite, Below the Repository Horizon, at the Waste Isolation Pilot Plant," Sandia National Laboratories, Albuquerque, NM., printed May, 1992.
- Borns, D.J., 1985, "Marker Bed 139: A Study of DrillCore From a Systematic Array," SAND 85-0023, Sandia National Laboratories, Albuquerque, NM,
- Borns, D.J., and Stormont, J.C., 1988, "An Interim Report on Excavation Effect Studies at the Waste Isolation Pilot Plant: Delineation of the Disturbed Rock Zone," SAND87-1375, Sandia National Laboratories, Albuquerque, NM.
- Pickens, J.F., Grisak, G.E., Avis, J.A., Belanger, D.W., and Thury, M., 1987, "Analysis and Interpretation of Borehole Hydraulic Tests in Deep Boreholes: Principles, Model Development, and Applications," Water Resources Research, 23(7), pp. 1341-1375.
- Stormont, J.C., Peterson, E.W., and Lagus, P.L., 1987, "Summary of and Observations About WIPP Facility Horizon Flow Measurements through 1986," SAND87-0176, Sandia National Laboratories, Albuquerque, NM.

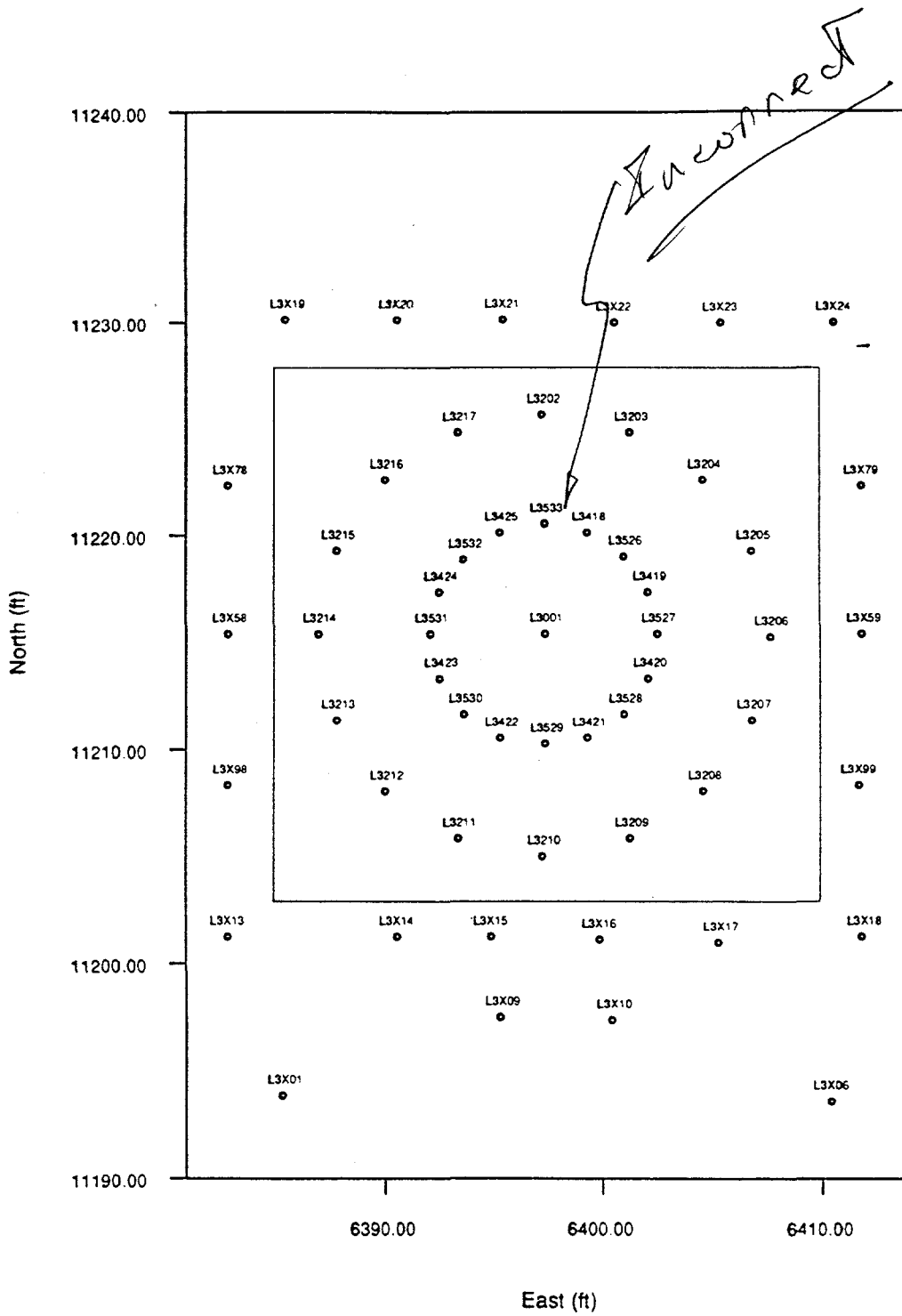


Figure 1. Concrete slab and borehole locations in Room L3.

TABLE 2. Results of on-slab gas flow characterization. Gas permeability estimates before (Jan/93) and after (Mar/93) primary holes grouted.

BOREHOLE	PEMEABILITY (m ²)		DIFFERENCE ORDER OF MAG.
	JAN/93	MAR/93	
L3202	2.3E-15	5.5E-16	0.62
L3203	1E-12	3E-13	0.52
L3204	5.45E-14	1.45E-14	0.58
L3205	3.75E-14	1.05E-15	1.55
L3206	1.95E-14	1E-18	4.29
L3207	5.15E-15	2.2E-15	0.37
L3208	5.5E-15	4E-16	1.14
L3209	4.25E-12	4E-13	1.03
L3210	1.25E-12	4.5E-13	0.44
L3211	9E-12	2E-11	+ 0.35
L3212	2.8E-13	9.5E-16	2.47
L3213	5.5E-15	1E-16	1.74
L3214	4.25E-15	9.5E-16	0.65
L3215	9E-14	2.85E-14	0.50
L3216	1.25E-13	6E-14	0.32
L3217	2.8E-13	5.15E-15	1.74
AVERAGE DIFFERENCE			1.14
L3001	1.825E-12	1.95E-15	2.97

TABLE 3. Table of tracer arrival maximum relative concentrations [REL] and time of arrival (min) for grout episodes through completion of primaries.

HOLE NO.	01/29/93 [REL]@time	02/05/93 [REL]@time	02/09/93 [REL]@time	02/15/93 [REL]@time	02/17-18/93 [REL]@time	03/10/93 [REL]@time
L3202	.188 @ 44	.078 @ 60	.016 @ 56	.015 @ 70	.008 @ 80	.012 @ 78
L3203	.148 @ 52	.273 @ 40	.152 @ 40	.109 @ 40	.035 @ 50	.031 @ 60
L3204	.129 @ 44	.039 @ 62	.012 @ 58	.016 @ 50	.004 @ 48	NO PEAK
L3205	.070 @ 40	.105 @ 60	.027 @ 74	.035 @ 60	NO PEAK	NO PEAK
L3206	.059 @ 50	.082 @ 46	.012 @ 82	.027 @ 56	NO PEAK	NO PEAK
L3207	.063 @ 44	.047 @ 52	.019 @ 72	.016 @ 62	NO PEAK	NO PEAK
L3208	.192 @ 44	.074 @ 60	.024 @ 62	.035 @ 60	NO PEAK	NO PEAK
L3209	.289 @ 34	.301 @ 36	.254 @ 32	.262 @ 32	.109 @ 44	.039 @ 68
L3210	.289 @ 34	.074 @ 60	.043 @ 46	.055 @ 40	.027 @ 64	.027 @ 70
L3211	.254 @ 40	.106 @ 50	.070 @ 38	.105 @ 42	.043 @ 48	.067 @ 56
L3212	.137 @ 44	.168 @ 60	.027 @ 72	.024 @ 54	.012 @ 78	NO PEAK
L3213	.153 @ 44	.223 @ 48	.117 @ 68	.070 @ 52	.035 @ 74	.011 @ 64
L3214	.133 @ 44	.137 @ 56	.062 @ 68	.055 @ 62	.024 @ 98	LATE RISE
L3215	.113 @ 36	.027 @ 72	.031 @ 70	.027 @ 58	NO PEAK	NO PEAK
L3216	.121 @ 40	.090 @ 68	.074 @ 74	.054 @ 74	.019 @ 72	NO PEAK
L3217	.160 @ 48	.195 @ 42	.101 @ 44	.145 @ 32	.051 @ 60	.039 @ 54

TABLE 1
Summary of On-Slab and Near-Slab Boreholes

<u>BOREHOLE #</u>	<u>DATE DRILLED</u>	<u>DATE GROUTED</u>	<u>DATE GAS FLOW TESTING*</u>	<u>COMMENTS</u>
L3X01	May, 92	NA	June-Aug, 92	off-slab
L3X06	May, 92	NA	June-Aug, 92	off-slab
L3X09	May, 92	NA	June-Aug, 92	off-slab
L3X10	May, 92	NA	June-Aug, 92	off-slab
L3X14	May, 92	NA	June-Aug, 92	off-slab
L3X17	May, 92	NA	June-Aug, 92	off-slab
L3X19	May, 92	NA	June-Aug, 92	off-slab
L3X20	May, 92	NA	June-Aug, 92	off-slab
L3X21	May, 92	NA	June-Aug, 92	off-slab
L3X22	May, 92	NA	June-Aug, 92	off-slab
L3X23	May, 92	NA	June-Aug, 92	off-slab
L3X24	May, 92	NA	June-Aug, 92	off-slab

SLAB CONSTRUCTED SEPT, 1992

L3X13	Oct, 92	NA	1/20-28/93	off-slab
L3X18	Oct, 92	NA	1/20-28/93	off-slab
L3X58	Oct, 92	NA	1/20-28/93	off-slab
L3X59	Oct, 92	NA	1/20-28/93	off-slab
L3X78	Oct, 92	NA	1/20-28/93	off-slab
L3X79	Oct, 92	NA	1/20-28/93	off-slab
L3X98	Oct, 92	NA	1/20-28/93	off-slab
L3X99	Oct, 92	NA	1/20-28/93	off-slab
L3X15	Oct, 92	NA	1/20-28/93	off-slab
L3X16	Oct, 92	NA	1/20-28/93	off-slab
L3001	Nov-Dec, 92	NA	1/20-28/93	tracer gas injection
L3202	Nov-Dec, 92	NA	1/20-28/93	"sniffer"
L3203	Nov-Dec, 92	NA	1/20-28/93	"sniffer"
L3204	Nov-Dec, 92	NA	1/20-28/93	"sniffer"
L3205	Nov-Dec, 92,	NA	1/20-28/93	"sniffer"
L3206	Nov-Dec, 92	NA	1/20-28/93	"sniffer"
L3207	Nov-Dec, 92	NA	1/20-28/93	"sniffer"
L3208	Nov-Dec, 92	NA	1/20-28/93	"sniffer"
L3209	Nov-Dec, 92	NA	1/20-28/93	"sniffer"
L3210	Nov-Dec, 92	NA	1/20-28/93	"sniffer"
L3211	Nov-Dec, 92	NA	1/20-28/93	"sniffer"
L3212	Nov-Dec, 92	NA	1/20-28/93	"sniffer"
L3213	Nov-Dec, 92	NA	1/20-28/93	"sniffer"
L3214	Nov-Dec, 92	NA	1/20-28/93	"sniffer"
L3215	Nov-Dec, 92	NA	1/20-28/93	"sniffer"
L3216	Nov-Dec, 92	NA	1/20-28/93	"sniffer"
L3217	Nov-Dec, 92	NA	1/20-28/93	"sniffer"

****TRACER GAS TEST, JAN 29, 1993 (20 psi)**

TABLE 1 (cont.)
Summary of On-Slab and Near-Slab Boreholes

BOREHOLE #	DATE DRILLED	DATE GROUTED	DATE GAS FLOW TESTING*	COMMENTS
L3422	2/1/93	2/3-4/93	NA	primary
	**TRACER GAS TEST - FEB 5, 1993 (20 psi)			
L3418	2/2/93	2/8/93	NA	primary
	**TRACER GAS TEST - FEB 9, 1993 (20 psi)			
L3424	2/10/93	2/11-12/93	NA	primary
	**TRACER GAS TEST - FEB 15, 1993 (20 psi)			
L3420	2/15/93	2/16/93	NA	primary
	**TRACER GAS TEST - FEB 17-18, 1993 (20 psi)			
L3421	2/18/93	2/19/93	NA	primary
L3423	2/19/93	2/23/93	NA	primary
L3419	2/23/93	2/24/93	NA	primary
L3425	2/25/93	2/25/93	NA	primary
GAS FLOW CHARACTERIZATION 3/3-8/93				
	**TRACER GAS TEST - 3/10/93 (20 psi)			
L3526	3/12-24/93	3/12-24/93	NA	secondary
L3527	3/12-24/93	3/12-24/93	NA	secondary
L3528	3/12-24/93	3/12-24/93	NA	secondary
L3529	3/12-24/93	3/12-24/93	NA	secondary
L3530	3/12-24/93	3/12-24/93	NA	secondary
L3531	3/12-24/93	3/12-24/93	NA	secondary
L3532	3/12-24/93	3/12-24/93	NA	secondary
L3533	3/12-24/93	3/12-24/93	NA	secondary

NOTES: * - Date first gas flow characterization performed.
 ** - Tracer gas tests always consist of injecting tracer spiked gas in L3001 and "sniffing" in holes L3202-L3217.

Primary and secondary refer to grouting episodes in either primary or secondary boreholes.

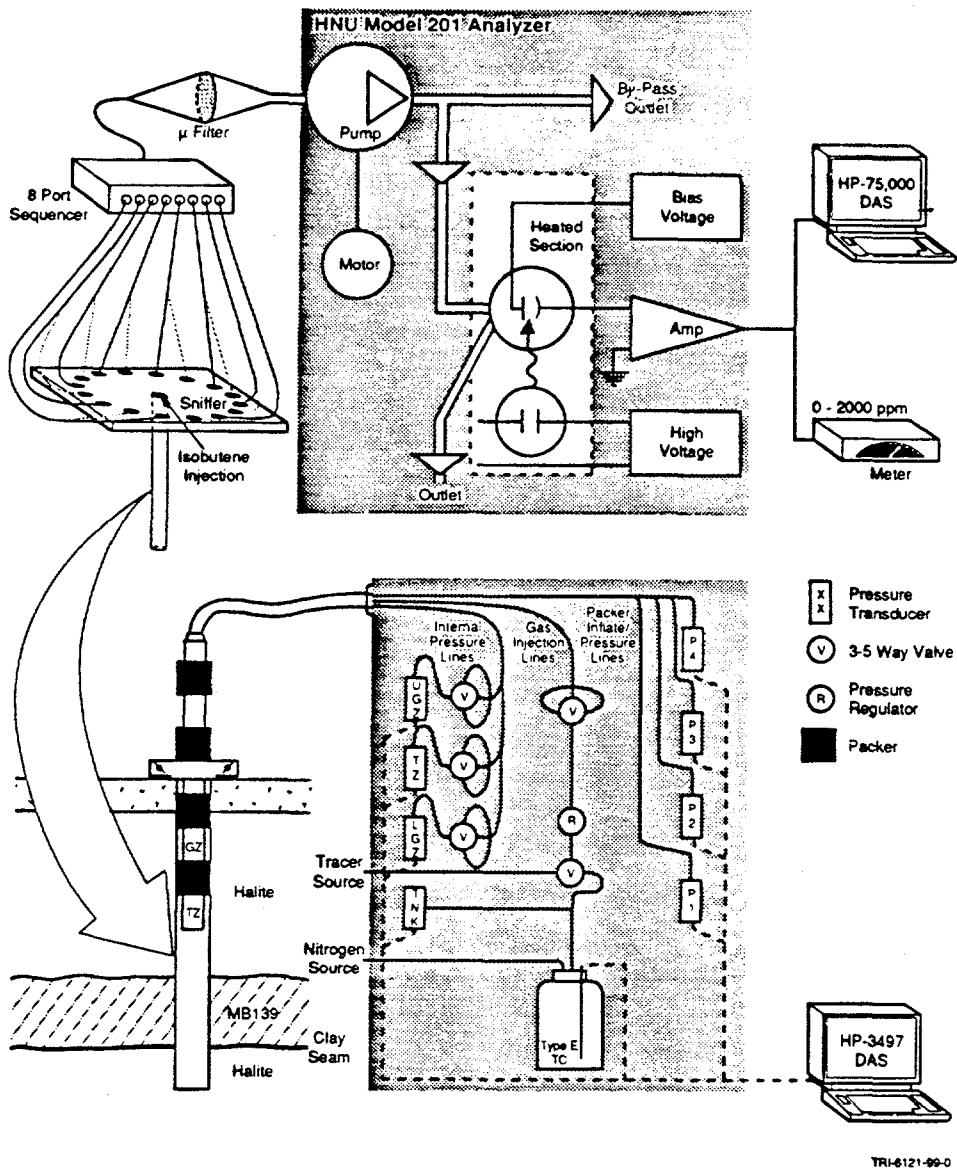


Figure 2. Schematic of equipment used for tracer gas injection/sampling (above) and gas flow characterization (below).

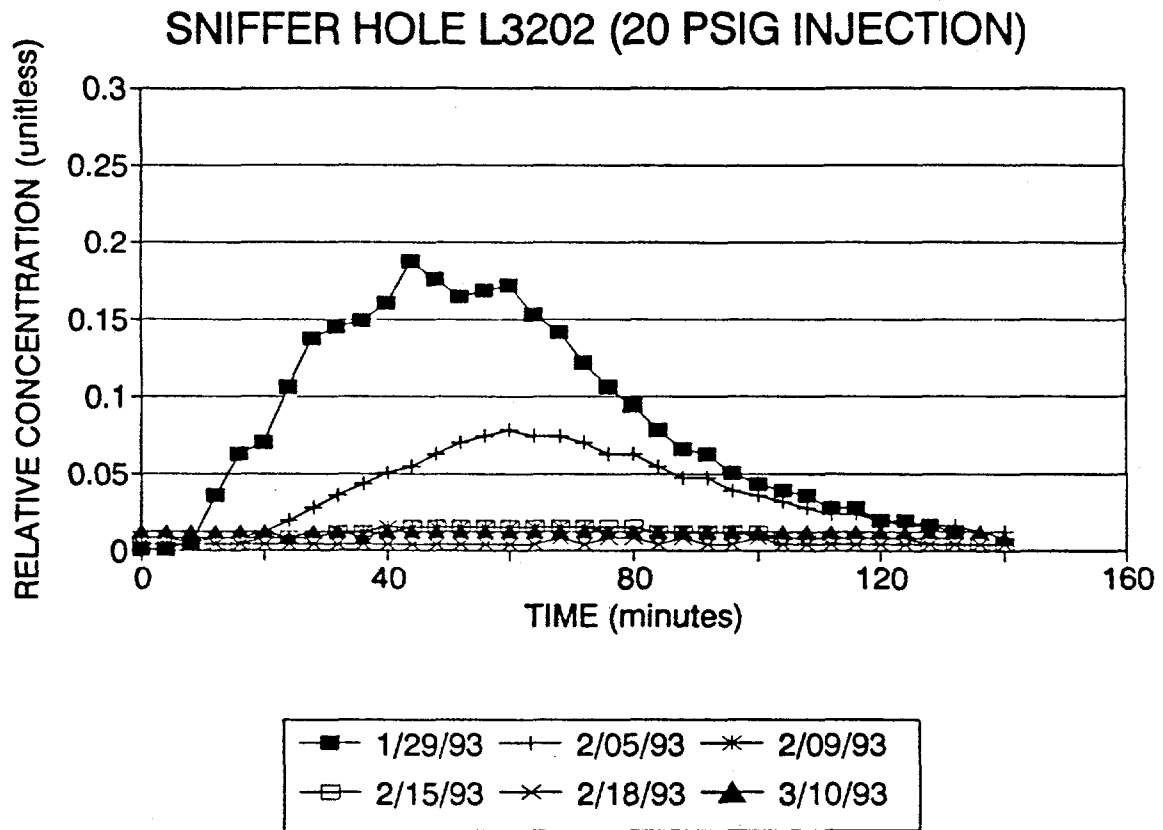


Figure 3. Tracer gas breakthrough curves - Borehole L3202

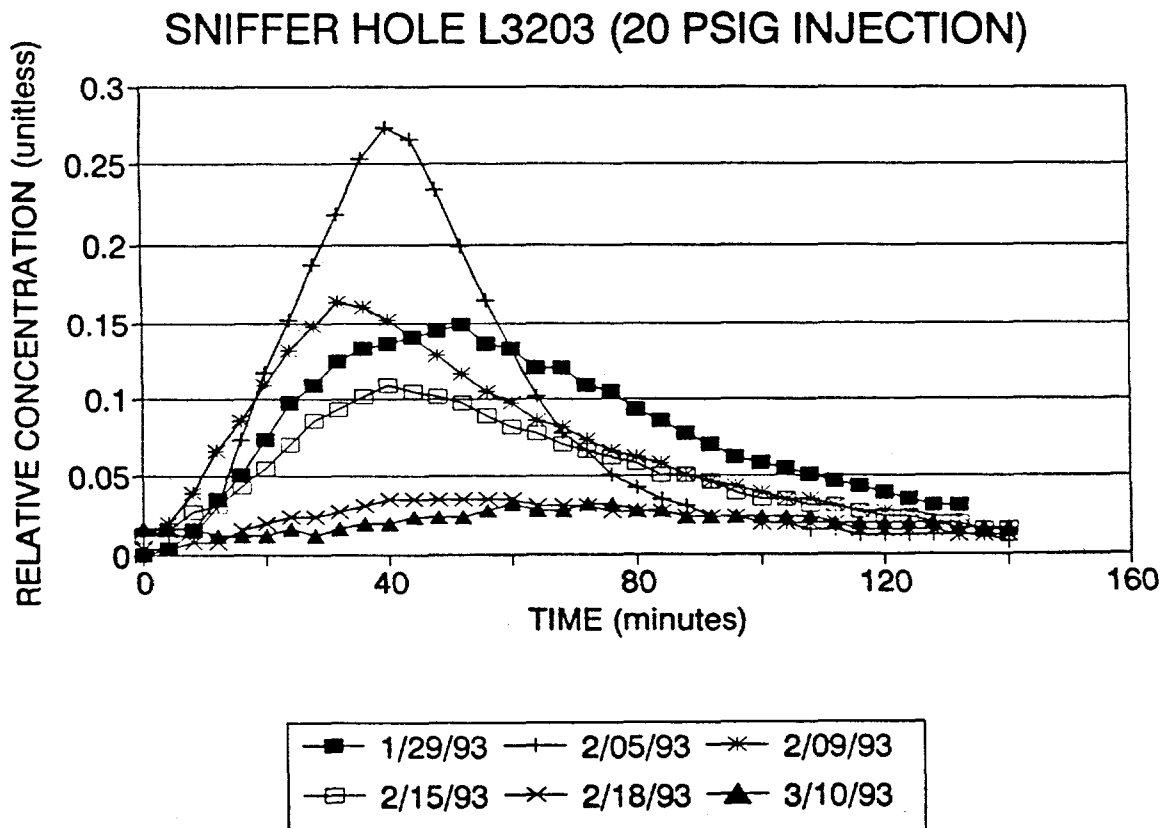


Figure 4. Tracer gas breakthrough curves - Borehole L3203

SNIFFER HOLE L3204 (20 PSIG INJECTION)

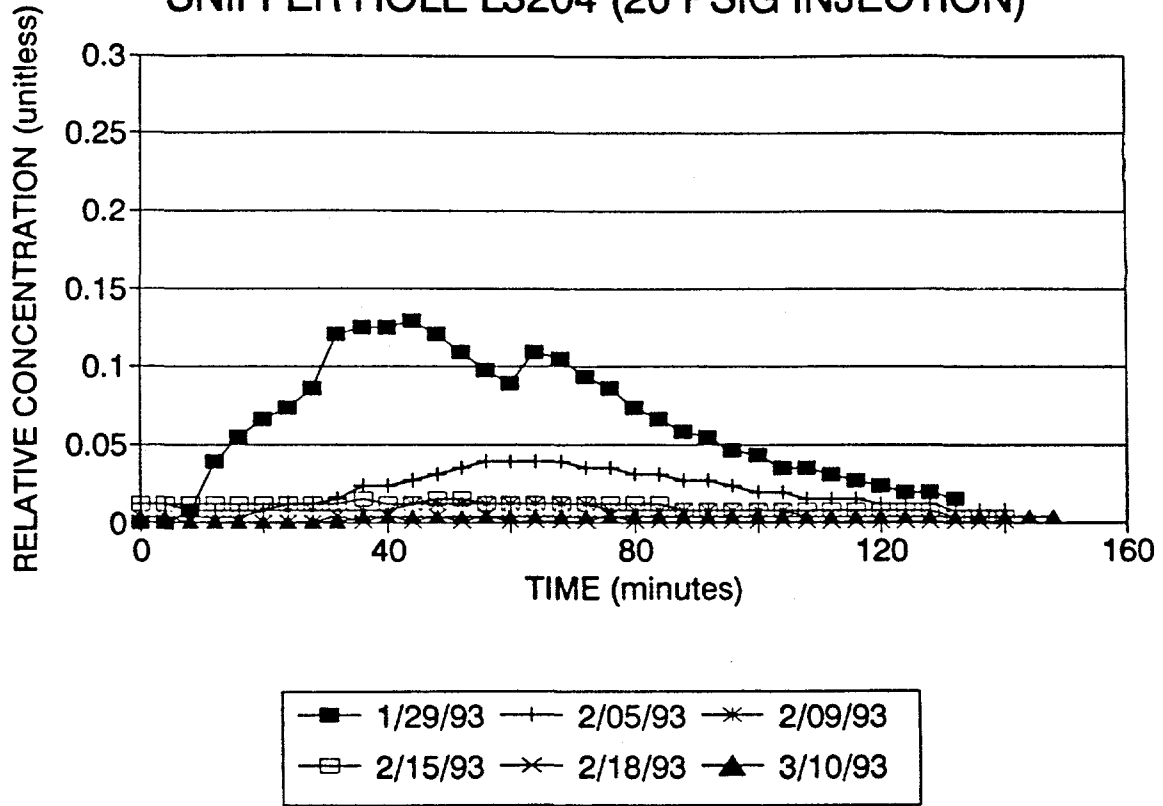


Figure 5. Tracer gas breakthrough curves - Borehole L3204

SNIFFER HOLE L3205 (20 PSIG INJECTION)

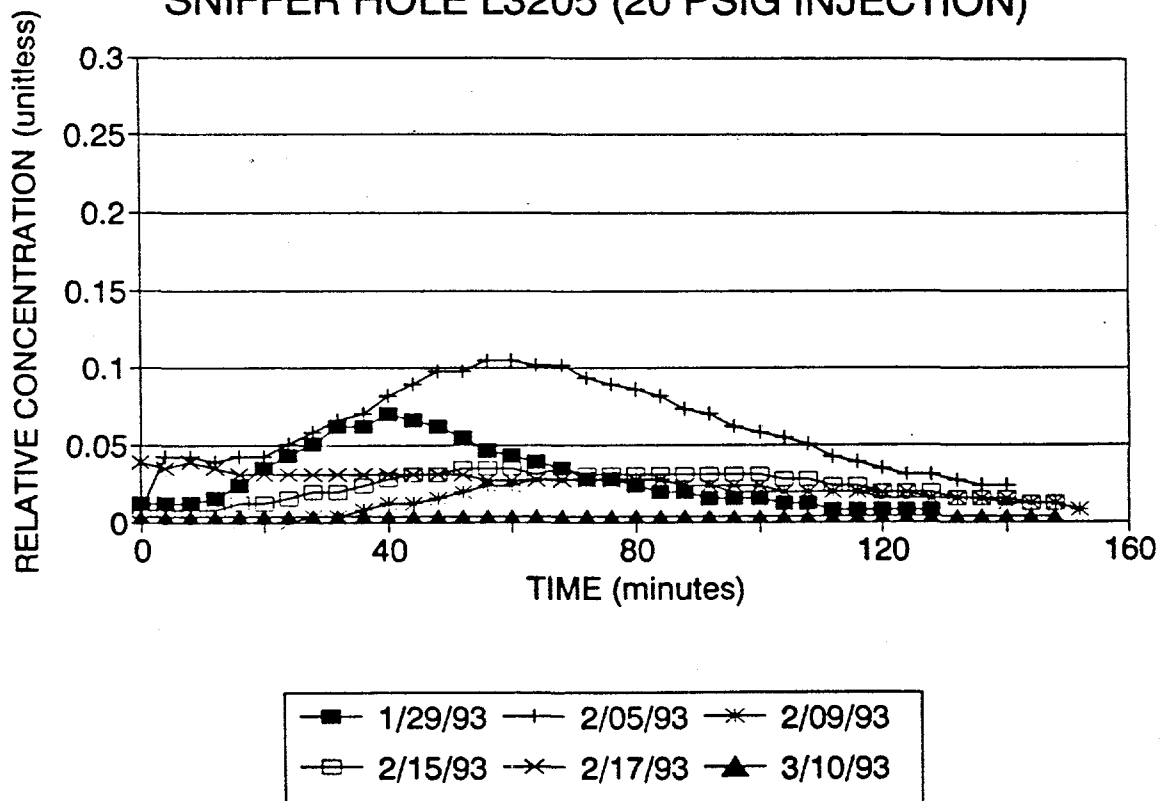


Figure 6. Tracer gas breakthrough curves - Borehole L3205

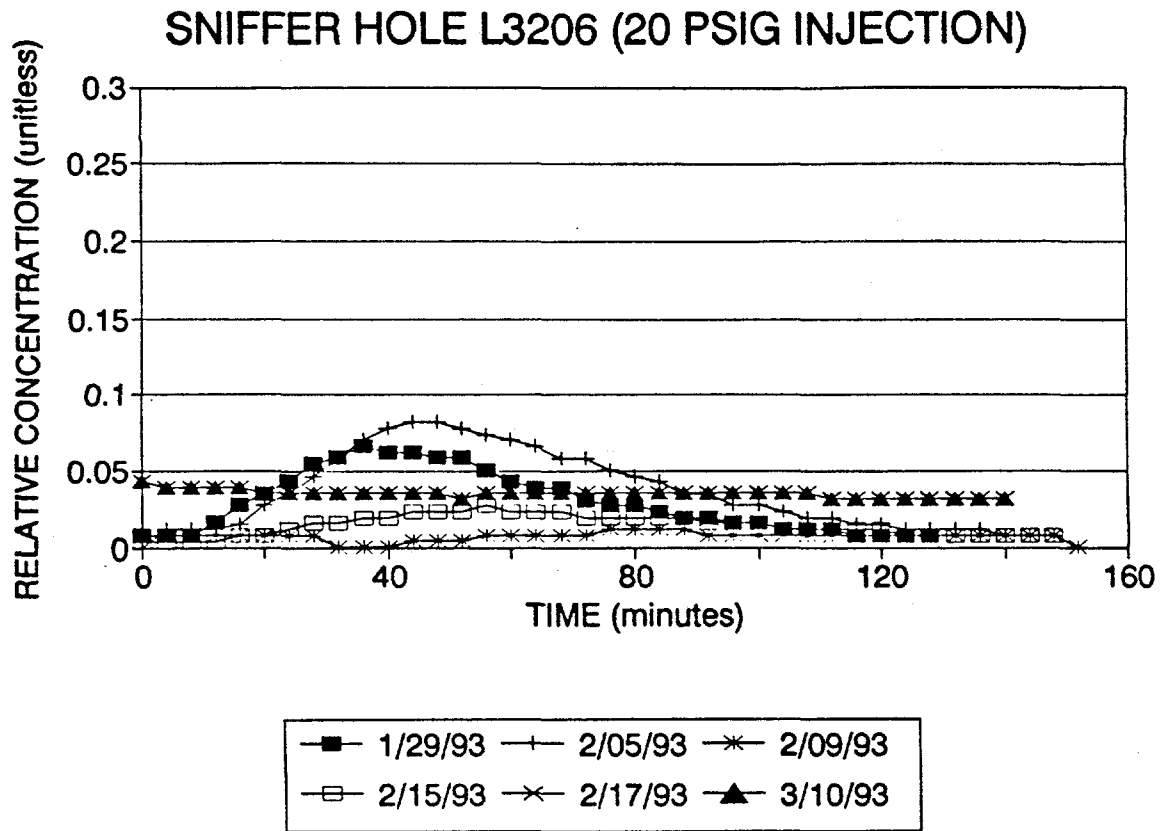


Figure 7. Tracer gas breakthrough curves - Borehole L3206

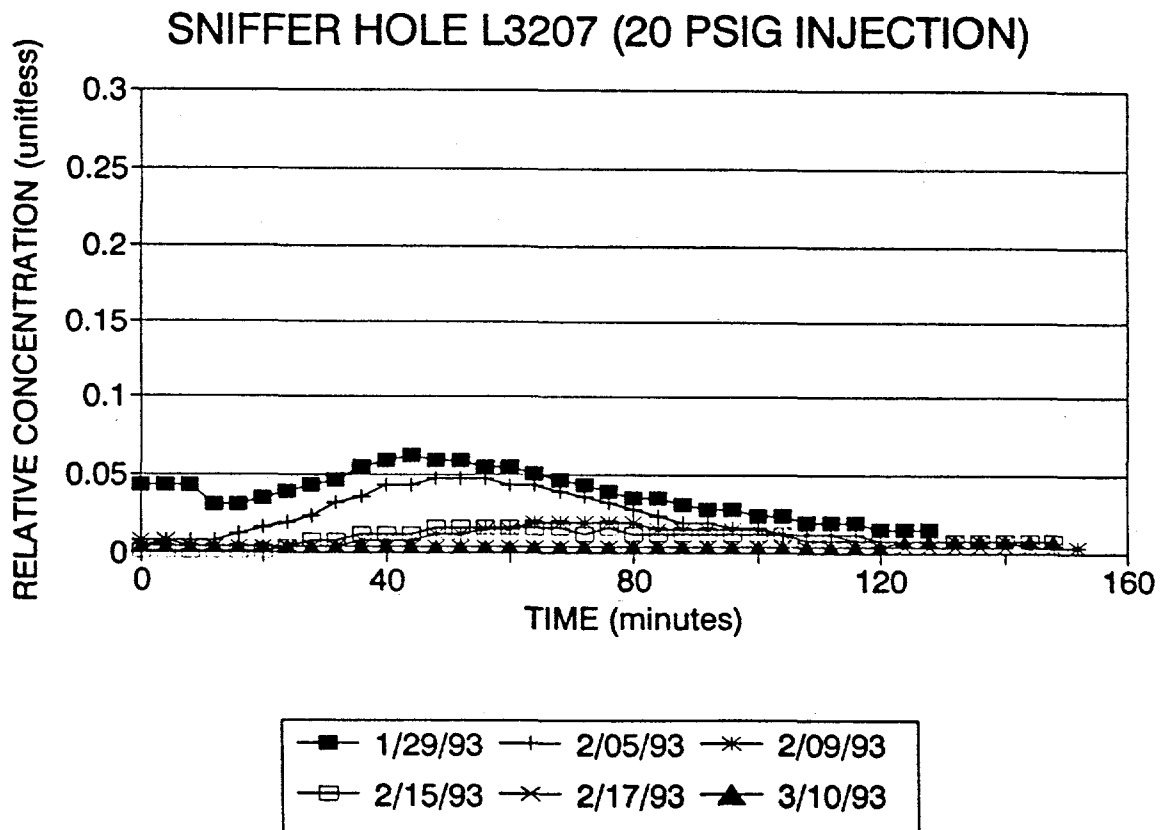


Figure 8. Tracer gas breakthrough curves - Borehole L3207

SNIFFER HOLE L3208

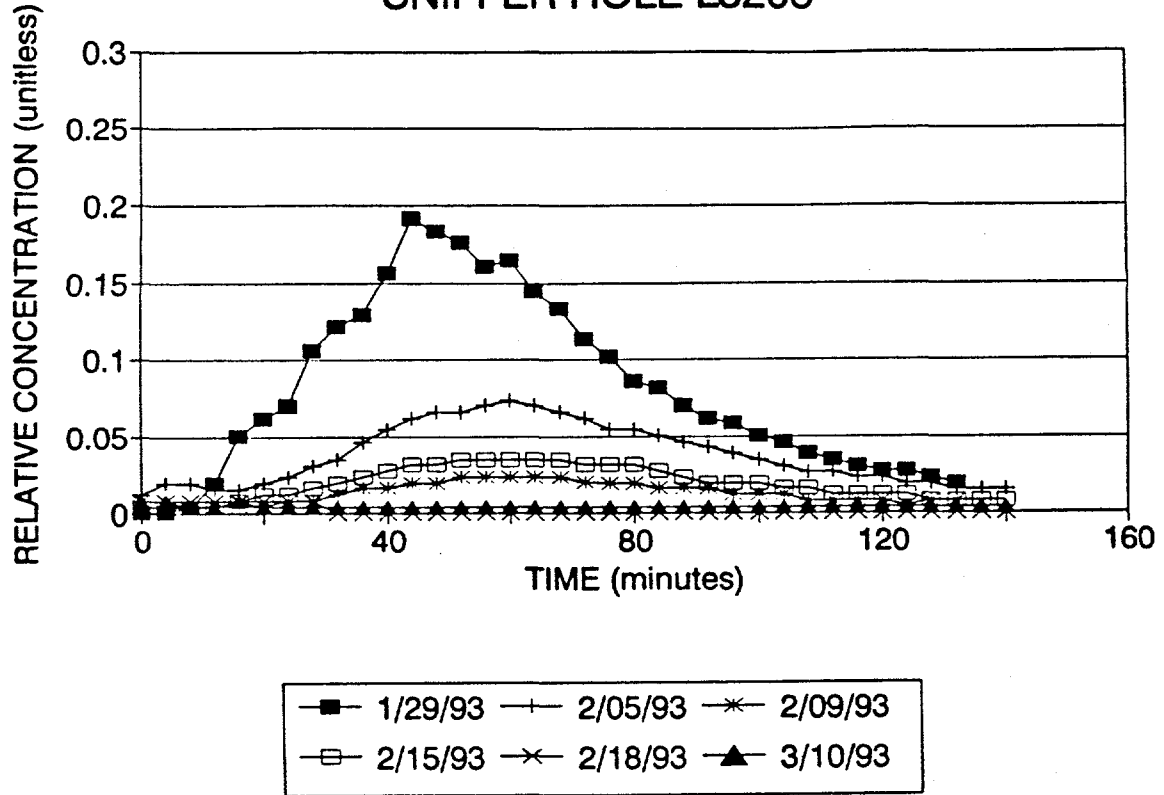


Figure 9. Tracer gas breakthrough curves - Borehole L3208

SNIFFER HOLE L3209 (20 PSIG INJECTION)

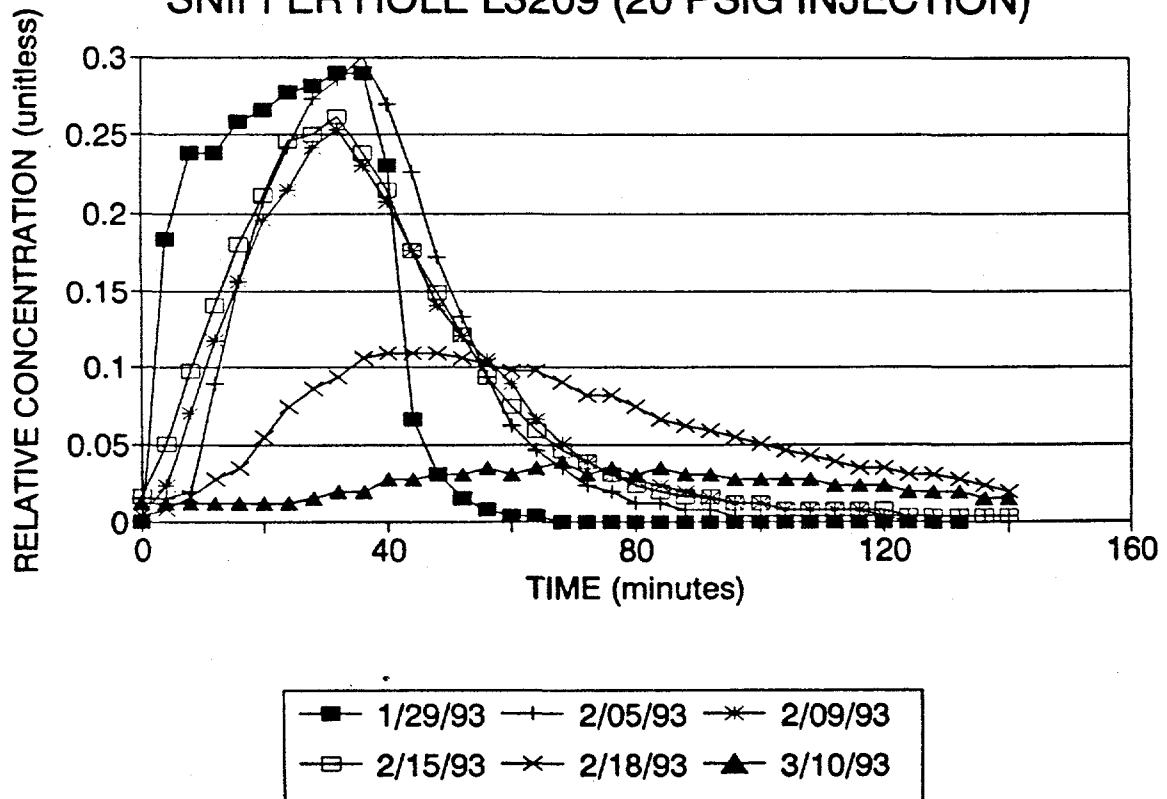


Figure 10. Tracer gas breakthrough curves - Borehole L3209

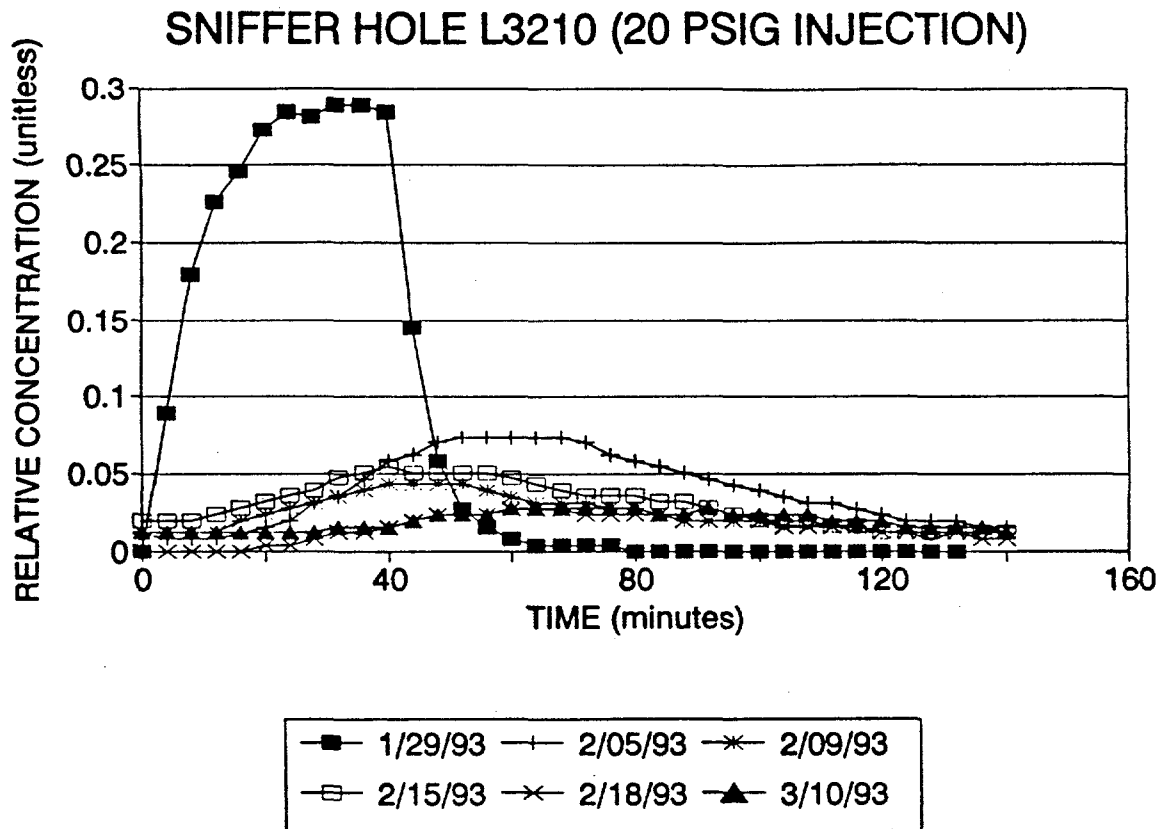


Figure 11. Tracer gas breakthrough curves - Borehole L3210

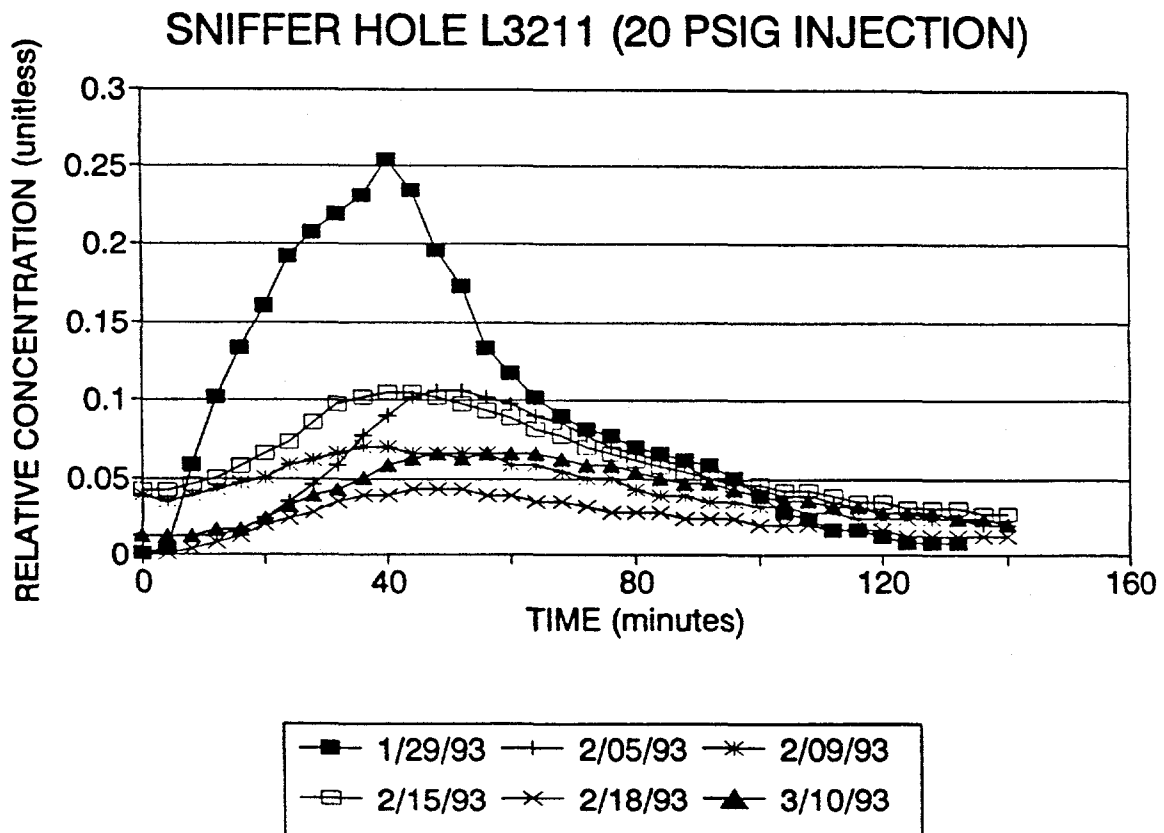


Figure 12. Tracer gas breakthrough curves - Borehole L3211

SNIFFER HOLE L3212 (20 PSIG INJECTION)

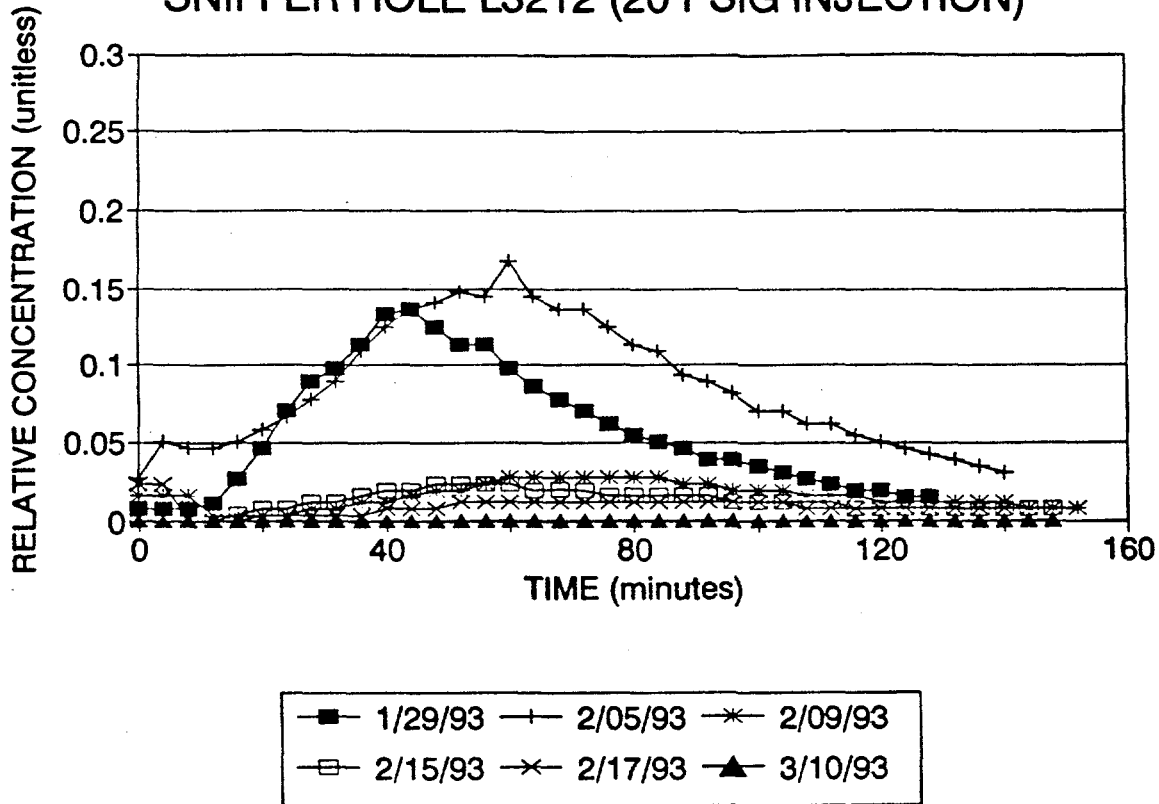


Figure 13. Tracer gas breakthrough curves - Borehole L3212

SNIFFER HOLE L3213 (20 PSIG INJECTION)

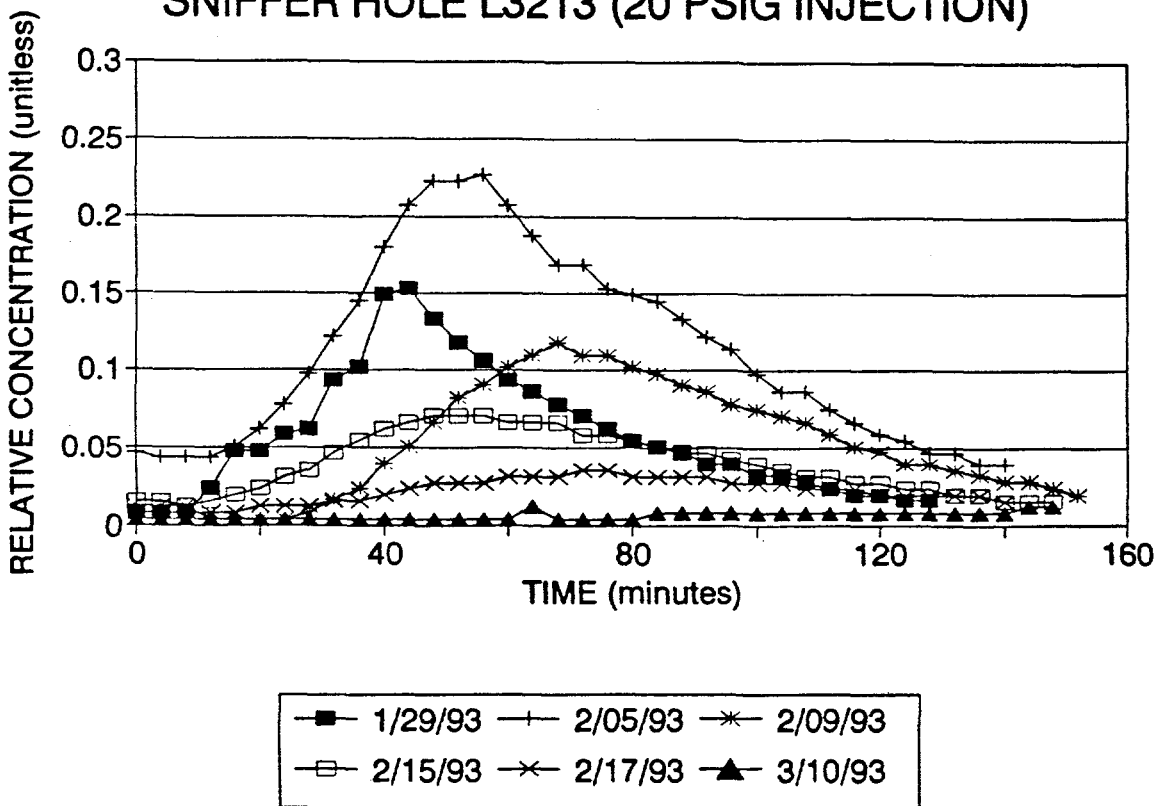


Figure 14. Tracer gas breakthrough curves - Borehole L3213

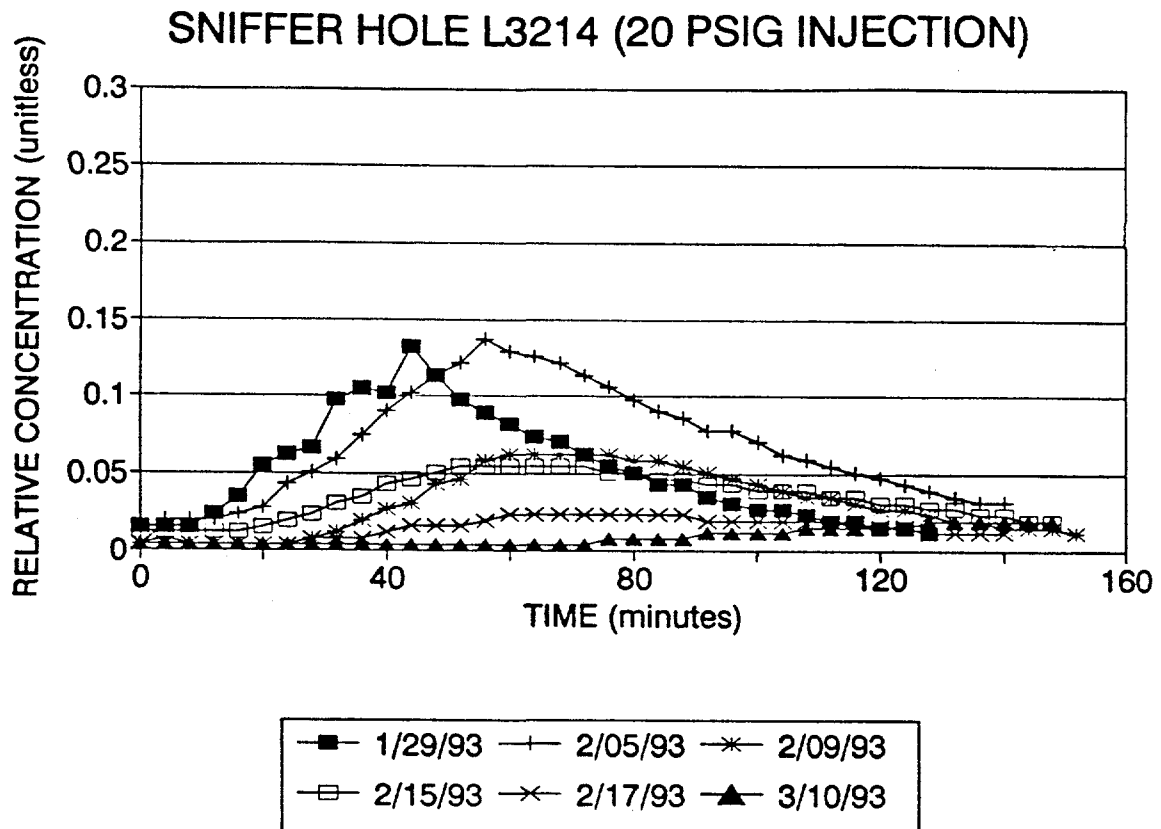


Figure 15. Tracer gas breakthrough curves - Borehole L3214

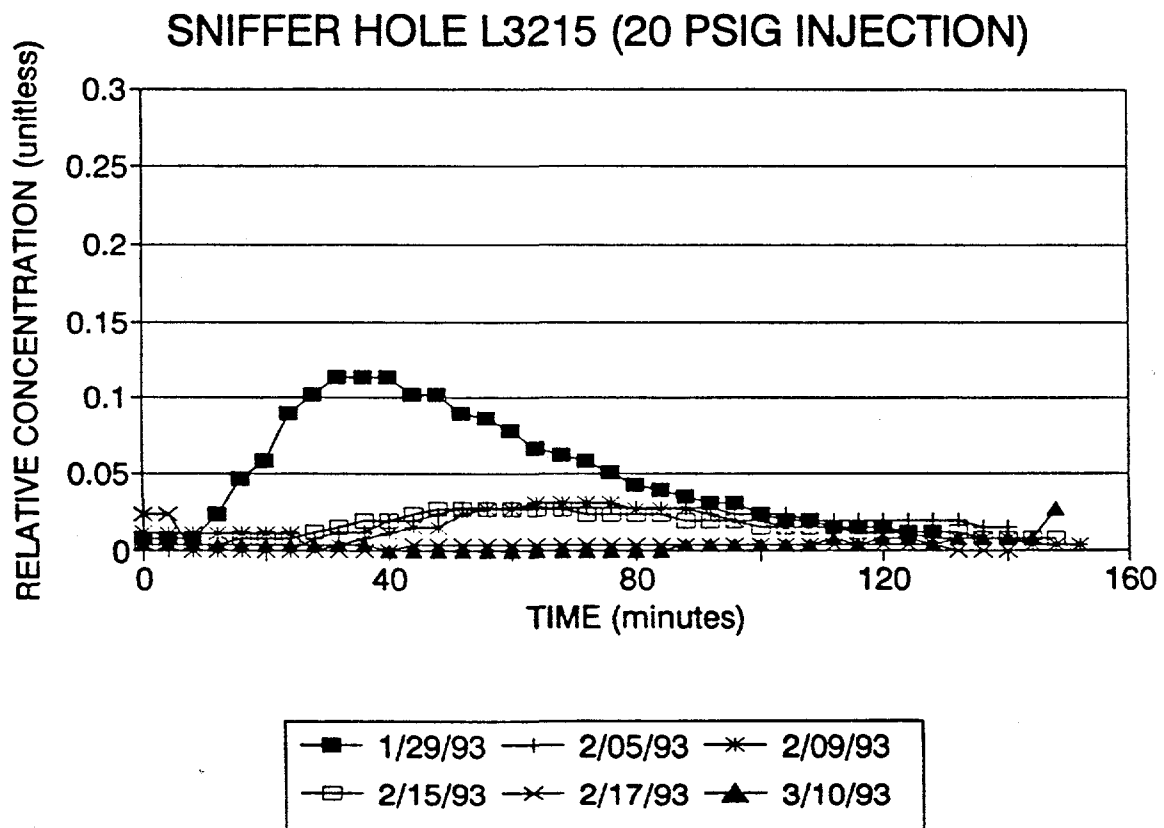


Figure 16. Tracer gas breakthrough curves - Borehole L3215

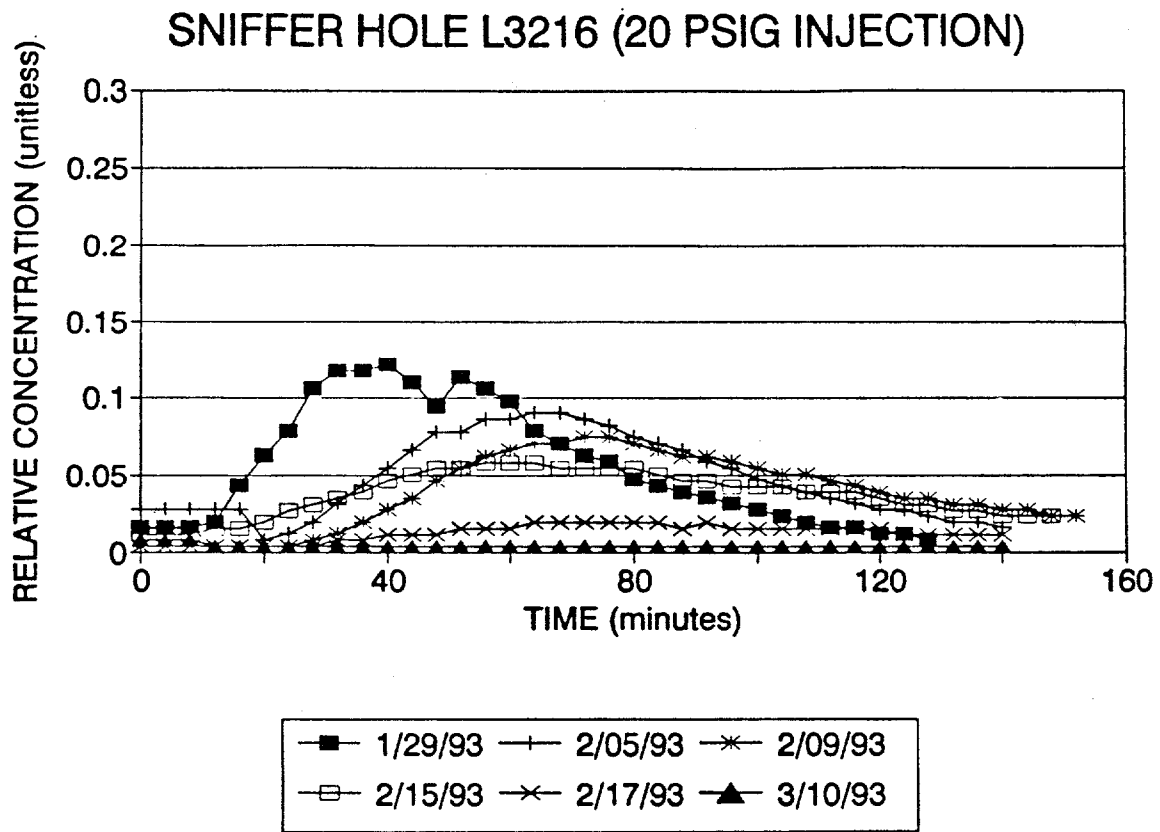


Figure 17. Tracer gas breakthrough curves - Borehole L3216

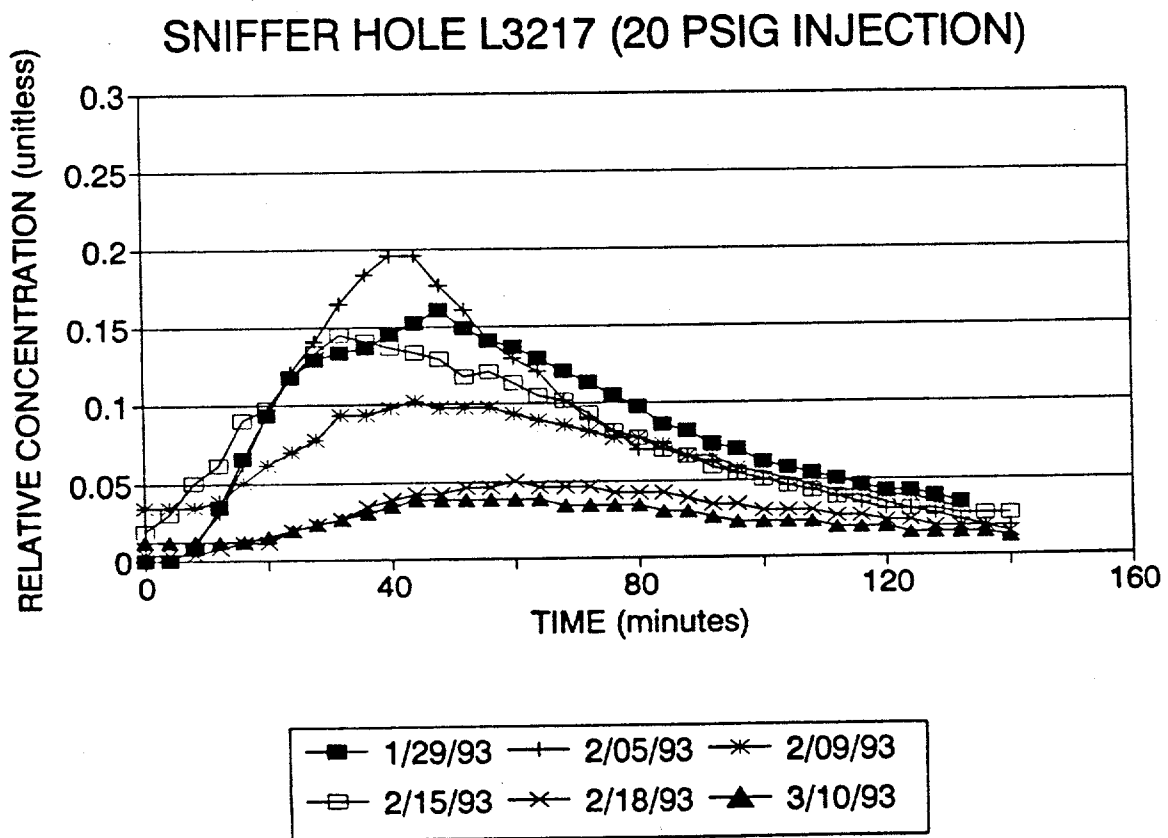


Figure 18. Tracer gas breakthrough curves - Borehole L3217

GENERALIZED CURVE TYPES

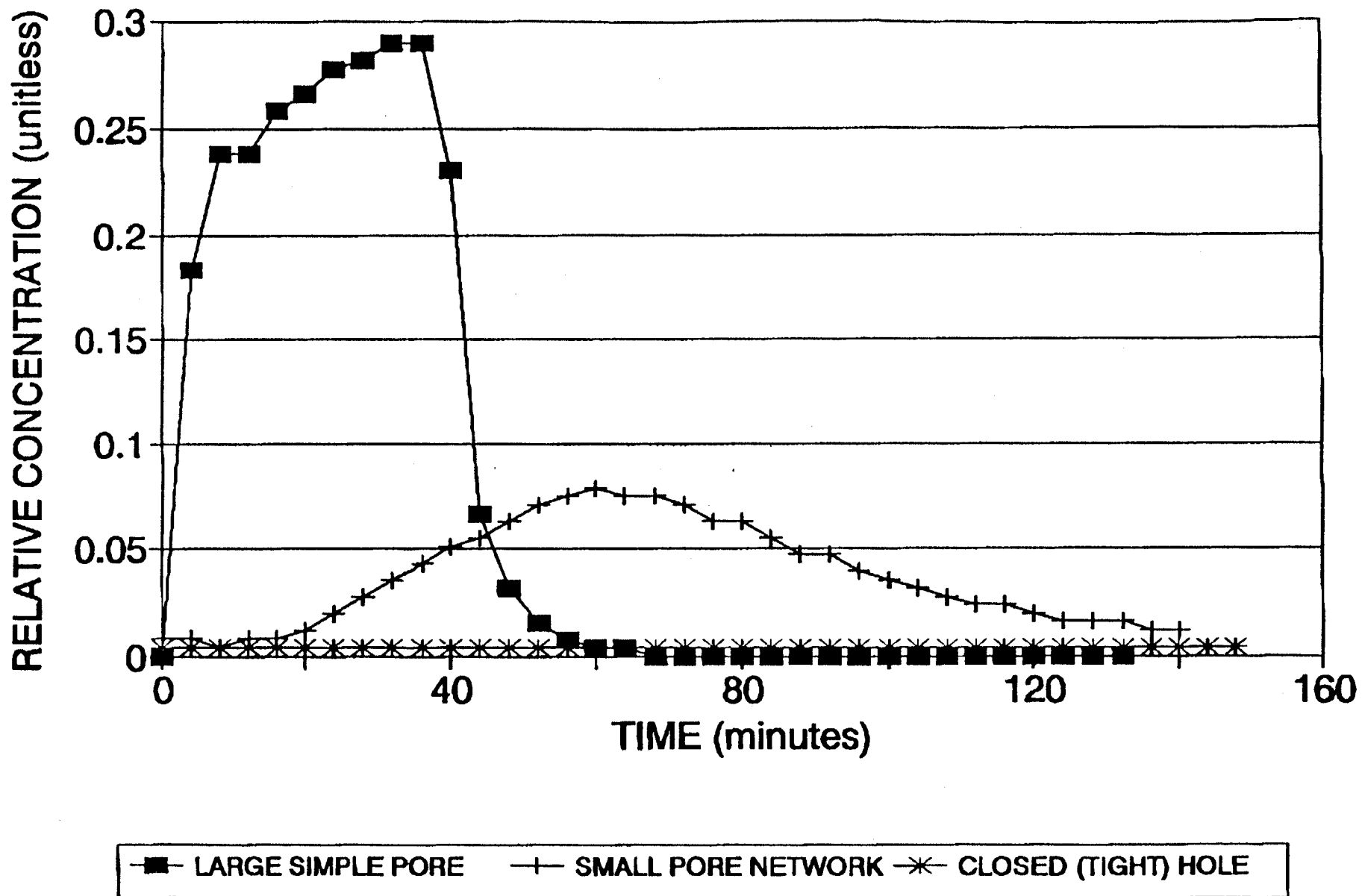


Figure 19. Generalized tracer gas breakthrough curve description.

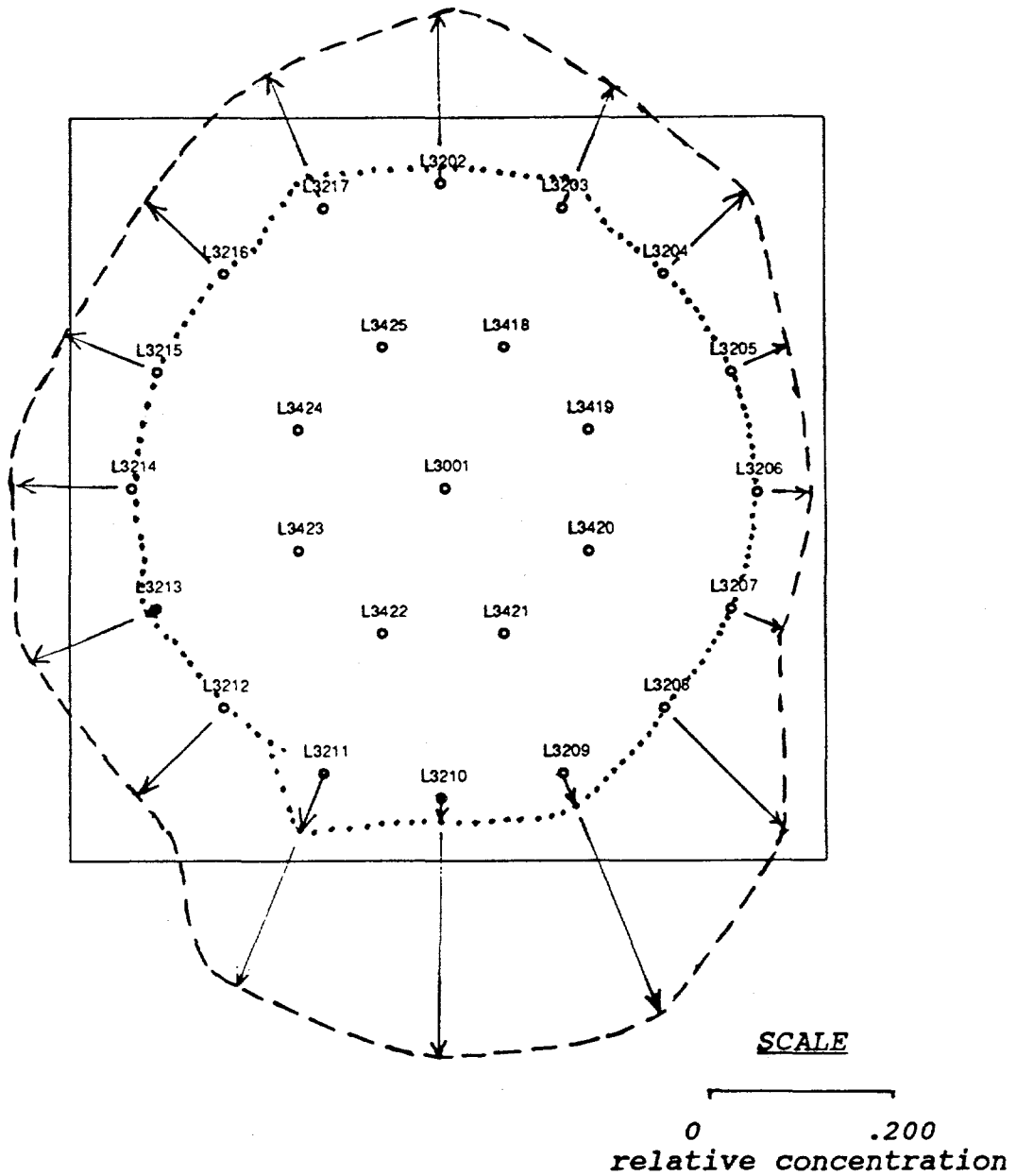


Figure 20. Plot of Peak Tracer Relative Concentrations Before and After Primary Hole Grouting.

- - - BEFORE GROUTING (tracer test 1/29/93)
- AFTER ALL PRIMARIES GROUTED (tracer test 3/10/93)

MEMORANDUM

DATE: June 16, 1994

TO: M.K. Pickens

cc: J.F. Pickens
R.S. Van Pelt
T.F. Dale
E. Ahrens ✓

FROM: G.J. Saulnier *GS*

RE: RESIMULATIONS OF THE 1993 GAS-INJECTION TESTS FOR PERMEABILITY CHARACTERIZATION OF MB-139 IN ROOM L3 IN SUPPORT OF THE SMALL-SCALE SEALS PERFORMANCE TEST (GROUTING EXPERIMENT)

This memorandum describes the results of the reanalysis of gas-injection tests performed by INTERA in January, March, and April of 1993 in support of the Small Scale Seals Performance Test (Grouting Experiment) . The reanalyses update preliminary analyses conducted during the period from April to August 1993 and provided to SNL in the form of a Technical Memorandum from G.J. Saulnier to R.S. Van Pelt dated August 3, 1993.

This Technical Memorandum covers the reanalyses of those tests using an enhanced, more relevant version of the test-analysis software, a discussion of transducer calibration and the data-acquisition program, and a review of the assumptions and limitations of these analyses. The text is accompanied by tabulations of the results of the reanalyses, including comparison with the preliminary analyses, and plots of the best matches between the observed data and the simulations developed by the test-analysis software.

TEST REANALYSES

Pre- and post-grout gas-injection tests of Marker Bed 139 were performed in Room L3 in the WIPP underground facility. The gas-injection tests were performed in boreholes drilled through the concrete slab installed in Room L3 to support the grouting experiment, and adjacent to the slab (off-slab boreholes). The boreholes were drilled in a radial pattern and numbered according to their position relative to the slab. The central borehole was borehole 001. The remainder of the slab boreholes were numbered 202 through 217. Off-slab boreholes were designated with a preceding X followed by numbers ranging from 12 through 99. The tests associated with each borehole are designated as L3 followed by the borehole number and the month and day of the 1993 testing date. For example, L3202126 refers to a test in borehole 202 on January 26, 1993.

Preliminary analyses were performed in 1993 using a version of INTERA's well-test-analysis code GTFM. The gas-injection tests were analyzed to provide preliminary estimates regarding the effectiveness of the grouting experiments and the estimates of formation parameter provided information with which to compare pre-test and post-test conditions in MB-139. The preliminary estimates of formation permeability indicated that the grouting succeeded in reducing the permeability of Marker Bed 139.

In early 1994, the GTFM subroutine for analyzing single-phase gas-flow tests was enhanced to include the ability to handle wellbore storage, model-boundary analysis, and, in addition, an optimization routine to facilitate estimation of formation permeability and porosity. Following the addition of these enhancements to GTFM, the 1993 gas-injection tests were reanalyzed. The results are included in this memorandum.

The principal changes incorporated in the reanalyses of the gas-injection tests were the extension of the model boundaries to beyond the area of influence of the modeled gas injection, simultaneous optimization of porosity and permeability, and inclusion of the effect of wellbore storage on the isolated test intervals. In addition, some matches between observed and simulated data were improved by reducing the effective test-zone volume. The effect of incorporating these changes was to improve confidence in the matches between the observed field data and the model-simulated data describing test-zone pressure versus time and the gas-injection flow rate versus time.

The preliminary analyses included permeability/porosity estimates using two complementary types of simulations. The tests were analyzed by both matching the observed injection rates while setting the model's the test-zone pressure equal to the observed test-zone pressure, and by matching the observed test-zone pressure setting the model's injection rate equal to the observed injection rate. The estimates of formation parameters developed from the two types of simulations were within a factor of 2 of each other and the matches between the observed and simulated data were satisfactory for preliminary analyses. The optimization improvements in the capability of the test-analysis software meant that the reanalyses required only one set of simulations to provide a best estimate of formation parameters. Because the test-zone pressure data was observed to be less noisy than the injection-rate data, the reanalyses were performed by setting the model's injection rate to the observed injection rate and simulating and matching the test-zone pressure to the observed test-zone pressure. In a majority of the reanalyses, a check simulation was performed to ensure that the formation parameters estimated in this way also would provide simulated injection-rate data that matched the observed injection rates.

In general, the reanalysis results support the results of the preliminary analysis and show that the grouting generally reduced the permeability of Marker Bed 139. Tables 1 and 2 summarize the results of the reanalysis showing a comparison of the reanalysis results compared with the preliminary estimates. The reanalysis results indicate formation permeabilities lower than the preliminary estimates by a factor of two to approximately one half order of magnitude.

TABLE 1. COMPARISON OF PRELIMINARY PERMEABILITY ESTIMATES FOR PRE-GROUTING GAS-INJECTION TESTS IN BOREHOLES ON THE ROOM L3 CONCRETE SLAB WITH ANALYSES PERFORMED WITH GTFM 5.10B

DRZ GAS-INJECTION TESTING (January to April 1993)
RESULTS OF GTFM SIMULATIONS FOR ON-SLAB BOREHOLES

BOREHOL	PERMEABILITY (m ²)											
	JAN/93				MAR/93				APR/93			
	Prelim.	Reanalysis	% Diff	Diff OM	Prelim.	Reanalysis	% Diff	Diff OM	Prelim.	Reanalysis	% Diff	Diff OM
L3202	2.3E-15	2.13E-15	7.39	0.03	5.5E-16	3.2E-16	41.82	0.24	4.8E-16	3.6E-16	24.21	0.12
L3203	1.0E-12	1.00E-12	0.00	0.00	3.0E-13	1E-12	-233.33	-0.52	8.8E-14	6E-14	31.43	0.16
L3204	5.5E-14	3E-14	44.95	0.26	1.5E-14	7E-15	51.72	0.32	1.3E-15	7E-16	46.15	0.27
L3205	3.8E-14	3E-14	20.00	0.10	1.1E-15	1E-15	4.76	0.02	4.3E-16	3E-16	29.41	0.15
L3206	2.0E-14	1.8E-14	7.69	0.03	1.0E-17	1E-17	0.00	0.00	6.0E-17	1.22E-17	79.67	0.69
L3207	5.2E-15	5E-15	2.91	0.01	2.2E-15	9.5E-16	56.82	0.36	7.5E-16	6E-16	20.00	0.10
L3208	5.5E-15	2E-15	63.64	0.44	4.0E-16	2.9E-16	27.50	0.14	1.5E-16	9E-17	40.00	0.22
L3209	4.3E-12	4E-12	5.88	0.03	4.0E-13	3.7E-13	7.50	0.03	9.8E-17	3E-17	69.23	0.51
L3210	1.3E-12	1.1E-12	12.00	0.06	4.5E-13	3.5E-13	22.22	0.11	3.0E-13	2.2E-13	26.67	0.13
L3211	9.0E-12	4E-12	55.56	0.35	2.7E-11	2.7E-11	0.00	0.00	2.7E-11	2.7E-11	0.00	0.00
L3212	2.8E-13	2.1E-13	25.00	0.12	9.5E-16	3.8E-16	60.00	0.40	9.5E-17	4E-17	57.89	0.38
L3213	5.5E-15	3.8E-15	30.91	0.16	1.0E-16	5E-17	50.00	0.30	3.5E-17	1.8E-17	48.57	0.29
L3214	4.3E-15	2.3E-15	45.88	0.27	9.5E-16	5.2E-16	45.26	0.26	1.0E-17	1E-17	0.00	0.00
L3215	9.0E-14	6E-14	33.33	0.18	2.9E-14	2.1E-14	26.32	0.13	1.5E-17	1E-17	33.33	0.18
L3216	1.3E-13	1E-13	20.00	0.10	6.0E-14	4.3E-14	28.33	0.14	2.0E-16	1E-16	50.00	0.30
L3217	2.8E-13	3E-12	-971.43	-1.03	5.2E-15	3.3E-15	35.92	0.19	2.2E-15	1.6E-15	27.27	0.14
L3001	1.8E-12	2.4E-12	-31.51	-0.12	2.0E-15	1.23E-15	36.92	0.20	1.1E-15	6.2E-16	43.64	0.25

TABLE 2. COMPARISON OF DIFFERENCES BETWEEN PRELIMINARY
AND REANALYSIS ESTIMATES OF PERMEABILITY

DRZ GAS-INJECTION TESTING (January to April 1993)
RESULTS OF GTFM SIMULATIONS FOR ON-SLAB BOREHOLES

BOREHOL	DIFF.(Jan-Mar) (Preliminary) ORDER OF MAG.	DIFF.(Jan-Mar) (Reanalysis) ORDER OF MAG.	DIFF.(Mar-Apr) (Preliminary) ORDER OF MAG.	DIFF.(Mar-Apr) (Reanalysis) ORDER OF MA
L3202	0.62	0.82	0.06	0.05
L3203	0.52	0.00	0.54	1.22
L3204	0.58	0.63	1.05	1.00
L3205	1.55	1.48	0.39	0.52
L3206	3.29	3.26	0.78	0.09
L3207	0.37	0.72	0.47	0.20
L3208	1.14	0.84	0.43	0.51
L3209	1.03	1.03	3.61	4.09
L3210	0.44	0.50	0.18	0.20
L3211	0.48	-0.83	0.00	0.00
L3212	2.47	2.74	1.00	0.98
L3213	1.74	1.88	0.46	0.44
L3214	0.65	0.65	1.98	1.72
L3215	0.50	0.46	3.28	3.32
L3216	0.32	0.37	2.48	2.63
L3217	1.74	2.96	0.37	0.31
L3001	2.97	3.29	0.25	0.30
AVERAGE DIFFERENCES				
	1.20	1.22	1.02	1.03

TRANSDUCER CALIBRATION AND DATA ACQUISITION

During a 1994 series of gas-injection tests in support of the Small-Scale Seals Testing Program, the CEC transducers used in the test tool were observed to indicate inaccurate ambient pressure. Similar transducers were used in the 1993 gas-injection tests whose interpretations are included in this report. R.S. Van Pelt of INTERA requested an independent evaluation of these transducers by M.D. Schuhen of ReSpec (Schuhen, May, 1994). The results of that investigation were presented to SNL in a Report which indicated that the transducers were temperature sensitive and that that sensitivity was not included either in the instruments' calibrations or in the data-acquisition software. In addition, the data-acquisition software was observed to include an unwarranted voltage compensation which had the effect of indicating lower pressures than actually occurred.

Two of the 1993 gas-injection tests in borehole 001, the central-injection borehole, were analyzed to determine whether or not the voltage compensation or the lack of a temperature compensation had a marked effect on test interpretation performed using the simulation software. The observed test-zone pressure data and the calculated injection-rate data from tests L3001121, a pre-grout-injection test, and L3001326, a post-grout-injection test, were simulated using the data as generated during the original testing period, using data which reversed the voltage compensation, and using data with a temperature compensation developed from the as-observed data and a pressure-versus-temperature relationship developed in the analysis by Schuhen (1994). The actual transducers used in the test series in question were not available for the type of analysis presented in Schuhen (1994) because they were rendered inoperable by having been subject to severe voltage fluctuations in subsequent testing operations. However, because the CEC transducers used in the 1993 tests were field calibrated by INTERA at ambient testing conditions using the transducer's internal indicator units, their calibrations were probably more relevant than the calibrations associated with the 1994 test series.

Figure 1 shows the pressure and injection-rate data from the three sets of data from the L3001121 test and the simulated test-zone pressure developed from the analysis of the data set including both voltage and temperature compensation. The plots show that the test data have the same form but are offset along the y-axis of the plots. The greatest difference in the observed transducers responses are observed to have been generated from the voltage compensation and only a slight difference is noted due to the temperature compensation. The analyses of the different data sets are summarized in Table 3 and the tabulated data indicating the differences in permeabilities determined from the as-recorded data and those estimated using the compensated data. The results are within one-half order of magnitude for the L3001121 data and very similar for the L3001326 data.

Because the original transducer calibrations for these transducers cannot be repeated and because the transducers are now inoperable and cannot be reevaluated, performing reanalyses on voltage- and temperature-compensated data for the entire series of gas-

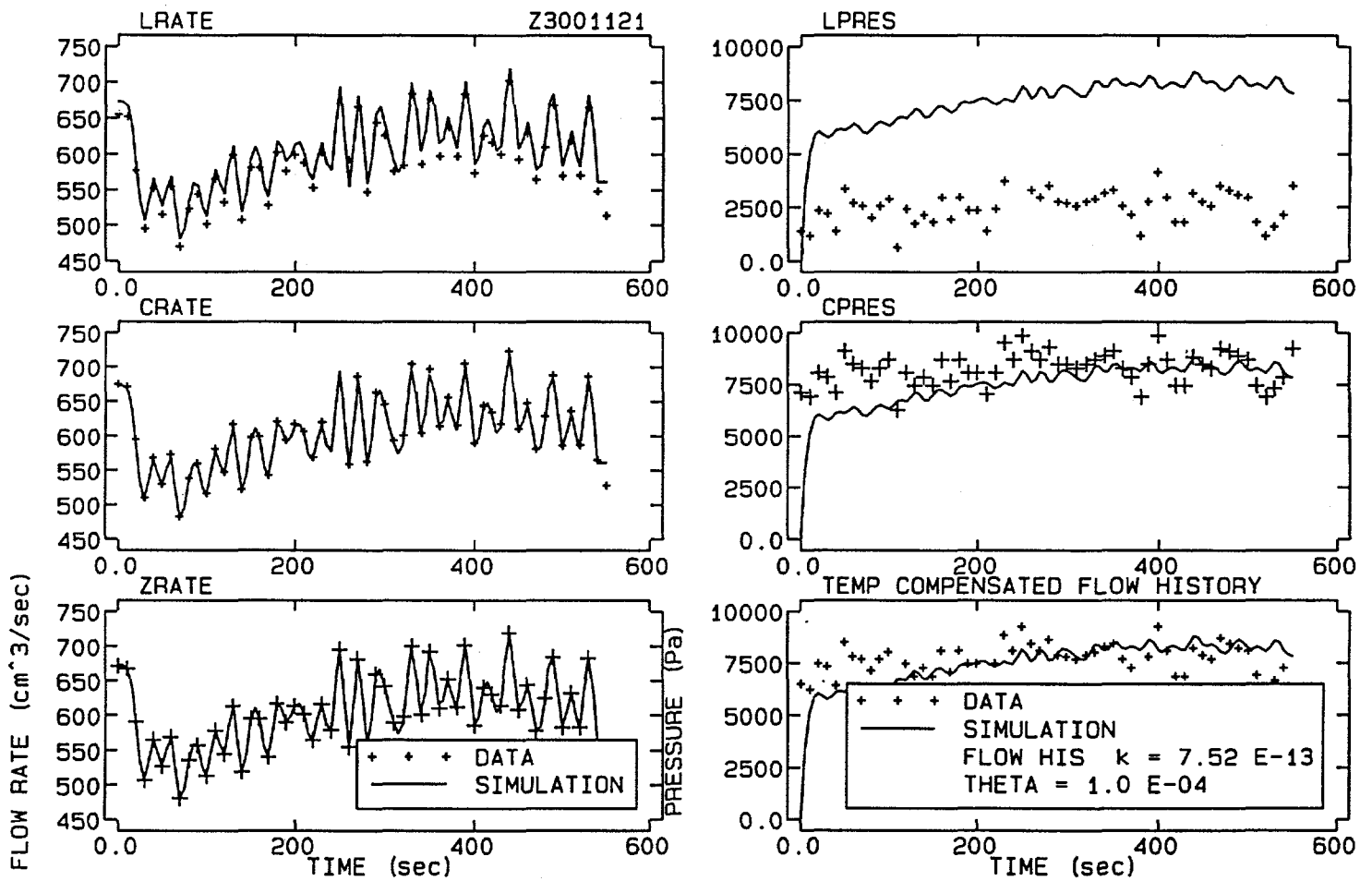


Figure 1. Comparison of as-observed data (LRATE, LPRESS), non-voltage-compensated data (CRATE, CPRESS) and temperature/non-voltage compensated data (ZRATE,ZPRESS) for test L3001121.

TABLE 3. Comparison of Permeability Estimates Derived From Compensated and Uncompensated Data

Borehole/Test	Permeability (m ²) Estimated Using:		
	As Recorded Data	Voltage-Compensated Data	Temperature-Compensated Data
L3001121	2.36E-12	6.66E-13	7.52E-13
L3001326	6.25E-16	6.03E-16	6.04E-16

reanalyses on voltage- and temperature-compensated data for the entire series of gas-injection-test data sets is not warranted. The consistent y-offset in both test-zone-pressure and injection-rate data indicate consistent relative differences in the interpreted formation parameters. The interpreted formation parameters are within the expected uncertainty for these types of tests and the implications relative to the effectiveness of the grout-injection experiments appear to be valid. Other uncertainties related the degree of moisture content in the injection host rock during this series of tests are presented below.

ASSUMPTIONS AND LIMITATIONS

The test-analysis software assume *radial, single-phase* conditions for the gas-injections tests. In Room L3, there are no data concerning the relative degree of saturation of Marker Bed 139. Shut-in and constant-pressure-withdrawal tests conducted in Room L4 indicate that saturated and two-phase conditions may exist in Marker Bed 139 (Beauheim and others, 1993), and tests in Waste Panel 1, Room 7 (Saulnier and others, 1992) indicate probable unsaturated conditions in Marker Bed 139 at that location. Because the gas-injection tests were conducted at pressures only two to three times ambient pressure, and because the tests were completed in from two to twenty hours, there was a reduced likelihood of observing whether or not confined or unsaturated conditions were present in the test zones. The initial shut-in data from the gas-injection tests, and the lack of pressure buildup in the guard zones when tests were shut in overnight indicates that confined conditions were not encountered. The use of reduced test-zone volumes to improve the matches between observed and simulated data could indicate the local presence of two-phase conditions due to trapped moisture in the primary and secondary porosity of Marker Bed 139. However, the need for a reduced test-zone volume could also reflect borehole closure since drilling, reduced fracture aperture with distance from some of the boreholes, and/or other uncertainties regarding borehole geometry and borehole infilling.

Another limitation regarding the testing is the lack of information concerning borehole and tool-system compressibility. The test tools used in conducting the higher pressure tests

reported in Saulnier and others (1991) and Stensrud and others (1992) were equipped with linear variable-differential transformers (LVDTs) which provided data for use in estimating the compressibility of various system components. The gas-injection-test test tool is not equipped with LVDTs but the test pressure were generally less than 50 psi (0.4 MPa), or seven times less than the packer-inflation pressure, indicating that system compressibility was probably minimal during the conduct of these tests.

REFERENCES

Beauheim, R.L., T.F. Dale, M.D. Fort, and R.M. Roberts, 1993. Hydraulic Testing of Salado Formation Evaporites at the Waste Isolation Pilot Plant Site: Second Interpretive Report. Sandia National Laboratories, Sandia Report SAND92-0533.

Beauheim, R.L., G.J. Saulnier, Jr., and J.D. Avis, 1991. Interpretation of Brine-Permeability Tests of the Salado Formation at the Waste Isolation Pilot Plant Site: First Interim Report. Sandia National Laboratories, Sandia Report SAND90-0083.

Saulnier, G.J., Jr., P.S. Domski, A.L. Jensen, J.B. Palmer, R.M. Roberts, and W.A. Stensrud, 1991. WIPP Salado Hydrology Program Data Report #1. Sandia National Laboratories, Contract Report SAND90-7000.

Stensrud, W.A., T.F. Dale, P.S. Domski, M.D. Fort, A.L. Jensen, J.B. Palmer, R.M. Roberts, and Saulnier, G.J., Jr., 1992. Waste Isolation Pilot Plant Salado Hydrology Program Data Report #2. Sandia National Laboratories, Contract Report SAND92-7072.

Schuhen, M.D., 1994. SNL WIPP Event Impact Statement No. 94-009, May 1994.

**TABULATED SUMMARY OF RESULTS
GAS-FLOW TESTING**

ROOM L3

**SMALL-SCALE SEALS
PERFORMANCE TEST**

JANUARY to APRIL 1993

TABLE 1. PERMEABILITY ESTIMATES FOR PRE-GROUTING GAS-INJECTION TESTS IN BOREHOLES
ON THE ROOM L3 CONCRETE SLAB

DRZ GAS-INJECTION TESTING (January 20 to 25, 1993)
RESULTS OF GTFM SIMULATIONS FOR ON-SLAB BOREHOLES

BOREHOLE (INTERVAL)	TEST DATE	ESTIMATED PERMEABILITY (m ²)	POROSITY	DELTA TEST- ZONE VOLUME (m ³)	COMMENTS
L3202	1/21/93	2.1E-15	0.0002	-0.0095	FLOW-RATE HISTORY/PRESSURE SIMULATION
L3203	1/21/93	1.0E-12	0.0010		FLOW-RATE HISTORY/PRESSURE SIMULATION
L3204	1/20/93	3.0E-14	0.0050		FLOW-RATE HISTORY/PRESSURE SIMULATION
L3205	1/20/93	3.0E-14	0.0006		FLOW-RATE HISTORY/PRESSURE SIMULATION
L3206	1/20/93	1.8E-14	0.0002		FLOW-RATE HISTORY/PRESSURE SIMULATION
L3207	1/20/93	5.0E-15	0.0001		FLOW-RATE HISTORY/PRESSURE SIMULATION
L3208	1/20/93	2.0E-15	0.0700		FLOW-RATE HISTORY/PRESSURE SIMULATION
L3209	1/21/93	4.0E-12	0.0010		FLOW-RATE HISTORY/PRESSURE SIMULATION
L3210	1/21/93	1.1E-11	0.0050		FLOW-RATE HISTORY/PRESSURE SIMULATION
L3211	1/21/93	4.0E-12	0.0050		FLOW-RATE HISTORY/PRESSURE SIMULATION
L3212	1/21/93	2.1E-13	0.0050	-0.0100	FLOW-RATE HISTORY/PRESSURE SIMULATION
L3213	1/20/93	3.8E-15	0.0010	-0.0110	FLOW-RATE HISTORY/PRESSURE SIMULATION
L3214	1/20/93	2.3E-15	0.0050		FLOW-RATE HISTORY/PRESSURE SIMULATION
L3215	1/20/93	6.0E-14	0.0050		FLOW-RATE HISTORY/PRESSURE SIMULATION
L3216	1/20/93	1.0E-13	0.0050		FLOW-RATE HISTORY/PRESSURE SIMULATION
L3217	1/21/93	3.0E-12	0.0001		FLOW-RATE HISTORY/PRESSURE SIMULATION
L3001	1/21/93	2.4E-12	0.0002		FLOW-RATE HISTORY/PRESSURE SIMULATION
L3001 (A2)	1/25/93	4.5E-15	0.0020	-0.0300	FLOW-RATE HISTORY/PRESSURE SIMULATION
L3001 (A3)	1/25/93	1.5E-12	0.0050		FLOW-RATE HISTORY/PRESSURE SIMULATION
L3001 (B1)	1/25/93	3.0E-12	0.0050		FLOW-RATE HISTORY/PRESSURE SIMULATION
L3001 (B2)	1/25/93	3.0E-13	0.0001	-0.0500	FLOW-RATE HISTORY/PRESSURE SIMULATION

TABLE 2. PERMEABILITY ESTIMATES FOR POST-GROUTING GAS-INJECTION TESTS IN BOREHOLES
ON THE ROOM L3 CONCRETE SLAB

POST-GROUTING DRZ GAS-INJECTION TESTING (March 3 to 8, 1993)
RESULTS OF GTFM SIMULATIONS FOR ON-SLAB BOREHOLES

BOREHOLE	TEST DATE	ESTIMATED PERMEABILITY (m ²)	POROSITY	DELTA TEST-ZONE VOLUME (m ³)	COMMENTS
L3202	3/03/93	3.2E-16	0.0050		FLOW-RATE HISTORY/PRESSURE SIMULATION
L3203	3/03/93	1.0E-12	0.0100		FLOW-RATE HISTORY/PRESSURE SIMULATION
L3204	3/04/93	7.0E-15	0.0200		FLOW-RATE HISTORY/PRESSURE SIMULATION
L3205	3/04/93	1.0E-15	0.0001		FLOW-RATE HISTORY/PRESSURE SIMULATION
L3206	3/04/93	1.0E-17	0.0010	-0.0065	FLOW-RATE HISTORY/PRESSURE SIMULATION
L3207	3/04/93	9.5E-16	0.0500	-0.0090	FLOW-RATE HISTORY/PRESSURE SIMULATION
L3208	3/05/93	2.9E-16	0.0100	-0.0100	FLOW-RATE HISTORY/PRESSURE SIMULATION
L3209	3/05/93	3.7E-13	0.0050		FLOW-RATE HISTORY/PRESSURE SIMULATION
L3210	3/05/93	3.5E-13	0.0050		FLOW-RATE HISTORY/PRESSURE SIMULATION
L3211	3/05/93	2.7E-11	0.0050		FLOW-RATE HISTORY/PRESSURE SIMULATION
L3212	3/05/93	3.8E-16	0.0150	-0.0100	FLOW-RATE HISTORY/PRESSURE SIMULATION
L3213	3/08/93	5.0E-17	0.0700	-0.0070	FLOW-RATE HISTORY/PRESSURE SIMULATION
L3214	3/08/93	5.2E-16	0.0050	-0.0100	FLOW-RATE HISTORY/PRESSURE SIMULATION
L3215	3/08/93	2.1E-14	0.0010		FLOW-RATE HISTORY/PRESSURE SIMULATION
L3216	3/08/93	4.3E-14	0.0050		FLOW-RATE HISTORY/PRESSURE SIMULATION
L3217	3/08/93	3.3E-15	0.0010	-0.0100	FLOW-RATE HISTORY/PRESSURE SIMULATION
L3001	3/03/93	1.2E-15	0.0012		FLOW-RATE HISTORY/PRESSURE SIMULATION

TABLE 3. PERMEABILITY ESTIMATES FOR SECOND ROUND OF POST-GROUTING GAS-INJECTION TESTS IN BOREHOLES ON THE ROOM L3 CONCRETE SLAB

SECOND ROUND - POST-GROUTING DRZ GAS-INJECTION TESTING (March 26 to April 13, 1993)

RESULTS OF GTFM SIMULATIONS FOR ON-SLAB BOREHOLES

BOREHOLE	TEST DATE	ESTIMATED PERMEABILITY (m ²)	POROSITY	DELTA TEST-ZONE VOLUME (m ³)	COMMENTS
L3202	4/01/93	3.6E-16	0.0002		FLOW-RATE HISTORY/PRESSURE SIMULATION
L3203	4/02/93	6.0E-14	0.0100		FLOW-RATE HISTORY/PRESSURE SIMULATION
L3204	4/02/93	7.0E-16	0.0100		FLOW-RATE HISTORY/PRESSURE SIMULATION
L3205	4/13/93	3.0E-16	0.0010		FLOW-RATE HISTORY/PRESSURE SIMULATION
L3206	4/02/93	1.2E-17	0.0140	-0.0100	FLOW-RATE HISTORY/PRESSURE SIMULATION
L3207	4/02/93	6.0E-16	0.0010	-0.0100	FLOW-RATE HISTORY/PRESSURE SIMULATION
L3208	4/06/93	9.0E-17	0.0300		FLOW-RATE HISTORY/PRESSURE SIMULATION
L3209	4/06/93	3.0E-17	0.0001	-0.0115	FLOW-RATE HISTORY/PRESSURE SIMULATION
L3210	4/06/93	2.2E-13	0.0050		FLOW-RATE HISTORY/PRESSURE SIMULATION
L3211	4/06/93	2.7E-11	0.0050		FLOW-RATE HISTORY/PRESSURE SIMULATION
L3212	4/06/93	4.0E-17	0.0050	-0.0110	FLOW-RATE HISTORY/PRESSURE SIMULATION
L3213	4/07/93	1.8E-17	0.0050	-0.0065	FLOW-RATE HISTORY/PRESSURE SIMULATION
L3214	4/07/93	1.0E-17	0.0010	-0.0100	FLOW-RATE HISTORY/PRESSURE SIMULATION
L3215	4/07/93	1.0E-17	0.0010	-0.0085	FLOW-RATE HISTORY/PRESSURE SIMULATION
L3216	4/08/93	1.0E-16	0.0050	-0.0100	FLOW-RATE HISTORY/PRESSURE SIMULATION
L3217	4/13/93	1.6E-15	0.0010	-0.0050	FLOW-RATE HISTORY/PRESSURE SIMULATION
L3001	3/26/93	6.2E-16	0.005	0.0190	FLOW-RATE HISTORY/PRESSURE SIMULATION

TABLE 4. PERMEABILITY ESTIMATES FOR POST-GROUTING GAS-INJECTION TESTS
IN OFF-SLAB BOREHOLES IN ROOM L3

DRZ GAS-INJECTION TESTING (April 14 to 21, 1993)

RESULTS OF GTFM SIMULATIONS FOR POST-GROUTING TESTS IN OFF-SLAB BOREHOLES

BOREHOLE	TEST DATE	ESTIMATED PERMEABILITY (m ²)	POROSITY	DELTA TEST-ZONE VOLUME (m ³)	COMMENTS
L3X13	4/21/93	1.5E-12	0.0010	-0.0075	FLOW-RATE HISTORY/PRESSURE SIMULATION
L3X15	4/21/93	5.0E-12	0.0050		FLOW-RATE HISTORY/PRESSURE SIMULATION
L3X16	4/20/93	8.0E-16	0.0010	-0.0130	FLOW-RATE HISTORY/PRESSURE SIMULATION
L3X58	4/14/93	1.0E-17	0.0010	-0.0060	FLOW-RATE HISTORY/PRESSURE SIMULATION
L3X59	4/19/93	1.0E-18	0.0010	-0.0050	FLOW-RATE HISTORY/PRESSURE SIMULATION
L3X78	4/14/93	5.0E-18	0.0010	-0.0100	FLOW-RATE HISTORY/PRESSURE SIMULATION
L3X79	4/16/93	5.0E-18	0.0050	-0.0050	FLOW-RATE HISTORY/PRESSURE SIMULATION
L3X98	4/22/93	5.0E-18	0.0010	-0.0035	FLOW-RATE HISTORY/PRESSURE SIMULATION
L3X99	4/19/93	1.0E-18	0.0030	-0.0040	FLOW-RATE HISTORY/PRESSURE SIMULATION

TABLE 5. PERMEABILITY ESTIMATES FOR POST-GROUTING GAS-INJECTION TESTS
IN SELECTED OFF-SLAB BOREHOLES IN ROOM L3

DRZ GAS-INJECTION TESTING

RESULTS OF GTFM SIMULATIONS FOR POST-GROUTING TESTS

BOREHOLE	TEST DATE	ESTIMATED PERMEABILITY (m ²)	POROSITY	DELTA TEST-ZONE VOLUME (m ³)	COMMENTS
L3X01	4/21/93	2.0E-17	0.0010	-0.0100	FLOW-RATE HISTORY/PRESSURE SIMULATION
L3X09	4/21/93	5.0E-12	0.0050		FLOW-RATE HISTORY/PRESSURE SIMULATION
L3X10	4/19/93	1.5E-12	0.0050		FLOW-RATE HISTORY/PRESSURE SIMULATION
L3X14	4/21/93	5.0E-12	0.0050		FLOW-RATE HISTORY/PRESSURE SIMULATION
L3X17	4/20/93	8.0E-16	0.0100		FLOW-RATE HISTORY/PRESSURE SIMULATION
L3X18	4/19/93	1.0E-18	0.0050	-0.0040	FLOW-RATE HISTORY/PRESSURE SIMULATION
L3X19	4/15/93	1.0E-17	0.0010	-0.0130	FLOW-RATE HISTORY/PRESSURE SIMULATION
L3X20	4/15/93	3.3E-15	0.0070	-0.0200	FLOW-RATE HISTORY/PRESSURE SIMULATION
L3X21	4/15/93	6.0E-14	0.0030	-0.0030	FLOW-RATE HISTORY/PRESSURE SIMULATION
L3X22	4/15/93	7.0E-14	0.0010		FLOW-RATE HISTORY/PRESSURE SIMULATION
L3X23	4/15/93	1.4E-15	0.0010		FLOW-RATE HISTORY/PRESSURE SIMULATION
L3X24	4/16/93	1.0E-17	0.0050	-0.0125	FLOW-RATE HISTORY/PRESSURE SIMULATION

TABLE 6. COMPARISON OF PRE- AND POST-GROUTING
GAS-INJECTION TESTS IN ON-SLAB BOREHOLES

GAS-PERMEABILITY COMPARISON
RESULTS OF TEST ANALYSES USING GTFM 5.10B

BOREHOLE	PEMEABILITY (m ²)		DIFFERENCE
	JAN/93	MAR/93	ORDER OF MAG.
L3202	2.13E-15	3.2E-16	0.82
L3203	1.00E-12	1E-12	0.00
L3204	3E-14	7E-15	0.63
L3205	3E-14	1E-15	1.48
L3206	1.8E-14	1E-17	3.26
L3207	5E-15	9.5E-16	0.72
L3208	2E-15	2.9E-16	0.84
L3209	4E-12	3.7E-13	1.03
L3210	1.1E-12	3.5E-13	0.50
L3211	4E-12	2.7E-11	-0.83
L3212	2.1E-13	3.8E-16	2.74
L3213	3.8E-15	5E-17	1.88
L3214	2.3E-15	5.2E-16	0.65
L3215	6E-14	2.1E-14	0.46
L3216	1E-13	4.3E-14	0.37
L3217	3E-12	3.3E-15	2.96
AVERAGE DIFFERENCE			1.09
L3001	2.4E-12	1.23E-15	3.29

TABLE 7. COMPARISON OF PRE- AND POST-GROUTING
GAS-INJECTION TESTS IN OFF-SLAB BOREHOLES

GAS-PERMEABILITY COMPARISON

 RESULTS OF TEST ANALYSES USING GTFM

BOREHOLE	PEMEABILITY (m ²)		DIFFEREN ORDER OF
	JAN/93	APR/93	
L3X13	1.0E-17	1.5E-17	-0.18
L3X15	7.0E-12	5.0E-12	0.15
L3X16	3.0E-14	8.0E-16	1.57
L3X58	1.1E-17	1.0E-17	0.04
L3X59	1.0E-17	1.0E-18	1.00
L3X78	2.0E-17	5.0E-18	0.60
L3X79	2.0E-18	5.0E-18	-0.40
L3X98	1.0E-17	5.0E-18	0.30
L3X99	1.0E-18	1.0E-18	0.00
AVG. DIFF			0.34

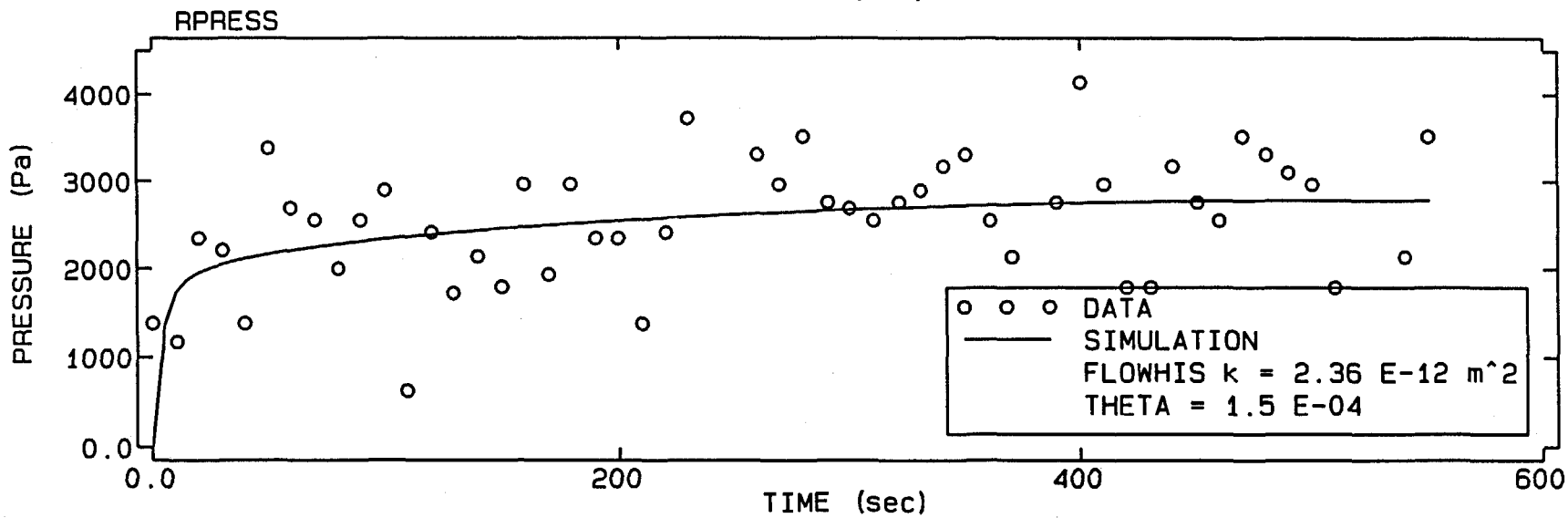
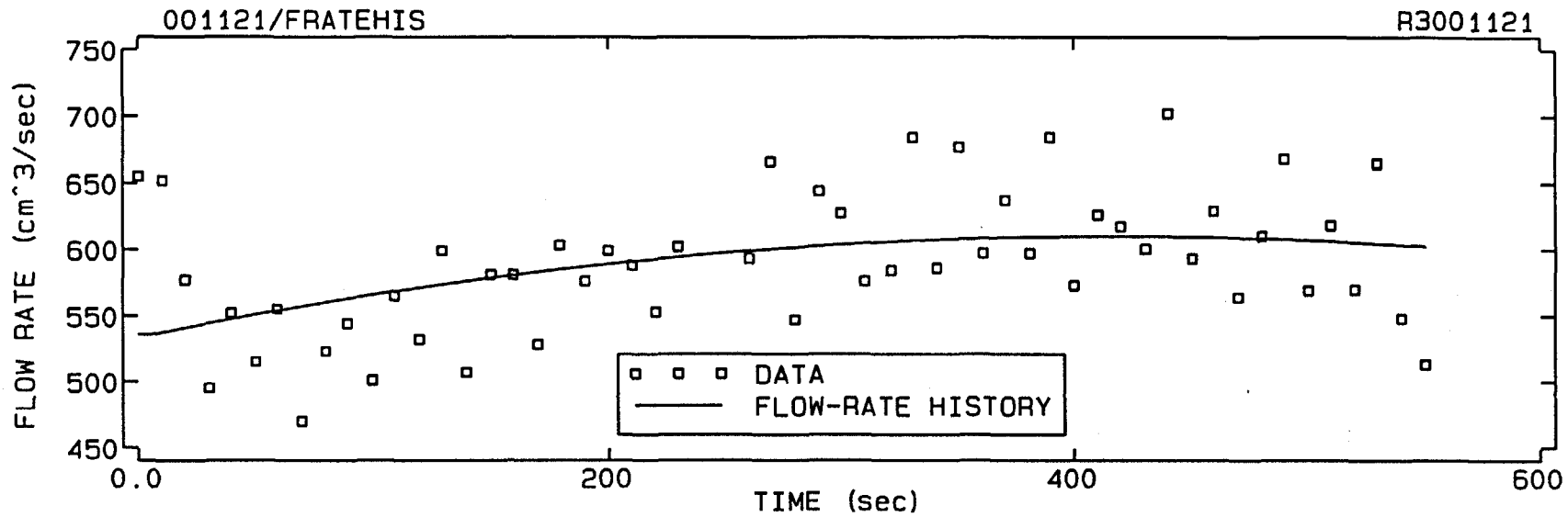
GAS-FLOW TESTING

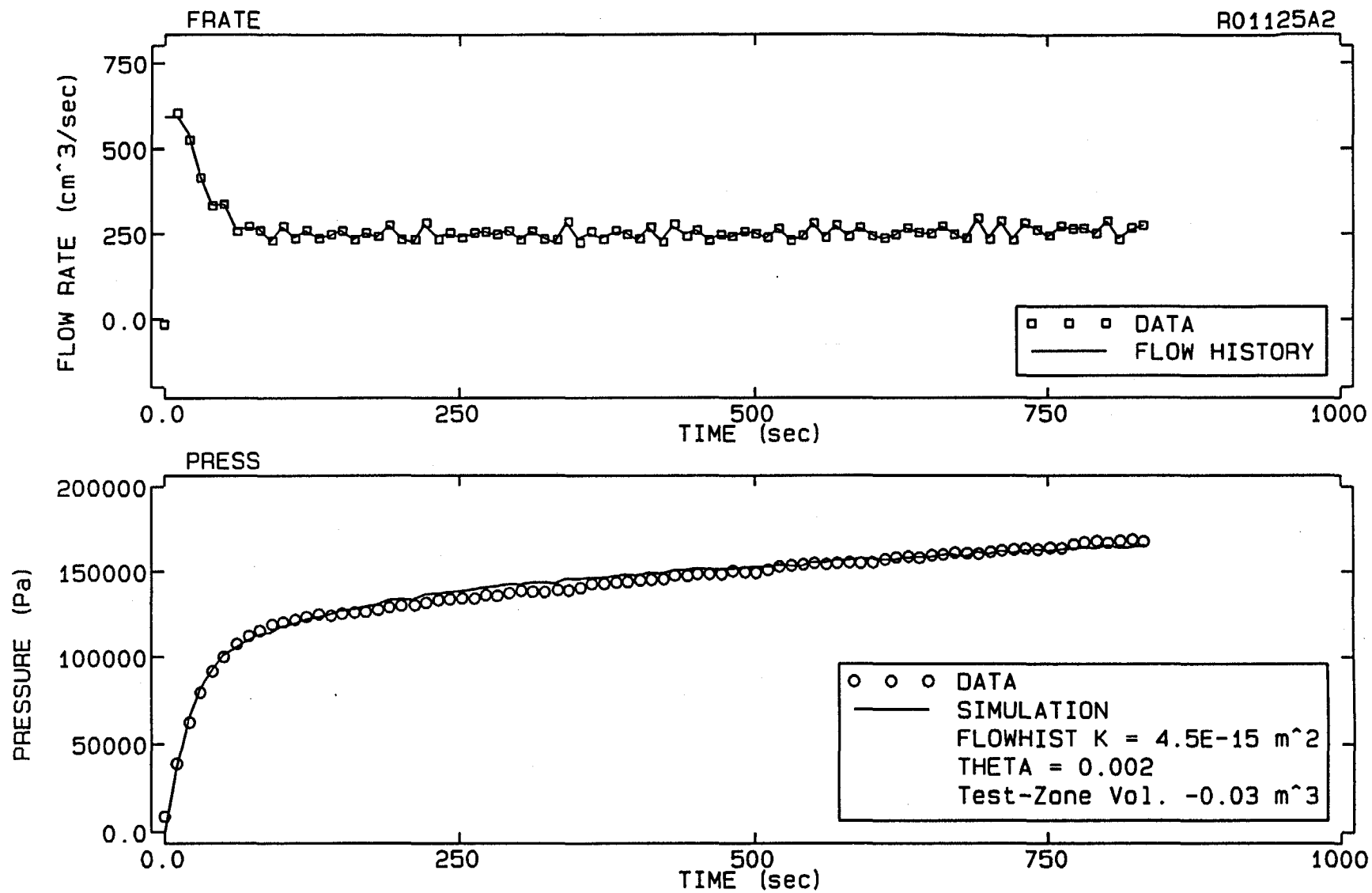
ROOM L3

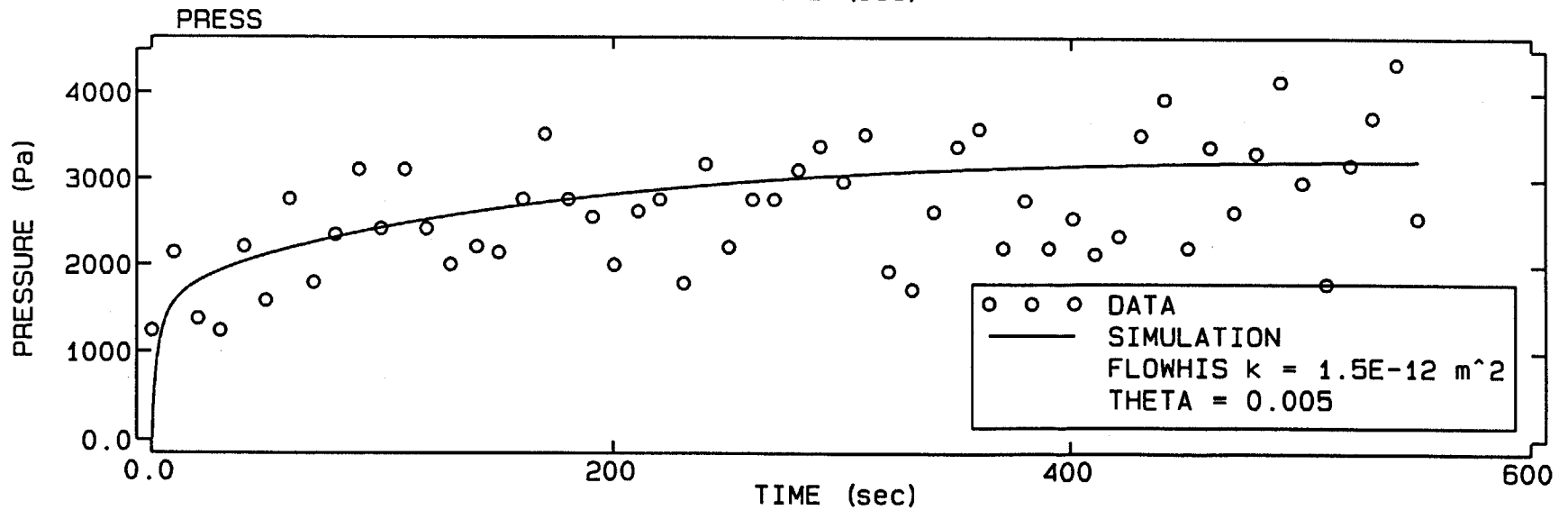
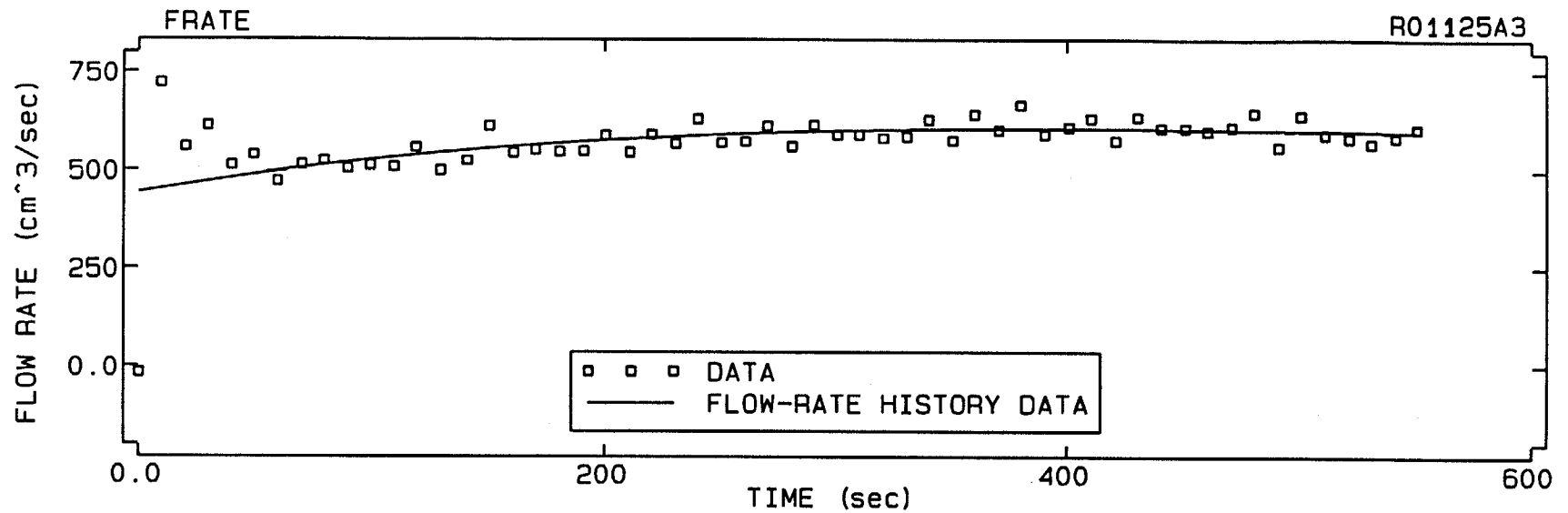
**SMALL-SCALE SEALS
PERFORMANCE TEST**

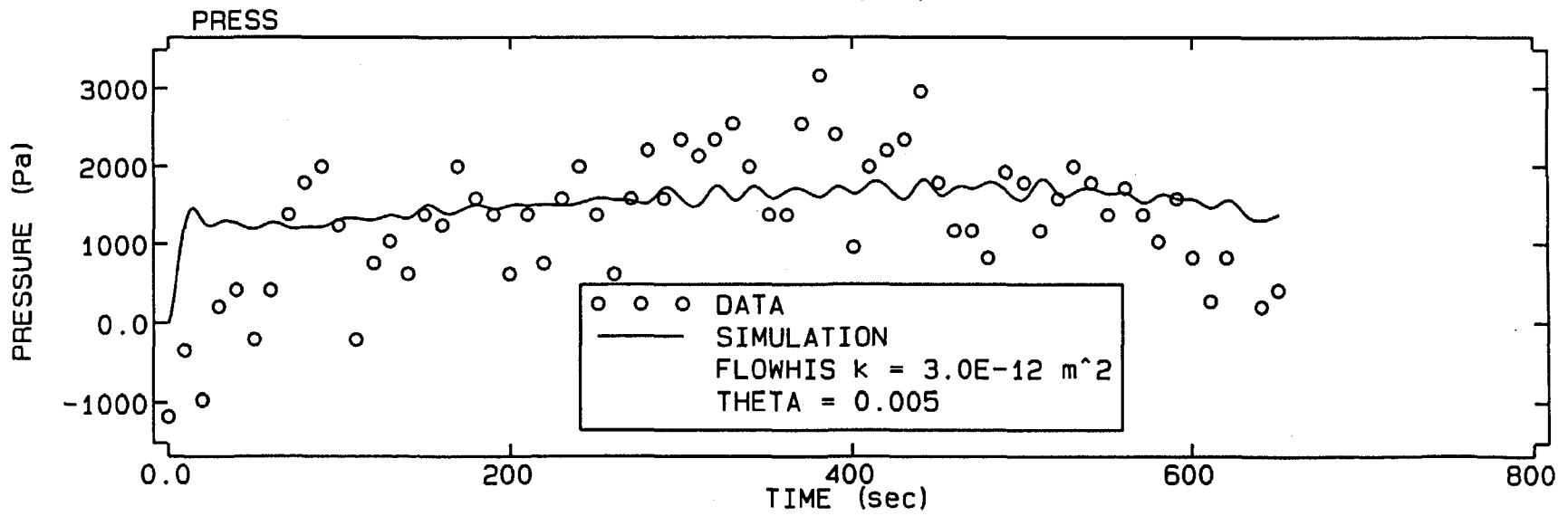
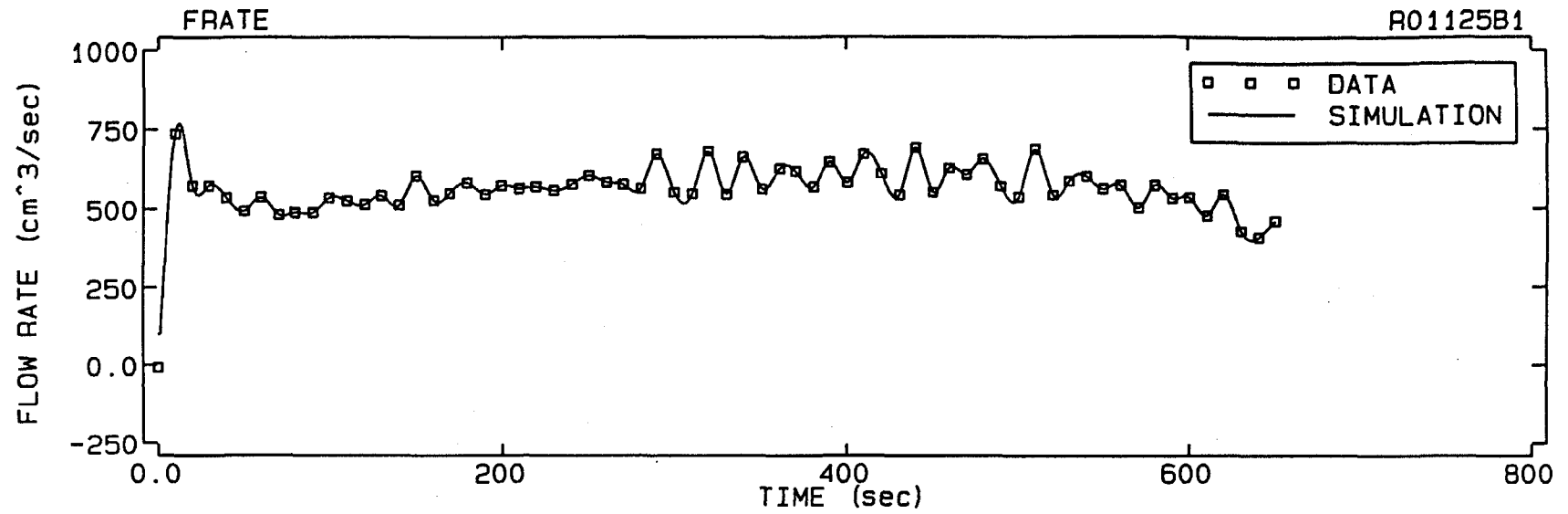
JANUARY to APRIL 1993

GTFM 5.10B TEST SIMULATIONS

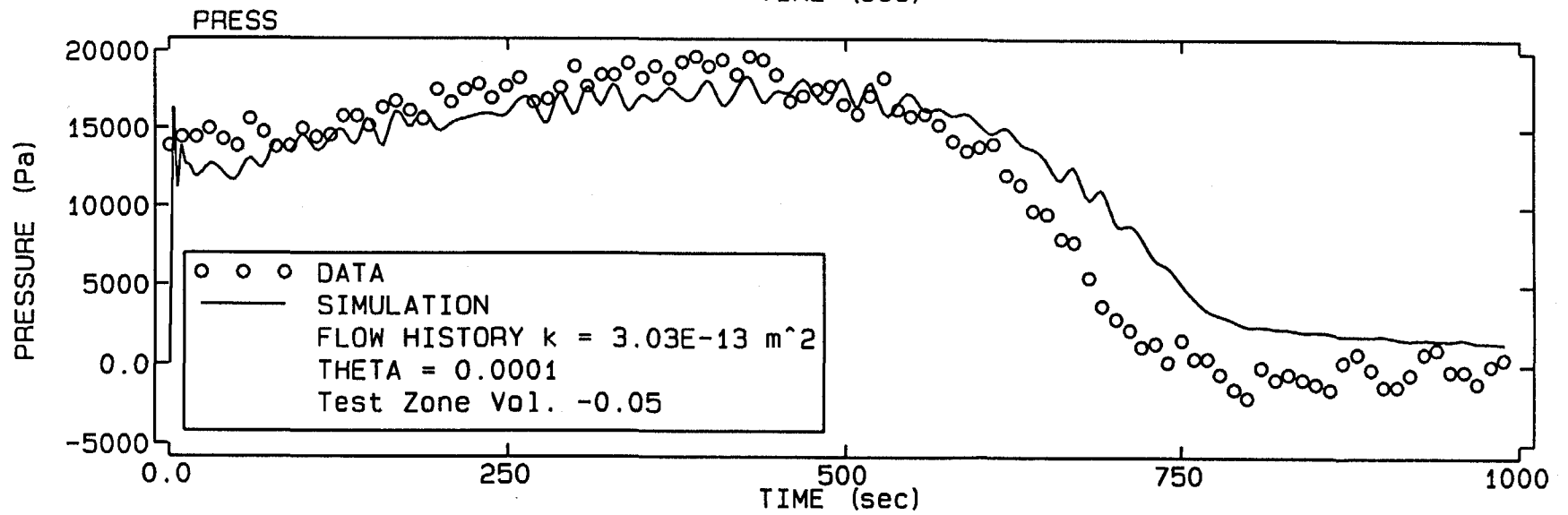
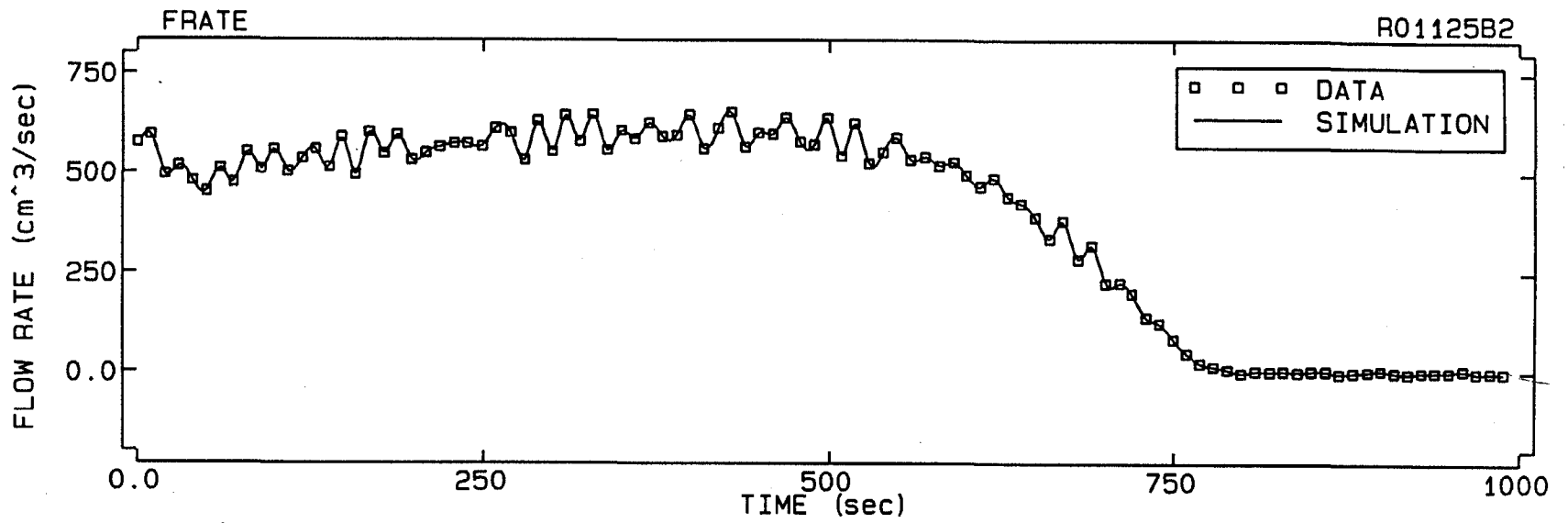


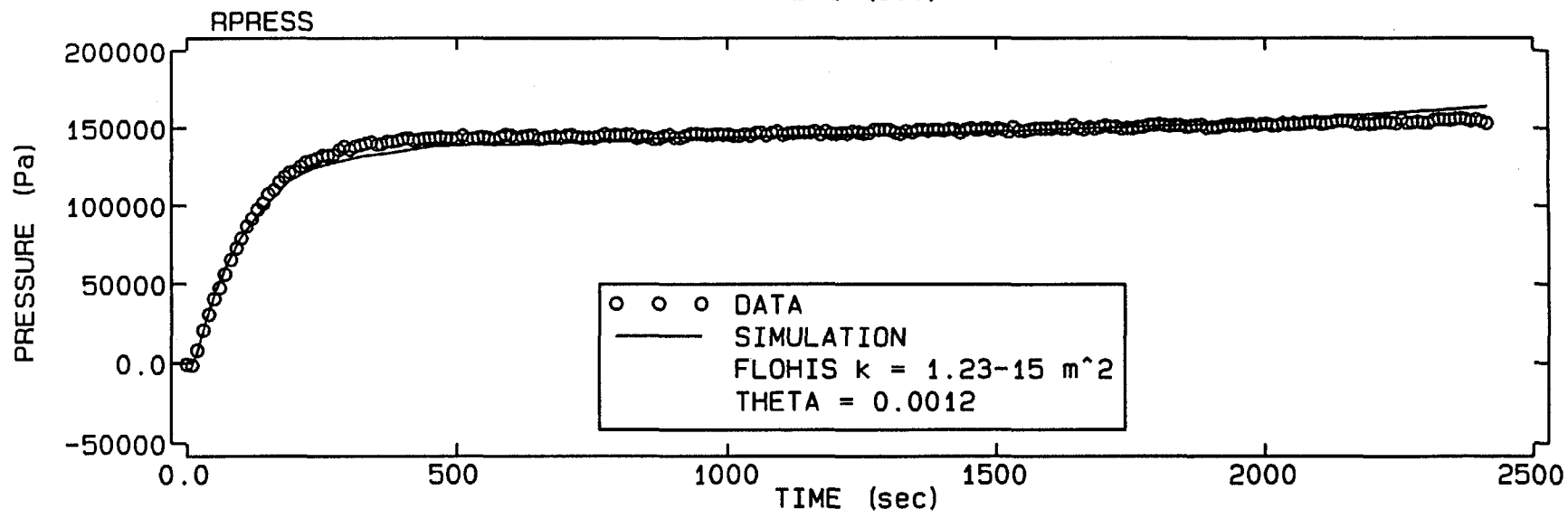
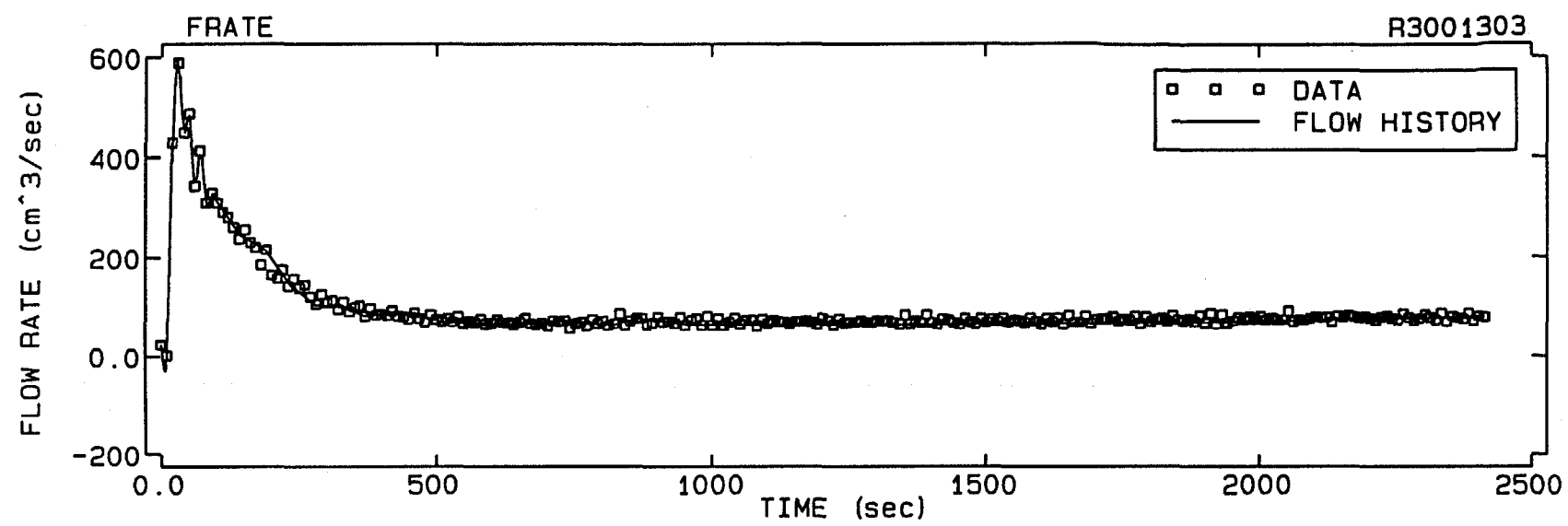


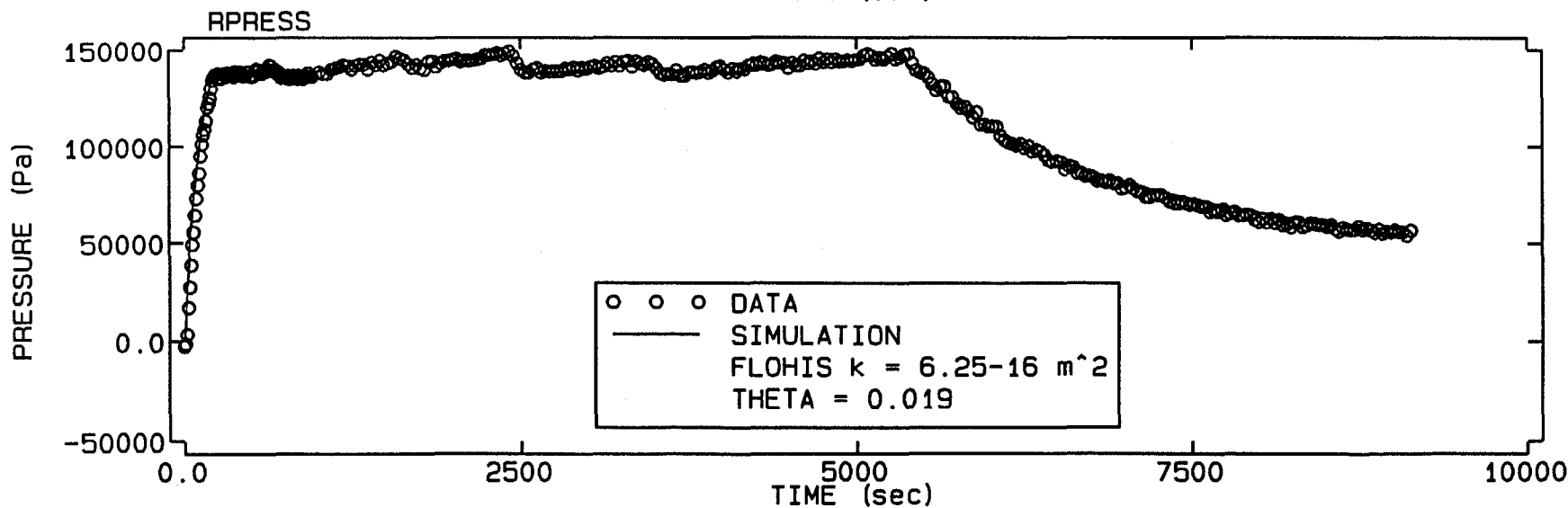
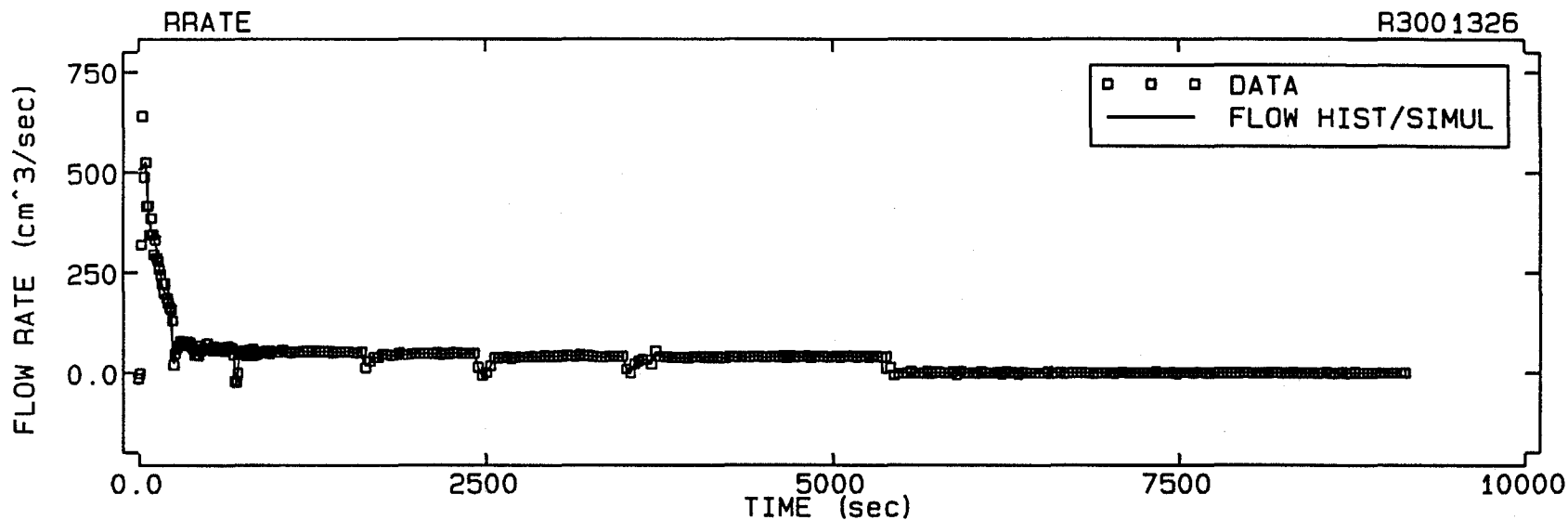


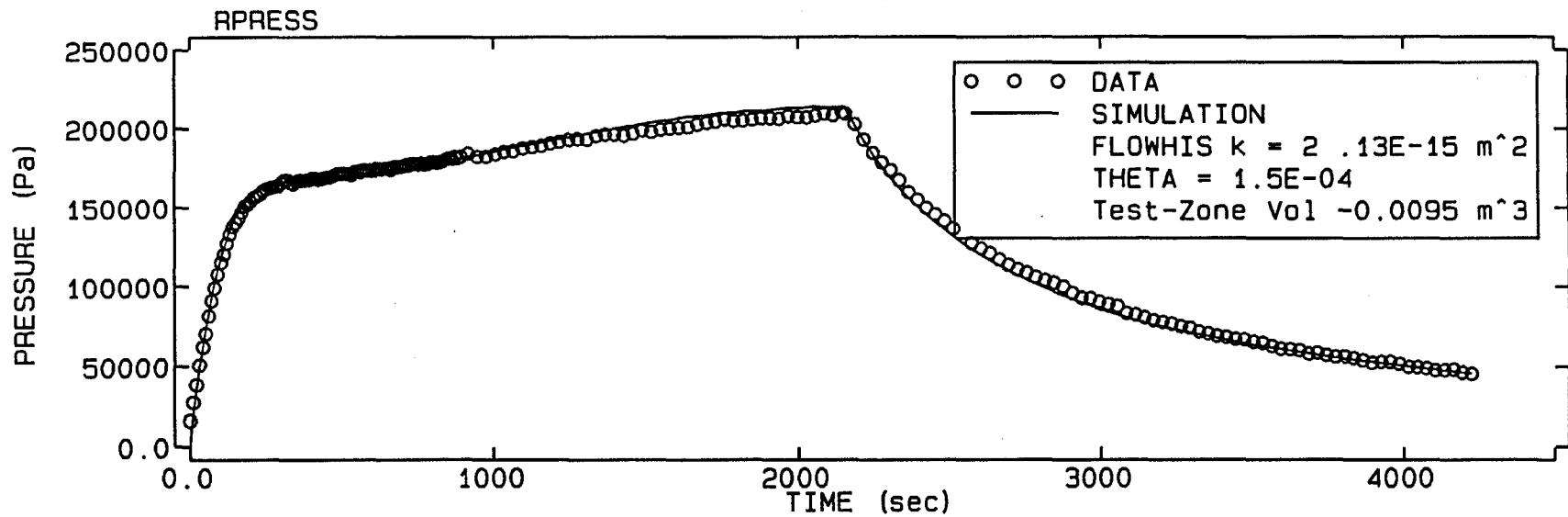
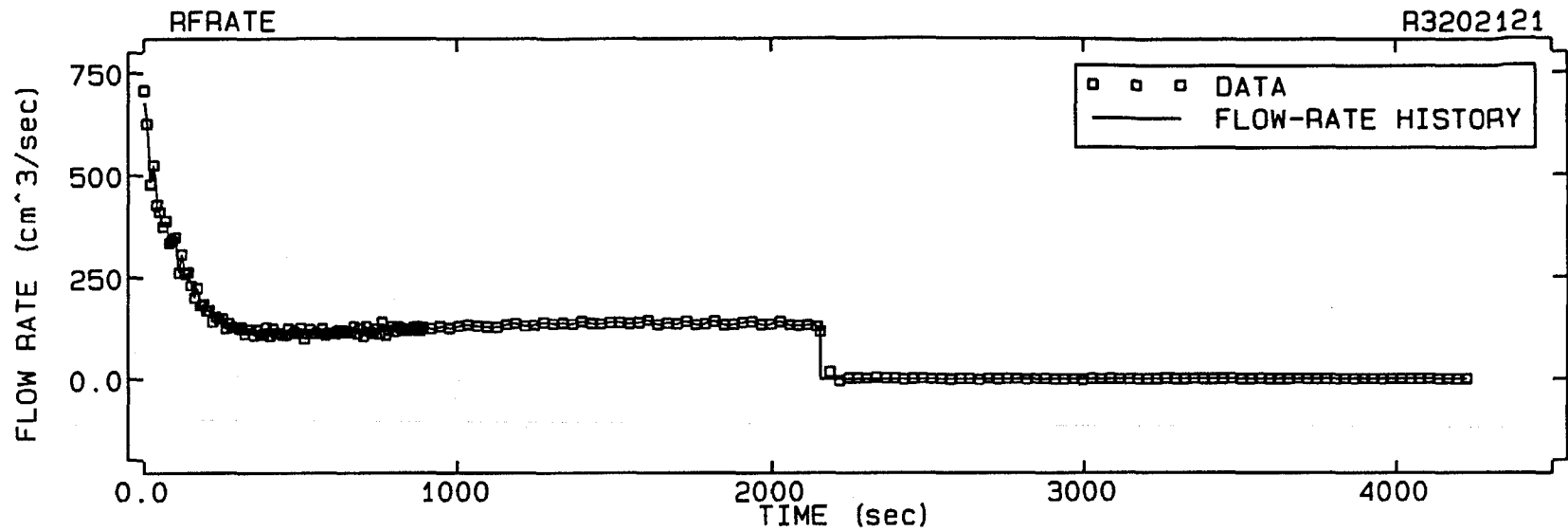


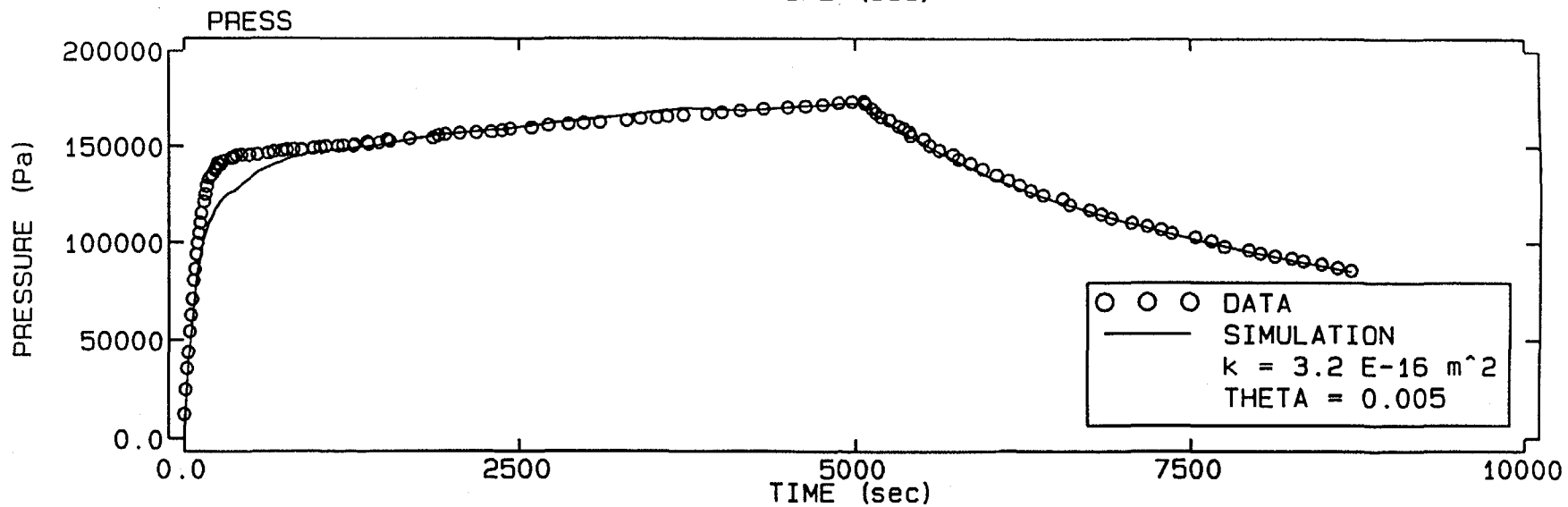
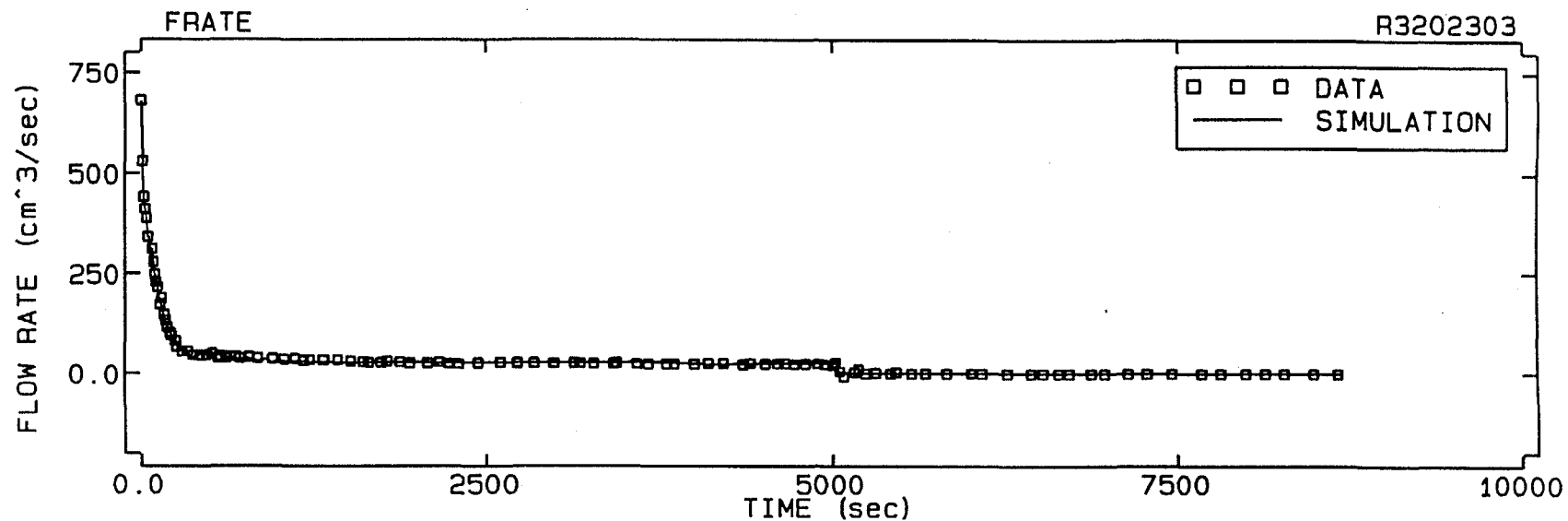
67-I

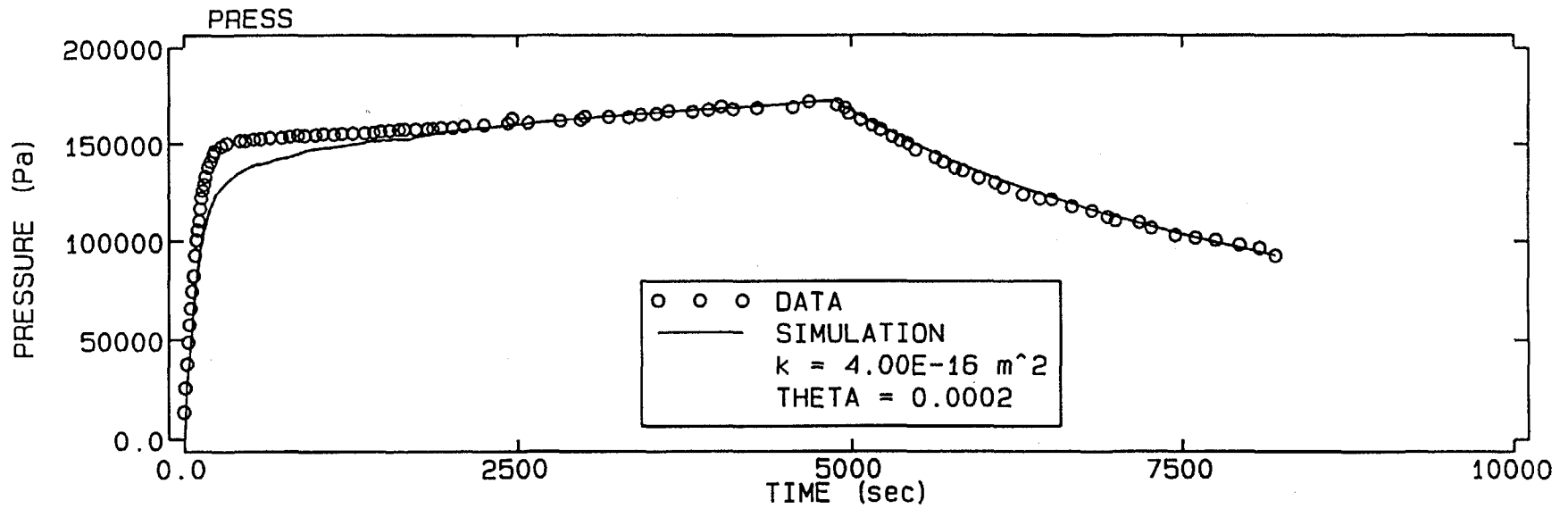
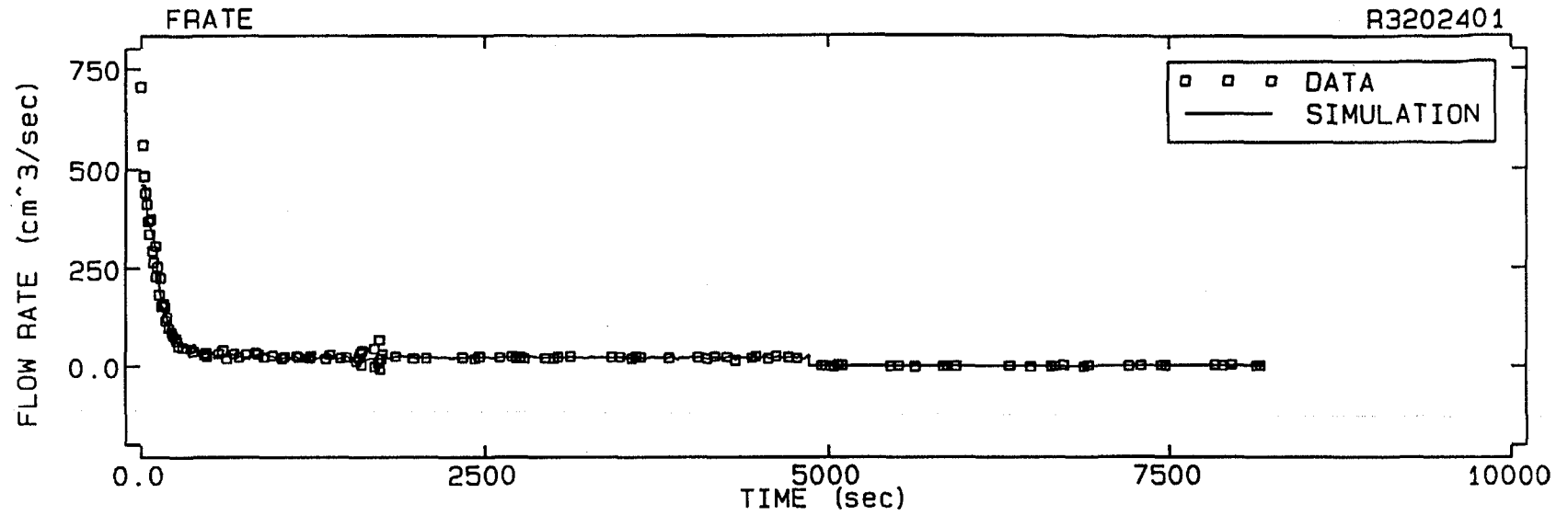


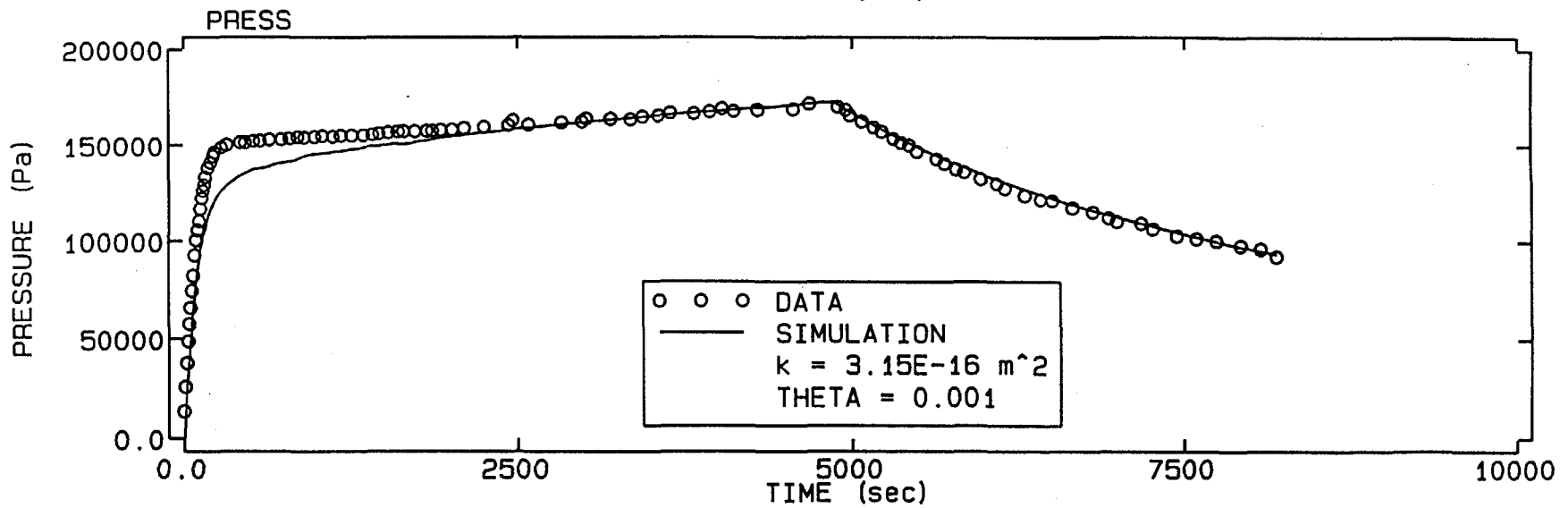
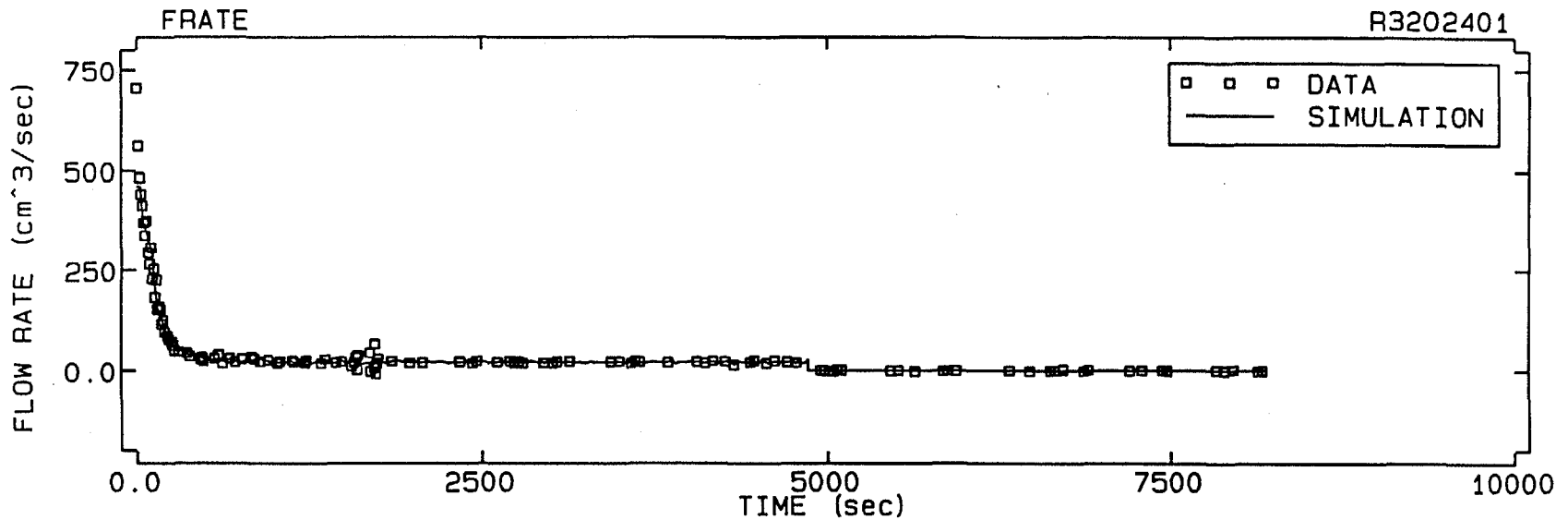


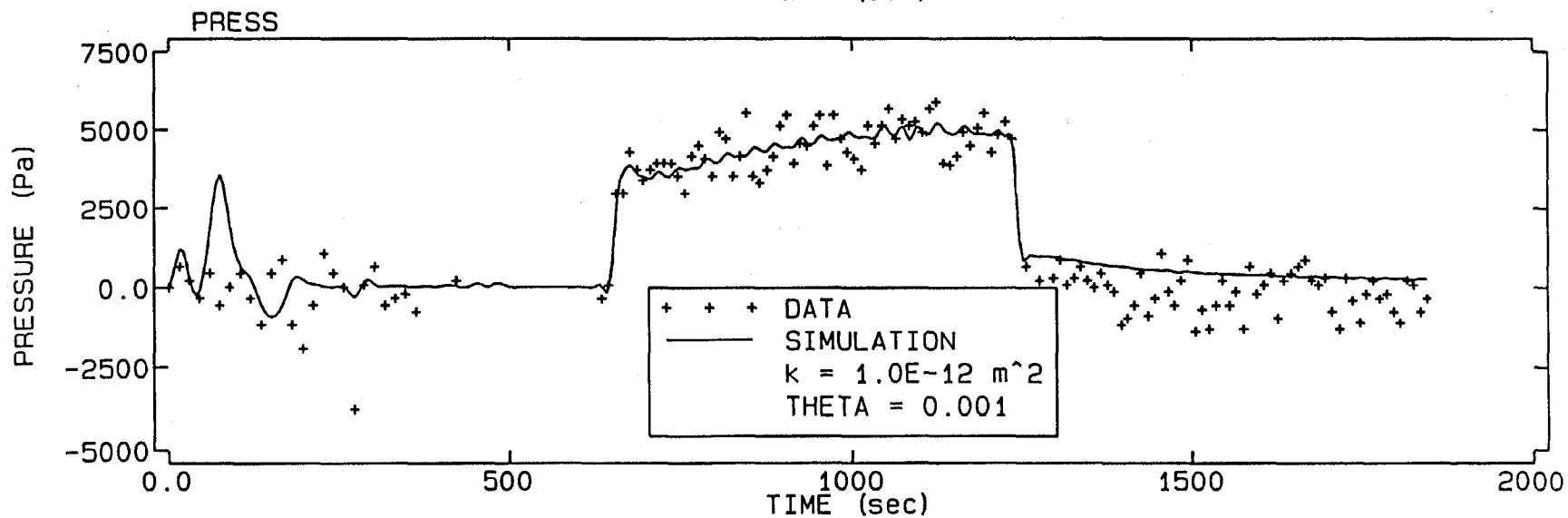
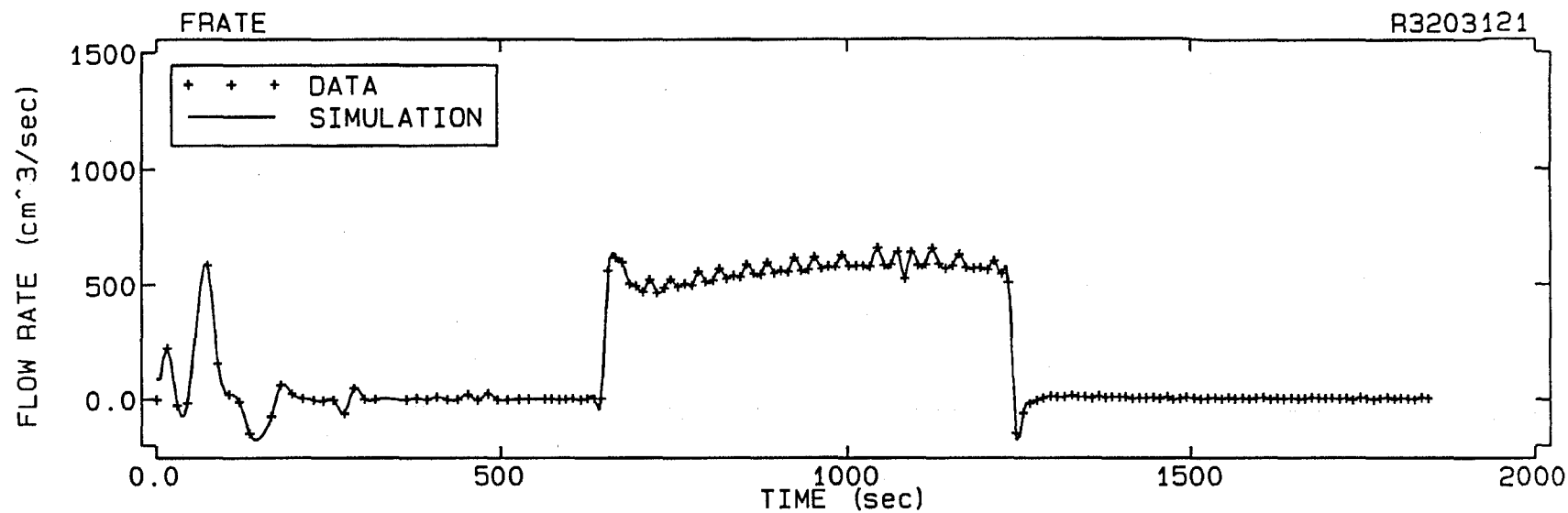


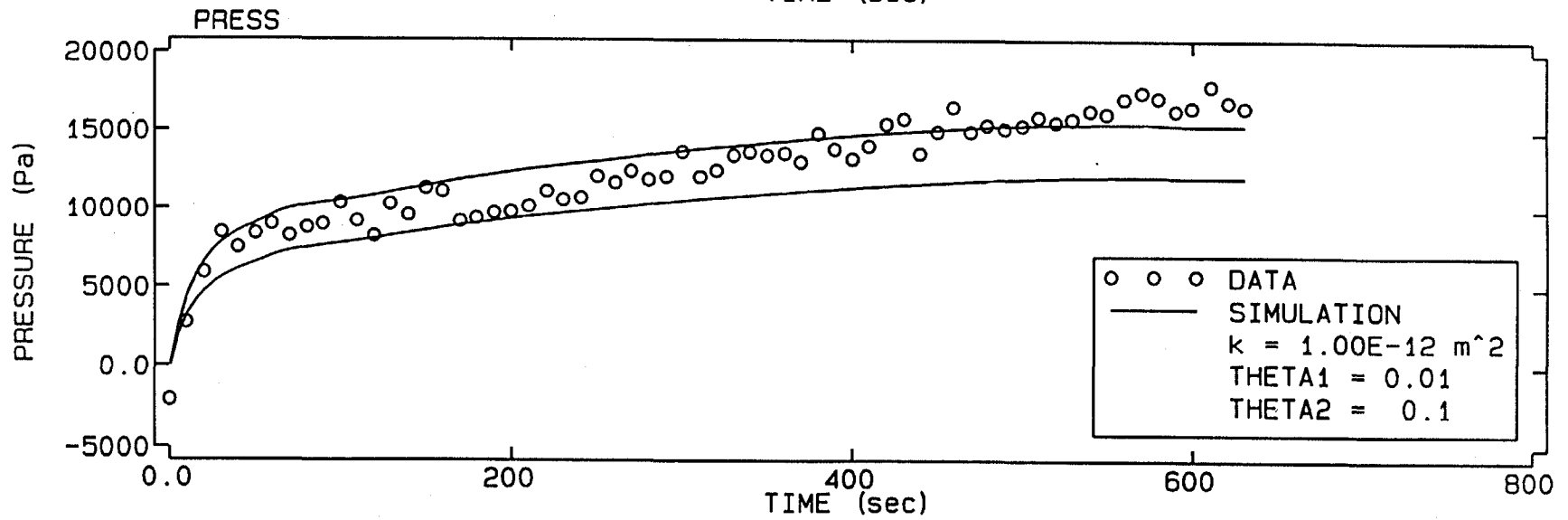
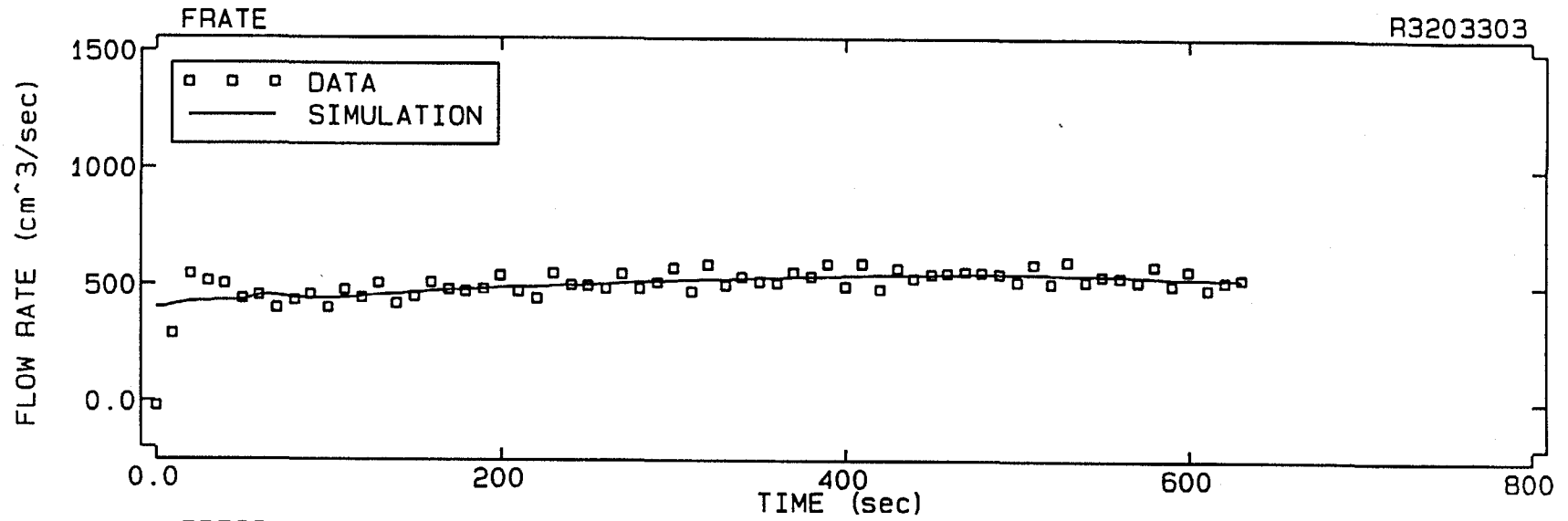


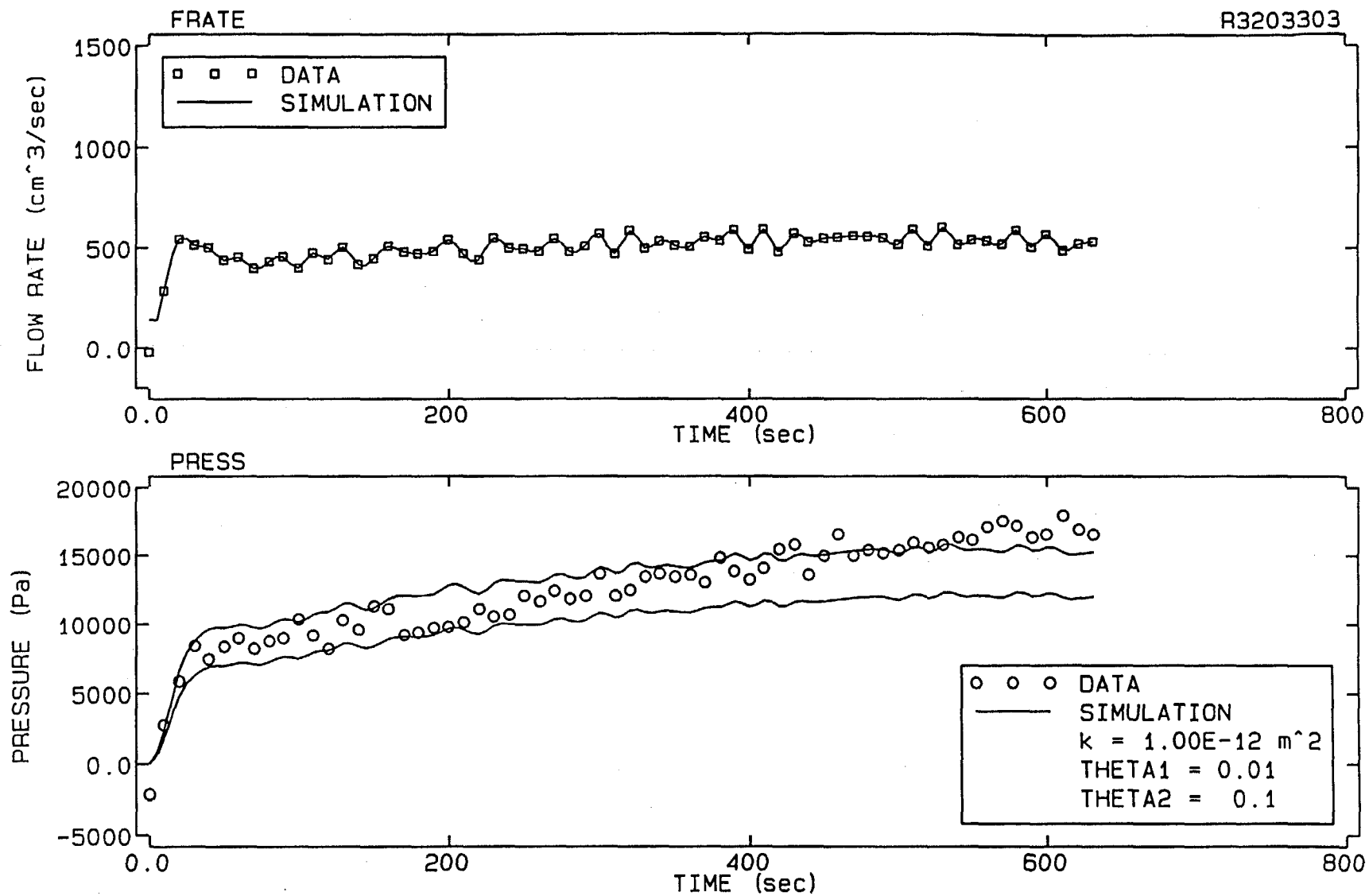


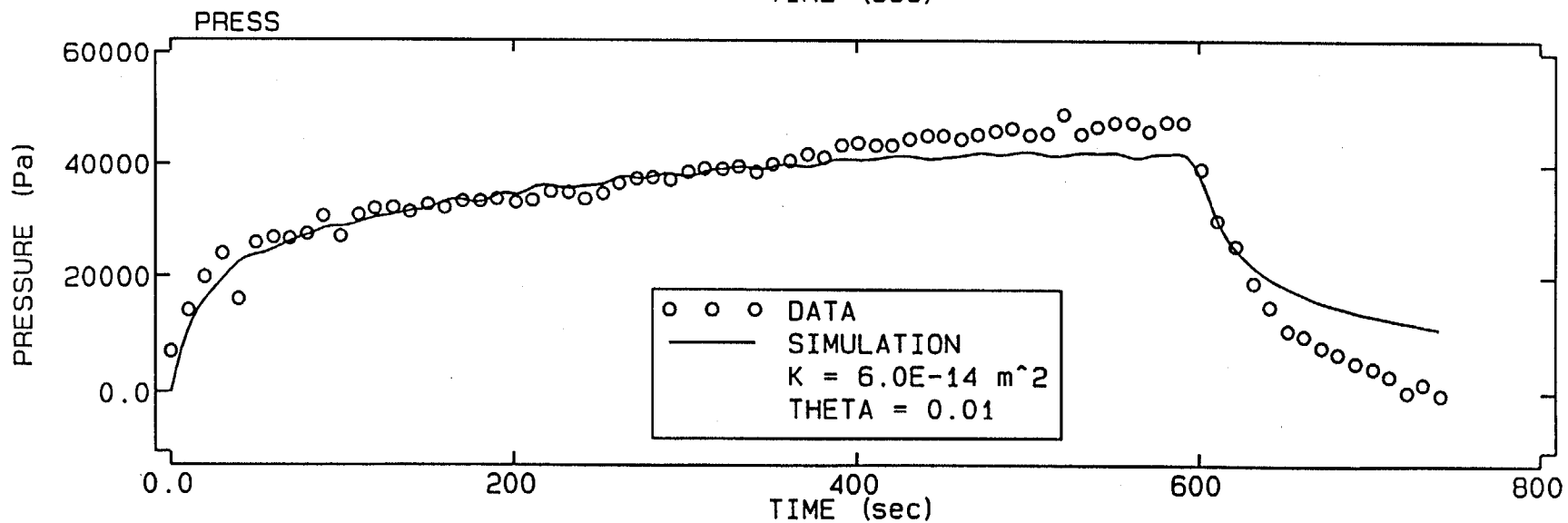
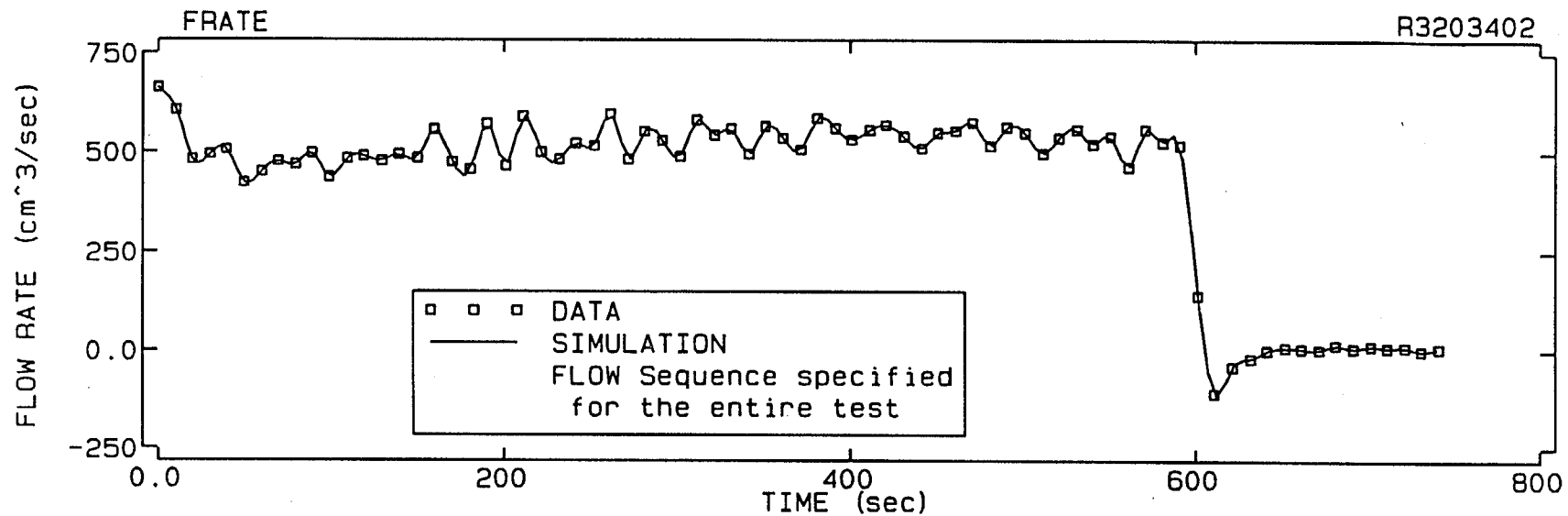


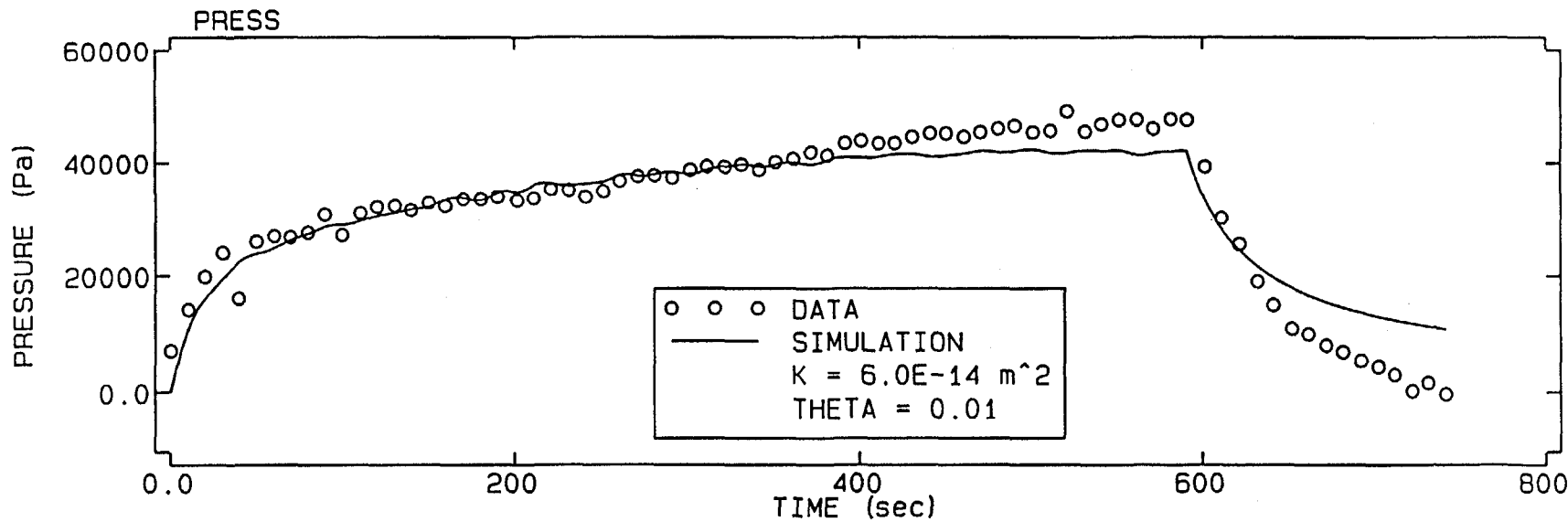
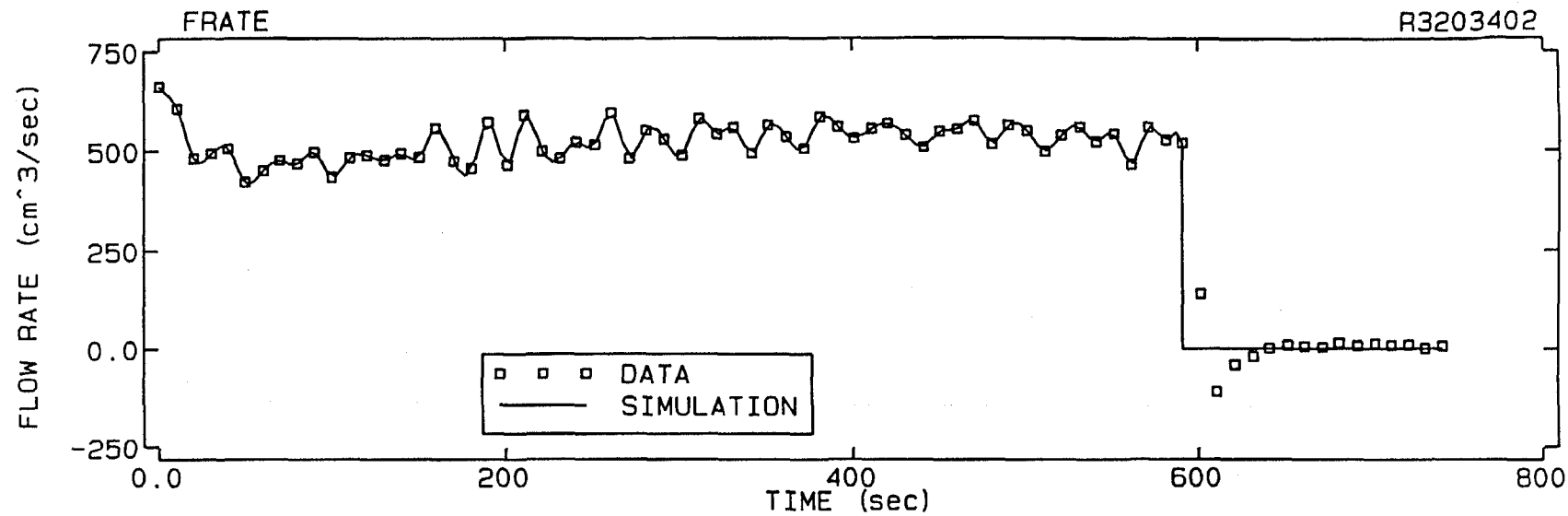




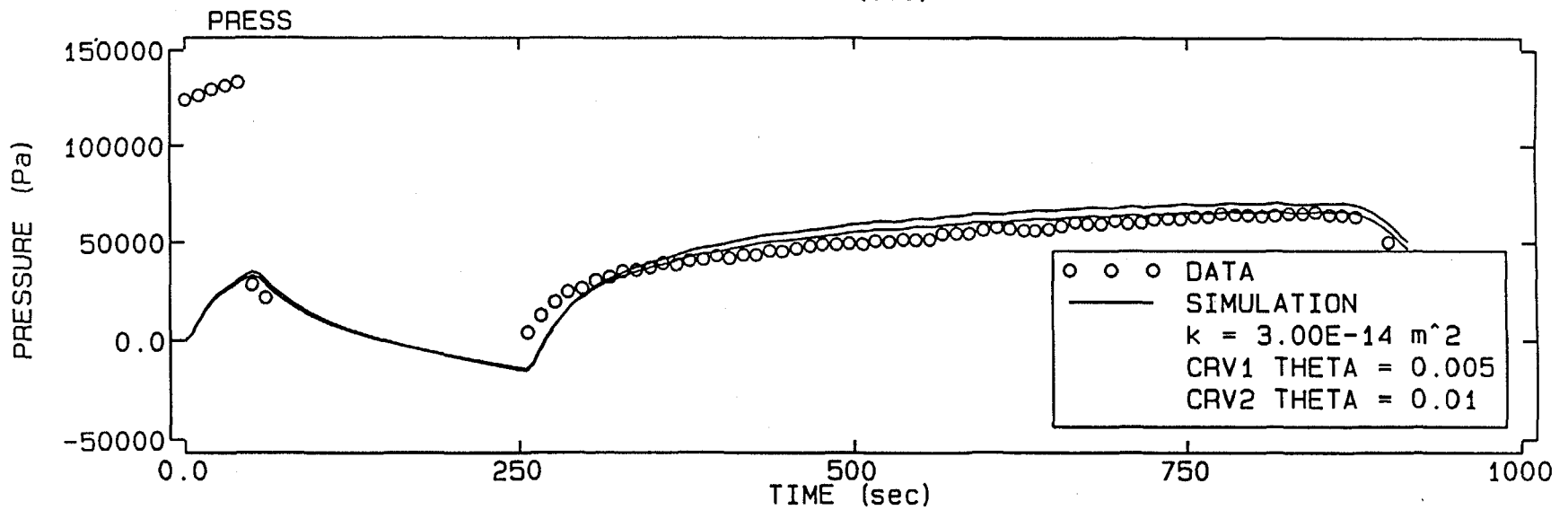
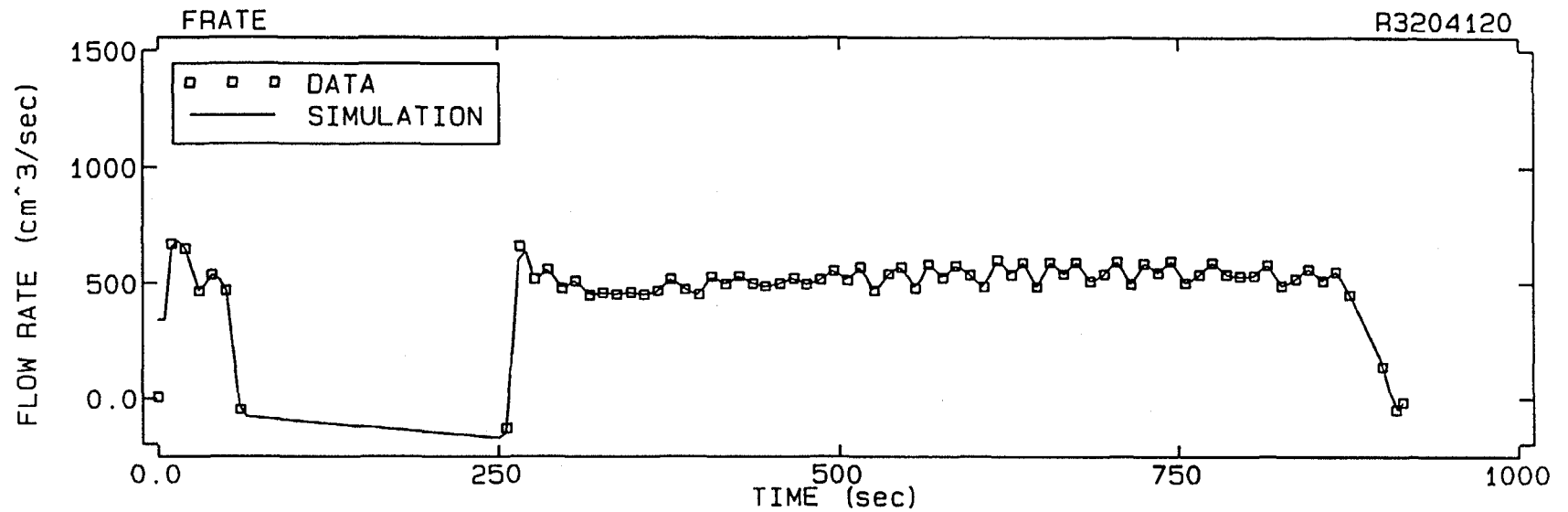






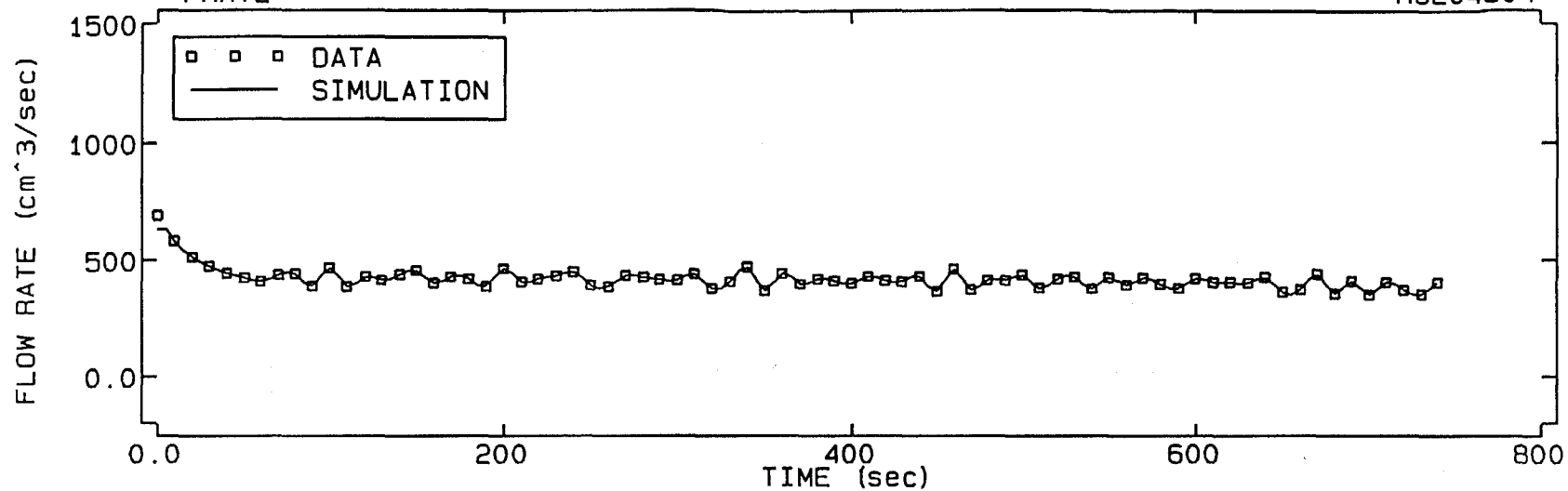


I9-I

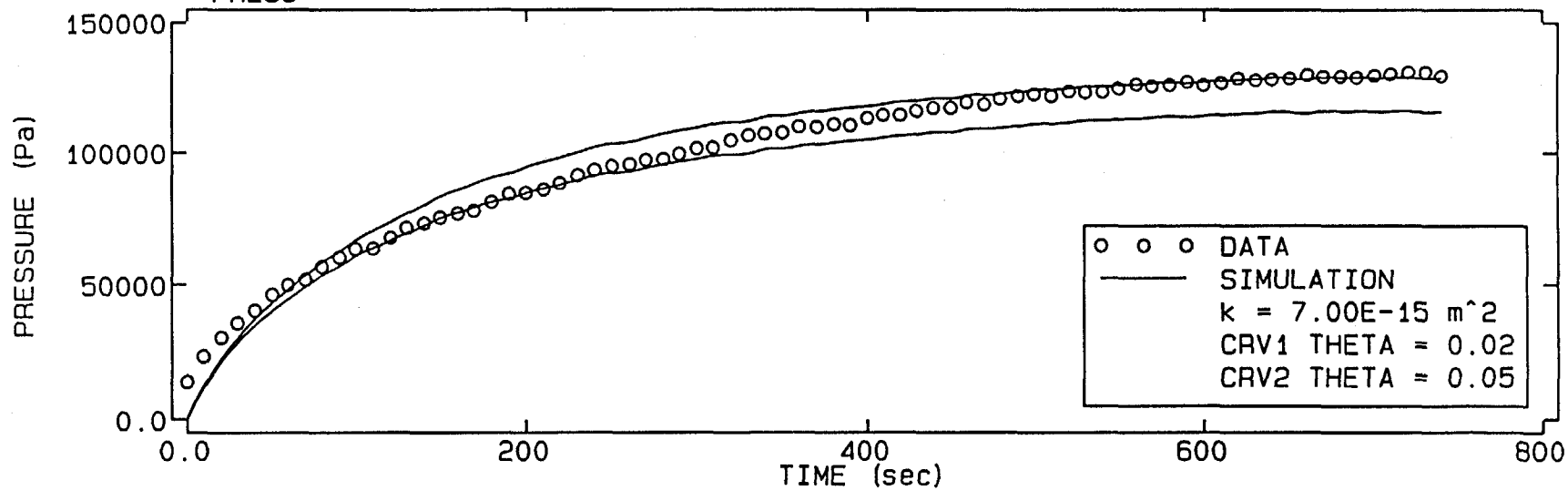


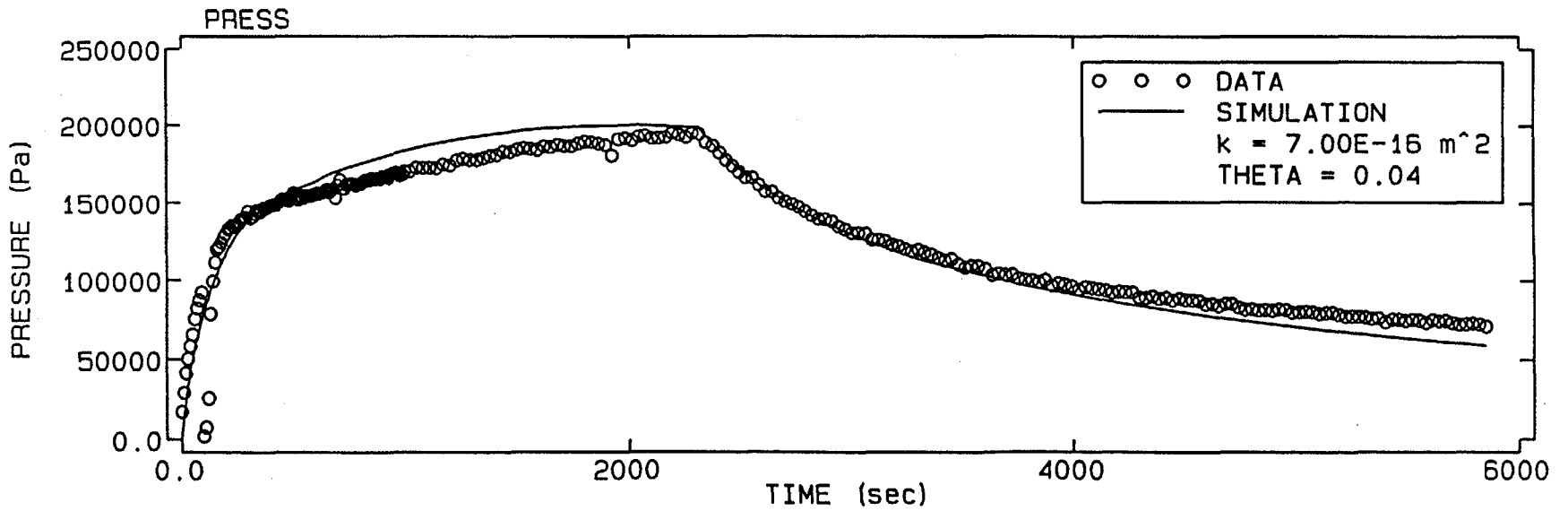
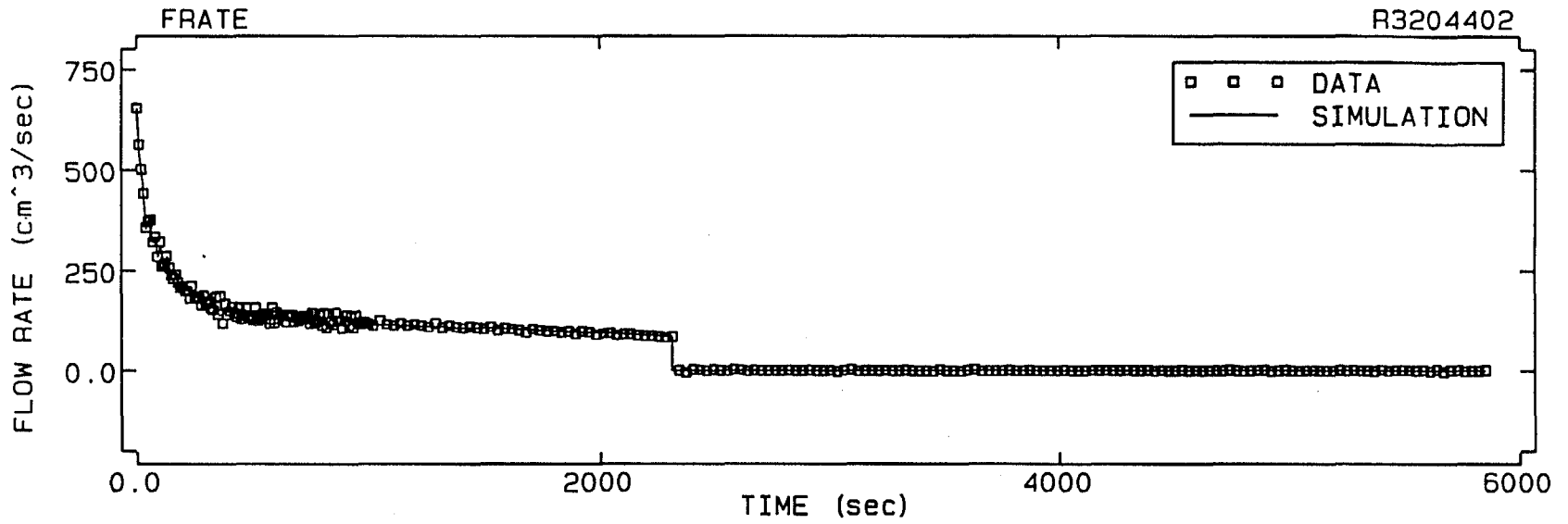
FRATE

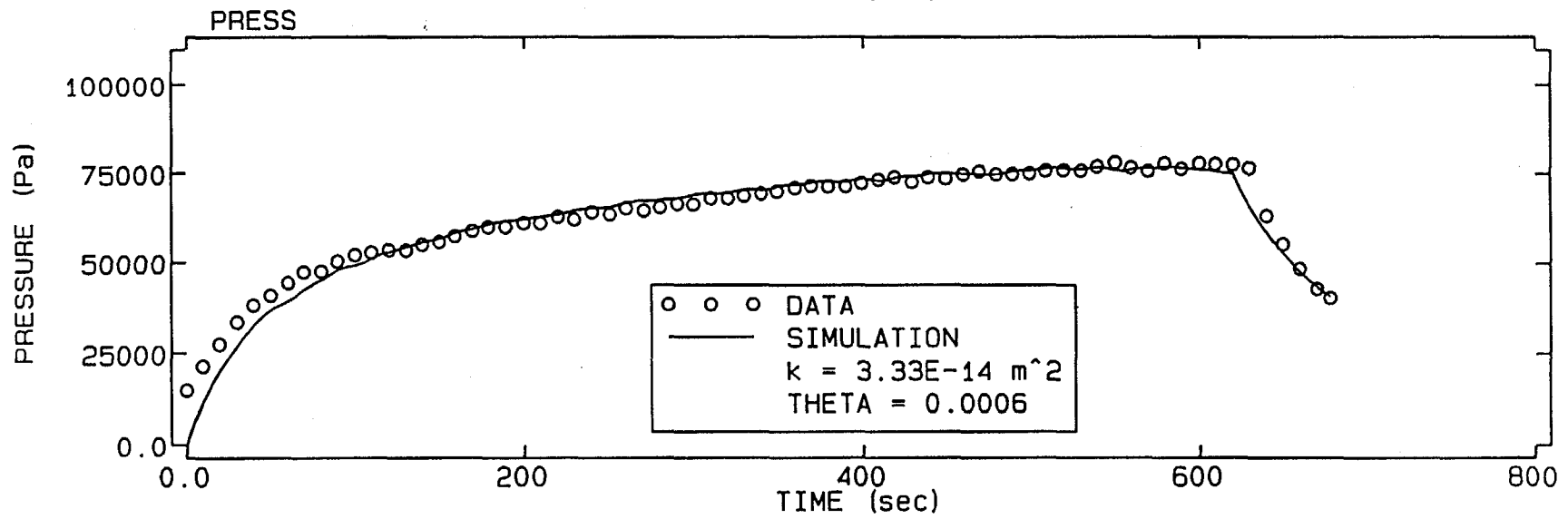
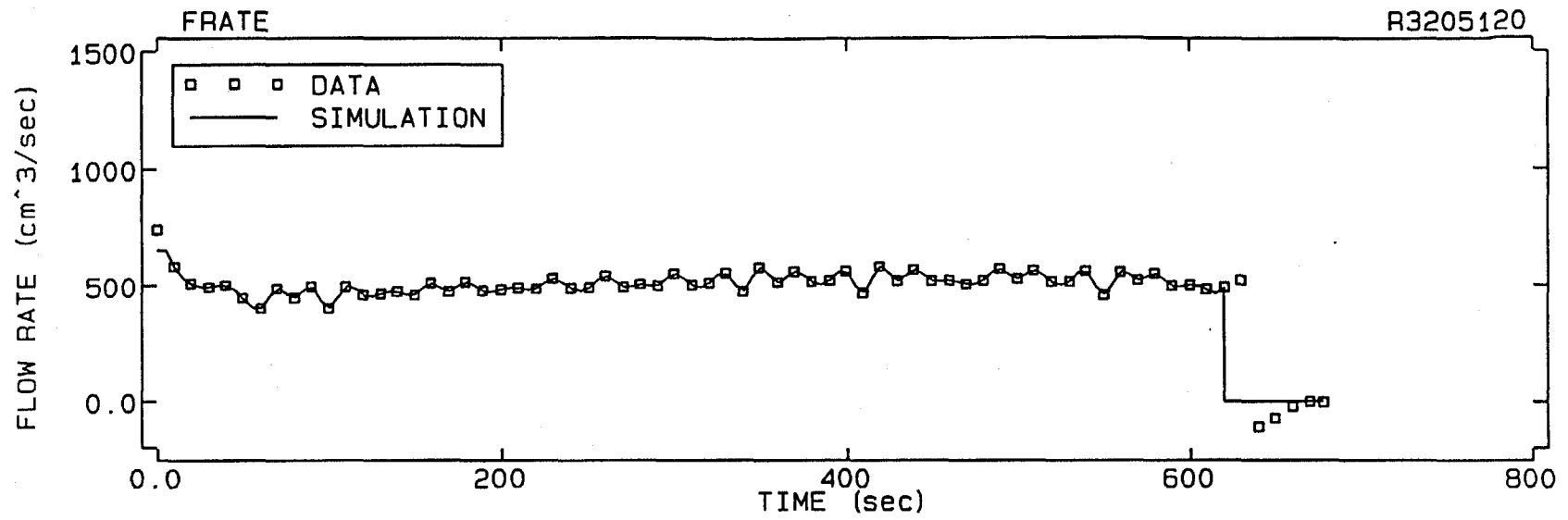
R3204304

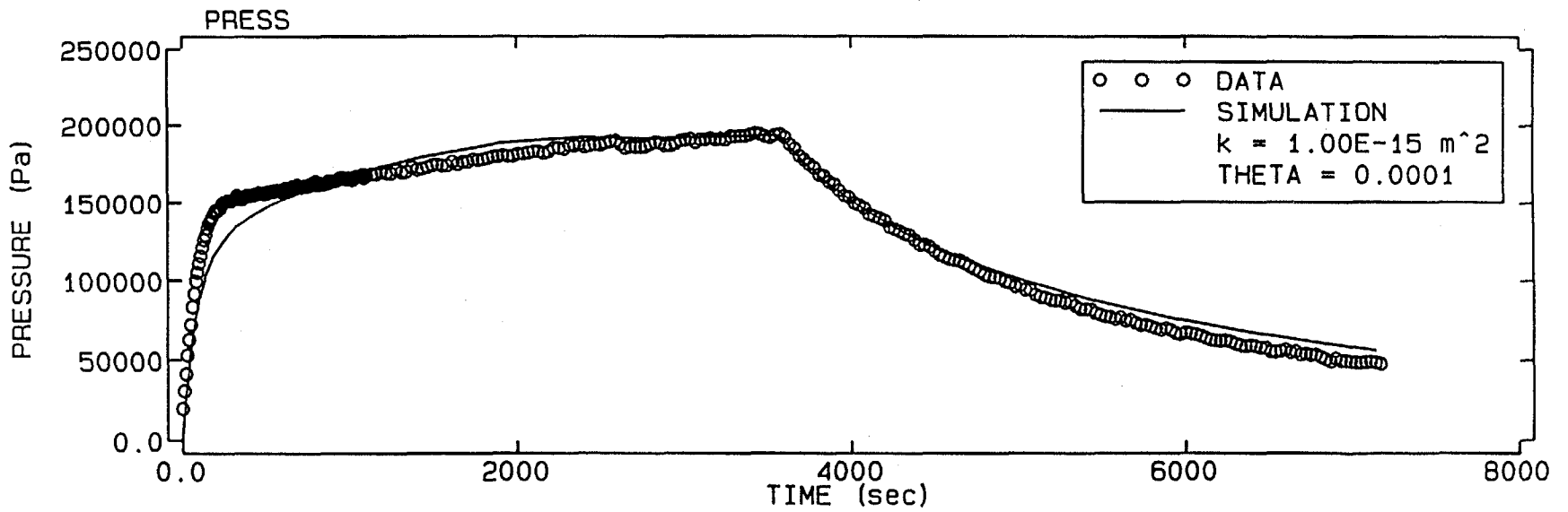
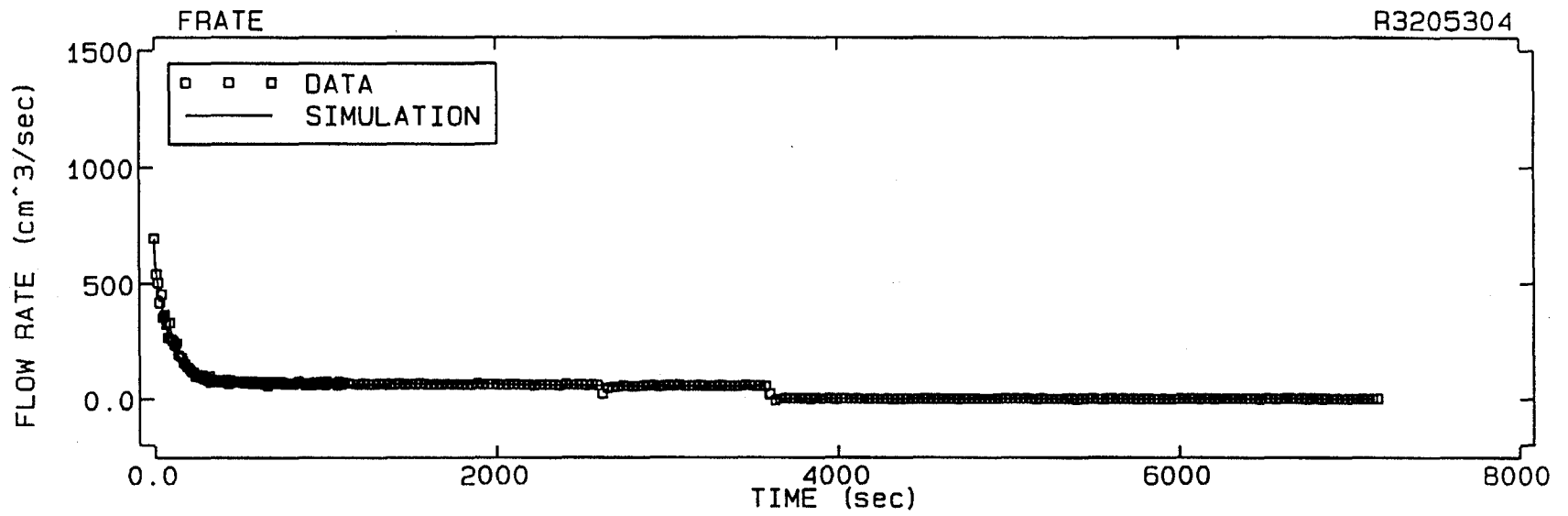


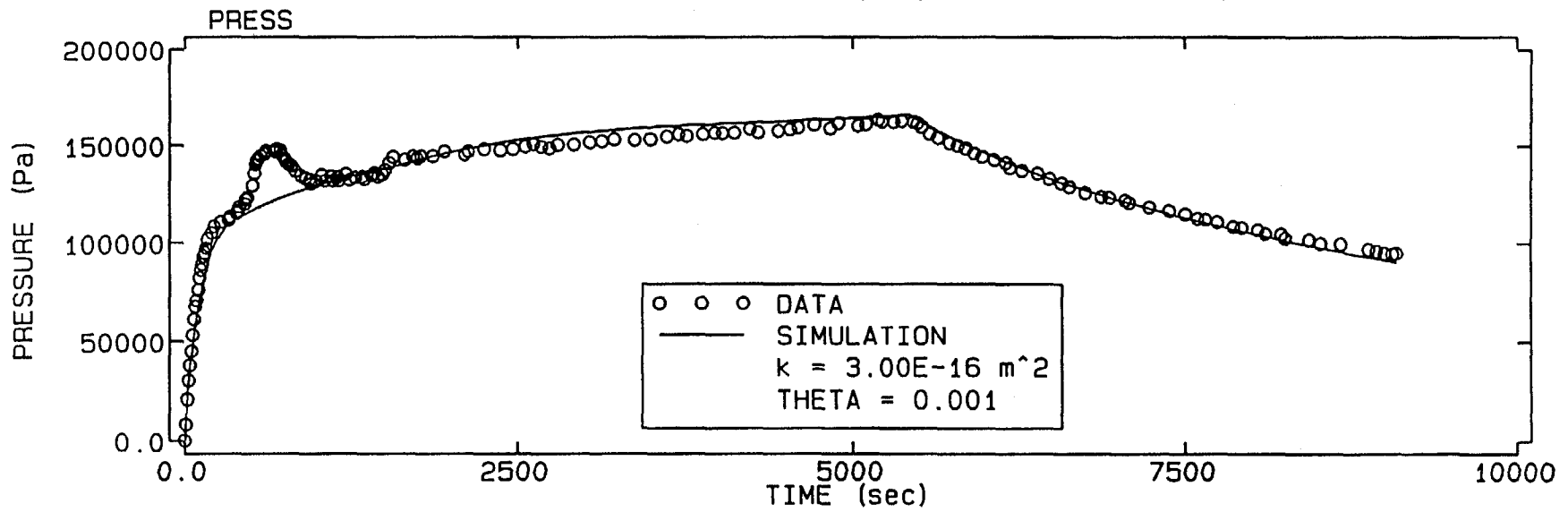
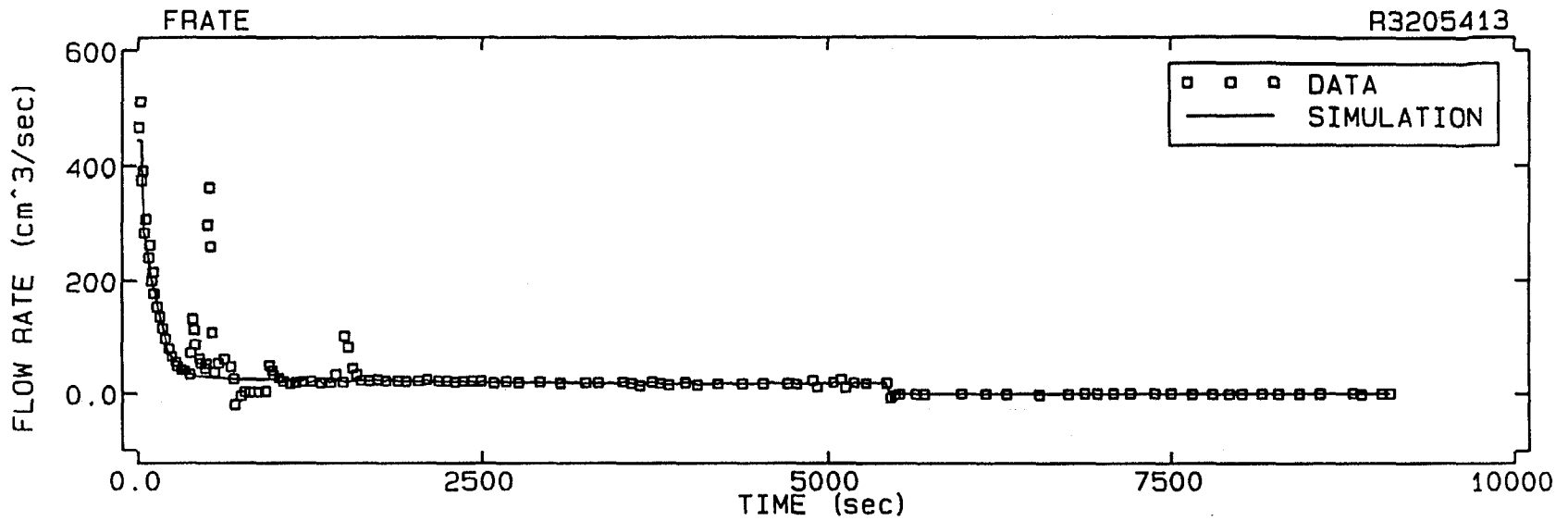
PRESS

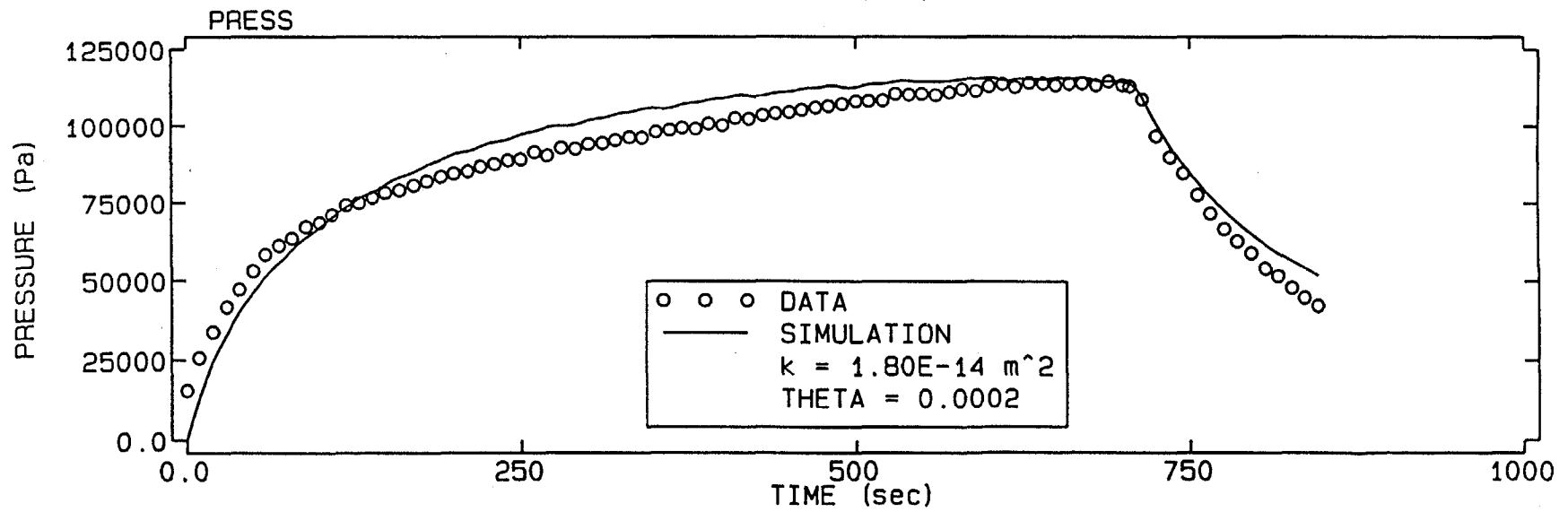
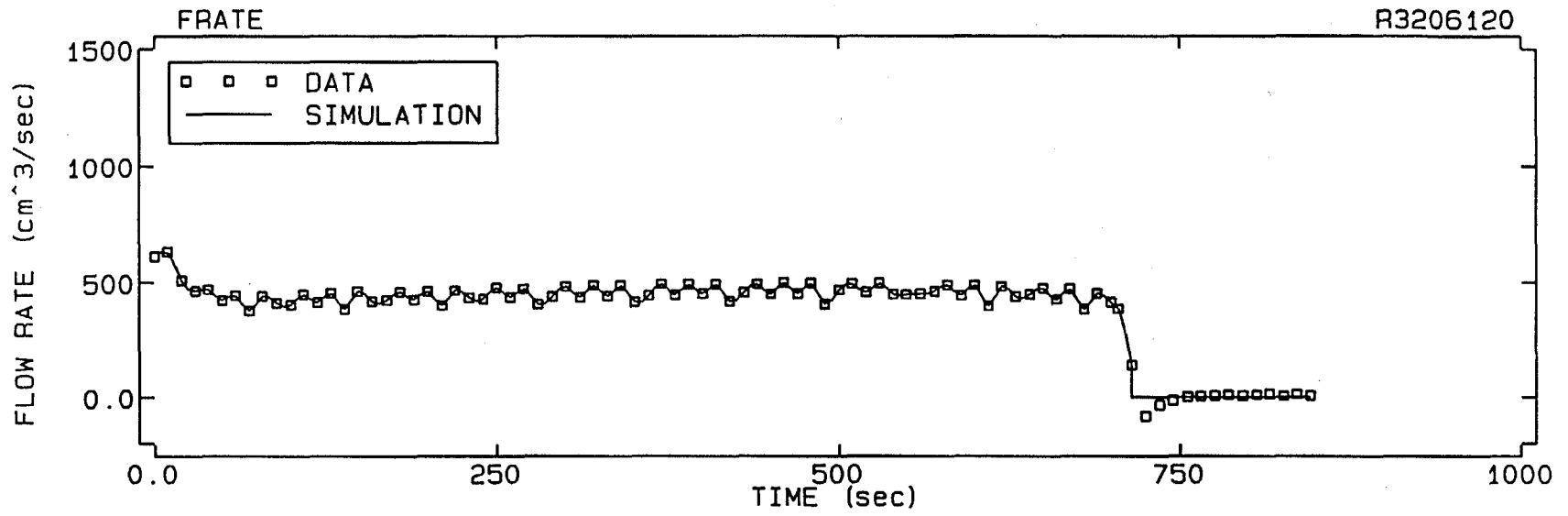


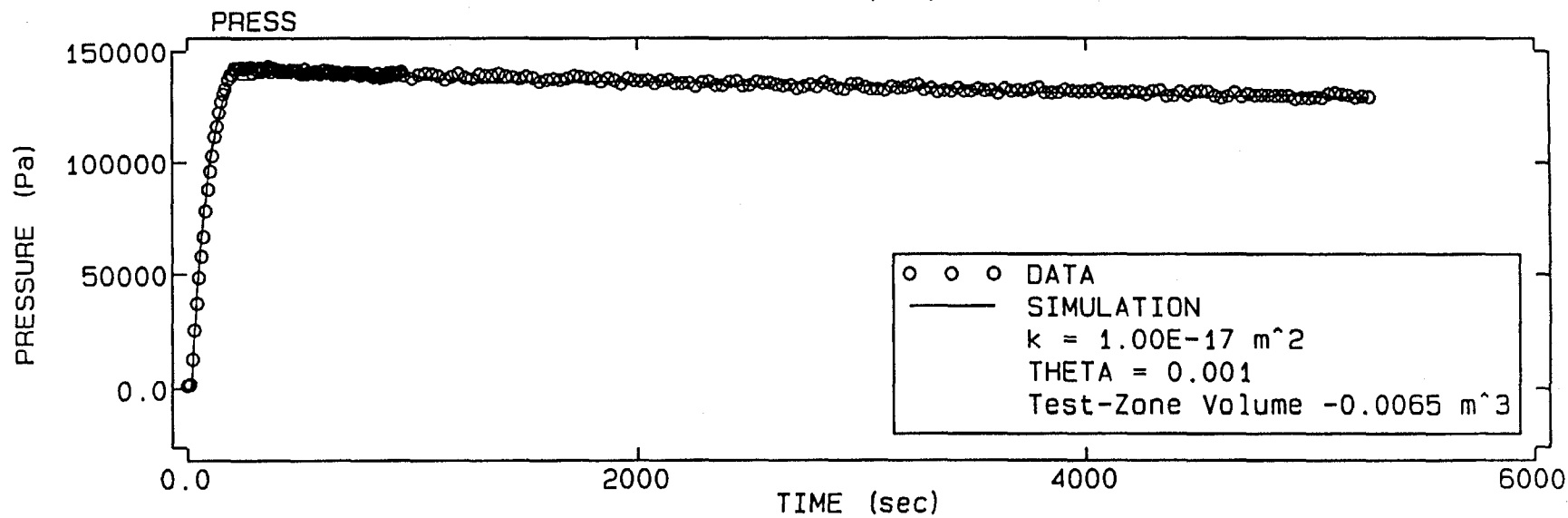
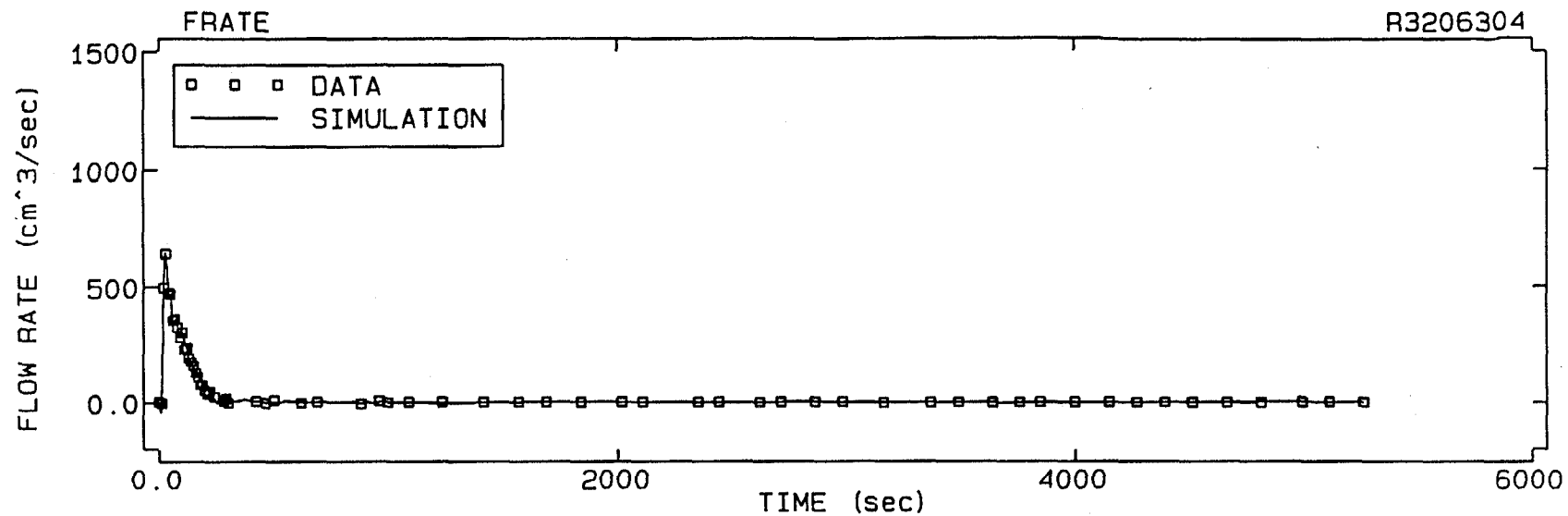


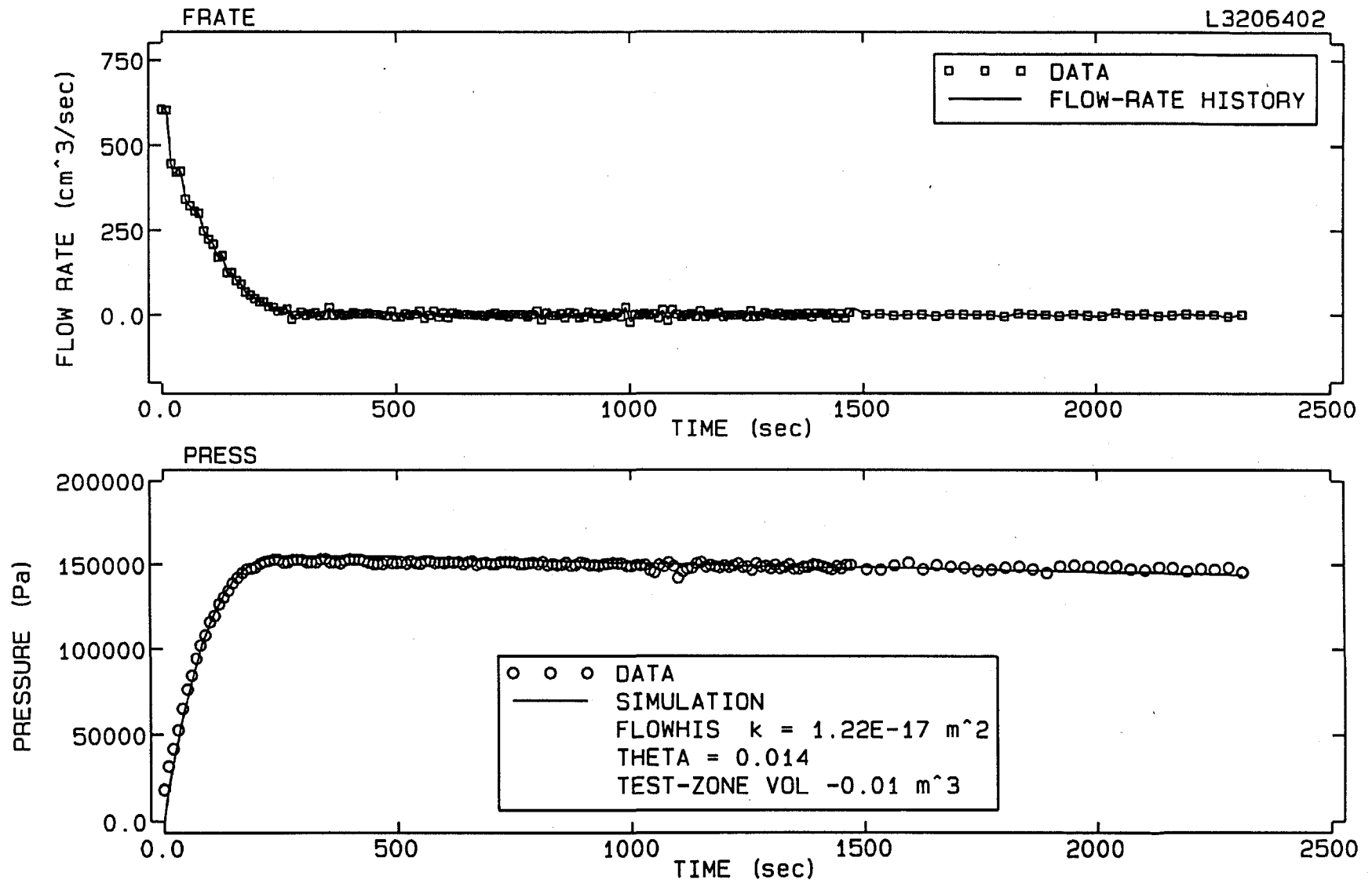




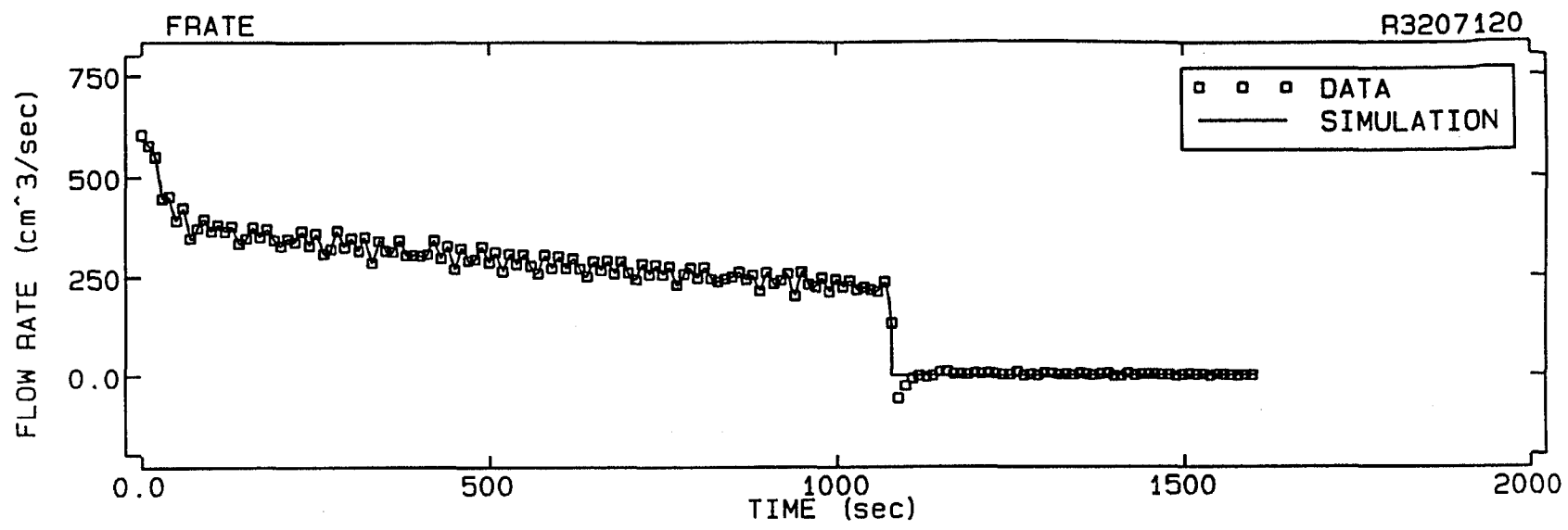




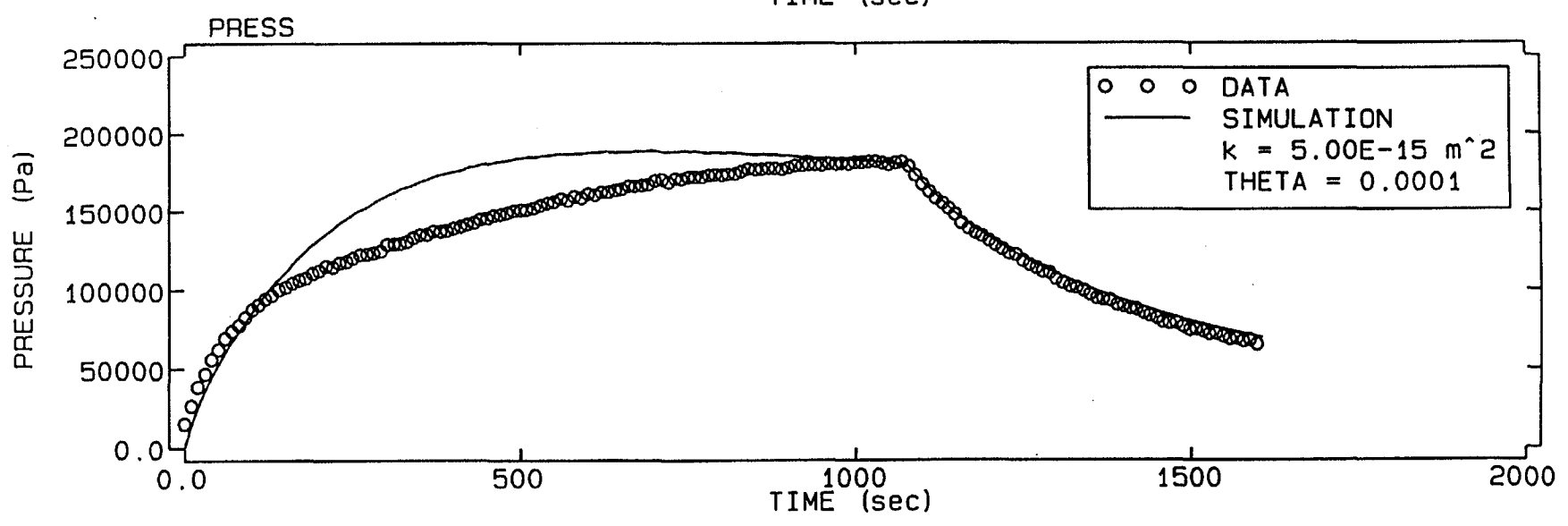


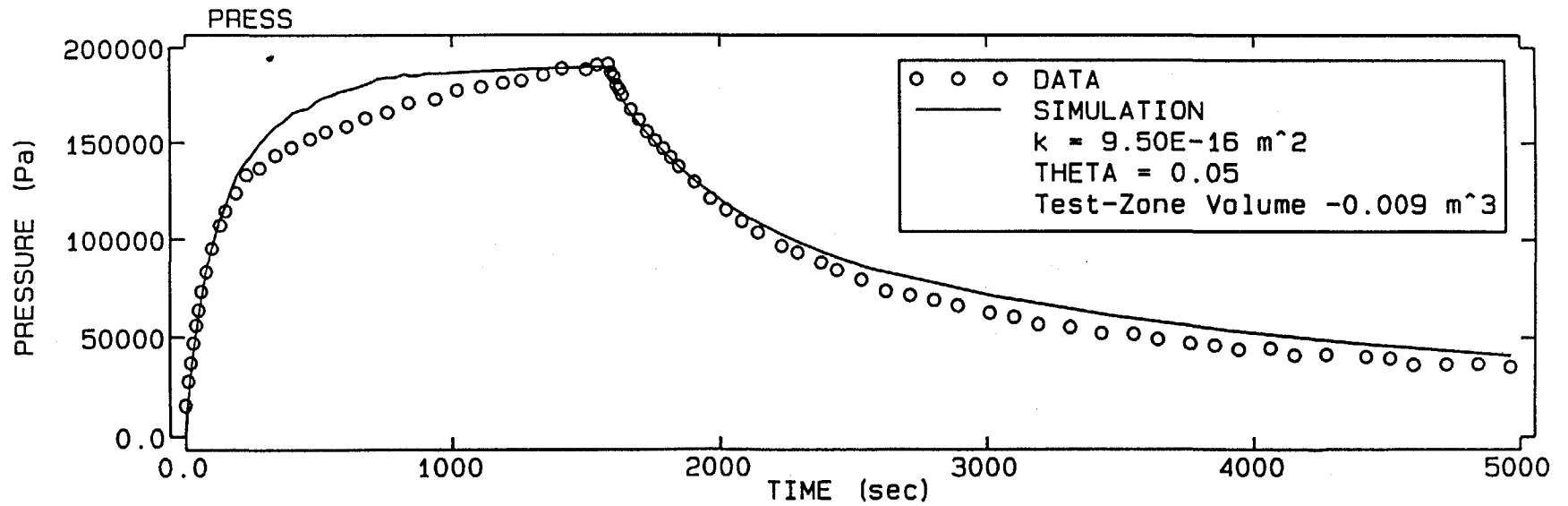
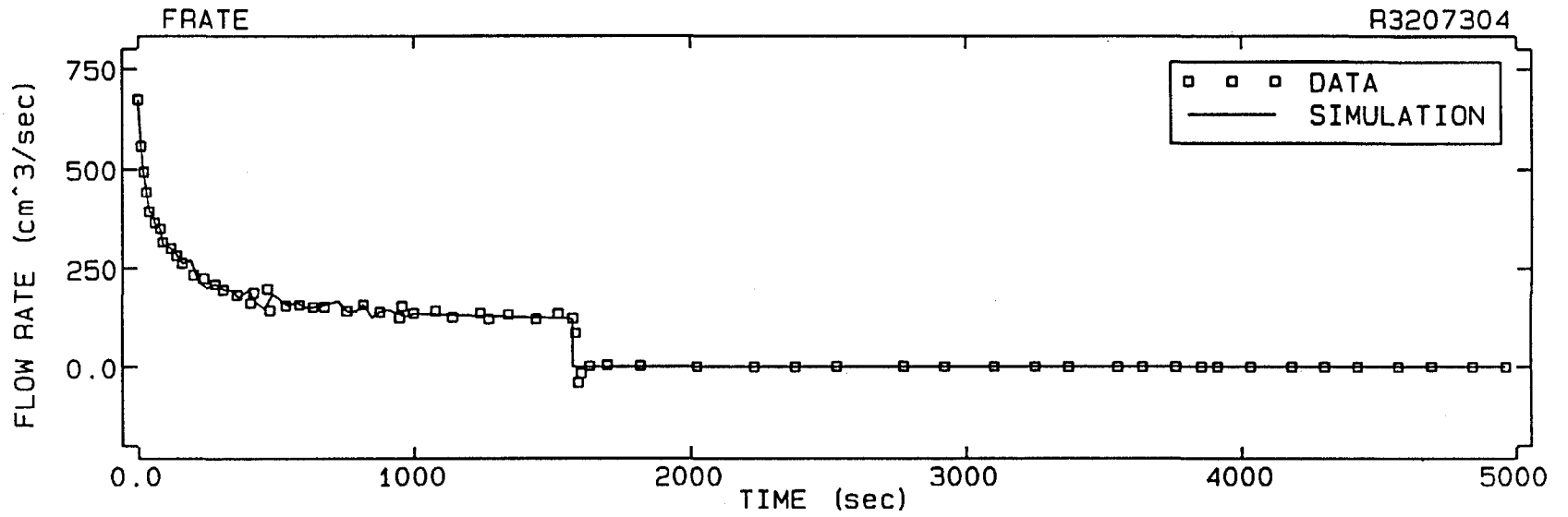


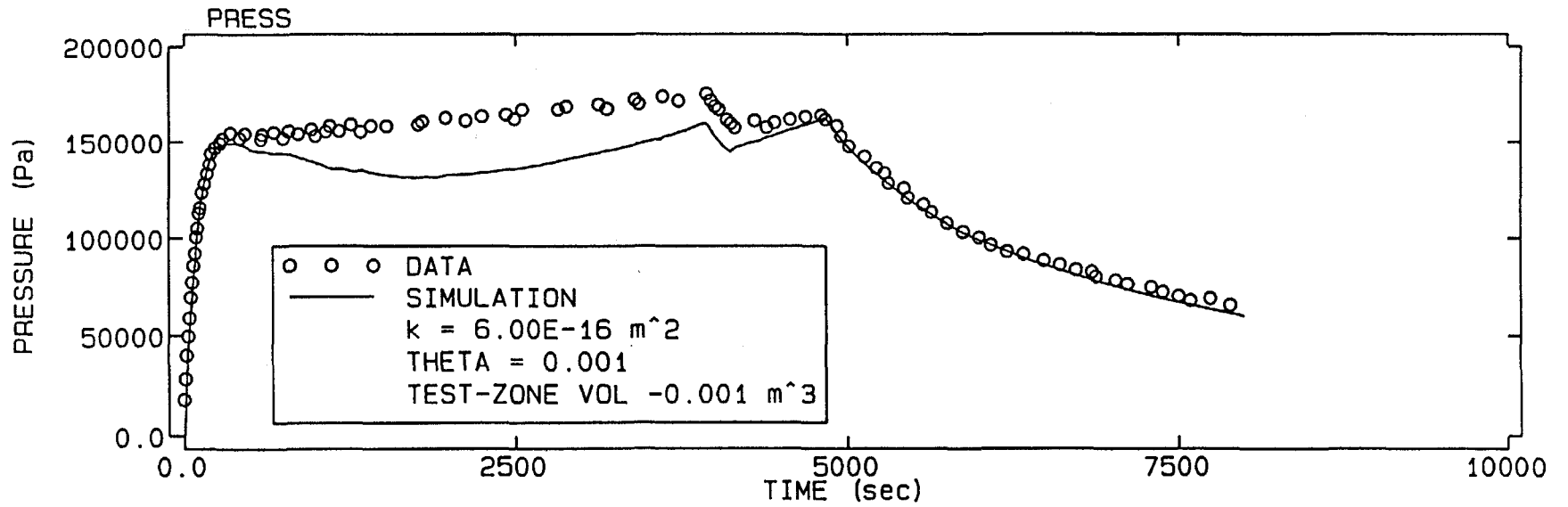
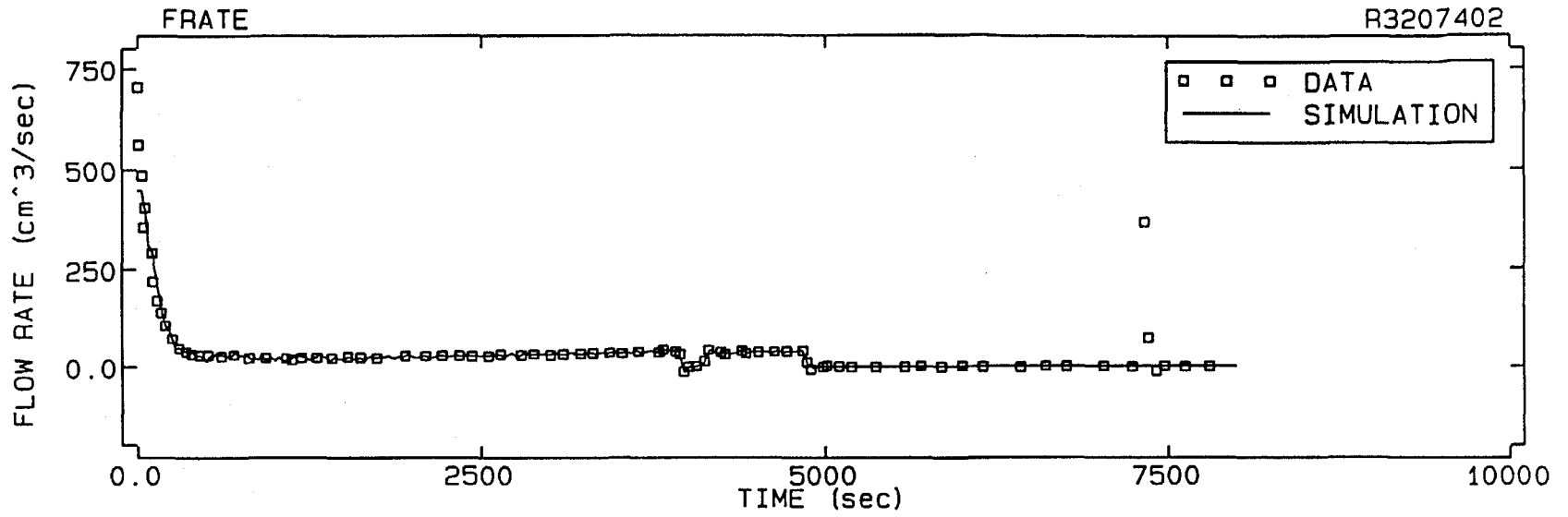
R3207120

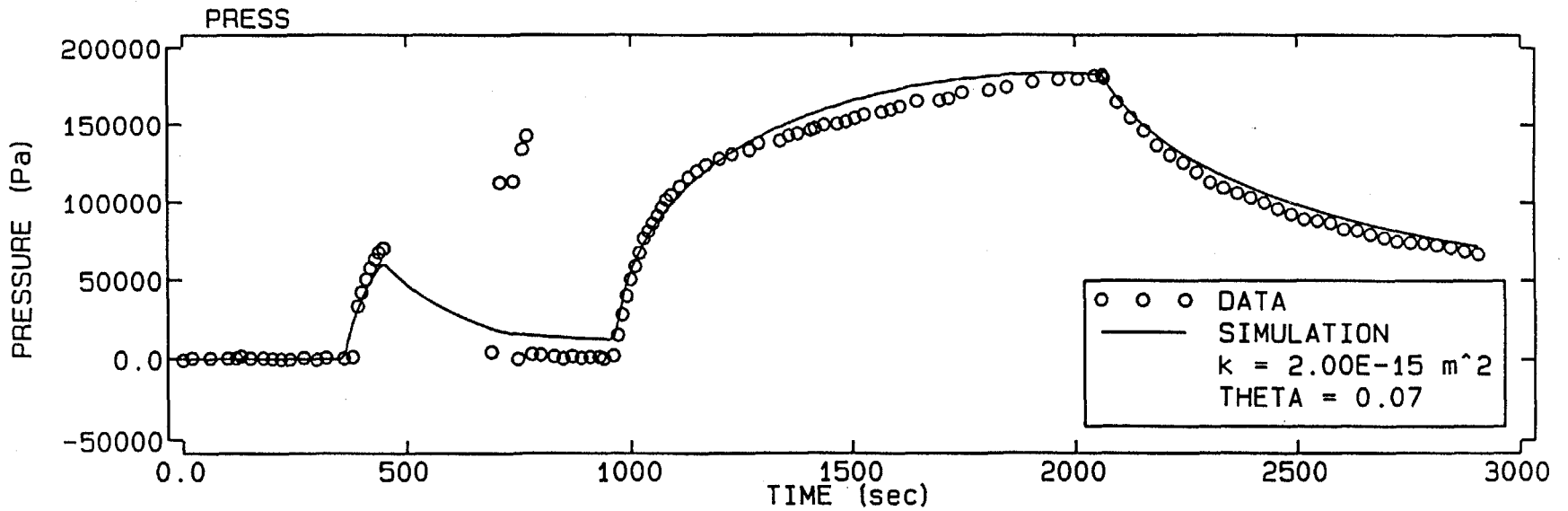
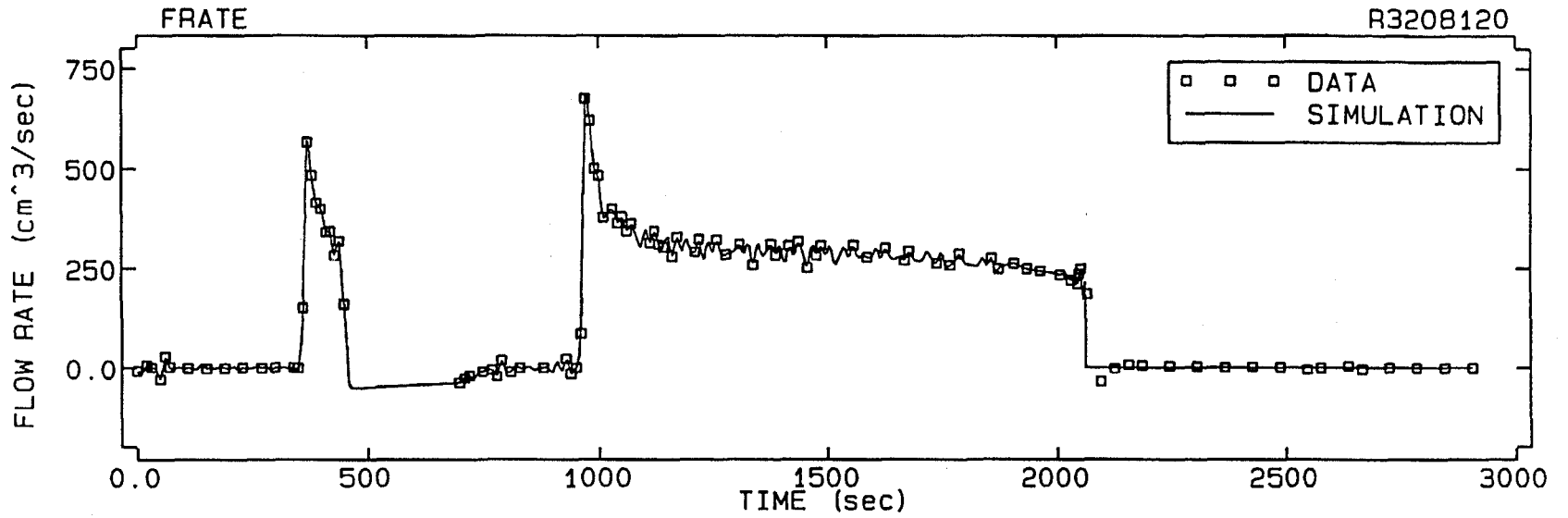


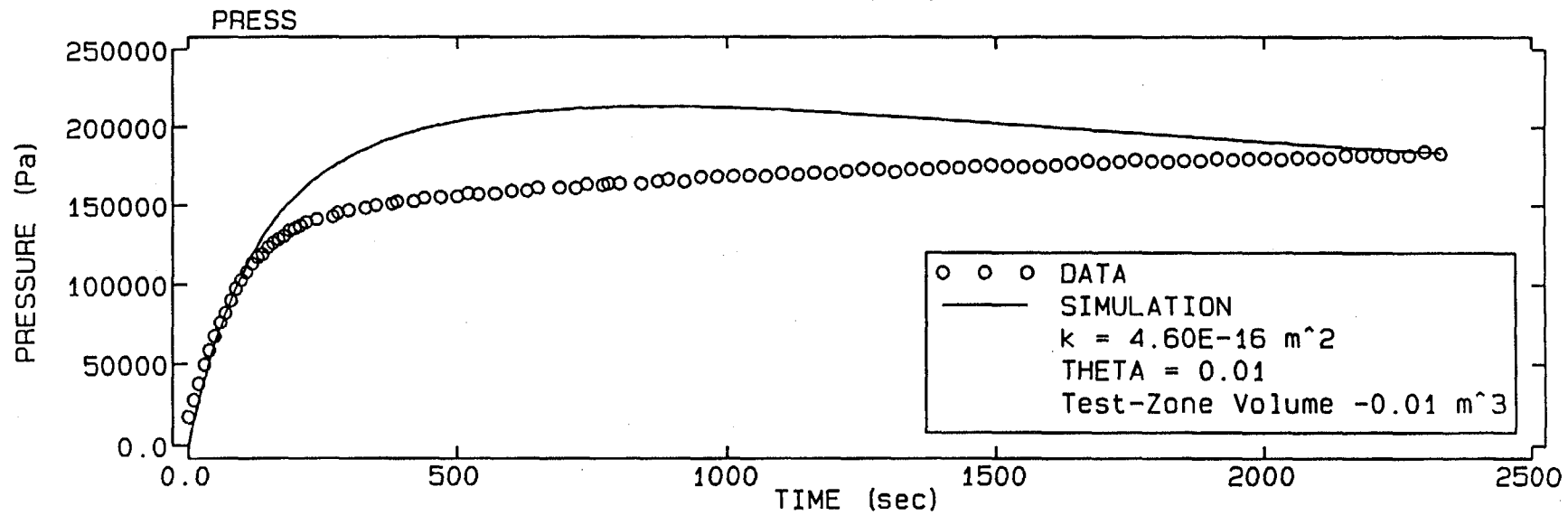
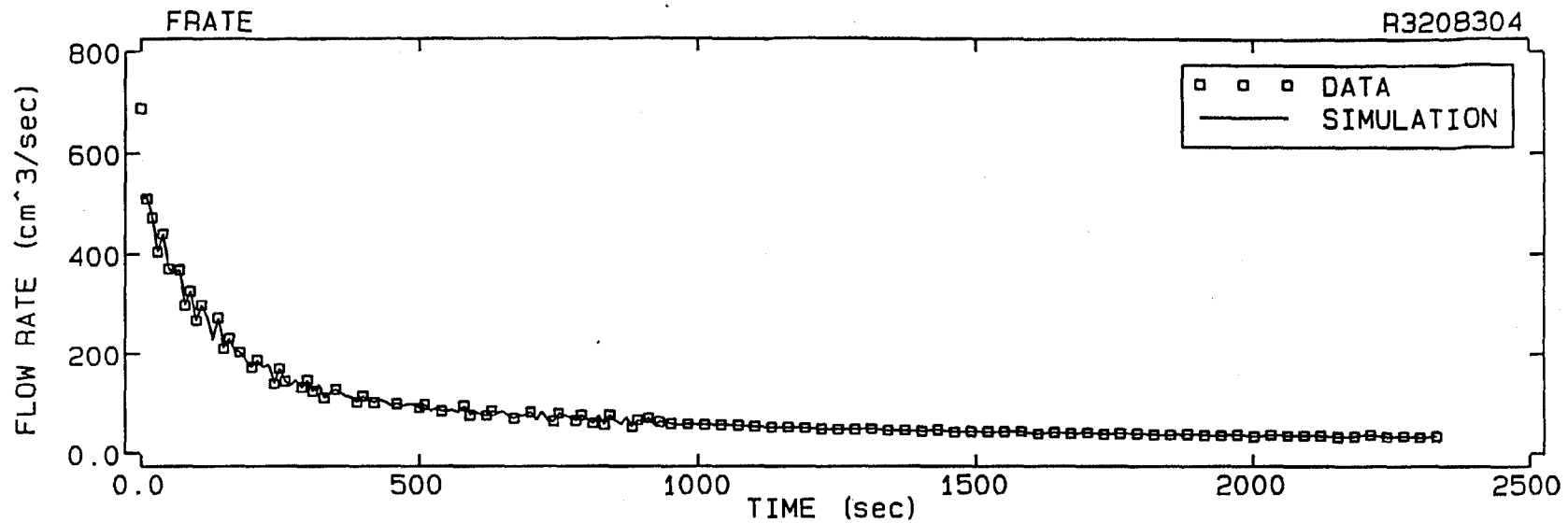
I-70

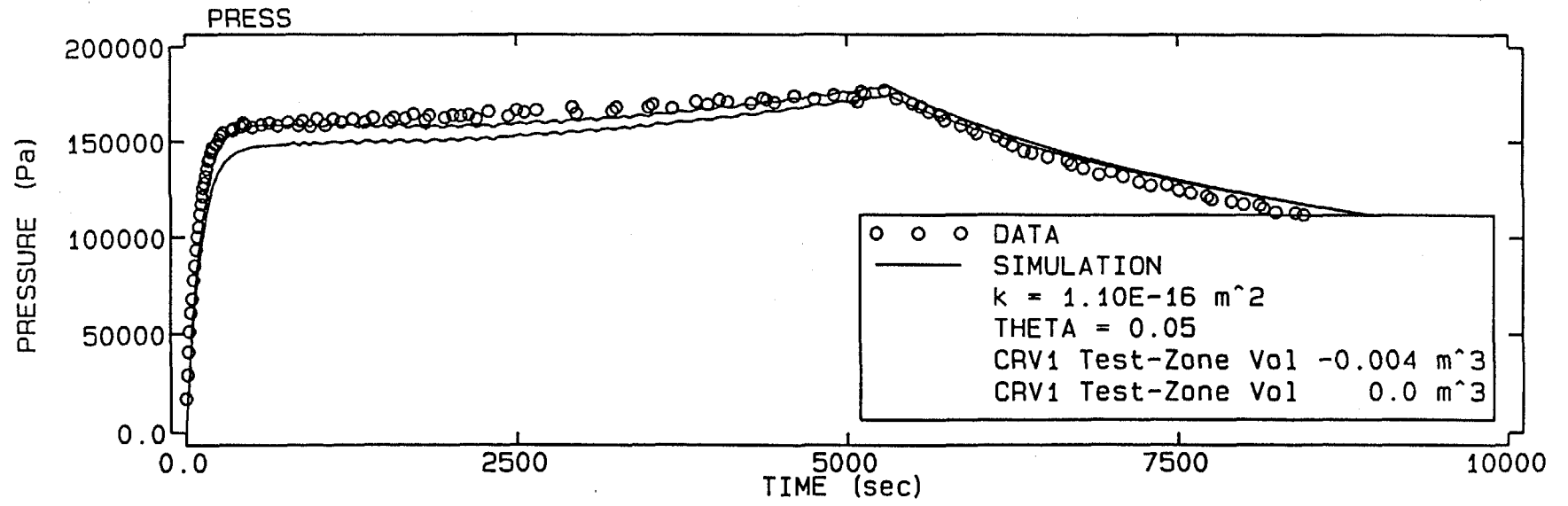
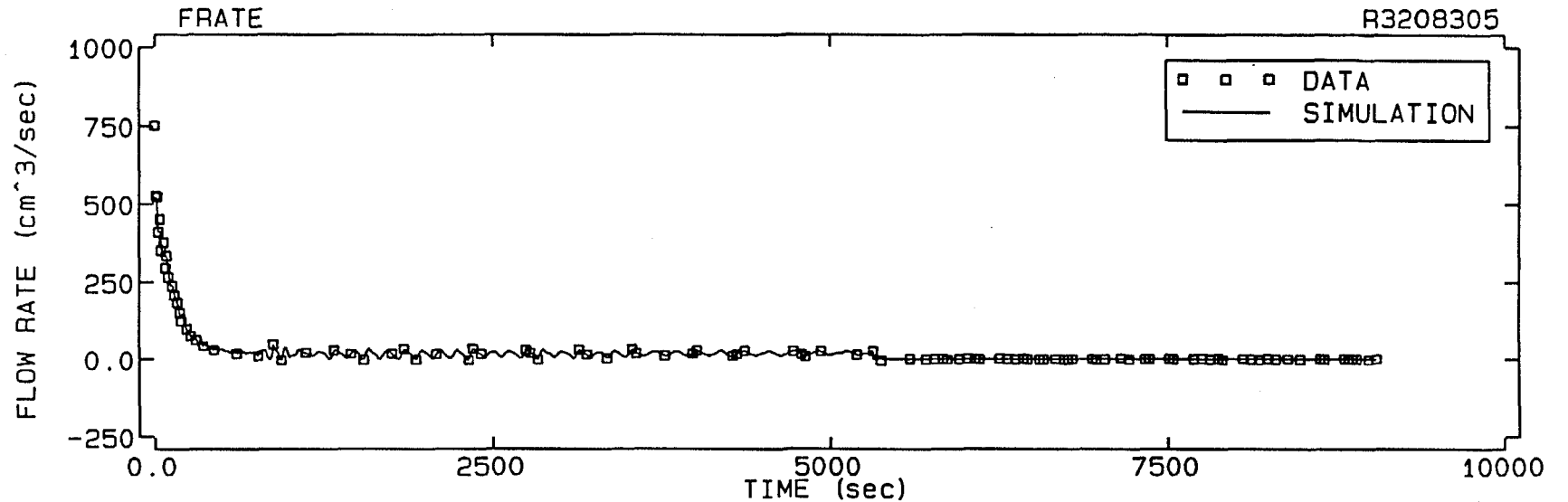


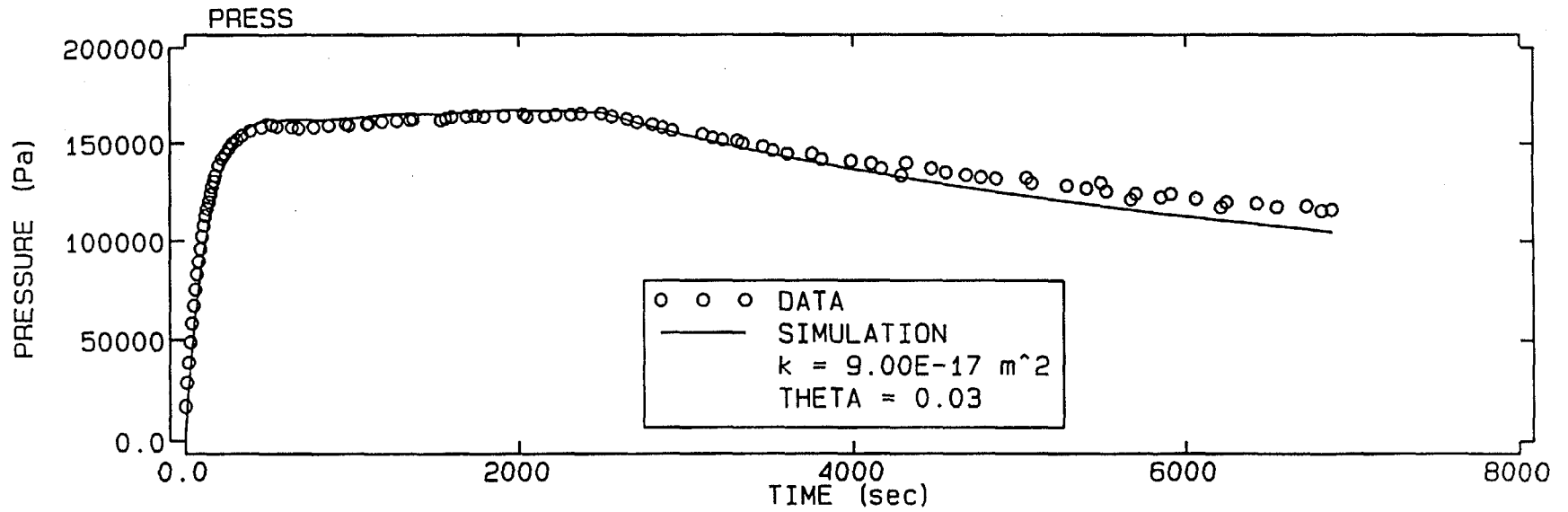
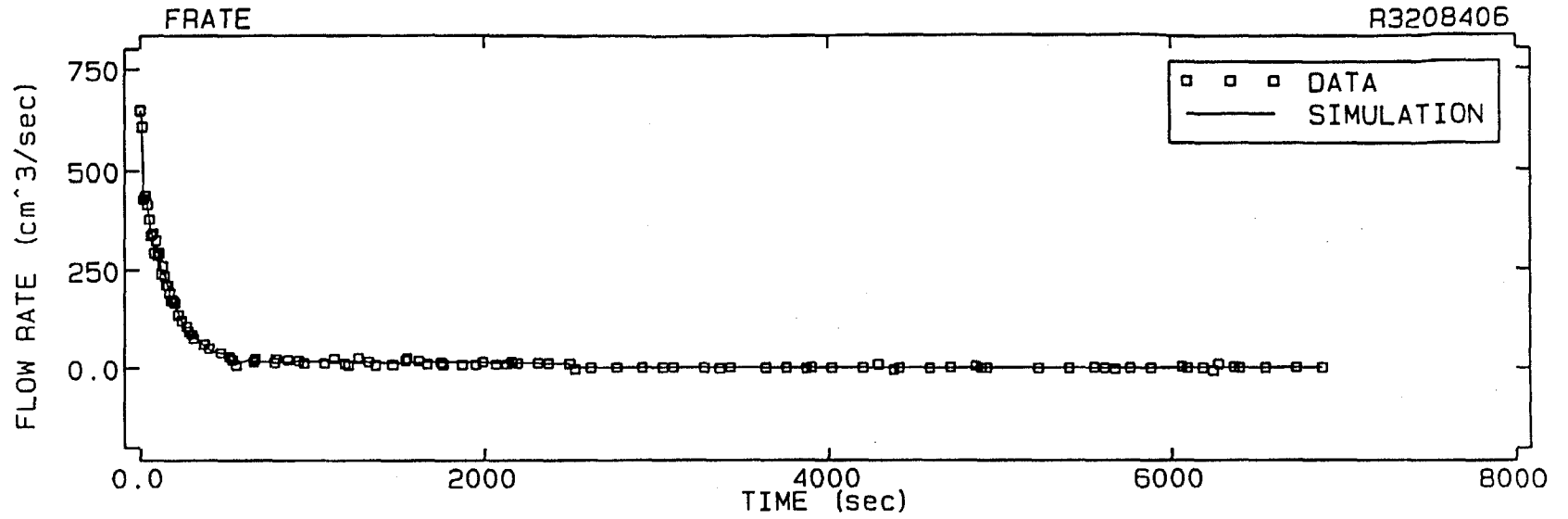


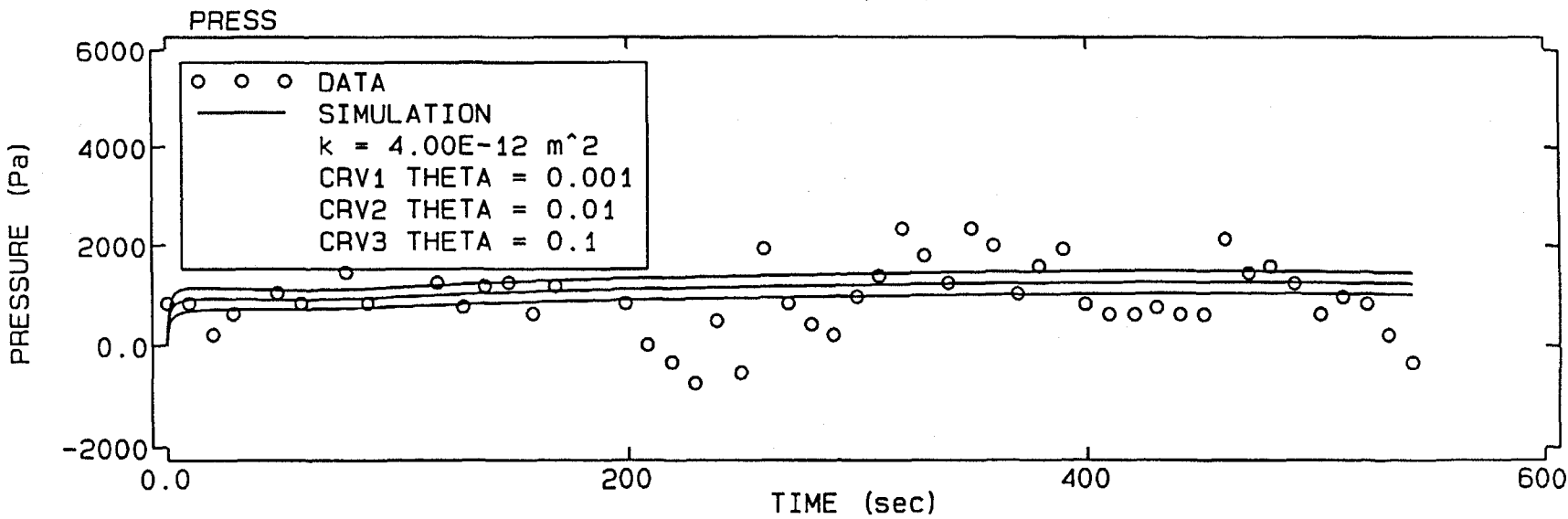
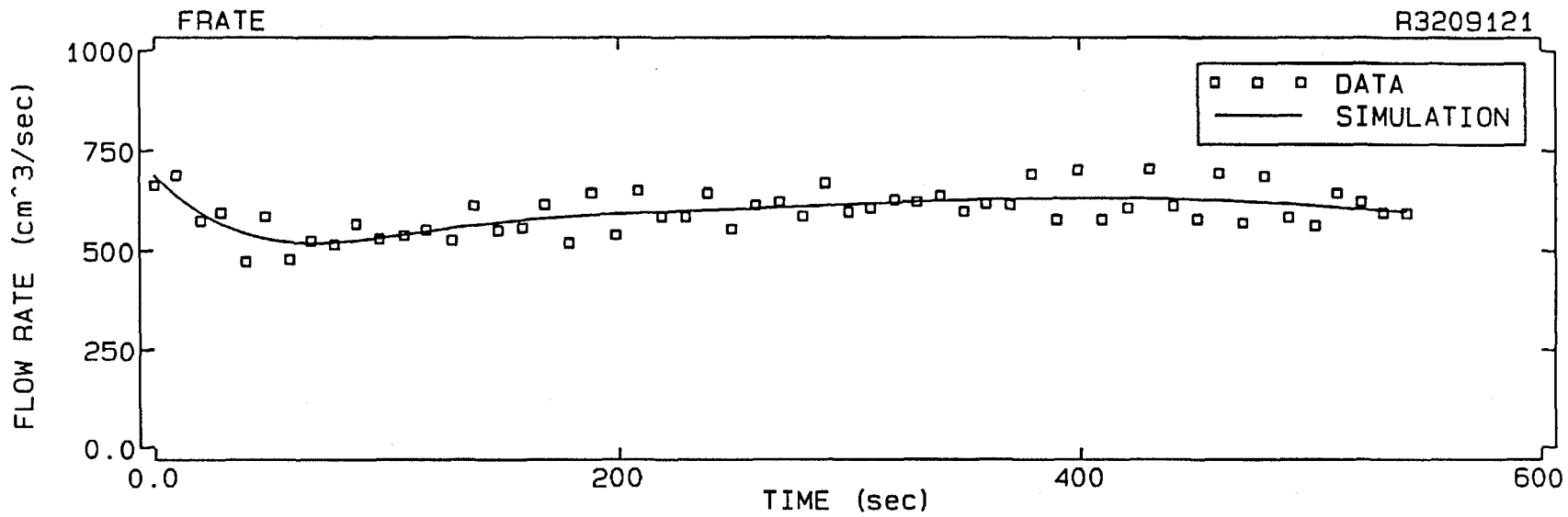


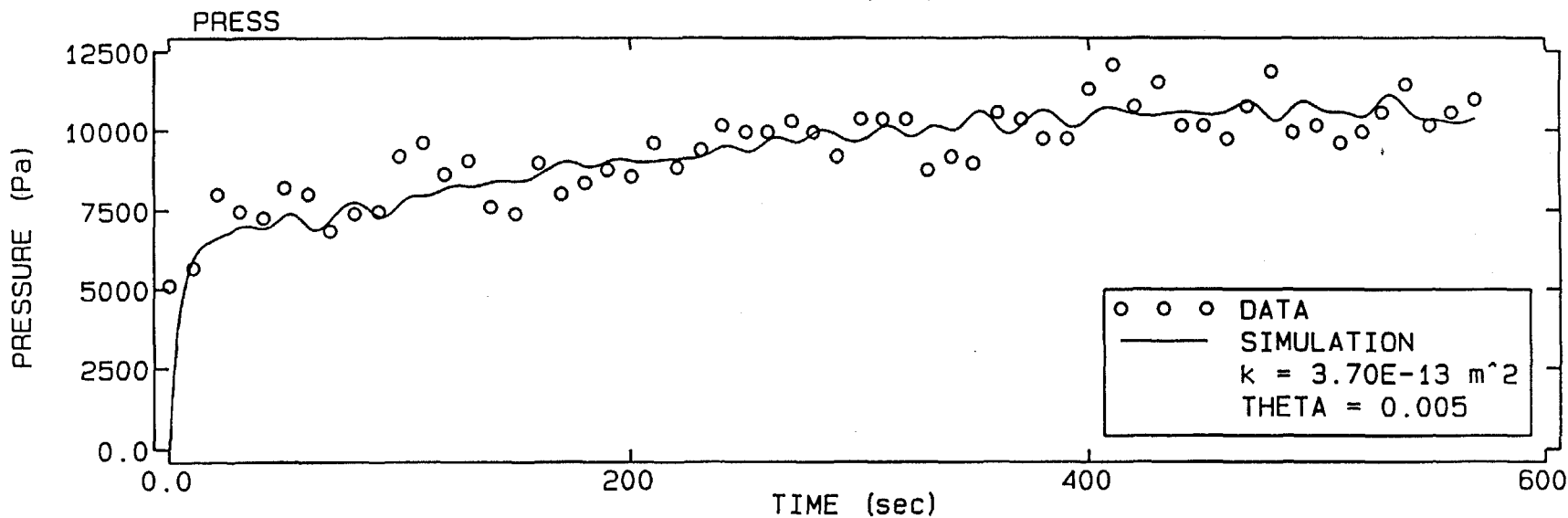
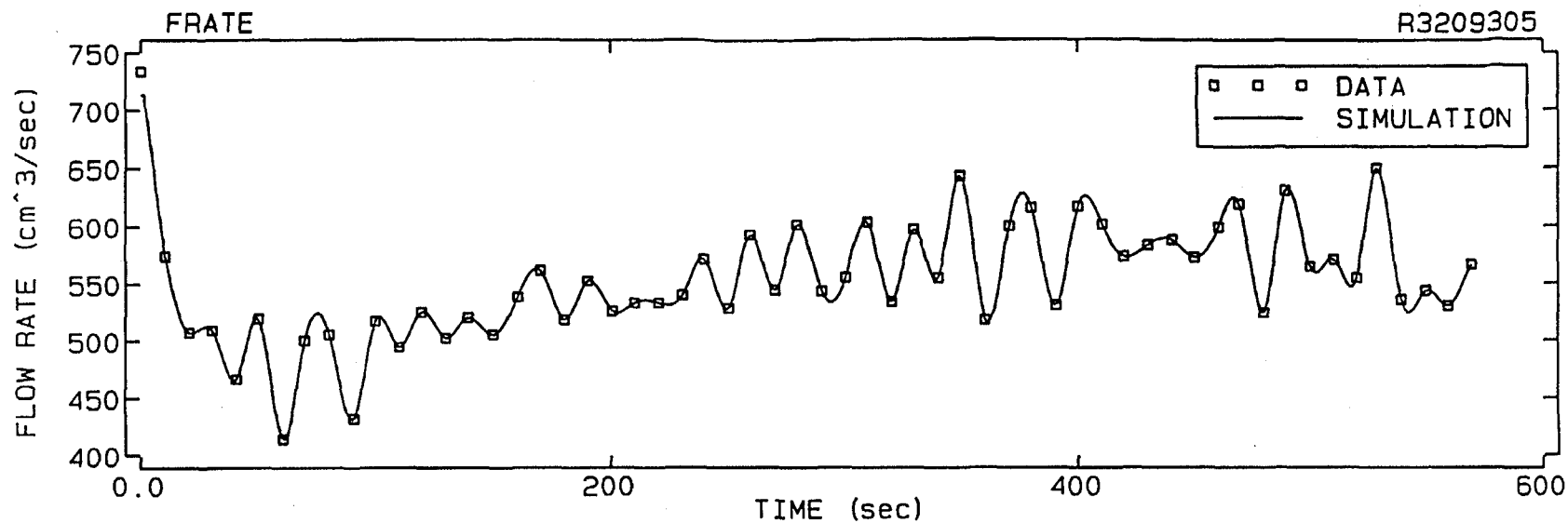


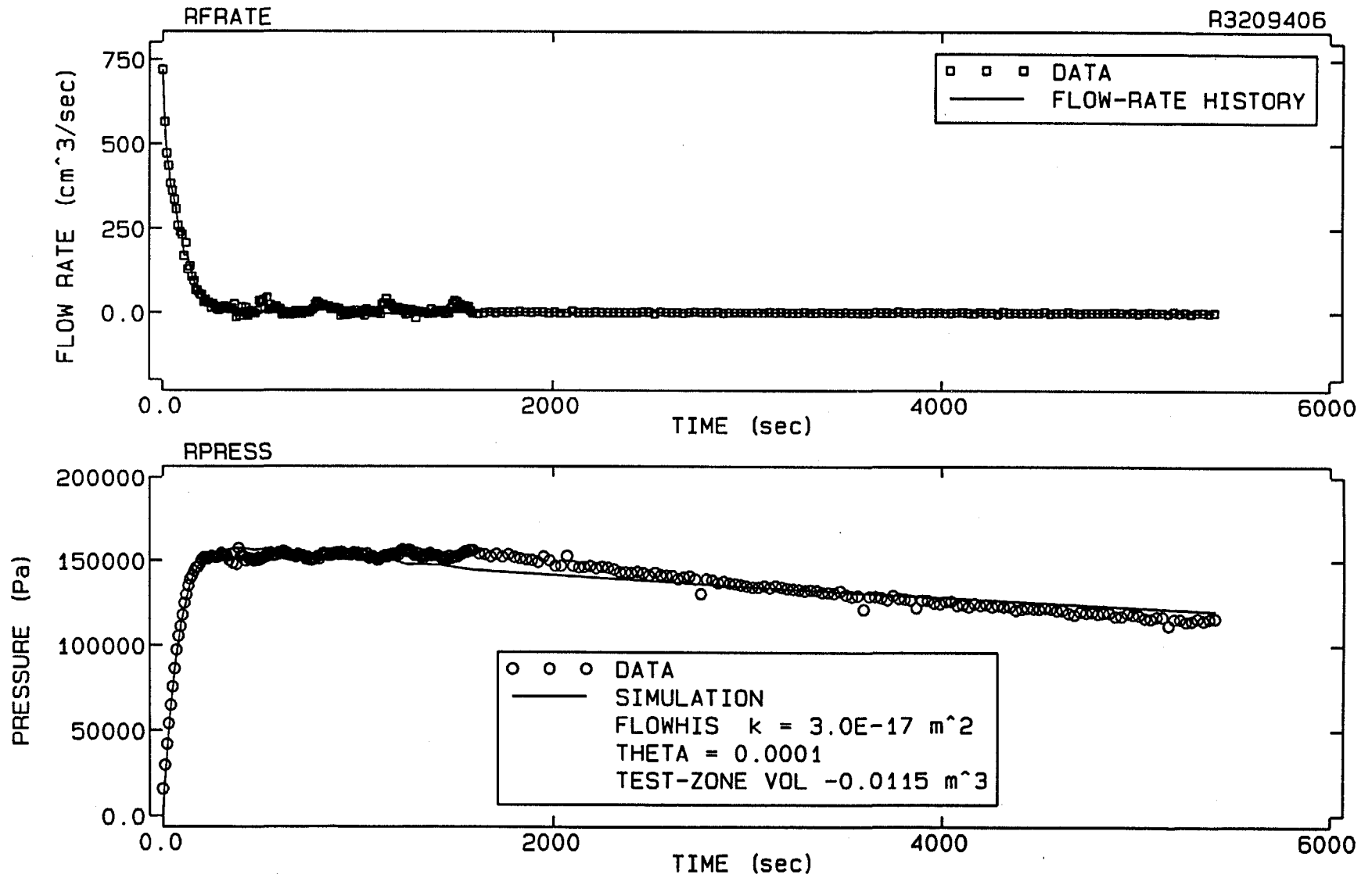




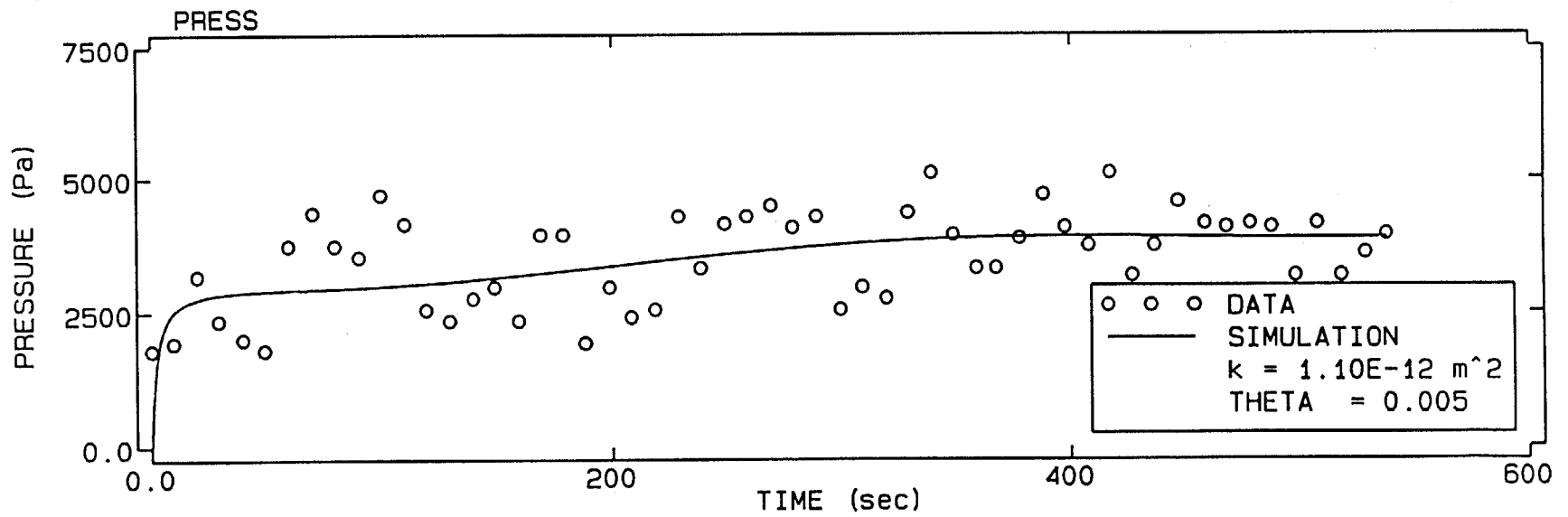
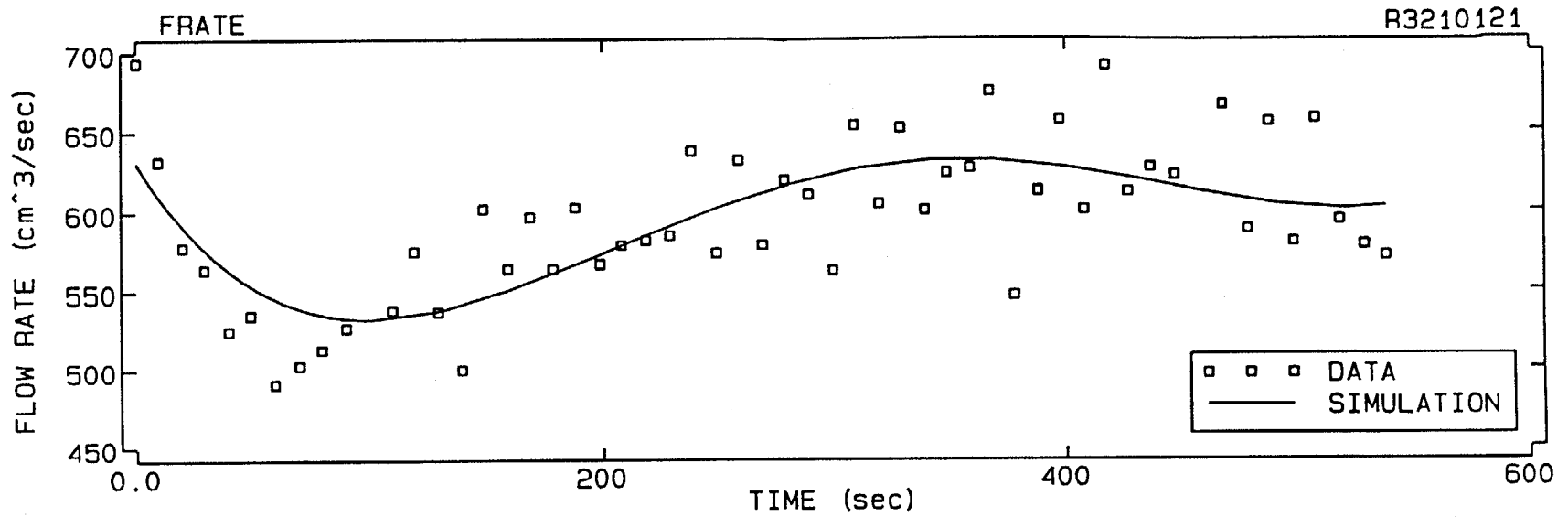


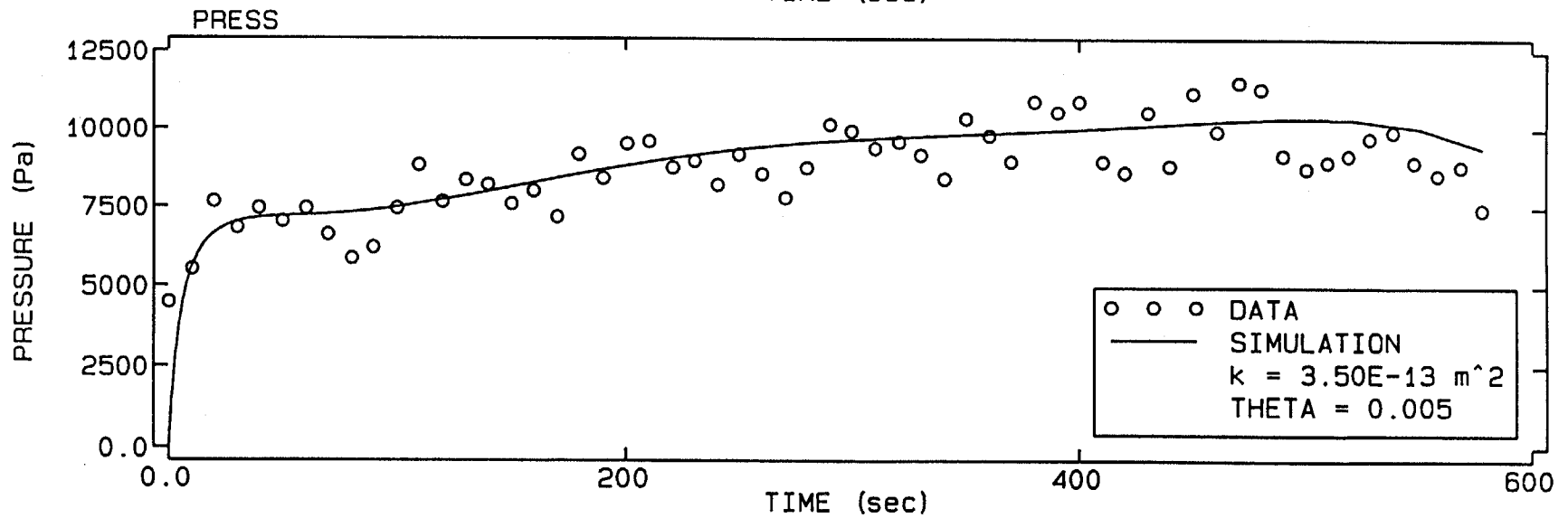
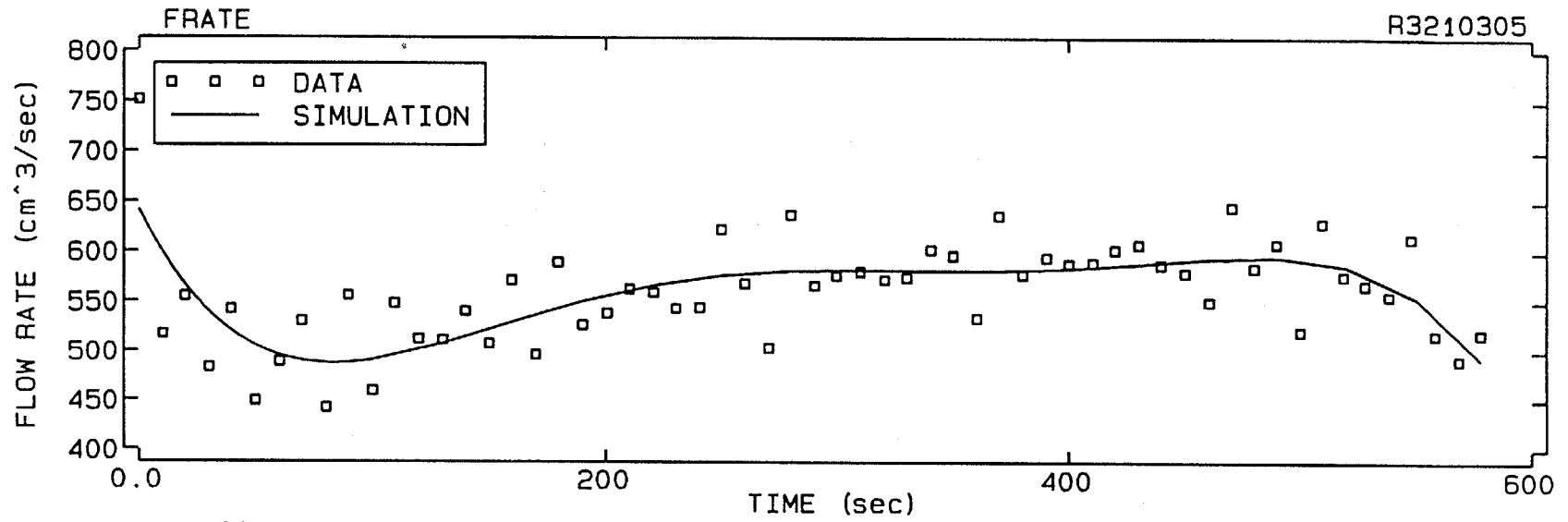


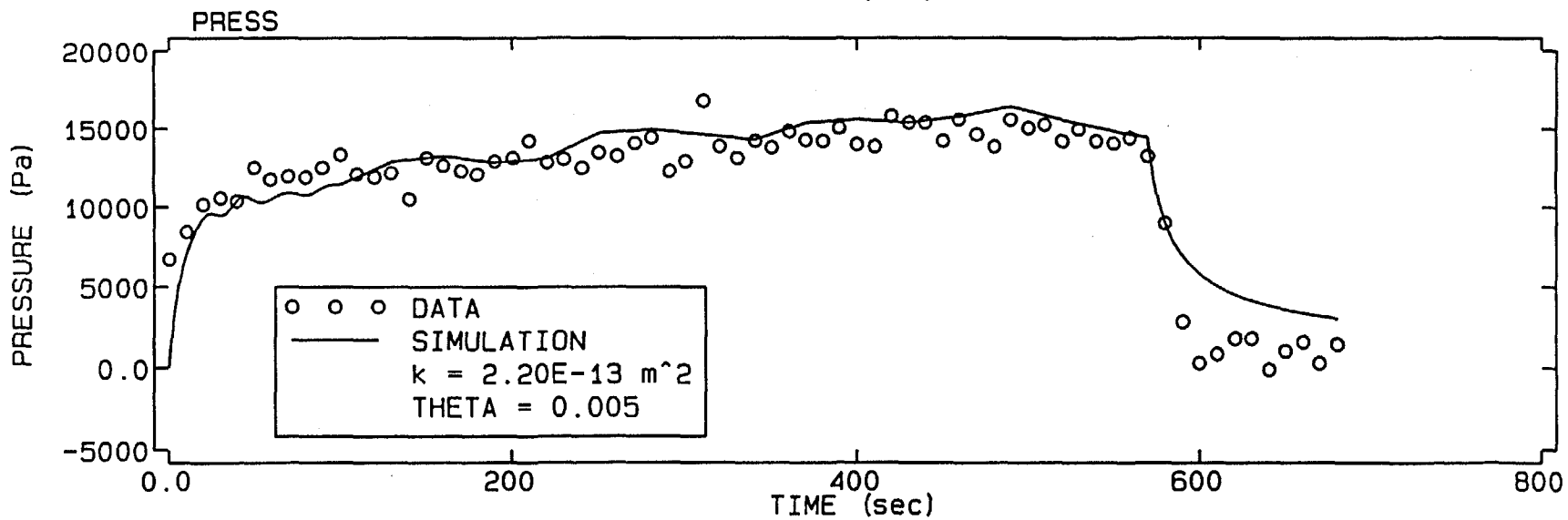
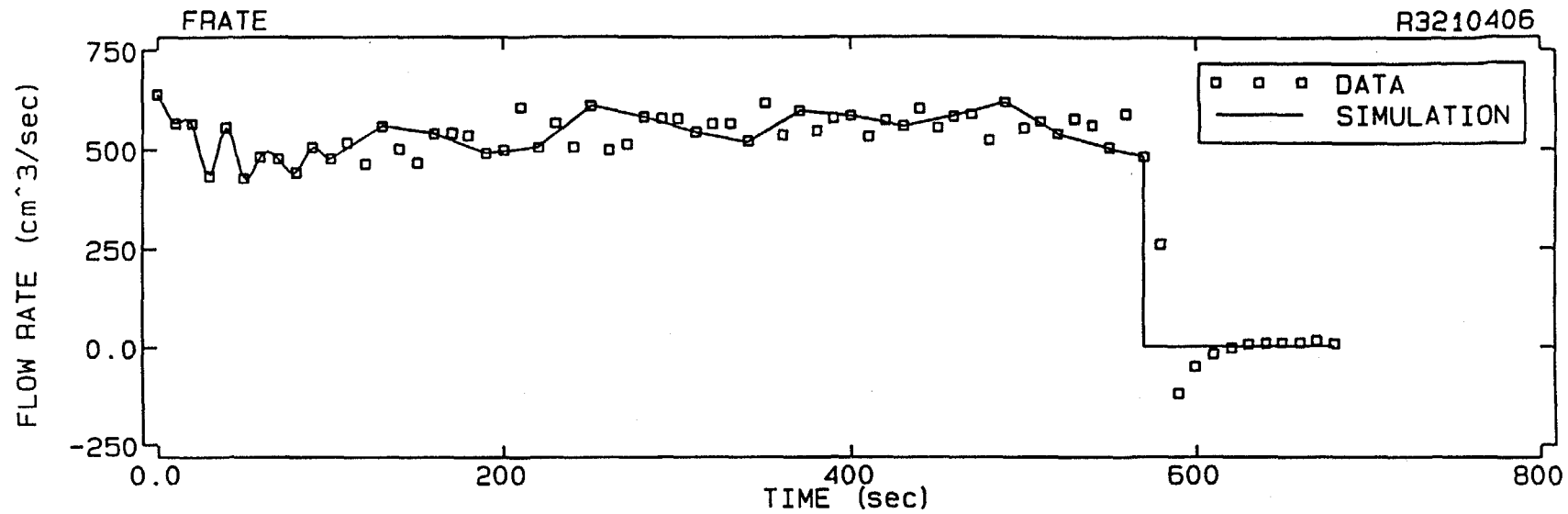


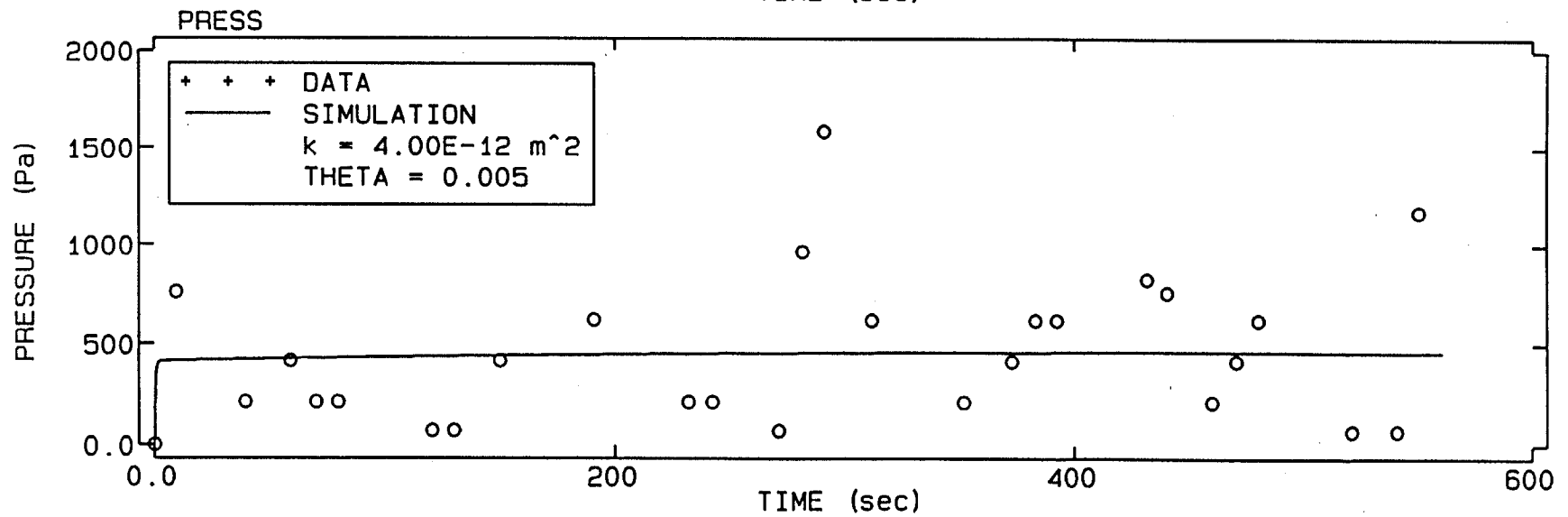
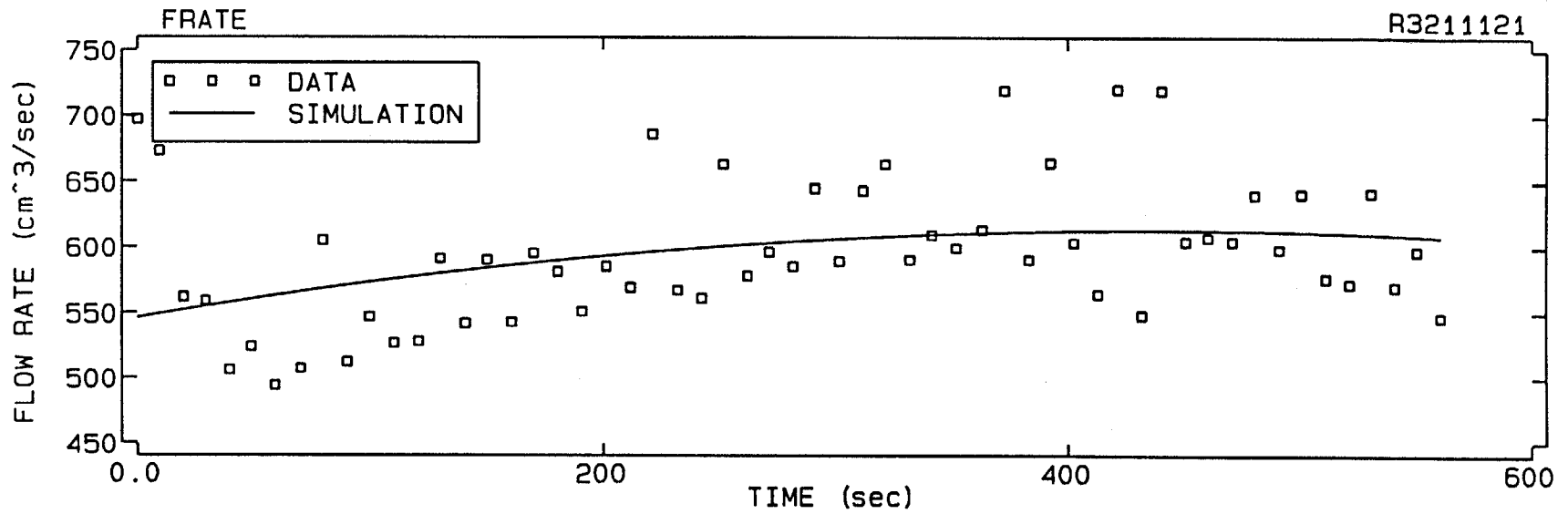


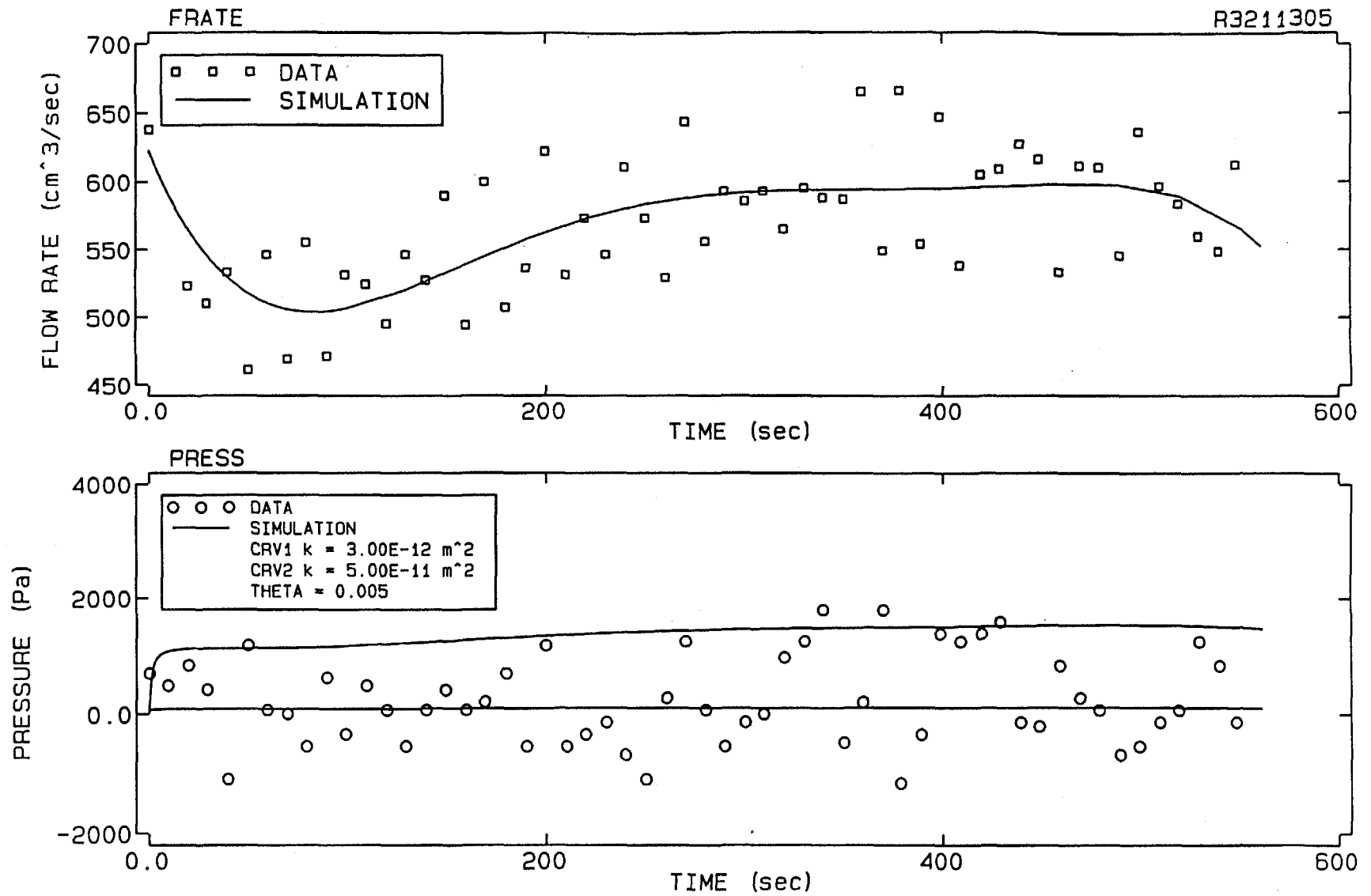
08-I

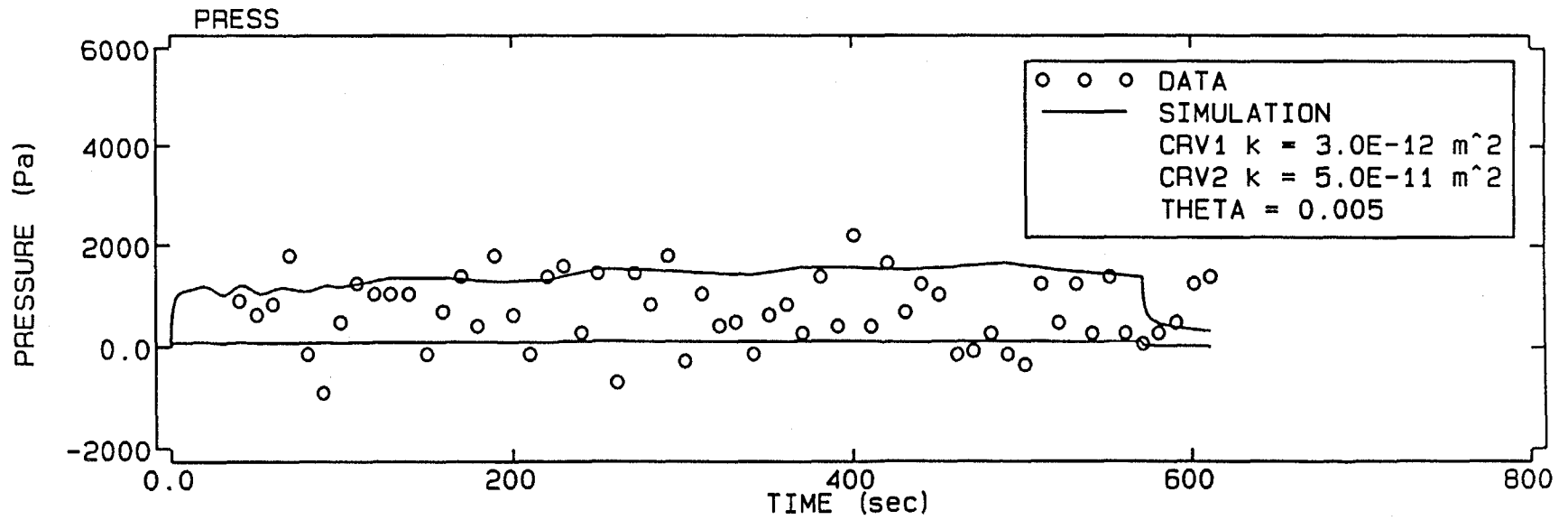
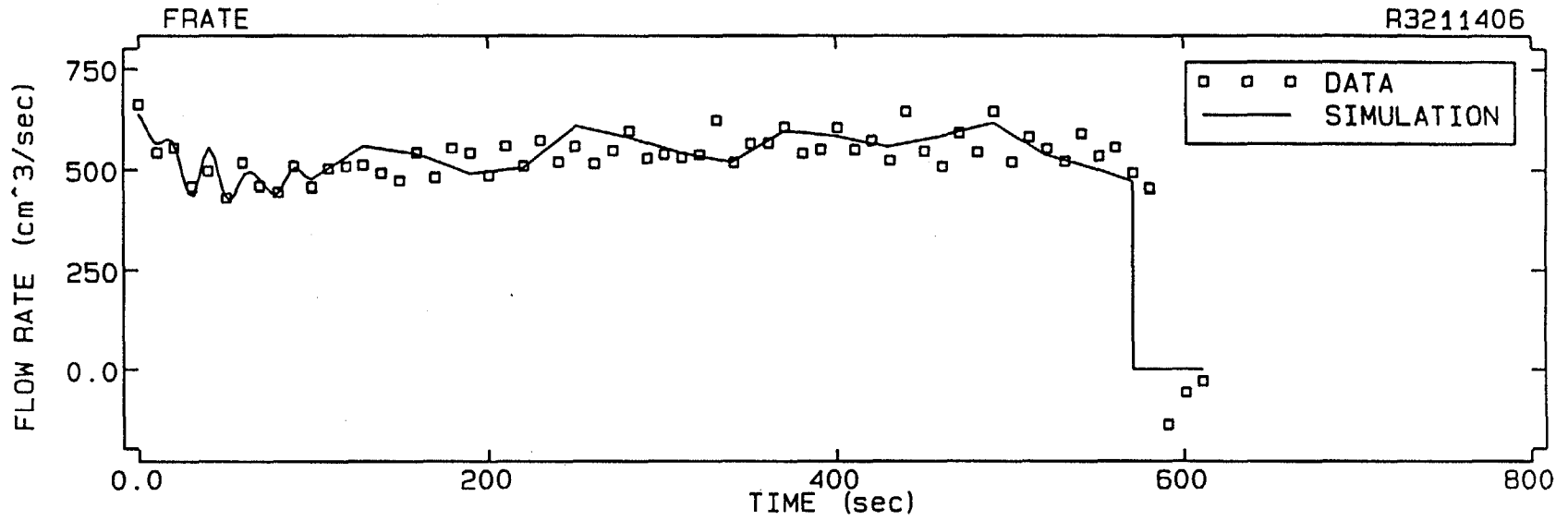


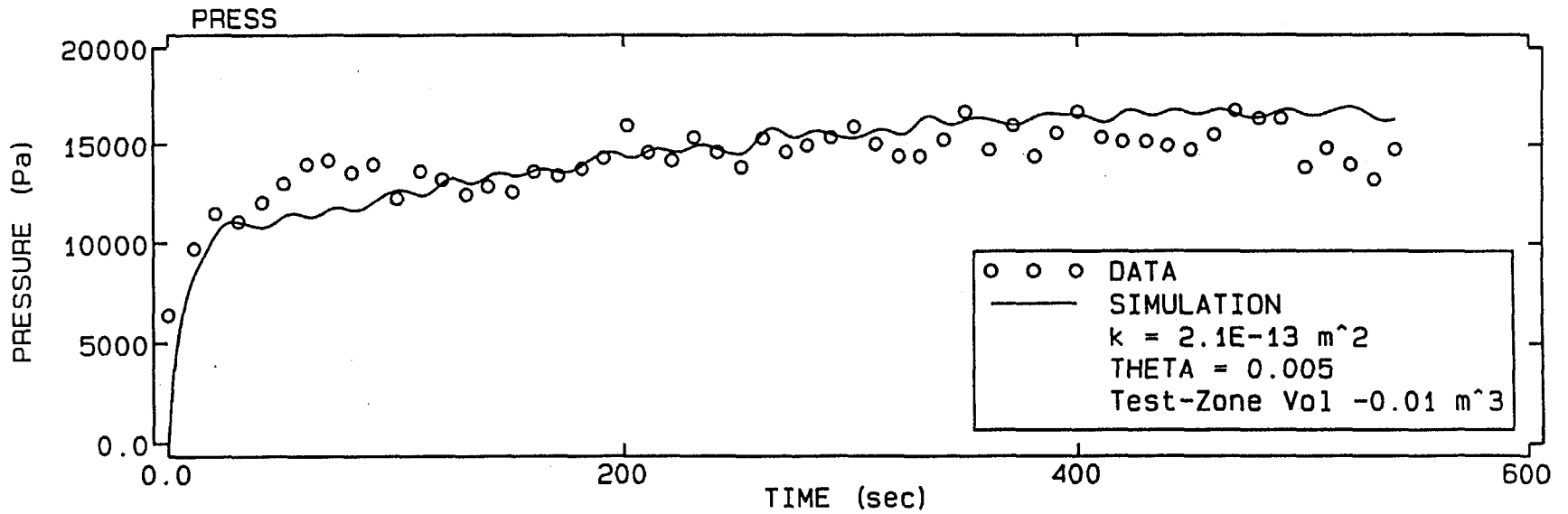
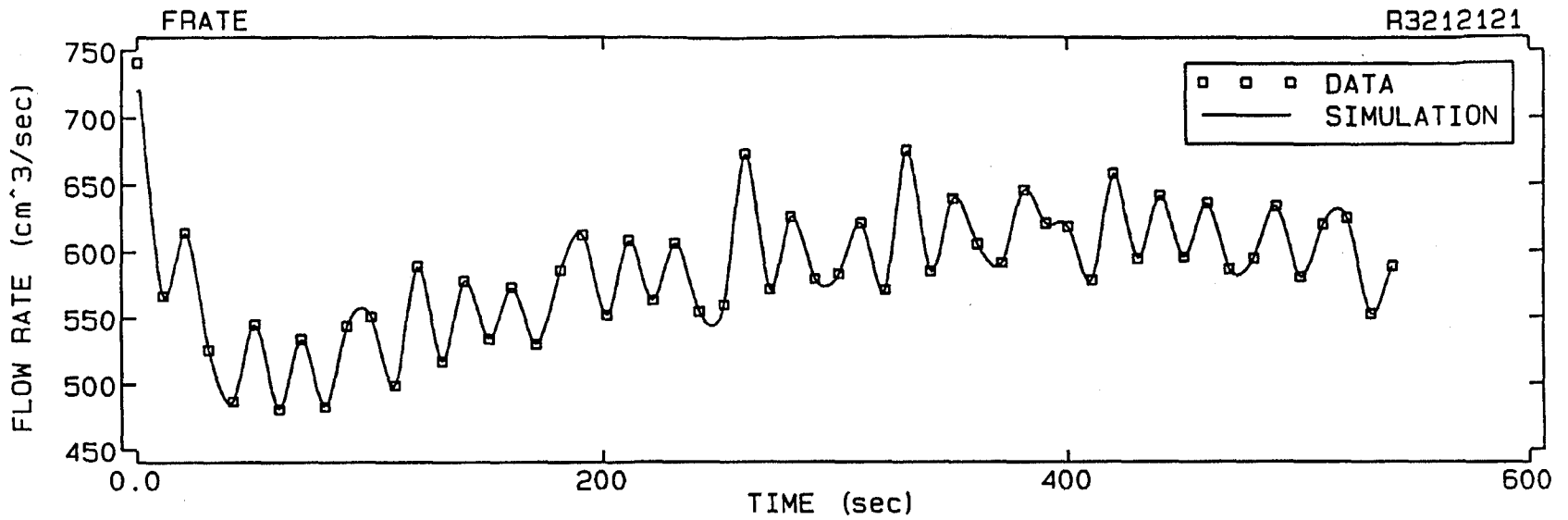


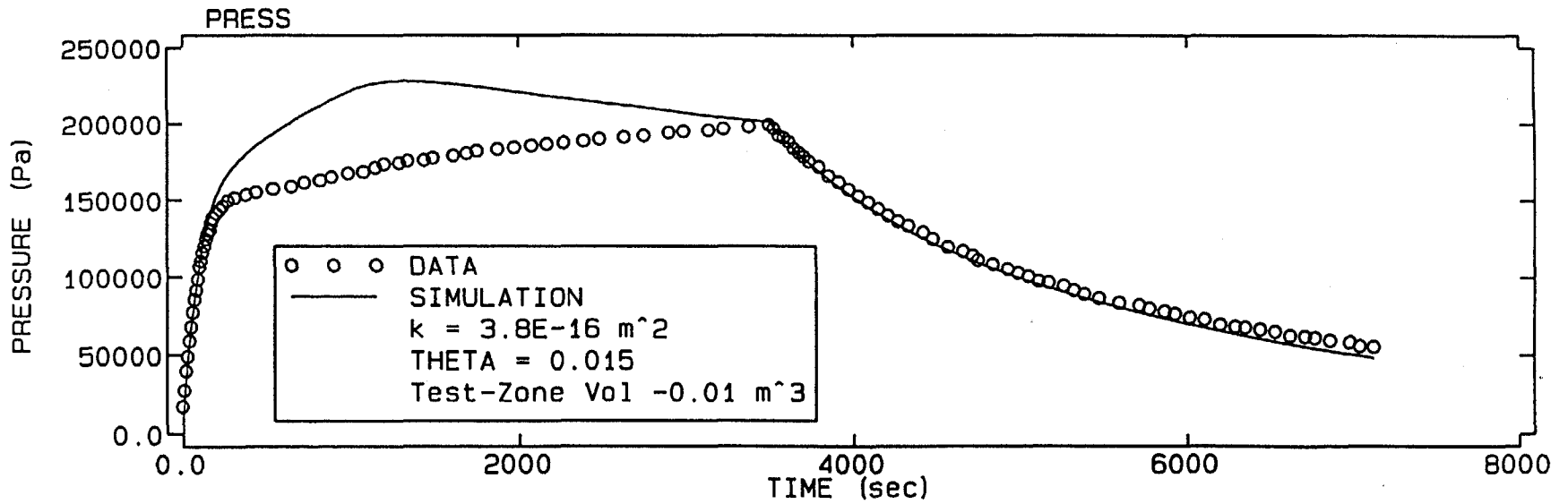
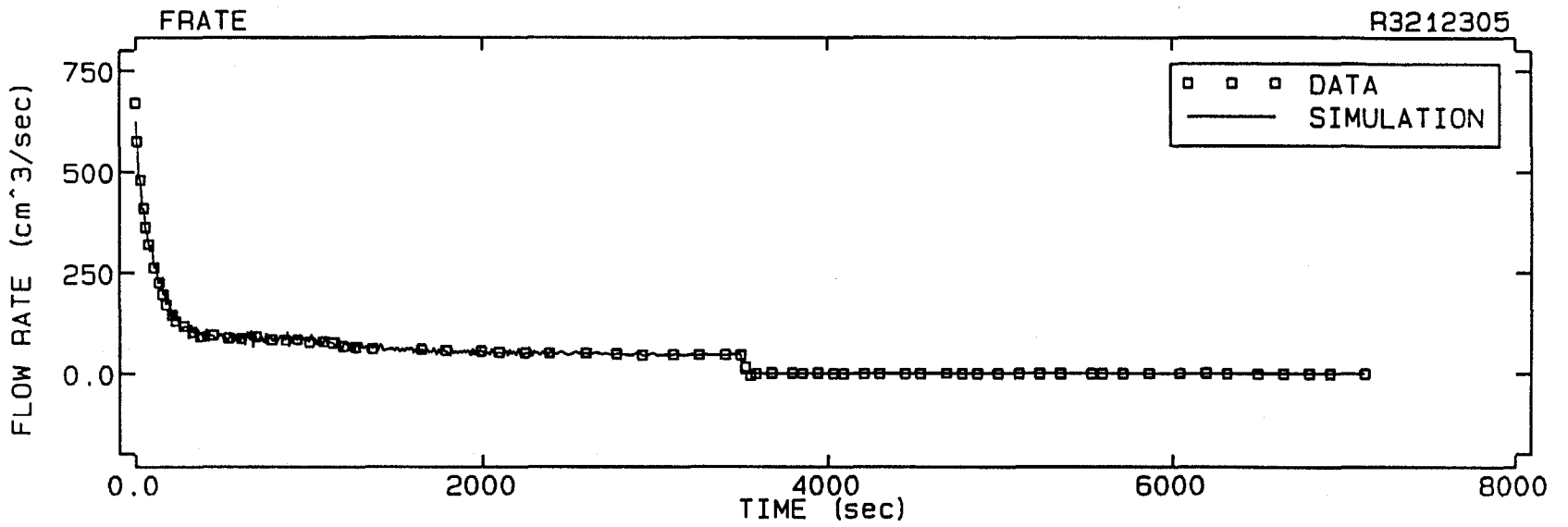


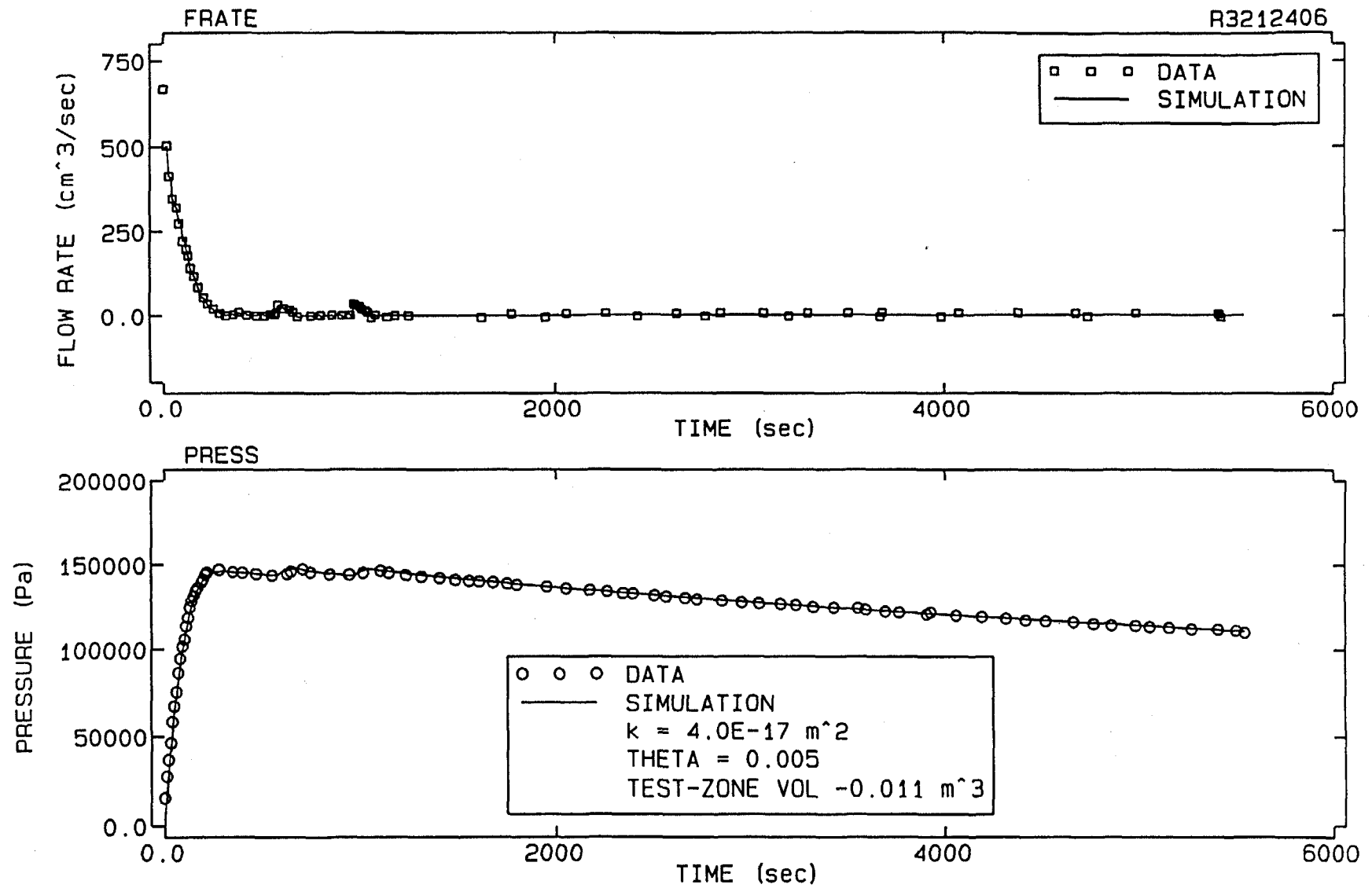


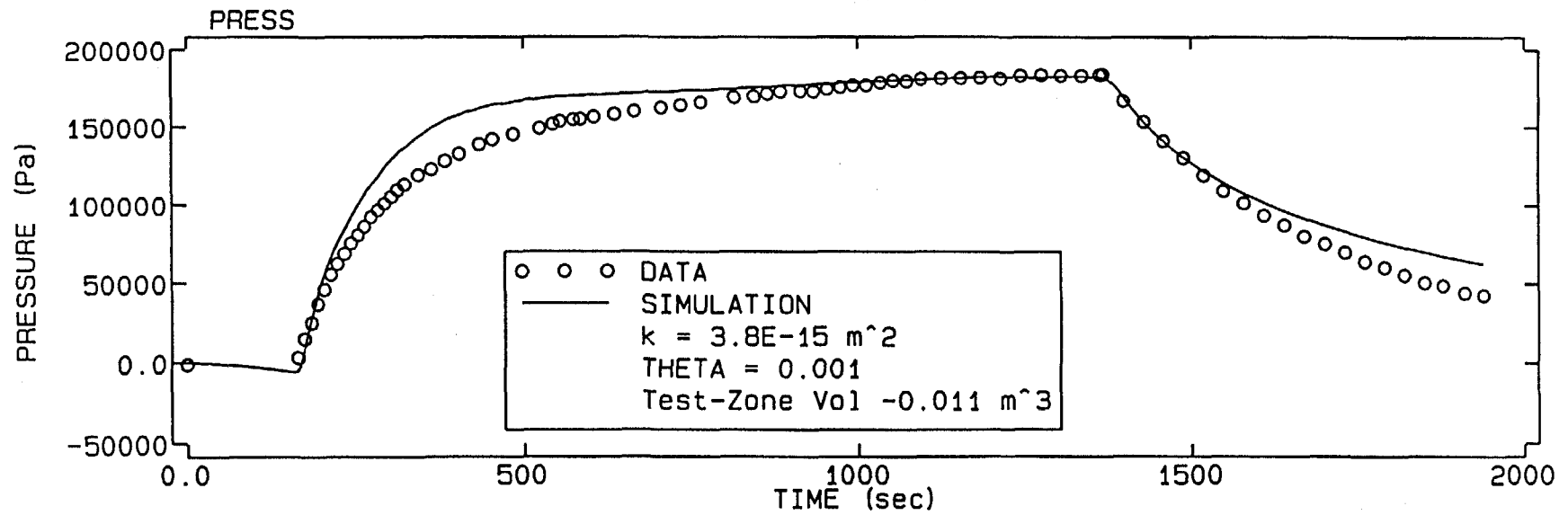
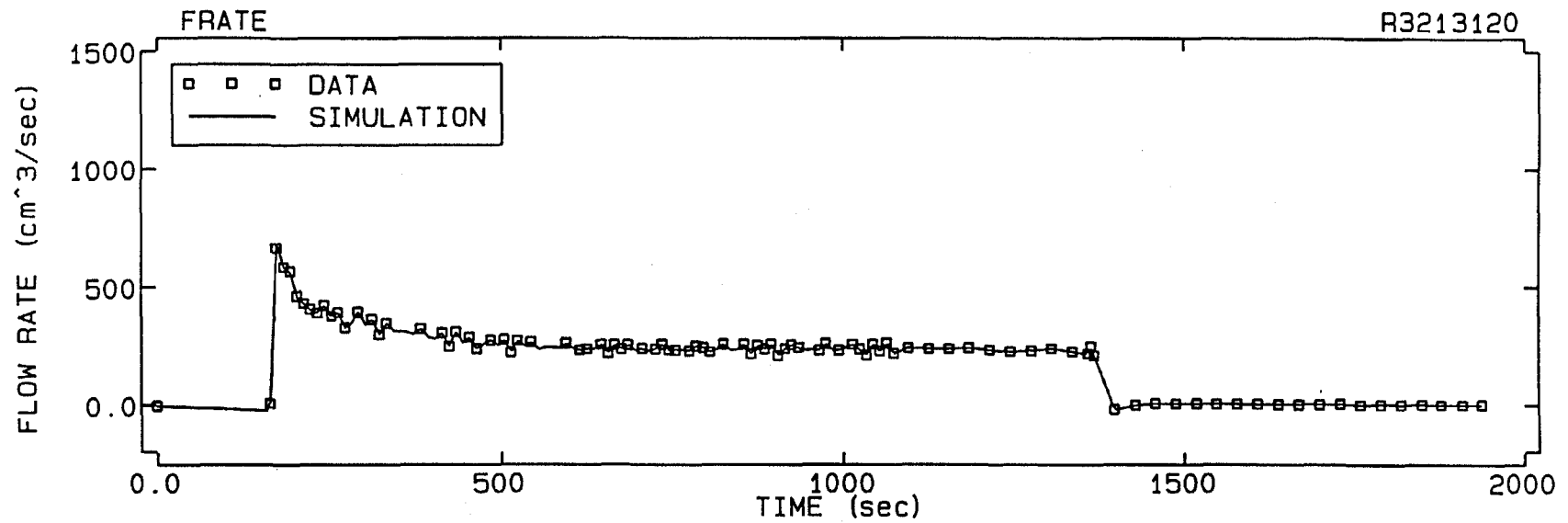




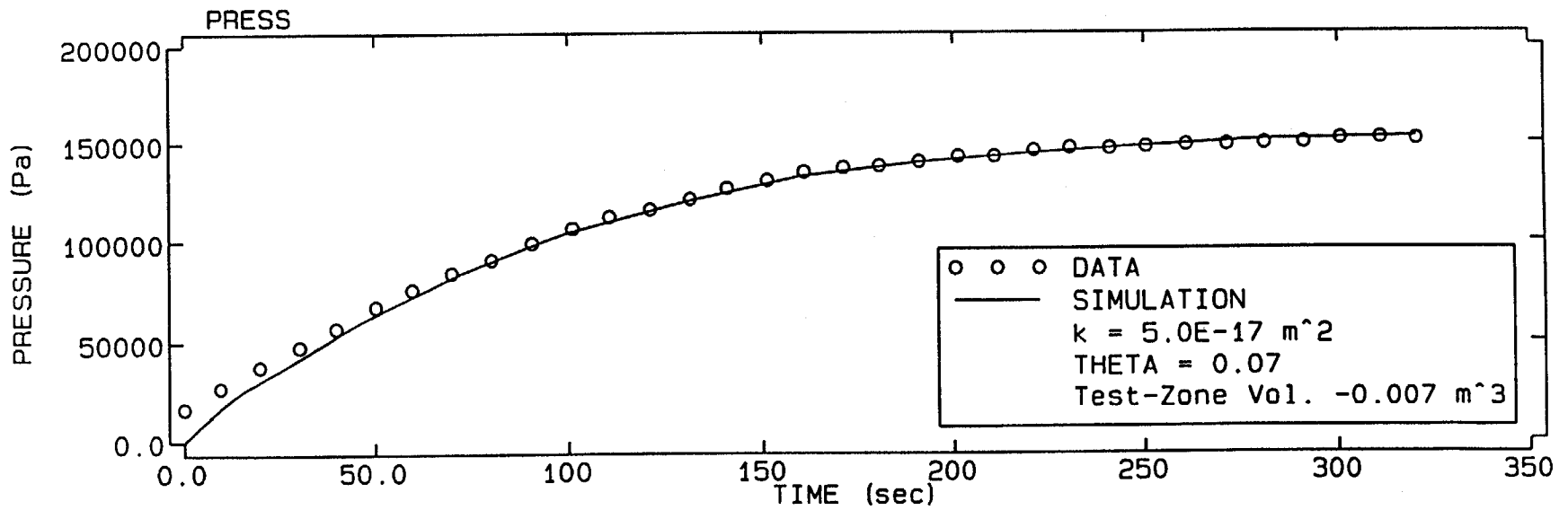
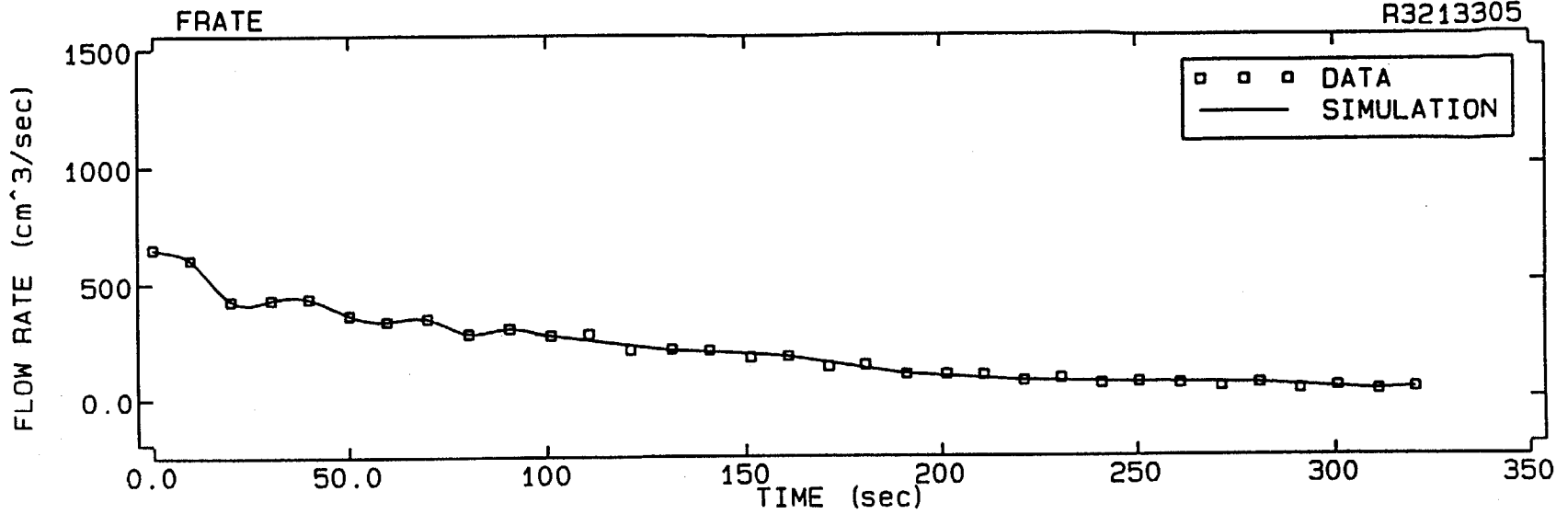




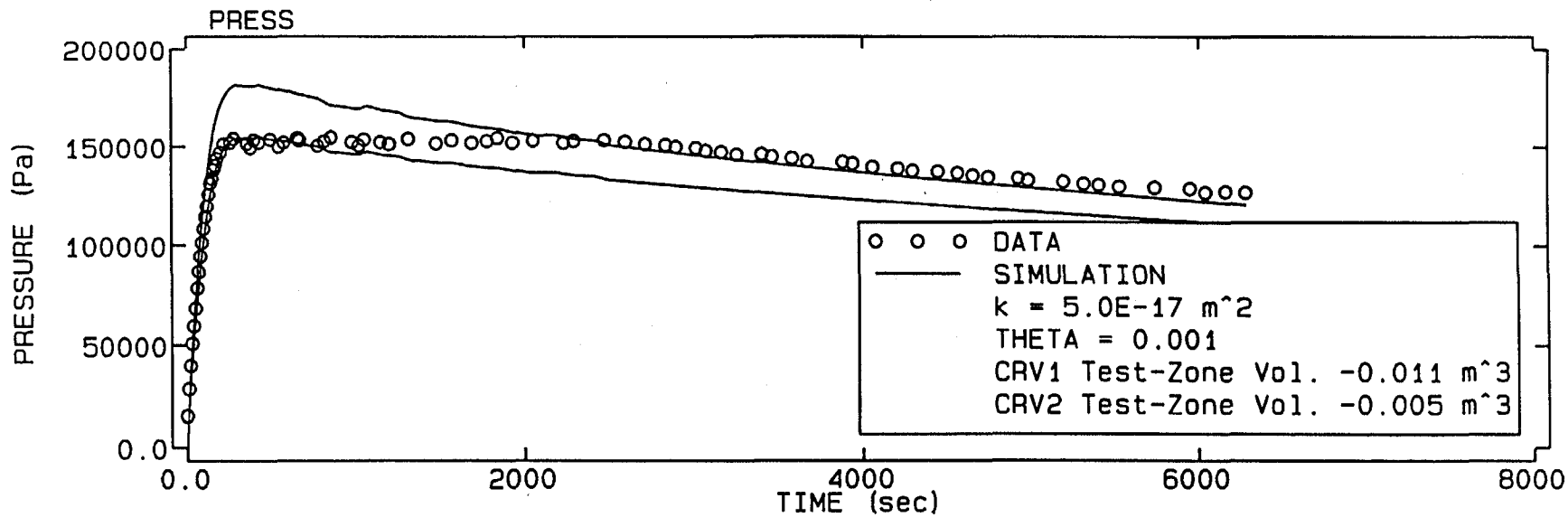
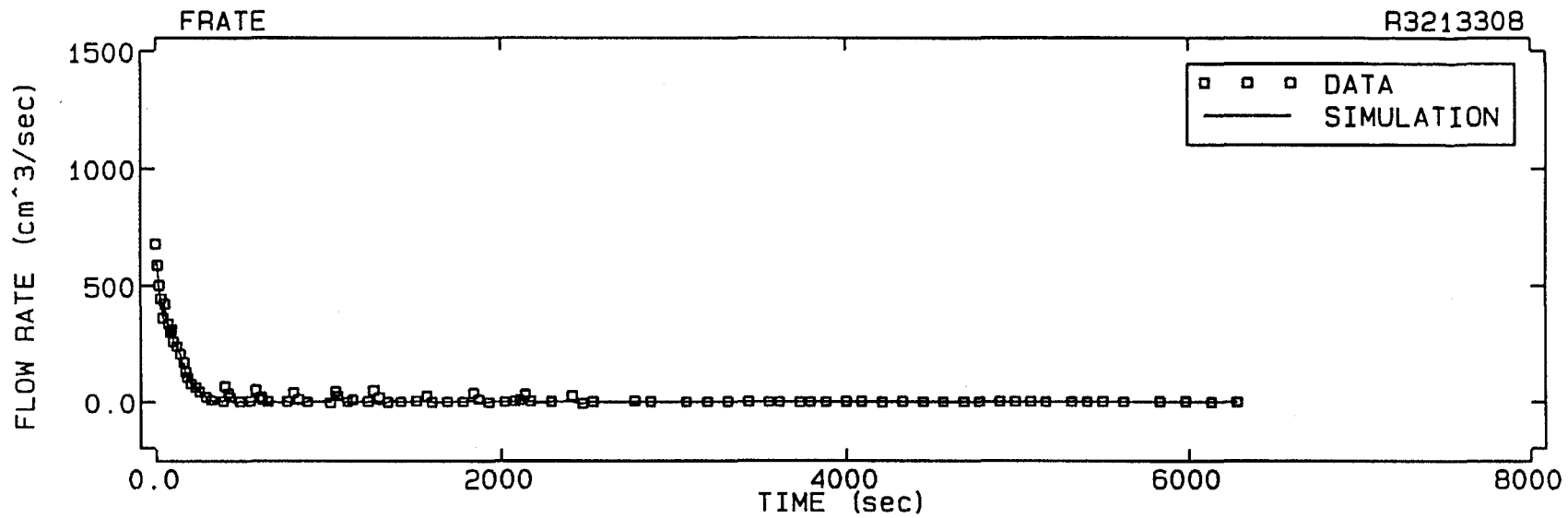


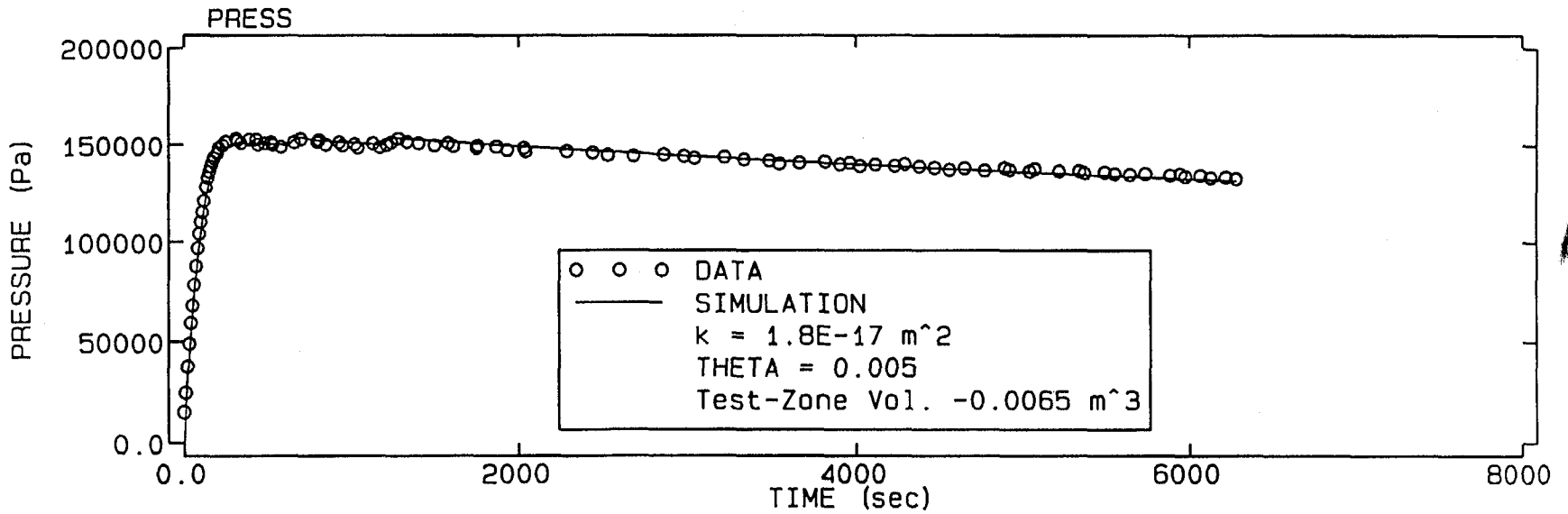
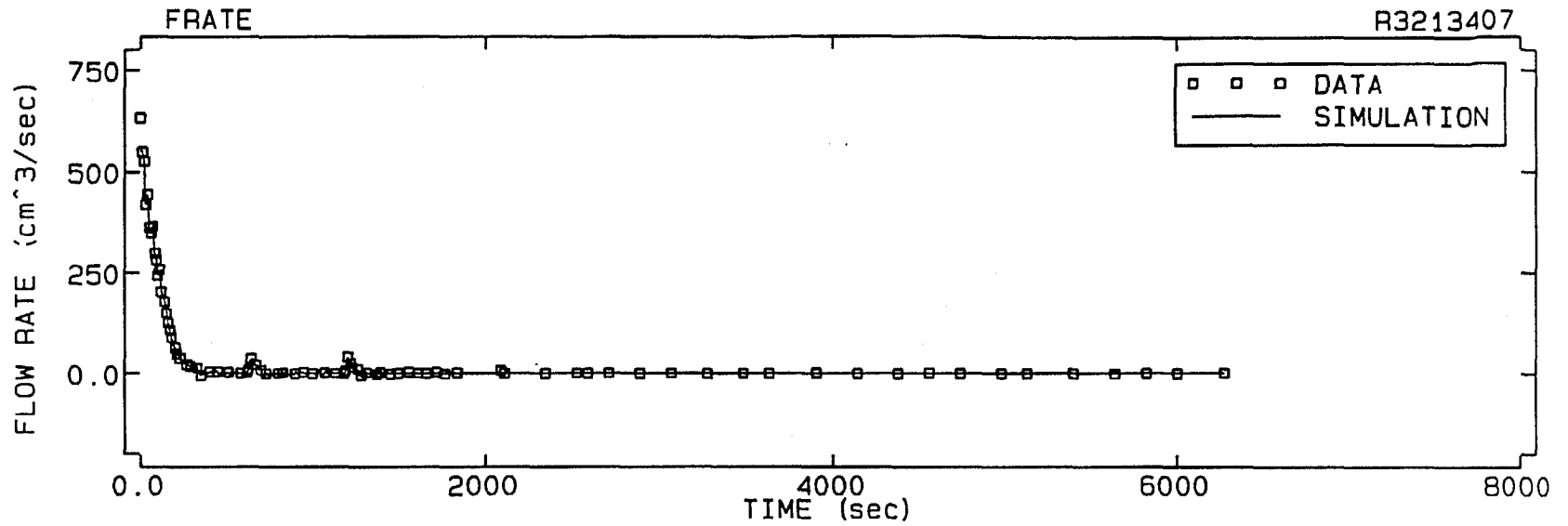


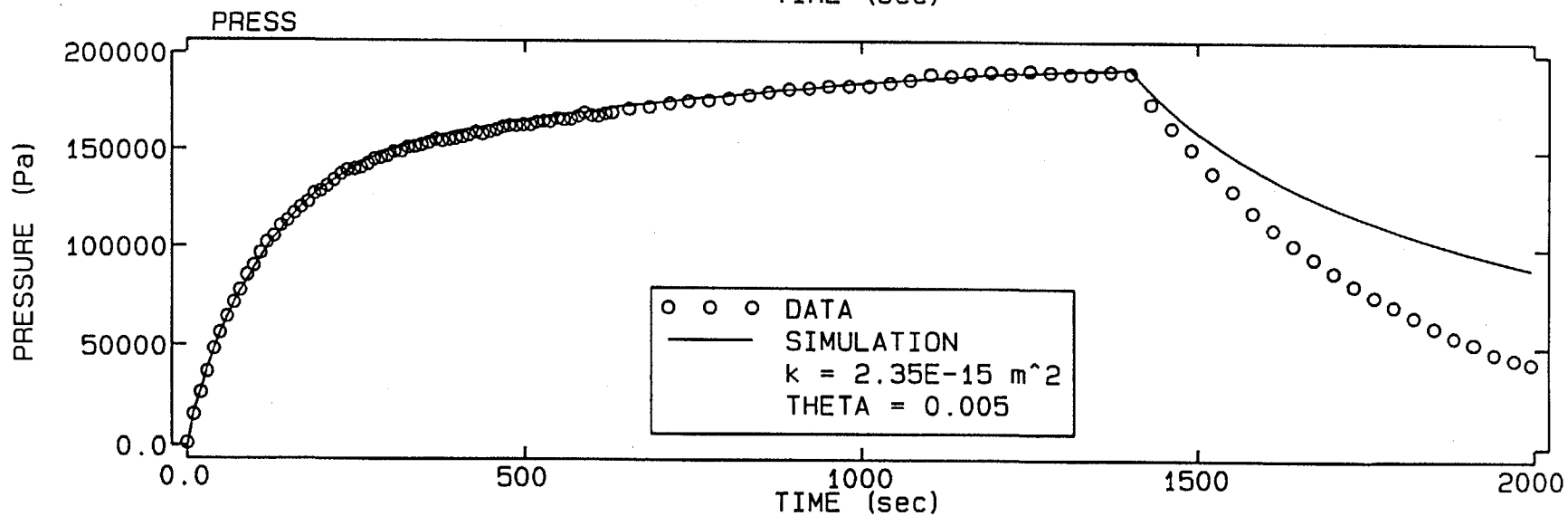
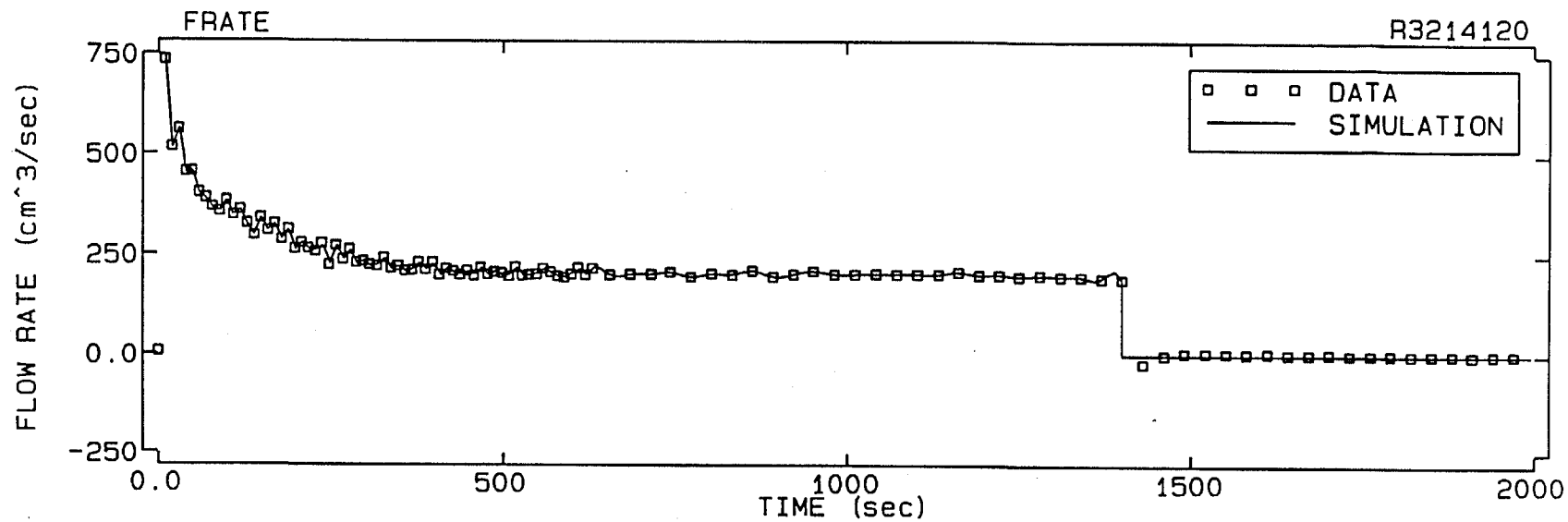
R3213305

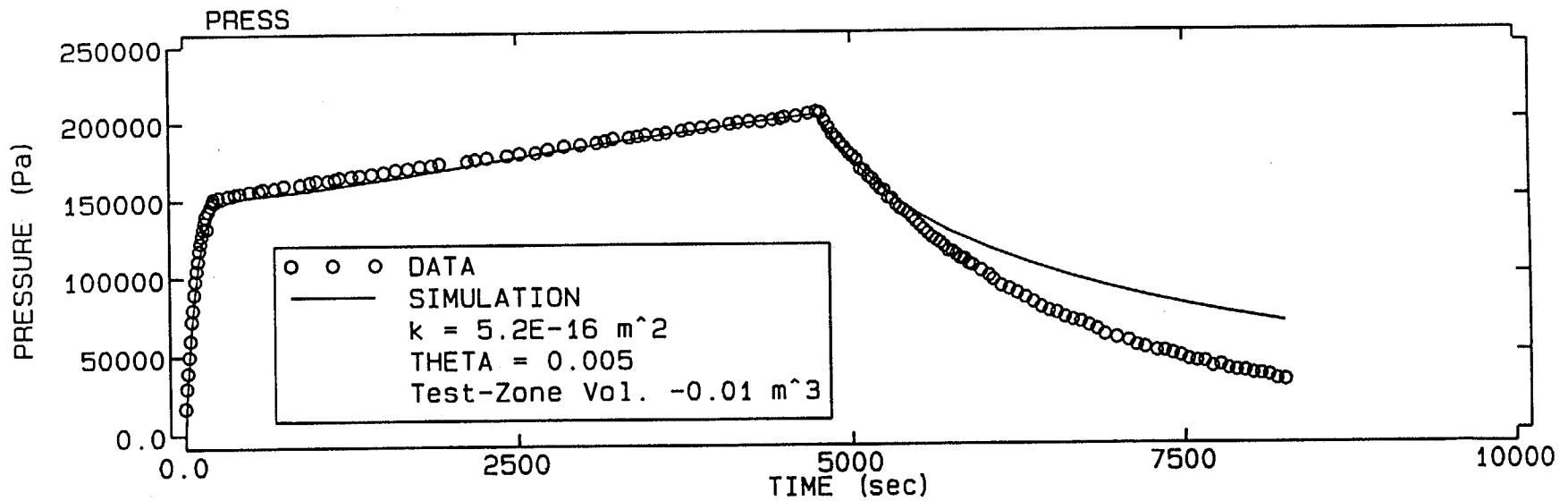
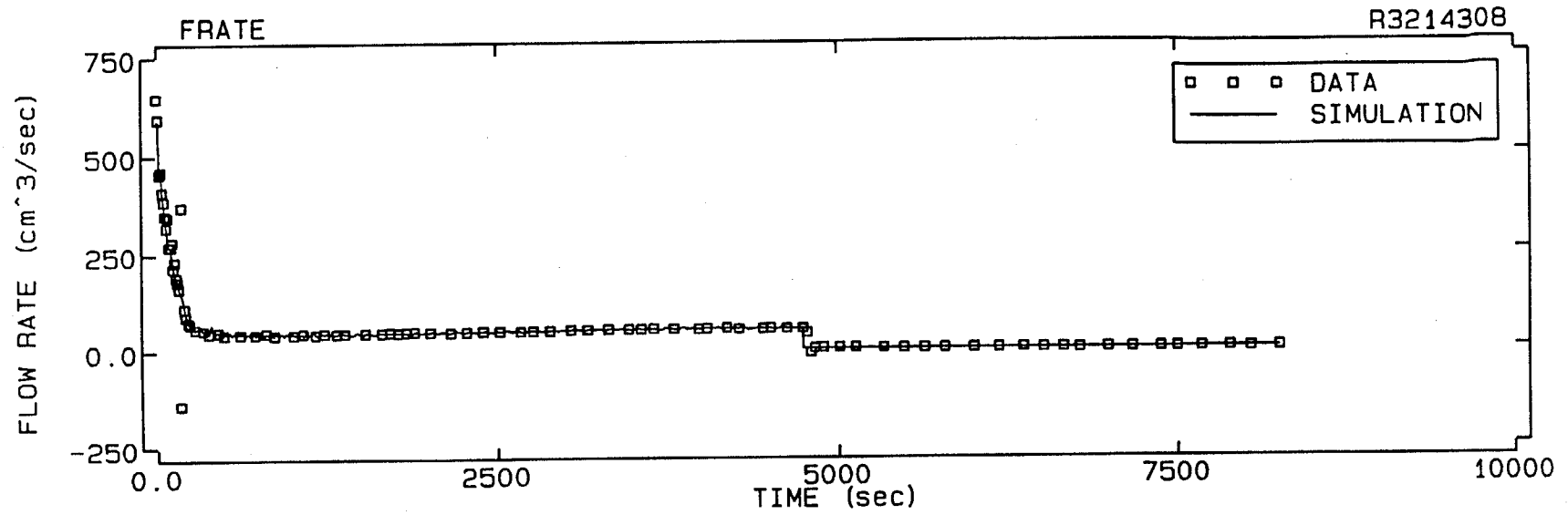


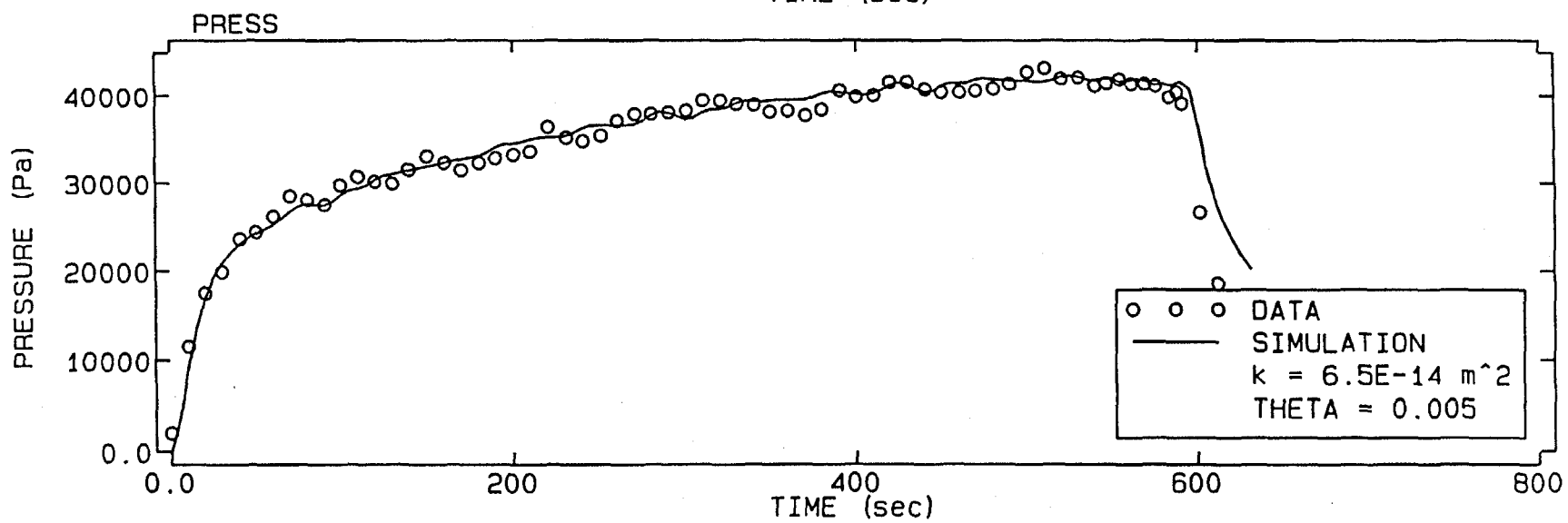
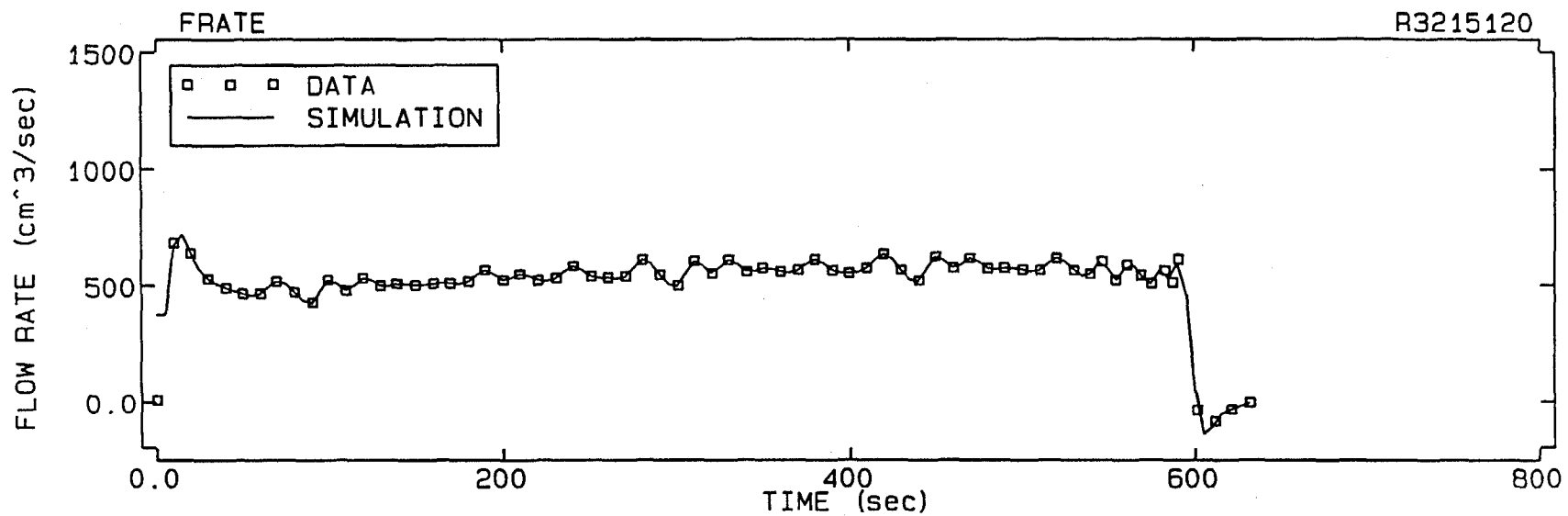
06-I

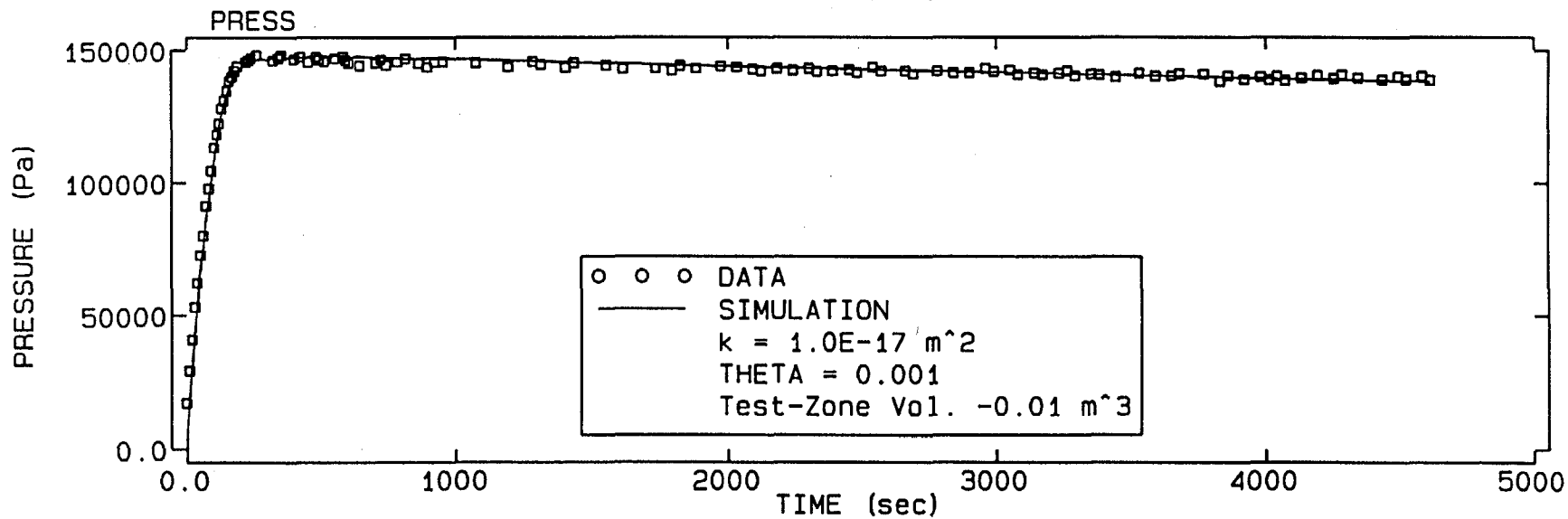
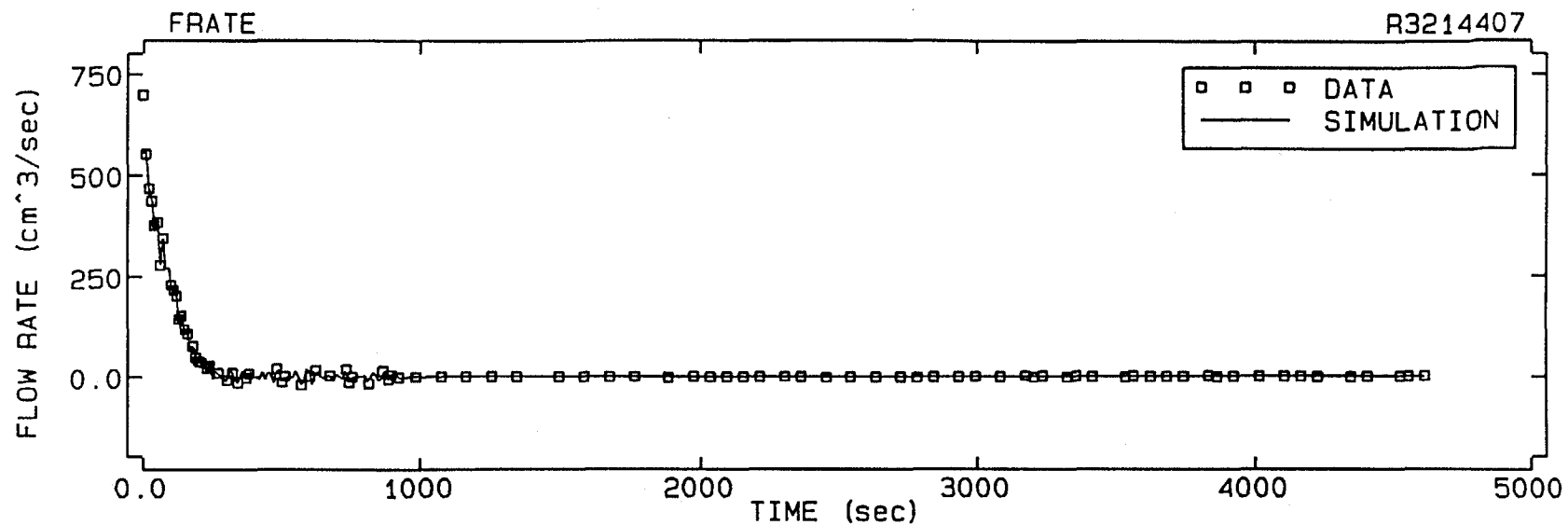


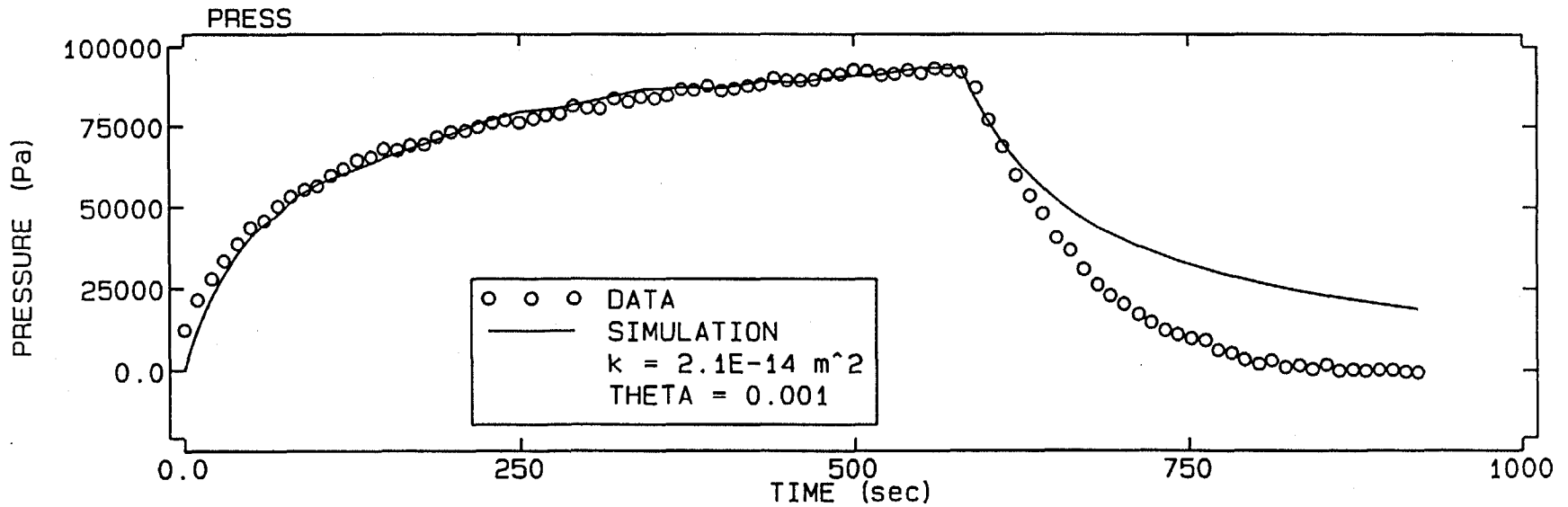
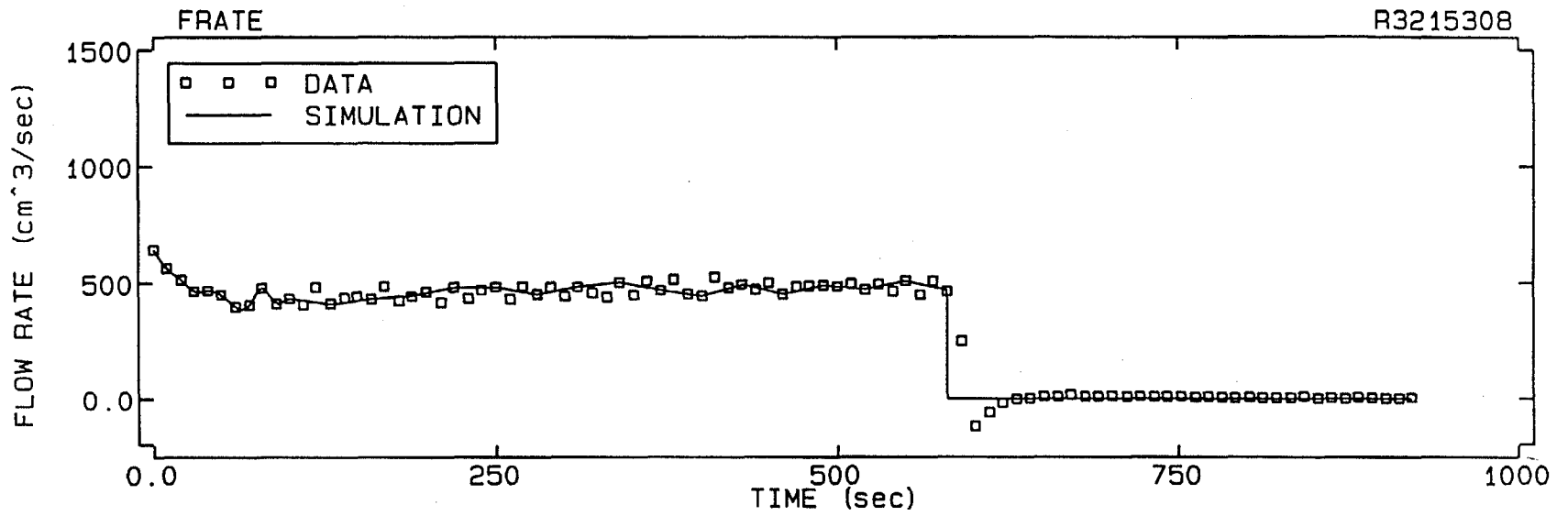


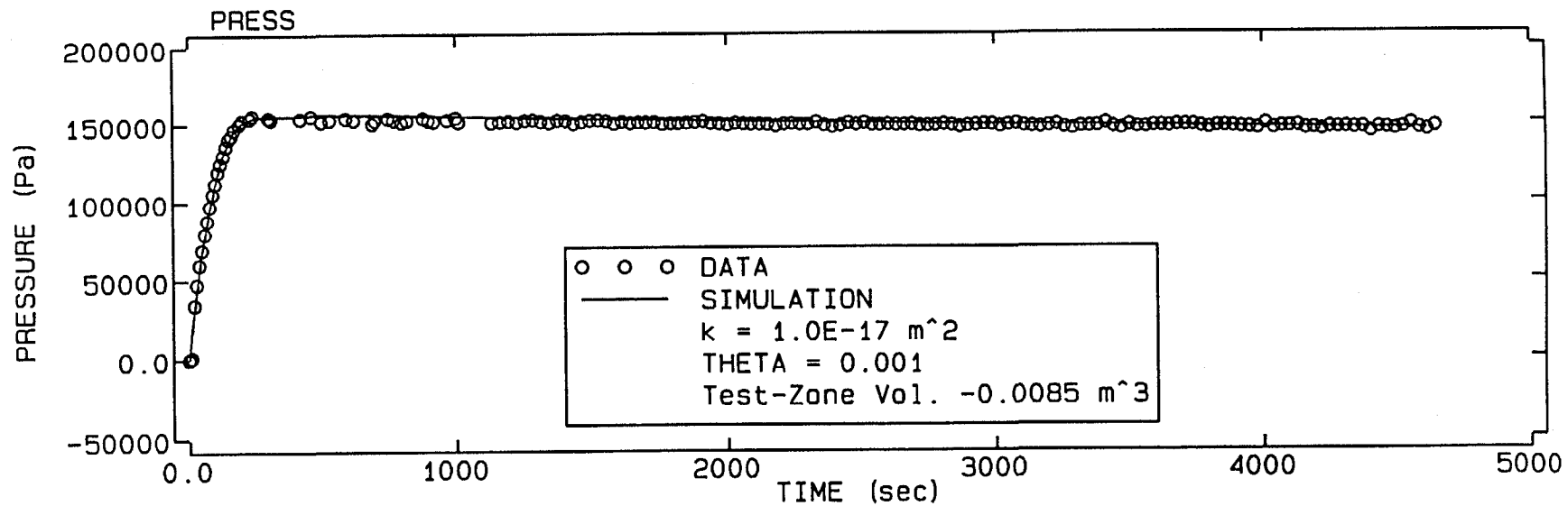
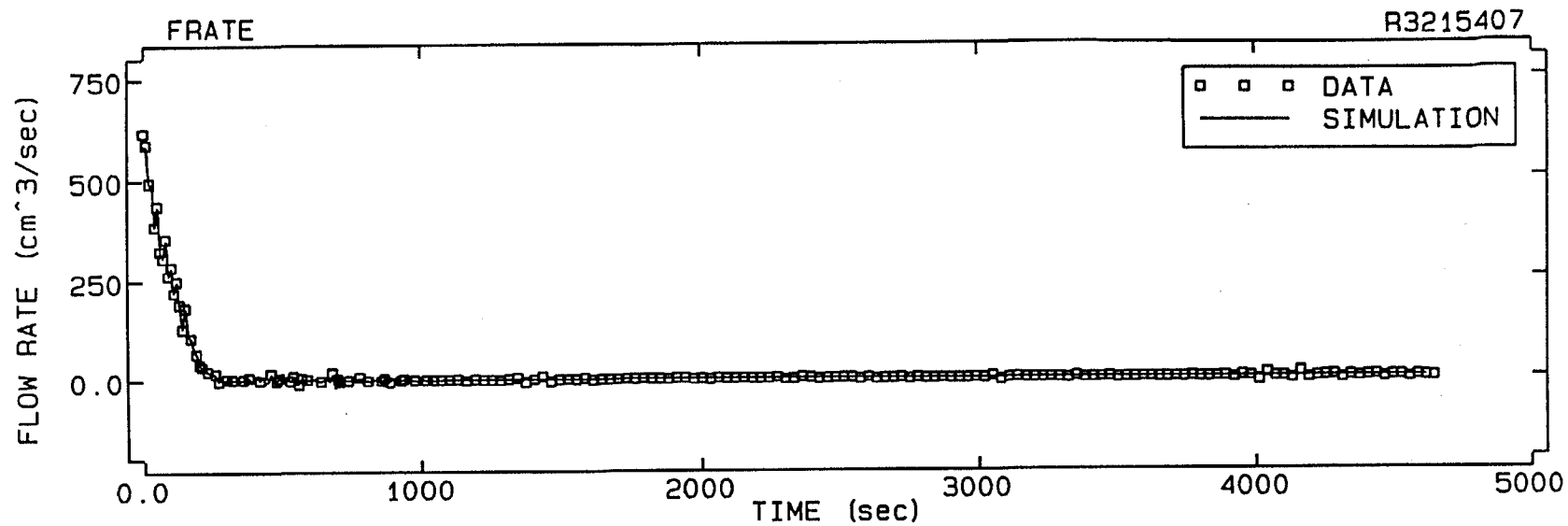


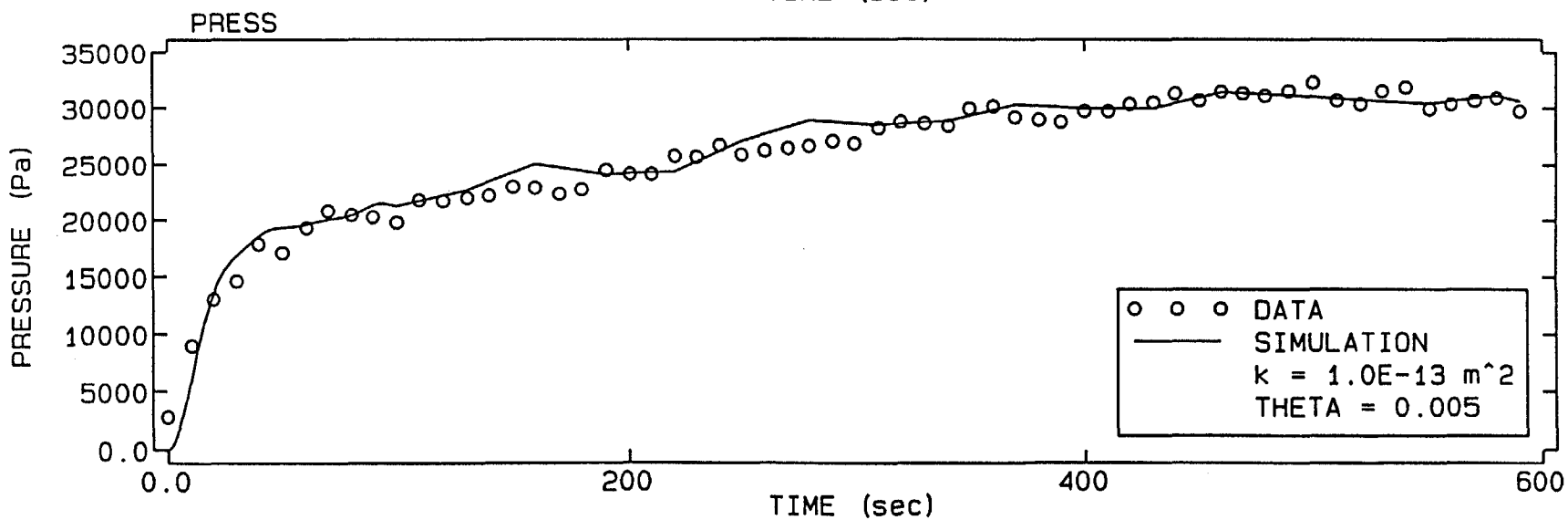
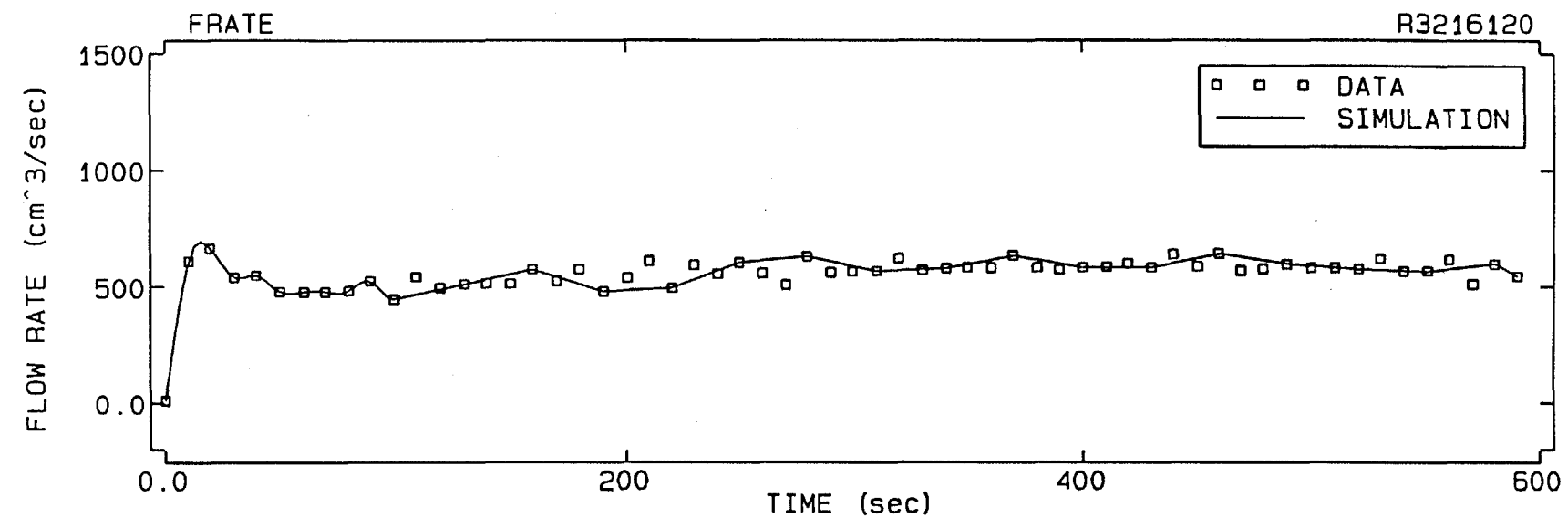




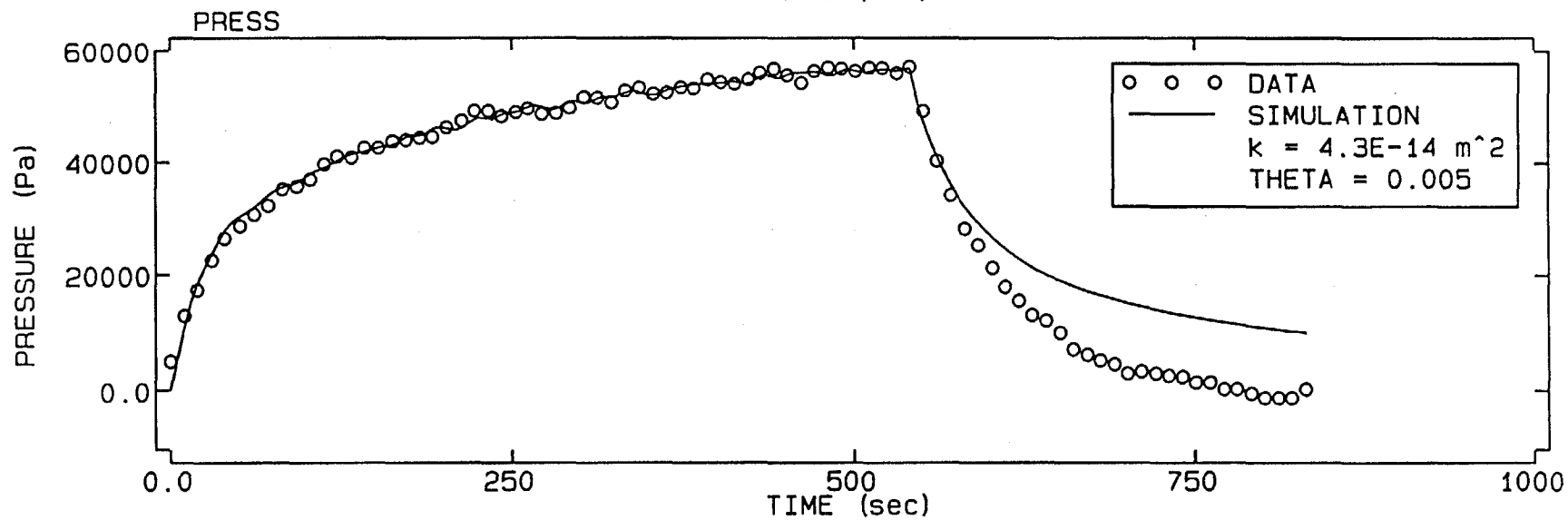
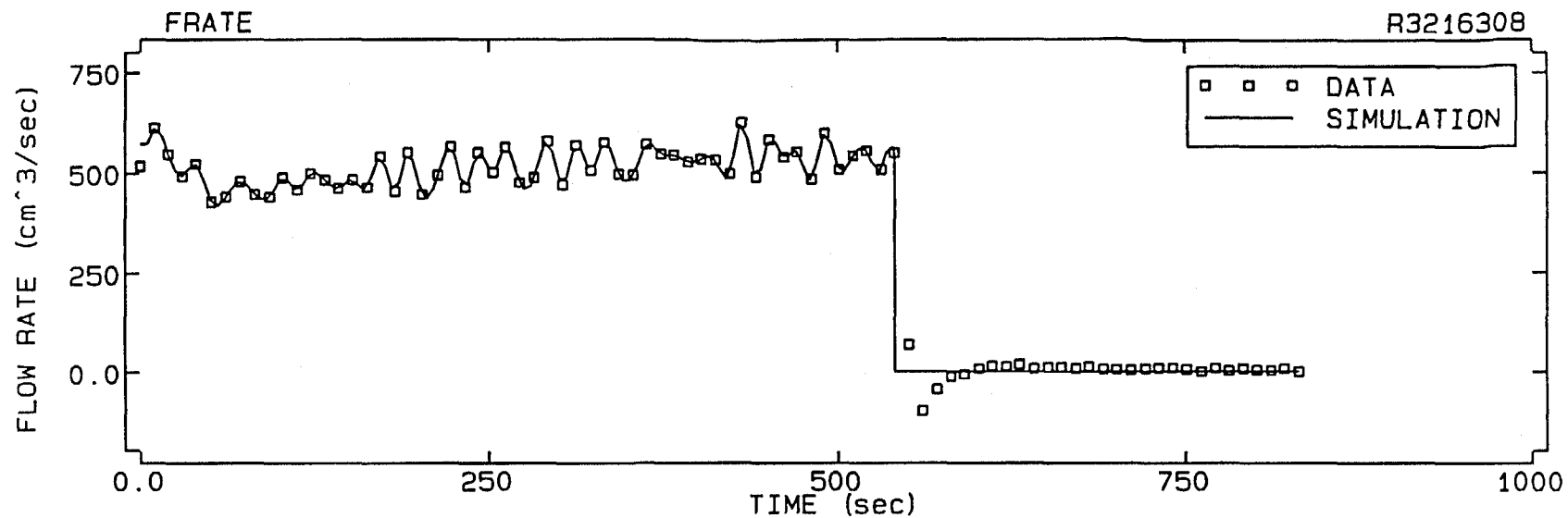


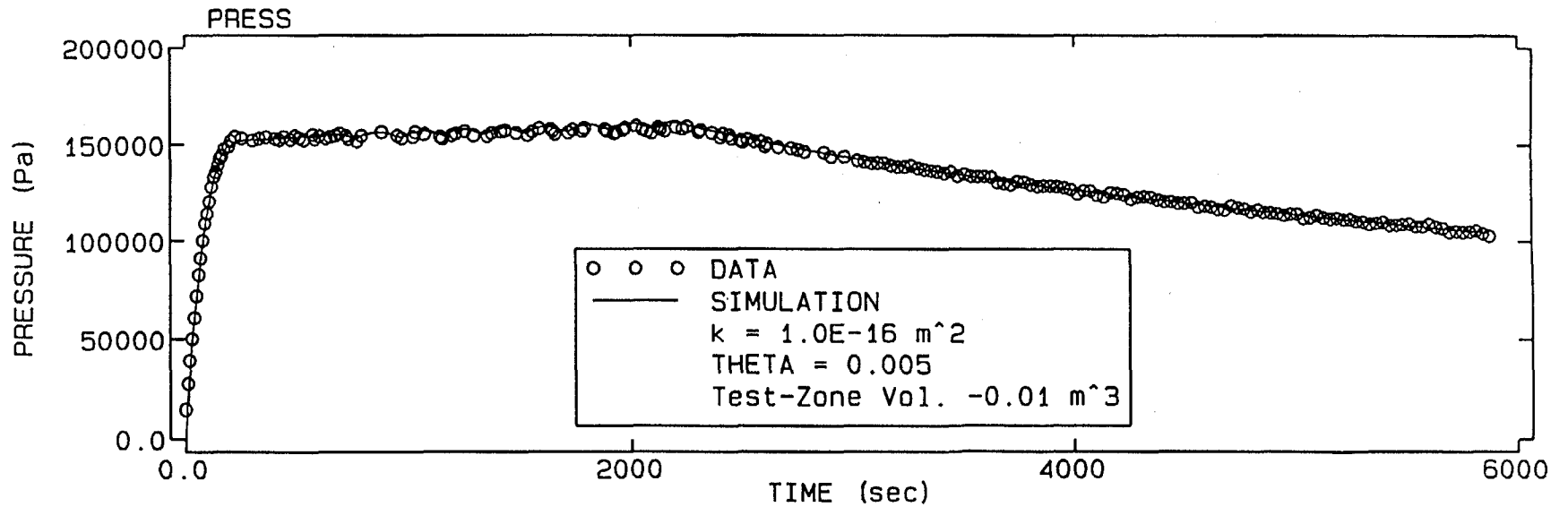
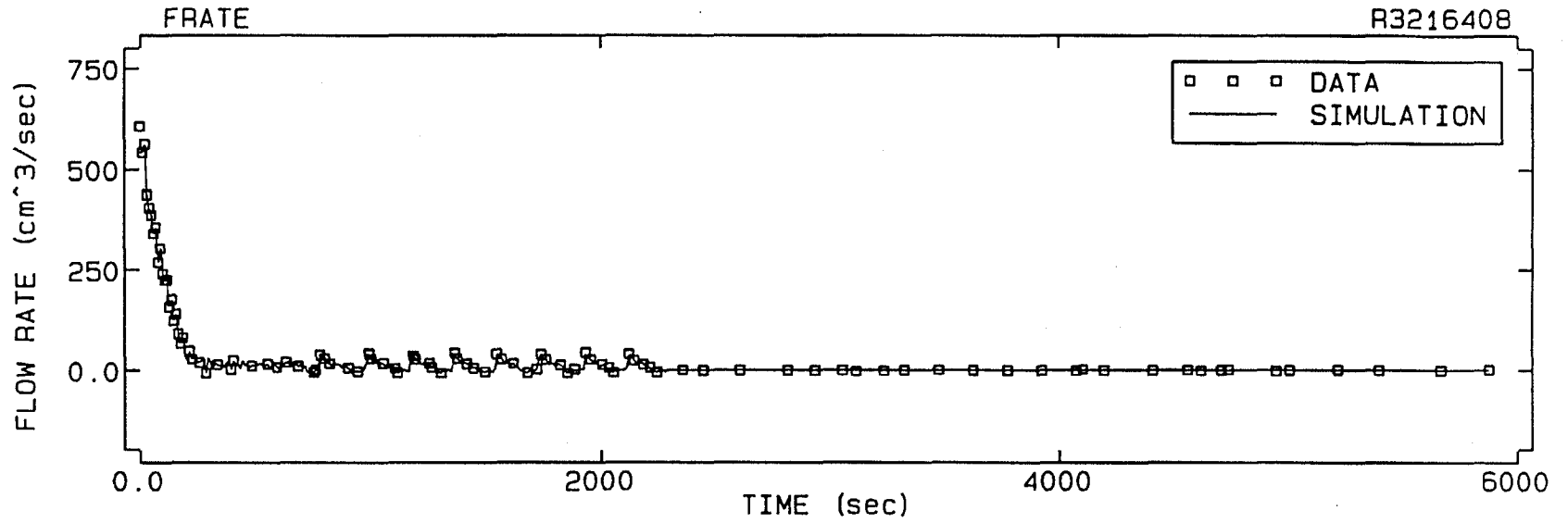


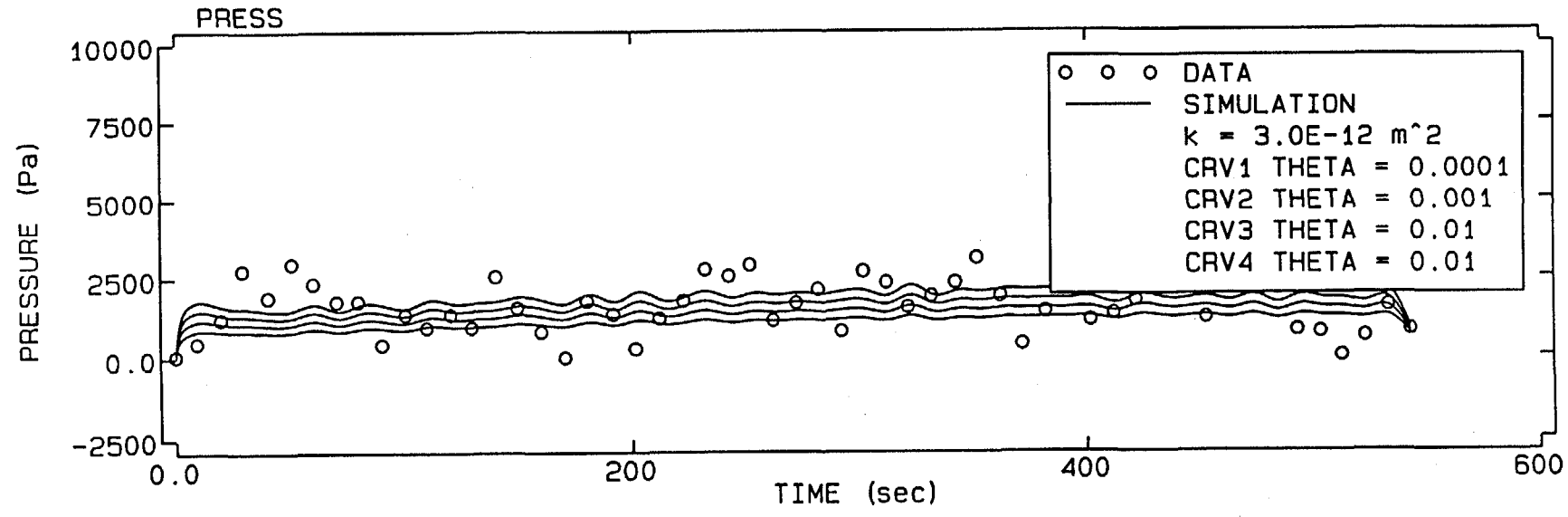
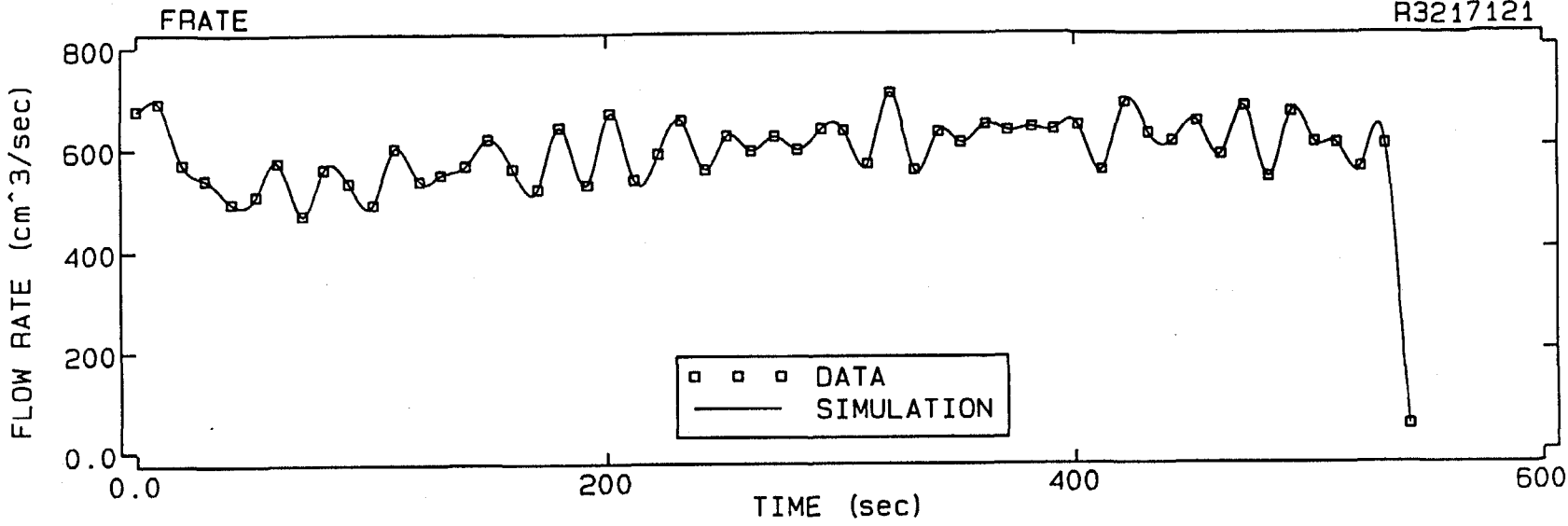


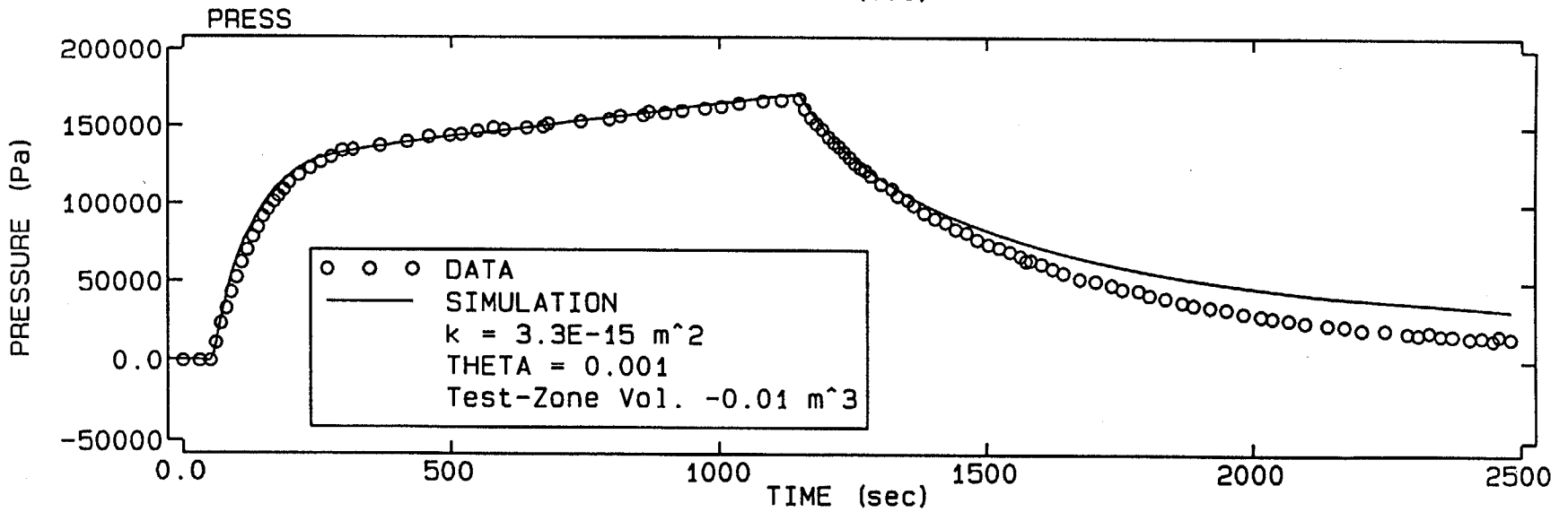
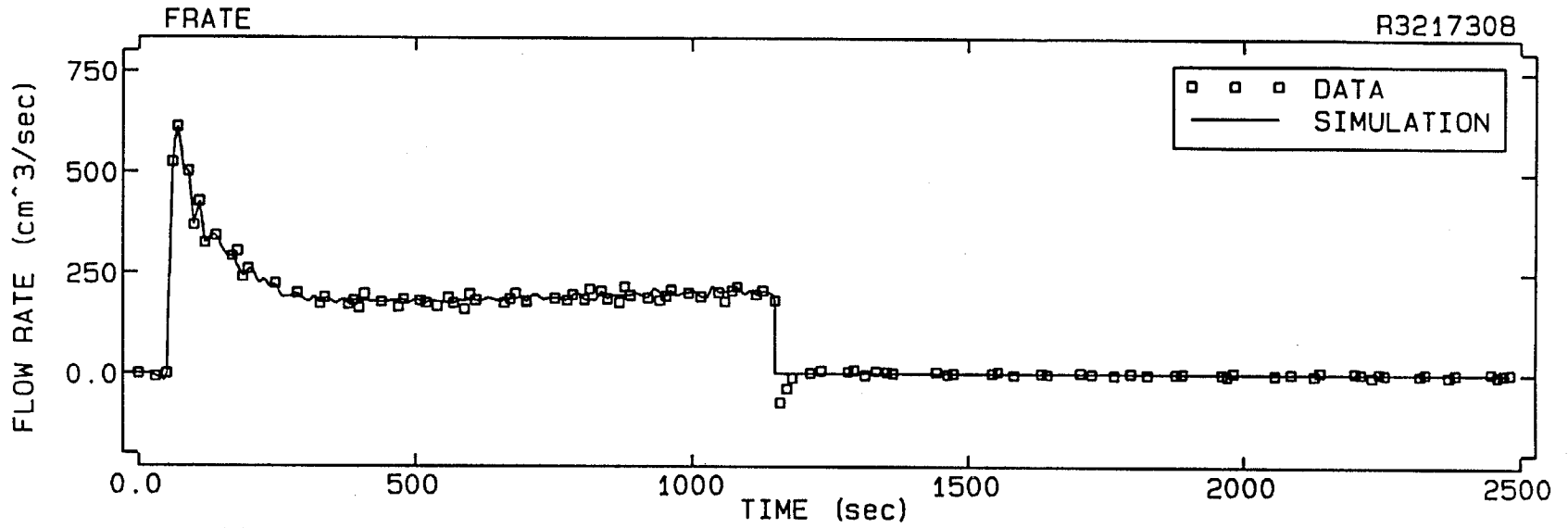


I-100

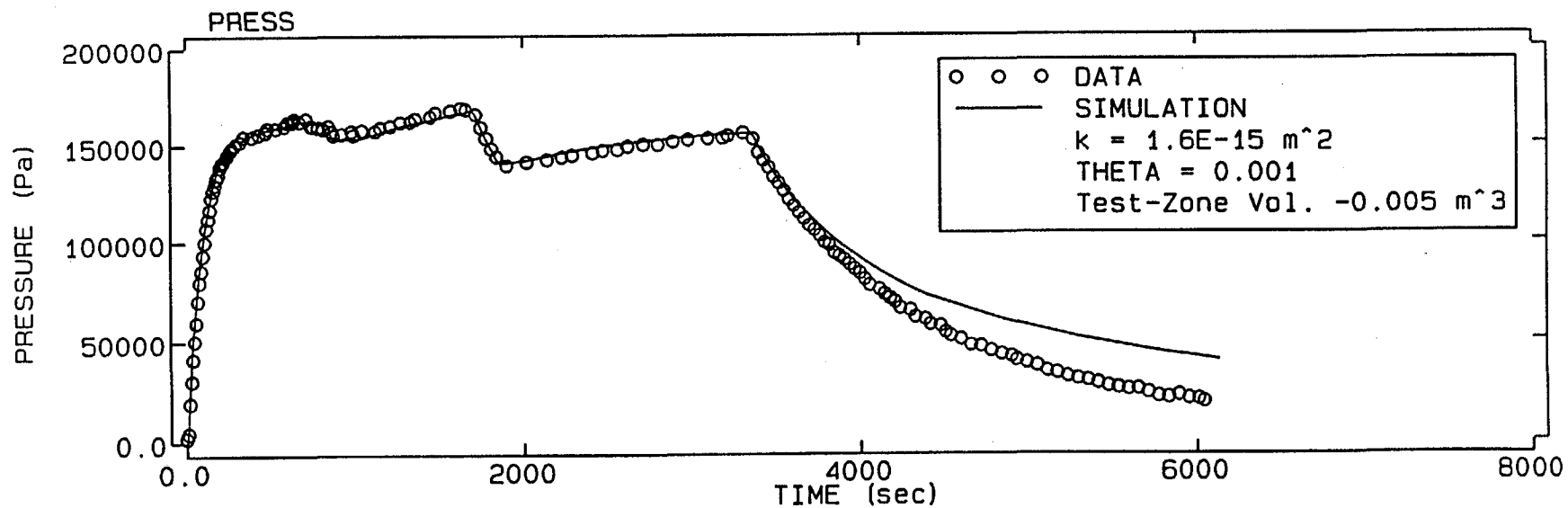
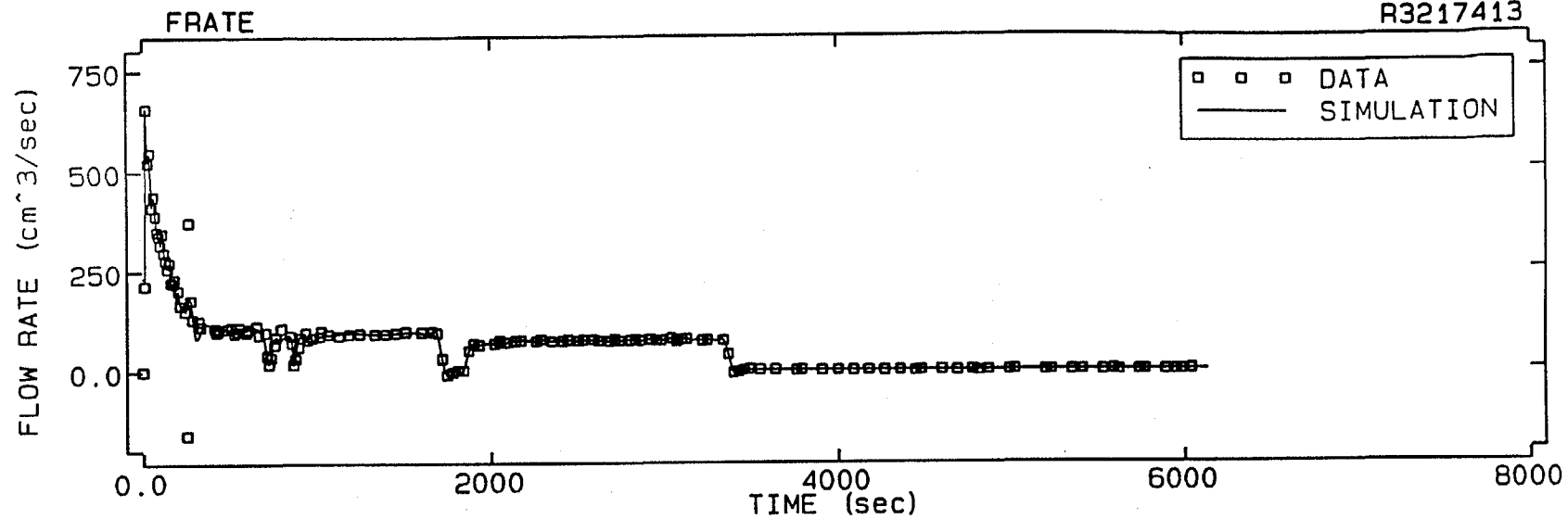




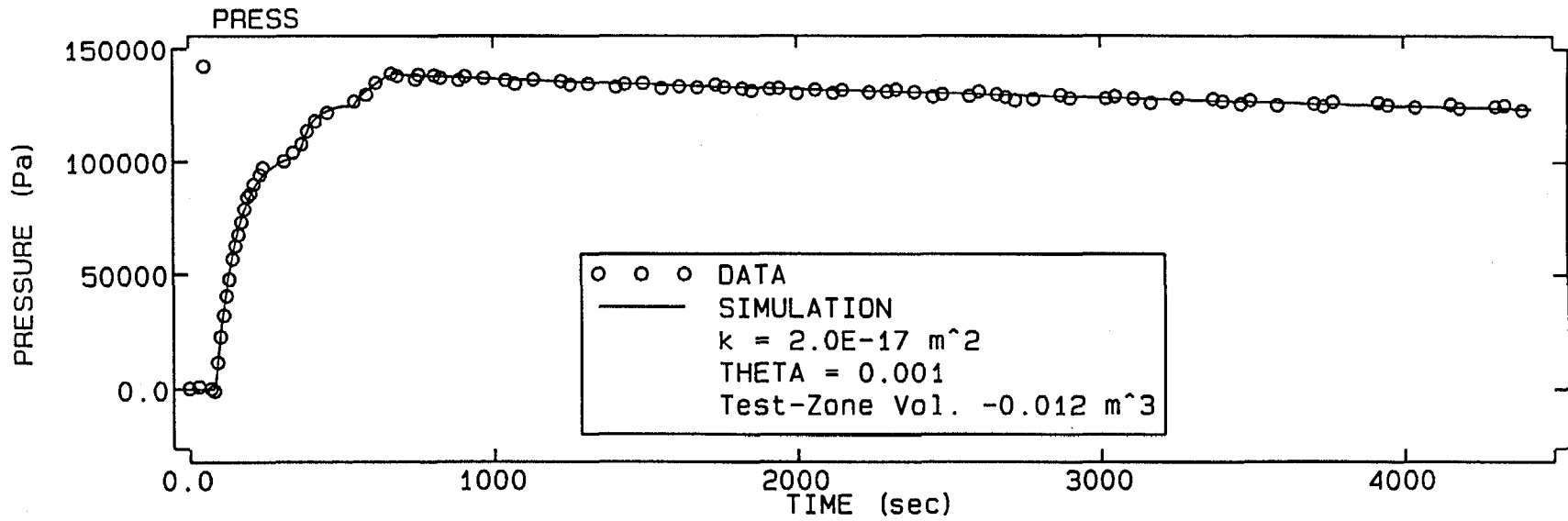
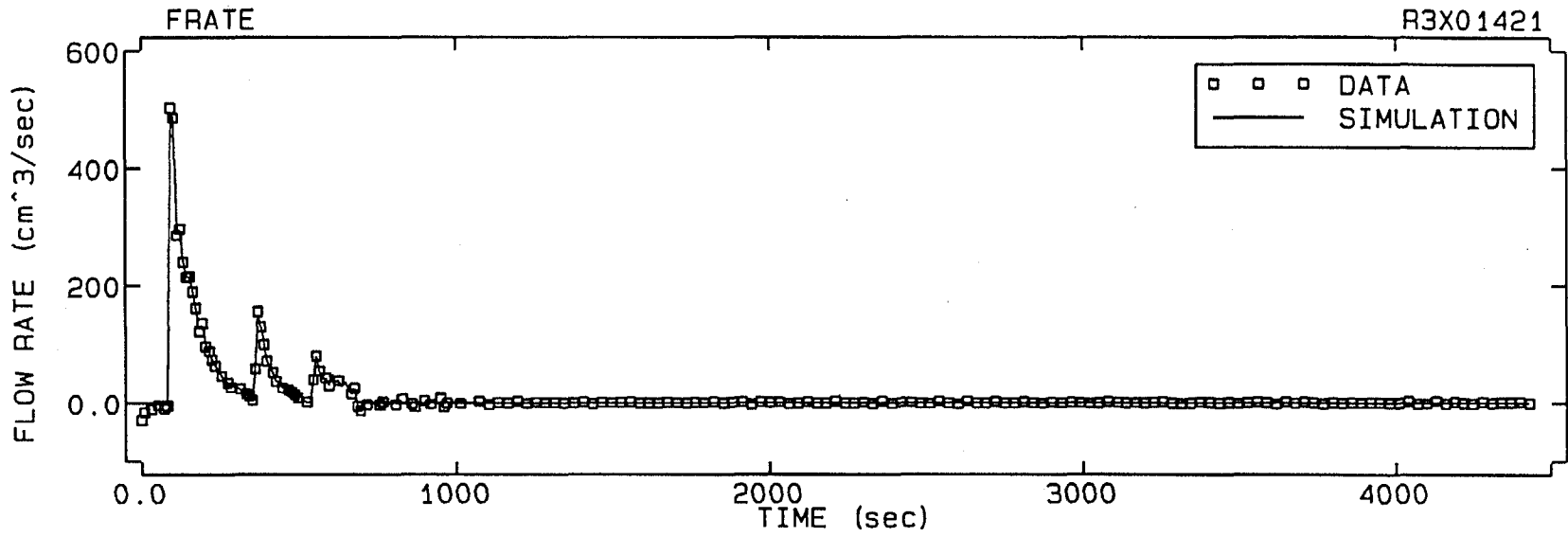


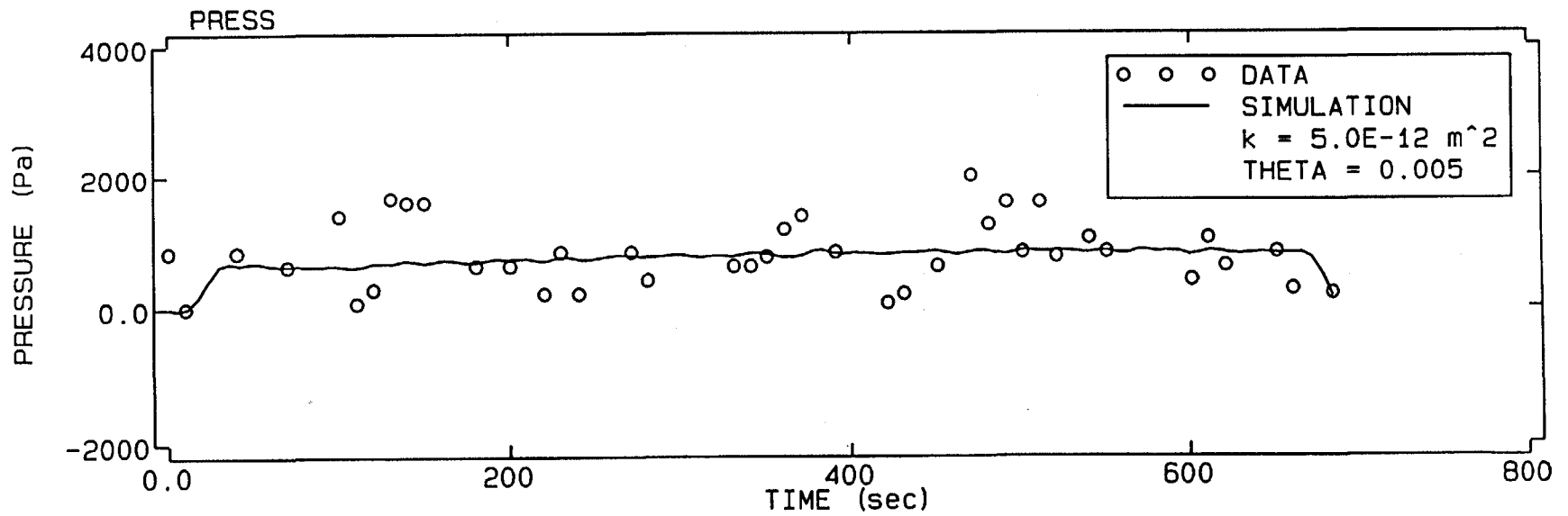
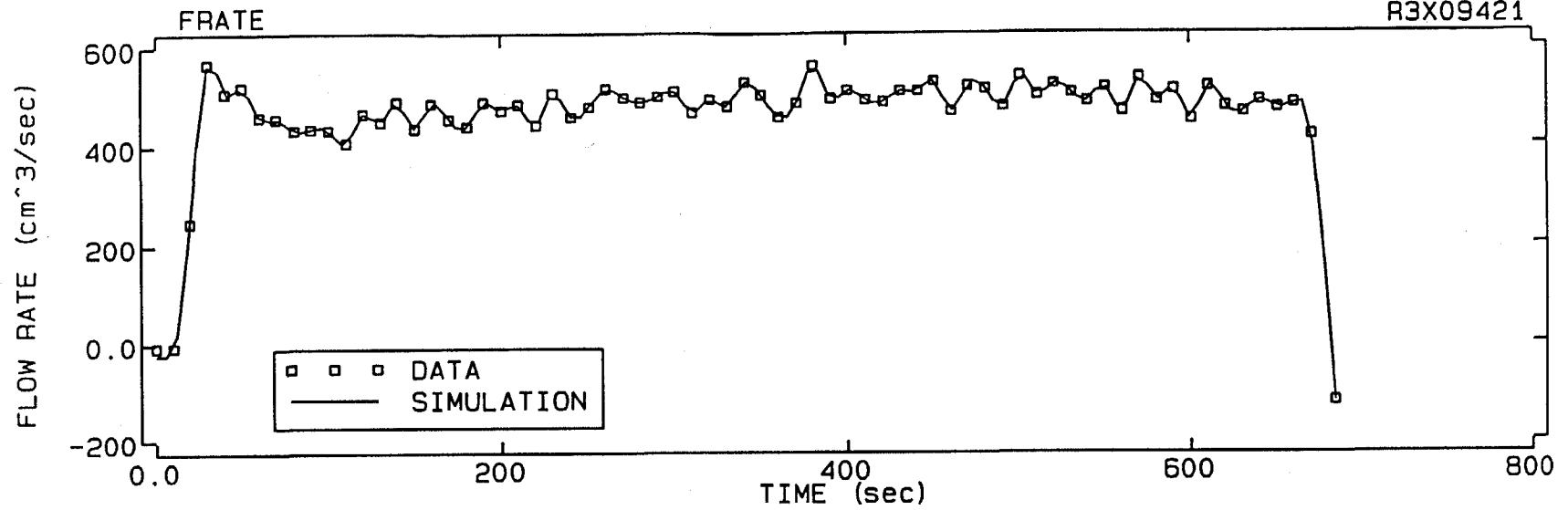


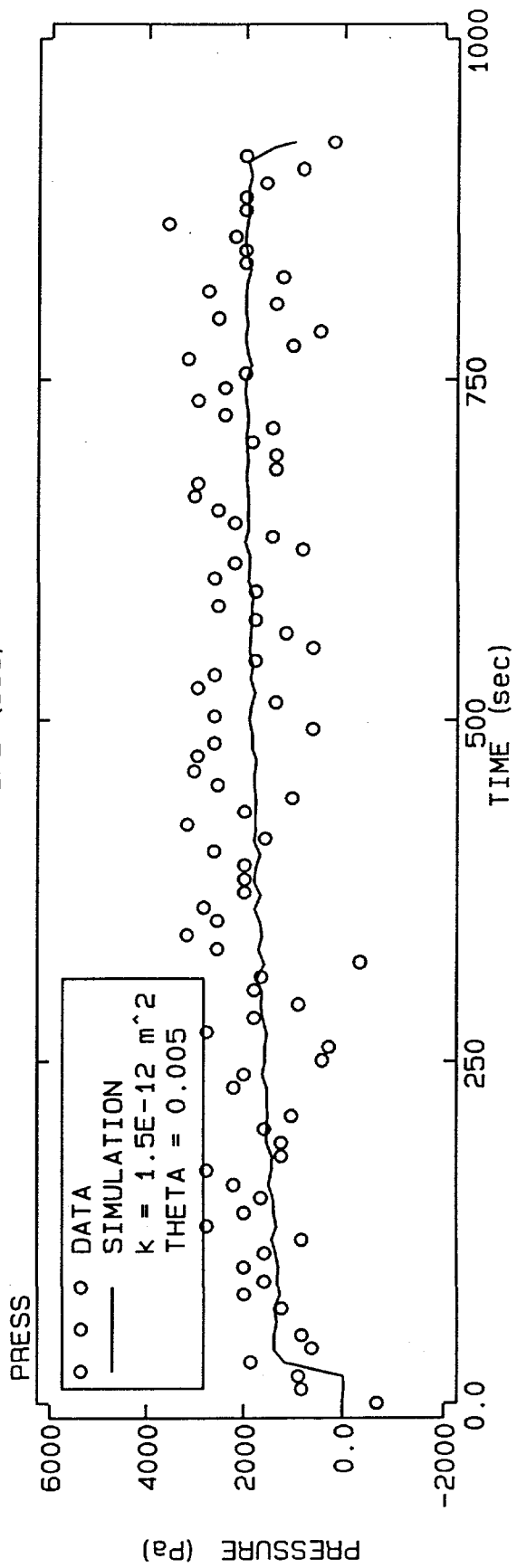
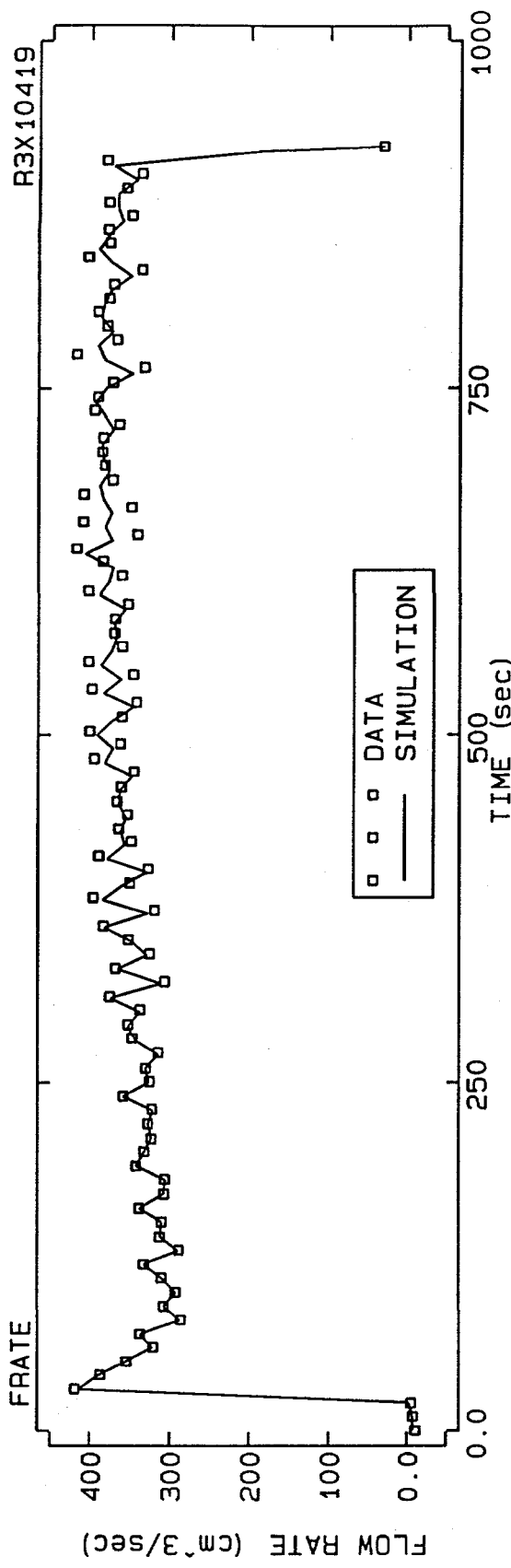
R3217413

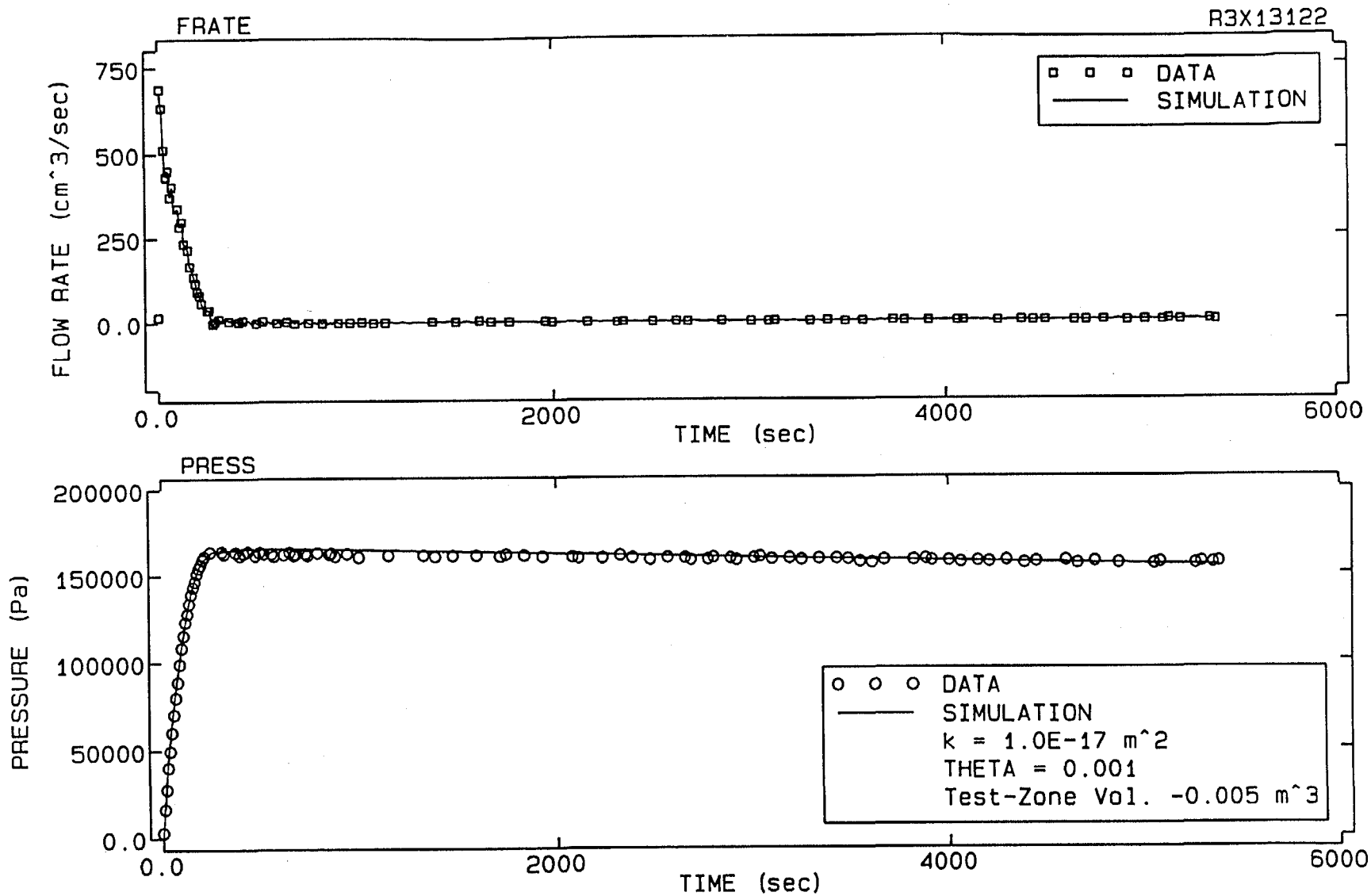


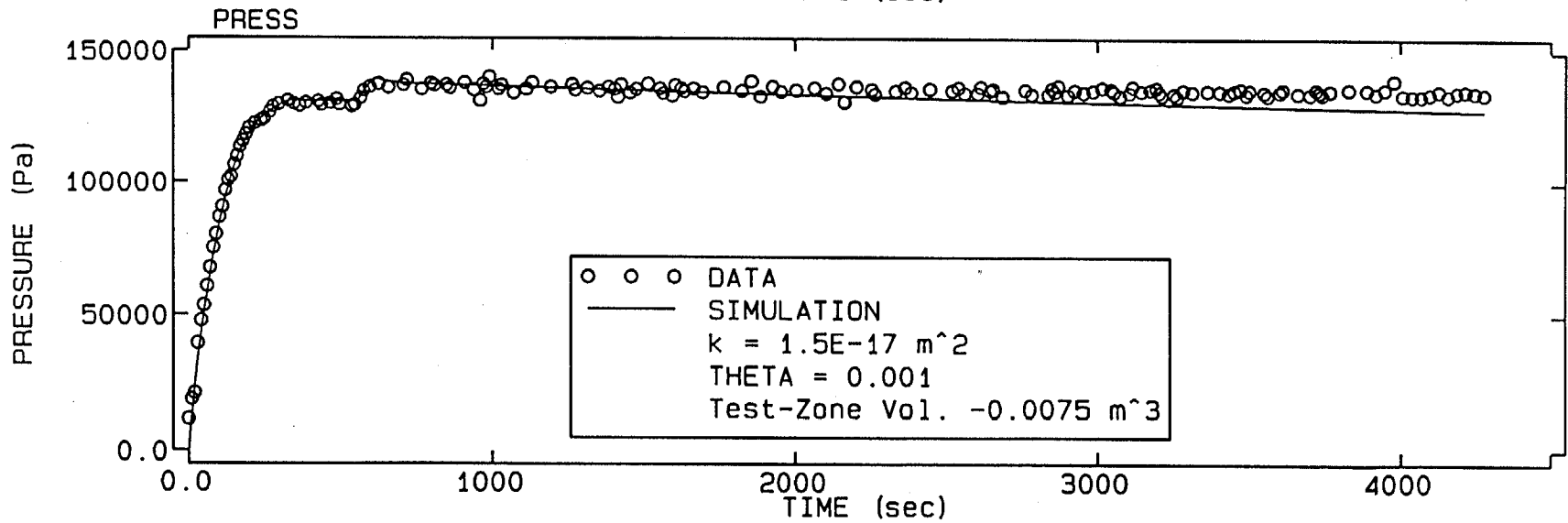
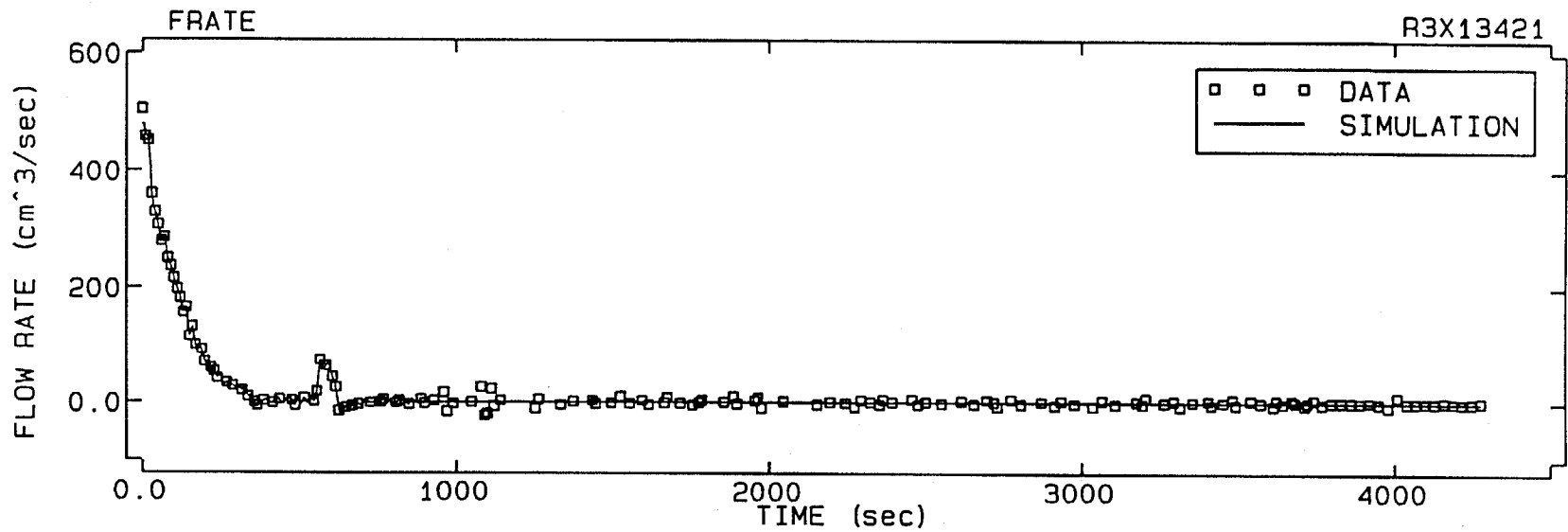
I-104

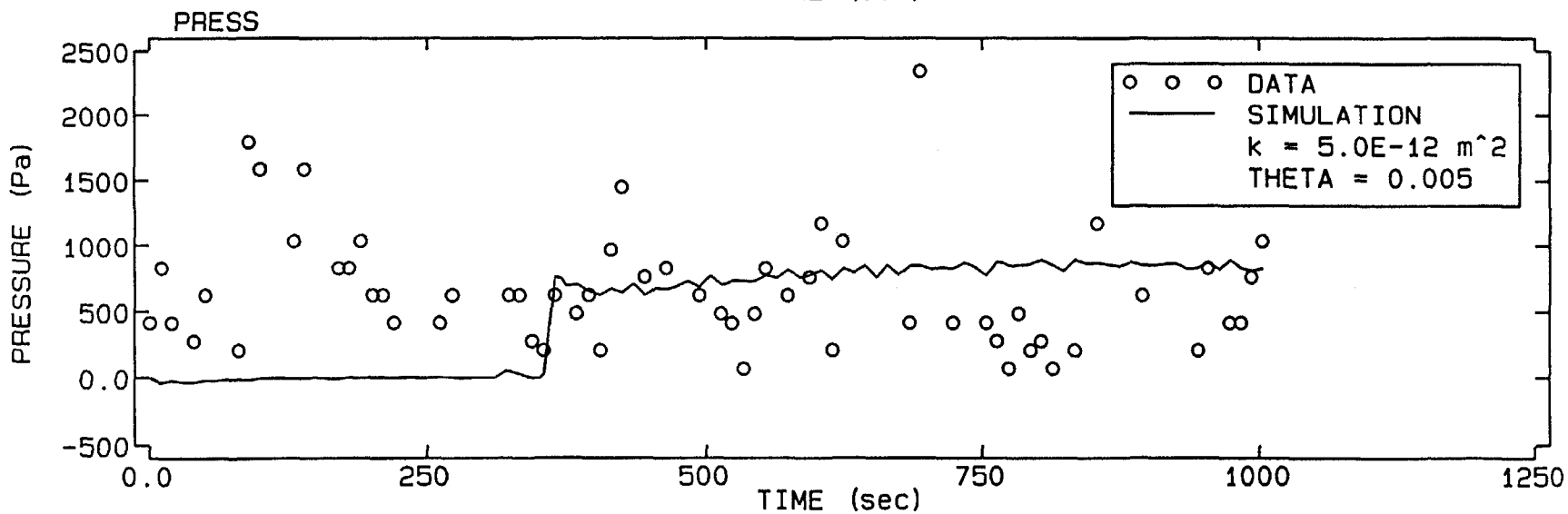
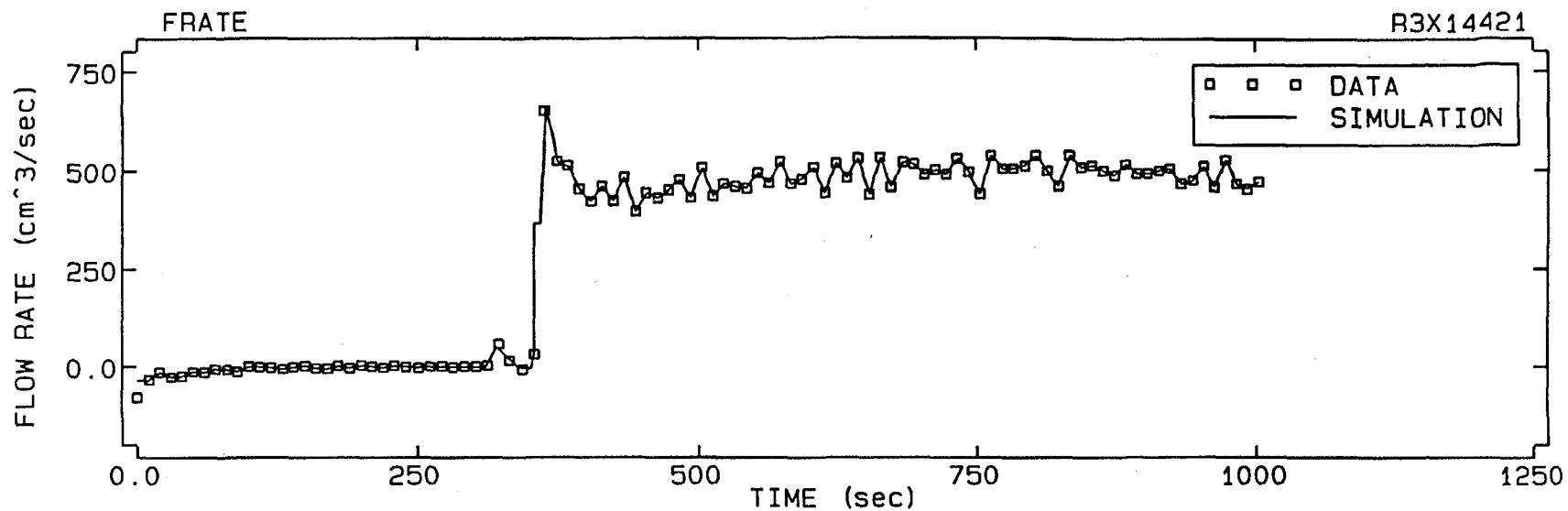


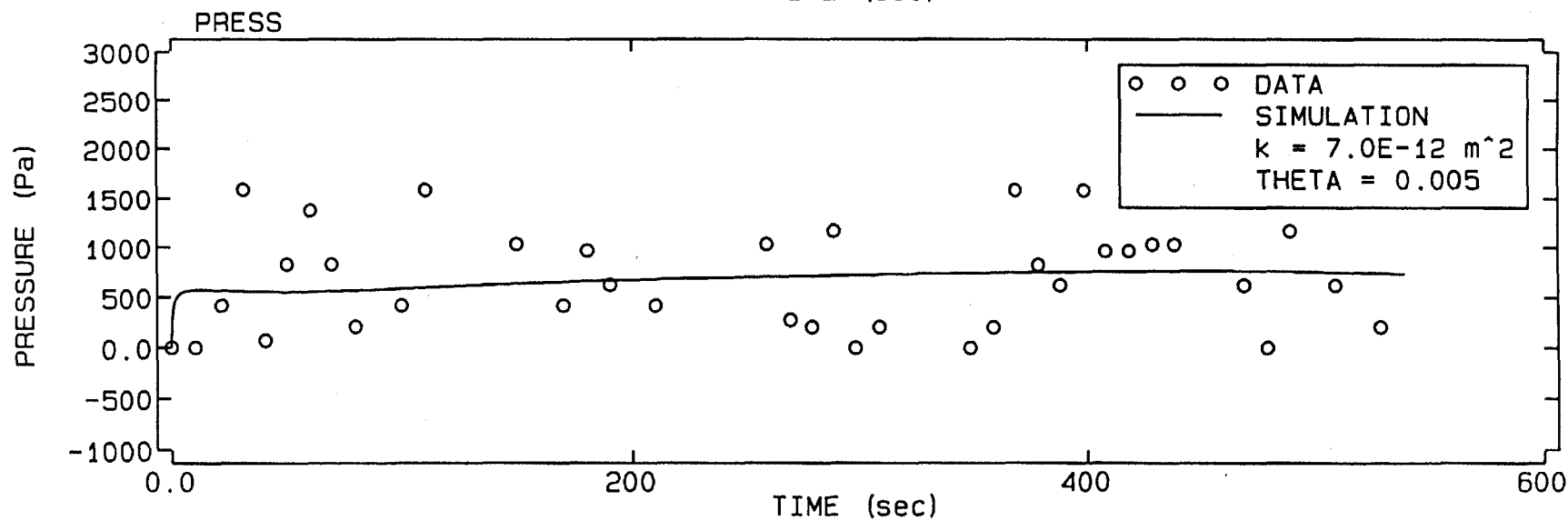
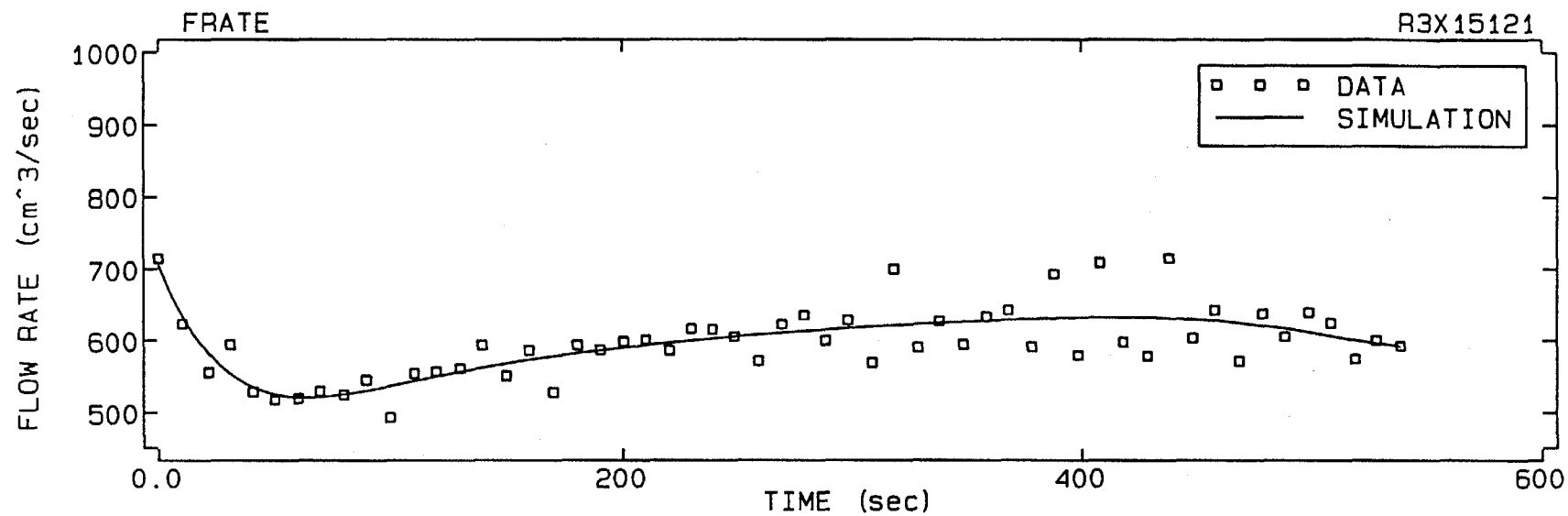


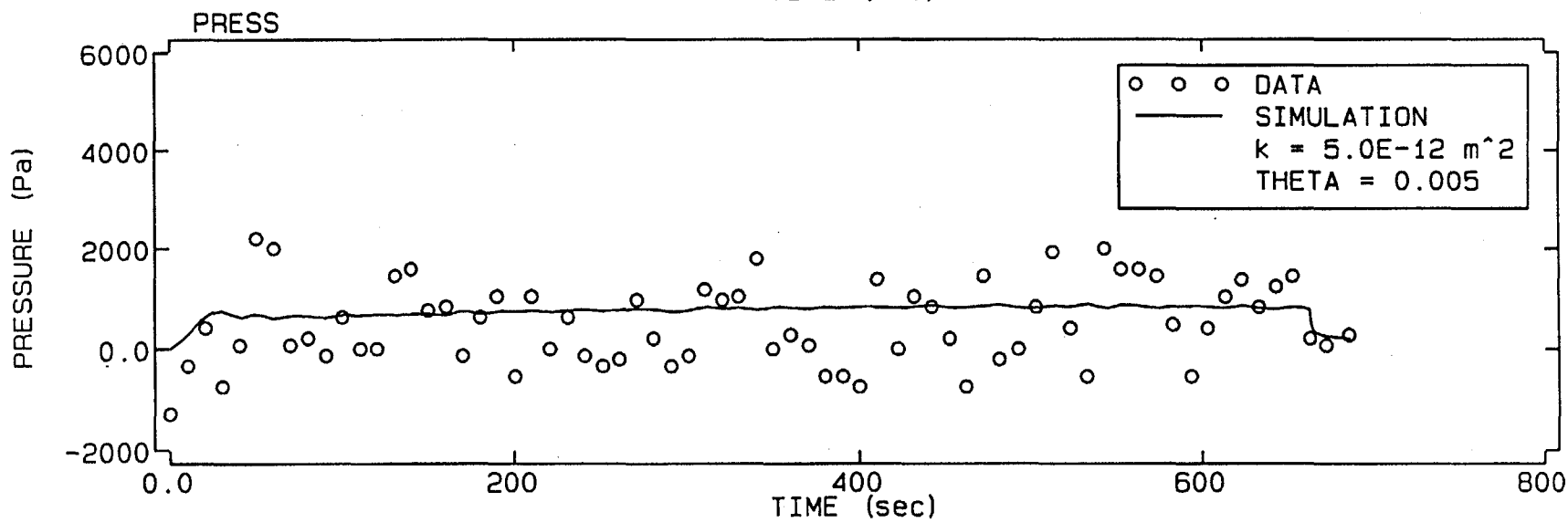
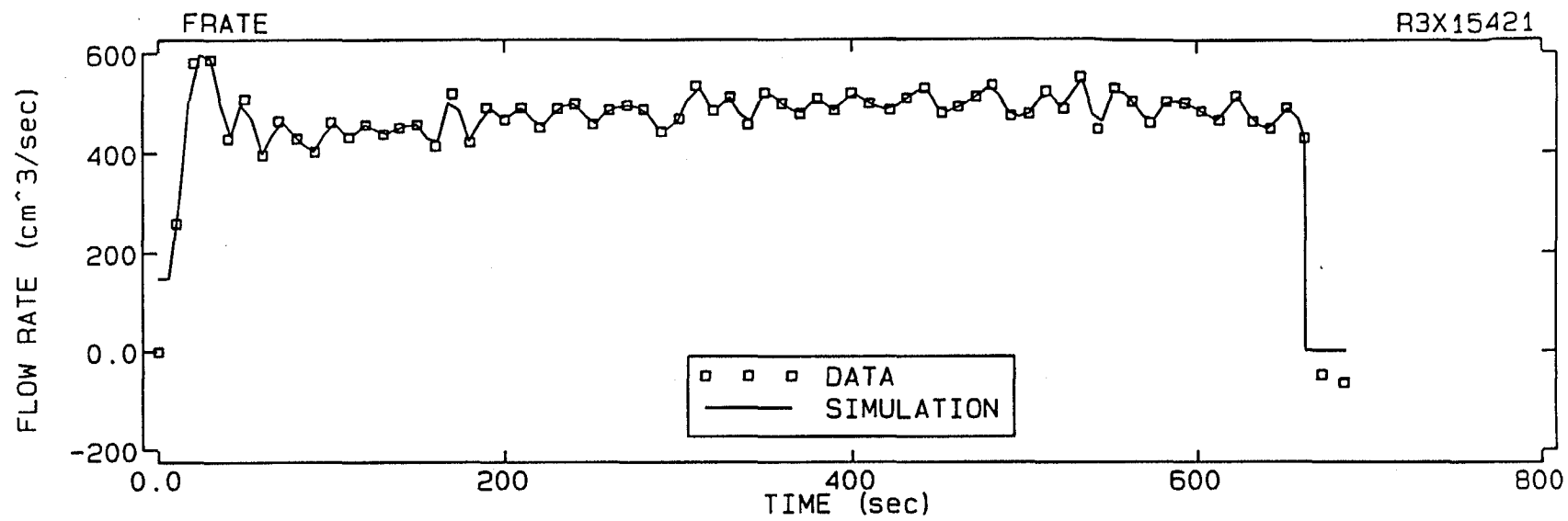


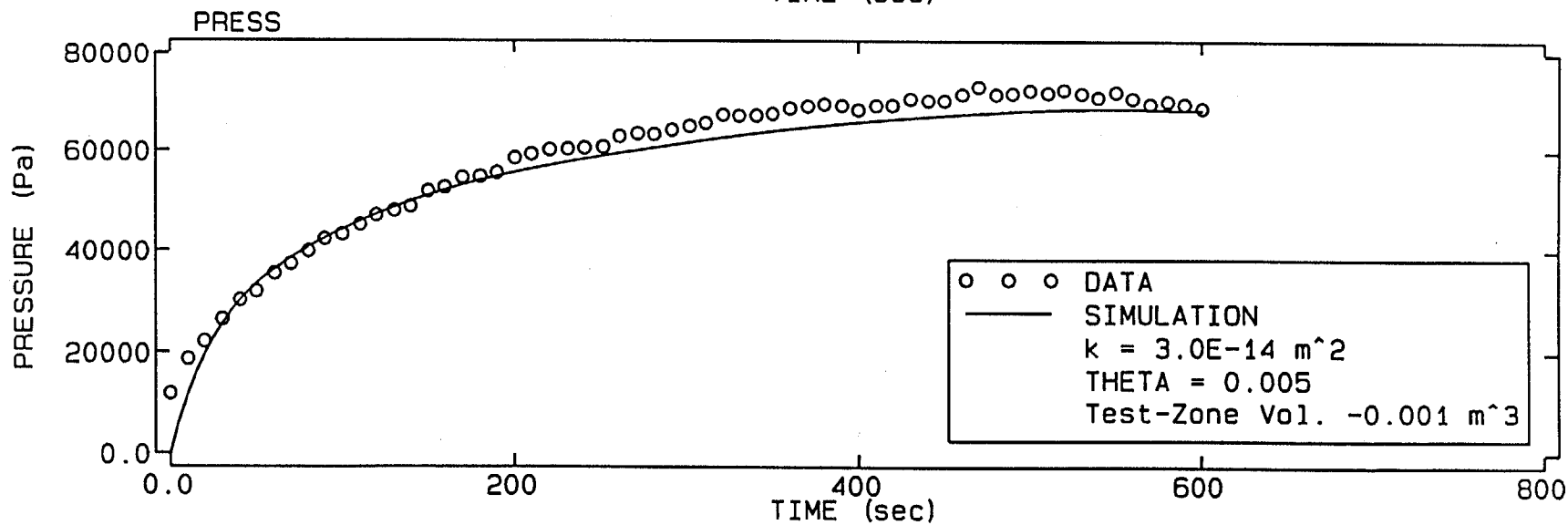
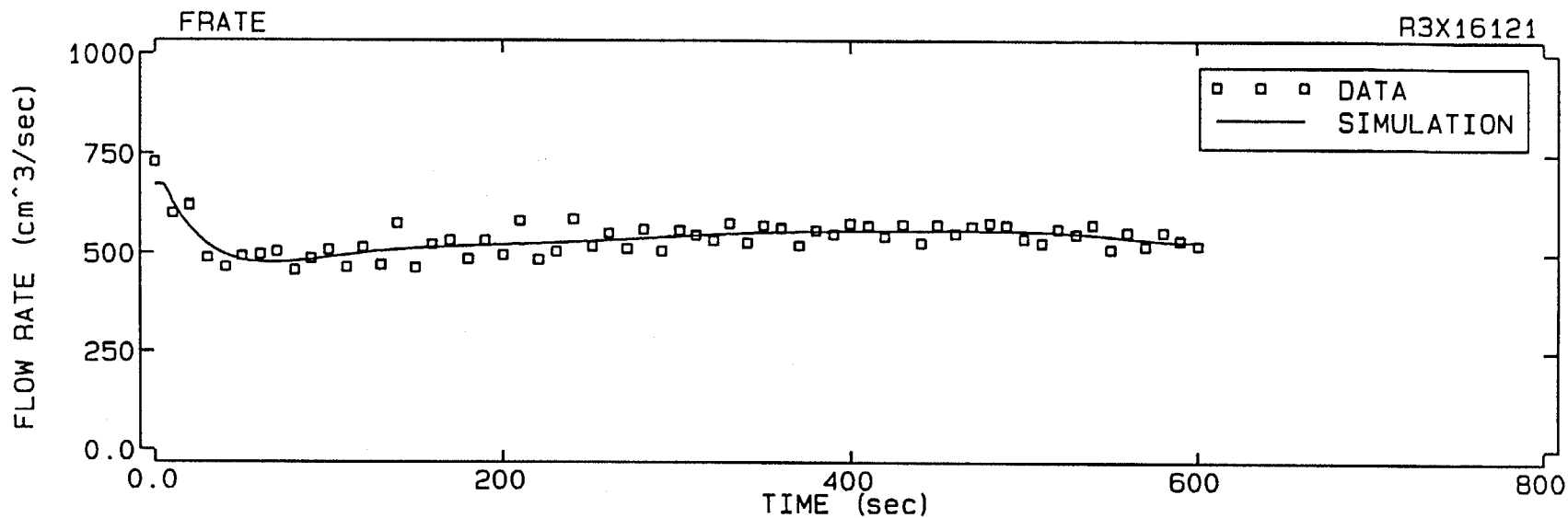


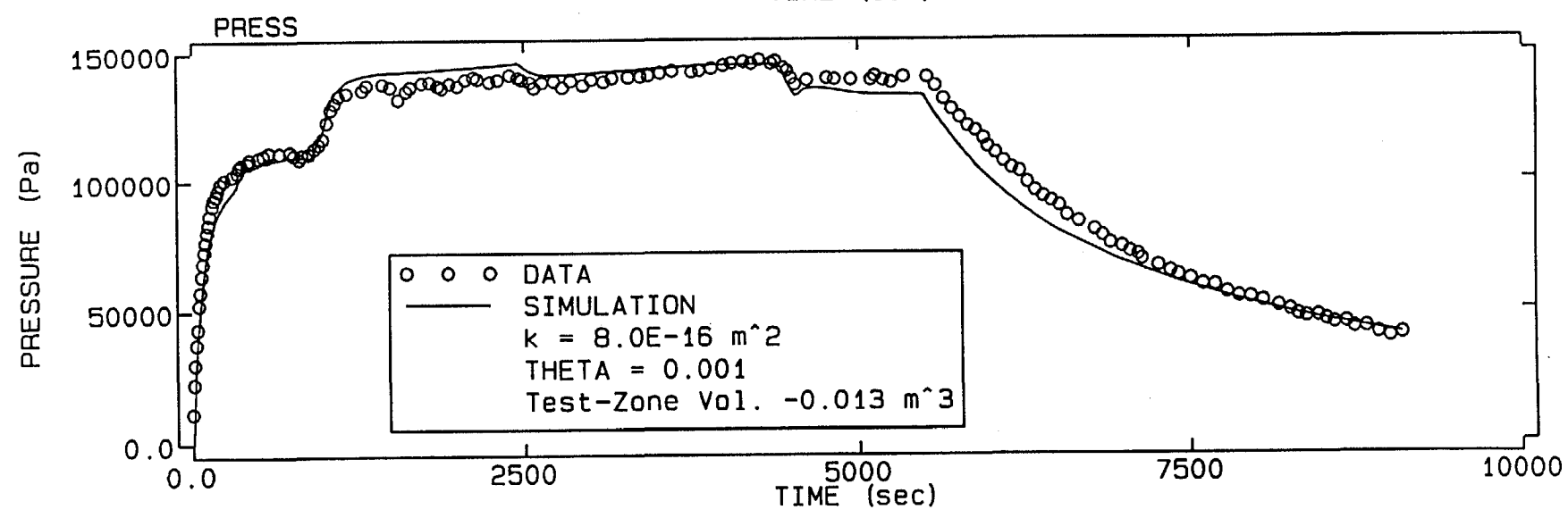
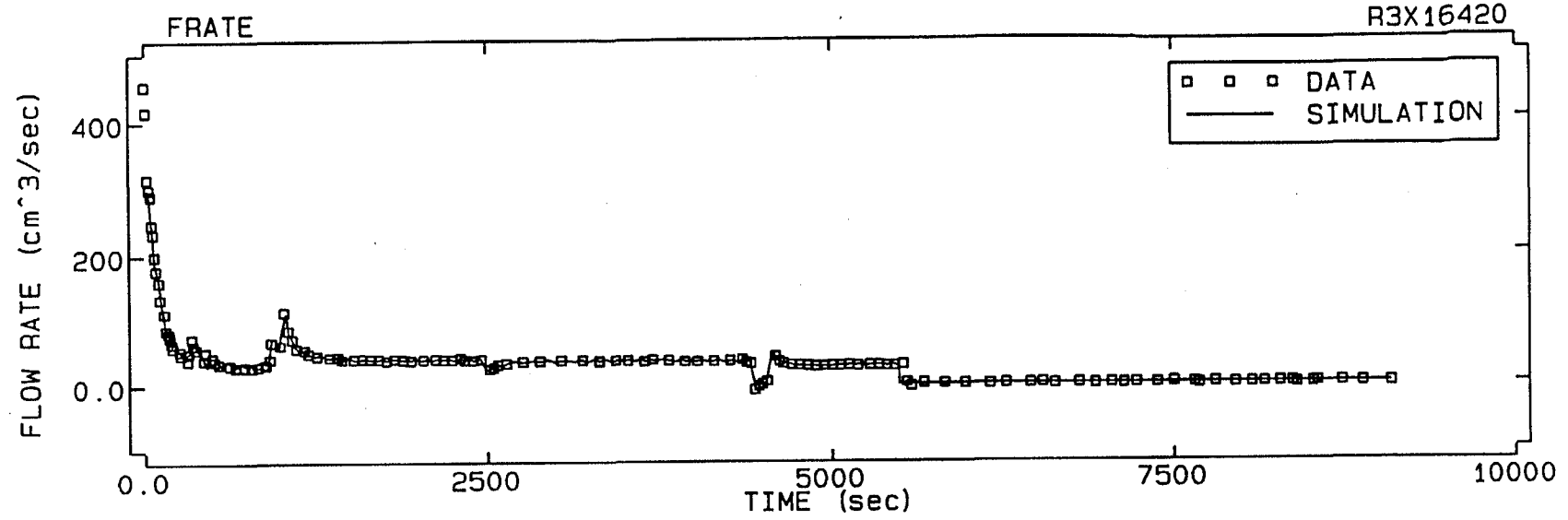


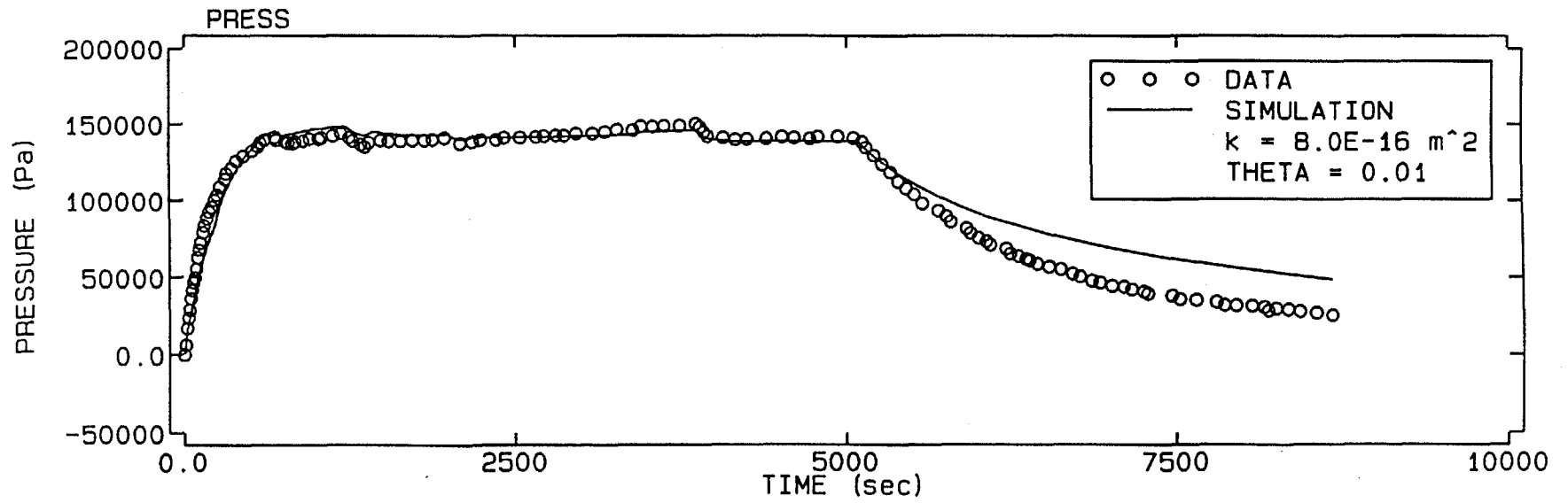
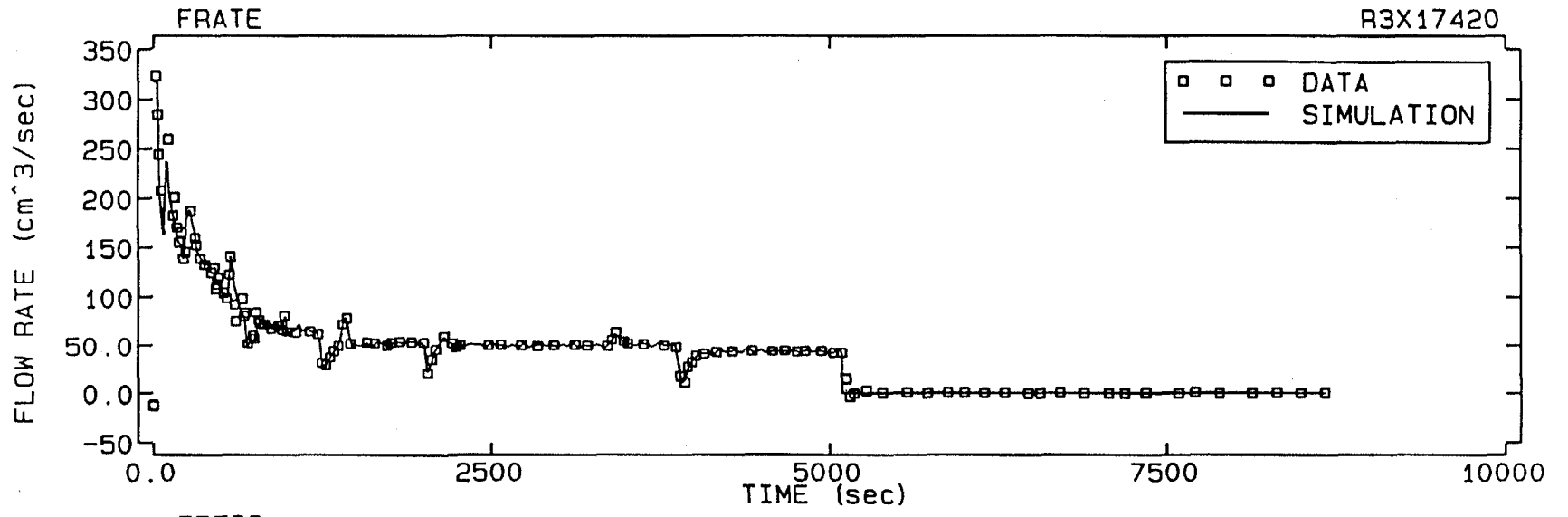


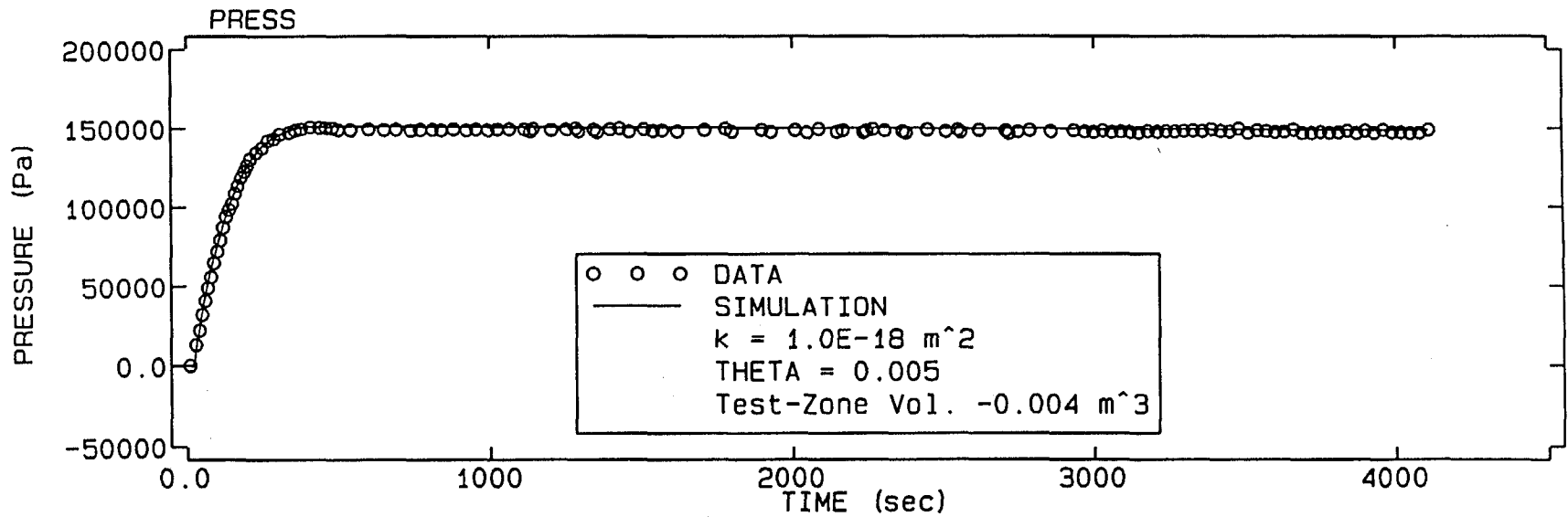
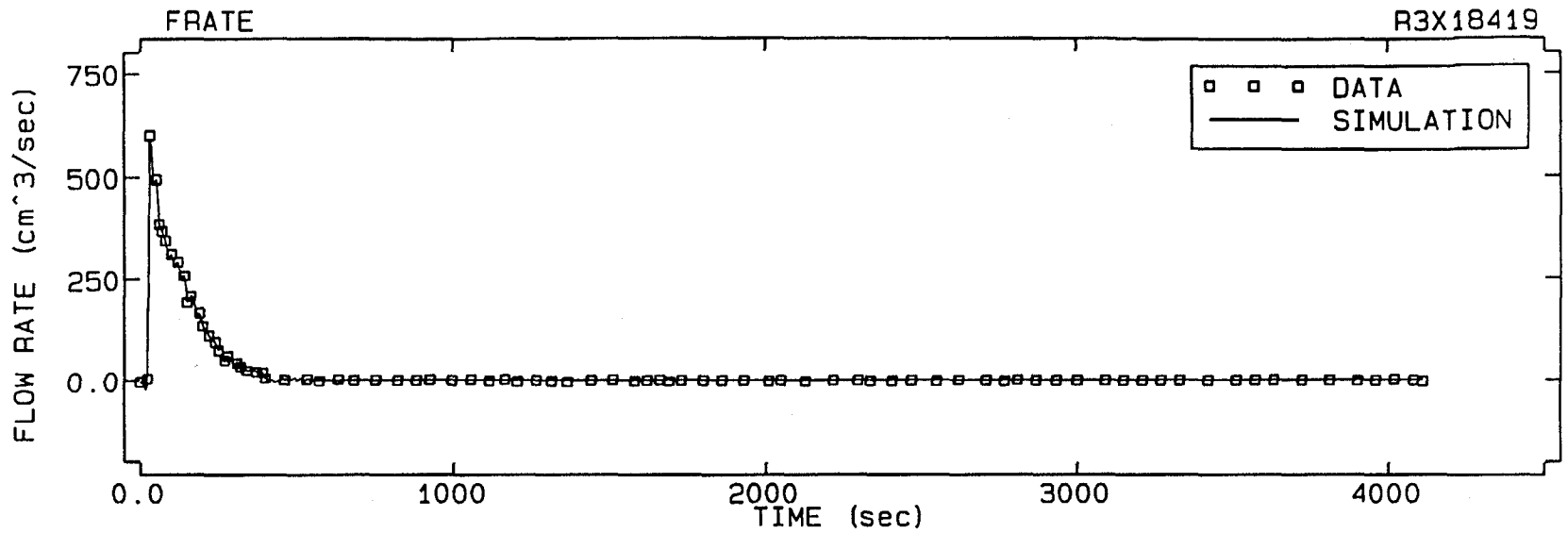


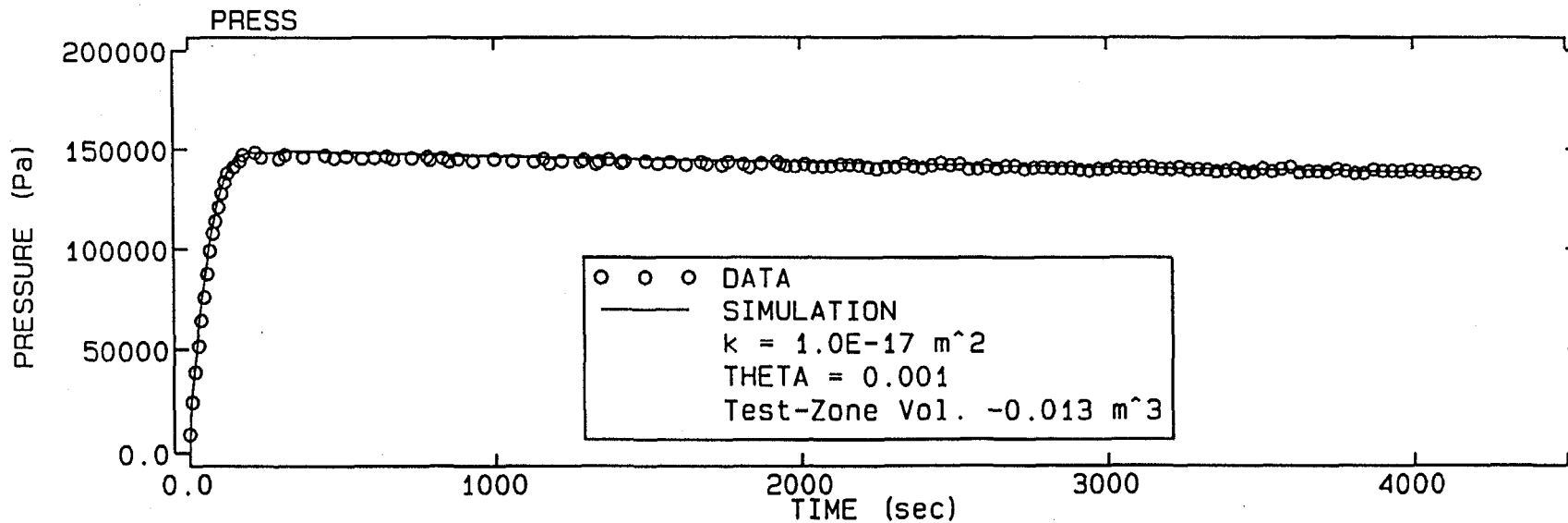
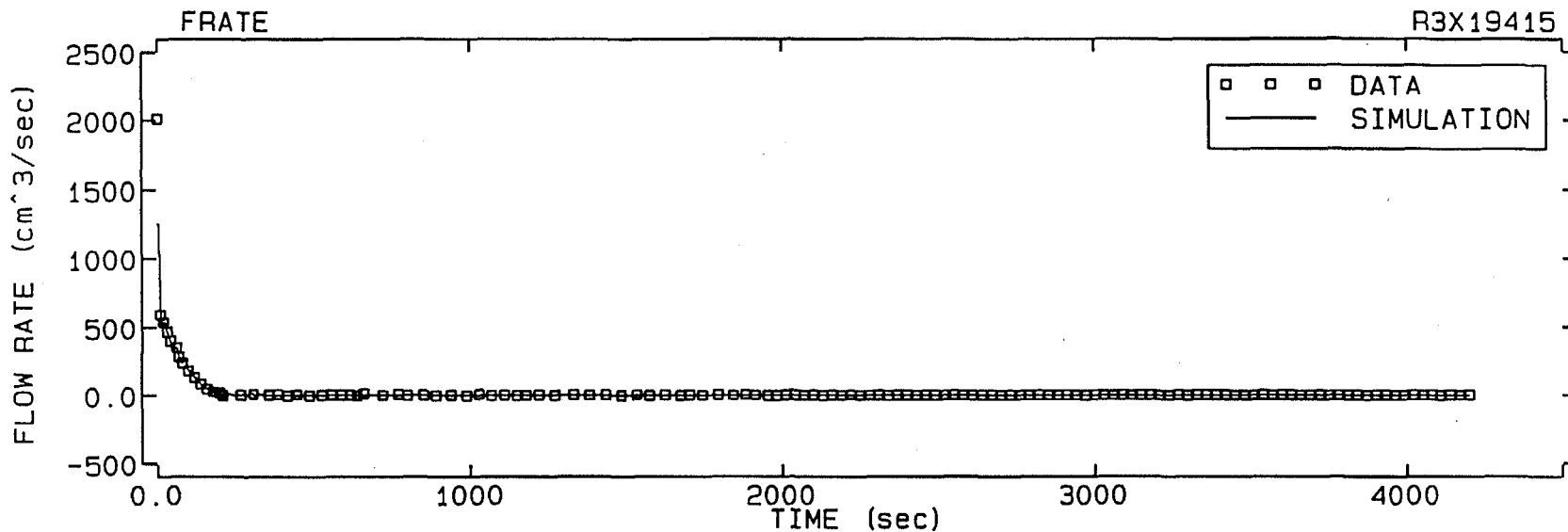


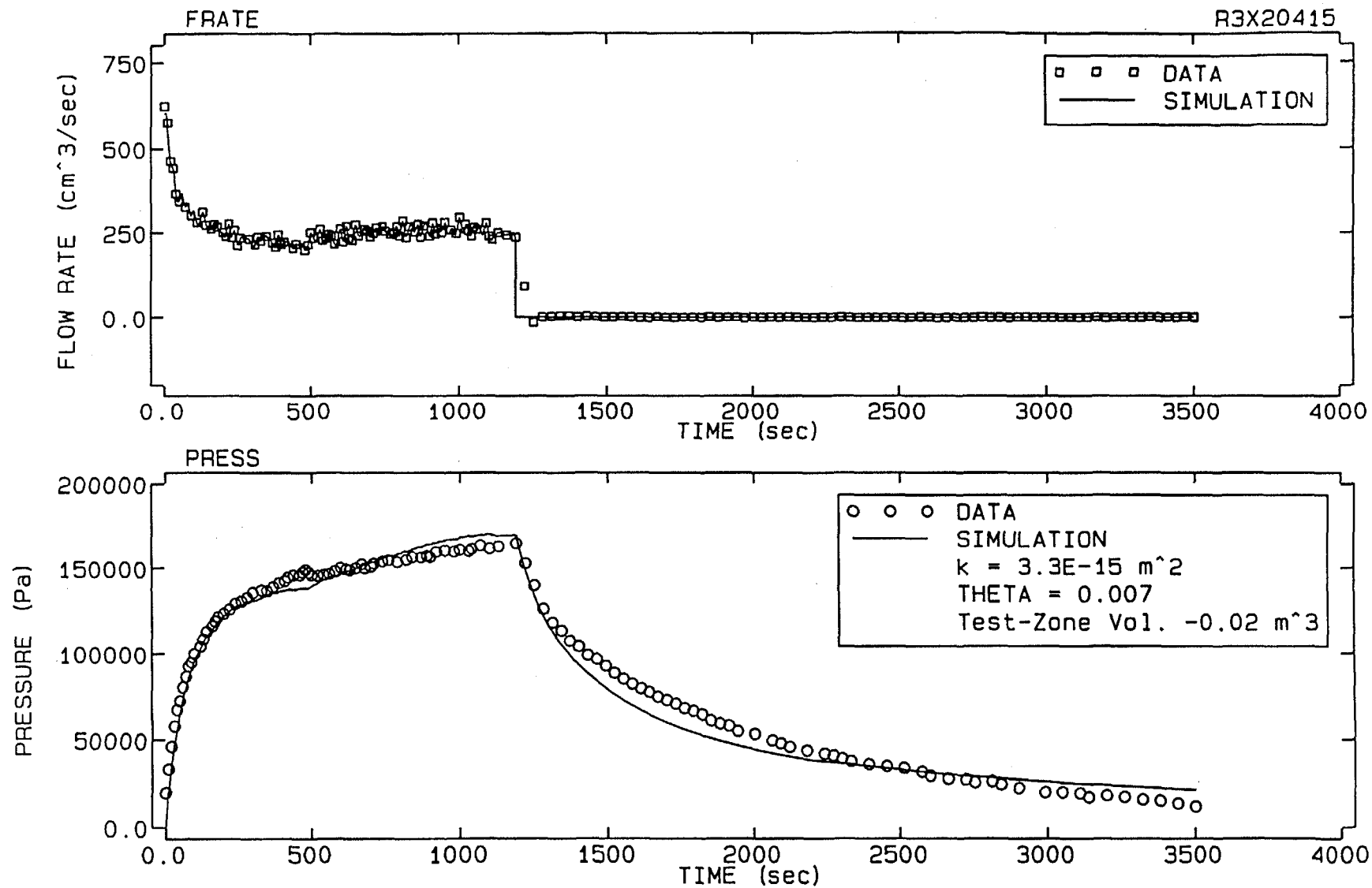


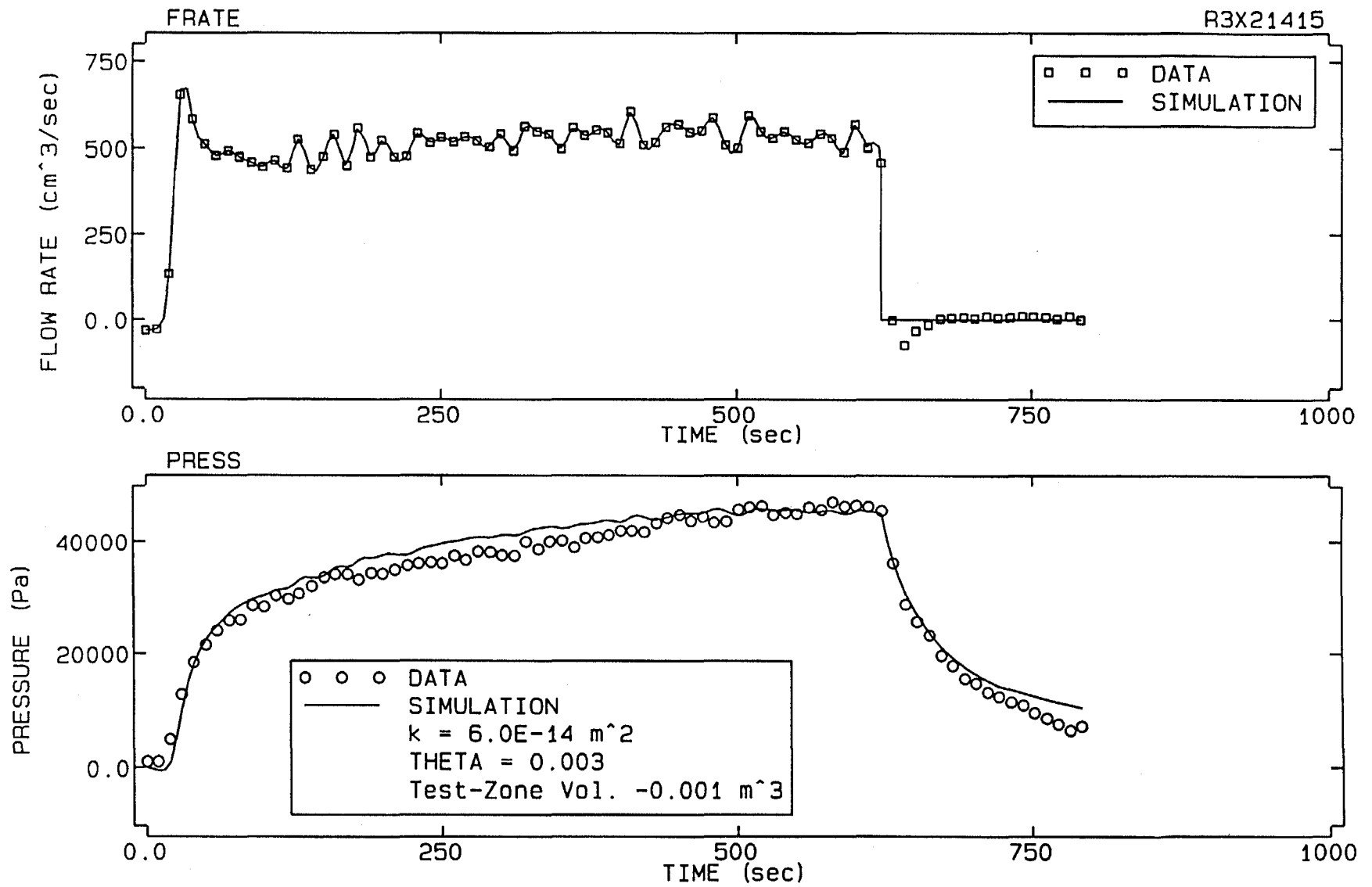






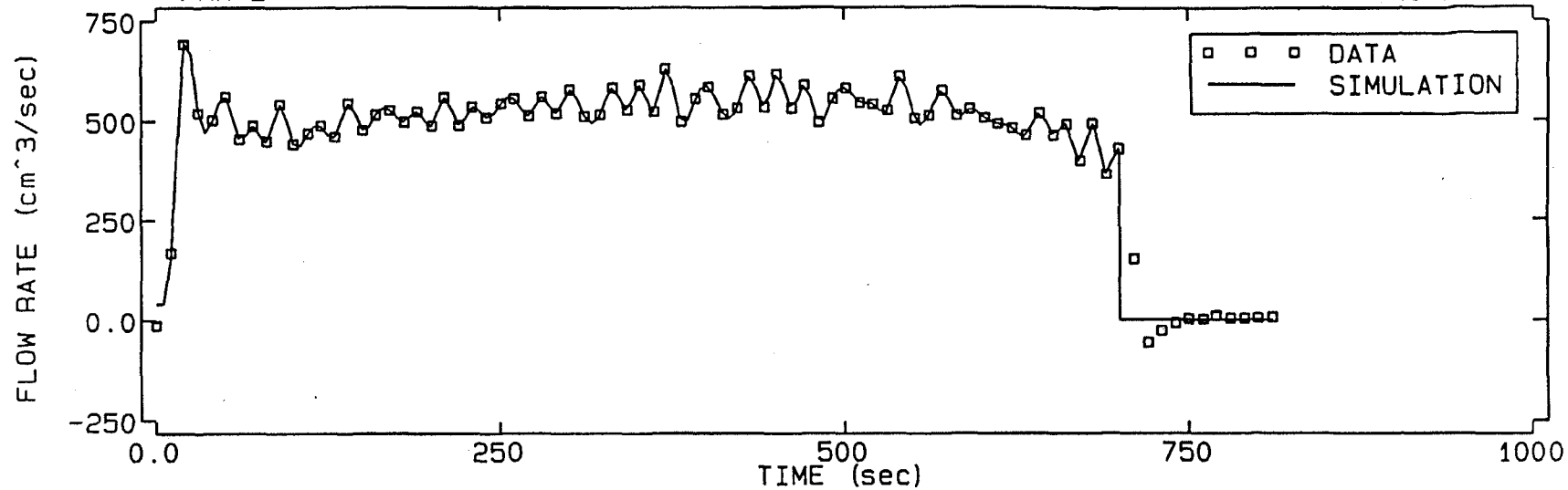




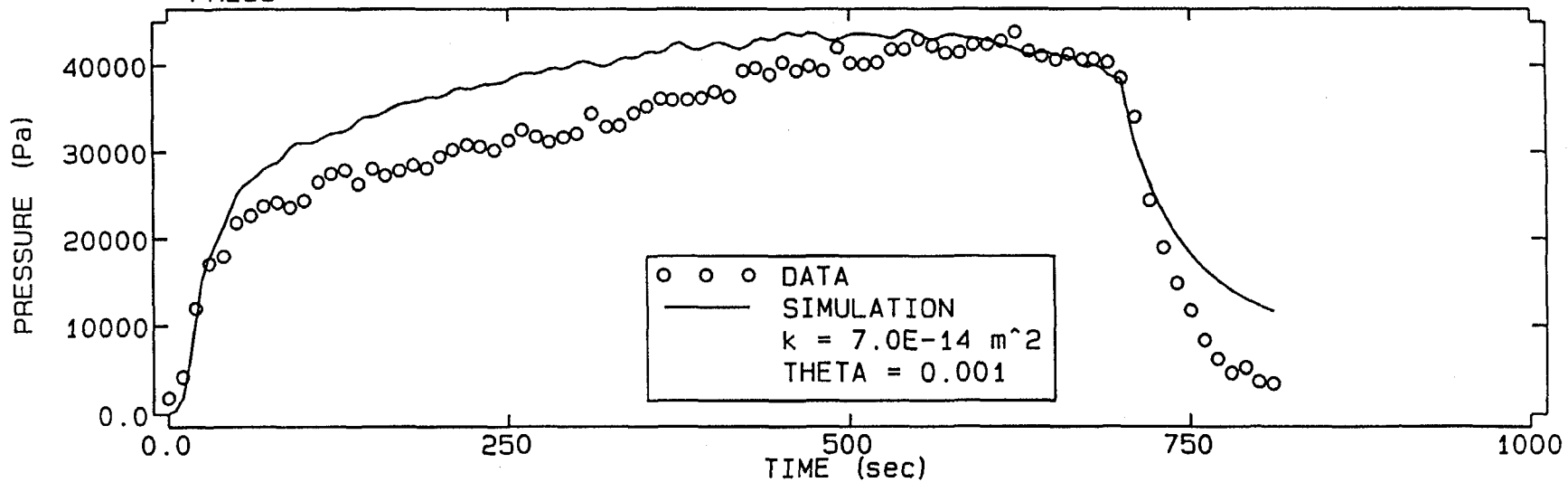


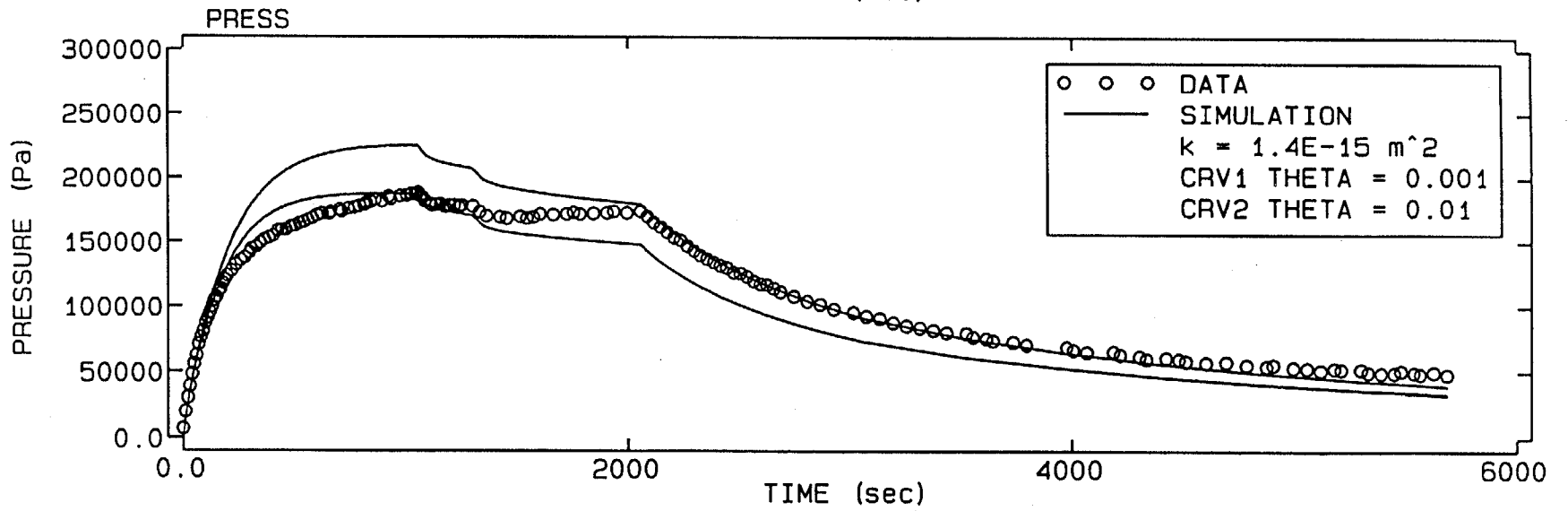
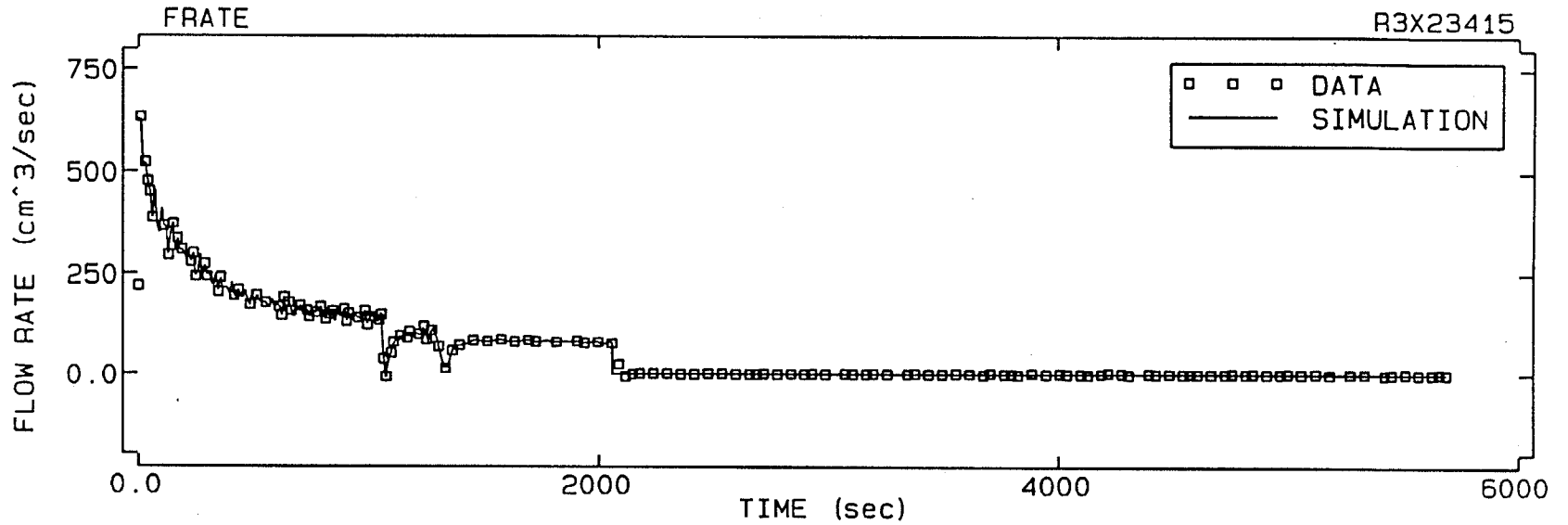
FRATE

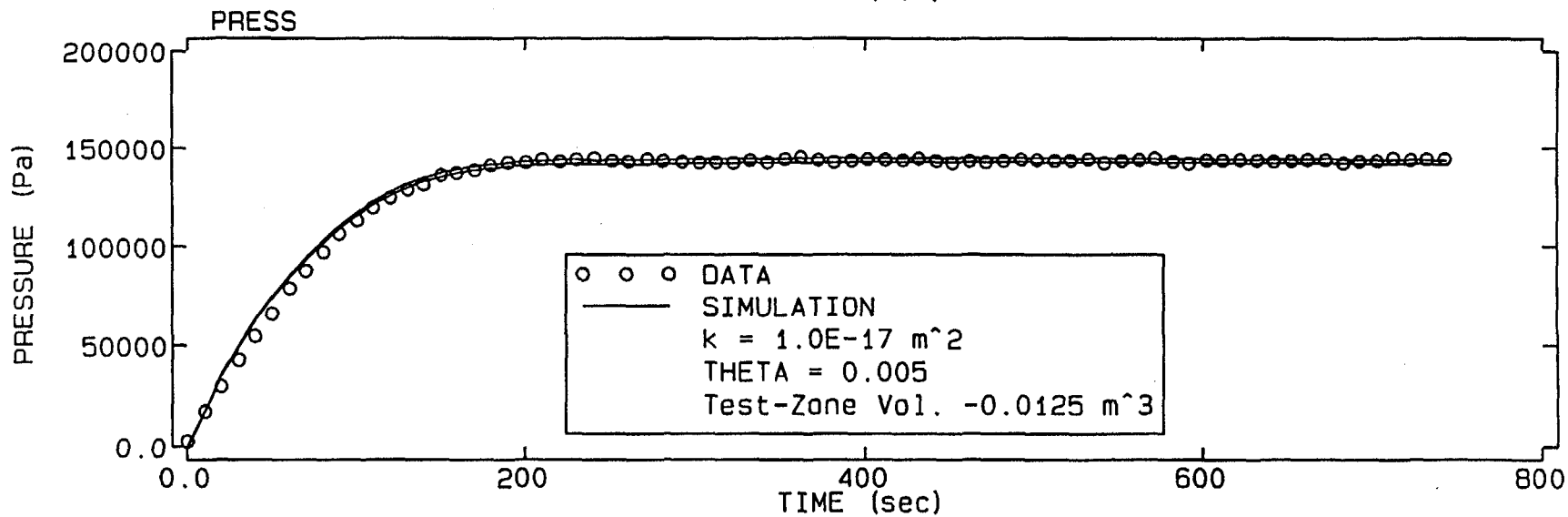
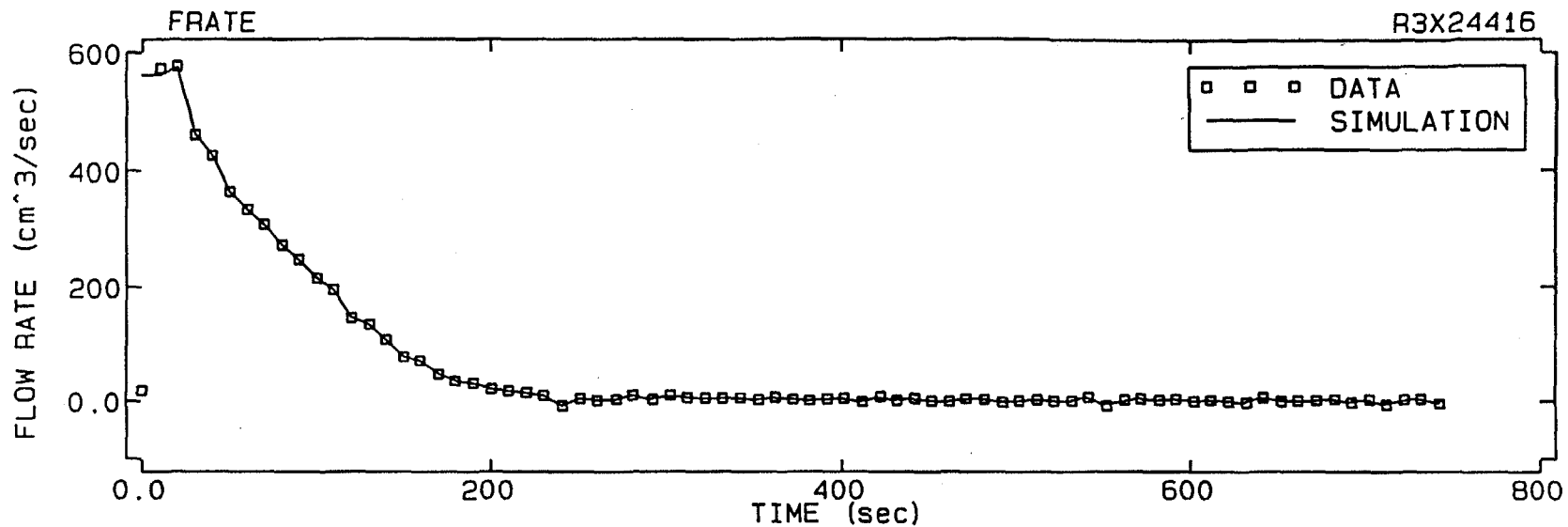
R3X22415

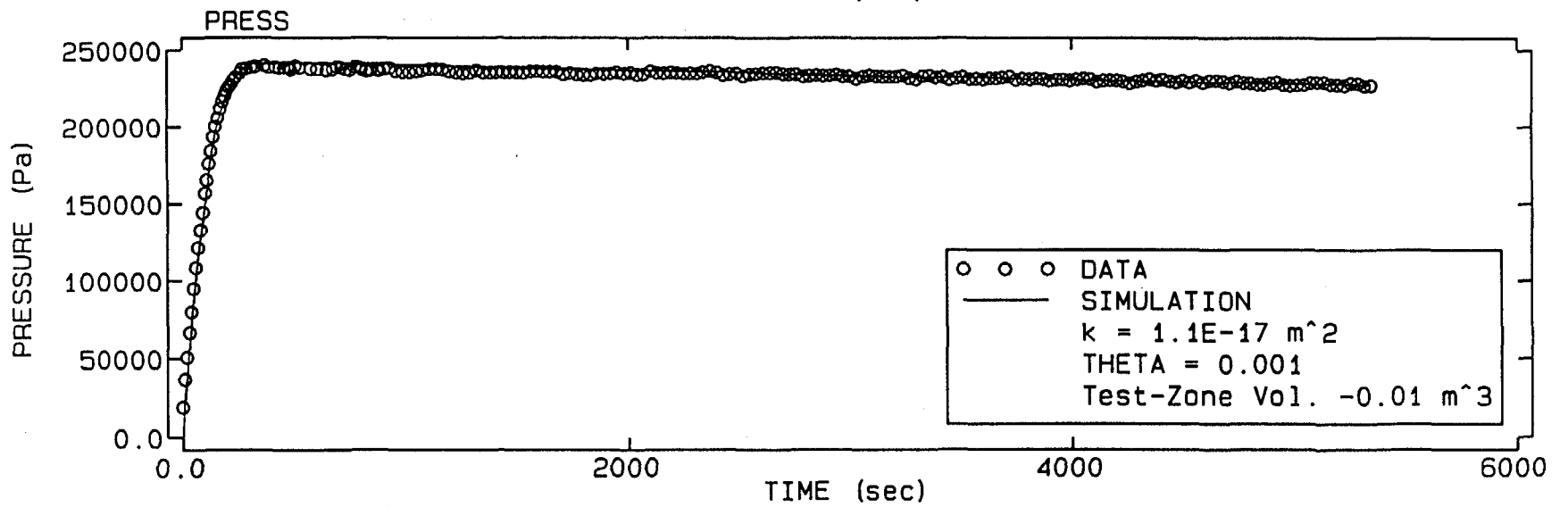
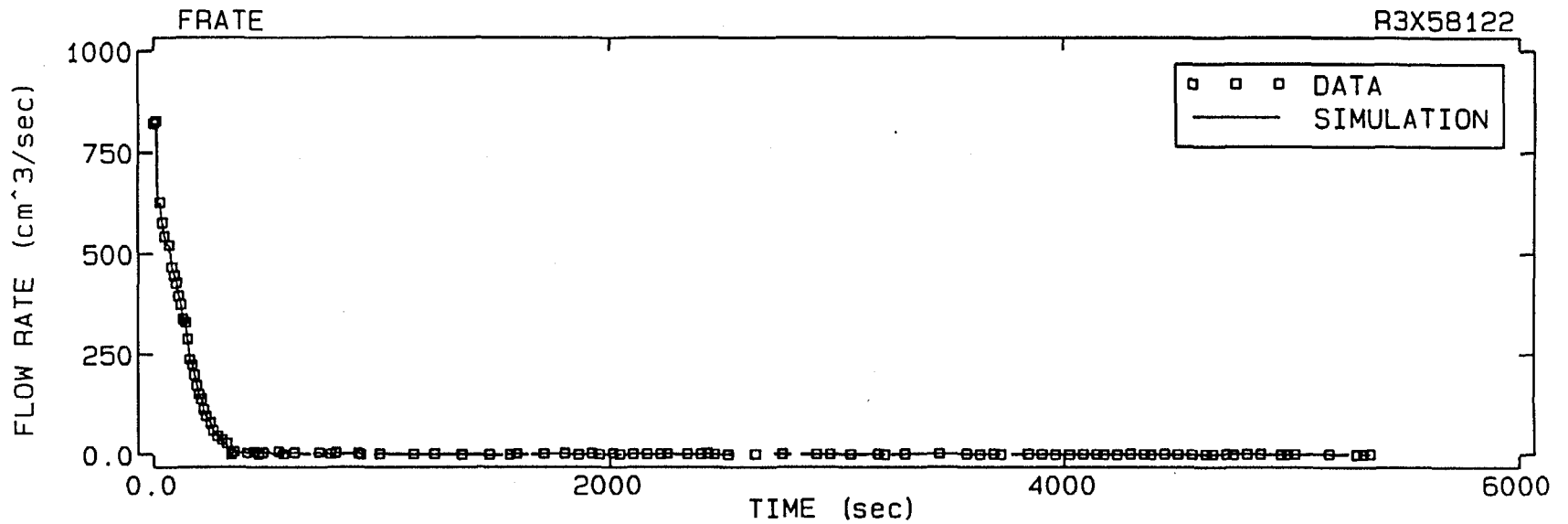


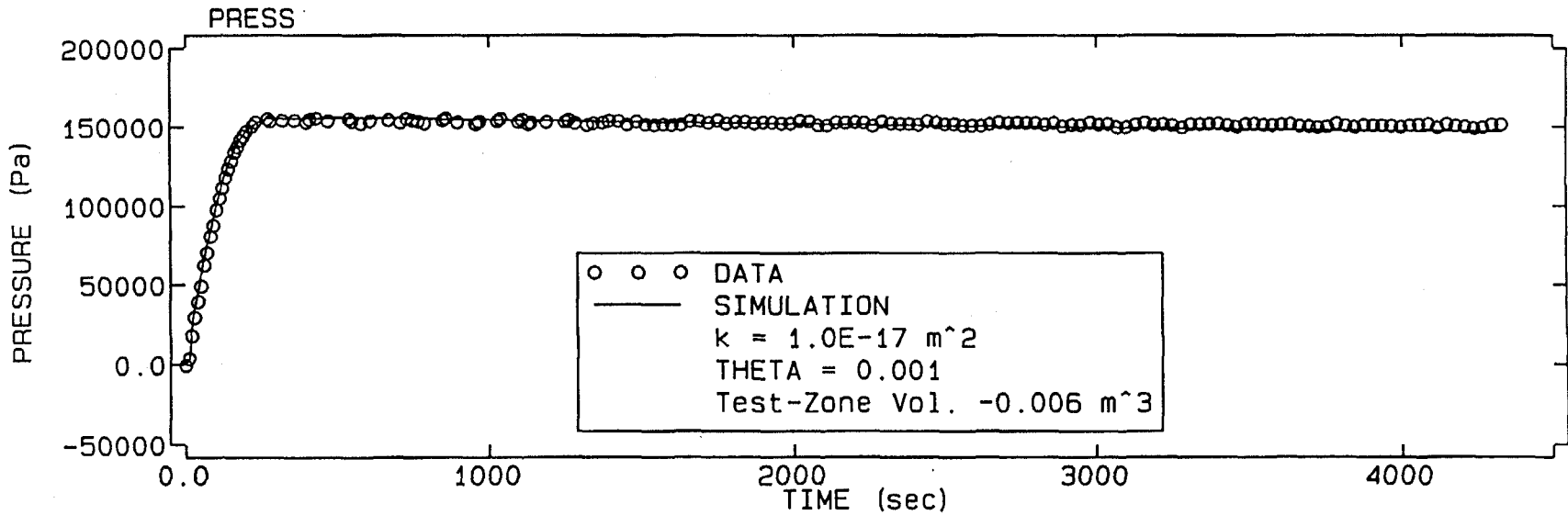
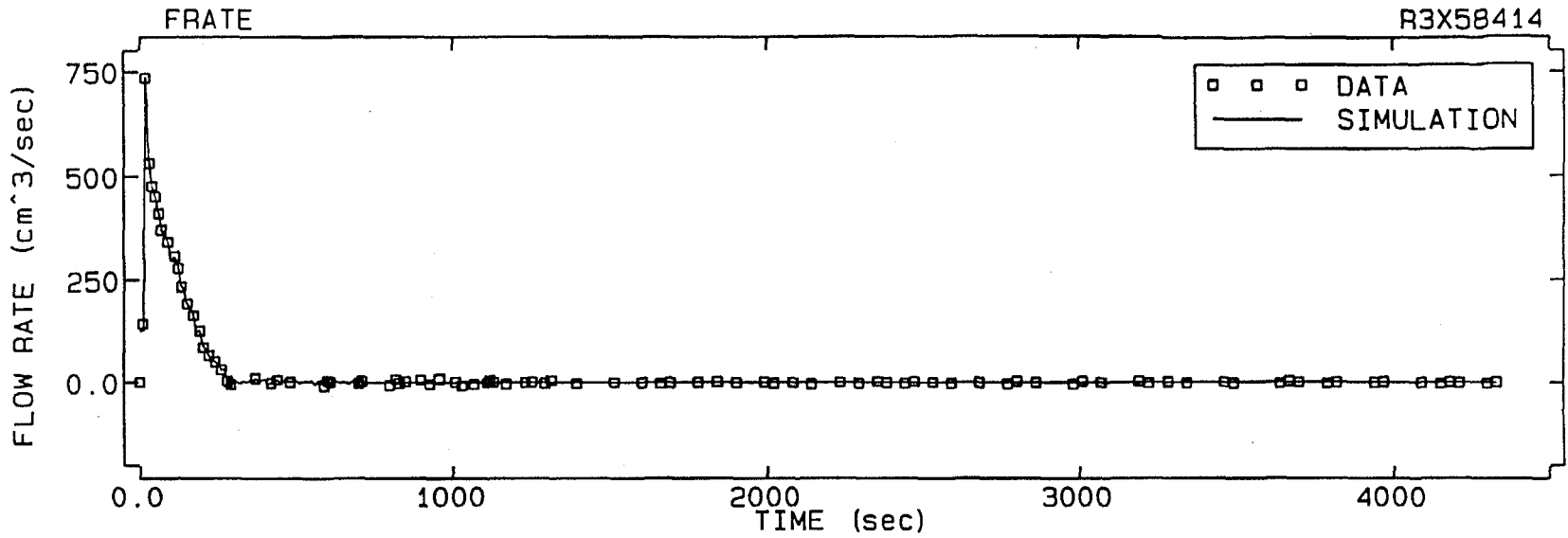
PRESS

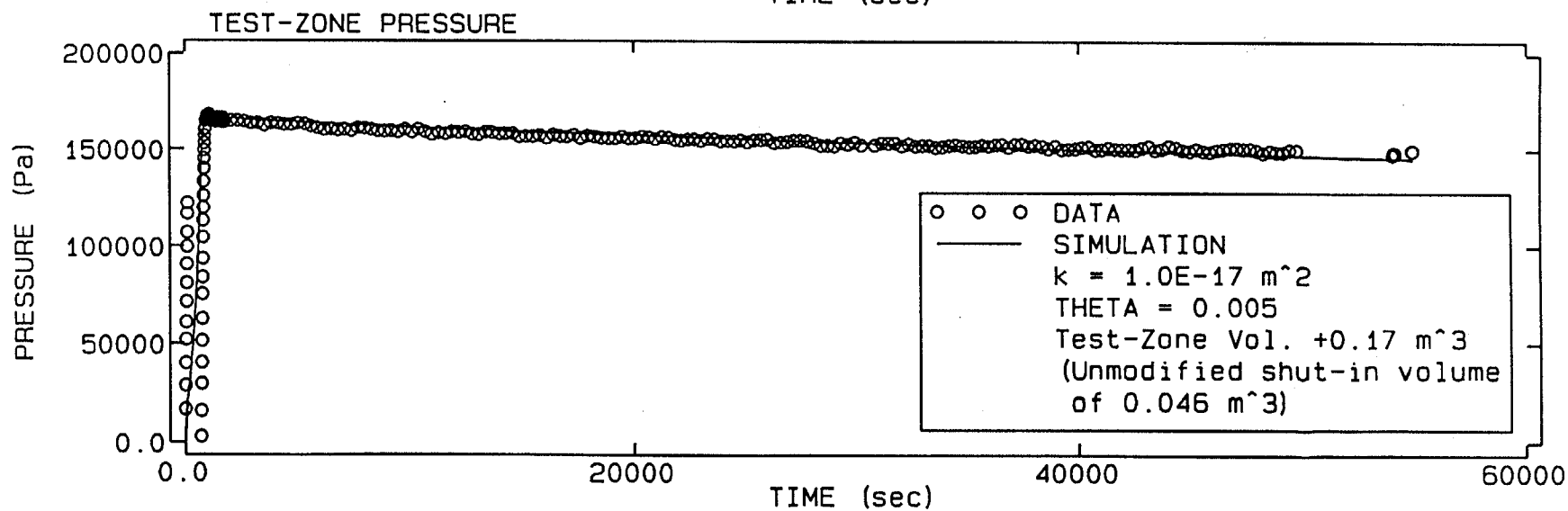
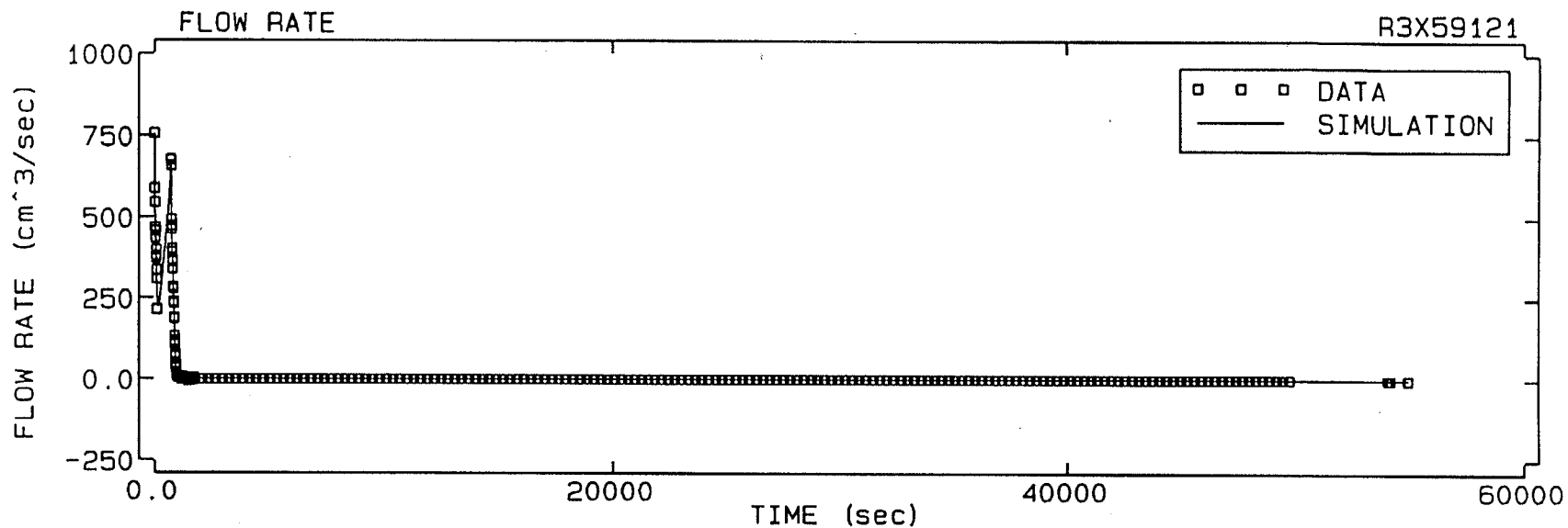


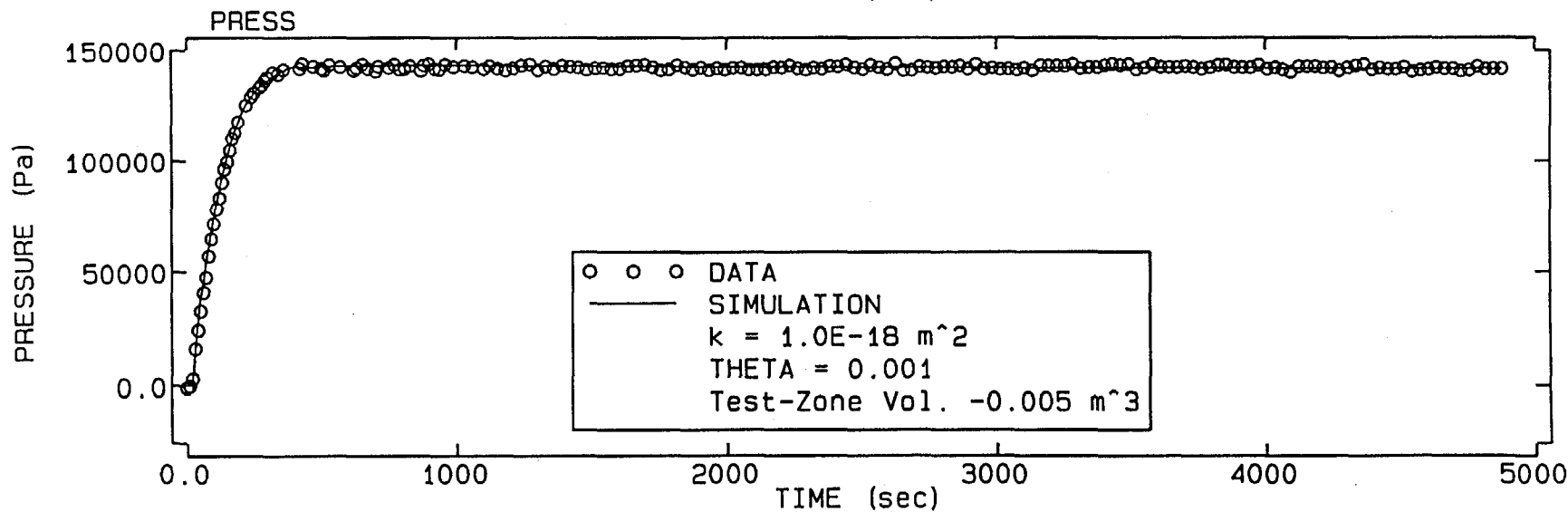
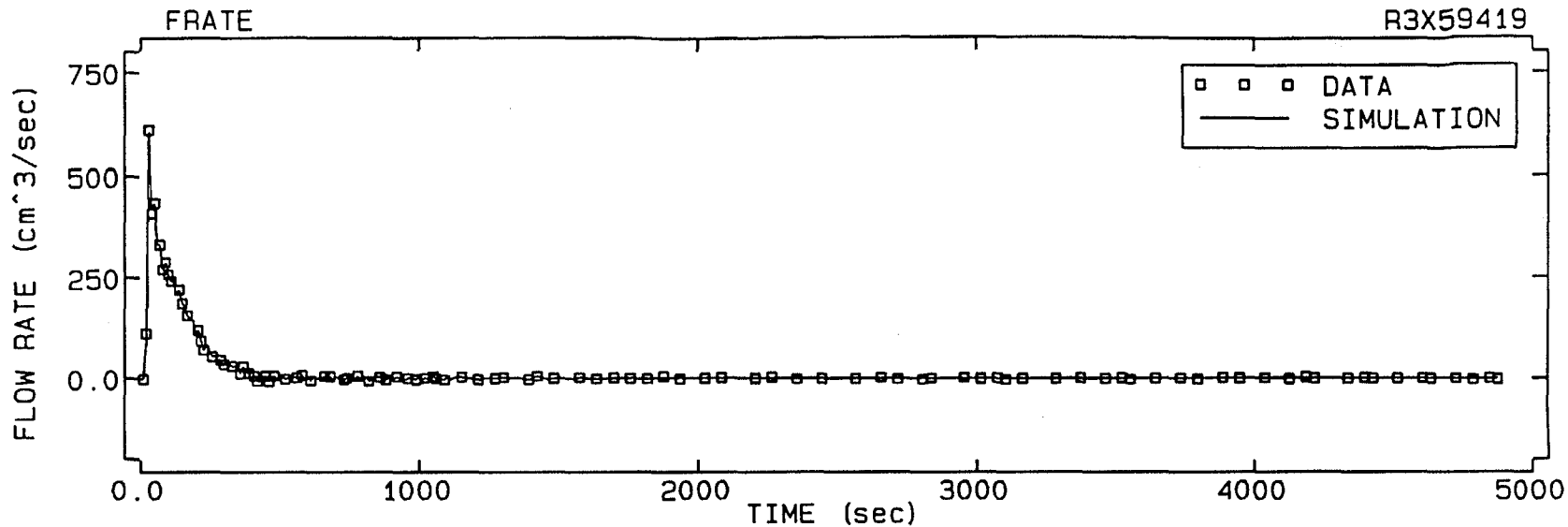


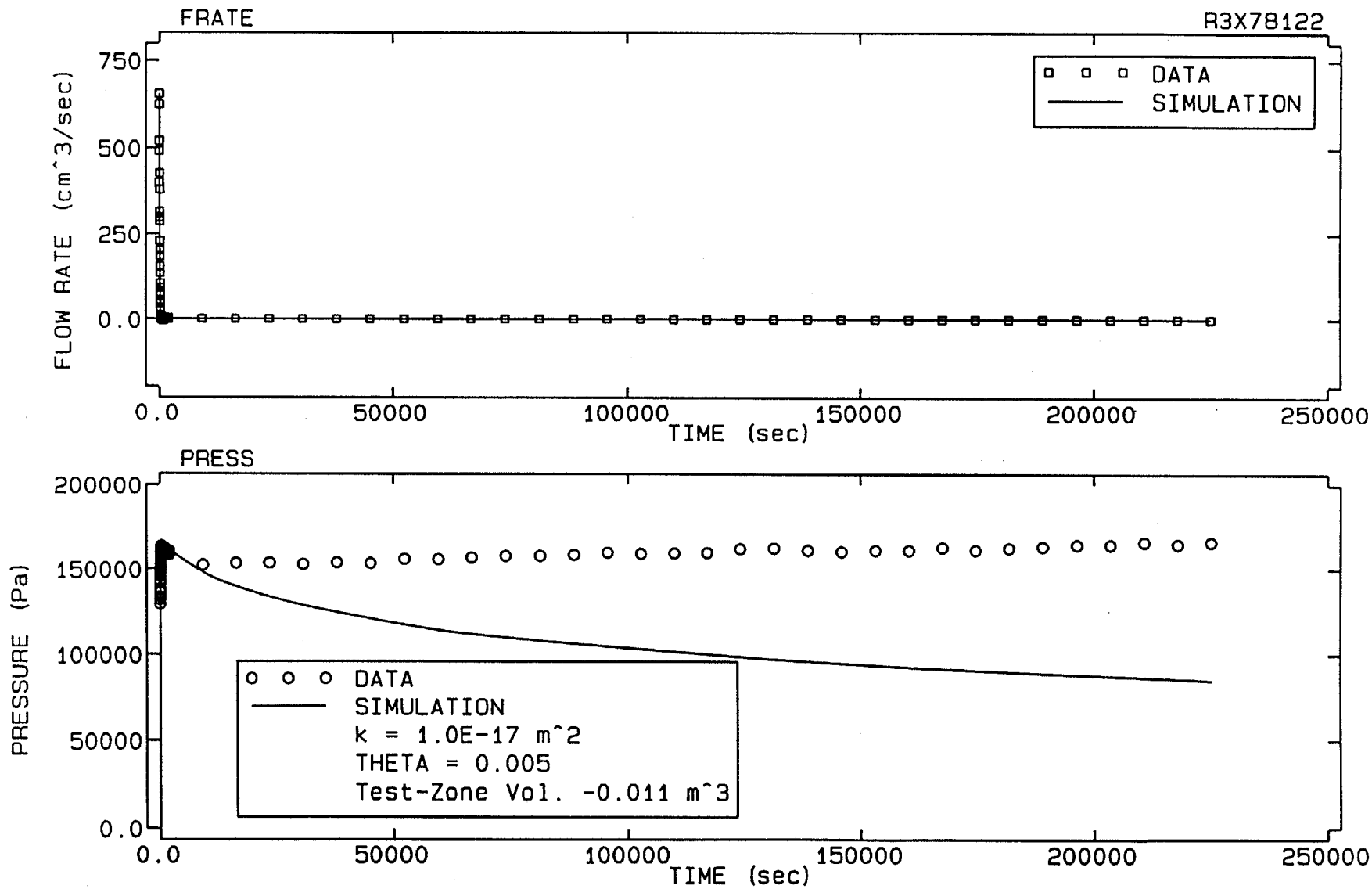


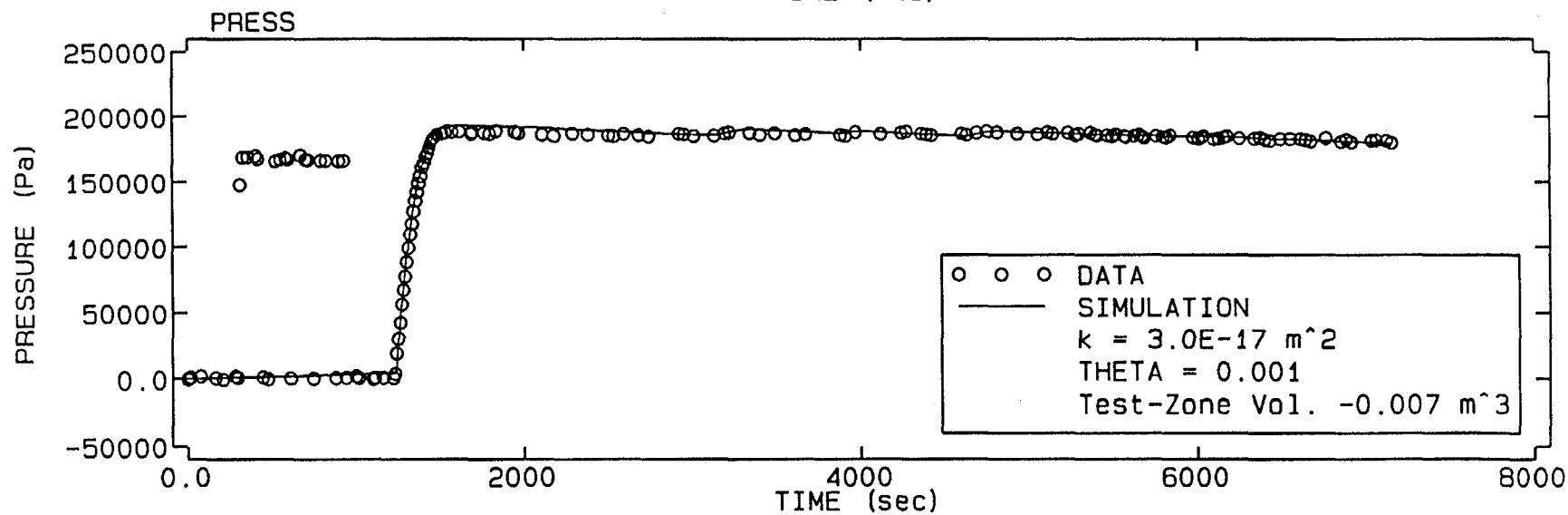
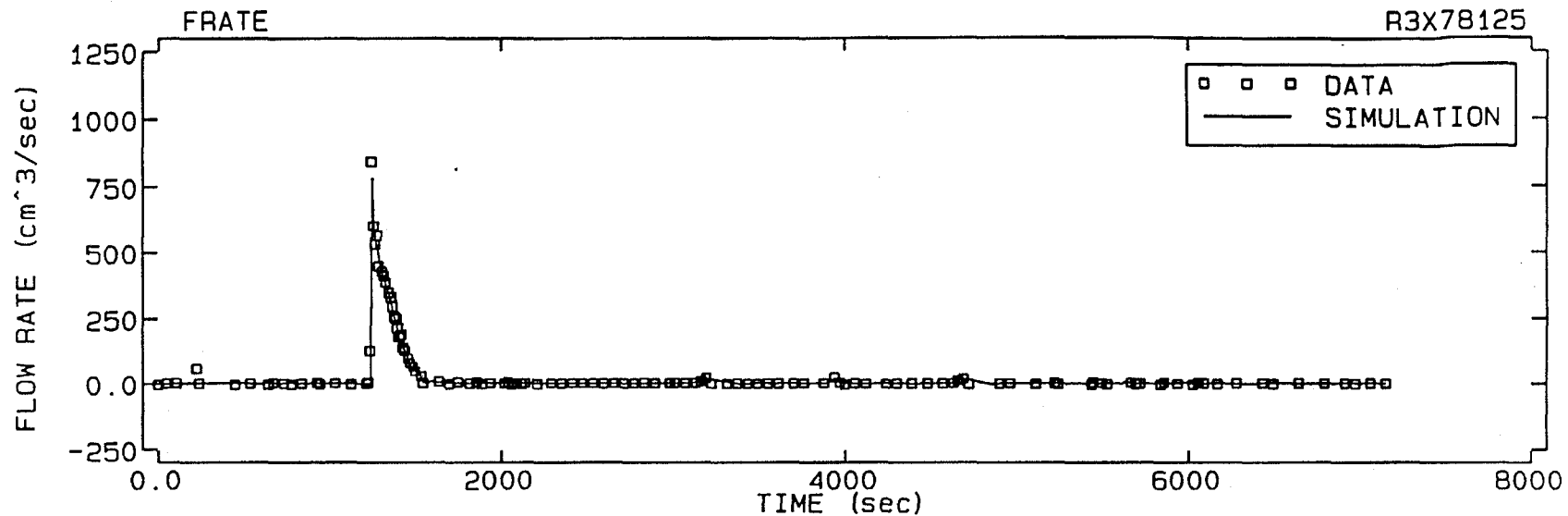


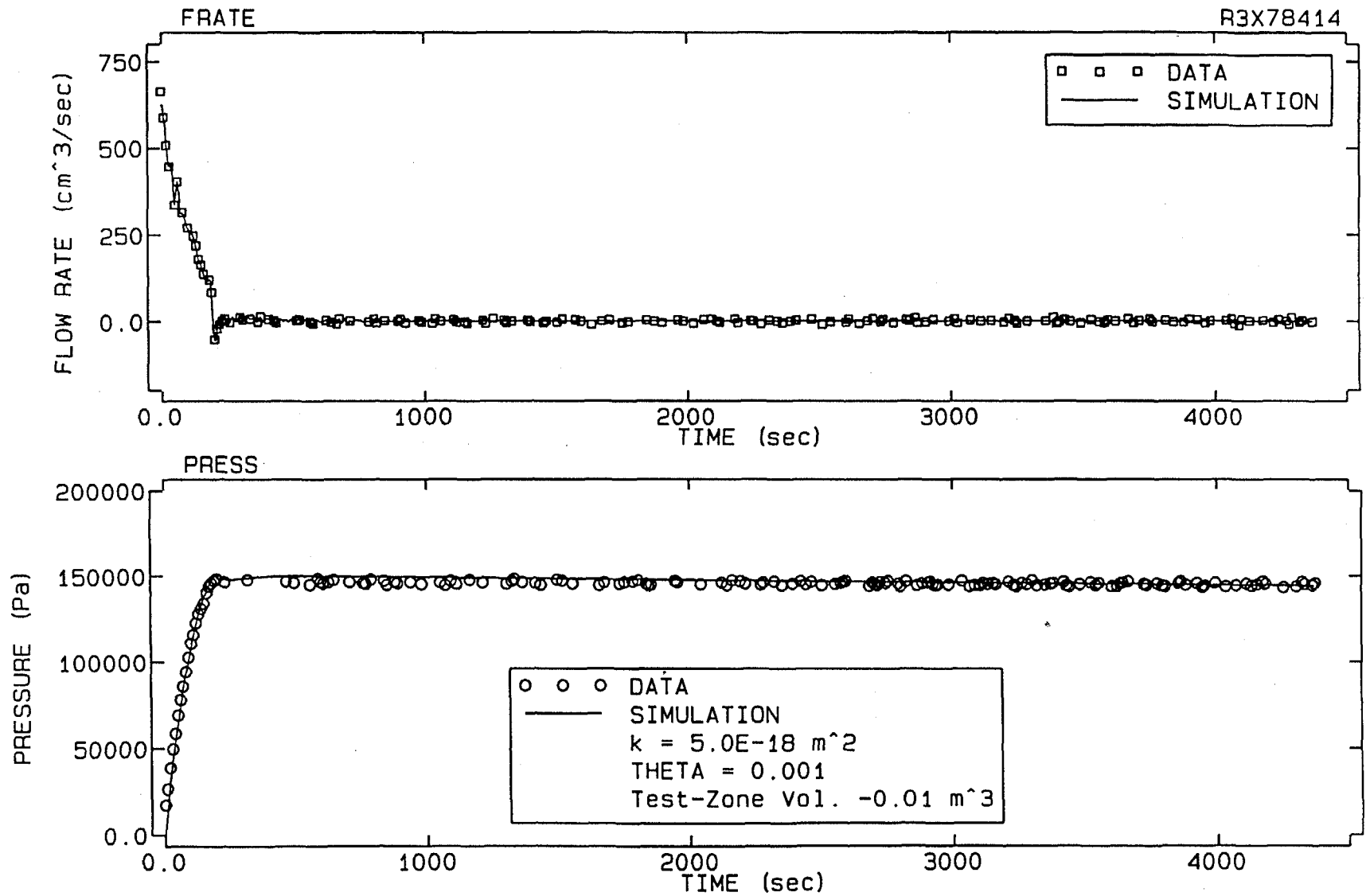


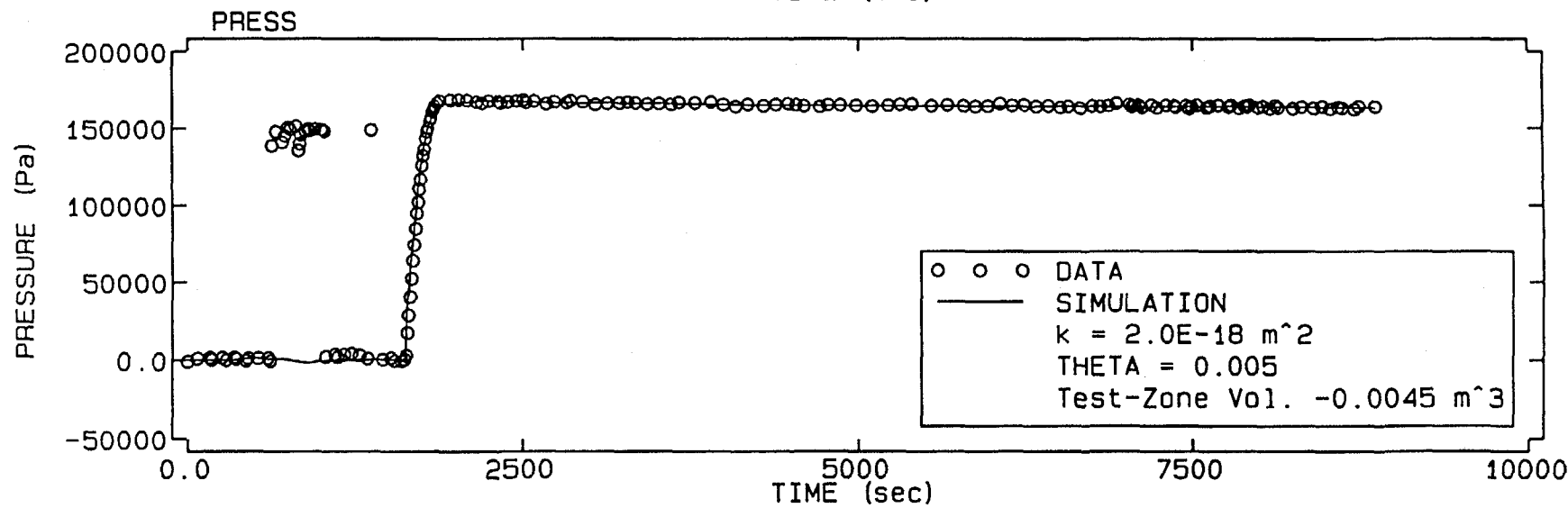
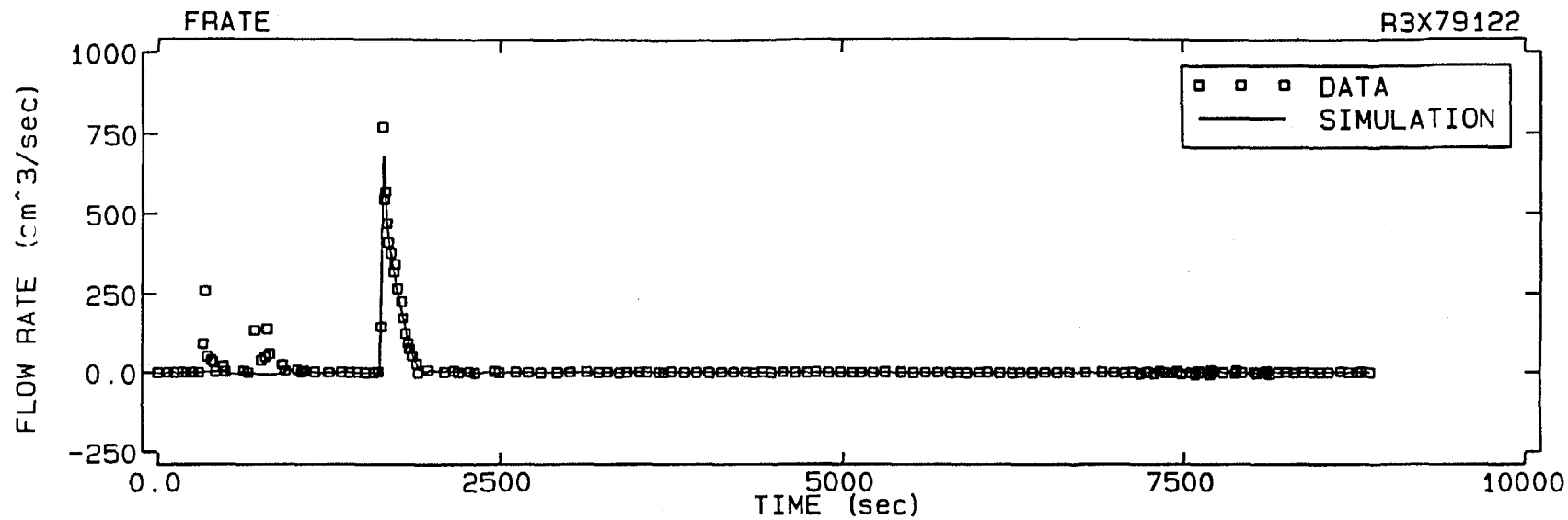


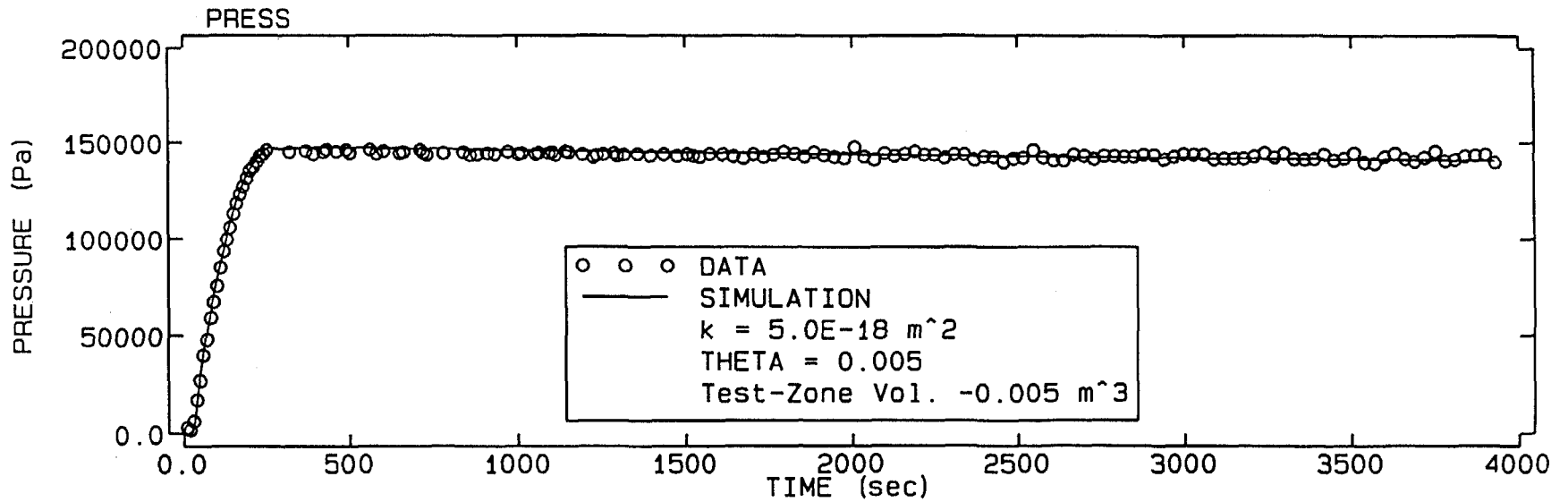
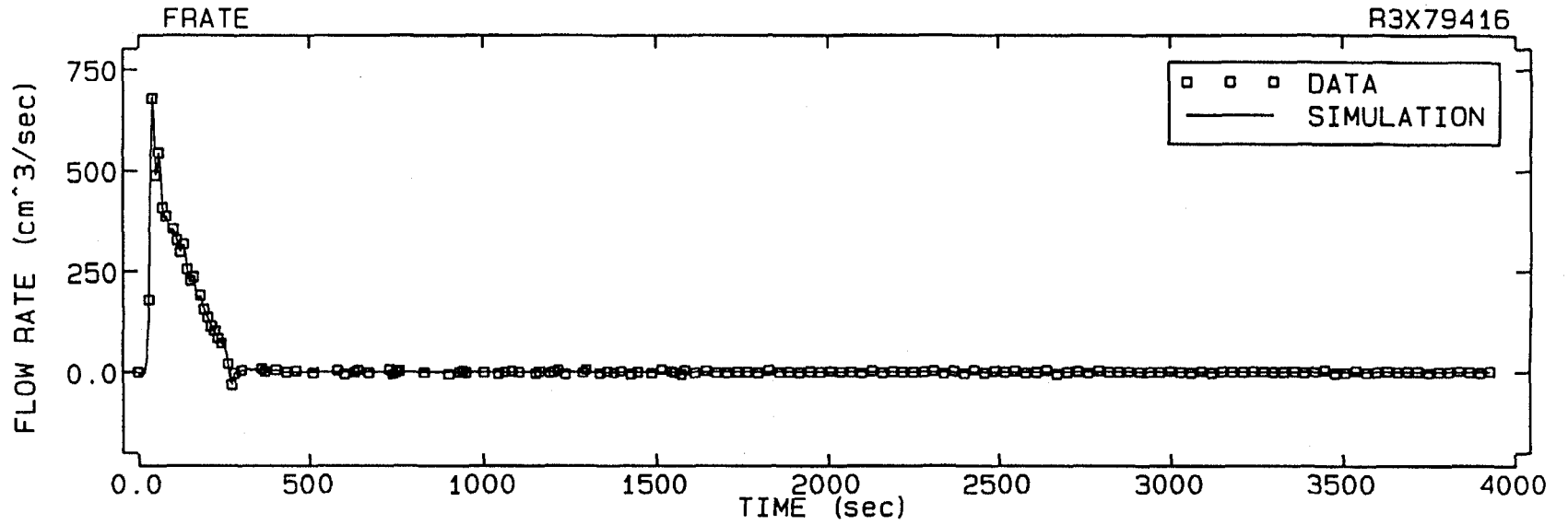


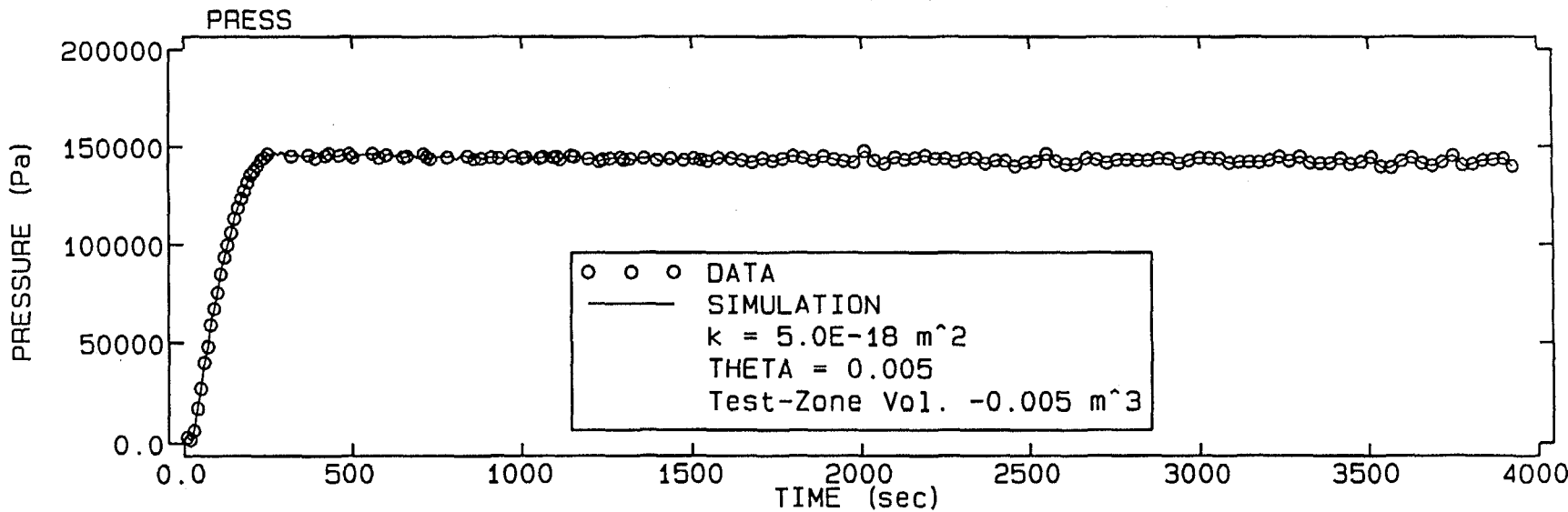
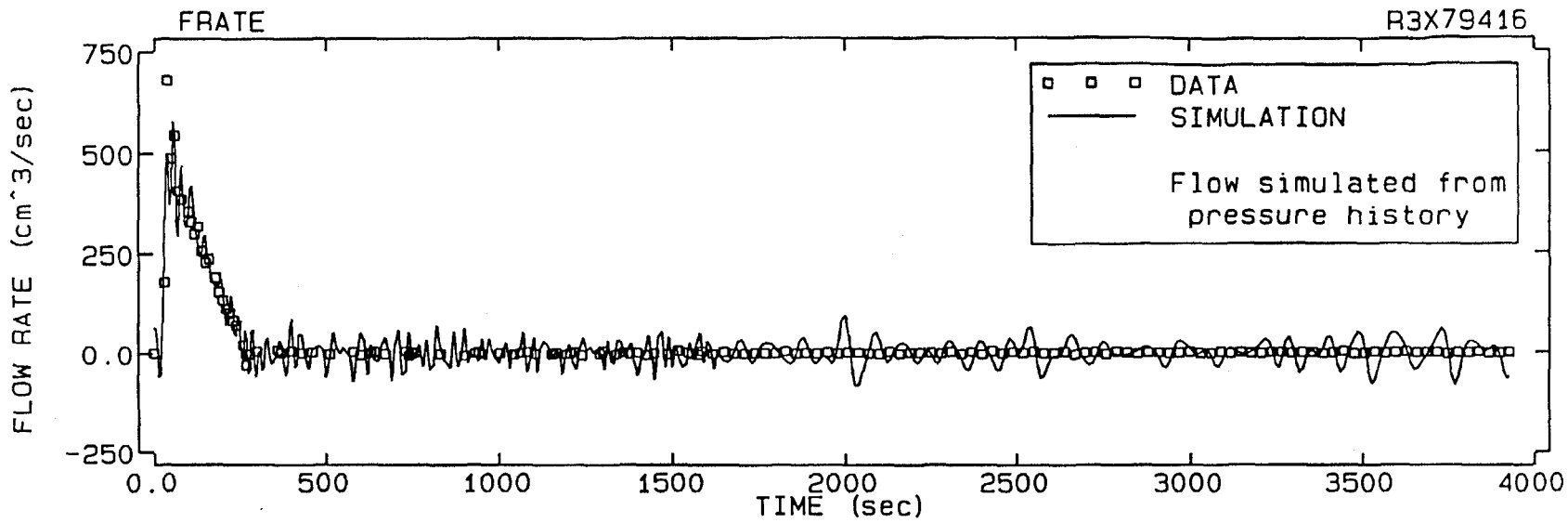


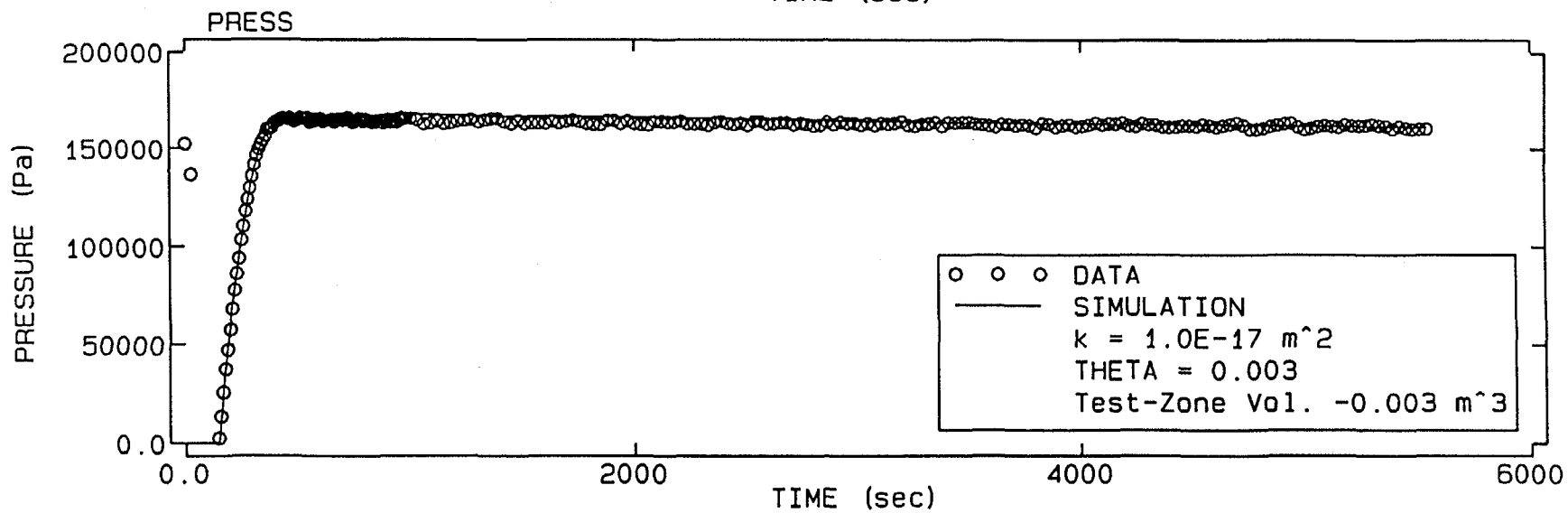
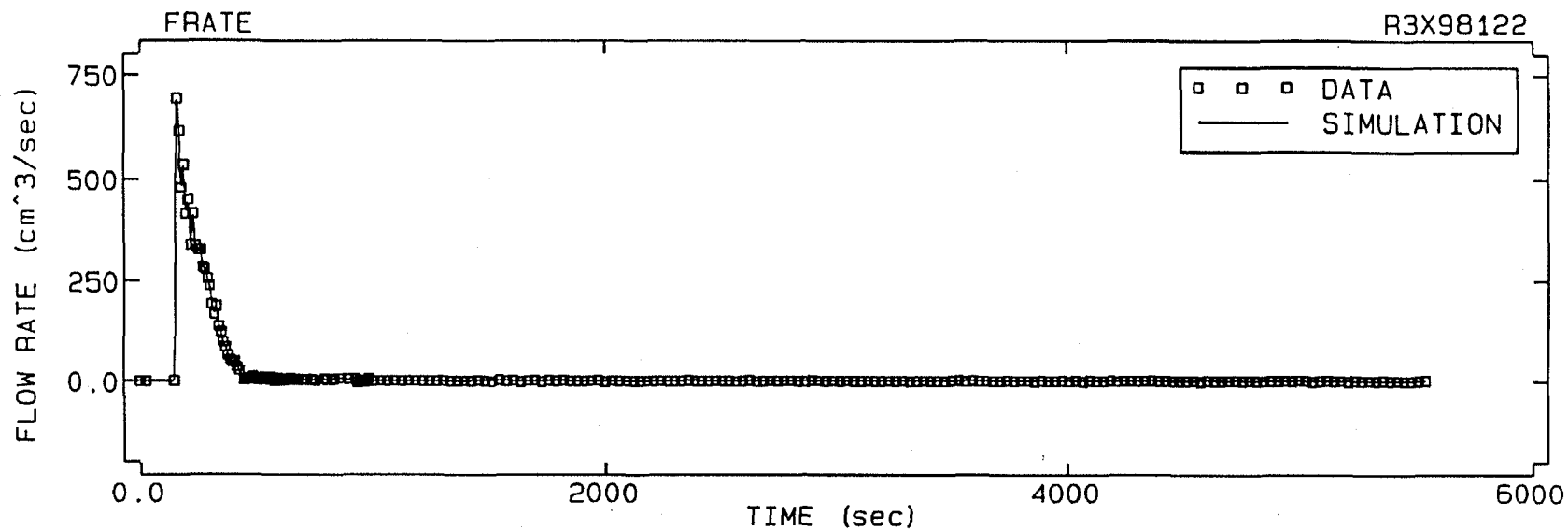


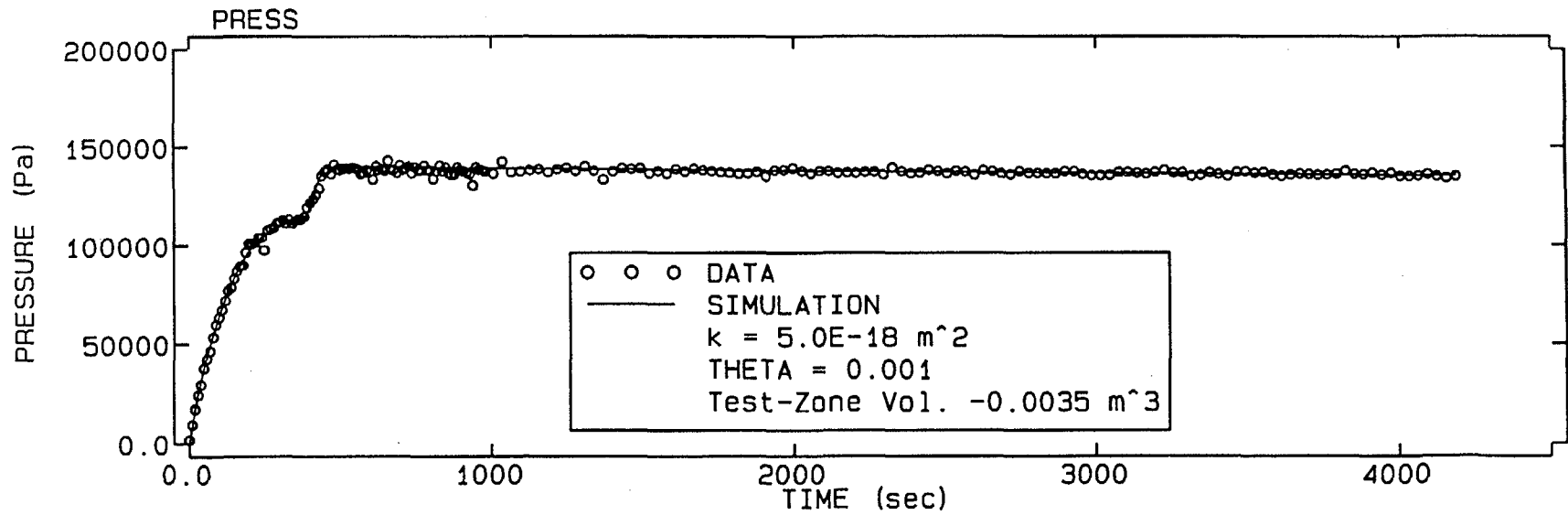
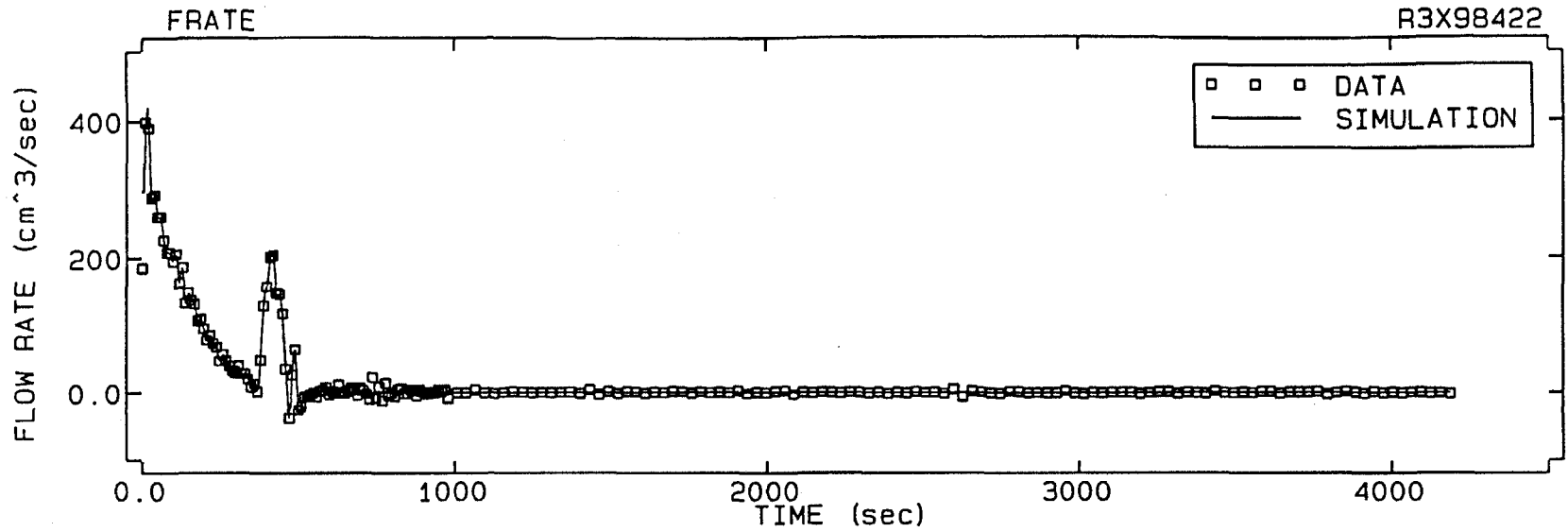


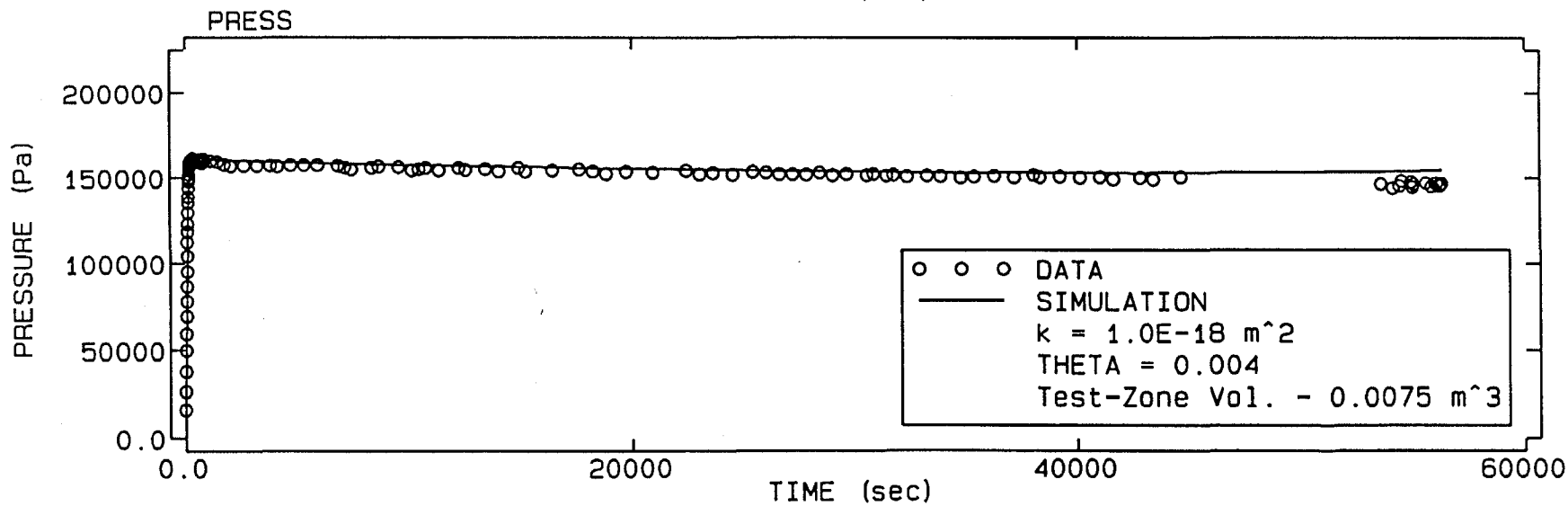
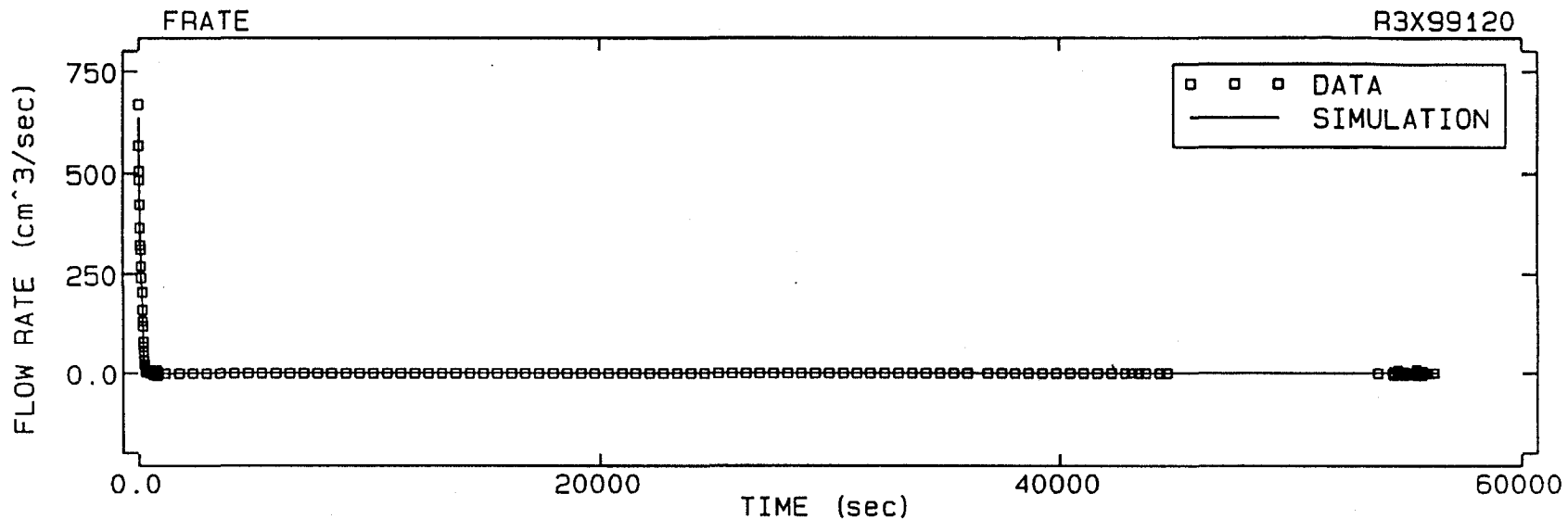


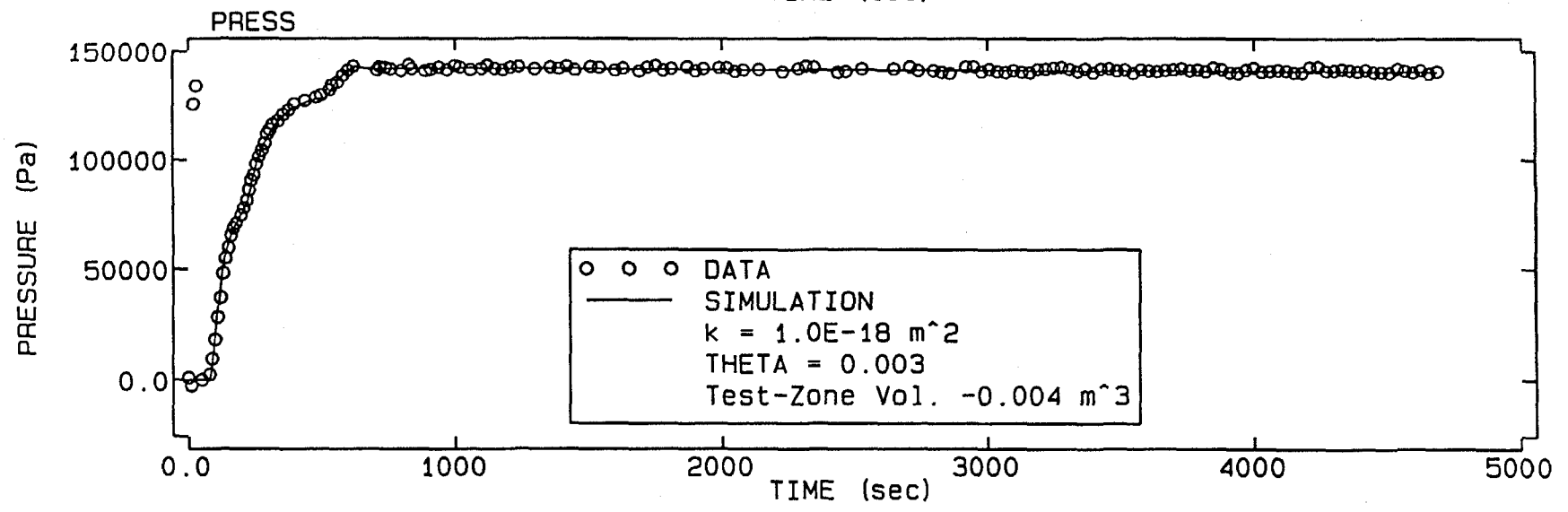
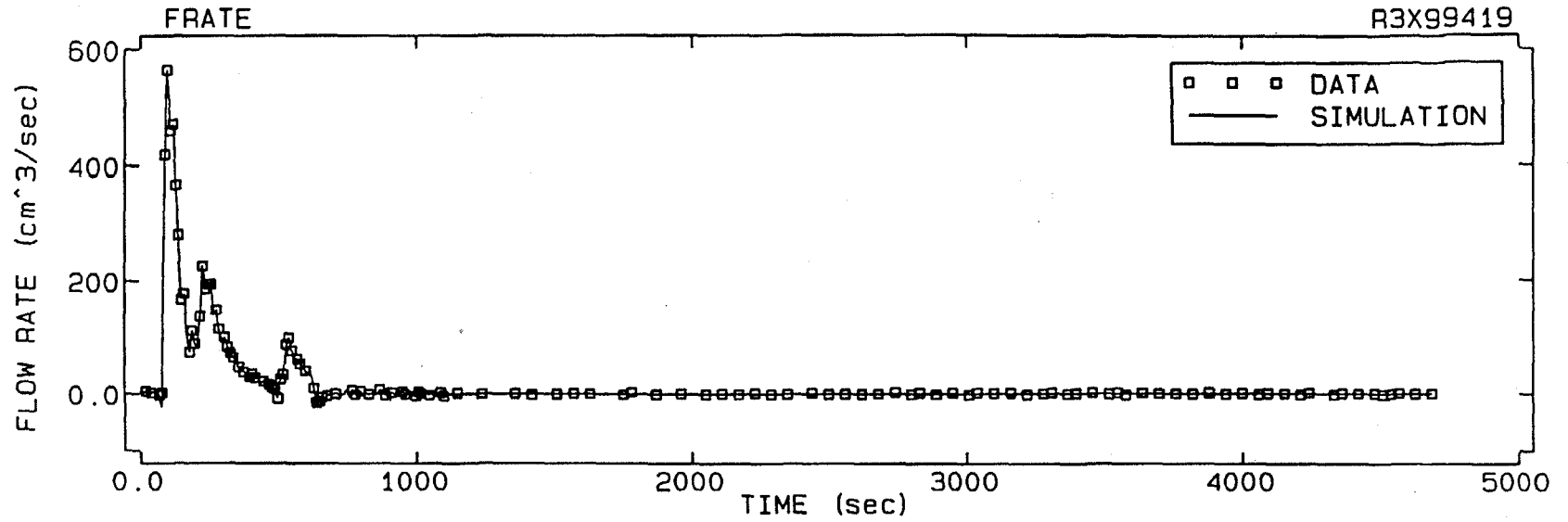






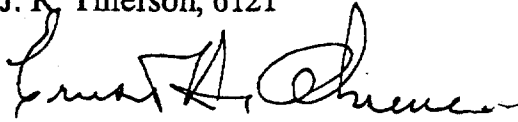






date: August 11, 1992

to: J. R. Tillerson, 6121




from: E. H. Ahrens, 6121


subject: Selection of Site for Grouting Experiment at the WIPP


A meeting was held today in the office of Organization 6121 at Sandia National Laboratories. This meeting, attended by Joe R. Tillerson, Scott Van Pelt (Intera), David Borns, 6116 and Ernst H. Ahrens, 6121, was held to finalize the exact location of the grout injection experiment.

Gas transmissivity has been determined by Mr. Van Pelt in the 20, vertical, diamond drill holes drilled through Marker Bed 139 below the floor of Room L3 at the WIPP (see attached Intera memorandum and sketch). Although additional data reduction will be accomplished prior to the issuance of a more detailed memo, his data on gas transmissivity convinced everyone present that the northern slab location is suitable for the grouting experiment. David Borns reported on electrical, geophysical survey results in Room L3 and essentially stated that the geophysical survey (see attached sketch) corroborates the gas flow information obtained by Van Pelt.

The decision was to situate the grout test in the northern position in Room L3 and to obtain the detailed memos on gas flow and geophysics as soon as they are available (estimate is approximately two weeks). These detailed memos will be filed, with this memorandum) in File 540, Organization 6121.

CONCURRENCE: Joe R. Tillerson 

Scott Van Pelt 

David Borns 

Copy to:
6121 file 540

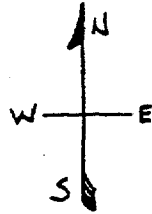
SSSPT-F

RSVP/INTERA
08/10/92

N₂ GAS FLOW RATES @ 20 PSIG (SCCM)

2E⁰ (14) 1.1E¹ (20) 2.9E¹ (21) 2.6E¹ (22) 1.1E² (23) 3.1E¹ (24)

10.4



1" = 10'

41 SHEETS 30 SHEETS 3 SQUARE
21 SHEETS 200 SHEETS 3 SQUARE
MATERIAL

PROPOSED
NORTHERN
LOCATION
FOR
SSSPT-F

3.2E¹ (14) 3.3E¹ (04) 2.4E¹ (10) 2.5E³ (17) 1.1E⁰ (06)

75.0
71.25
67.5

1.6E¹ (67) 7.0E² (74) 7.6E¹ (76) 6.6E¹ (62) 4.2E² (63) 3.7E² (65)

38.5
34.75
31.0

20
18
16
14
12
10
8
6
4
2

5.5E¹ (82) 3.9E¹ (83)

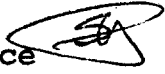
1 9 14 19 24 29

N 1420

September 2, 1992

MEMORANDUM

To: Ray Finley
Sandia National Laboratories 6121

From: Scott Van Pelt
Intera, Inc. WIPP Site Office 

Re: Gas Flow Results from Room L3

Gas flow testing of the first 20 boreholes in room L3 was completed on August 7, 1992 and gas flow rates were calculated on August 8. These results were presented to and discussed with Ernst Ahrens, Joe Tillerson, and Dave Borns on August 11.

Estimated gas permeabilities in the borehole arrays adjacent to the proposed slab location ranged from a minimum of 9.32×10^{-8} darcy near the rib to a maximum of 3.21×10^{-1} darcy near the center of the room. These figures are very similar to estimated permeabilities reported for other locations of similar age and room dimensions (Peterson et. al. 1985; Stormont, Peterson, and Lagus, 1987; Stormont, 1990). Permeability estimates are presented by borehole on the attached diagram of room L3.

Estimated gas permeabilities were calculated from gas flow data based upon the closed form solution presented in Stormont, Peterson, and Lagus 1987 and referenced to Zeigler, 1976. The equation used was:

$$k = \frac{dV}{dt} \frac{\mu P_a \ln(r_a/r)}{\pi L (P^2 - P_a^2)}$$

Where: k is permeability given in m^2 ;
 dV/dt is the gas flow rate given in m^3s^{-1} ;
 μ is the dynamic viscosity of nitrogen given in Pa s;
 P_a is the ambient atmospheric pressure given in Pa;
 P is the test zone absolute pressure given in Pa;
 r_a is the effective radius of influence given in m;
 r is the borehole radius given in m;

π is equal to 3.1416; and
L is pressurized test zone length given in m.

The permeabilities were converted to darcy by dividing the k expressed in m^2 by a factor of 9.87×10^{-13} . This solution requires the estimation of the effective radius of influence, r_a , for the ratio of effective radius of influence to well radius, r. This ratio varies with the formation permeability and, using data presented in Quality Assurance (QA) documents, was fit for permeabilities from 10^{-7} to 10^{-4} darcy. For permeabilities above 10^{-4} darcy, the ratio was assumed to be 20, a reasonable figure considering the spacing of the boreholes. These estimates should only be regarded as order of magnitude estimates due to the uncertainty inherent in estimating the effective radius of influence.

REFERENCES:

Peterson, E., et. al., 1985. WIPP Horizon In Situ Permeability Measurements Final Report. SAND85-7166.

Stormont, J.C., E.W. Peterson, and P.L. Lagus, 1987. Summary of and Observations About WIPP Facility Horizon Flow Measurements Through 1986. SAND87-0176.

Stormont, J.C., 1990. Summary of 1988 WIPP Facility Horizon Gas Flow Measurements. SAND89-2497.

cc Ernst Ahrens, 6121
Joe Tillerson, 6121
Dave Borns, 6116
George Saulnier, Intera

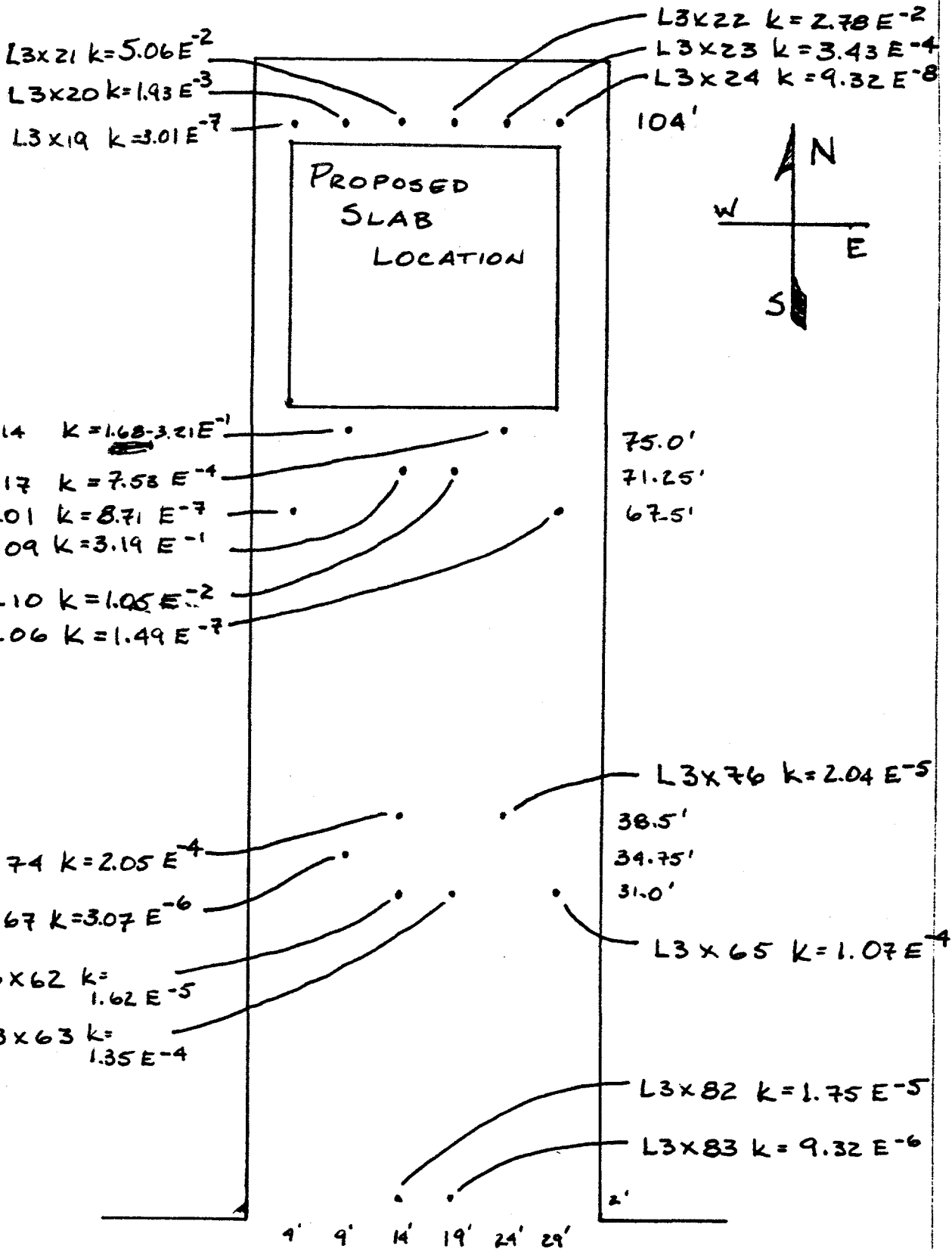
INTERA

ESTIMATED PERMEABILITIES IN ROOM L3 RSVP/INTERA

SSSPT-F

(PERMEABILITIES EXPRESSED IN DARCIES)

09/02/92



43 SHEETS 10 SHEETS 3 SQUARE
43 SHEETS 100 SHEETS 3 SQUARE
43 SHEETS 200 SHEETS 3 SQUARE
NATIONAL

N 1420

This page intentionally left blank.

APPENDIX J: GTFM FLOW MODEL

This page intentionally left blank.

APPENDIX J: GTFM FLOW MODEL

Flow Model Description

The Graph Theoretic Field Model (GTFM) numerical well-test interpretation model of Pickens et al. (1987) was used to analyze the gas-permeability tests. GTFM allows for complex pre-test pressure history and boundary conditions to be incorporated into the analysis. This feature permits the interpretation of sequential permeability tests without the need for pressure distributions within the testing formation to return to equilibrium conditions. GTFM simulates both Darcy flow and flow resulting from storage. For liquid phase simulations, GTFM is formulated based on the volumetric flow rate with storage a function of liquid and rock compressibility. For gas phase simulations, GTFM is based on either a volumetric flow rate or a mass flow rate with storage a function of only gas compressibility. The gas-permeability test interpretations presented in this report were all generated using the volumetric flow rate option for gas flow.

GTFM is a radial flow model with a flow system centered about a vertical, fully-penetrating wellbore within a formation of constant thickness. The flow system is partitioned into a specified number of radially centered cylindrical rings based on a multiplicative factor that incrementally increases the ring thickness as the distance from the wellbore increases. GTFM can simulate an unsaturated single porosity system when using the gas phase option (single phase only). For gas phase simulations, GTFM assumes ideal gas behavior under isothermal conditions with constant test-zone volume. The viscosity and permeability can be specified as either constant or pressure-dependent. The pressure dependence of permeability is based on the Klinkenberg equation.

Because GTFM assumes a constant-thickness single-layer system centered about the wellbore, boundary conditions must be specified within the wellbore, at the outer boundary, and along the upper and lower formation boundaries. Boundary conditions for the upper and lower formation boundaries are specified internal to the code as no-flow boundaries. The outer radial boundary condition can be specified as either constant-pressure or no-flow. The wellbore boundary conditions can be specified as a function of pressure or flow rate. The boundary conditions within the wellbore are specified by selecting the sequence of events that occurred during testing. Two sequence options within GTFM used for the gas-permeability test interpretations presented in this report are history and pulse. The history option applies a pressure or flow-rate boundary condition within the wellbore. This boundary condition can be either constant or a transient based on a curve fit through

measured field data. A history pressure boundary condition specification could be used to maintain atmospheric conditions within the borehole to account for an open hole prior to the start of testing. A history flow-rate boundary condition specifies a constant or transient flow rate being either injected or produced from the wellbore. In the gas-permeability tests presented in this report, a transient history flow boundary condition based on the measured gas-injection rates was specified within the wellbore during the gas-injection portion of the test. Using the specified wellbore flow rates, GTFM propagated the pressure disturbance out into the formation. The pulse sequence specifies that the wellbore is shut-in and the pressure between the wellbore and the formation are allowed to equilibrate. The pulse boundary condition was used in the gas-permeability test interpretations and was specified at the end of the gas injection portion of the tests. When the gas injection was terminated, the wellbore was shut-in and allowed to equilibrate with the static formation pressure.

The necessary input parameters for GTFM are used to describe the model configuration, the hydrological flow system configuration, and the simulation specifications. The model parameters are the wellbore radius, the distance to the outer boundary condition, the number of radial nodes (or rings) between the wellbore and the outer radial boundary, and the type of boundary condition specified at the outer radial boundary. The flow system parameters include the wellbore radius, formation thickness, test-zone volume, formation gas permeability, formation porosity, formation compressibility, and formation static pressure. The gas properties include the viscosity, the reference temperature and pressure for the viscosity value, and atmospheric pressure. The simulation parameters include specification of the testing sequence (history or pulse) in the proper order, the duration of each sequence, and the types of output data to capture (e.g., wellbore flow rate, wellbore pressure, pressure distribution within the formation).

Most of the flow-system parameters can be entered into the model as either constant values or as a suite of multiple values. GTFM allows for only a suite of two parameters at one time. This suite option allows for the generation of one simulation per value entered. If two gas-permeability and two formation porosity values were entered, GTFM would produce four different simulation runs. This feature allows the user to narrow the estimated parameter values of the suited parameters after only a few simulation runs have been performed.

Assumptions Used in Gas-Permeability-Testing Analyses

The assumptions used in the interpretations of the gas-permeability tests mirror those assumptions used in the formulation of GTFM, along with additional test-specific assumptions. The model assumptions included a single-phase gas simulation based on flow occurring by Darcy flow and caused by storage effects. The flow system was centered on a wellbore of known diameter and volume that fully penetrated a horizontal formation of constant thickness. This formation was assumed to be homogeneous and isotropic in nature with a far-field gas pressure assumed equal to atmospheric pressure. The simulations were generated assuming isothermal conditions within the borehole and formation. The gas-permeability and viscosity were held constant for each simulation and not given as a function of pressure. Therefore, the Klinkenberg effects on the gas permeability as a function of pressure were not incorporated into the solution.

The gas flow into the formation was assumed to be occurring over the entire length of the test zone. However, because of the potential fractured nature of MB139, this assumption is not completely valid. The formation was modeled within GTFM as a single porosity system. The gas-permeability analyses resulted in porosity values in the range of 0.015 to 0.005. Because of the overall qualitative nature of the gas-permeability testing approach, a more quantitative approach would be necessary to obtain greater certainty about exactly where flow was occurring within MB139.

The formational area of influence for each test is the area of rock that had a change in pressure from the gas-permeability testing. GTFM assumes that the area of influence is radially centered about the borehole and that no other pressure sinks or sources are incorporated beyond that of the outer constant-pressure boundary. Both of these assumptions are not completely valid for the flow system that developed under the concrete slab in Room L3. Depending on the borehole proximity to the rib, the pressure distribution in the formation may not be symmetrical. If the borehole is near the rib, a higher pressure region could exist under the rib as compared to under the center of the room, and this condition could have an effect on the test results. If the borehole is located in the center of the room, then the formation under the rib would have less impact on the test. GTFM assumes that no pressure sinks are incorporated into the solution. However, in the borehole array drilled into the slab, the distance between boreholes is from one to two meters. If the area of influence encompassed during a gas-permeability test is great enough, one or more boreholes may be at atmospheric pressure conditions and acting as pressure sinks. The presence

of these boreholes within the system was neglected in the analysis because the model assumes that the entire formation is at atmospheric pressure conditions.

Gas Properties Used in Test Analyses

Industrial-grade nitrogen gas was used for the gas-permeability testing. Nitrogen has an atomic weight of 14.0067 g/mole and a dynamic viscosity of 1.76×10^{-5} Ns/m². The viscosity of nitrogen is not affected in the pressure ranges used in this series of tests.

Instrument grade air with a 200 mg/Kg spike of isobutene was used for the tracer-gas injection testing. Its estimated dynamic viscosity is 1.784×10^{-5} Ns/m². The viscosity of air is not affected in the pressure ranges used in this series of tests.

Gas-Flow-Rate Calculations

Data from the internal reservoir pressure and temperature histories of individual tests, in conjunction with the volume of the internal reservoir and associated plumbing (up to the panel regulator), were used to calculate gas-flow rates at standard temperature and pressure during the constant-pressure injection portion of the tests. To calculate the number of moles of gas in the reservoir at each data sampling point, the Ideal Gas Law was used:

$$n = \frac{PV}{R(T+273)}$$

where

- n = the number of moles of nitrogen gas (moles)
- P = the internal-reservoir absolute pressure (Pa)
- V = the internal-reservoir volume at pressure P (m³)
- R = the universal gas constant (8314 J/Kg K)
- T = the reservoir temperature (°C)

The number of moles calculated was used to determine the volume that this nitrogen gas would occupy at a standard temperature of 20°C and a standard pressure of 0.10 MPa. Using the Ideal Gas Law and the number of moles at standard conditions, the volume of gas in the internal reservoir at each time step was calculated. The calculated volumes at each time step were used to calculate a change in reservoir volume from the previous time step. This calculated change was divided by the time between measurements to yield a gas-flow rate at standard temperature and pressure.

**WIPP
UC721 - DISTRIBUTION LIST**

Federal Agencies

US Department of Energy (6)
Office of Civilian Radioactive Waste Mgmt.
Attn: Deputy Director, RW-2
Associate Director, RW-10/50
Office of Prog. & Resources Mgmt.
Office of Contract Business Mgmt.
Director, RW-22
Analysis & Verification Division
Associate Director, RW-30
Office of Systems & Compliance
Associate Director, RW-40
Office of Storage & Transportation
Director, RW-4/5
Office of Strategic Planning and
International Programs
Office of External Relations

Forrestal Building
Washington, DC 20585

US Department of Energy
Albuquerque Operations Office
Attn: National Atomic Museum Library
P.O. Box 5400
Albuquerque, NM 87185-5400

US Department of Energy
Research & Waste Management Division
Attn: Director
P.O. Box E
Oak Ridge, TN 37831

US Department of Energy (5)
Carlsbad Area Office
Attn: G. Dials
D. Galbraith
M. McFadden
R. Lark
J. A. Mewhinney
P.O. Box 3090
Carlsbad, NM 88221-3090

US Department of Energy
Office of Environmental Restoration and
Waste Management
Attn: J. Lytle, EM-30
Forrestal Building
Washington, DC 20585-0002

US Department of Energy (3)
Office of Environmental Restoration and
Waste Management
Attn: M. Frei, EM-34, Trevion II
Washington, DC 20585-0002

US Department of Energy
Office of Environmental Restoration and
Waste Management
Attn: S. Schneider, EM-342, Trevion II
Washington, DC 20585-0002

US Department of Energy (2)
Office of Environment, Safety & Health
Attn: C. Borgstrom, EH-25
R. Pelletier, EH-231
Washington, DC 20585

US Department of Energy (2)
Idaho Operations Office
Fuel Processing & Waste Mgmt. Division
785 DOE Place
Idaho Falls, ID 83402

US Environmental Protection Agency (2)
Radiation Protection Programs
Attn: M. Oge
ANR-460
Washington, DC 20460

Boards

Defense Nuclear Facilities Safety Board
Attn: D. Winters
625 Indiana Ave. NW, Suite 700
Washington, DC 20004

Nuclear Waste Technical Review Board (2)
Attn: Chairman
S. J. S. Parry
1100 Wilson Blvd., Suite 910
Arlington, VA 22209-2297

State Agencies

Attorney General of New Mexico
P.O. Drawer 1508
Santa Fe, NM 87504-1508

Environmental Evaluation Group (3)
Attn: Library
7007 Wyoming NE
Suite F-2
Albuquerque, NM 87109

NM Energy, Minerals, and Natural
Resources Department
Attn: Library
2040 S. Pacheco
Santa Fe, NM 87505

NM Environment Department (3)
Secretary of the Environment
Attn: Mark Weidler
1190 St. Francis Drive
Santa Fe, NM 87503-0968

NM Bureau of Mines & Mineral Resources
Socorro, NM 87801

NM Environment Department
WIPP Project Site
Attn: P. McCasland
P.O. Box 3090
Carlsbad, NM 88221

Laboratories/Corporations

Battelle Pacific Northwest Laboratories
Attn: R. E. Westerman, MSIN P8-44
Battelle Blvd.
Richland, WA 99352

INTERA, Inc.
Attn: G. A. Freeze
1650 University Blvd. NE, Suite 300
Albuquerque, NM 87102

INTERA, Inc.
Attn: J. F. Pickens
6850 Austin Center Blvd., Suite 300
Austin, TX 78731

INTERA, Inc.
Attn: W. Stensrud
P.O. Box 2123
Carlsbad, NM 88221

Los Alamos National Laboratory
Attn: B. Erdal, INC-12
P.O. Box 1663
Los Alamos, NM 87544

RE/SPEC, Inc
Attn: Angus Robb
4775 Indian School NE, Suite 300
Albuquerque, NM 87110-3927

RE/SPEC, Inc
Attn: J. L. Ratigan
P.O. Box 725
Rapid City, SD 57709

Tech Reps, Inc. (3)
Attn: J. Chapman (1)
Loretta Robledo (2)
5000 Marble NE, Suite 222
Albuquerque, NM 87110

Westinghouse Electric Corporation (5)
Attn: Library
J. Epstein
J. Lee
B. A. Howard
R. Kehrman
P.O. Box 2078
Carlsbad, NM 88221

S. Cohen & Associates
Attn: Bill Thurber
1355 Beverly Road
McLean, VA 22101

National Academy of Sciences, WIPP Panel

Howard Adler
Oxyrase, Incorporated
7327 Oak Ridge Highway
Knoxville, TN 37931

Bob Andrews
Board of Radioactive Waste Management
GF456
2101 Constitution Ave.
Washington, DC 20418

Rodney C. Ewing
Department of Geology
University of New Mexico
Albuquerque, NM 87131

Charles Fairhurst
Department of Civil and Mineral Engineering
University of Minnesota
500 Pillsbury Dr. SE
Minneapolis, MN 55455-0220

Universities

B. John Garrick
PLG Incorporated
4590 MacArthur Blvd., Suite 400
Newport Beach, CA 92660-2027

Leonard F. Konikow
US Geological Survey
431 National Center
Reston, VA 22092

Carl A. Anderson, Director
Board of Radioactive Waste Management
National Research Council
HA 456
2101 Constitution Ave. NW
Washington, DC 20418

Christopher G. Whipple
ICF Kaiser Engineers
1800 Harrison St., 7th Floor
Oakland, CA 94612-3430

John O. Blomeke
720 Clubhouse Way
Knoxville, TN 37909

Sue B. Clark
University of Georgia
Savannah River Ecology Lab
P.O. Drawer E
Aiken, SC 29802

Konrad B. Krauskopf
Department of Geology
Stanford University
Stanford, CA 94305-2115

Della Roy
Pennsylvania State University
217 Materials Research Lab
Hastings Road
University Park, PA 16802

David A. Waite
CH₂ M Hill
P.O. Box 91500
Bellevue, WA 98009-2050

Thomas A. Zordon
Zordan Associates, Inc.
3807 Edinburg Drive
Murrysville, PA 15668

University of New Mexico
Geology Department
Attn: Library
141 Northrop Hall
Albuquerque, NM 87131

University of Washington
College of Ocean & Fishery Sciences
Attn: G. R. Heath
583 Henderson Hall, HN-15
Seattle, WA 98195

Libraries

Thomas Brannigan Library
Attn: D. Dresp
106 W. Hadley St.
Las Cruces, NM 88001

Government Publications Department
Zimmerman Library
University of New Mexico
Albuquerque, NM 87131

New Mexico Junior College
Pannell Library
Attn: R. Hill
Lovington Highway
Hobbs, NM 88240

New Mexico State Library
Attn: N. McCallan
325 Don Gaspar
Santa Fe, NM 87503

New Mexico Tech
Martin Speere Memorial Library
Campus Street
Socorro, NM 87810

WIPP Public Reading Room
Carlsbad Public Library
101 S. Halagueno St.
Carlsbad, NM 88220

Foreign Addresses

Atomic Energy of Canada, Ltd.
Whiteshell Laboratories
Attn: B. Goodwin
Pinawa, Manitoba, CANADA R0E 1L0

Francois Chenevier (2)
ANDRA
Route de Panorama Robert Schumann
B. P. 38
92266 Fontenay-aux-Roses, Cedex
FRANCE

Claude Sombret
Centre d'Etudes Nucleaires de la Vallee Rhone
CEN/VALRHO
S.D.H.A. B.P. 171
30205 Bagnols-Sur-Ceze, FRANCE

Commissariat a L'Energie Atomique
Attn: D. Alexandre
Centre d'Etudes de Cadarache
13108 Saint Paul Lez Durance Cedex
FRANCE

Bundesanstalt fur Geowissenschaften und
Rohstoffe
Attn: M. Langer
Postfach 510 153
D-30631 Hannover, GERMANY

Bundesministerium fur Forschung und
Technologie
Postfach 200 706
5300 Bonn 2, GERMANY

Institut fur Tieflagerung
Attn: K. Kuhn
Theodor-Heuss-Strasse 4
D-3300 Braunschweig, GERMANY

Gesellschaft fur Anlagen und Reaktorsicherheit
(GRS)
Attn: B. Baltes
Schwertnergasse 1
D-50667 Cologne, GERMANY

Shingo Tashiro
Japan Atomic Energy Research Institute
Tokai-Mura, Ibaraki-Ken, 319-11
JAPAN

Netherlands Energy Research Foundation ECN
Attn: J. Prij
3 Westerduinweg
P.O. Box 1
1755 ZG Petten
THE NETHERLANDS

Svensk Karnbransleforsorjning AB
Attn: F. Karlsson
Project KBS (Karnbranslesakerhet)
Box 5864
S-102 48 Stockholm
SWEDEN

Nationale Genossenschaft fur die Lagerung
Radioaktiver Abfalle (2)
Attn: S. Vomvoris
P. Zuidema
Hardstrasse 73
CH-5430 Wettingen
SWITZERLAND

AEA Technology
Attn: J. H. Rees
D5W/29 Culham Laboratory
Abington, Oxfordshire OX14 3DB
UNITED KINGDOM

AEA Technology
Attn: W. R. Rodwell
044/A31 Winfrith Technical Centre
Dorchester, Dorset DT2 8DH
UNITED KINGDOM

AEA Technology
Attn: J. E. Tinson
B4244 Harwell Laboratory
Didcot, Oxfordshire OX11 0RA
UNITED KINGDOM

Individuals

Hassan Alief
ALNICO Geo Services
8400 Manual NE
Albuquerque, NM 87112

Dave Ankeny
Elkin Manufacturing, Inc.
2431 Route 286 West
Indiana, PA 15701

Henry Backe
Cambrian Equipment Co.
137 Hughes Road
King of Prussia, PA 19406

John Baldwin
Pier-A-Mid Rehabilitation, Inc.
908 Tulane
Houston, TX 77008

Dirk Balzer
Bundesanstalt fur Geomissenschafren
(030) 46501329
Invalidenstrasse 44
70775 Berlin GERMANY

Mark Boscardin
GEI Consultants, Inc.
1021 Main Street
Winchester, MA 01890

Matt Bravenic
GZA Environmental Tech, Inc.
3200 Needham St.
Neptown Falls, MA 02164

Michael Chang
Kewell Geotechnical Engineering
96-1416 Waiihona Place
Pearl City, HI 96782

Paul Chung
Geotech Engineers, Inc.
10617 Duvall St.
Glendale, MD 20769

William J. Clarke
GEO/CHEM
162 Spencer Pl.
Ridgewood, NJ 07450

S. Cohen and Associates, Inc.
Attn: W. C. Thruber
1355 Beverley Rd.
McLean, VA 22101

Community Environmental Council
Attn: Chris Webb
930 Miramonte Drive
Santa Barbara, CA 93109

John Del Val
Del Val Grouting Consultants, Inc.
6299 Crampton Dr. North
Salem, OR 97303

Farrokh Djahanguri
U. S. Bureau of Mines
Denver Federal Center
Building 20
Denver, CO 80225

David Eastwood
Geotech Engineering & Testing, Inc.
5889 West 34th Street
Houston, TX 77092

Peter Emmons
Structural Preservation Systems
3761 Commerce Dr.
Baltimore, MD 21227

Peter S. Gaillard
Martin Marietta Magnesia, Inc.
P. O. Box 15470
Baltimore, MD 21220-0470

Tom Griffin
Senior Staff Engineer
Dowell Schlumberger, Inc.
P.O. Box 4378
Houston, TX 77210-4378

Kay Harkcom
3M Government R&D Contracts
3M Center Bldg.
224-2S-25
St. Paul, MN 56144-1000

Warren L. Harrison, P. E.
Commercial Pantex Sika, Inc.
P. O. Box 3315
4901 Dry Creek Rd.
Littleton, CO 80161-3315

A. C. Houlsby
A.S.T.C., F.I.E. Aust., F. ASCE
32 Apps Ave.
Turramurra, N.S.W. 2074
AUSTRALIA

Pete Iovion
Delm Geotechnical Services
22 Dradock Ave.
Boston, MA 02210

Stephan Jeffries
Golder & Associates, Ltd.
54 Moorbridge Road
Maidenhead, Berkshire
ENGLAND SL6 8BN

Don Jones
Progressive Industries, Inc.
Gene E. Stewart Blvd.
P. O. Box 1329
Sylacauga, AL 35150

Bill Larsen
U. S. Bureau of Mines
5629 Minnehaha Ave., South
Minneapolis, MN 55417

Glen Lau
Pacific Geotechnical Engineers
1030 Kohou St., SE101
Honolulu, HI 96817

K. Licklitter
400-C 8th St. SW
Tacoma, WA 98439

Don Mack
Avanti International
822 Bay Star Blvd.
Webster, TX 77598-1528

Steve Maranowski
Spartan Specialties, Ltd.
P. O. Box 3715
Centerline, MI 48015

Bruce McDonald
P. O. Box 1266
Milton, WA 98354

Richard McGaw
McGaw Civil & Geotechnical Engineers
3 Prospect St.
Shanover, NH 03755

M. Mohrmann
Fugro McClelland
P.O. Box 740010
Houston, TX 77274

Paul Moore
Phelps Dodge Morenci, Inc.
4521 U. S. Highway 191
Morenci, AZ 85540

Trevor A. Moss
Senior Engineering Specialist
Redpath-McIntosh Engineering, Inc.
1347 North Alma School Rd., Suite 100
Chandler, AZ 85224

Alex Naudts
ECO GEO Consulting, Ltd.
73 Credit Road
Cheltenham, Ontario LOP 1CO
CANADA

W. W. Poimboeuf
Liquid Waste Disposal, Inc.
214 Arthur Street
Manistee, MI 49660

Ronald D. Powell
TVA
1101 Market Street
Chattanooga, TN 37402

D. W. Powers
Star Route Box 87
Anthony, TX 79821

David E. Ridenour, P. E.
Fernald Environmental Management Project
7400 Willey Road
P. O. Box 398704
Cincinnati, OH 45239

Richard Sheets, Vice President
Soil Technology
7865 NE Day Road West
Bainbridge Island, WA 98100

Joe Stevenson
J. B. Stevenson & Sons
P. O. Box 4740
Senora, CA 95370

Fred Sherill
Surecrete, Inc.
155 N. E. 100T11, Suite 300
Seattle, WA 98125

James Villar
Balvac
3517 Genesee Street
Buffalo, NY 14225

1395 6700 P. Brewer
1395 6800 L. Shephard
1395 6707 M. Marietta
1395 6841 V. H. Slaboszewicz

James Warner
Consulting Engineer
P. O. Box 1208
Mariposa, CA 95338

1330 6752 C. B. Michaels (2)
1330 6752 NWM Library (20)
9018 8523-2 Central Technical Files
0899 4414 Technical Library (5)
0619 12615 Print Media
0100 7613-2 Document Processing (2)
for DOE/OSTI

Peter T. Yen, Chief Geologist
Bechtel Corporation
50 Beale Street
P. O. Box 193965
San Francisco, CA 94119-3965

Maria Onofrei
Whiteshell Laboratories
Pinawa Manitoba
CANADA ROE ILO

Parson Brinckerhoff
303 Second Street
Suite 850 North
San Francisco, CA 94107-1368

Internal

<u>MS</u>	<u>Org.</u>	
0701	6100	R. Lynch
0705	6114	R. Harding
0706	6113	J. Linn
0715	6603	R. Luna
0719	6621	J. Nelson
0720	6609	T. Sanders
0726	6600	J. K. Rice
0728	6602	D. Berry
0743	6907	D. Engi
0743	6907	R. Matalucci
0750	6116	M. Walck
0750	6118	H. Westrich
0751	6117	W. Wawersik
1003	6604	D. Weaver
1033	6111	D. Glowka
1320	6719	E. J. Nowak
1322	6121	J. R. Tillerson
1322	6121	E. Ahrens (25)
1324	6115	P. B. Davies
1328	6749	D. R. Anderson
1328	6741	H. N. Jow
1335	6705	M. Chu
1341	6811	A. L. Stevens
1341	6748	J. T. Holmes

